Technical Report
TR-19-07
December 2019

Past and future impact of glacial erosion in Forsmark and Uppland

Final Report

Adrian M Hall
Karin Ebert
Bradley W Goodfellow
Clas Hättestrand
Jakob Heyman
Maarten Krabbendam
Seulgi Moon
Arjen P Stroeven

SVENSK KÄRNBRÄNSLEHANTERING AB

SWEDISH NUCLEAR FUEL
AND WASTE MANAGEMENT CO

Box 3091, SE-169 03 Solna
Phone +46 8 459 84 00
skb.se

SVENSK KÄRNBRÄNSLEHANTERING

ISSN 1404-0344
SKB TR-19-07
ID 1718396

December 2019

Past and future impact of glacial erosion in Forsmark and Uppland

Final report

Adrian M Hall[1], Karin Ebert[2], Bradley W Goodfellow[3], Clas Hättestrand[1], Jakob Heyman[4], Maarten Krabbendam[5], Seulgi Moon[6], Arjen P Stroeven[1, 7]

1 Geomorphology and Glaciology, Department of Physical Geography, Stockholm University
2 Department of Natural Sciences, Technology and Environmental Studies, Södertörn University
3 Sveriges Geologiska Undersökning
4 Department of Earth Sciences, University of Gothenburg
5 British Geological Survey
6 Department of Earth, Planetary, and Space Sciences, University of California
7 Bolin Centre for Climate Research, Stockholm University

Keywords: Glacial erosion, Cambrian, Unconformity, sub-Cambrian peneplain, Cosmogenic nuclides, Exposure dating, Sheeting, Geomorphology, GIS, Long-term landscape development, Stress modelling, Forsmark.

Preface

The following report constitutes a final report of a comprehensive study on denudation and glacial erosion conducted at Forsmark and in the surrounding Uppland province, Sweden, between 2015 and 2019. The aim was to quantify the amount of past denudation at the Forsmark site and the broader Uppland region, with special focus on glacial erosion, by employing a range of methodologies. The methods included geomorphological mapping and analysis of the bedrock surface and Quaternary deposits, cosmogenic exposure dating, bedrock fracture mapping, and shallow bedrock stress modelling. The results were also used together with results from a long-term climate modelling study to quantify the potential amount of glacial erosion at Forsmark over the coming one million years.

The study was initiated by Jens-Ove Näslund (SKB) and it was jointly designed by Jens-Ove Näslund, Adrian Hall (Stockholm University), Karin Ebert (Södertörn University), Bradley Goodfellow (Stockholm University, SGU), Clas Hättestrand (Stockholm University), Jakob Heyman (University of Gothenburg) and Arjen Stroeven (Stockholm University). Adrian Hall coordinated the scientific work within the study, and also conducted the studies on long-term burial and erosion history (Chapter 2) and glacial erosion (Chapter 4). Karin Ebert developed the digital elevation models of the unconformity and derived the glacial erosion estimates derived from summit erosion surfaces. Bradley Goodfellow contributed across the project and conducted the study of topographic stress perturbation, with mathematical modelling by Seulgi Moon (University of California, Los Angeles) (Chapter 3). Clas Hättestrand developed geomorphological maps of the unconformity and of glacial bedforms. Maarten Krabbendam (British Geological Survey) contributed to Chapter 2 on the long-term burial and erosion history and to Chapter 4 on glacial erosion and mapped landforms associated with glacial ripping in Uppland. Sample site selection and cosmogenic nuclide sample collection was carried out by Jakob Heyman, Bradley Goodfellow, Arjen Stroeven, Marc Caffee and Adrian Hall. Jakob Heyman conducted the modelling of cosmogenic nuclide erosion and burial histories. Bradley Goodfellow was involved in cosmogenic nuclide sample preparation at Purdue University. Reporting and interpretation of cosmogenic nuclide results in Chapter 5 was done by Jakob Heyman, Arjen Stroeven and Bradley Goodfellow. All authors contributed to the final revision of the report.

The study includes several additional important contributions. Marc Caffee (Purdue University) was responsible for all cosmogenic isotope laboratory analyses and guided and participated in the discussions of interpretation of results (Chapter 5). Stephen Martel (University of Hawaii) and Taylor Perron (Massachusetts Institute of Technology) were involved in the fracture mapping and modelling (Chapter 3). Mikis van Boeckel (Stockholm University) produced many of the figures in the report from digital elevation model data from the Swedish mapping, cadastral and land registration authority (Lantmäteriet) and SGU.

In connection to the present study, two additional studies have been performed employing similar methods (e.g. geomorphological analysis and cosmogenic exposure dating) for studying the sub-Cambrian unconformity in the Trollhättan area in south-western Sweden. The two associated studies will be published in separate reports (Goodfellow et al. 2019, Hall et al. 2019a).

The results will be used, together with other published scientific information, for constructing future scenarios of climate and climate-related processes in SKB's work on assessing long-term safety of nuclear waste repositories in Sweden. The safety assessments performed for the planned repository for spent nuclear fuel in Forsmark, Sweden, cover a total time span of one million years. Since this time span covers the timescales relevant for glacial cycles, the effect of future glacial erosion needs to be analysed in the safety assessments. In this context, the present study provides important results on the potential amount of glacial erosion that may be expected in the topographical, geological, and glaciological setting of the Forsmark site. A separate study models changes in climate over the next 1 million years and has been published ahead of this report (Lord et al. 2019).

The report was scientifically reviewed by Prof. Paul Bishop (School of Geographical and Earth Sciences, University of Glasgow), Prof. Dr. Miriam Dühnforth (Department für Geo- und Umweltwissenschaften, Ludwig-Maximilians-Universität, München), Prof. Neil Glasser (Department of Geography and Earth Sciences, Aberystwyth University), and Assoc. Prof. Henriette Linge (Department of Earth Science, University of Bergen). Input to an earlier version of the manuscript was provided by Jens-Ove Näslund (SKB), Raymond Munier (SKB), Diego Mas Ivars (SKB), Assen Simeonov (SKB), and Christina Truedsson (Tintra consult).

Stockholm, December 2019

Jens-Ove Näslund
Coordinator Climate Research Programme SKB

Summary

We provide estimates of past and projections of future depths and rates of glacial erosion in the Uppland province in east central Sweden. We focus on the area around Forsmark, the proposed site for a geological repository for spent nuclear fuel in Sweden and the site for the existing repository for low- and intermediate level radioactive waste (SFR). The project is built on four research strands: (i) use of the Cambrian basement unconformity as a reference surface against which to estimate Pleistocene glacial erosion, (ii) control of basement fractures on past and future glacial erosion patterns, (iii) mapping of the distribution, form and characteristics of glacial landforms on the shield surface to understand patterns, processes and depths of glacial erosion and (iv) use of cosmogenic nuclide inventories for bedrock surfaces and erratic boulders to estimate erosion rates and total depths of erosion beneath the last ice sheet through the last glacial cycle (100 ka) and cumulatively over multiple glacial-interglacial cycles (1 Ma).

The Fennoscandian craton stabilised in east central Sweden after the Svecokarelian orogeny at ~ 1.9 Ga. The basement was reduced to hilly and low relief by 1.5 Ga at the sub-Jotnian unconformity (U1) and was subsequently buried by kilometre thick sediments consisting mainly of arkosic sandstones. Small outliers of Jotnian sandstone occur to the west of Singö in grabens bounded to the north by the Singö Deformation Zone. The presence of Ordovician limestone in these grabens, and those in Gävle Bay, indicates the reactivation of bounding faults. The proximity of U1 and the present basement surface around the edge of the Bothnian basin indicates that total denudation of basement since 1.5 Ga has been low.

From the final stages of the Sveconorwegian Orogeny at ~ 960 Ma onwards, much of Scandinavia was subjected to long-term uplift and erosion that led eventually to removal of Jotnian and Sveconorwegian foreland basin cover from Uppland. Previous (U-Th)/He data from surface samples at Forsmark indicate cooling below 70 °C between 750 and 530 Ma. By the late Neoproterozoic, large areas of Baltica, in common with Laurentia, had been reduced to low relief shield surfaces that stood close to base level. In Estonia, the shield surface became deeply weathered after ~ 580 Ma and was then transgressed by 548 Ma as sea level rose by ~ 50 m in the Late Ediacaran, with burial by quartz sandstones. Those parts of Baltica that now lie in Sweden were flooded later, starting in the Early Cambrian (541 Ma) in the first of numerous transgressive-regressive cycles that continued into the Late Ordovician. Geological evidence for the remarkable extent and low relief of the sub-Cambrian unconformity surface (U2) over wide areas of Baltica comes from strike sections around outliers and from the stratigraphic architecture of the overlying sedimentary cover, with continuity of unit thicknesses and facies between the Bothnian Sea and southern Sweden. U2 developed after prolonged subaerial denudation in the Late Neoproterozoic. Final grading of the already low-relief basement occurred during shoreline erosion during multiple transgression-retrogression cycles.

Burial of the basement of Uppland from the Early Cambrian onwards is indicated by Early Cambrian sandstone dykes in basement fractures around its eastern periphery, widespread asphaltite fracture coatings derived from Middle Cambrian and younger Alum Shales and the presence of small outliers of Early to Middle Ordovician limestone offshore that overlie a gently inclined basement surface on the seabed off Forsmark. During early Middle Cambrian emergence of Uppland, an unconsolidated Early Cambrian cover was removed by erosion during the Hawke Bay sea level low-stand before the basement was reburied by Alum Shale and limestone during renewed marine transgression. At the time of the Caledonian orogeny, Uppland formed part of a foreland basin. U2 and its Early Palaeozoic cover were buried to kilometre depth.

In basement areas around early Palaeozoic outliers in south-central Sweden, U2 has a distinctive morphology where it emerges from beneath cover rocks. At the regional scale (1–10 km), U2 is seen in Digital Elevation Models (DEMs) as a low-relief surface displaying a widespread accordance of basement summit elevations. Where seen near to outliers at the local scale (0.1–1 km) in Västergötland, the unconformity has relief as low as metre-scale. U2 is broken by minor, post-Cambrian faulting into mosaics of inclined, flat-topped fault blocks. A similar basement morphology with inclined, fault blocks with accordant summits, and vertical displacement of a few tens of metres, exists in north-east Uppland. This morphology indicates proximity between the present basement surface (UQ) and U2. The former U2 surface is mapped from Digital

Elevation Models (DEMs) across dislocated rock blocks. Models of the former sub-Cambrian unconformity, with its minimum elevation, are also constructed using present basement summit heights as pinning points to produce summit envelope surfaces. The summit envelope surfaces provide reference surfaces for estimation of depths of glacial erosion required to form UQ. The models of U2 rest on assumptions that U2 was originally a near planar surface, without deep Neoproterozoic weathering at the time of burial, overlain by Ordovician limestone and broken by minor, post-Ordovician faulting.

The elevation differences between U1, U2 and UQ around Forsmark are small. As below UQ today, fractures were likely opened beneath the antecedent unconformities. Similarly, fracture coatings may also have developed during basement exposure beneath U1 and U2 but currently are not recognised in the literature as representing distinct generations of fracture coatings. Previous detailed analysis of the geochemistry of fracture coatings indicates that the late Palaeozoic and early Mesozoic were important periods for brine circulation and fracture mineralisation. The absence of saprolite remnants from the dense network of boreholes at Forsmark indicates that the basement was not re-exposed to weathering prior to Pleistocene glaciation. Evidence for recent re-exposure to weathering of U2 from beneath Ordovician limestone at locations on the western fringes of the Baltic is given by the persistence of calcite fracture coatings of Palaeozoic age found at shallow depth around Forsmark and by the mobilisation of U oxides over the last 300 ka at Äspö, Oskarshamn.

Fracture sets at Forsmark have a highly complex history of formation, opening, and mineralisation that spans the last 1.9 Ga due in part to the limited denudation of the basement and its prolonged and deep burial by sedimentary cover rocks. However, the modification of pre-existing topography by Pleistocene glacial erosion may contribute to further fracturing in ways that could influence future glacial erosion. This is because theoretical calculations and field observations elsewhere indicate that topographic features such as ridges and valleys cause vertical and lateral variations in the shallow subsurface stress field. If these stress perturbations are large enough (and perhaps aided by elevated groundwater pressure) they may modify near-surface bedrock fracture patterns, which in turn can influence glacial erosion. Whereas the regional surface gradient and present topographic relief in the Forsmark area are low (1 m/km and less than 20 m, respectively), both parameters increase in the adjacent offshore region and topographic curvatures are frequently high, particularly on the flanks of trenches and basins and on hills and ridges. In addition, Forsmark is characterized by high maximum horizontal compressive stresses in the shallow subsurface. The depth to which topography influences the stress field and bedrock fracturing is determined by the combination of horizontal compressive stresses and topographic wavelength.

We assess how present topography may perturb near-surface stress fields at Forsmark to impart control on which fractures may open and where in the landscape and subsurface they open. We did this using a three-dimensional boundary element model and considered influences from pore pressure and sediment loading on the near-surface stress fields. This modelling showed that topography may strongly perturb near-surface stress-fields in the uppermost 100 m, even in this low relief landscape. The topographic perturbation declines with depth and is minor at depths below 400 m. The model predicts that sub-horizontal fractures will more likely open beneath convex landforms perpendicular to the maximum horizontal compressive stress (directed NW-SE), i.e. particularly those landforms with long axes oriented NE-SW. This may produce higher erosion rates on ridges and lower erosion rates in valleys that display this orientation and might result in overall relief reduction through glacial erosion. Conversely, the higher magnitudes of the least compressive horizontal stress beneath ridges and valleys oriented parallel to the maximum horizontal compressive stress may mean they are more resistant to glacial erosion and relief may persist or increase, rather than decrease. Finally, it appears that some valleys might be in tension, which would favour opening of sub-vertical fractures in these locations. Glacial erosion rates might therefore be higher in these valleys, potentially increasing local relief. In summary, even in this low-relief landscape, topography may exert control on near-surface bedrock fracturing and patterns and depths of glacial erosion. Further research is needed to explore other controls on present fracture openness including the important contributions of antecedent conditions as far back as 1.9 Ga. Topographic stress perturbations are also likely to have interacted with groundwater overpressure underneath the Fennoscandian Ice Sheet, which has been modelled previously to extend to depths of 500 m.

During the Pleistocene, erosion by the Fennoscandian Ice Sheet led to development of a nested hierarchy of glacial landforms set mainly within relative relief of less than 20 m. Mapping of

landscapes and landforms of glacial erosion at the regional (1–10 km) and local (0.1–1 km) scales using LiDAR-based DEMs reveals the pattern of modification of antecedent topography and the development of new glacial landforms. Progressive erosion of basement blocks involved the lowering and roughening of block top surfaces via the excavation of narrow trenches and shallow basins along fracture zones, the crenulation and indentation of block edges and the excavation of 15–20 m deep bounding trenches and basins. Mapping of local landforms shows a strong zonation of features within three terrain types: (i) ice-roughened, (ii) weakly streamlined and (iii) disrupted terrain. *Ice-roughened terrain* is dominated by roches moutonnées and box hills, with fracture-guided trenches and box and star basins. *Weakly streamlined terrain* includes elongate hills, with till tails, and parallel trenches aligned with fracture sets and former ice flow direction. *Glacially disrupted terrain* is characterised by extensive spreads of large, angular boulders that mask underlying bedrock. An inventory of glacial landforms is provided based on DEMs and field observations at the local (0.1–1 km), macro (10–100 m), meso (1–10 m) and micro (less than 1 m) scales. Landform assemblages seen across these scales are linked to sets of glacial processes grouped as abrasion, plucking, ripping and meltwater erosion. Glacial meltwater has acted together with other subglacial erosional processes to excavate fracture-guided trenches. Glacial ripping is a newly recognised process set that involves the jacking, disruption and entrainment of rock blocks, with the formation of extensive spreads of large, angular boulders. The process of ripping requires groundwater overpressure, possibly associated with high volumes of meltwater, beneath the retreating margin of the Fennoscandian Ice Sheet. The ripping process set is an important, perhaps locally dominant agent of glacial erosion in the Forsmark area that operated to depths of at least several metres during deglaciation.

Field observations on roche moutonnée surfaces allow assessment of the likely processes operating on these surfaces in relation to erosion depths and rates estimated from cosmogenic nuclide inventories. The micro to macro forms currently displayed on these rock surfaces mainly reflect the operation of the erosional processes late in the last glacial cycle and evidence of earlier modification are normally obliterated. Abrasion microforms, including polished and striated surfaces, are ubiquitous but the frequency and extent of lacunae such as chips, crescentic fractures and shallow cavities indicate that other processes may be more important for micro-erosion budgets. Some roches moutonnées mapped in drone surveys on the shoreline at Forsmark display numerous 0.5–5 m wide prismatic and box sockets that probably relate to block removal under conditions of high sub-glacial meltwater pressures. Plucking has generated cliffs and sockets on roche moutonnée flanks and lee slopes. Features indicating the operation of ripping or thrusting are largely absent from roche moutonnée tops at our cosmogenic nuclide sample sites.

Depths of Pleistocene glacial erosion include the removal of Ordovician limestone and the underlying hard, fractured basement. Removal of soft, bedded and jointed sedimentary cover involved the loss of at least several tens of metres of cover rock based on the 20–40 m depths of sub-Jotnian and -Ordovician rock basins in the Öregrund archipelago. Fault-bounded basement blocks found offshore and beneath Ordovician cover have sharp edges to fault scarps. On the re-exposed unconformity, these exhumed fault scarp edges are rounded and eroded leeward, with loss to glacial erosion of wedges of rock up to 20 m in thickness. Some adjoining fault blocks in NE Uppland, however, have raised edges that differ in elevation by less than 10 m. A deeper glacial erosion in basement can be expected to have erased these slightly upstanding features.

Depths of glacial erosion in basement are also estimated using summit envelope surface models of the dislocated sub-Cambrian unconformity as a reference surface. A summit envelope surface model indicates that an average of 14 m of basement rock has been lost to glacial erosion across north-east Uppland, with increasing depths of erosion towards the south. In the Forsmark area, the equivalent depth is 12 m. The largest depths of glacially eroded rock came from rock trenches and basins, 10–20 m deep, excavated along fracture zones. To these estimates should be added the depth of rock lost from summits in the current landscape used to construct the model of U2. Evidence from height differences between still-buried U2 surfaces and exposed basement summits nearby and the low elevation ranges of summits at increasing distances from Early Palaeozoic outliers in southern Sweden, and assuming U2 to be a planar surface, indicate that losses of basement from summits are <10 m. Similar losses, less constrained by outliers, are indicated by the elevation range of basement summits on the inclined basement ramp, with patches of Ordovician limestone, found offshore from Forsmark and by the preservation of low, exhumed fault scarps, along with gently inclined fault block tops with less than 5 m relief. A preliminary estimate of 10 m is adopted in the Forsmark area for the rock lost from above basement summits. However, if model assumptions are invalid or if

integrated glacial erosion since exhumation has been spatially uniform then the upper limit for basement summit erosion could potentially be higher.

Paired ^{10}Be and ^{26}Al cosmogenic nuclide data are available for 32 surface bedrock samples along a transect that extends south from Forsmark for ~50 km, and three boulder samples at the coast. Three of these samples were collected within or on the edges of the planned waste repository at the Forsmark site. Compared to the expected cosmogenic nuclide concentration based on the detailed timing of deglaciation and postglacial emergence from water, all but one sample have ^{10}Be and ^{26}Al concentrations that show inheritance, with the mid-range being 3.4–9.6 ka too old. We use the cosmogenic nuclide data from the bedrock samples to simulate the range of rates and depths of glacial erosion that are consistent with the measured ^{10}Be and ^{26}Al concentrations. We adopt a range of scenarios, with simulation start times ranging from 10 Ma to 130 ka before present, interglacial erosion rates of 0–5 mm/ka, a range of ice cover histories determined by the benthic δ^{18}O global ice volume proxy (LR04: 4.4–4.6 ‰) and by ice sheet modelling for the last glacial cycle, and with glacial erosion either scaled against duration of ice cover or scaled against number of ice cover periods. The samples are primarily collected from local high points in the landscape and because of sediment cover we have no samples from basin floors. Sample elevations range from 0–67 m a.s.l. There is no relationship between inheritance/glacial erosion and sample elevation. For one hill with seven analysed samples, the pattern of nuclide inheritance indicates low erosion across the hill top and more intense erosion around its base. Nineteen samples from low elevation (0–24 m a.s.l.) within 5 km of the location of the planned spent nuclear fuel repository yield total erosion since 100 ka of 0–8.6 m. Two samples located directly above the repository footprint yield total erosion over the last 100 ka of 1.0–5.6 m (based on ^{10}Be and ^{26}Al). Thirteen samples at 25–67 m a.s.l. along a transect SSW of Forsmark yield similar erosion from the paired nuclides with 0.6–8.1 m of erosion since 100 ka. Three boulder samples from the Forsmark coast all yield inheritance of similar magnitude to the bedrock samples equivalent to 2–41 ka of surface exposure. This supports an interpretation of limited glacial erosion as the boulders must have experienced exposure prior to the last ice-cover period and thereby have been located at shallow depth. Under the assumption that all glaciations that covered the Forsmark area and Uppland region erode the basement with similar mode and intensity, the typical total erosion over the last 100 ka appears to be 1.6–3.5 m and 13–27 m erosion over the last 1 Ma. The erosion depths over 1 Ma are larger than the estimate of 10 m lowering of basement summits below U2 based on geomorphological evidence. The higher 1 Ma erosion depths derived from cosmogenic nuclides may include removal of cover rocks or simply reflect erosion of basement rock. If the latter, the 10 m estimate for U2 lowering based on geomorphological evidence is too low. Both options are consistent with re-exposure of basement from below Early Palaeozoic cover rocks by glacial erosion within the last 1.1 Ma. The ranges of erosion derived from the simulations represent variation of simulated erosion from point samples and illustrate that glacial erosion has varied spatially. However, given the number of samples and their wide spatial distribution, the ranges of erosion are well-clustered and indicate limited glacial erosion in this low relief landscape.

The safety assessments made for the planned repository for spent nuclear fuel for the proposed nuclear waste repository site require consideration of glacial erosion under projected future glacial conditions. Assuming re-exposure of basement at 1.1 Ma before present, estimated average depths of glacial erosion per glacial cycle based on geomorphological evidence are ~2 m. In basins and trenches, erosion rates may exceed 3 m per glacial cycle. Cosmogenic nuclide data indicate that erosion rates on rock surfaces at Forsmark, including those within the proposed repository site, were 0–8.6 m over the past 100 ka. The end member values of 0 and 8.6 m of erosion apply to sites spaced at <2.5 km distance and appear to reflect stochastic variations in erosion depths and processes. Hence, erosion rates averaged over multiple glacial cycles probably fall within this range.

To estimate potential future depths of glacial erosion at the Forsmark site, we combine simulations of glacial erosion based on ^{10}Be and ^{26}Al cosmogenic nuclides with projections of future ice sheet cover at Forsmark over the coming 1 Ma from ice sheet modelling based on IPCC emission scenarios and future variations in insolation (Lord et al. 2019). Projected depths of total erosion for the Forsmark site over the coming 100 ka is less than 1 m. Over the coming 1 Ma, the mid- range of total erosion depth is 5–28 m, and the wider range of total erosion depth is 2–43 m. It is important to note that these projected depths of erosion are highly dependent on the assumption that glacial erosion depths in the past are representative of glacial erosion depths in the future.

Sammanfattning

I denna rapport redovisas beräkningar av den glaciala erosionens omfattning i Uppland, såväl i historisk tid som i framtiden. Geografiskt fokus för undersökningarna är området kring Forsmark, som idag utgör platsen för lagring av svenskt låg- och mellanaktivt radioaktivt avfall (SFR), och som föreslagits som framtida plats för slutförvar av använt kärnbränsle i Sverige. Projektet bygger på fyra metodologiska forskningsspår: 1. Användandet av den kambriska inkonformiteten som en referensyta, mot vilken den pleistocena glaciala erosionen kan uppskattas. 2. Spricksystem i urberget som en indikator på glaciala erosionsmönster. 3. Kartering av utbredning, form och egenskaper hos glaciala landformer i urberget, i syfte att förstå mönster, processer och djupet hos den glaciala erosionen. 4. Mätning av kosmogena nuklider i berggrund och i block i syfte att uppskatta erosionshastighet och erosionsdjup under den senaste glaciala cykeln (ca 100 000 år sedan; 100 ka), liksom den totala kumulativa erosionen över flera glaciala-interglaciala cykler (1 000 000 år sedan; 1 Ma).

Den fennoskandiska kratonen stabiliserades i östra Svealand efter den svekokarelska orogenesen omkring 1,9 miljader år sedan (Ga). Urberget var nederoderat till en relativt låg relief vid 1,5 Ga, markerat av den sub-jotniska inkonformiteten (U1), och blev därefter täckt av tjocka sedimentlager som sedermera gav upphov till framförallt kvartsitiska sandstenar. Närheten till U1 i förhållande till dagens urbergsyta längs kanterna av den Bottniska bassängen indikerar att den totala denudationen under de senaste 1,5 Ga varit begränsad. Mindre förekomster av jotnisk sandsten finns väster om Singö, i djupområden mellan Singö och Forsmark deformationszoner, i samma tektonisk miljö som i området omkring Forsmark. Neoproterozoiska förkastningar ledde till förskjutningar av bergblock i södra Bottenhavet, vilket sannolikt påverkade även bergblocken kring Forsmark.

Från slutet av den svekonorvegiska orogenesen, vid ca 960 Ma, påverkades stora delar av Skandinavien av långvarig upphöjning och erosion, vilket ledde till att de jotniska och svekonorvegiska pålagringssedimenten eroderades bort i det som är dagens Uppland. Tidigare (U-Th)/He-data från ytprover vid Forsmark har visat att en avsvalning till under 70 °C inträffade mellan 750 och 530 Ma. Under sen neoproterozoikum hade stora delar av Baltica, i likhet med Laurentia, reducerats till ett sköldområde med låg topografisk variation i en nivå nära basytan. I Estland blev sköldens yta utsatt för djupvittring efter 580 Ma och utsattes sedan för transgression vid 548 Ma, i takt med att havsytan steg med ca 50 m i sen ediacara, och urbergsytan begravdes av kvartssandstenar. De svenska delarna av Baltica översvämmades något senare, med start i tidig kambrium (541 Ma), i den första av ett flertal transgressions-regressionscykler som fortsatte i yngre ordovicium. Den kambriska inkonformiteten (U2) har en anmärkningsvärt plan yta och vidsträckt utbredning över stora delar av Baltica. Geologiska bevis för detta finns i skärningar där paleozoiska bergarter vilar på urberget och genom stratigrafin hos överliggande sedimentär berggrund, som uppvisar kontinuitet i mäktighet och facies från Bottenhavet ner till södra Sverige. U2 utvecklades efter långvarig subaeril denudation i sen-proterozoikum. Slutlig avplaning av den redan flacka ytan skedde i samband med upprepade transgressions-regressionscykler under loppet av några tiotals millioner år.

Urberget i Uppland blev täckt av sediment från och med tidig kambrium, vilket indikeras av tidig-kambriska sandstensgångar i urberget i områdets östligaste delar, av utbredd sprickfyllnad av asfaltit som härstammar från alunskiffer från mellankambrium och senare, samt av mindre förekomster av kalksten från undre och mellersta ordovicium. Denna kalksten ligger ovanpå en flackt sluttande urbergsyta på havsbotten öster om Forsmark. I samband med regression i tidiga delen av mellersta kambrium eroderades okonsoliderade sediment innan urberget återigen blev täckt av alunskiffer och kalksten under förnyad marin transgression i ordovicium. Under den kaledoniska orogenesen utgjorde Uppland en del av en större depression i Östersjöbäckenet öster om kollisionszonen och såväl U2 som pålagrade tidigpaleozoiska sediment överlagrades som ett resultat av bergskedjebildningen av kilometertjocka sediment.

I urbergsområden omkring rester av tidig-paleozoiska sedimentbergarter i södra Sverige, har U2 en distinkt morfologi där den kommer fram under täckbergarterna. På regional skala (1–10 km) kan U2 ses i digitala höjdmodeller som en mjuk och generellt flack yta som framträder genom utbredd överensstämmelse av höjden på urbergets toppar. Där urberget kan ses nära täckberg på lokal skala (0,1–1 km) i Västergötland, har inkonformiteten en ytrelief på bara någon meter. U2 är uppbruten av mindre post-kambriska förkastningar i en mosaik av flacka bergblock. En liknande urbergsmorfologi,

med flacka bergblock med överensstämmande topphöjder och vertikala höjdskillnader på några tiotal meter, finns i nordöstra Uppland. Denna morfologi indikerar en närhet mellan den nutida urbergsytan (UQ) och U2. U2 har karterats utifrån morfologiska kriterier i en digital höjdmodell såväl över enskilda bergblock som mellan bergblock av olika höjd. Genom att använda maxhöjder inom och mellan bergblocken som ankarpunkter har det också varit möjligt att rekonstruera en ungefärlig ursprungsyta. Denna ursprungsyta används som en referensyta mot vilken en uppskattning av den glaciala erosionen kan göras, och som resulterat i den inkonformitet (UQ) som den nutida urbergsytan utgör. Modellerna av U2 bygger på antagandet att U2 från början var en nästan plan yta utan djup neoproterozoisk vittring, innan den täcktes av ordovicisk kalksten och bröts upp av mindre post-ordoviciska förkastningar.

Höjdskillnaden mellan U1, U2 och UQ är relativt liten i området kring Forsmark. Liksom under UQ har sprickor öppnats i berggrunden även under bildandet av tidigare inkonformiteter. På samma sätt kan sprickfyllnader ha bildats även då U1 och U2 ursprungligen var exponerade, även om de inte har identifierats eller beskrivits i litteraturen som tillhörande distinkta generationer av sprickfyllnader. Tidigare studier av geokemin hos mineralisering i sprickor indikerar att senare delen av paleozoikum och tidiga delen av mesozoikum var viktiga perioder för cirkulation av lösningar och utfällning av sprickfyllnader. Avsaknaden av rester av saprolit i det täta nätverk av borrhål som finns kring Forsmark indikerar att urbergsytan inte återexponerades för vittring innan de pleistocena glaciationerna startade. Ytterligare indikationer på att ytan UQ återexponerades i sen tid i de västra delarna av Baltiska bassängen, från att ha varit täckt med ordoviciska sedimentbergarter, är de paleozoiska sprickfyllnader av kalcit som är vanligt förekommande i ytliga sprickor omkring Forsmark, i kombination med mobilisering av uranoxider under de senaste 300 ka som påträffats vid Äspö, Oskarshamn.

Sprickmönstret i Forsmark har en mycket komplex bildningshistoria med öppning av sprickor och mineraliseringar som spänner över 1,9 Ga. Det är ett resultat av att denudationen av urberget varit mycket begränsad samt att området under lång tid varit täckt av täckbergarter. Den pleistocena glaciala erosionens påverkan på topografin kan ha medfört ytterligare sprickbildning vilken i sin tur kan påverka glacial erosion under framtida glaciationer. Såväl teoretiska beräkningar som fältobservationer indikerar att topografiska element som ryggar och sänkor orsakar både vertikala och horisontella variationer i det ytnära spänningsfältet. Om dessa spänningsvariationer är tillräckligt stora (eventuellt i kombination med förhöjt subglacialt grundvattentryck) kan de medföra ytnära sprickbildning som i sin tur kan påverka den glaciala erosionen. Den generella lutningen av det storskaliga landskapet i norra Uppland är låg (~1 m/km), liksom reliefen i landskapet (<20 m), men värdena på båda dessa parametrar ökar i angränsande marina delar av landskapet där den topografiska kurvaturen vanligtvis är hög, särskilt längs kanterna av djupränno r, djupområden och angränsande kullar och ryggar. Forsmarksområdet karakteriseras dessutom av höga maximalvärden på den ytnära horisontella tryckspänningen. Det djup till vilket topografin påverkar tryckspänning och tillhörande uppsprickning av berggrunden är beroende av en kombination av horisontella tryckspänningar och den topografiska våglängden.

Vi har analyserat hur dagens topografi påverkar de ytliga spänningsfälten kring Forsmark, i syfte att få en bild av vilka sprickor som kan komma att öppnas och var detta kan ske. Vi har gjort detta genom att använda en tredimensionell *boundary element model*, samt genom att ta hänsyn till hur de ytliga spänningsfälten påverkas av porvattentryck och tryck från ovanförliggande sediment. Modelleringen visar att den topografiska faktorn kan påverka spänningsfälten i hög utsträckning ner till 100 m djup, även i ett flackt landskap. Topografins påverkan avtar med djupet och är mycket begränsad under ca 400 m djup. Modellen visar också att subhorisontella sprickor är mer benägna att öppnas under konvexa landformer vinkelrätt mot den maximala normalspänningen, och särskilt under sådana landformer som är utsträckta i nordost-sydvästlig riktning. Detta kan leda till högre erosion på ryggar och mindre erosion i svackor som följer denna riktning, och kan därmed leda till minskad relief över tid genom glacial erosion. Dalgångar och ryggar som är parallella med den största horisontella tryckspänningen kan däremot vara mer motståndskraftiga mot glacial erosion, med bibehållen eller ökad relief som följd. Det förefaller också som om vissa dalgångar är utsatta för tension, vilket kan leda till öppnandet av sprickor. Den glaciala erosionen kan därför vara större i dessa dalar, och potentiellt öka den lokala reliefen. Modelleringen av spänningsfälten visar alltså att även i ett landskap med så låg relief som i nordöstra Uppland kan topografin ha en påverkan på sprickbildning och därmed mönstret och omfattningen av den glaciala erosionen. Vidare undersökningar behövs dock för att utreda på vilket sätt dagens topografi, liksom topografin kopplad till U1 och U2, interagerade

med de strukturella elementen i urberget som bildats de senaste 1,9 Ga kring Forsmark för att utveckla och öppna sprickor. Topografiskt styrda spänningsfält har sannolikt också interagerat med det ökade grundvattentryck som enligt tidigare modeller påverkade underlaget ner till 500 m djup under de fennoskandiska inlandsisarna.

Erosionen under de pleistocena fennoskandiska inlandsisarna bildade en stor mängd glaciala landformer i olika skalor, men företrädesvis former med mindre än 20 m relativ relief. Vi har karterat glaciala landformer på regional (1–10 km) och lokal (0,1–1 km) skala med hjälp av terrängmodeller från LiDAR-data och kan visa att vissa områden domineras av glacial modifikation av preexisterande former medan andra områden domineras av nybildade glaciala landformer. Överytorna på bergblocken runt Forsmark har utsatts för gradvis erosion i form av såväl generell sänkning som reliefförstärkning genom urgröpning av sprickdalar och grunda sänkor längs förkastningszoner, urgröpning av mindre sprickor längs bergblockens kanter, samt djupare erosion (15–20 m) av omgivande sprickdalar och sänkor. Karteringen i lokal skala visar på en tydlig landformszonering i tre olika landskapstyper; (1) småkuperad, (2) svagt strömlinjeformad och (3) uppbruten terräng. Den glacialt eroderade småkuperade terrängen domineras av rundhällar och rektangulära kullar samt förkastningsstyrda svackor och rektangulära och stjärnformade sänkor. Den svagt strömlinjeformade terrängen består av avlånga bergkullar med moränsvansar samt långsträckta svackor som är parallella med berggrundens sprickmönster och tidigare isrörelseriktningar. Den glacialt uppbrutna terrängen karakteriseras av fält av stora kantiga block som täcker underliggande terräng.

Vi har även karterat enskilda glaciala landformer på makro- (10–100 m), meso- (1–10 m) och mikroskalan (< 1 m), i fält och i digitala höjdmodeller. Sammansättningen av landformer i olika skalor kan länkas till olika glaciala processgrupper, som abrasion, plockning, uppslitning (*ripping*), och smältvattenerosion. Glaciala smältvattenprocesser har agerat tillsammans med andra subglaciala processer i erosionen av förkastningsstyrda sänkor och dalgångar. Glacial uppslitning är resultatet av en kedja av processer som här beskrivs för första gången och som involverar lyftprocesser, fragmentering av berggrunden och upplockning och transport av block i isen, vilket leder till utbredda täcken av stora kantiga block. Uppslitningsprocessen kopplas till ett förhöjt grundvattentryck under iskanten, eventuellt i kombination med stora smältvattenvolymer, i samband med att den fennoskandiska inlandsisen drog sig tillbaka under den senaste deglaciationen. Uppslitningsprocessen identifieras här som en viktig, och lokalt dominerande, komponent för den glaciala erosionen kring Forsmark och som ställvis påverkat berggrunden ner till flera meters djup.

Genom fältobservationer på rundhällar kan slutsatser dras om de glaciala processer som sannolikt opererat i området och som kompletterar uppskattningar av erosionsdjup och erosionshastighet från mätningar av kosmogena nuklider. Mikro- och makroformerna som kan ses på rundhällarna härör framför allt från senare delen av den sista glaciationen i området. Spår från tidigare glaciala skeenden har vanligtvis eroderats bort. Mikroformer relaterade till abrasion i form av till exempel isräfflor och polerade ytor är mycket vanligt förekommande. Den relativt utbredda förekomsten av andra erosionsformer som kaviteter, musselbrott, och andra former av grund plockning av mindre partier av berggrundsytan, vittnar dock om att andra erosionsprocesser kan ha varit än viktigare för mikroerosionen. Rundhällar längs Östersjöns strandlinje utanför Forsmark, som karterats i detalj från bilder tagna med drönare, uppvisar talrika 0,5–5 m stora triangulära och rektangulära håligheter i den abraderade bergrundsytan och som sannolikt bildats genom urplockning av bergfragment under högt subglacialt vattentryck. Plockning har också skapat skarpare kanter och håligheter längs rundhällarnas laterala sidor och läsidor. Tecken på uppslitning saknas i stort sett på de rundhällar som provtagits i området för analys av kosmogena nuklider.

Den pleistocena erosionen av berggrunden i området inkluderar såväl erosion av ordovicisk kalksten som det underliggande spruckna urberget. Erosionen av mjukare, lagrade och uppspruckna sedimentära täckbergarter omfattade sannolikt några tiotals meter berg. Denna uppskattning baseras på förekomsten av sub-jotniska och subordoviciska sedimentavlagringar på 20–40 m djup i sänkor på havsbotten öster om Forsmark (i Öregrunds skärgård). Förkastningsstyrda bergblock som är begravda av sedimentbergarter på havsbotten öster om Forsmark har observerats ha skarpa kanter intill förkastningsbranterna. Där inkonformiteten istället är exponerad, är kanterna på förkastningskanter avrundade och eroderade i lälägen, och djupet på den glaciala erosionen kan uppgå till 20 m längs inskärningar i bergskanterna. Andra bergblock, som i nordöstra Uppland, avgränsas av branter som är mindre än 10 m i höjd. En djupare glacial erosion av urberget borde ha eroderat bort dessa lägre uppstickande bergblock.

Omfattningen av erosionen i urberget kan uppskattas genom att använda den kambriska inkonformiteten (U2) som en referensyta. I genomsnitt skiljer det i nordöstra Uppland 14 m i höjd mellan dagens urbergsyta (UQ) och den teoretiska modell av landskapet som fås av en yttäckande länkning av topografiska höjdpunkter inom området (*summit envelope surface*), och som antas ligga nära ytan U2. I området närmast Forsmark är motsvarande siffra 12 m. Den volymmässigt största glaciala erosionen har skett i de djupa (10–20 m) dalar och sänkor som bildats längs sprickzoner. Till dessa siffror ska adderas det berg som eroderats från topparna i dagens landskap och som har använts för att konstruera modellen av U2. I södra Sverige är höjdskillnaden mellan fortfarande täckta ytor av U2 och intilliggande exponerade urbergsytor begränsad, och variationen i absoluthöjd på urbergskullar är låg vid ökande avstånd från paleozoiska rester. Detta indikerar, under förutsättning att U2 ursprungligen var en plan yta, att erosionen av urberg från toppytor på kullar i området varit mindre än 10 m. Liknande erosionsdjup indikeras i Forsmarksområdet, dock inte lika välbestämt genom närvaro av täckbergarter, av variationen i absoluthöjd hos urbergskullar på den sluttande urbergsytan, där ordovicisk kalksten förekommer på havsbotten öster om Forsmark, samt av den ringa glacialerosionen av återexponerade förkastningsbranter med mindre än 5 m relief. Preliminärt uppskattas därför att 10 m berg har eroderats ovanför urbergshöjderna i Forsmarksområdet. Om modell-antaganden är felaktiga eller om den glaciala erosionen efter återexponering har varit geografiskt uniform kan dock den maximala erosionen vara högre.

Analys av kosmogena nuklider (^{10}Be och ^{26}Al) har gjorts på 32 ytliga berggrundsprover som samlats in längs en ca 50 km lång transekt i sydlig riktning från Forsmark samt på tre prover från block vid kusten. Tre av proverna samlades in inom eller längs kanten av området där Forsmarks slutförvar är planerat att ligga. Alla prover utom ett har halter av kosmogena nuklider som är högre än vad som är förväntat i förhållande till tidpunkten för deglaciationen och den efterföljande landhöjningen. De flesta prover har skenbara åldrar som är 3,4–9,6 ka för gamla. Vi använder dessa nukliddata från berggrundsproverna för att simulera de glaciala erosionshastigheter respektive erosionsdjup som är möjliga med hänsyn till uppmätta koncentrationer av ^{10}Be och ^{26}Al. Vi har använt ett antal olika scenarier med en starttid från 10 Ma till 130 ka, interglaciala erosionshastigheter mellan 0 mm/ka och 5 mm/ka, ett antal olika scenarier för nedisning av Forsmark baserat på beräkningar av global isvolym utifrån bentiska δ^{18}O data (LR04: 4.4–4.6 ‰) och inlandsismodellering för den senaste glaciala cykeln, samt glacial erosion beräknad proportionerligt mot tiden som området varit täckt av inlandsis eller mot antal istäckningsperioder.

Proverna för mätning av kosomgena nuklider är huvudsakligen tagna från lokala höjdpunkter i landskapet och eftersom svackor i terrängen i allmänhet är fyllda av sediment finns inga prover från landskapets lågpunkter. Lägsta provet är taget vid havsnivån 0 m ö h och högsta provet är taget på 67 m ö h. Det finns inget samband mellan storleken på den glaciala erosionen och provernas höjd över havet. För en kulle som provtagits på 7 olika platser visar data på låg erosion på kullens högre delar medan erosionen varit mer intensiv längs kullens bas. Nitton av proverna är tagna på lägre höjd (0–24 m ö h), inom 5 km från området där Forsmarks slutförvar är planerat att ligga, och de visar på en total erosion på 0–8,6 m sedan 100 ka. Två prover tagna direkt ovanför slutförvaret visar på en total erosion på 1,0–5,6 m sedan 100 ka. Tretton prover tagna på högre höjd (25–67 m ö h) längs en transekt mot sydsydväst från Forsmark visar på liknande erosionshastigheter på 0,6–8,1 m sedan 100 ka. De tre proverna från block i närheten av Forsmark visar alla på nedärvd exponering av samma storleksordning som berggrundsproverna, motsvarande 2–41 ka med tidigare exponering. Detta stödjer tolkningen om begränsad glacialerosion i området, eftersom blocken måste ha exponerats innan den senaste glaciala cykeln, och därmed ha varit belägna i ett ytnära läge.

Förutsatt att samtliga glaciationer som täckt Forsmark och Uppland har eroderat berggrunden med samma intensitet och på samma sätt, kan det typiska totala erosionsdjupet sedan 100 ka uppskattas till 1,6–3,5 m, och det typiska totala erosionsdjupet sedan 1 Ma uppskattas till 13–27 m. Det senare värdeintervallet är högre än det erosionsdjup på 10 m urberg som rekonstruerats baserat på geomorfologiska metoder. Den högre erosion sedan 1 Ma som analysen av de kosmogena nuklider indikerar skulle kunna inkludera erosion av täckbergarter eller enbart urberg. Om det beräknade djupet på 13–27 m erosion helt härrör från erosion i urberget så är storleken på erosionen baserad på geomorfologi för låg. Båda alternativen är förenliga med en händelseutveckling där täckbergarterna i området eroderades bort under de senaste 1,1 Ma. Spännvidden i värdena för erosionshastighet och erosionsdjup beräknat från halten kosmogena nuklider är ett resultat av variationen i de resultat som erhållits för de enskilda provpunkterna, vilket illustrerar att graden av erosion har en rumslig

variation. Trots detta kan det konstateras att med tanke på det stora antalet prover, och den vida geografiska utbredningen av dem, är resultaten väl sammanhållna och de tyder på en låg erosionsgrad i detta landskap med låg relief.

De säkerhetsbedömningar som görs med anledning av det planerade slutförvaret av använt kärnbränsle kräver att hänsyn tas till glacialerosion under framtida nedisningar. Baserat på geomorfologin, och under antagande att urberget återexponerades för 1,1 Ma, uppskattas den genomsnittliga glaciala erosionen till ca 2 m per glacial cykel. I djupare delar av terrängen kan denna siffra vara 3 m eller mer. Resultaten från kosmogena nuklider tyder på ett erosionsdjup av urbergsytorna i terrängen kring Forsmark på 0–8,6 m sedan 100 ka. Min- och max-värdena på 0 respektive 8,6 m erosion härrör från undersökningslokaler som ligger mindre än 2,5 km från varandra, och verkar reflektera stokastiska variationer i erosionsdjup och erosionsprocesser. Det är därför rimligt att anta att över flera glaciala cykler kommer värdena i genomsnitt att ligga inom detta spann.

För att uppskatta den potentiella framtida glacialerosionen i Forsmark kan vi kombinera simulationerna baserade på ^{10}Be- och ^{26}Al-nukleider med modellering av nedisningen över Forsmark över de kommande 1 Ma, baserad på IPCCs utsläppsscenarier och framtida variationer i instrålning (Lord et al. 2019). Baserat på detta kan den totala erosionen för Forsmark över de kommande 100 000 åren uppskattas till mindre än 1 m. Över de kommande 1 Ma kan den totala erosionen i huvudsak beräknas ligga mellan 5 och 28 m, med min-/max-värden på 2 respektive 43 m. Det ska dock påpekas att dessa uppskattningar av erosionsdjup är starkt kopplade till antagandet att den rekonstruerade glaciala erosionen är representativ även för den glaciala erosionen i framtiden.

Contents

1 Introduction

The Swedish Nuclear Fuel and Waste Management Company, SKB, is planning to build a geological repository for spent nuclear fuel in Forsmark in south-central Sweden. As part of the safety assessments made for this repository, and for the existing repository for low- and intermediate level waste (SFR) and a planned repository for a low level long-lived nuclear waste (SFL), it is necessary to constrain the erosional impact of future glaciations on the repository site. The present study aims to provide well-founded estimates of past depths and rates of glacial erosion in the Forsmark area (Figure 1-1) by using several methodologies, and to use these estimates for projections for glacial erosion in the distant future (100–1 000 ka).

This study was originally based on three research strands:

1. The use of the sub-Cambrian unconformity as a reference surface against which to estimate Pleistocene glacial erosion.
2. Mapping of the distribution, form and characteristics of glacial landforms on the shield surface to identify patterns and processes of glacial erosion.
3. The use of cosmogenic nuclide inventories from bedrock surfaces to estimate erosion depths and rates beneath the last, and from earlier ice sheets.

During the first year of the project a new research strand was included:

4. Topographic control of bedrock fracturing and its significance for past and future glacial erosion patterns.

This final report summarises findings for each of the four research strands and provides projections for future glacial erosion rates. Chapter 2 considers the erosion and burial history of the basement in the Uppland province from its first exposure at ~ 1.5 Ga until re-exposure in the Pleistocene. Chapter 3 examines topographic perturbations of near-surface bedrock stresses, fracture development, and possible links to glacial erosion at Forsmark, Chapter 4 investigates glacial bedforms in Uppland as indicators of patterns and depths of glacial erosion at different scales. Chapter 5 provides estimates from cosmogenic nuclides for inheritance attributable to incomplete resetting during the last glacial cycle (130 ka) and, using modelling, constrains total erosion and erosion rates over the past 10 Ma, 2.588 Ma, 1 Ma, and 130 ka, Chapter 6 provides an overview of our conceptual understanding across the research strands and includes estimates of depths and rates of glacial erosion in future glaciations derived from geomorphic evidence and from cosmogenic nuclide- and ice sheet modelling. The main conclusions are presented in Chapter 7.

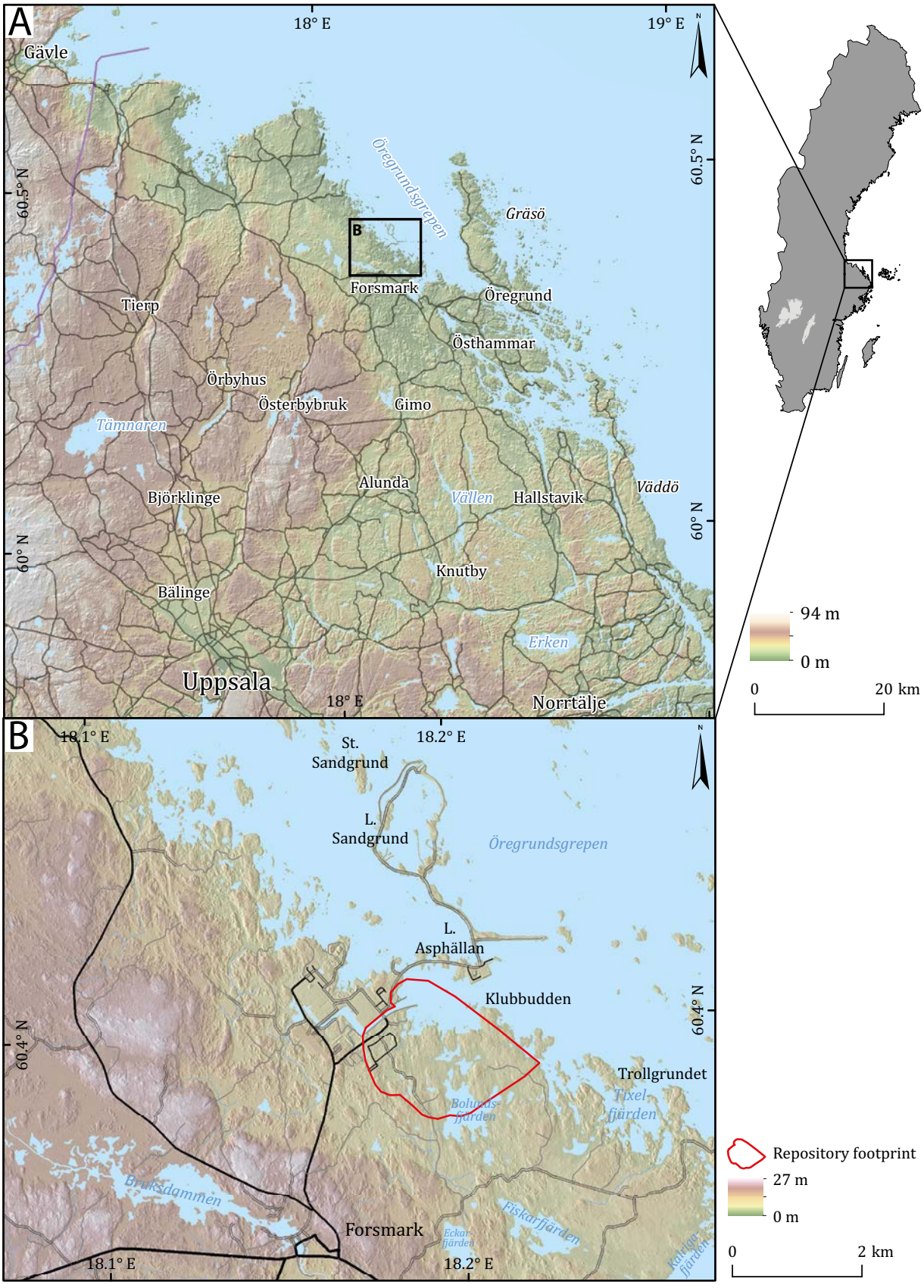

Figure 1-1. *Location maps of the Uppland province and the Forsmark area. Elevations in m a.s.l.*

2 Erosion and burial history of the basement in the Uppland province

2.1 Introduction

Understanding of the erosion and burial history over the last 1.5 Ga is important for constraining erosion rates and depths on the craton in Uppland province through the Proterozoic and Phanerozoic. Major basement unconformities represent culminations of very long periods of weathering and erosion (Gabrielsen et al. 2015). Fractures may develop and open beneath unconformities and be exploited by weathering (Parnell et al. 2014). Burial by sedimentary cover may protect the basement from erosion over very long time periods during which circulating groundwater may deposit mineral coatings on fracture surfaces to depths of tens of hundreds of metres below the contemporary land surface (Sandström et al. 2010). The inherited Cambrian basement unconformity surface, widely referred to in the Swedish literature as the sub-Cambrian peneplain (SCP) (Lidmar-Bergström et al. 2012) is of key importance for this study as it provides a reference surface for identification of post-Ordovician block faulting and against which to estimate depths of glacial erosion since re-exposure of basement.

2.1.1 Aims

The proximity of the present erosion level to that of the SCP, or more specifically the sub-Cambrian unconformity, in the Forsmark area is referred to widely in SKB reports (Sandström et al. 2006a, Söderbäck 2008, Stephens 2010). Yet little detailed attention has been given previously to geomorphological evidence for the exposure of the basement in the Mesoproterozoic and late Neoproterozoic despite the importance of these unconformities for understanding rates of cratonic denudation, fracturing, mineralisation of fractures and hydrogeology. The sub-Cambrian unconformity also has not been mapped in detail previously in Uppland, nor linked to the Ordovician outliers that lie close offshore (Söderberg and Hagenfeldt 1995). The SCP has been used as a reference surface for identification of patterns of Phanerozoic fault block movement in the basement (Beckholmen and Tirén 2009, 2010a, b, Grigull et al. 2019). Here we examine the denudation history of the basement in Uppland and model the sub-Cambrian unconformity (U2). The modelled unconformity surface is used later to establish patterns and depths of glacial erosion since its re-exposure in Uppland.

The main aims of this research strand are to:

- Identify the extent, positions and form of major Mesoproterozoic (U1) and Early Palaeozoic (U2) basement unconformities and to link these to exposure and burial history, faulting and fracture formation.
- Model the dislocated surface of U2 in NE Uppland and around Forsmark.

The continuity of the U2 across the lowlands of south-central Sweden means that other areas proximal to outliers of Early Palaeozoic cover rocks provide analogues for understanding the history, position and form of the U2 surface in Uppland. Those analogue areas are also examined separately in forthcoming Technical Reports for the Trollhättan area (Goodfellow et al. 2019, Hall et al. 2019a).

2.1.2 Terminology

A major goal of this study is to use the Cambrian basement unconformity as a reference surface against which to constrain or estimate Pleistocene glacial erosion. We first define three regional unconformities as follows:

1. The *sub-Jotnian unconformity* (U1) of Mesoproterozoic age (~1.5Ga), where Jotnian sandstones rest on basement.
2. The *sub-Cambrian unconformity* (U2), where Cambro-Ordovician sedimentary rocks lie on basement, or on Jotnian sandstones, where these are still present.
3. The *present basement surface* (UQ), developed after exhumation from cover rocks and modified by glacial erosion. UQ is locally covered by Quaternary sediments.

Our main focus is on U2. This unconformity is diachronous, with Late Ediacaran cover in the Baltic States, Early Cambrian cover in southern Sweden and Early Ordovician cover in east-central Sweden and neighbouring parts of south-west Finland. In this report dealing with Sweden, we use the term *sub-Cambrian unconformity*.

Where U2 remains covered by Cambrian and Ordovician sedimentary rocks, we refer to the *buried unconformity*. We acknowledge that all regional basement unconformities were once buried, and our usage refers to the unconformity remaining buried by Early Palaeozoic sedimentary rocks at the present day. Where the unconformity has been exhumed, but little modified by further erosion, this is termed the *exposed unconformity*. Where the unconformity is reconstructed from basement summit heights, this is termed the *modelled unconformity*. Where the different surfaces can be constrained in a particular area, then the depth of erosion of basement rocks is represented by the elevation difference between the modelled U2 and the UQ. The components of its re-exposure and erosion in Uppland require removal of layers of (i) Cambro-Ordovician and younger sedimentary cover, (ii) any weathered crystalline bedrock at shallow depth below the surface of U2 that may have been present and (iii) unweathered, fractured basement from below any regolith. UQ displays the glacial bedforms produced by Pleistocene ice sheet glaciation.

The term *Sub-Cambrian peneplain* (SCP) is used widely in the geological and geomorphological literature to refer to the generally flat bedrock surface that emerges from below the Cambrian cover in Sweden (e.g. Lidmar-Bergström 1988, Gabrielsen et al. 2015, Japsen et al. 2016). Its use arguably has become somewhat ambiguous (Ebert 2009). Some use the term *Sub-Cambrian peneplain* to describe the buried unconformity itself (e.g. Gabrielsen et al. 2015); another more widespread use is for the present-day basement that mimics, and is inherited from, the sub-Cambrian unconformity where it became re-exposed in recent geological time, but remains little modified by subsequent erosion (e.g. Rudberg 1970, Lidmar-Bergström 1988, Johansson et al. 1999). Arguably, the latter meaning always remains an interpretation based on a model of the former unconformity surface. The term *peneplain* also brings complications in its use both as a landform descriptor and as a genetic term (Ebert 2009). Some have argued that, in places, U2 is an actual plain and too flat to be a peneplain (Rudberg 1970), which is “almost a plain” (Fairbridge and Finkl 1980). Recent usage has also drifted to include planation surfaces in southern Sweden with many hills and >100 m relief (Lidmar-Bergström et al. 2017). The original use of *peneplain,* following Davis (1902), also refers to subaerial planation whereas U2 is overlain directly by marine sediment, suggesting that shoreline erosion had a role in the final shaping of the unconformity. In this study of post-exhumation erosion, we prefer to use the more neutral term *sub-Cambrian unconformity* (U2).

2.1.3 Geological history

The geology of Uppland is dominated by anisotropic gneisses of granite to granodiorite composition, with minor amphibolite (Figure 2-1). Major structural and tectonic units around Forsmark have been described and mapped in detail (Stephens et al. 2008a, Sandström and Tullborg 2009). The rocks first formed in the Palaeoproterozoic (Figure 2-2) during the Svecokarelian orogeny and have been affected by multiple episodes of ductile and brittle deformation (Stephens 2010). Brittle fractures first developed during post-orogenic cooling at 1.8–1.6 Ga (Welin 1964, Sandström et al. 2009) (Figure 2-3). $^{40}Ar/^{39}Ar$ biotite ages from boreholes indicate cooling in response to uplift and erosion at rates of ~25–30 m/Ma for the 1.70–1.62 Ga time period (Page et al. 2007). The Paleoproterozoic crust was eroded close to the present-day levels before Mesoproterozoic sediments were deposited unconformably on basement in alluvial, fluvial or aeolian environments. (Buntin et al. 2019.)

The Mesoproterozoic basins (the ‘Jotnian-Dala sandstone’) of the Bothnian and Åland Seas represent failed rifts (Korja et al. 2001). The western margins of the Mesoproterozoic basin in Uppland is bounded by regional deformation zones that were formed during the Svecokarelian orogeny (Juhlin and Stephens 2006) and by faults that were repeatedly reactivated during and after the Mesoproterozoic (Söderberg 1993, Beckholmen and Tirén 2009, Grigull et al. 2019). After ~1.5 Ga, the basement surface was buried by a Mesoproterozoic platform sequence. The term *Jotnian* is also used to refer to these sedimentary rocks (Amantov et al. 1996) (Figure 2-2). The Mesoproterozoic sandstones at Gävle show prehnite-pumpellyite facies metamorphism, indicating burial to depths of several kilometres (Nyström and Levi 1980) (Figure 2-3). Major events of dolerite intrusion in central Sweden are dated at 1.60–1.59, 1.27–1.25 (termed *post-Jotnian*) and 0.98–0.95 Ga (Söderlund 2006).

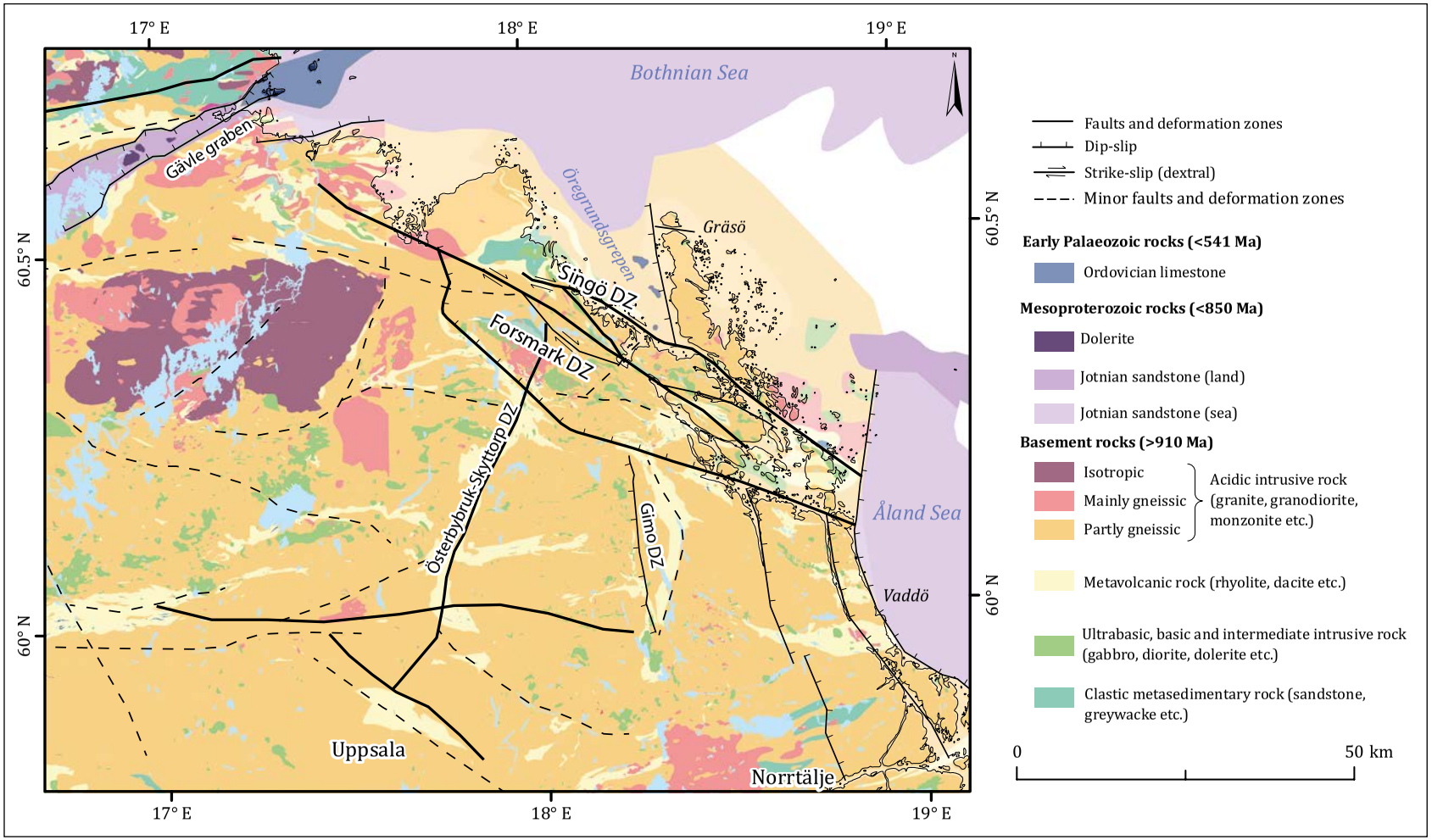

Figure 2-1. *Geology of Uppland and the adjacent seabed based on SGU data.*

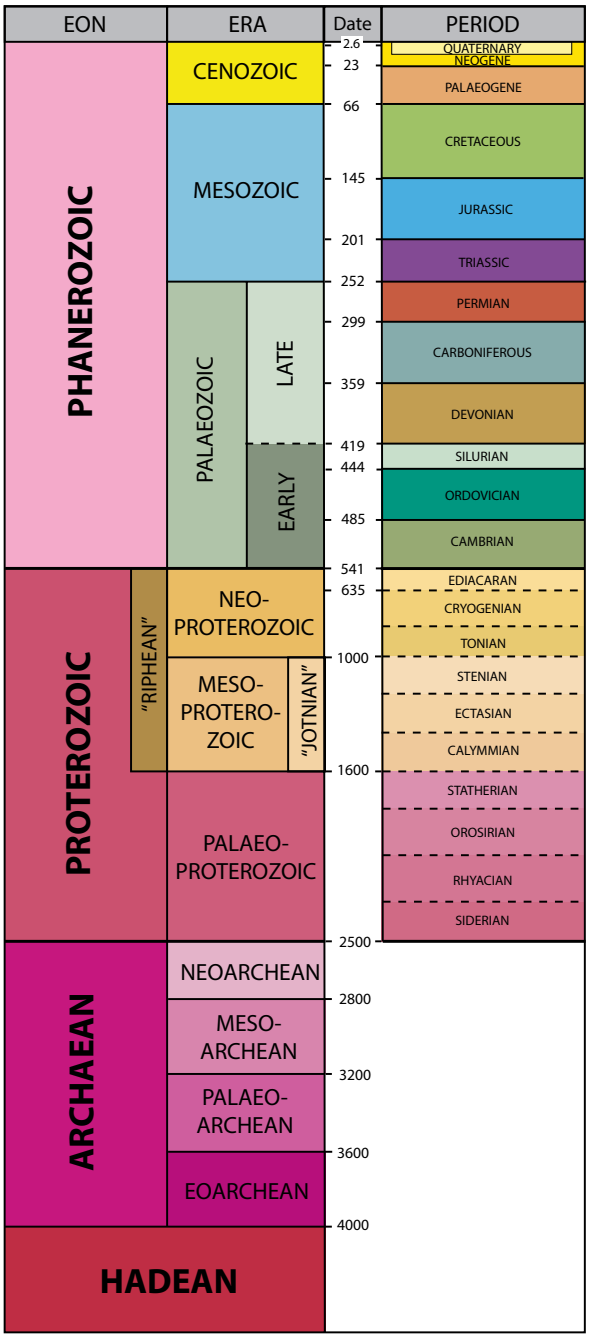

Figure 2-2. *A geological timescale from the British Geological Survey based on The Geologic Time Scale 2012 (Gradstein et al. 2012). Dates are in millions of years.*

During the Sveconorwegian orogeny, Uppland formed part of the Fennoscandian foreland (Bingen et al. 2008) and was likely deeply buried by sediments that accumulated in a foreland basin (Larson et al. 1999). (U-Th)/He ages obtained from surface samples in the Forsmark area indicate cooling below 70 °C between 750 and 530 Ma, without subsequent reheating above this temperature during Palaeozoic burial (Page et al. 2007). An intra- plate carbonatite volcanic centre at Alnö, Sundsvall (Andersson et al. 2013), about 250 km N of Forsmark, indicates contemporaneous, localized high mantle heat flow on the craton at ~584 Ma (Nystuen et al. 2008). Around 500 m of overburden has been removed since the time of emplacement but rapid erosion is typical of similar active alkaline volcanic centres on Earth today (Kresten and Troll 2018). This volcanic activity was likely associated with minor uplift and erosion of surrounding basement.

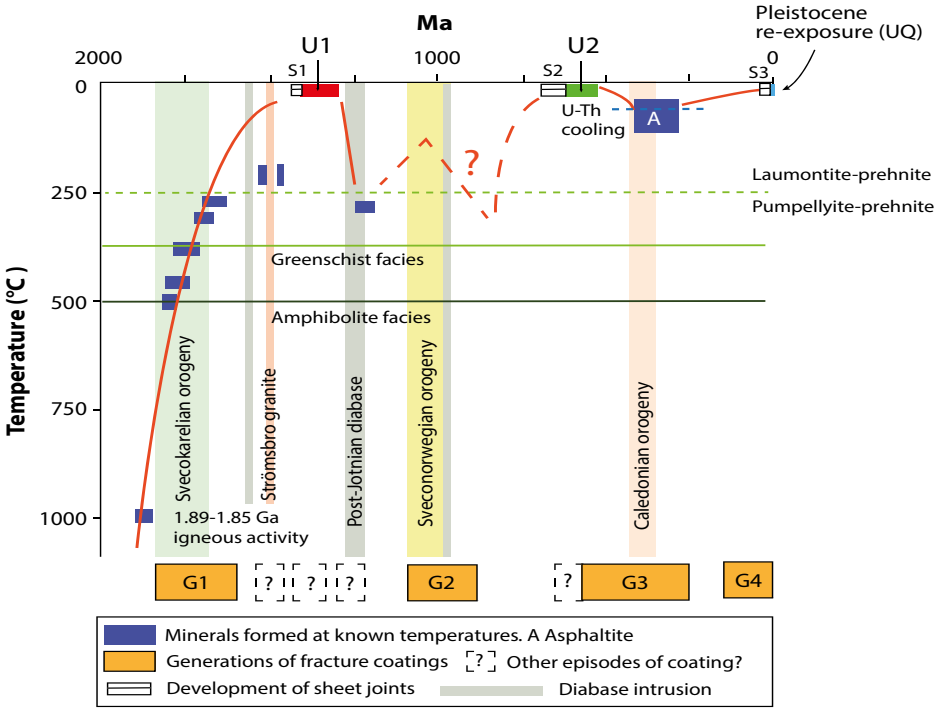

Figure 2-3. *Bedrock thermal history of Uppland. The temperature curve is constrained by metamorphic facies and mineral ages and the main generations (G1–G4) of fracture minerals. Modified from Stephens (2010). Diabase intrusion ages from Söderlund (2006). Strömsbro Granite age from Andersson (1997). Unconformities U1–UQ may be linked to phases of sheet jointing (S1–S3) and fracture opening beneath exposed basement surfaces. Possible additional phases of mineral coating in fractures are identified for U1 and U2 and during post-Jotnian diabase intrusion at 1 260 Ma (Karhu 2000).*

By the end of the Neoproterozoic (Figure 2-2), prolonged denudation had reduced much or all of Baltica to a landscape of extremely low relief that stretched from western Norway to western Russia (Amantov et al. 1995, Nielsen and Schovsbo 2011). During the global late Ediacaran-Ordovician transgression, during which global sea level rose slowly but step-wise by ≥200 m (Haq and Schutter 2008), Baltica was progressively flooded from the periphery towards the centre. This denudational plain, subsequently covered by Cambro-Ordovician deposits, is often referred to as the *sub-Cambrian peneplain* in the literature (Section 2.1.2).

By the Ediacaran Period (635–541 Ma) (roughly equivalent in earlier usage to the former *Vendian* stage) (Kohonen and Rämö 2005), Baltica was situated at 35°S to 60°S (Torsvik and Cocks 2013), with a warm temperate to moderately humid climate (Dreyer 1988). Marine transgression and the eventual burial of the basement unconformity was diachronous (Nielsen and Schovsbo 2011), commencing with a sea-level rise of ~50 m through the late Ediacaran after 548 Ma in Estonia (Meidla 2017) but delayed until after the Lower Cambrian boundary (541 Ma) in Sweden (Slater et al. 2018). The extremely low relief of the shelf in this part of Baltica during marine transgression is indicated by (i) the limited thickness of the Early and Middle Cambrian sequence of Norway, Sweden and the eastern Baltic, (ii) the near-horizontal dip and very wide lateral extent of many of the facies (for example, the lack of lateral facies variations) (Ormö et al. 2017), and (iii) the general lack of coarse clastic sediment, indicating a general lack of higher ground as source areas (Cocks and Torsvik 2005).

The sub-Cambrian unconformity was buried by ~0.25 km of platform sediments, including sandstone, shale and limestone, in the Cambrian and Ordovician (Nielsen and Schovsbo 2006). The preservation of Ediacaran marine sedimentary rocks in impact structures at Karikkoselkä (Uutela 2001) and Iso-Naakkima (Elo et al. 1993) in Finland indicates that these rocks formerly extended continuously from the Lake Ladoga area across southern Finland (Puura et al. 1996), towards basins in the Baltic Sea (Paulamäki and Kuivamäki 2006, Klein et al. 2015) and onto terrain now

buried beneath the Caledonide nappes (Nielsen and Schovsbo 2011). The presence of these outliers also demonstrates limited post-Ordovician erosion of basement. From the Silurian onwards, up to 2 km of deposits were added during the development of the foreland basin to the Caledonide mountains (Larson et al. 1999), although no remnant of these deposits is preserved in Sweden today. Circulation of groundwater brines through fractures in the basement led to the formation of multiple generations of fracture coatings at Forsmark in the Phanerozoic (Erlström 1987, Sandström et al. 2009). Rifting of the Oslo Graben in the Early Permian was accompanied by widespread tectonics and erosion across southern Fennoscandia (Gabrielsen et al. 2018), with re-magnetization of fault zones in S Finland (Preeden et al. 2009). Dolerite dykes are seen in seismic sections to cut Ordovician strata in the western part of the Bothnian Sea off Sundsvall (Winterhalter et al. 1981): an Early Permian age is likely for this magmatism. Hence, the post-Ordovician block faulting around the southern Bothnian Sea and in Uppland may include Early Permian extension (Saintot et al. 2011). (U-Th)/He thermochronology (Page et al. 2007) and apatite fission-track analysis (Cederbom 2001, Japsen et al. 2016) indicate that the Palaeozoic cover in Uppland (including the Caledonide foreland basin deposits) was thinned around or after 250–240 Ma (Söderbäck 2008). (U-Th)/He results from boreholes at Forsmark suggest slow exhumation at ~2 m/Ma between ~500 and 250 Ma (Page et al. 2007). However, there is no evidence of Mesozoic or Palaeogene re-exposure of the basement in this part of Sweden or in neighbouring parts of SW Finland (Nironen 2017). The Dellen impact structure (Figure 2-13) in Hälsingland, dated to 109.6±1.0 Ma (Müller et al. 1990), lacks evidence for sedimentary cover at the time of impact, indicating that the basement here was exposed to weathering and erosion in the Early Cretaceous (Henkel 1992).

Opening of the North Atlantic was associated with uplift of the western margin of Fennoscandia after the Late Cretaceous (Sømme et al. 2013), the development of a set of epeirogenic domes further away from the margin (Figure 2-4) and the progressive exhumation of the sub-Cambrian unconformity in southernmost Sweden (Lidmar-Bergström et al. 2012). Neogene uplift of Fennoscandia (Gibbard and Lewin 2016) led to reduction of sedimentary cover across eastern Sweden and to the re-emergence of the South Swedish Dome (Japsen et al. 2016). Early Miocene (23–15 Ma) cooling in the Stockholm region inferred from fission track data (Japsen et al. 2016) indicates further thinning of remaining sedimentary cover across Uppland. Final exhumation of basement around the present Bothnian Sea coast may have occurred as late as Pleistocene time (Olvmo 2010, Amantov et al. 2011).

Critical evidence for the timing of fracturing in Uppland comes from sequences of fracture mineralisation identified at the Forsmark site. Four main generations (G1–G4) of fracture minerals have been recognised (Sandström et al. 2008, 2009, Sandström and Tullborg 2009). G1 was formed during the Precambrian between 1.8–1.1 Ga ago (Figure 2-3), at temperatures above 150–200 °C. The main G1 minerals are epidote, chlorite, and quartz. G2 was formed during oxidising hydrothermal events at 1.1–1.0 Ma at temperatures between ~150–280 °C. The main G2 minerals are adularia, prehnite, laumontite, chlorite, and calcite. G2 minerals coat new brittle fractures formed during the Sveconorwegian Orogeny (Sandström et al. 2010). G3 minerals were precipitated at temperatures of ~60–190 °C and are dominated by quartz, calcite and pyrite, with minor corrensite, adularia, analcime, and asphaltite. G3 minerals were precipitated as layered coatings between ~460 and 277 Ma in reactivated and new fractures (Krall et al. 2015, Drake et al. 2017). Pyrite, formed under reducing conditions, occurs almost exclusively as a G3 mineral. Solution of Ordovician limestone by circulating brines may have provided a source for younger calcite veins. Where pyrite is not precipitated onto existing G1 and G2 mineral coatings, the formation of new fractures during the Palaeozoic is indicated. Support for late brittle deformation, mainly resulting in reactivation of pre-existing deformation zones, is provided by a $^{40}Ar/^{39}Ar$ age of 276.9±1.1 Ma for an adularia filling of a NE–SW striking, steeply dipping fracture in a deformation zone at Forsmark (Sandström et al. 2006a) and by extensive brecciation and hydrothermal alteration along the Österbybruk–Skyttorp fault zone (Persson and Sjöström 2003). G4 minerals formed at temperatures below 50 °C, likely from the late Palaeozoic to the Pleistocene. Clay minerals, chlorite/corrensite and thin coatings of calcite dominate, together with small amounts of pyrite and goethite. They are often found in hydraulically conductive structures, many of which are reactivated fractures containing G1–G3 minerals (Sandström et al. 2008, Tullborg et al. 2008, Sandström and Tullborg 2009).

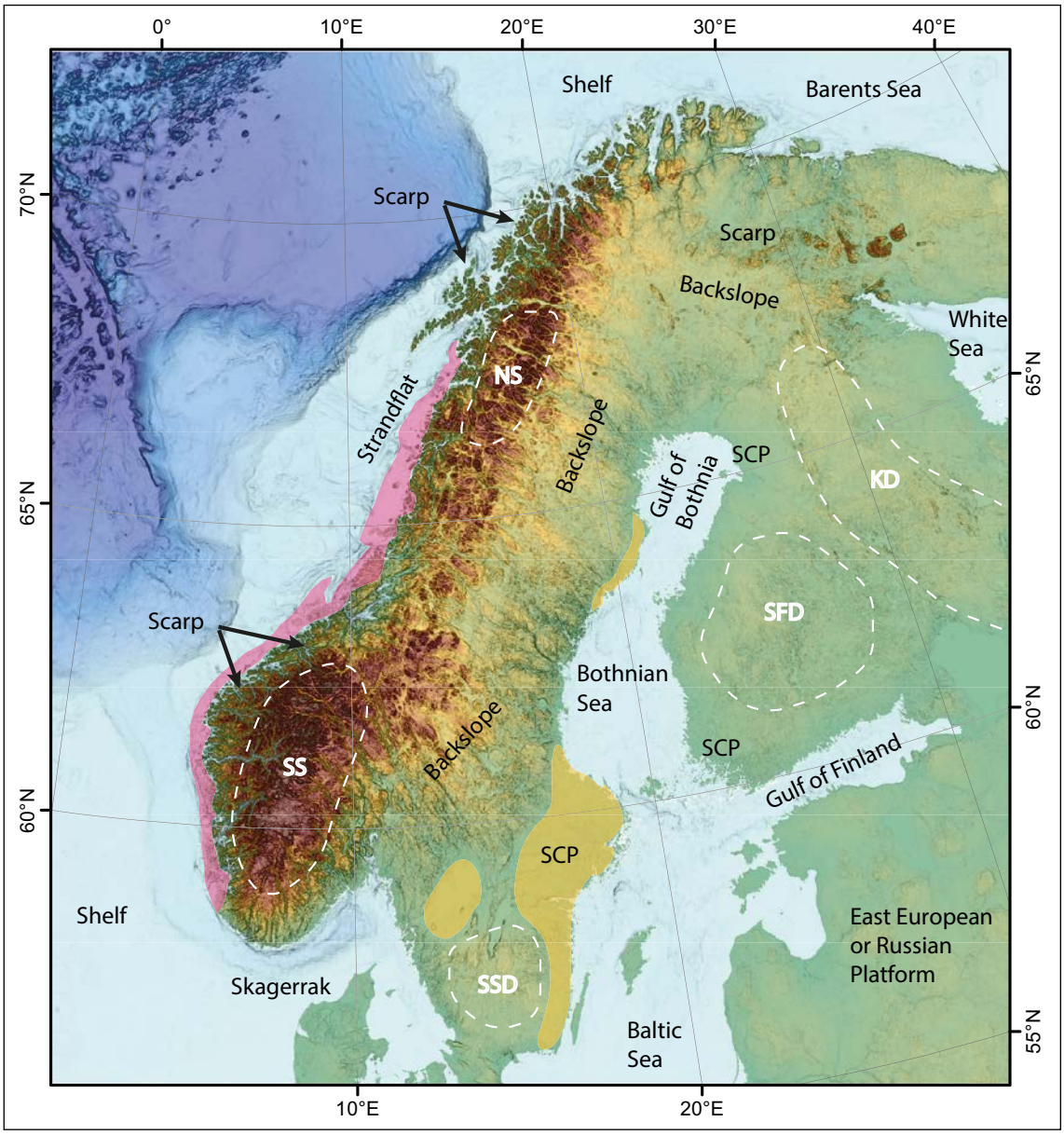

Figure 2-4. *Main topographic features of Fennoscandia showing major epeirogenic domes and basins. Domes: Southern Scandes (SS), Northern Scandes (NS), Karelian Dome (KD), South Finnish (SFD) and South Swedish (SSD) domes. SCP: Sub-Cambrian peneplain, after Lidmar-Bergström and Näslund (2002).*

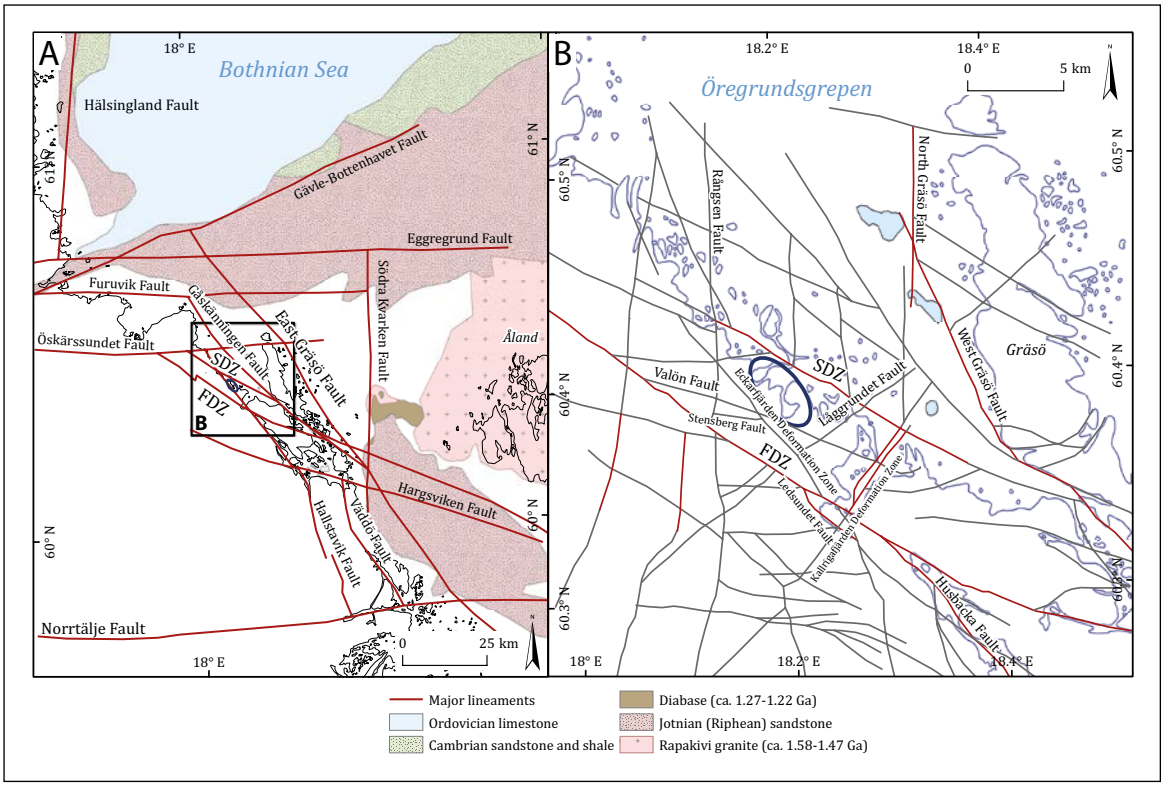

Figure 2-5. *Major deformation zones, faults and fractures in NE Uppland and the Forsmark area based on SGU data. Fault names given here are informal and based on local place names. FDZ Forsmark Deformation Zone. SDZ Singö Deformation Zone. Forsmark area shown by blue oval.*

Whilst the deformation, fracturing and mineralisation history of the basement of NE Uppland is complex, the erosion history appears less so. Only three major basement unconformities are recognised in the Mesoproterozoic (U1), the Cambrian (U2) and the Quaternary (UQ) (Figure 2-3). U1 and U2 were each deeply buried beneath foreland basin sediments after formation. Around the Bothnian Mesoproterozoic basin (Högbom 1910), in Dalarna (Lundmark and Lamminen 2016) and in S Finland (Nironen 2017), U1, U2 and UQ are found in vertical and horizontal proximity. Erosion depths in basement rocks have remained low since U1 formed at ~1.5 Ga.

Evidence is presented below that the present basement surface in Uppland coincides in broad terms with U2, with only minor glacial modification (Rudberg 1954, Lidmar-Bergström 1997). Such spatial coincidence of stacked basement unconformities is a product of cratonic stability and extremely slow erosion during periods of basement exposure and of very long periods of burial by sedimentary sequences in the Neoproterozoic and Phanerozoic.

2.2 The sub-Jotnian unconformity (U1)

The Mesoproterozoic, sub-Jotnian unconformity refers to the unconformity of the metamorphic basement rocks and the overlying low-grade metamorphic Mesoproterozoic sandstone sequence generally referred to as Jotnian (or Dala) sandstone (Lundmark and Lamminen 2016). The Jotnian sandstone sequence was deposited sometime between 1.58 and 1.26 Ga (Söderlund et al. 2006, Lundmark and Lamminen 2016), so the unconformity was formed in the Early-Mid Mesoproterozoic.

This section examines the form and dislocation of the sub-Jotnian unconformity around the edge of the southern part of the Bothnian Sea, on the exposed basement in Uppland and in the intervening hinge zone between Uppland and the Mesoproterozoic basins to the N and E (Beckholmen and Tirén 2009). The U1 surface has received limited attention in the geological literature for Forsmark (Milnes 2002) despite the presence of Jotnian sandstone within 20–25 km of the site (Figure 2-6).

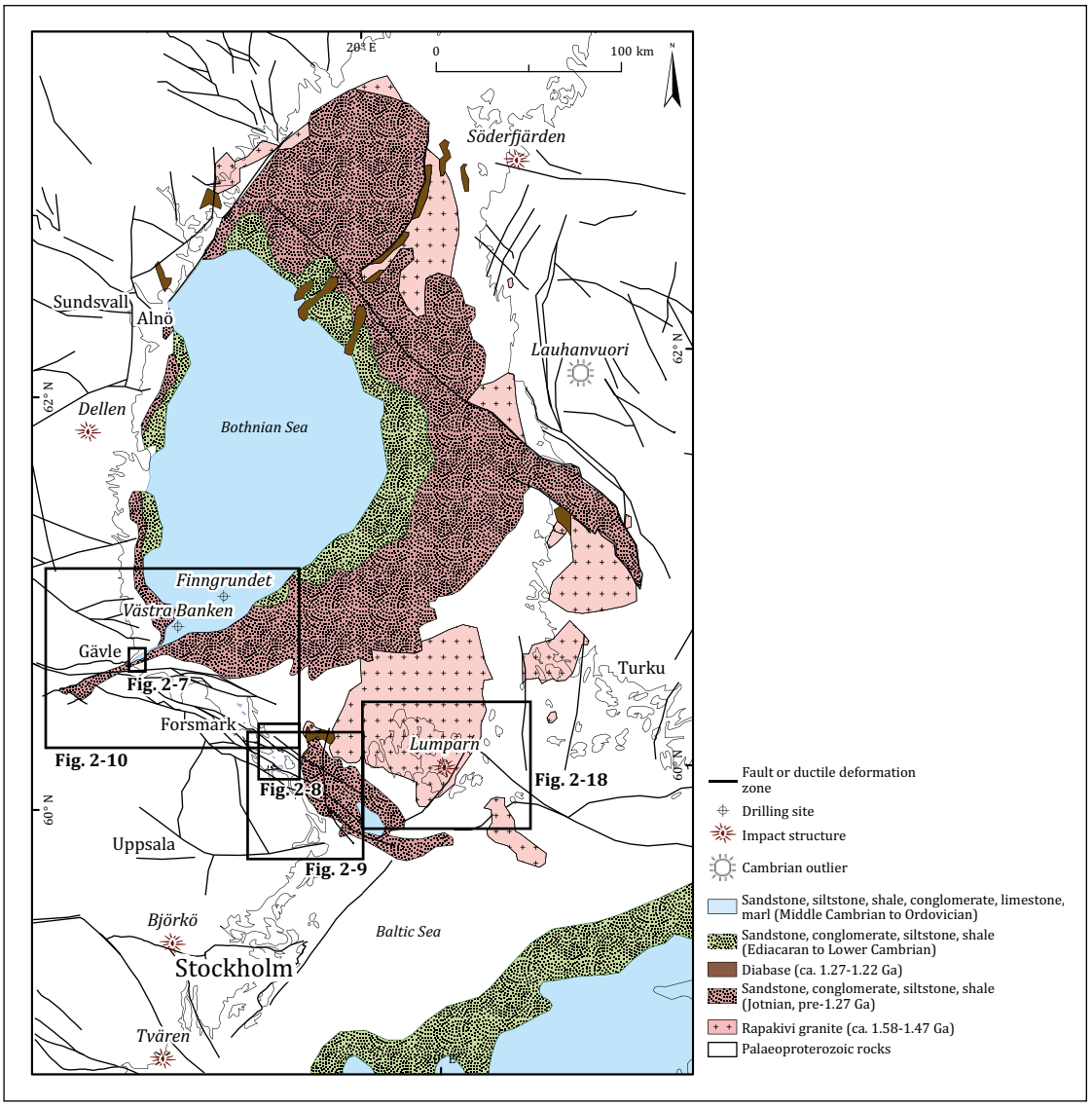

Figure 2-6. *Geology of the Bothnian Sea, modified from Paulamäki and Kuivamäki (2006). See text below for references to the Lauhanvuori outliers and the impact structures.*

2.2.1 U1 in the Bothnian Sea

The Jotnian sedimentary rocks deposited before 1.5 Ga are present below Early Palaeozoic rocks in the southern Bothnian basin as a submarine continuation of the 'Jotnian' sandstone formations in the Gävle area on the east coast of Sweden (Paulamäki and Kuivamäki 2006) (Figure 2-6). The rocks are typical red bed arkosic sandstones displaying low-grade metamorphism (Nyström and Levi 1980). Seismic refraction survey indicates a thickness of 900 m in the Gävle half-graben (Gorbatschev 1967). Outside the graben, in the SW part of the Bothnian Sea, the sandstone thins to ~100 m (Winterhalter 1972), and, on the Finngrundet (Figure 2-6). Early Palaeozoic sedimentary rocks rest directly on crystalline basement (Flodén 1977). Mesoproterozoic sandstones are seen in seismic sections to rest on the basement surface of U1 (Winterhalter et al. 1981). U1 has a relief of > 100 m around the Finngrundet, with the shoals representing partially buried hills, and over a wider areas of the southern Bothnian Sea but has low relief on the sea bed W of Åland (Flodén 1977). U2 has a much more even surface in seismic images (Winterhalter et al. 1981). U2 is cut across basement and Jotnian sandstone, indicating that the Jotnian sequence was down faulted before the Early Cambrian transgression. Similar relationships between U1 and U2 exist around the Åland islands (Flodén 1977). U1 is of low relief on the margins of and around inliers within the Satakunta basin (Pokki et al. 2013a) (Figure 2-6) and locally around other Mesoproterozoic outliers in Sweden (von Eckermann 1937). The presence of Early Cambrian sandstone dykes in SW Finland indicates also that the erosion levels of the U1 and U2 basement surfaces are similar in this area (Kohonen and Rämö 2005).

2.2.2 U1 in Gävle Bay

In the inner part of Gävle Bay, the Jotnian sandstones occupy narrow grabens, locally overlain by thin Ordovician limestones, sitting between basement horsts (Figure 2-7). Faults are oriented ENE–WSW (Flodén 1977). The sub-Cambrian unconformity is cut in basement and Jotnian sandstones and across intra- and post-Jotnian fault blocks (Figure 2-7). E of Finngrundet, post-Ordovician fault block displacement is ~100 m (Winterhalter et al. 1981). Towards the S, post-Ordovician displacement is only a few tens of metres (Figure 2-7), reaching a maximum of 50–60 m (Flodén 1977). The present basement surface (UQ) along the southern coast of Gävle Bay coincides approximately with U1 and closely to U2.

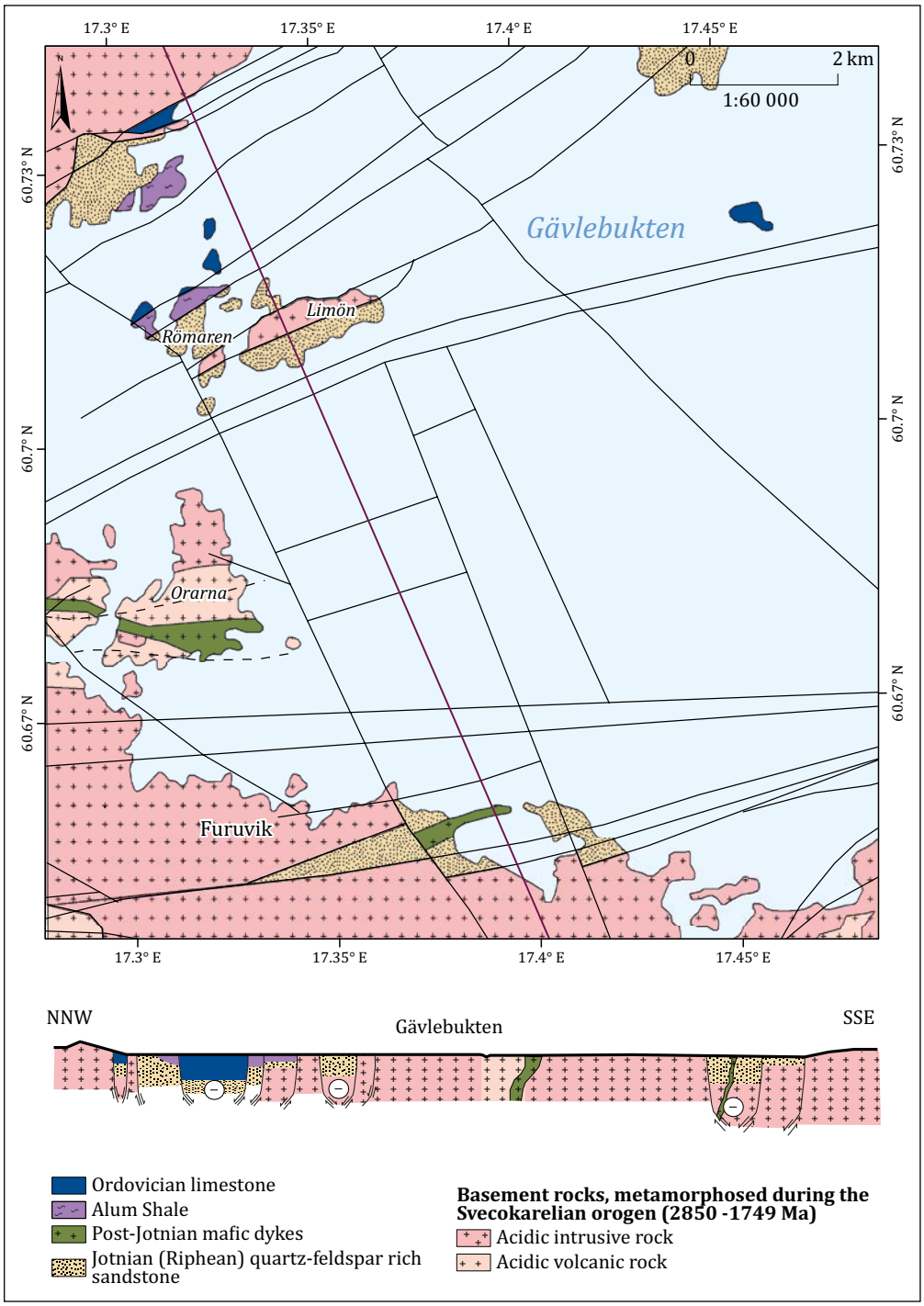

Figure 2-7. *Mesoproterozoic sandstones and Ordovician limestone in Gävle Bay (Gävlebukten). Terrestrial geology based on SGU maps. Schematic section shown from NNW to SSE (purple line). Location of Figure 2-7 is portrayed in Figure 2-6.*

2.2.3 U1 between Öregrund and Singö

The archipelago between Öregrund and Singö (termed the Öregrund archipelago) stands within the zone of NW–SE oriented major faults and deformation zones that delimit the western margin of the Mesoproterozoic basin in the Åland Sea (Söderberg 1993). Regional structures, with a trace length greater than 10 km, include the Forsmark, Eckarfjärden and Singö Deformation Zones (Stephens 2010) (Figure 2-5). Horizontally bedded Jotnian sandstones occur in narrow half grabens, with a single sandstone dyke recorded on the basement surface (Figure 2-8). These grabens correspond to small fault blocks in the basement (Grigull et al. 2019). The southern Mesoproterozoic outliers in Galtfjärden are greater than 100 m in thickness (Söderberg and Hagenfeldt 1995). Widespread block faulting and dislocation of U1 is indicated in the hinge zone between Uppland and the main Mesoproterozoic basin in the Åland Sea.

2.2.4 U1 around Väddö

The Mesoproterozoic basin of the Åland Sea has a western margin parallel to the coast of the island of Väddö in eastern Uppland (Figure 2-9). Jotnian sandstones approach to within 3 km of the coast (Söderberg and Hagenfeldt 1995) and terminate against a set of NNW–SSE oriented faults, with a 90 m offset (Beckholmen and Tirén 2010a), part of a major N–S fracture system in Uppland. The N–S faults extend into the northern part of the Stockholm archipelago (Hagenfeldt and Söderberg 1994) where Jotnian sandstones >30 m thick occur in fault zones and local concentrations of erratics indicate that other small outliers are present (Hagenfeldt 1995). Ordovician limestones also are present in several small fault-bounded or –guided basins or depressions (Söderberg and Hagenfeldt 1995). The disposition of the southern outliers in relation to the NNW–SSE oriented faults at Väddö indicates initial displacement of U1 during and after Jotnian sandstone deposition and also a later, lesser phase of dislocation of U2 after deposition of Early Cambrian sandstone (Hagenfeldt and Söderberg 1994) and Late Ordovician limestone (Söderberg and Hagenfeldt 1995).

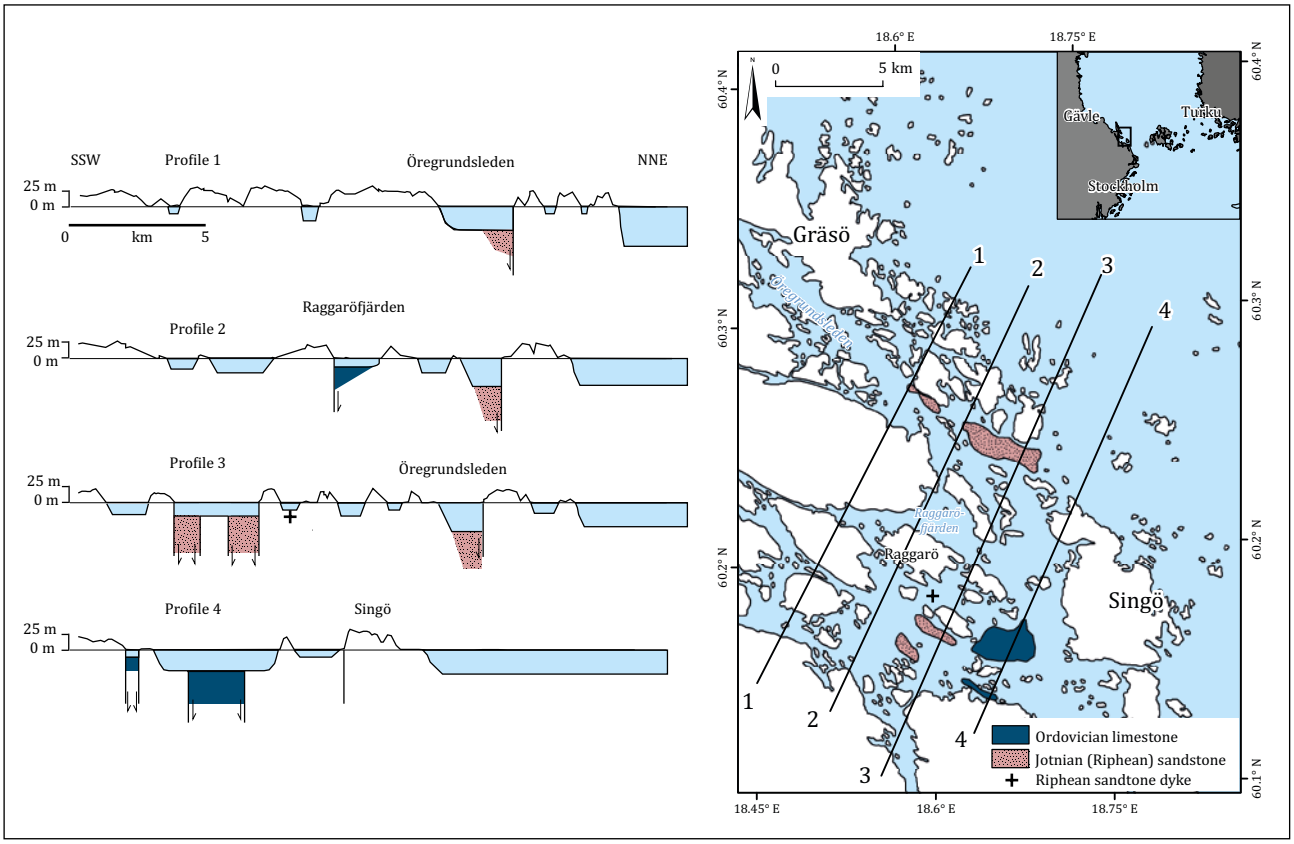

Figure 2-8. *Schematic profiles of block-faulted basement W of Singö, with Mesoproterozoic and Ordovician sedimentary rocks after Söderberg and Hagenfeldt (1995).*

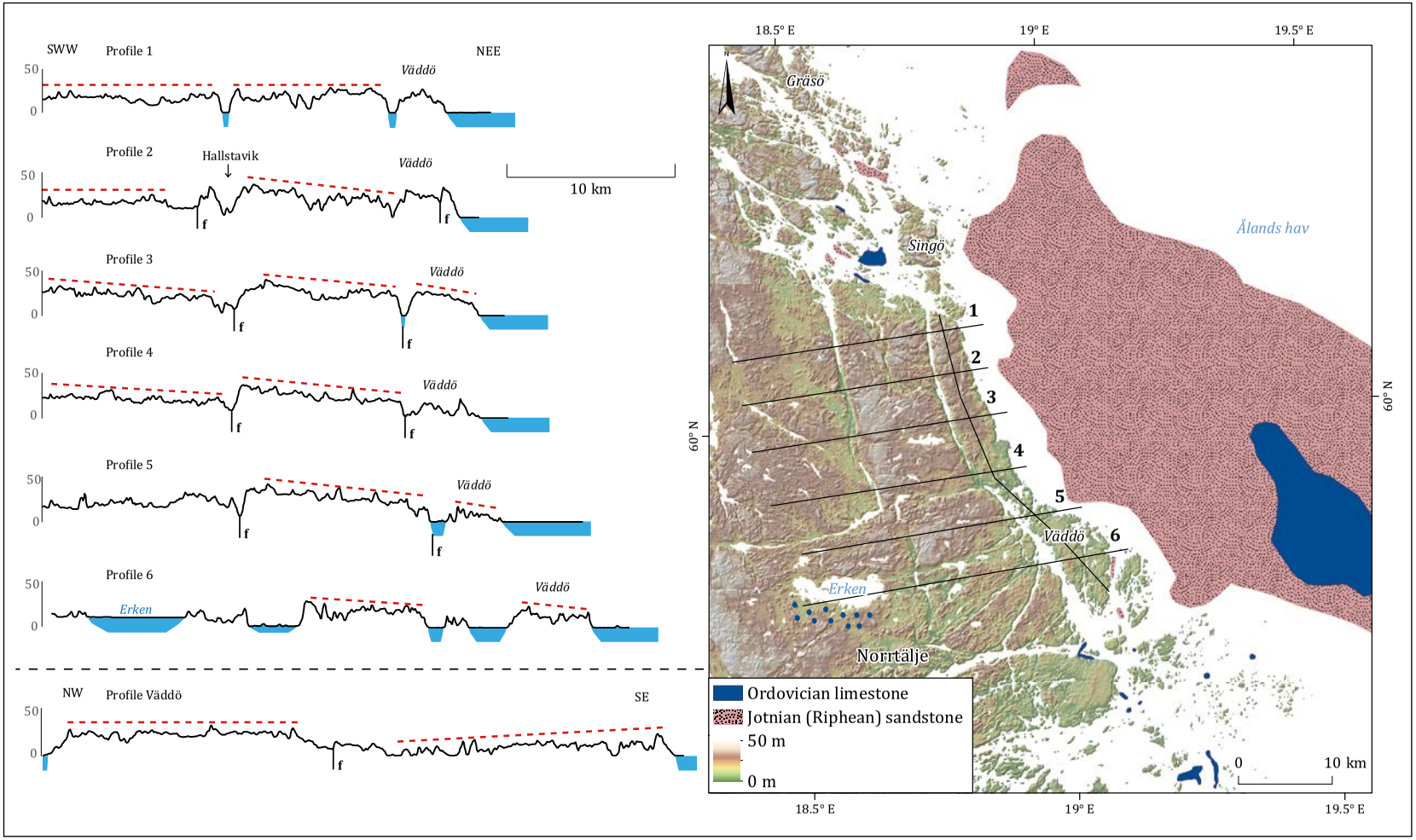

Figure 2-9. *Geology and topography on the margin of the Åland Sea at Väddö. Red dotted lines show block inclinations. Offshore Mesoproterozoic and Ordovician sedimentary rocks after Söderberg and Hagenfeldt (1995). High concentrations of Ordovician limestone boulders south of Lake Erken may indicate the local presence of a limestone outlier (Asklund 1930). The location of the map area is shown in Figure 2-6.*

2.2.5 U1 over Uppland

The distribution of Mesoproterozoic sandstones and the thickness of these rocks in the Bothnian and Åland Sea basins (Figure 2-6) indicate that Mesoproterozoic sedimentary rocks formerly buried the basement in Uppland. Extensive cover is also indicated by a Mesoproterozoic infill of the Björkö impact structure at Lake Mälaren, 35 km W of Stockholm, formed more than 1.2 Ga ago (Figure 2-6). The hilly surroundings of the crater were eroded and the crater was infilled by sandstone (Flodén et al. 1993) with a basal boulder conglomerate (Wiman 1942). Based on the model of Degeai and Peulvast (2006), this impact structure, with a diameter of ~8 km, likely had an original depth of ~0.6 km, providing a maximum depth for basement erosion at this location through the 1.2–0.5 Ga interval. Very slow (< 1 m/Ma) average rates of subsequent basement denudation are consistent with prolonged post-impact burial.

On the seabed off northern Uppland, U1 emerges from below Mesoproterozoic cover as a low relief surface at similar elevation and within 4 km distance of an Ordovician outlier on the sea bed off Gräsö (Figure 2-10). The edge of the Jotnian sandstone off NE Uppland is smooth and apparently without major fault displacements (Figure 2-11A). A profile in basement along this edge shows a relief of less than 15 m (Figure 2-11B). U1 is here coincident with U2 that extends towards the present coastline as a gently inclined basement ramp (Figure 2-11C). Along the present Uppland coast at Gävle and between Forsmark and Väddö, the Mesoproterozoic sandstones are largely confined to small fault-bounded basins between large basement horsts (Figure 2-8). Forsmark stands between the Singö and Eckarfjärden Deformation Zones and, with its surroundings, shows a similar rock block topography to the parts of the archipelago to the SE which retain Jotnian and Ordovician outliers (Beckholmen and Tirén 2009). The dislocated Phanerozoic rock blocks recognised across Uppland (Beckholmen and Tirén 2010a, Grigull et al. 2019) include reactivated Mesoproterozoic fault blocks. No Mesoproterozoic outliers are known in Uppland W of the present coastline. Traces of former red bed cover, however, may be present locally as fracture coatings (Figure 2-12). Oxidation of U(IV) to U(VI) minerals at Forsmark is dated to ~1.25 Ga (Krall et al. 2018) and may also relate to secondary mineralisation at shallow depth beneath the former U1 surface. Further south, the depth of post-impact erosion at Björkö indicates that U1 stood several hundred metres above the present basement surface in its surrounding area.

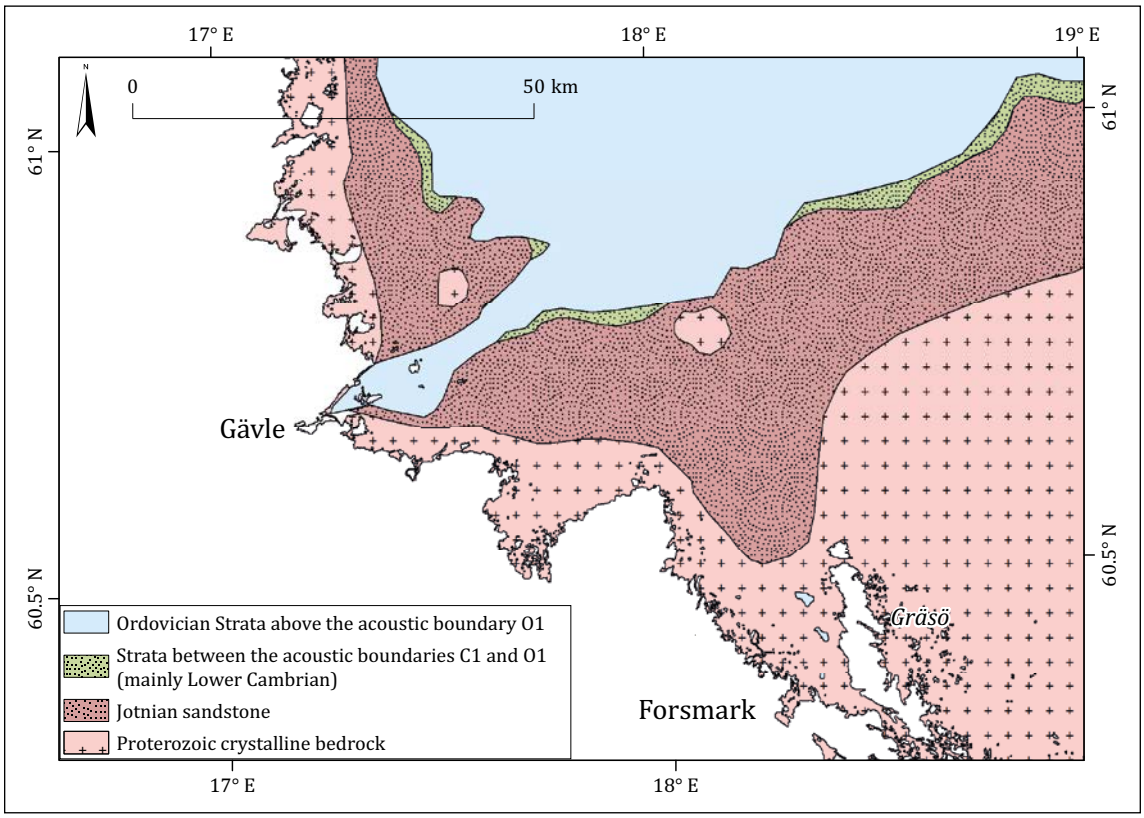

Figure 2-10. *Geology of the SW Bothnian Sea, after Thorslund and Axberg (1979).*

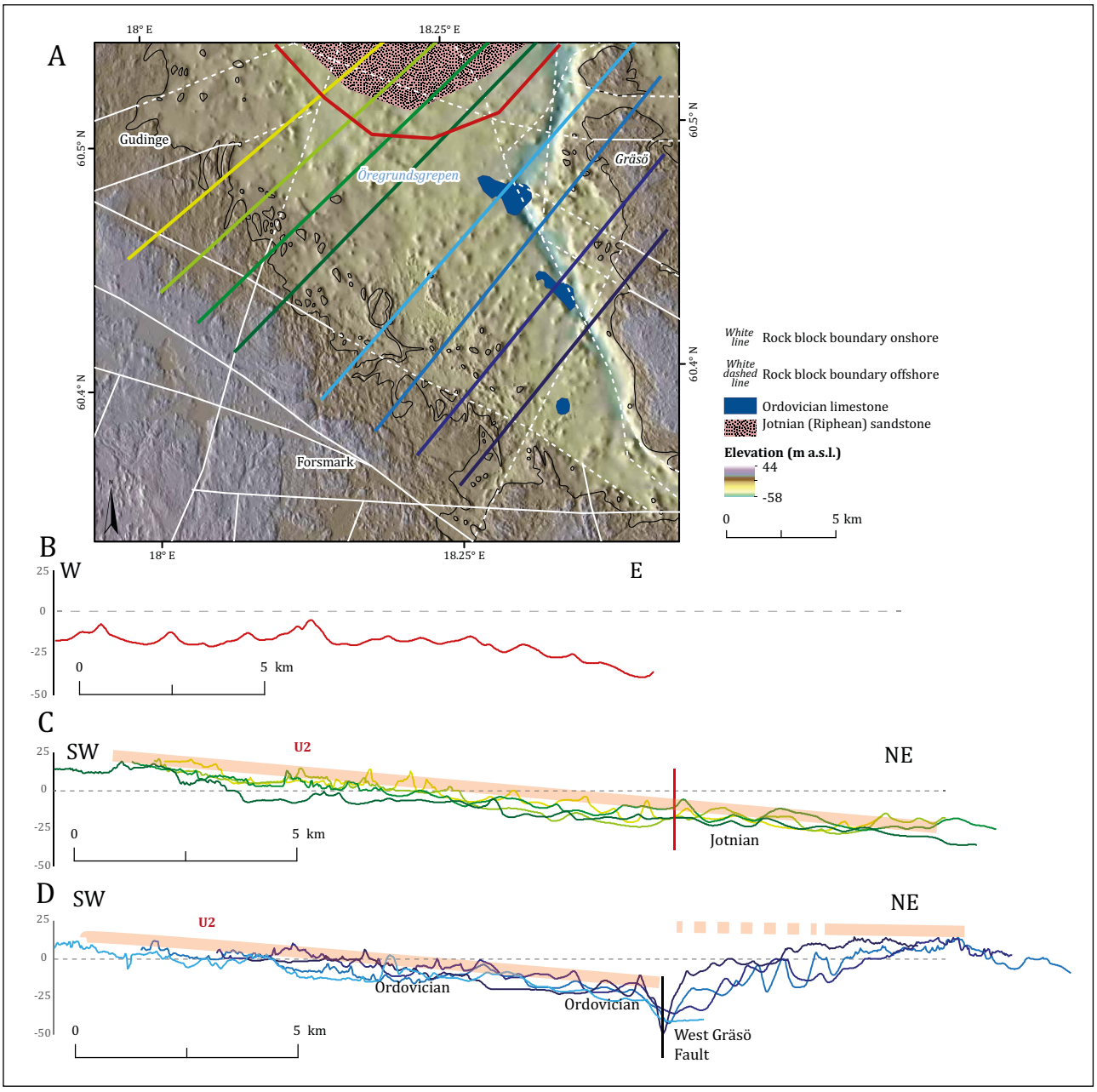

Figure 2-11. *U1 and U2 on the sea bed between Gräsö and Forsmark. A. DEM based on the terrestrial and bathymetric data. Topographic profile lines run SW–NE. The positions for the Ordovician are orthorectified from Söderberg and Hagenfeldt (1995) but may not be exactly positioned. Fault block boundaries from Grigull et al. (2019). Note the proximity of the edge of the Jotnian to the northernmost Ordovician outlier and of Ordovician outliers to Forsmark. B. Topographic profile for the sea bed around the edge of the Jotnian cover showing the low relief of U1 where the basement emerges from cover (red curve in panel A across the Öregrundsgrepen). C. Superimposed topographic profiles across basement and Jotnian sandstone. D. Superimposed topographic profiles across basement and Ordovician limestone. The general position and form of U2 is indicated by the coincident elevations of bedrock highs along the band. The average gradient of U2 to the NE is ~0.2 %. Slight tilting towards the SE is also indicated.*

The coincident elevations of the U1, U2 and UQ surfaces around the Mesoproterozoic basin of the Bothnian Sea requires very limited erosion of basement since ~1.5 Ga. Average basement erosion rates for other cratons (Flowers et al. 2006) indicate this part of the Fennoscandian Shield is amongst one of the slowest eroding cratonic areas known on the Earth's surface. Ultra-slow basement denudation in this part of Sweden is fundamentally a product of protection from erosion by prolonged burial. Jotnian and Palaeozoic sedimentary cover rocks were originally of km thickness and their removal required deep erosion. Exhumation from Palaeozoic cover at Forsmark was slow, with estimated rates of exhumation of ~2 m/Ma between 500 and 250 Ma based on U-Th/He thermochronology (Page et al. 2007).

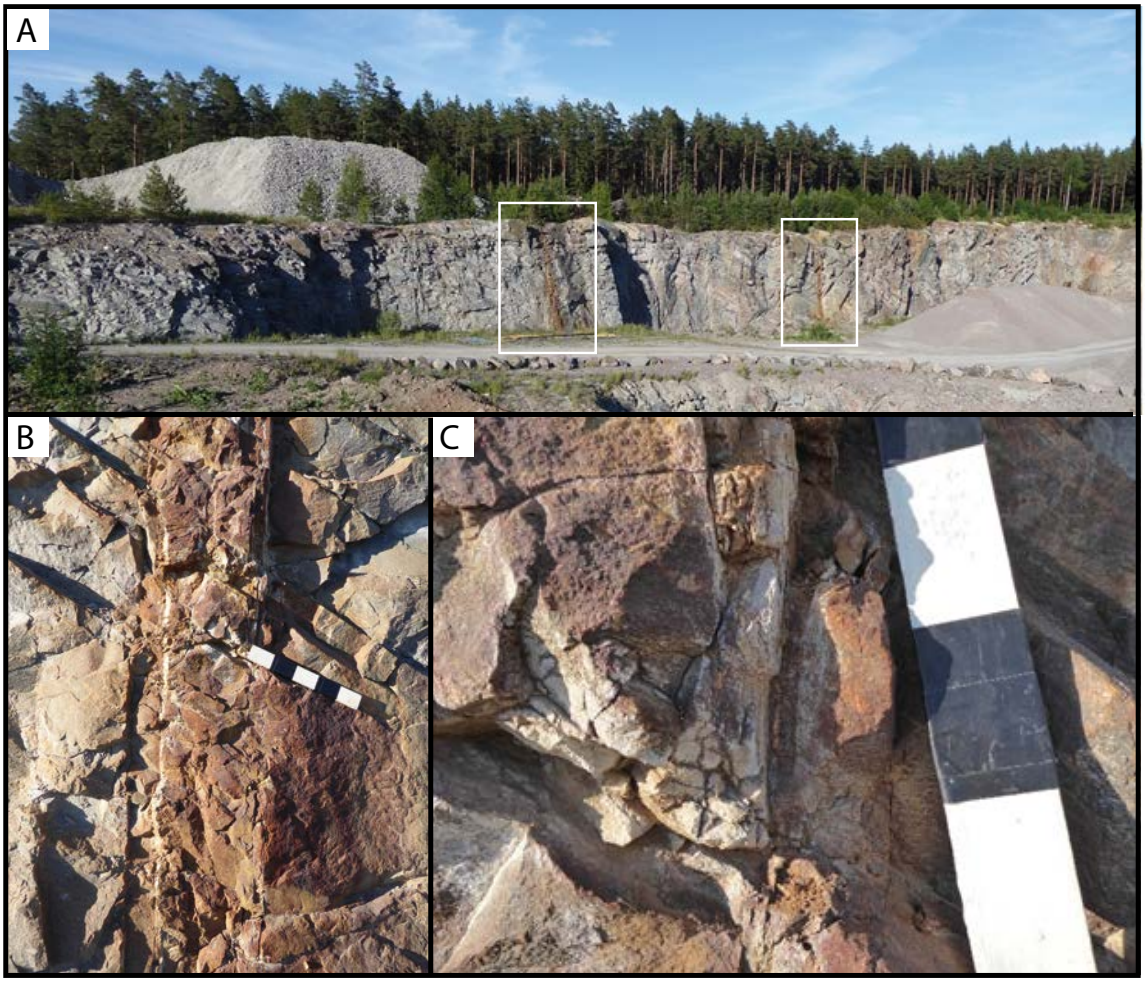

Figure 2-12. *Griggebo Quarry, Vavd (60.466361°N, 17.8952970°E, 20 m a.s.l. For location see Figure 2-22). The quarry stands ~20 km S of the edge of the Mesoproterozoic sedimentary rocks offshore. Major fractures are oriented NW–SE in this area (Beckholmen and Tirén 2010b). A. Near-vertical fractures are exposed, oriented to 35° and with minor (0–25 cm) displacements. B and C. The fractures display undated hematite coatings and breccia (G1?) that are cut by younger calcites (G2 or G3?) and iron oxides (G4). The hematite coating may have developed originally below a cover of Mesoproterozoic red beds. The scale bar is 50 cm long.*

2.3 The sub-Cambrian unconformity (U2)

This section first examines the re-exposed sub-Cambrian unconformity (U2) in the wider context of earlier interpretations of the sub-Cambrian. The form and subsequent dislocation of U2 is then assessed in Uppland where it remains buried on the sea bed E of Forsmark (Figure 2-11), within the tectonic hinge zone that includes Forsmark and across Uppland. The original form of U2 is modelled from summit elevation data and provides a reference surface for estimating depths and patterns of glacial erosion in basement rocks across Uppland.

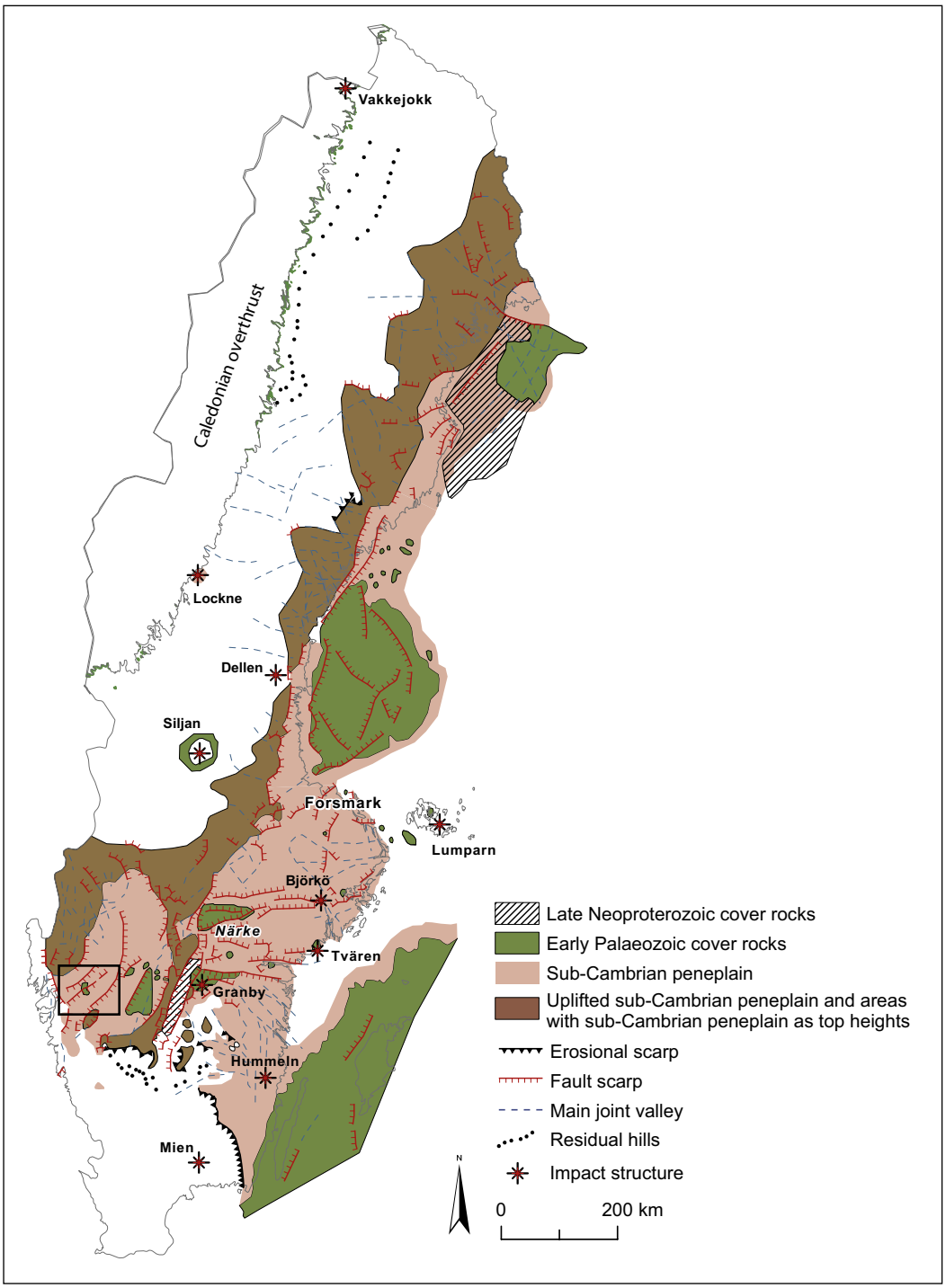

Figure 2-13. *Mapped extent of the sub-Cambrian peneplain in Sweden, modified from Lidmar-Bergström and Olvmo (2015). Impact structures from Abels et al. (2002). Box indicates Trollhättan study area location in Västergötland (Goodfellow et al. 2019, Hall et al. 2019a).*

2.3.1 The form and cover of the sub-Cambrian unconformity in Fennoscandia from geological evidence

The sub-Cambrian unconformity is cut across heterogeneous basement lithologies and, locally, Mesoproterozoic sedimentary rocks (Lidmar-Bergström 1996). The sub-Cambrian unconformity is widely regarded as an exceedingly flat surface in Fennoscandia, and in North America (Nielsen and Schovsbo 2011, 2015, Peters and Gaines 2012). The relief on an unconformity surface can be constrained along strike in exposures, from the gross stratigraphic architecture of the strata that cover the unconformity, as well as from seismic section where the unconformity is buried.

On the sub-Cambrian unconformity, relief of less than 10–20 m per km is found widely along strike close to the edge of Cambrian cover rocks in eastern Sweden in the Öland–Gotland area (Flodén 1980), at Kalmar (Tirén and Beckholmen 1992), from Kalmar northwards to Västervik (Munier and Talbot 1993) and at Närke (Figure 2-13). In northernmost Sweden, the buried sub-Cambrian unconformity is described as "exceedingly flat" along strike for over 400 km (Ormö et al. 2017). In Estonia, the buried sub-Ediacaran unconformity has a relief of less than 10 m per km (Puura et al. 1996, Tuuling and Flodén 2016) and an average gradient of 0.15 % over a distance of 200 km (Kirsimäe et al. 1999). The buried sub-Ediacaran unconformity on the Onega peninsula, NW Russia has an average gradient of 0.1 % over a distance of 200 km (Grazhdankin 2003). On the Hardangervidda, SW Norway, the sub-Cambrian unconformity at Finse is close to planar in form (Rosendahl 1934). The buried sub-Cambrian unconformity between northern Jutland and Bohuslän is also described as exceptionally flat in seismic sections (Lassen and Thybo 2012).

In Västergötland, the relief on the buried sub-Cambrian unconformity is most tightly constrained along the edges of Cambrian outliers (Figure 2-13). Around the edges of the Halleberg and Hunneberg mesas, the basement unconformity that emerges from below Early Cambrian cover is described as "extremely flat" (Johansson 1999). Available evidence indicates a relief of <2 m per 100 m on km long sections of the buried unconformity at Kinnekulle (Högbom and Ahlström 1924). Lake shore exposures at Kinnekulle show that the ribbed bedrock unconformity surface, with less than 2 m relief, retains thin patches of quartz sandstone and conglomerate (Högbom and Ahlström 1924), giving the appearance of an extensive and flat platform, with minor surficial roughness. At Närke, the basal Early Cambrian Mickwitzia sandstone rests upon "an almost perfectly plane surface of denudation" (Thorslund and Jaanusson 1960).

Although the relief on the sub-Cambrian unconformity was low to extremely flat across large areas, some palaeo-valleys and isolated inselbergs occur locally. Valleys of up to 40 m depth and tens of kilometres in length are developed on U2 on the Hardangervidda, SW Norway (Gabrielsen et al. 2015). Widely-spaced inselbergs occur in the Gulf of Finland (Pokki et al. 2013b) and below Late Ediacaran cover in Estonia (Puura et al. 1996). North of Kalmar, Sweden, a single granite inselberg more than 90 m high forms the islet of Jungfrun (Elvhage and Lidmar-Bergström 1987). Smaller, isolated, granite hills, many with sandstone dykes (Friese et al. 2011), rise 10–20 m above surrounding basement summits at lower, accordant elevations along the edge of Cambrian cover west of Mönsterås (Martinsson 1974). The low granite hills are exhumed landforms that have been modified by glacial erosion (Lidmar-Bergström 1997).

The sub-Cambrian unconformity became progressively covered during the Cambrian transgression. The extent and character of the cover sediments provides additional information on the geometry of the unconformity surface. A high/medium-relief unconformity will be typically covered by a sequence showing high-energy fluvial deposits such as alluvial fans and/or abrupt lateral facies changes: the early Neoproterozoic sub-Torridon unconformity in Scotland is a good example (Stewart 2002). In contrast, a flat unconformity surface should result in a cover sequence with large areal extent, with thin units with wide geographic extent and few lateral facies changes. The broad sequence deposited onto U2 in Sweden in the Early Palaeozoic is a cover of sandstone, shale and limestone. The sandstone sequence is characterised by well-sorted, mature quartz sandstones, with thin basal pebble conglomerates (Thorslund and Axberg 1979). Deposition took place in a storm dominated, shallow (less than 10 m depth) water environment (Artyushkov et al. 2000, Nielsen and Schovsbo 2011). As an example of the lateral extent and lack of lateral facies variations, the File Haidar sandstone formation, deposited onto the U2 surface in south-central Sweden (Figure 2-14) varies in thickness between 16 and 38 m (with most values between 22 and 26 m) in sections and boreholes in an area stretching from Kinnekulle, including the Vänern and Vättern area towards the boreholes in the Bothnian Sea (Nielsen

and Schovsbo 2011). Only in the Baltic Sea area did formation thickness reach 50 m or more. Thus, in south-central Sweden all available sections and boreholes indicate that the File Haidar Formation was of uniform thickness over a very wide area.

An hiatus, the Hawke Bay unconformity, is widely recorded within Cambrian sequences late in the Early Cambrian (Nielsen and Schovsbo 2015), with non-deposition and erosion across large areas of southern Sweden, Estonia and the St Petersburg region (Artyushkov et al. 2000). This hiatus is a result of combined minor (< 40 m) epeirogenic uplift and ≥ 100 m sea level fall (Artyushkov et al. 2000, Nielsen and Schovsbo 2015). This hiatus was of limited (≤ 6 Ma) temporal range and low erosional impact, with a maximum of 5–10 m of strata removed by erosion (Nielsen and Schovsbo 2015), but nevertheless the disconformity is recorded over a very wide area, again attesting to the flatness of the landscape at the time across large parts of Scandinavia, (Figure 2-14). Typical regional gradients are estimated at only 0.5–1 m per km (Nielsen and Schovsbo 2015).

Marine transgression and deposition resumed in the early Middle Cambrian. The former continuity of the Alum Shale from Forsmark towards Uppsala is indicated by asphaltite fracture fills (Sandström et al. 2006b). The onset of deposition in Uppland of the organic-rich Alum Shale took place under anoxic conditions at or below storm-wave base (Nielsen and Schovsbo 2015). Deposition of Alum Shale across Uppland and directly onto basement implies conditions with low wave energy and limited clastic sediment supply.

The Ordovician sequence is today c. 200 m thick in the Bothnian Sea basin and more than 133 m thick at Siljan (Juhlin et al. 2012) (Figure 2-4). The uppermost parts of these sequences are missing and hence the preserved thicknesses represent the minimum thickness of Ordovician cover originally present in Uppland. Extensive deposition of shallow water limestones attests to a lack of clastic sediment supply, indicating complete burial of basement during deposition and hence a lack of basement hills to supply clastic sediment.

In summary, evidence from the buried sub-Cambrian unconformity, as well as the occurrence of thin sandstone units of extraordinary lateral extent (Figure 2-14), directly overlying the unconformity points to the sub-Cambrian unconformity being an exceedingly flat plain of great extent.

2.3.2 Weathering remnants on the sub-Cambrian unconformity

Weathering and alteration of the surface of the basement unconformity are recorded in exposures and boreholes. Thick, kaolinitic weathering profiles more than 40 m deep, thinning southwards, have been documented in Estonia and are buried by Ediacaran sandstones that date from ca. 560 Ma (Liivamägi 2015, Liivamägi et al. 2015). No reports of similar thicknesses of late Neoproterozoic weathering are known from Norway and Sweden. Instead, in southern Norway (Gabrielsen et al. 2015) and in southern Sweden (Elvhage and Lidmar-Bergström 1987), weathering profiles below the sub-Cambrian unconformity are absent across extensive areas and the sub-Cambrian unconformity is developed across unweathered basement rocks. Where present, as at Närke, saprolite remnants are < 5 m thick (Elvhage and Lidmar-Bergström 1987, Gabrielsen et al. 2015). Boreholes in Gävle Bay indicate that the saprolite layer beneath Early Cambrian sandstone is only 1–2 m thick (Thorslund and Axberg 1979). The general presence of diagenetic minerals in shallow saprolite on the buried unconformity (Gabrielsen et al. 2015) indicate fluid migration across the unconformity surface after burial. No remnant of Late Neoproterozoic or early Cambrian weathering has been reported (Söderbäck 2008) or observed on the basement in Uppland, including from the dense network of boreholes drilled in the Forsmark area.

The absence of late Neoproterozoic deep weathering on U2 in Sweden may indicate removal by wave erosion during the Early Palaeozoic marine transgression. This is consistent with the storm-dominated facies of the clastic Cambrian deposits that cover much of the unconformity (Nielsen and Schovsbo 2011; see also Peters and Gaines 2012 for North America). Alternatively, thick weathering mantles may not have developed widely on this part of Baltica due to the efficiency of sheet wash and wind erosion operating on rock surfaces without vegetation cover at a time before the evolution of vascular plants (Rudberg 1970). Evidence for wind erosion is provided by the presence of ventifacts in Early Cambrian basal conglomerates in southern Sweden (Hadding 1929, Martinsson 1974). Such processes may also have acted in combination with shoreline erosion to keep basement surfaces free of soil and saprolites during transgressive-regressive phases of the Cambrian. The removal of remaining regolith from the unconformity surface by storm and wave erosion during the Cambrian marine transgression contributed to the final grading of U2.

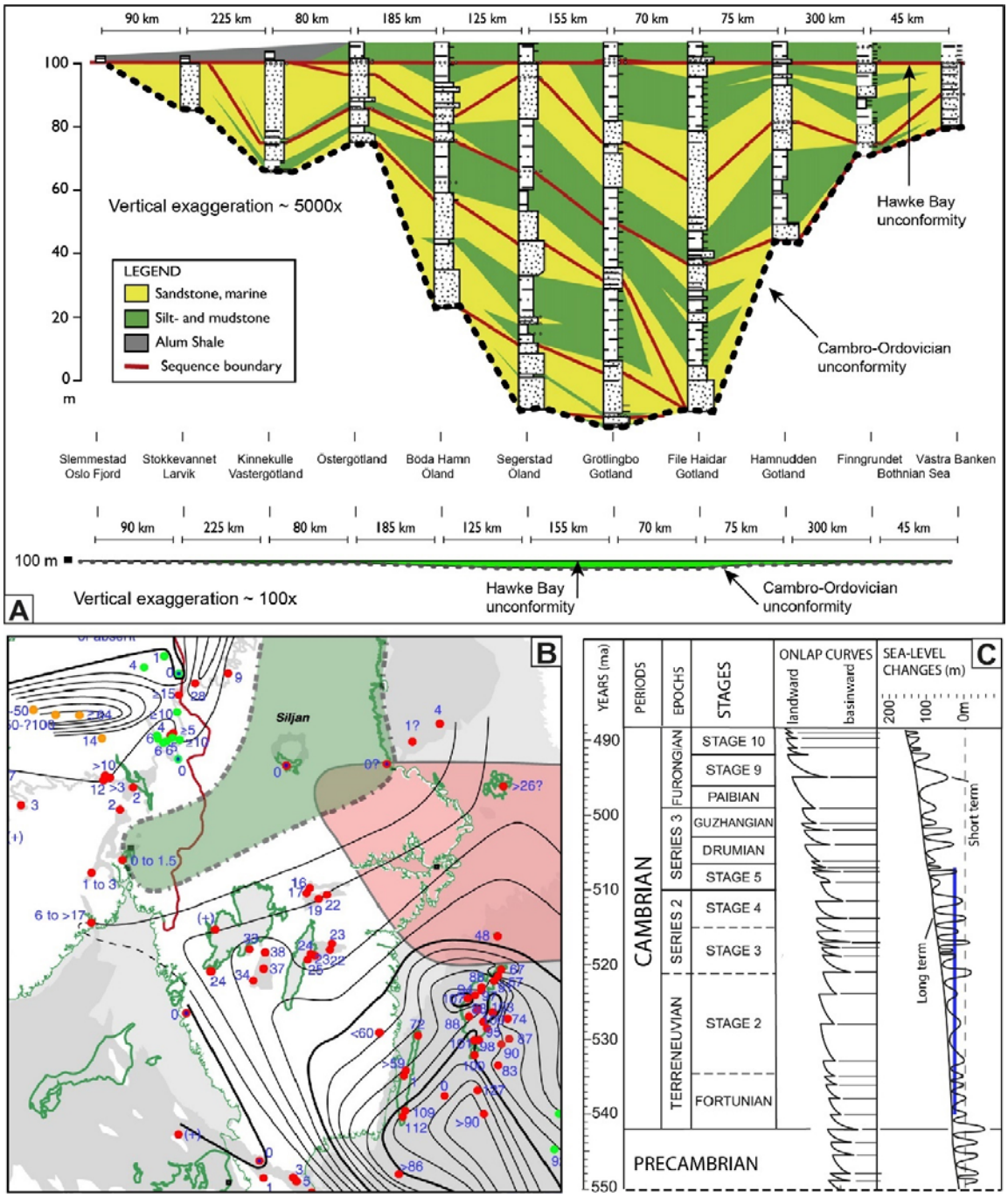

Figure 2-14. *Early Cambrian transgression in southern Sweden and neighbouring areas. A. Correlation diagram (sequence stratigraphy correlations) of the File Haidar Formation between the sub-Cambrian unconformity and the Hawke Bay intra-basinal unconformity. The section extends from the Oslo region, across Västergötland, Öland–Gotland and south-central Sweden to the Bothnian Sea. Top diagram with 5 000× vertical exaggeration; bottom diagram with 100 × vertical exaggeration. Modified after Nielsen and Schovsbo (2011). B. Isopach map (5 m contours) and measured thickness in sections and boreholes (red points) of the File Haidar sandstone formation and correlative units in southern Sweden. Modified after Nielsen and Schovsbo (2011). Red shaded area has experienced later erosion, so thicknesses are minima. Green area shows no evidence of deposition of the File Haidar Formation and it is interpreted to have remained emergent. C. Cambrian sea level changes modified after Haq and Schutter (2008). Sea level curves show a long-term overall transgression, and short-term retrogression-transgression cycles, based on onlap curves, based on sequence stratigraphic analysis of sections and boreholes that document base level changes. The blue line is an imaginary datum, which (if the datum is stable) experienced 14 flooding and retrogression cycles.*

2.3.3 Origin and formation of the sub-Cambrian unconformity in Fennoscandia

The extraordinary flatness of both the Fennoscandian and Laurentian sub-Cambrian unconformities begs the question as to the origin and formation of these surfaces. Whilst much recent attention has been given to the scale of cratonic denudation through the Neoproterozoic that led to the formation of Great Unconformities on Laurentia and Baltica (Peters and Gaines 2012, DeLucia et al. 2017), the question of the origins of the flatness of the basement unconformities has been largely ignored.

In Fennoscandia, the late Ediacaran to Ordovician unconformity represents an hiatus of ~400 Ma or more in the geological record, between 900 Ma (the end of the Sveconorwegian Orogeny) and the onset of Ediacaran-Cambrian deposition, indicating that much of Scandinavia was subjected to long-term uplift and erosion (Kohonen and Rämö 2005). Several rift-basins developed across Baltica, but major rifts were located distal to south-central Sweden (Cocks and Torsvik 2005). During much of the late Neoproterozoic, Baltica was surrounded by passive margins, with any subduction zones distal to the continent (Greiling et al. 1999, Cocks and Torsvik 2005). Thus, Baltica experienced a long period of cratonic stability, and was subjected to a very long period of denudation. The proximity of U1 and U2 on the basement around the Mesoproterozoic basin of the Bothnian Sea indicates that Neoproterozoic erosion in this area was largely confined to sedimentary cover rocks.

Deep denudation culminated in formation of extensive low relief terrain prior to the onset of marine transgression. As on Laurentia (Keller et al. 2019), glacial erosion through the Cryogenian contributed to deep denudation on Baltica (Gabrielsen et al. 2015). Uneven basement topography with low, asymmetric hills showing stoss-lee forms typical of roches moutonnées emerge from beneath tillite in northern Norway (Laajoki 2003). Glaciation on Baltica, however, largely ceased at the end of the Cryogenian (Gabrielsen et al. 2015). By the Late Ediacaran, shallow marine conditions extended for hundreds of kilometres across eastern Baltica (Pehr et al. 2018). No tillites rest on the sub-Cambrian unconformity surface in southern Sweden (Nielsen and Schovsbo 2011). Hence, glacial erosion played no part in the later stages of shaping of the sub-Cambrian unconformity here.

Cessation of carbonatite magmatism at Alnö after 584 Ma coincides generally with the onset of deep kaolinisation in the Baltic states and likely marks the start of a >30–40 Ma long period prior to marine transgression in which the shield surface remained stable. The balance between weathering and erosion, leading to denudation, was likely different in the Precambrian from today, prior to the development of terrestrial vegetation (Liivamägi et al. 2015). On the one hand, atmospheric CO_2 levels were at least periodically high during the Neoproterozoic (Liivamägi et al. 2015), enhancing weathering rates. On the other hand, lack of plants may have made weathering less efficient (see discussion in Berner 1992). Lack of vegetation also implies that removal of saprolite by sheet wash and wind erosion would have been highly efficient (Lidmar-Bergström 1993, Martinsson 1974), leading to increased denudation rates. Whilst the mechanisms remain obscure, erosion acting over long timescales across a stable craton resulted in levelling of the surface of Baltica.

Final grading of the shield surface was achieved through the Cambrian transgression, a result of a long-term (>50 Ma) overall sea level rise (with a total of 200 m sea level rise), superimposed on a series of repeated short-term high-stands and low-stands of 20–70 m amplitude (Haq and Schutter 2008). Any particular datum (palaeo-horizontal) would have been subjected to 10–20 short-term transgression-retrogression cycles over tens of millions of years (Figure 2-14) ; each of these cycles would result in a phase of coastal erosion (the so called ‘wave-base razor’) sweeping across exposed basement surfaces, before they became covered by sediment (Peters and Gaines 2012). This is consistent with the mature, well-sorted nature of the storm-dominated Cambrian sandstone (Dott 2003), as described above (Nielsen and Schovsbo 2015). The depth of erosion involved in final marine grading of the basement unconformity remains uncertain

2.3.4 Peneplains, planation surfaces and buried unconformities

The term *sub-Cambrian peneplain* has been used to refer to the present-day expression of the U2 unconformity as a regional geomorphic feature. The exhumed sub-Cambrian unconformity surface is regarded as a primary inherited landform (as the SCP) of the Fennoscandian shield (Lidmar-Bergström 1988), extending across much of southern and eastern Sweden and on to the flanks of the South Finland Dome (Figure 2-4). The unconformity, as modelled in regional profiles (Elvhage and Lidmar-Bergström 1987), trend surfaces (Johansson et al. 1999) and seen in DEMs (Figure 2-15) is flat, with less than

5–20 m relief per km over wide areas and with only isolated hills and ridges. This flatness distinguishes U2 from exhumed sub-Mesozoic unconformities found in southern Sweden which show hilly relief due to a development in response to Mesozoic and Neogene deep weathering and erosion that exploited differences in rock resistance (Lidmar-Bergström et al. 2012, 2017). The flat exhumed surface of U2 is also distinct from the rougher terrain of hills and fracture-guided valleys produced by erosion from the Fennoscandian Ice Sheet of the weathered basement during the Pleistocene (Lidmar-Bergström 1997, Olvmo et al. 1999). The extensive, near-planar form has allowed the modelled unconformity to be used as a reference surface in southern and east-central Sweden for analysis of later tectonics and block movements (Ahlin 1987, Lidmar-Bergström et al. 2012, Jarsve et al. 2014, Japsen et al. 2016, Tuuling 2017), impact crater depths (Sturkell and Lindström 2004), patterns of Phanerozoic denudation (Lidmar-Bergström 1991, Amantov and Fjeldskaar 2013, Japsen et al. 2016) and depths of Pleistocene glacial erosion (Amantov 1995, Johansson et al. 2001b). The basement terrain around Trollhättan is a type area for the SCP (Johansson et al. 2001b). This area is considered critical for understanding the local morphology of the sub-Cambrian unconformity and its modification by faulting and glacial erosion and so provides a valuable analogue for Uppland considered in forthcoming reports (Goodfellow et al. 2019, Hall et al. 2019a).

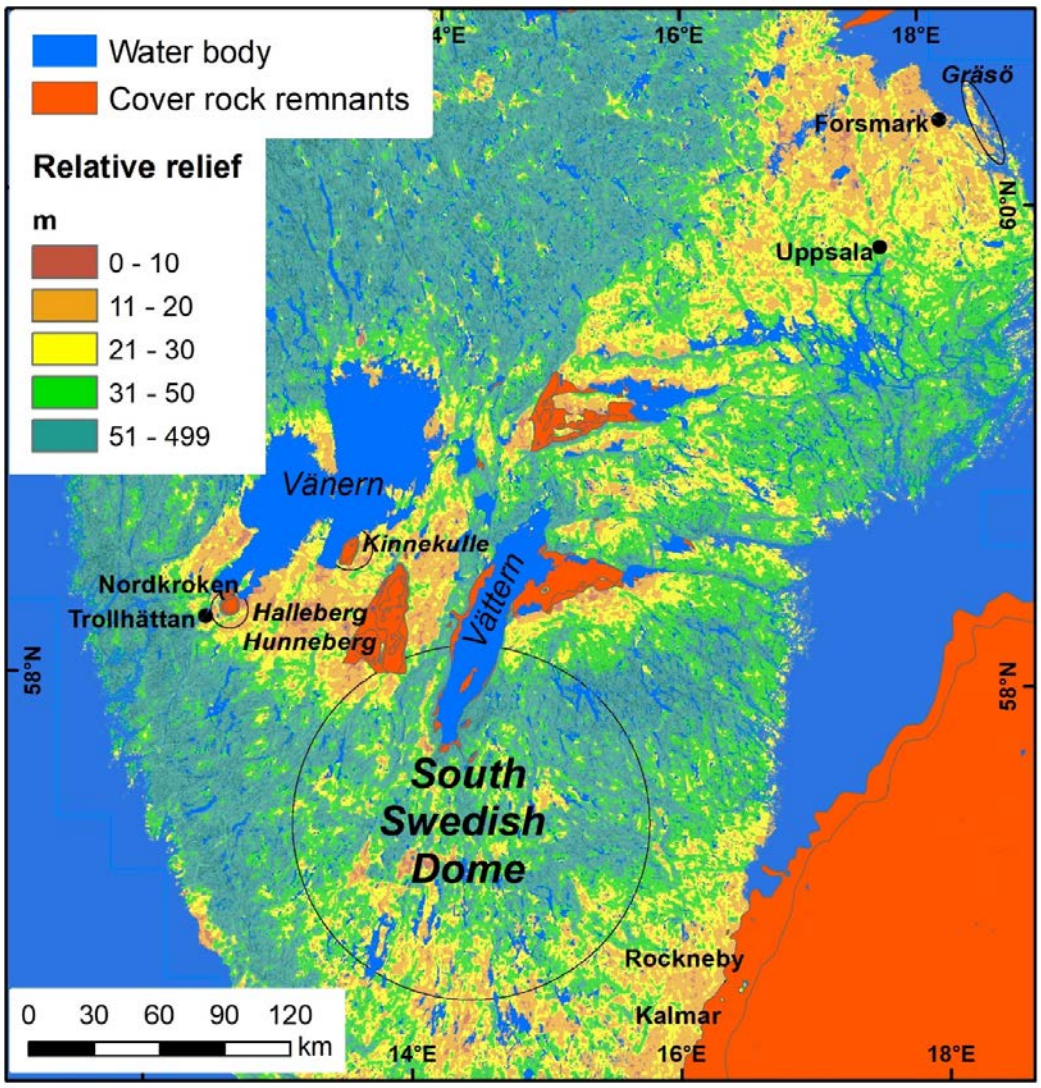

Figure 2-15. *Relative relief in southern and east-central Sweden. Relative relief is less than 20 m in the areas closest to Early Palaeozoic cover rocks. The relative relief is calculated by the range (vertical distance between lowest and highest pixel) in circular search windows of 1 km diameter around each pixel. The calculation is based on a DEM with 50 m resolution from the Swedish mapping, cadastral and land registration authority (Lantmäteriet). Distribution of Early Palaeozoic cover rocks from SGU. The approximate extent of the South Swedish Dome is indicated, along with the small Early Palaeozoic outliers on the Vänern shoreline, and the island of Gräsö.*

In southernmost Sweden, the sub-Cambrian unconformity was exhumed earlier than in Uppland and exposed to weathering and erosion at intervals through the Phanerozoic (Japsen et al. 2016). Early Miocene uplift of basement domes in southern Sweden (Migoń and Lidmar-Bergström 2001) and southern Finland (Gilg et al. 2013) led to exhumation and re-exposure of the basement to subaerial weathering and erosion under prevailing warm to temperate humid climates. In other parts of Fennoscandia, including large parts of southern and east-central Sweden, the basement remained covered by Palaeozoic and younger sedimentary rocks thorough the Mesozoic and much of the Cenozoic. In Uppland and, specifically, in the many SKB boreholes around Forsmark, there are no known records of Neogene deep weathering (Söderbäck 2008). Calcite fracture coatings remain widespread in the near-surface (Sandström et al. 2008) and indicate a lack of contact with circulating acidic groundwater. The absence of weathering, and the presence of calcite together indicate that covers of Early Palaeozoic limestone persisted into the Pleistocene in the Forsmark area and probably also more widely across Uppland. Continued burial of the basement prevented deep weathering and, on its re-exposure, provided a hard, fractured, low relief crystalline substrate as the bed of the Fennoscandian Ice Sheet. Glacial erratics sourced from Uppland are components of Elsterian and younger tills in E-central Poland (Czubla et al. 2019), indicating that at least part of the regional basement was already re-exposed to erosion by the Fennoscandian Ice Sheet by the Middle Pleistocene.

2.3.5 Faulting of the sub-Cambrian unconformity in south-central Sweden

Major tectonic disruption of the sub-Cambrian unconformity is recognised on the backslope of the shoulder of the North Atlantic passive margin in southern Norway where the unconformity has been displaced vertically by hundreds of metres in places (Jarsve et al. 2014, Gabrielsen et al. 2015). Lesser disruption of the unconformity on the cratonic lowlands was first characterised in southern Sweden (Rudberg 1970, Elvhage and Lidmar-Bergström 1987, Tirén and Beckholmen 1989). To the north of the South Swedish Dome in Västergötland (Figure 2-15), the unconformity is broken into gently-inclined, flat-topped blocks by major NNE–SSW trending-faults marked by prominent, exhumed fault-line scarps (Ahlin 1987, Johansson 1999, Lidmar-Bergström 1999). Fault displacements of < 70 m of the unconformity are recognised (Ahlin 1987). At Billingen, fault displacement across an Early Permian sill is 25–30 m (Andersson et al. 1985). In Uppland, the bedrock terrain has been mapped previously as a large tract of the SCP (Rudberg 1954) (Figure 2-13) that has been dislocated by minor block faulting (Ahlbom and Tirén 1991, Lidmar-Bergström and Olvmo 2015, Grigull et al. 2019) of possible Permian age (Saintot et al. 2011). Minor dislocation of the sub-Cambrian unconformity is widespread across southern Sweden.

Block faulting and tilting of U2 is well displayed in the Närke district, 200 km SW of Forsmark, Here the topography closely resembles parts of Uppland, with gently inclined, low relief surfaces on large rock block tops. Each topographic block is bounded by linear scarps (Figure 2-16). Comparison with the geology map shows that the topography at Närke is an expression of the exhumation of fault blocks from beneath Early Palaeozoic cover (Figure 2-17). The topographic blocks exposed as basement inliers and beyond the margins of the sedimentary cover represent fault blocks that have been re-exposed by stripping of the overlying Cambrian sandstone, Alum Shale and Ordovician limestone (Figure 2-17). The buried sub-Cambrian basement surface is flat (Thorslund and Jaanusson 1960). The sub-Cambrian unconformity has been broken along a series of W–E oriented faults with vertical displacements of 30–70 m. The impact of glacial erosion on the exhumed fault blocks at Närke is considered further in Chapter 4.

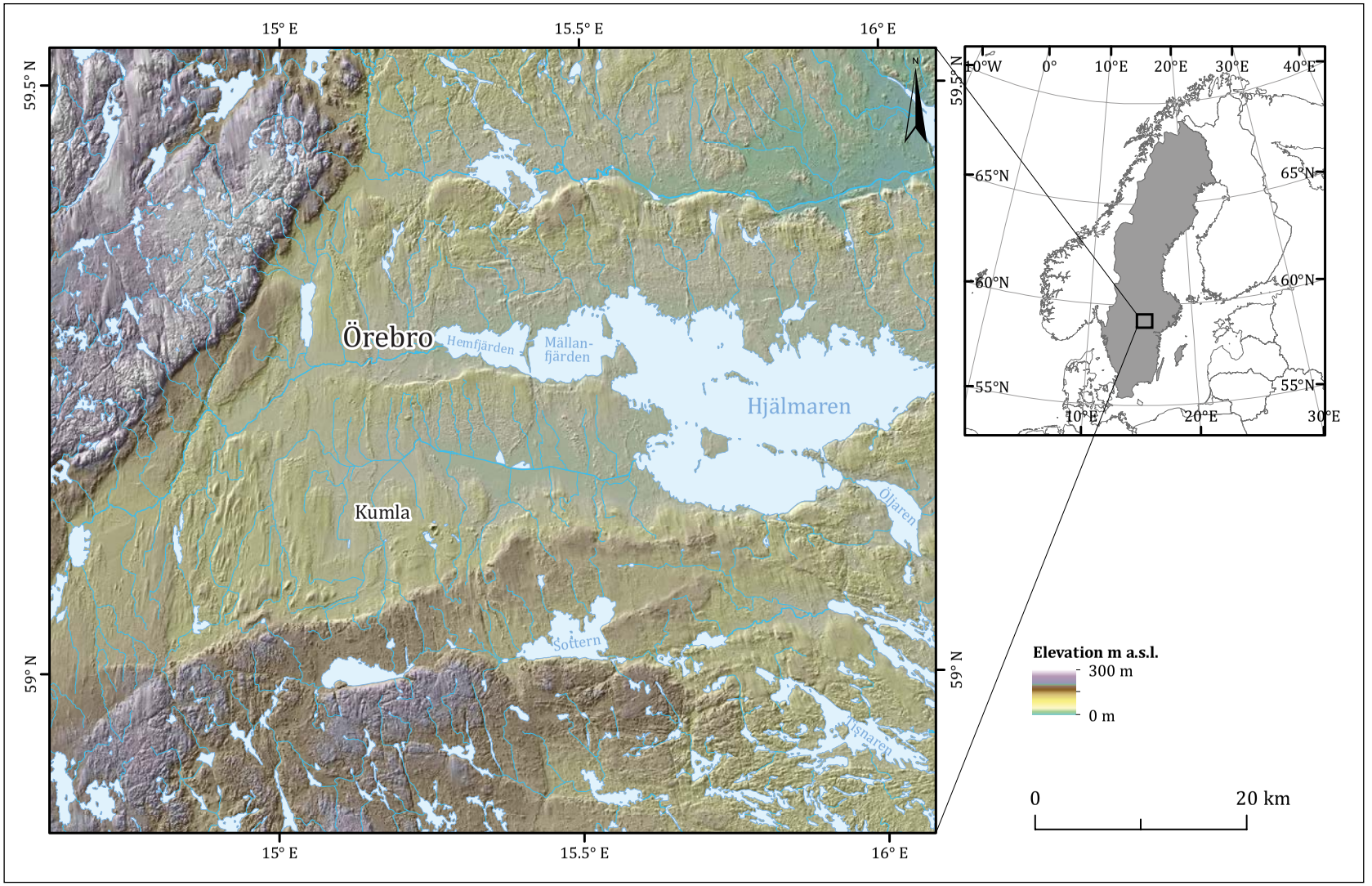

Figure 2-16. *DEM of the topography of the Närke district. The northward facing scarps and gently-inclined fault blocks are landforms exhumed from beneath Cambrian and Ordovician sedimentary cover. Erosion by the Fennoscandian ice sheet flowing to the south has modified the basement scarps and the block tops.*

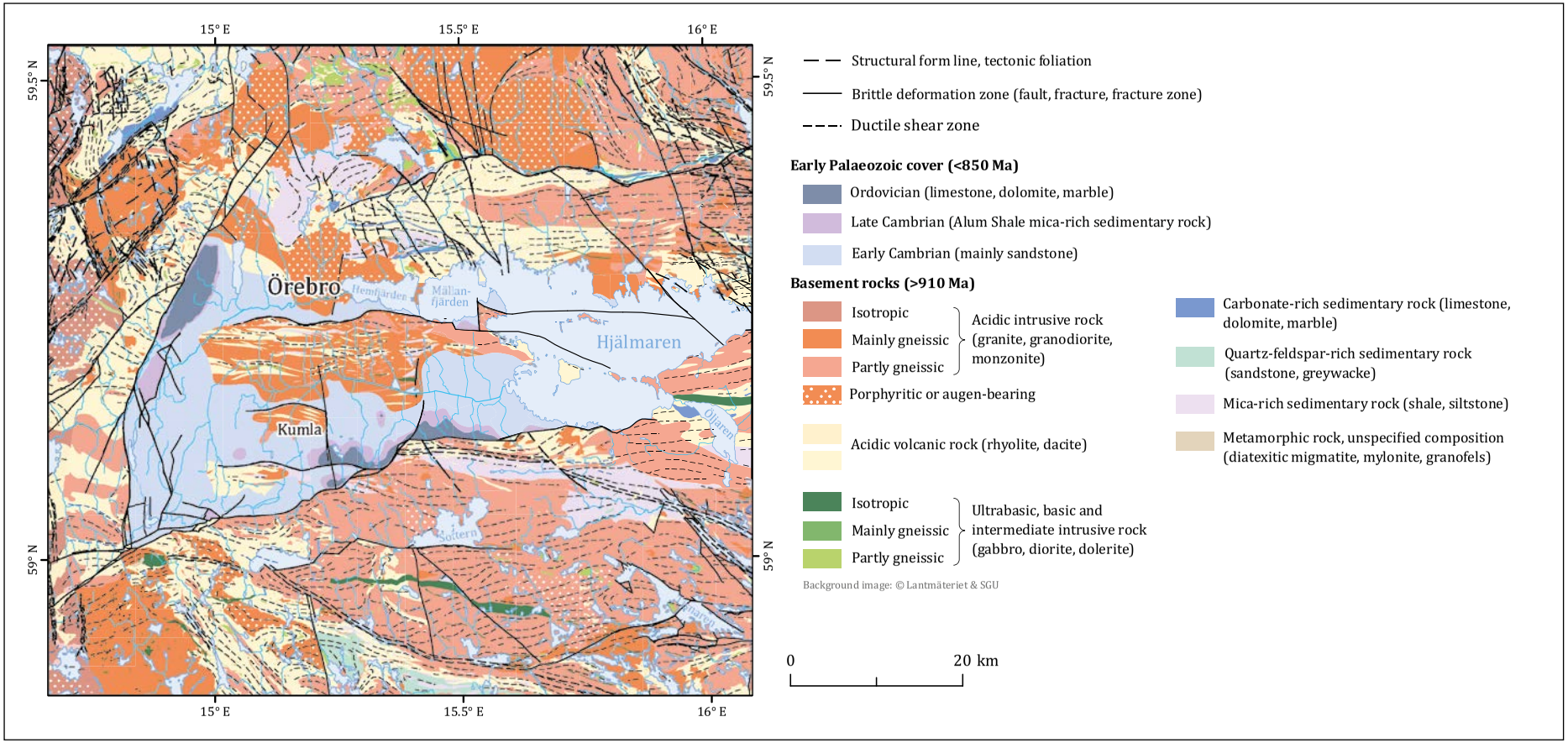

Figure 2-17. *Geology of the Närke district based on SGU data. The basement was planated in the late Neoproterozoic and buried during the Early Palaeozoic marine transgression. The planar unconformity and its cover were dislocated by minor faulting in the Palaeozoic but remained buried until the Pleistocene. Progressive glacial erosion has stripped away the sedimentary cover to partly reveal fault blocks on the dislocated surface of the sub-Cambrian unconformity.*

2.3.6 U2 in the Bothnian and Åland Seas

In the Bothnian Sea, Early Cambrian to Late Ordovician sediments lie within the older structure of the Mesoproterozoic intracratonic basin (Figure 2-6). Early Cambrian outliers and sandstone dykes are reported from Åland (Bergman 1982) and from parts of SW Finland (Kohonen and Rämö 2005). The sandstone dykes occur in vertical basement fractures and indicate former covers of Early Cambrian sands in these areas. Outliers of Early Ordovician limestone also occur near Forsmark, in the northern part of the Stockholm archipelago (Hagenfeldt 1995) and on Åland (Tynni 1982). At Lake Kultebo, on the Hälsingland coast 100 km NNW of Forsmark, Middle Ordovician limestone apparently rests directly on basement, overstepping faults on the W margin of Bothnian Sea (Löfgren and Laufeld 2007). Ordovician strata formed part of the target geology (Uutela 1990) in the Late Cretaceous Lappajärvi impact structure in W Finland (Kenny et al. 2019). The widely scattered Early Palaeozoic outliers indicate formerly continuous covers on basement surrounding the Bothnian basin (Paulamäki and Kuivamäki 2006). On the Swedish side of the Bothnian Sea, the sub-Cambrian unconformity dips gently E whereas on the Finnish side the dip is to the W (Figure 2-6), indicating minor post-Ordovician sag of the southern Bothnian basin.

Preserved remnants of the Early Cambrian marine sedimentary sequence vary in thickness from 20 to 30 m in the southern Bothnian Sea at Finngrundet and from 15–18 m at Närke (Nielsen and Schovsbo 2011). Quartz sandstones are dominant, with thin basal pebble conglomerates (Thorslund and Axberg 1979). Deposition took place in a storm dominated, shallow (less than 10 m deep) water environment (Artyushkov et al. 2000, Nielsen and Schovsbo 2011). In Gävle Bay (Thorslund and Axberg 1979), and in the Tvären (Lindström et al. 1994) and Söderfjärden (Lehtovaara 1982) impact structures, the horizontally-bedded Early Cambrian clays, with subordinate layers of sandstone, remain weakly consolidated to unconsolidated.

Coarse, arkosic beds intercalated in the clayey sediments comparatively high above the base of the sequence at Finngrundet probably indicate the persistence of small, exhumed sub-Jotnian basement hills in the vicinity (Figure 2-10).

In the Åland Sea, U2 is imaged in sonar surveys as an gently-inclined, even basement surface at ~90 m below sea level (Flodén 1977), and formed in Upper Jotnian to Vendian sedimentary rocks (Söderberg 1993). Sandstone dykes occur widely in basement fractures in the Stockholm archipelago, in the northern part of the Stockholm archipelago and towards Åland and SW Finland at distances of 40–160 km from the northern edge of the Cambrian in the Baltic Sea (Martinsson 1974).

The Lumparn impact on Åland probably dates from the Late Ediacaran (~580 Ma) (Abels et al. 1998) and so predates the sub-Cambrian unconformity (Tynni 1982). The impact structure is filled by poorly lithified Lower Cambrian siltstone and overlain by Lower and Middle Ordovician limestone (Tynni 1982). Sandstone dykes are commonly observed in vertical fractures in rapakivi granite at the present waterline in the Åland archipelago (Bergman 1982) (Figure 2-18). A few dykes contain Early Cambrian and Early Ordovician marine mollusca (Martinsson 1968), indicating proximity of the surfaces of Early Palaeozoic rock shorelines. Granite terrain on Åland mainland today rises to 90 m a.s.l. (Figure 2-18). This topography likely existed as a large hill or hills on U2. The Lumparn impact, however, generated large fault displacements (Abels et al. 1998) and, alternatively, the high ground may represent post-Ordovician reactivation of a horst in the rapakivi granite. Galena-bearing calcite veins found in vertical fractures cross-cut and so post-date the Early Cambrian to Early Ordovician sandstone dykes (Bergman and Lindberg 1979) and are markers for more widespread Permian hydrothermal activity (Alm et al. 2005).

2.3.7 U2 in Uppland

The sub-Cambrian unconformity in Uppland has been identified previously as a basement surface with less than 10–20 m of relief per km^2 that extends over an area of 10 000 km^2 along the edge of the Åland Sea from the edge of Gävle Bay towards Stockholm and Mälaren (Rudberg 1954) (Figure 2-13). The present basement surface is inclined at average gradients of ~0.1 % E of Uppsala (Figure 2-19) and towards the Bothnian Sea (Rudberg 1970). The terrain rises abruptly across faults W of Uppsala and Gävle to elevations that exceed 100 m a.s.l. (Figure 2-19). A set of W–E oriented topographic steps seen W of Stockholm indicate where the unconformity is dislocated by a series of W–E faults (Figure 2-13) (Lidmar-Bergström 1994).

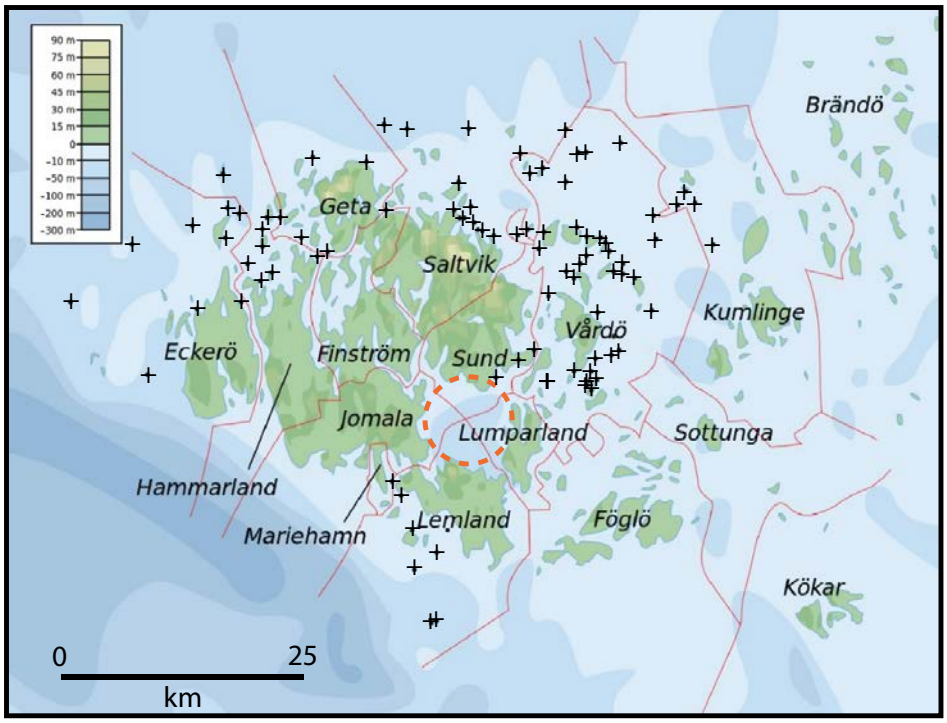

Figure 2-18. *Topography of Åland (Figure 2-6). Crosses represent sites where Early Cambrian and Early Ordovician sandstone dykes are recorded in vertical fractures in granite on shorelines and skerries (Bergman 1982). Red dashed line denotes the outline of the Late Ediacaran impact structure at Lumparn.*

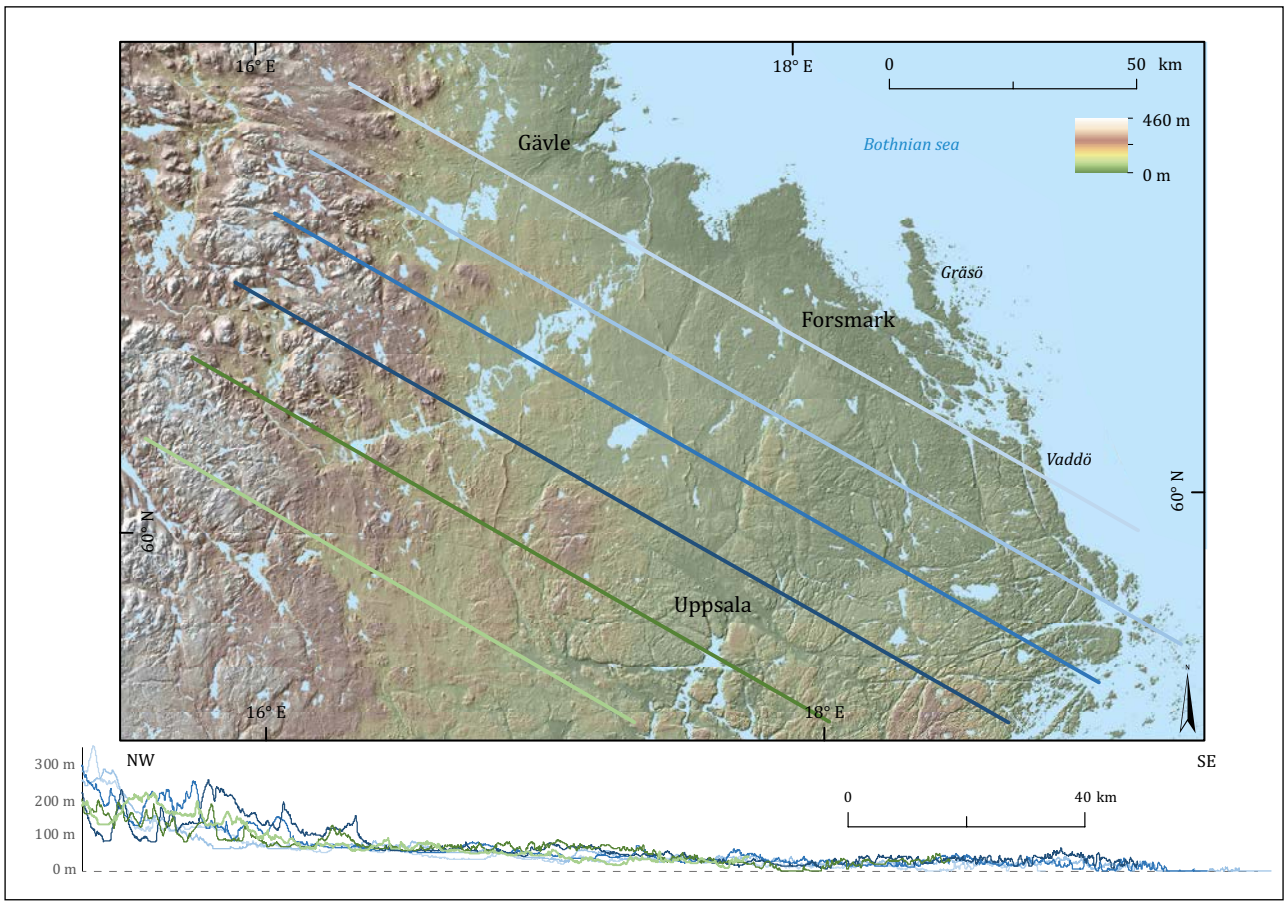

Figure 2-19. *Superimposed NW–SE topographic profiles across Uppland.*

Evidence of former Early Palaeozoic cover

In NE Uppland, the Singö and Forsmark deformation zones stand between the submerged Mesoproterozoic basin and the upstanding basement of Uppland (Figure 2-5). The boundary zone is itself broken into small fault blocks (Figure 2-6) (Beckholmen and Tirén 2010b). To the E and NE is an area, now largely submerged, that includes the Öregrundsgrepen and the Gräsö block and extends eastwards towards Åland and southwards towards Ålands hav (Beckholmen and Tirén 2010a). The eastern area is dominated by dislocated blocks of various dimensions, with small half grabens and basins holding outliers of Jotnian, Cambrian and Ordovician rocks (Söderberg and Hagenfeldt 1995). Early Ordovician limestones, more than 30 m thick in Singöfjärden, rest on Mesoproterozoic sandstone and basement (Söderberg and Hagenfeldt 1995) (Figure 2-8). Three small outliers, also more than 30 m thick, of horizontally-bedded Lower to Middle Ordovician limestone occur on the sea bed between Gräsö and Forsmark (Persson 1985, Söderberg and Hagenfeldt 1995). It is not known if the limestone here is underlain by Alum Shale. The outliers are taken from regional outline maps (Söderberg and Hagenfeldt 1995) and so may not be located exactly on Figure 2-11 but each rests on the lower part of an inclined basement surface that rises at a gradient of 0.2 % towards Forsmark. The inclined surface is interpreted as the sub-Cambrian unconformity, with minor modification by Pleistocene glacial erosion.

To the W and SW of the boundary zone is an area, largely above sea level, that extends towards Uppsala where U2 is dislocated into fault blocks of different sizes (Beckholmen and Tirén 2010b, Grigull et al. 2019). Outliers of Early Cambrian sedimentary rocks are restricted to one locality near Vattholma where a more than 3 m wide mass of brecciated and bituminous fine-grained, grey sandstone was found in a down-faulted position during quarrying (Wiman 1918). In addition, a possible outlier of Early Ordovician limestone is indicated by a dense concentration of glacial erratics at Lake Erken (Asklund 1930) (Figure 2-9). Dolomitic limestone erratics also occur frequently along the Uppland coast and may derive from sources that are more proximal that the southern Bothnian Sea (Hagenfeldt 1995). Asphaltite, derived from a former cover of Alum Shale (Late Cambrian to Early Ordovician in age) is recorded over a depth of 148 m in the Singö fault zone (Erlström 1987, Sandström et al. 2006b) and at shallower depths at numerous other locations in Uppland (Wiman 1918, Welin 1966, Ahlbom et al. 1986) (Figure 2-20). Limestone outliers and the asphaltite fracture coatings in fractures demonstrate that the basement in Uppland has been exhumed from beneath a former cover of early Middle Cambrian to Early Ordovician sedimentary rocks.

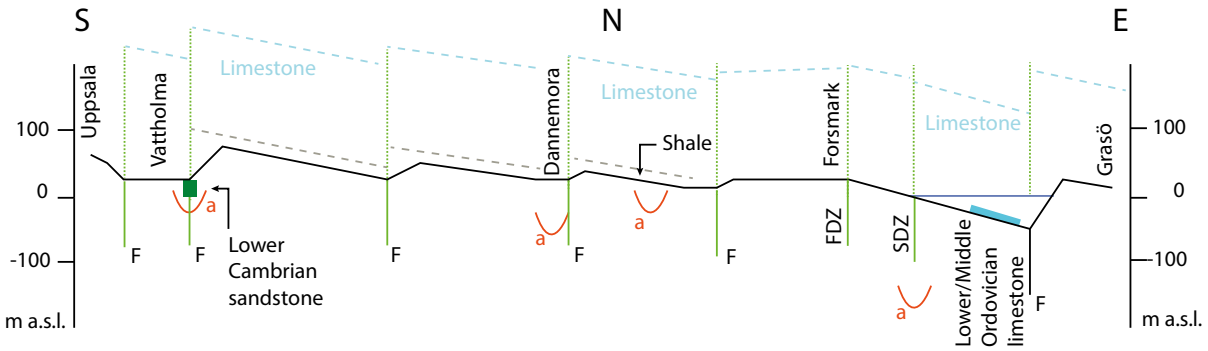

Figure 2-20. *Schematic section between Uppsala and Gräsö (Figure 1-1) showing tilted rock blocks, deformation zones and major faults, the schematic position of the former Late Cambrian Alum Shale and the Ordovician limestone cover prior to Pleistocene glaciation, and present day outliers and the maximum depths of asphaltite (a) fracture coatings. FDZ Forsmark Deformation Zone, SDZ Singö Deformation Zone, F fault.*

A formerly continuous Early Cambrian sandstone cover is indicated by the presence around the periphery of Uppland of outliers (Hagenfeldt and Söderberg 1994) and sandstone dykes (Martinsson 1974) in the northern part of the Stockholm archipelago, on Åland (Bergman 1982) and in Gävle Bay (Thorslund and Axberg 1979). The former continuity of the Alum Shale from Forsmark towards Uppsala is also demonstrated by asphaltite fills found in basement fractures (Figure 2-20) (Sandström et al. 2006b). The numerous outliers of Early Ordovician limestone must also have been part of a formerly continuous cover in eastern Uppland. South of Stockholm, the small (2 km diameter) Tvären Bay impact structure dates from 457 Ma (Grahn et al. 1996). The impacted sedimentary sequence at Tvären consisted of Middle Ordovician carbonates resting on non-lithified sands of Early to earliest Middle Cambrian age (Lindström et al. 1994). The Early Palaeozoic outliers indicate formerly continuous covers of these rocks in Uppland, with little post-Ordovician erosion of surrounding basement.

A widespread hiatus, the Hawke Bay regression, is recorded in Cambrian sequences late in the Early Cambrian (Nielsen and Schovsbo 2015) (Figure 2-14), with non-deposition and erosion across large areas of southern Sweden, Estonia and the St Petersburg region (Artyushkov et al. 2000), a result of combined epeirogenic uplift and sea level fall (Artyushkov et al. 2000, Nielsen and Schovsbo 2015). The absence of Early Cambrian sandstone in Uppland and below Ordovician limestone in offshore outliers is consistent with the removal of unconsolidated Early Cambrian clays and sands in this Hawkes Bay event (Söderberg and Hagenfeldt 1995). It is unlikely that the Early Cambrian basement unconformity was significantly lowered during emergence as erosion of weakly consolidated sedimentary rocks amounted to less than 5–10 m in depth (Nielsen and Schovsbo 2015). Subsequent deposition in Uppland of the organic-rich Alum Shale took place under anoxic conditions at or below storm-wave base (Nielsen and Schovsbo 2015). Deposition of Alum Shale directly onto basement implies conditions with very low wave energy and limited clastic sediment supply. Extensive deposition of shallow water limestones indicates complete burial of basement during the Ordovician and a lack of basement hills to supply clastic sediment.

Faulting of the sub-Cambrian unconformity

The basement terrain across Uppland and offshore has been broken by Phanerozoic faulting into a mosaic of rock blocks of different sizes (25–70 km^2) (Figures 2-21 and 2-22). In northern Uppland, fault blocks are bounded by pronounced and slightly curved N–S trending edges, with a higher ground surface on their W side than the block to the E (Ahlbom and Tirén 1991). Block edges follow topographic lineaments that locally coincide with faults (Figure 2-5) (Grigull et al. 2019). Many blocks have tilted surfaces visible in DEMs in 10 km^2 windows (Figure 2-22). Strong support for the interpretation of rock blocks as fault blocks is provided by the different elevations and inclinations of the fault block tops (Figure 2-21) (Beckholmen and Tirén 2010b) and by the apparent lack of lithological and structural control over the position and form of hill masses that is typical for hills otherwise produced by differential weathering and erosion (Twidale 1982). The displacement and rotation of the ground surface indicate that the WNW trending structures and the curved N–S structures are listric faults (Beckholmen and Tirén 2010b). The shallow depths and limited thicknesses of Ordovician outliers in Gävle Bay and the Singö area indicate that block movements were post-Ordovician. Cumulative relative displacements were of the order of no more than a few tens of metres (Beckholmen and Tirén 2010b).

Reactivation of faults by late- and post-glacial neotectonics in response to isostatic rebound has been proposed during several major palaeo-seismic events in eastern Sweden (Mörner 2004, 2011). The main evidence presented for these events comes from fault scarps, disrupted roches moutonnées, angular boulder spreads and sediment deformation and liquefaction (Mörner et al. 2000). Straight-edged scarps of likely neotectonic origin have not been identified in Uppland (Lagerbäck et al. 2005, Mikko et al. 2015, Öhrling et al. 2018). Moreover, the morphological features and distribution of disrupted roches moutonnées and boulder spreads indicate formation during a late phase of glacial erosion and transport beneath the last Fennoscandian Ice Sheet (Lagerbäck et al. 2005), rather than in earthquakes. Supporting evidence is presented below (Section 4.4.3) for a glacial origin for these features as part of the newly recognised glacial ripping process set. No deformations related to seismically induced liquefaction of sand and silt beds have been observed in trenches excavated in the Forsmark area (Lagerbäck et al. 2005). Firm evidence is lacking in Uppland for late- and post-glacial neotectonic disturbance in this part of Uppland.

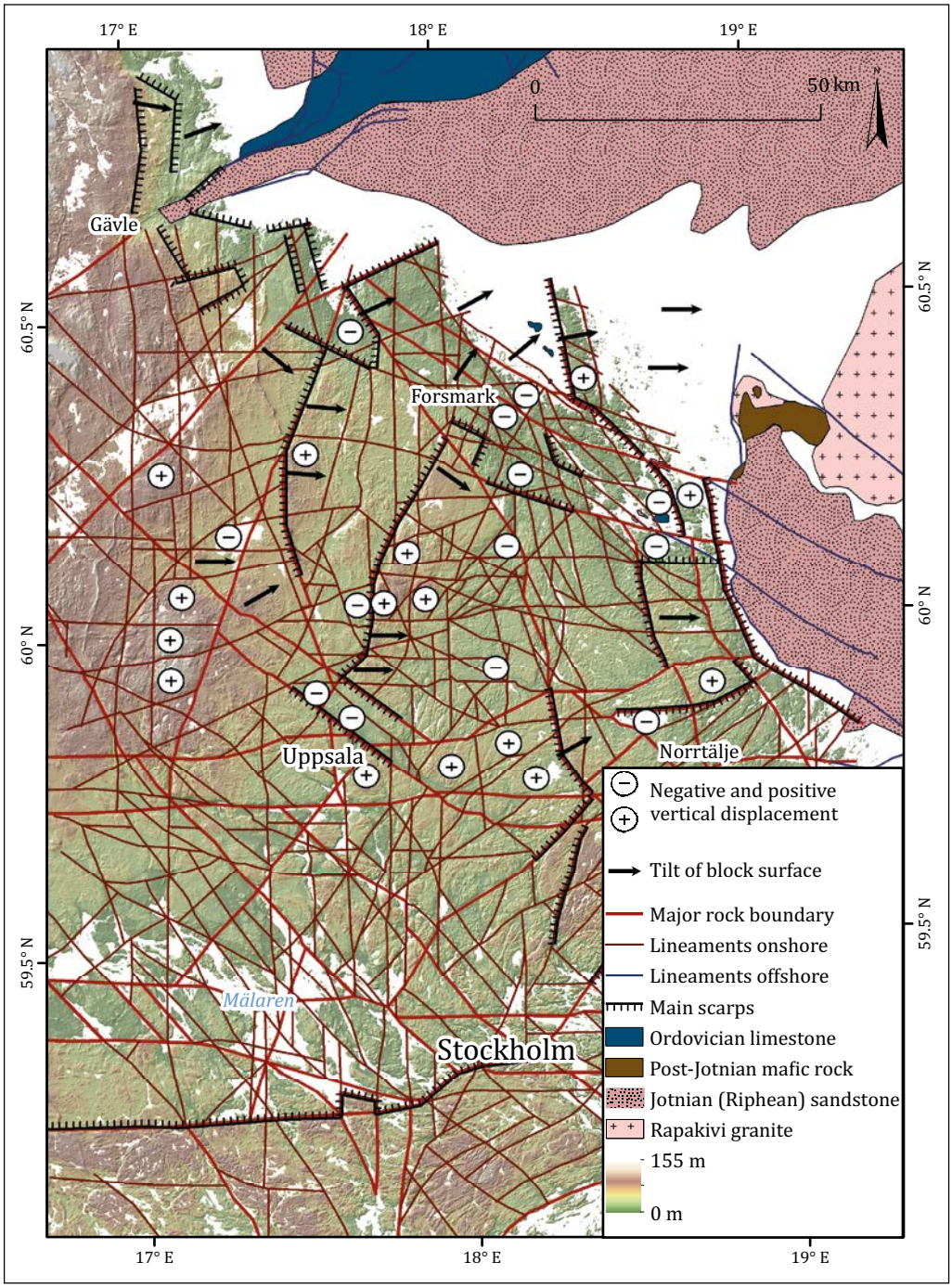

Figure 2-21. *Rock block map of Uppland and surrounding areas (Beckholmen and Tirén 2010b), with main fault scarps and positive and negative movements added on the basis of relative topographic position. Elevations in meters above sea level.*

Differences exist between the relative displacement of faults and in the elevation of basement floors of depressions across the boundary zone between the Forsmark and Singö deformation zones. Within the boundary zone in the Forsmark candidate area, the relative displacement of the ground surface is ~10 m between rock blocks (Beckholmen and Tirén 2010b). Across Uppland, apparent displacement rarely exceeds 20 m (Beckholmen and Tirén 2010a, b, Grigull et al. 2019). Moreover, low rock blocks have basement floors with elevations of high points that mainly remain within 10 to 20 m of equivalent summits on adjacent high rock blocks (Grigull et al. 2019). The magnitude of relative displacements is larger NE of the boundary zone. The Öregrund–Singö fault shows displacements of 40–70 m E of Singö. The Forsmark–Granfjärden fault zone, located less than 10 km S (Figure 2-5), has 20 m of post-Ordovician displacement across its trace. The Hargshamn–Herräng–Grisslehamn

fault zone displaces Ordovician outliers in Galtfjärden by ~20 m (Figure 2-8). The island of Gräsö rises to 27 m a.s.l, ~50 m above the Ordovician outliers that rest SW of the West Gräsö Fault (Figure 2-5). The island in its broad form is a tilted basement block (Söderberg and Hagenfeldt 1995), with ~50 m of post-Ordovician displacement across the fault along its SW edge. Similar displacements are found along faults with similar orientations in Palaeozoic rocks in the Bothnian Sea (Axberg 1980). The depth to basement on the floors of low rock blocks in the archipelago is up to 50–60 m below summits on adjacent high rock blocks. The different displacements across the boundary zone indicate that differential movements occurred across the Forsmark and Singö deformation zones in the Phanerozoic.

Small outliers of horizontally-bedded Ordovician limestone rest locally on this surface off Gräsö and Singö (Söderberg and Hagenfeldt 1995) (Figure 2-8). U2 is broken by post-Ordovician block faulting in the Åland Sea and similarly dislocated by NW–SE faults in the hinge zone at the Uppland coast (Beckholmen and Tirén 2010a) (Figure 2-5). Displacements are low E of Forsmark with relative offsets in the order of some tens of metres and rotation of fault blocks by up to a few degrees (Beckholmen and Tirén 2010a). Previous interpretations are supported that the basement relief of Uppland represents minor post-Ordovician dislocation of U2 (Persson and Sjöström 2003, Beckholmen and Tirén 2010a). The buried sub-Cambrian unconformity in the Bothnian Sea also has been dislocated by post-Ordovician faulting into flat-topped, gently-tilted blocks (Winterhalter et al. 1981). Similar post-Early Palaeozoic jostling of basement fault blocks that represents the dislocation of U2 is recorded around Äspö, Oskarshamn, SE Sweden (Munier and Talbot 1993) and around Trollhättan, SW Sweden (Ahlin 1987). Small (10–15 m) offsets across post-Ordovician faults are reported from the Baltic Sea and at Oskarshamn (Tirén et al. 2001).

The fault blocks show internal relief of less than 20 m but many block tops retain accordant hill summit elevations within very low (less than 5 m) height ranges (Figure 2-22). On the Ironworks block, the upper surface stands at up to 45–55 m a.s.l. to the E of a 15 m high fault scarp (Figure 2-23).

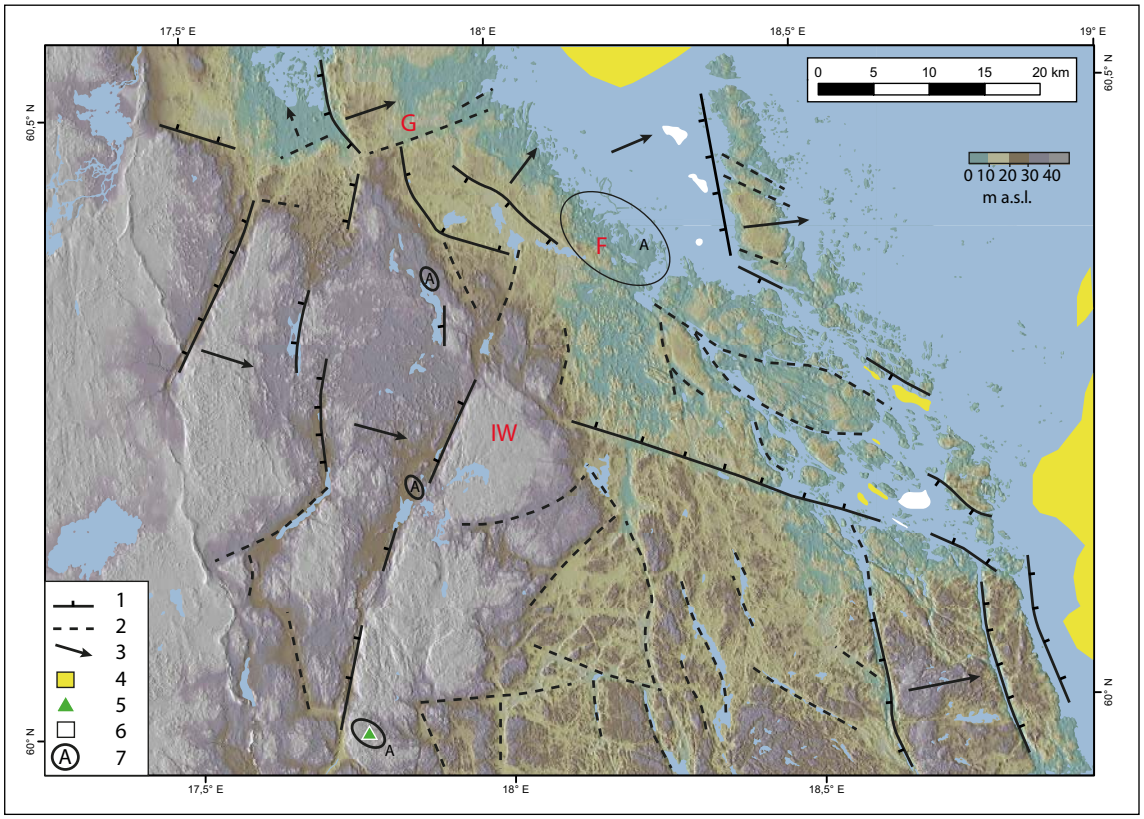

Figure 2-22. *The dislocated surface of the sub-Cambrian unconformity in NE Uppland. 1. Exhumed fault scarp along edge of rock block. 2. Fracture without clear dislocation of opposing blocks. 3. Direction of tilt of rock block. 4. Jotnian sandstone. 5. Early Cambrian sandstone. 6. Early Ordovician limestone. 7. Asphaltite fracture coatings derived from a former cover of Late Cambrian to Early Ordovician Alum Shale. F Forsmark. G Griggebo. IW Ironworks.*

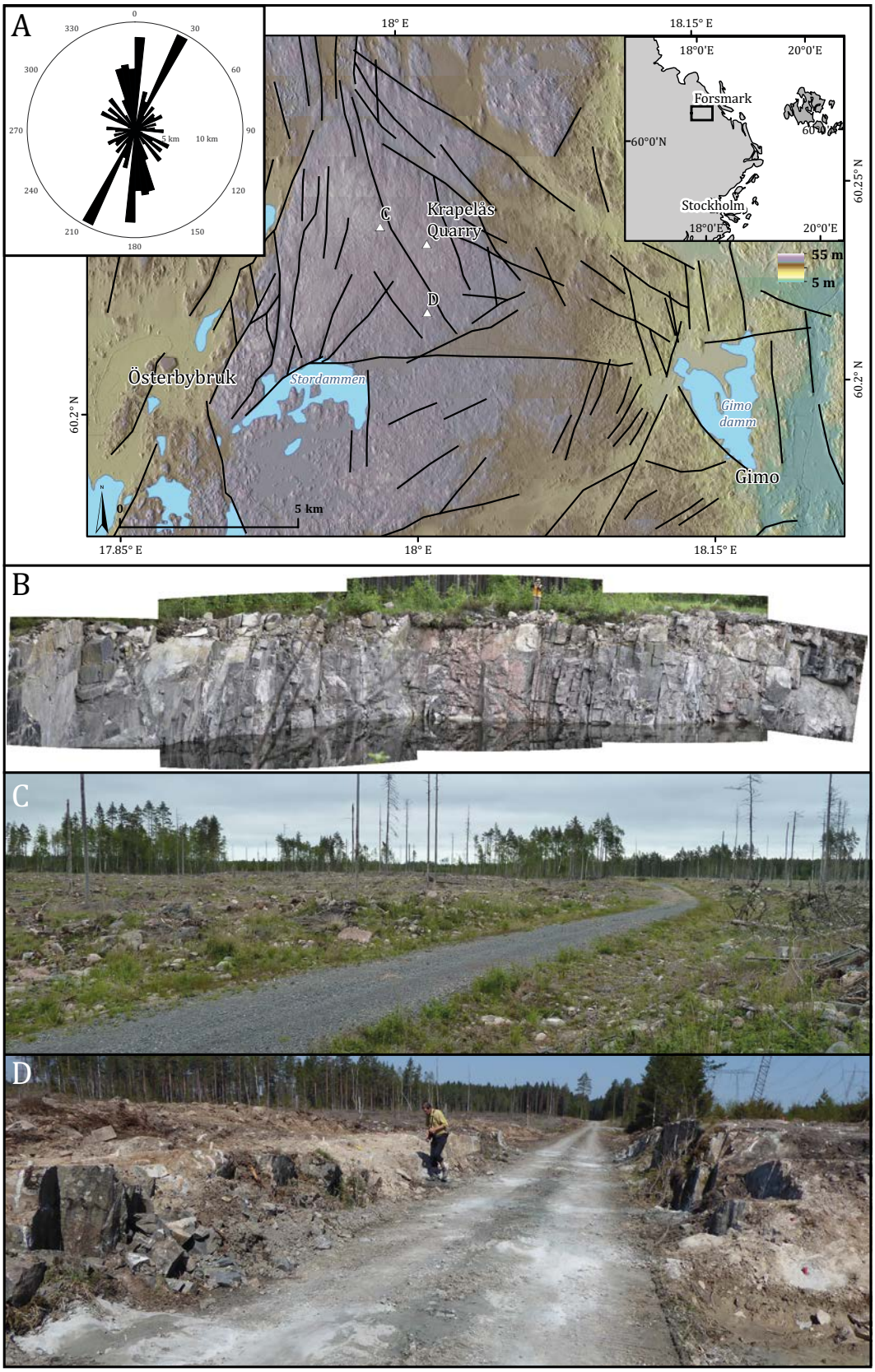

Figure 2-23. *Little-modified surface of U2 on the elevated Ironworks fault block (Figure 2–22), with only minor glacial modification. A. DEM (in m a.s.l.) showing the low relief of the block surface that extends over an area of ~30 km^2. B. Granite gneiss in Krapelås Quarry, with closely spaced vertical and inclined fractures. Photo montage by Stephen Martel. C. Topography W of Krapelås Quarry, with 1–2 m of till and very low relief rock surfaces developed in intermediate to acid gneisses. D. Topography S of Krapelås Quarry, with low roches moutonnées and thin till cover on an extensive low relief surface.*

The terrain shows low (less than 2 m high), small roches moutonnées with only thin till cover. At Krapelås Quarry and in its wider surroundings, the exposed granite gneiss has fracture spacings of mainly less than 2 m and lacks prominent sub-horizontal fractures (Figure 2-23B). The upstanding position of the Ironworks Block is clearly not a result of rock resistance or structural control. At Griggebo, similar low relief topography is seen to be associated with closely fractured gneiss but here the rock block is in a down-faulted position (Figure 2-24). At Griggebo also, low relief is not controlled by sub-horizontal fractures (Figure 2-24). Along the E coast of Väddö, the basement surface rises abruptly from below sea level to 30–35 m a.s.l. and maintains this general elevation inland (Figure 2-9), with only minor offset across a number of tilted rock blocks. Further examples of flat-topped fault blocks in Uppland are described in Section 3.3.1. Isolated hills that rise more than 20 m high above surrounding summits are absent from NE and E Uppland (Figure 2-22). Perhaps the most prominent hill is on Väddö, where Kasberget has a summit at 50 m a.s.l. and stands ~20 m above surrounding summits (Figure 4-43). The Cambrian basement surface that rises at a gradient of 0.2 % towards Forsmark has a relative relief of ~10 m (Figure 2-11). Near-planar basement surfaces are apparent in seismic images below Ordovician strata in the Bothnian Sea (Winterhalter et al. 1981). The morphology of the exposed basement surfaces on the fault blocks is similar to that on the edge of and below the Cambrian basement surfaces.

The occurrence of low relief surfaces developed across gneisses with closely spaced vertical and inclined fractures is typical of exhumed facets of U2 in southern Sweden. Close analogues to Ironworks and Griggebo are found on U2 near Trollhättan and Kalmar at sites in closely-fractured gneisses that stand 50 m to 10 km distant from the edge of the buried sub-Cambrian unconformity (Figure 2-25). The basement topography of NE Uppland shows many similarities with other basement terrain around the edges of Cambrian outliers in Västergötland, Kalmar and Närke in terms of a near absence of large hills, extensive near-planar surfaces and post-Cambrian dislocation evident from tilted, flat-topped fault blocks. Available evidence from Uppland is largely consistent with long established interpretations of the basement terrain as inherited from the sub-Cambrian unconformity (Rudberg 1988, Lidmar-Bergström 1994, Olvmo 2010).

2.3.8 Unconformities and fractures at Forsmark

The present basement surface elevation on the sea bed within 10 km of Forsmark is coincident with the sub-Jotnian (U1) and Cambrian (U2) unconformities on the lower part of a basement ramp that rises towards Forsmark (Figure 2-11). The planned repository site at Forsmark is bounded by major deformation zones that form the hinge zone between the basement of Uppland and the Mesoproterozoic basin that lies to the NE. The U1 unconformity likely stood within tens of metres of the present basement surface around Forsmark (Figure 2-8). U2 also stood close to the highest present-day summits of dislocated fault blocks, as slightly upstanding, flat-topped blocks have experienced only minor erosion since exhumation. The former basement surfaces of U1 and U2 likely developed over conditions of erosion operating over tens of millions of years on an existing structural fabric, including gneissic foliation and layering and Proterozoic fractures.

Like on the present UQ basement surface (Chapter 3), existing and new fractures opened and formed in the near surface beneath U1 and U2. Despite the proximities of U1 and U2 to the present basement surface around the flanks of the Mesoproterozoic basin in the southern Bothnian Sea (Figure 2-6), little consideration has been given previously to the legacy of fracture sets and mineral coatings inherited from the Jotnian and Cambrian unconformities at Forsmark. It is noteworthy that new Ca-U(VI)-ages identify a ~1.25 Ga U(IV) to U(VI) oxidation event at Forsmark (Krall et al. 2018). Oxidation may have involved oxygenated groundwater circulating beneath U1.

Much attention has been directed to the origins of the spectacular sub-horizontal fracture sets (Figure 2-26) exposed during the excavation for the cooling water intake canal at Forsmark in the 1970s (Carlsson 1979, Pusch et al. 1990, Juhlin and Stephens 2006). This specific case is unusual in Uppland, where extensive sub-horizontal fracture sets are not widely exposed in the near surface.

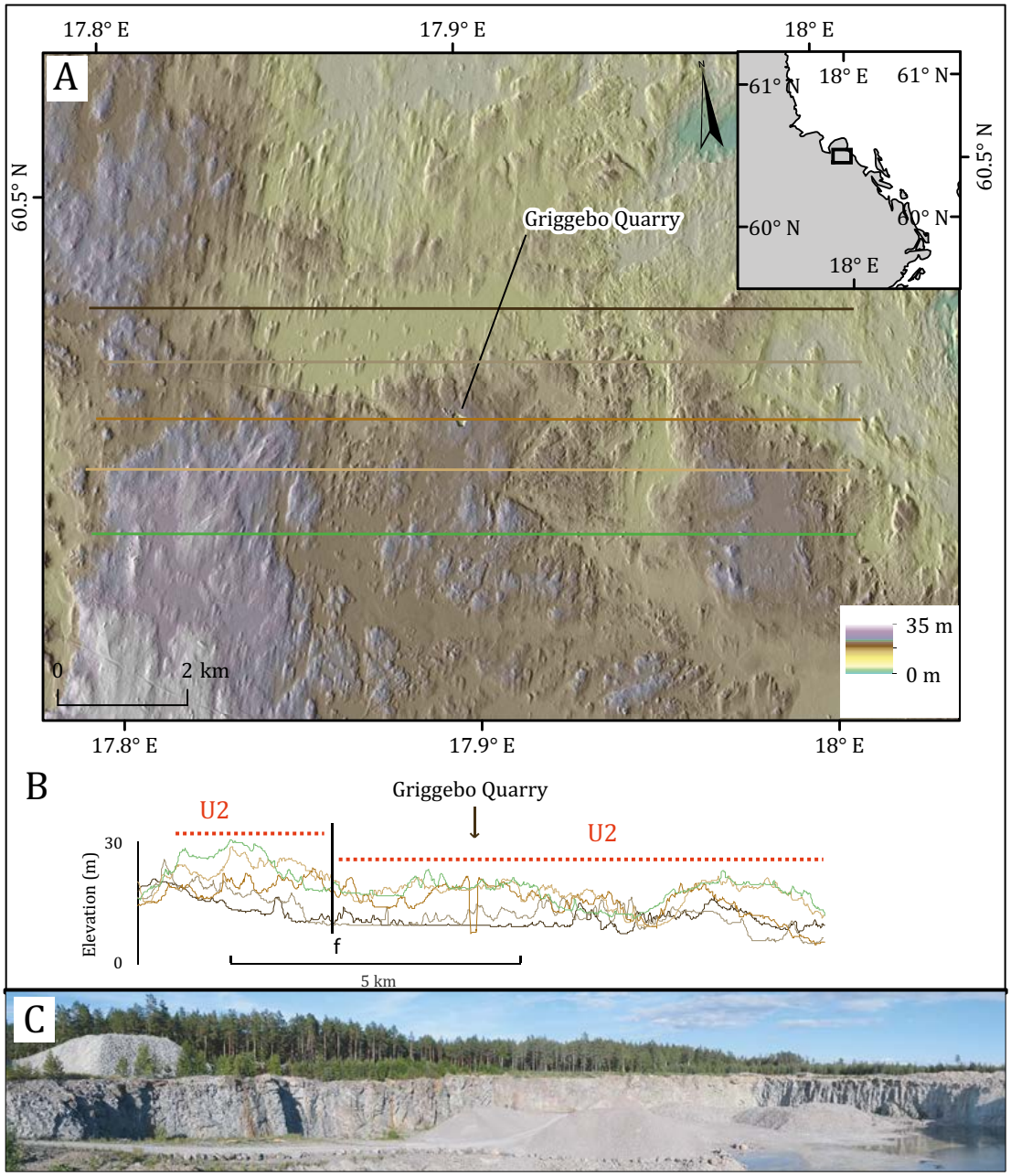

Figure 2-24. *Little-modified fragment of U2 on a down-faulted block at Griggebo, Vavd (60.466361°N, 17.8952970°E, 20 m a.s.l.). A. DEM (in m a.s.l.) of low relief basement terrain with thin till cover at Griggebo. Roches moutonnées less than 4 m high in the vicinity of the quarry are aligned N–S with a fracture set and former ice flow. B. W–E profiles at Griggebo, showing the likely former position of U2 and minor (~5 m) displacement by faulting. C. North face of Griggebo Quarry. Granite gneisses with vertical and inclined fractures spaced 1–4 m apart. For detail of the quarry face see Figure 2-12.*

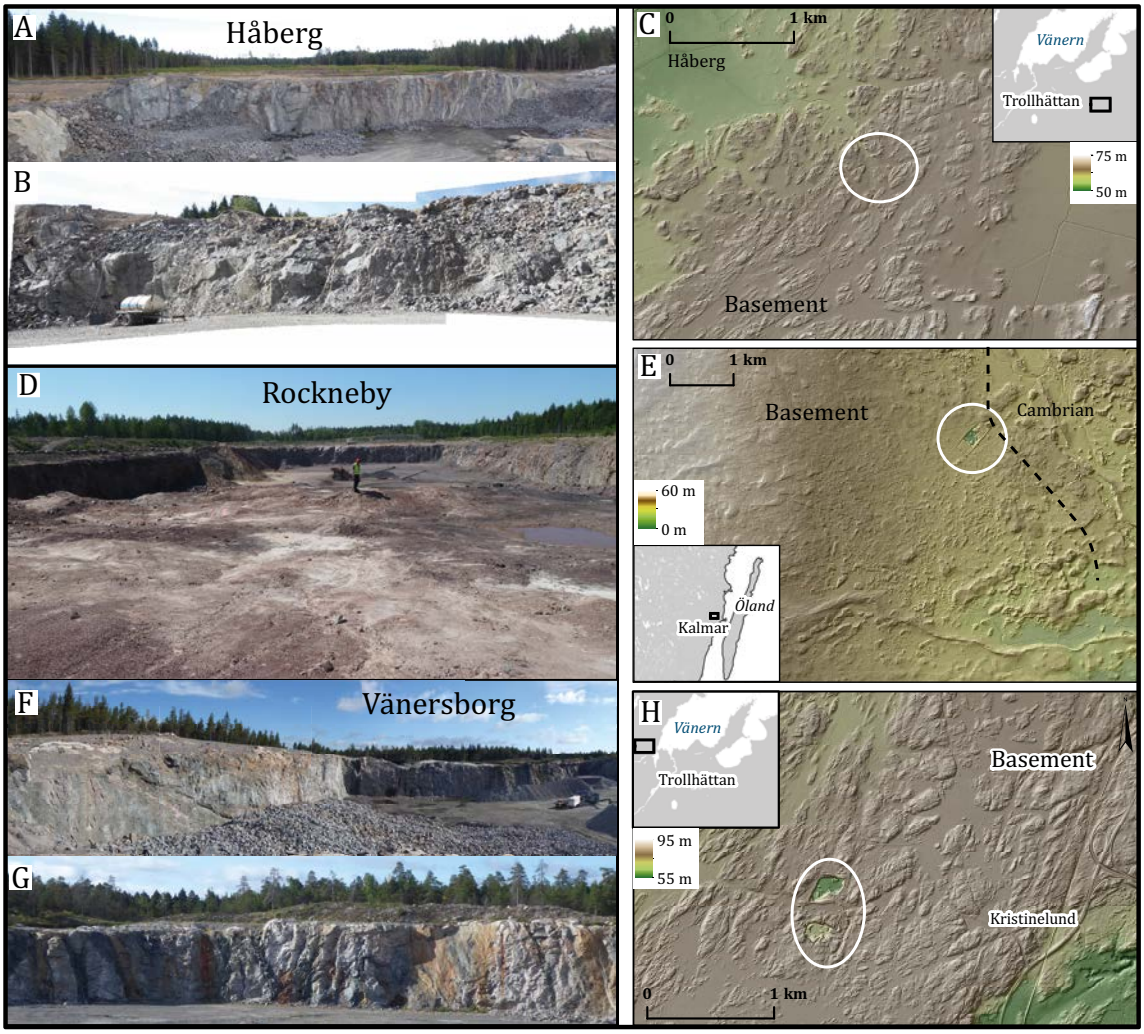

Figure 2-25. *Analogue sites on the sub-Cambrian unconformity in southern Sweden. A–C. Håberg Quarry, 5 km E of the buried sub-Cambrian unconformity at Hunneberg, Trollhättan (Lat. 58.313675° N Long. 12.613221° E). A. East face. Ice flow towards camera. B. West face, with closely spaced vertical and inclined fractures. C. DEM of the area surrounding Håberg. Bedrock summit elevations fall gently northward at a gradient of ~0.3 %. D. Rockneby Quarry, near Kalmar (see also Goodfellow et al. 2019) (Lat. 56.830397° N Long. 16.294236° E). Photo looking SW from ~50 m W of the edge of the buried sub-Cambrian unconformity. The bedrock surface shows ~2 m of relief. A layer of till and loose rock, 1–3 m thick, has been stripped to make the rock surface ready for quarrying. E. DEM of the Rockneby area. Bedrock summit elevations rise gently westward at a gradient of ~0.6 %. F. Vänersborg Cross Quarry, 10 km W of the buried sub-Cambrian unconformity at Halleberg, Trollhättan (Lat. 58.386241° N Long. 58.386241° E). F. North quarry, W and N faces. Low domes with up to 10 m relief in granite gneiss developed across inclined fractures. G. South quarry, SE face. Low relief surface developed across steeply inclined fractures. H. DEM of the area surrounding Vänersborg Cross Quarry. Bedrock summit elevations fall gently northward at a gradient of ~0.4 % Elevations in panels E and H are in m a.s.l.*

Figure 2-26. *Horizontal fractures along the excavation made during the construction of the ca. 8 m deep and more than 1 km long canal at present sea level between the nuclear power plant at Forsmark and the Öregrundsgrepen. The section is located in the north-western part of the Forsmark tectonic lens (Figure 3-3); outcrops 0.2–0.5 km to the SE lack extensive sheeting. Photo: A. Carlsson.*

The gently dipping fracture zones with ENE and NE strike in the Forsmark area are 1.2–4 km in length and occur in 6–185 m thick zones at up to 950 m in depth (Carlsten et al. 2004) (Figure 2-26). Similar fracture systems occur at Finnsjön (Tirén 1991). The deep low angle fractures are considered by Juhlin and Stephens (2006) to represent minor thrust faults developed during the latest stages of the Svecokarelian orogeny, produced once cooling had progressed sufficiently for this part of the crust to respond in a brittle manner to the regional stress field. The presence of epidote (G1) as a mineral filling along fractures in the gently dipping zones confirms that at least some of these fractures are deep-seated geological structures of Palaeoproterozoic age (Sandström et al. 2009) and part of the structural fabric of the basement. Sub-horizontal fractures found at shallow depth below the current landsurface include more closely spaced, open fracture sets, with corrensite coatings on some shallow fractures (Carlsson 1979) which indicate a later (G2 to G3) formation or opening in the Sveconorwegian orogeny and in the Palaeozoic (Sandström et al. 2009). The proximity of U1 and U2 to the present erosion level at Forsmark allows the possibility that these shallow fracture sets may have opened as sub-horizontal fractures beneath low relief unconformities in the Mesoproterozoic and the latest Neoproterozoic (Figure 2-3). The presence of G3 minerals (asphaltite and goethite) as coatings along vertical fractures in the uppermost part of the bedrock (Stephens et al. 2015) provides some support for contemporaneous, open and crossing sub-horizontal fractures. In this context, it is noteworthy that horizontal to sub-horizontal fractures are prominent in granites below the buried planar unconformity of the sub-Cambrian unconformity on Hardangervidda (Øvretveit 2016) and on the exposed unconformity in E Sweden (Kresten and Chyssler 1976, Wahlgren 2010) and in SW and SE Finland (Selonen et al. 2011, 2014). The very long time intervals since fractures first opened is indicated by evidence of episodic microbial processes deep in the fracture system. Rb–Sr dates of 396 ± 7 Ma for secondary adularia–calcite coated fractures in borehole sample KFM24:399 indicate that fractures at a present depth of 0.4 km were open in the Palaeozoic (Drake et al. 2018). The sub-horizontal fractures at Forsmark may have been reactivated or formed as joints within an existing structural fabric in the current stress regime (Claesson Liljedahl et al. 2011) in response to high rock stresses (Follin et al. 2014), deep burial (Stephens et al. 2015), Pleistocene ice sheet unloading (Stephens et al. 2015), high subglacial groundwater pressures and hydraulic jacking (Juhlin and

Stephens 2006, Hökmark et al. 2010) and/or changing topography in response to glacial erosion (Section 3). In summary, the sub-horizontal fracture sets at Forsmark have a highly complex history of formation, opening and mineralisation that spans the last 1.9 Ga as a consequence of very limited denudation of the basement and its prolonged and deep burial by sedimentary cover rocks.

Fracture coatings may provide key evidence for the timing of re-exposure of the U2 surface. A former thin cover of Alum Shale is the likely source of asphaltite found at shallow depth in Uppland (Erlström 1987, Sandström et al. 2006b) (Figure 2-22). The much thicker former cover of Ordovician limestone (Figure 2-20) likely provided the main source of Ca for thick G3 and G4 calcite coatings. In SE Sweden, the isotopic characteristics of calcite coatings down to 100 m depth are consistent with deposition from circulating Ca-enriched groundwater below a thinning limestone cover during the Pleistocene (Drake et al. 2009a). Leaching above the redox front of calcite and mobilisation of U after re-exposure of the basement has been largely confined to depths of 30 m. U oxidation has occurred within the last 300 ka in the upper 20 m of the boreholes and locally down to 55 m along fractures with high transmissivity (Drake et al. 2009a). At Forsmark, U minerals were mobilised and redeposited during the past 1 Ma (Smellie et al. 2008, Tullborg et al. 2017). Low Pb-contents in Ca-U(VI)-silicate minerals indicate recent or on-going interaction between these minerals and carbonate-rich fluids (Krall et al. 2018). In these mainly acid basement rocks, an eroding Ordovician limestone cover is potentially the main source for Ca-rich groundwater. Along the Uppland coast, carbonates have been thoroughly leached from the upper 3–6 m of tills in the post-glacial period (Ingmar and Moreborg 1976). The onset of calcite leaching from near-surface vertical fractures around Forsmark likely postdates final removal of Ordovician cover and the timing of U oxidation in SE Sweden suggests that this removal dates from the Middle Pleistocene. Late re-exposure of basement is consistent with the apparent absence of saprolite from fracture zones in the basement of NE Uppland.

2.3.9 Reconstructing U2 based on the current basement topography

The form of the sub-Cambrian unconformity across Scandinavia, including its dislocation across fault blocks, has been modelled previously in topographic profiles, trend surfaces, digital elevation models (DEMs) and maps using the present elevations of bedrock summits (Elvhage and Lidmar-Bergström 1987, Lidmar-Bergström 1994, Johansson et al. 2001b). The use of summit elevations as pinning points relies on three basic assumptions that:

1. The buried Early Cambrian to Ordovician basement unconformity is one of very low relief.
2. The wider exposed basement was originally of similar relief to that below the buried unconformity.
3. Erosion of basement summits subsequent to re-exposure has been minor.

Assumption 1 is supported by the low relief of the buried unconformity across fault blocks in the Bothnian Sea and observed below and around the edges of Early Palaeozoic outliers across Fennoscandia (Section 2.3.1). Assumption 2 is consistent with the continuity of low relief at the regional scale away from the edge of the buried U2 unconformity off Forsmark and from Early Palaeozoic outliers elsewhere in Sweden, also described above. Assumption 3 can be tested for scenarios of 1, 10 and 50 m of erosion under three circumstances: (i) where the U2 basement surface emerges from below Early Palaeozoic covers in close proximity to outliers,(ii) at increasing distances from outliers where planar form and inclination of the unconformity remains well defined by summit accordance and (iii) where exhumed fault block topography is observed on the present basement surface. A 1-metre erosion depth requires complete preservation of the detailed form of U2. Key evidence for such preservation includes remnant patches of cover rocks, such as the Early Cambrian pebble conglomerates and sandstones found on the lake shoreline within 200 m of the buried U2 surface at Kinnekulle (Högbom and Ahlström 1924). Cambrian sandstone dykes occur widely in basement fractures but because dykes can occur not only immediately below the buried unconformity surface but also to depths of several tens of metres (Friese et al. 2011), it is only those sandstone fills that include fossil molluscs (Bergman 1982) or found within sub-horizontal fractures (Mattsson 1962) at the present basement surface that can be confidently regarded as lying within metres of the former buried unconformity. A 1-metre erosion depth is not possible at locations where

the buried U2 has a near planar form but stands at a higher elevation than nearby basement summits. This is the case in Västergötland where ongoing research indicates that basement summits close to outliers stand a few metres below the buried basement unconformity (Hall et al. 2019a). The near-planar form of the buried unconformity is maintained over a surrounding area of ~1 000 km^2 in Västergötland, with consistent inclinations across exhumed fault block tops (Johansson et al. 1999). Relative relief in trend surfaces across individual fault blocks around Halleberg and Hunneberg is <20 m (Johansson et al. 1999) and ongoing research indicates that summit elevation ranges are <10 m. A similar elevation range of the summits on the basement surface that emerges from beneath the submerged Ordovician outliers E of Forsmark (Figure 2-11). The mosaic of exhumed fault scarps in NE Uppland (Figure 2-21) and at Närke (Figure 2-16) include features that are 10–20 m high that have not been destroyed by Pleistocene glacial erosion (Section 4.3.5). Summit erosion depths of 50 m are incompatible with the much lower relative relief around Early Palaeozoic outliers (Figure 2-15), the observed elevation differences between the buried and exposed U2 surface at Forsmark and around other Early Palaeozoic outliers in southern Sweden, the integrity of near-planar surfaces identified in summit profiles and trend surfaces (Johansson et al. 1999) and with the survival of slightly upstanding fault blocks found in NE Uppland and around Early Palaeozoic outliers in southern Sweden. A provisional estimate of 10 m is adopted in NE Uppland for the depth of rock removed from U2 above present rock summits. Reconstructions of U2 derived from the present basement summit elevations rest on assumptions that U2 in Uppland was originally a near planar surface, without deep Neoproterozoic weathering prior to burial, overlain by Ordovician limestone and broken by minor, post-Ordovician faulting.

Modelling has uncertainties when applied to Forsmark and to the wider area of Uppland. Available information to test Assumptions 1 and 2 comes mainly from shallow high (5 m) resolution 2D marine seismic surveys (Flodén 1980). Reprocessing of similar vintage data in the SE Baltic and comparison to drill core logs indicates good matches with the main reflectors and differences of <10 m in the elevation of reflector tops (Sopher and Juhlin 2013). Hence, the relief on the buried U2 offshore from Forsmark and the exposed U2 in the surroundings has uncertainties of <10 m. The sparsity of 2D marine seismic data from Öregrundsgrepen (Söderberg and Hagenfeldt 1995), offshore from Forsmark (Figure 1-1), means, however, that more reliance is placed on comparisons with the topography on the buried and exposed unconformities found around other Early Palaeozoic outliers in Sweden.. For Assumption 3, the height difference between the buried and exposed parts of U2 cannot be estimated on the land area as all outliers lie on the seabed (Figure 2-11). The planar form and inclination of the basement unconformity and the fault bock mosaic are features characteristic of basement terrain around other Early Palaeozoic outliers in southern Sweden and provide strong geomorphological support for low erosion of the basement surface since its exhumation. The 10 m estimate adopted is provisional, however, and further work is needed to better constrain the depths of gneiss eroded from summits.

2.3.10 Model of U2 in Uppland based on summit elevations

The model of the dislocated sub-Cambrian unconformity in Uppland is generated as a summit envelope surface on the basis of a modelled DEM of the bedrock surface (Table *2-1*). The bedrock surface DEM was generated by subtraction of the 2 m resampled 20 m soil depth (source: SGU) from the 2 m resolution LIDAR elevation model (source: Lantmäteriet). Summit envelope surfaces were then generated by firstly calculating maximum surfaces of elevation on search windows of different radii, and secondly calculating a mean surface from the maximum surface with the same radius. The resulting maximum-mean surface represents a summit envelope surface. All calculations were conducted in the GIS-software ArcGIS Pro. The effect of the summit envelope surface (the maximum-mean surface) is to fill in low points in the terrain that have been eroded by the Fennoscandian Ice Sheet. The procedure gives DEMs that show smoothed surfaces at different scales that represent models of the former unconformity (the former bedrock surface). (See Table 2-1 for a step-by-step description). The procedure has been followed for a large area of Uppland and for NE Uppland and the neighbouring seabed. Search windows of 0.5 and 1 km radius were used as a check on which provided the best visualisation of fault blocks on the dislocated sub-Cambrian unconformity.

Table 2-1. Summary of the steps taken to generate a summit envelope surface in Uppland.

Input Data (source)	Calculation(s)	Result
2 m LIDAR DEM (Lantmäteriet) 20 m soil depth (Swedish Geological Survey)	Resampling of the 20 m soil depth to 2 m Subtraction of the soil depth from the 2 m LIDAR DEM	2 m DEM of the present bedrock surface
2 m DEM of the present bedrock surface	Focal statistics: Generating a maximum surface using circular search windows of different radii. The GIS picks the highest pixel value within the circle of the given radius.	A 2 m maximum surface with circles and steps between them
2 m maximum surface	Focal statistics: Generating a mean surface using a circular search window with the identical radius that the input maximum surface was based on	A 2 m maximum-mean (smoothed) surface (a summit envelope surface)

U2 model for eastern Uppland

The DEM of the present topography (Figure 2-27A) highlights the main fault blocks, lineaments and basins. Soil depths are less than 5 m over wide areas but thicken to the W and S (Figure 2-27B). Hence the bedrock surface lies close to the present topographic surface in much of NE Uppland (Figure 2-27C). The summit envelope surface for a 1 km radius circular search window shows the edges of the main rock blocks (Figure 2-27D) but does not match the detail of the reconstruction shown in Figure 2-22. This difference is likely a result of the low topographic relief in which subtle (smaller than 10–20 m) differences in the elevation of the original unconformity on rock blocks are masked by equivalent depths of glacial erosion between and around the edges of blocks. The model likely underestimates the elevation of U2 in depressions where all summits have been lowered by glacial erosion but the restricted area of depressions seen in the model (Figure 2-27D) suggests that this error is small. Across all summits, the depth of erosion below U2 is ignored. Our best estimate of a depth of less than 10 m is added later in estimates of glacial erosion.

U2 model for Forsmark and its surroundings

In the Forsmark area, we use a 20 m surface model to match the available resolution of the bathymetry of adjacent parts of the Bothnian Sea (Figure 2-28A). A bedrock surface model is generated by subtracting the thickness of sediment from the surface model (Figure 2-28B).

A maximum surface (Table *2-1*) was created using a search window of 1 km, where each pixel in the elevation model shows the highest value found in this search window (Figure 2-28C). A 1 km search window was used to capture widely spaced high points regarded as closest in elevation to the former unconformity. Next, a mean surface was created from this maximum surface (Figure 2-28D) to achieve a more realistic modelled land surface without artefact circles (Figure 2-28C) but which displays maximum elevations. The same search window of 1 km was used so that each pixel of the maximum surface shows the mean elevation within a circle of 1 km.

The smoothed summit envelope surface **(**Figure 2-28D**)** shows the general slope of the unconformity to the NE (Figure 2-11) and the steps at the edges of the rock block SW of Forsmark and along the edge of the island of Gräsö that are also well displayed in topographic profiles (Figure 2-11). Comparison with the bedrock surface model (Figure 2-28B) and with the mapped unconformity surface (Figure 2-22) indicates that, at this scale and in this area, the summit envelope surface provides only a low resolution representation of the sub-Cambrian unconformity.

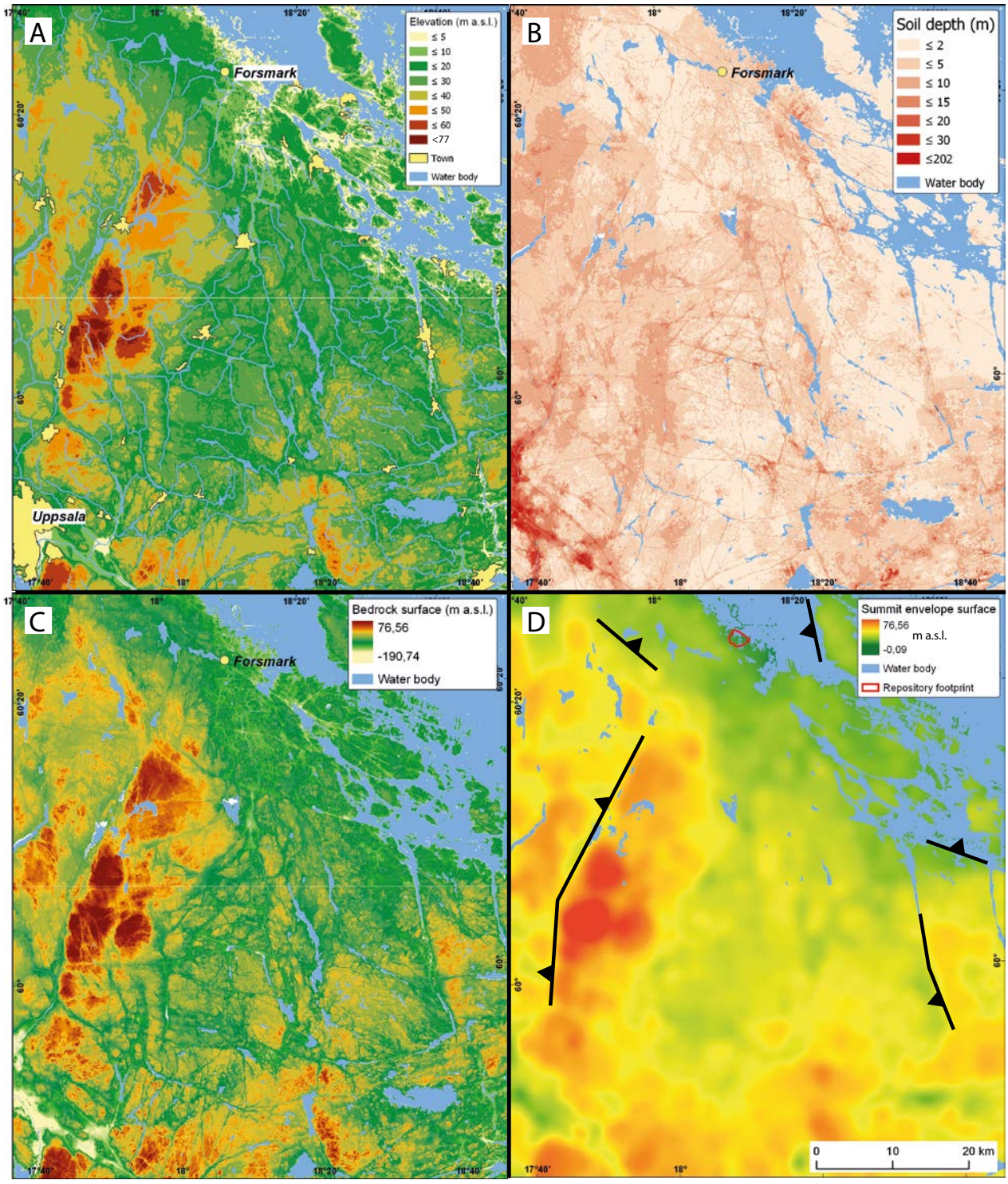

Figure 2-27. *A. Uppland area 2 m resolution DEM. B. Soil depth from SGU data, resampled to 2 m resolution. C. Bedrock surface (2 m resolution DEM minus soil depth). D. Summit envelope surface for NE Uppland (max mean of a 1 km radius circular search window) constructed using the methodology in Table 2-1. Main fault scarps shown in black.*

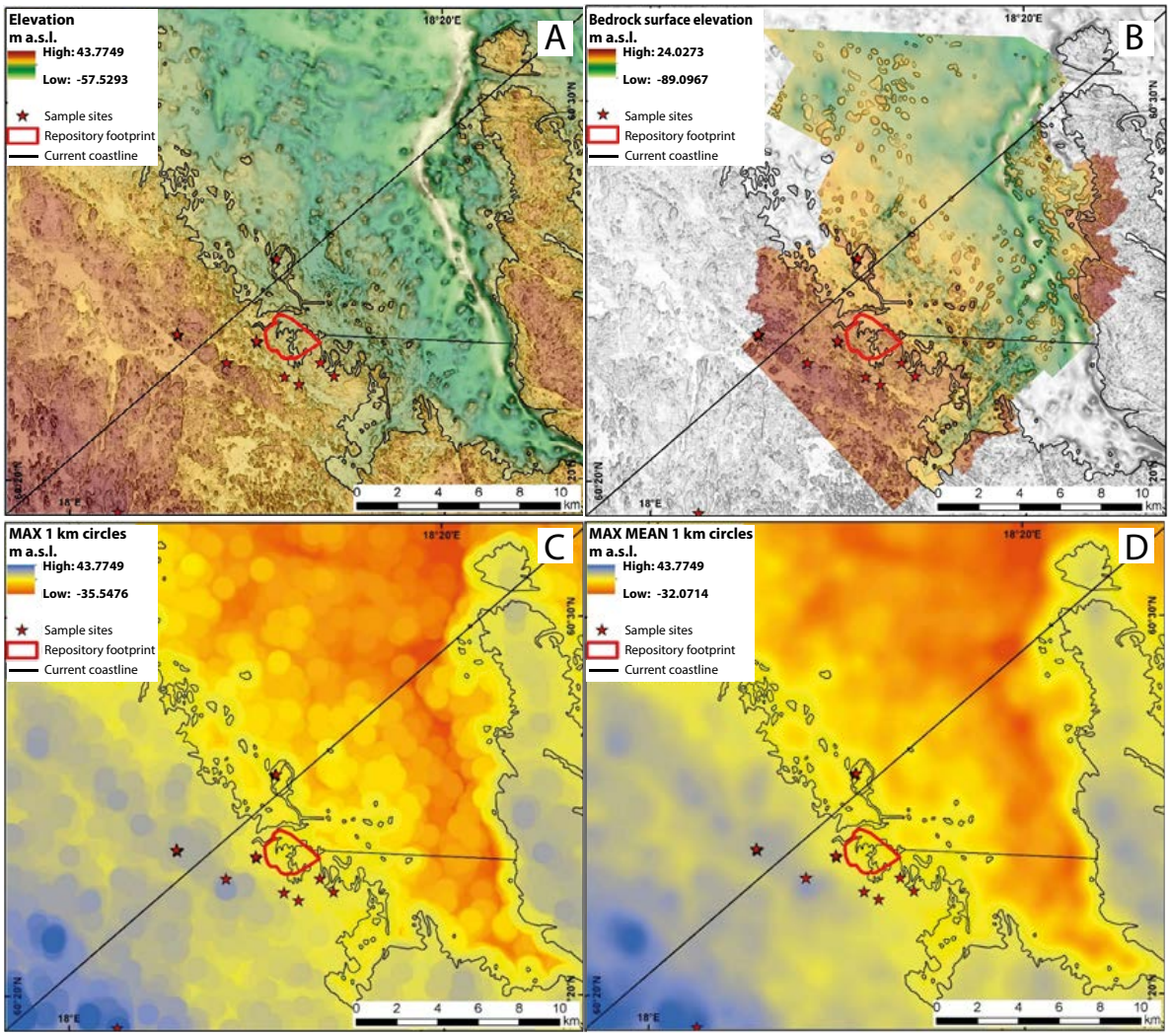

Figure 2-28. *A. Current surface elevation of the Forsmark area including bathymetry. The footprint of the planned spent nuclear fuel repository is shown. B. Bedrock surface model of the Forsmark area (data by SKB). Highest elevations, represented by bedrock outcrops, are the same as in the DEM of Figure 2-21. Lowest areas in the Baltic are more than 30 m deeper than in the DEM with sediments. C. Reconstruction of an envelope surface from local summits using the maximum values within a circular search window of 1 km diameter. D. Reconstruction of a smoothed summit envelope surface from local summits using the mean values within a circular search window of 1 km diameter with the maximum surface (C) as input. Line of section shown in Figure 4-47. Cosmogenic nuclide sample sites indicated by red stars.*

2.4 Summary

The Fennoscandian craton in Uppland stabilised after the Svecokarelian orogeny. The basement was reduced to low relief by 1.5 Ga at the sub-Jotnian (U1) unconformity and was subsequently buried by km thick Jotnian red beds. The proximity of U1 and the present basement surface on the edge of the Bothnian Mesoproterozoic basin indicates that total Neoproterozoic and Phanerozoic denudation of basement has been very limited (Welin 1992). Small outliers of Jotnian sandstone occur in grabens to the W of Singö between the Singö and Forsmark Deformation Zones. Late Meso- to Neoproterozoic block faulting caused vertical dislocation of fault blocks by up to 100 m in the southern Bothnian Sea and similar displacements likely affected the blocks around Forsmark.

The sub-Cambrian unconformity, U2, is cut across Jotnian sandstones and basement on the seabed N of Forsmark. U2 formed initially as part of an extensive peneplain across eastern Baltica after a period of more than 40 Ma of subaerial weathering and erosion had reduced the basement surface

close to base level. Further grading of the unconformity, including removal of regolith, likely took place on extensive rock shelves during marine transgression in the Early Cambrian. During Middle Cambrian emergence, the unconsolidated Early Cambrian cover was removed before the basement was reburied by Late Cambrian to Early Ordovician Alum Shale and Early Ordovician limestone. The basement remained deeply buried throughout the Phanerozoic and there is little evidence that the basement was exposed to weathering prior to the Pleistocene. U2 has been dislocated through the jostling of numerous, small fault blocks by post-Ordovician fault movements, with displacements of a few tens of metres. Some rock blocks S of Forsmark retain surfaces with less than 5 m bedrock relief over km wide areas and most closely represent the re-exposed U2 surface.

The mosaic of tilted, flat-topped basement fault blocks seen in NE Uppland continues beneath the bed of the Bothnian Sea where seismic surveys show that fault-bounded basement blocks remain covered by Cambrian and Ordovician sedimentary rocks (Winterhalter et al. 1981). The fault block mosaic also closely resembles bedrock topography seen around other Early Palaeozoic outliers in southern Sweden. The similarities in form indicate that, as in earlier reconstructions (Rudberg 1970, Lidmar-Bergström 1996), the present basement surface in Uppland is inherited from U2, with modification by Pleistocene glacial erosion. The pattern of dislocation of U2 in Uppland is apparent from the differential movement and tilting of individual fault blocks previously mapped across Uppland (Beckholmen and Tirén 2010a, Grigull et al. 2019) (Figure 2-21). The U2 surface in NE Uppland is mapped from DEMs (Figure 2-22) and displays several fault blocks that retain inclined surfaces with extensive low relief that represent the least modified facets of U2 in this area. Basement summit heights are used as pinning points in models of the former U2 surface in E Uppland (Figure 2-27) and at Forsmark (Figure 2-28). Evidence from height differences between still-buried U2 surfaces and exposed basement summits nearby and the low elevation ranges of summits at increasing distances from Early Palaeozoic outliers in southern Sweden indicate losses of < 10 m of basement from summits. Similar losses are indicated by the elevation range of basement summits on the inclined basement ramp, with outliers of Ordovician limestone, found off Forsmark (Figure 2-11) and by the survival of low fault scarps despite glacial erosion after exhumation (Section 4.3.5). A preliminary estimate of 10 m is adopted for the rock lost from above basement summits. The summit envelope surfaces provide reference surfaces for estimation of depths of glacial erosion below the former unconformity but the estimate for lowering of the basement summits below U2 requires further investigation.

Brittle deformation of the basement after 1.9 Ga led to development of fracture sets that provided the structural framework for later fracture development, opening and mineralisation. Fracture opening likely took place beneath the sub-Jotnian (U1) and sub-Cambrian (U2) unconformities. As U1 and U2 remain close to the present erosional level, near-surface, sub-horizontal fracture sets at Forsmark may relate in part to these antecedent topographies. However, fracture coatings developed during exposure of U1 and U2 are not recognised currently as distinct generations of fracture coatings (Drake et al. 2009b). The G2-G4 generations of fracture coatings record a complex history of fracture opening and groundwater circulation since 1.2 Ga. The persistence of calcite fracture coatings at shallow depth around Forsmark, combined with mobilisation of U oxides after ~ 300 ka at Äspö, Oskarshamn may provide evidence that the final removal of Ordovician limestone from U2 at these locations was a result of glacial erosion during the Middle Pleistocene.

3 Topographic perturbations of near-surface bedrock stresses, fracture development, and possible links to glacial erosion at Forsmark

3.1 Introduction

The fracturing and faulting of bedrock is a crucial control on processes and rates of glacial erosion (Dühnforth et al. 2010, Becker et al. 2014, Leith et al. 2014) and the resulting morphology of glacial bedforms (Gordon 1981, Krabbendam and Bradwell 2011, Krabbendam et al. 2016). Important characteristics of bedrock fractures in the context of understanding their potential impact on the spatial distribution of glacial erosion include: spacing; whether they are steeply-dipping or surface-parallel; their location and orientation with respect to glacier flow direction; dimensions and apertures; and whether they are accessible to water (Rastas and Seppälä 1981, Sugden et al. 1992, Dühnforth et al. 2010, Krabbendam and Bradwell 2011, Hooyer et al. 2012, Lönnqvist and Hökmark 2013). Perturbation of the ambient near-surface stress fields by bedrock surface topography may open existing bedrock fractures and nucleate new ones, making them accessible to fluids and erosive processes (Miller and Dunne 1996, Slim et al. 2015, St Clair et al. 2015, Martel 2016). Here, we assess this perturbation at Forsmark with a view to understanding which fractures may be open in the present landscape and are therefore available to future glacial erosion. We do not imply that topographic stress perturbations are the only control on near-surface bedrock fracturing. Others are also important such as those related to glaciation, some of which are dealt with in Chapter 4.

3.2 Regional structural setting

The basement rock at Forsmark comprises thick, stable, cratonic crust that displays a present-day relief of less than 20 m on the onshore part of the landscape. The present fracture characteristics of the Forsmark bedrock reflect a complex 1.89 billion-year history (Section 2.3.8). Orogeny accompanying crustal shortening was followed by multiple periods of rifting with associated sediment loading, interspersed with periods of exhumation related to far-field orogenic events (Stephens et al. 2007). These oscillatory loading and unloading cycles have continued up to the Holocene, during which the Fennoscandia has been repeatedly loaded and unloaded by thick ice sheets and the changing level of the Baltic Sea (Kleman et al. 2008). Because of this history, most of the bedrock fractures at Forsmark are old and occur as three main sets. The different orientations of these fracture sets reflect temporal variations in the magnitude and orientation of maximum compressive stress (Stephens et al. 2007). The oldest fracturing and faulting occurred late during the Svecokarelian orogeny at 1.80–1.70 Ga, when NNW–SSE regional transpression and associated clockwise stress deviation inside a tectonic lens produced dextral slip along WNW-ESE and NW-SE deformation zones (Saintot et al. 2011). This was followed by transpression along a NE–SW axis during 1.7–1.6 Ga and then further transpression along a WNW-ESE axis during the Sveconorwegian orogeny at 1.1–0.9 Ga, which produced sinistral reactivation along WNW-ESE and NW-SE zones (Saintot et al. 2011). Fracture mineralization indicates that episodes of fracture opening have continued from the late Phanerozoic up to the Pleistocene, related to oscillatory sedimentary loading and erosional unloading (Section 2.1.1; Stephens et al. 2007, Sandström et al. 2008). Where new fractures have formed during Quaternary ice sheet loading and unloading, they frequently nucleate off pre-existing ones (Carlsson 1979, Leijon 2005, Sandström et al. 2008), as may be expected for fracture-saturated bedrock.

3.2.1 Fracture domains in the Forsmark area

The repository site is located in the Forsmark tectonic lens, which is comprised of three fracture domains (Figure 3-1) (Martin 2007). The rock in fracture Domain FFM01 is sparsely fractured, apart from steeply dipping minor deformation zones containing sealed fractures. Sub-horizontal fractures may only occur locally and there are few hydraulically connected fractures. In contrast, fracture Domain FFM02, which thickens towards the SE, displays abundant sub-horizontal fractures in the

uppermost 150 m. These fractures are frequently open and hydraulically conductive. Open fractures are those defined as having apertures greater than hairline and which can be distinguished by the naked eye as open on the borehole image processing system (BIPS) used by SKB (for example, Martin 2007). Fracture domain FFM03 comprises abundant gently dipping minor deformation zones where fractures are open and hydraulically connected over a broad area. These fracture domains are enveloped to the north and south by the Singö and Forsmark deformation zones, respectively (Figure 3-1). Deformation in these latter zones has occurred under both ductile and brittle regimes (Stephens et al. 2007). Other smaller deformation zones, formed in the brittle regime, occur approximately transverse to the regional Singö and Forsmark deformation zones (Figure 3-1) (Stephens et al. 2007, 2008b). Collectively, the deformation zones comprise parcels of weaker, more densely fractured, rock surrounding harder, more sparsely fractured, rock (Martin 2007). These spatial variations in fracture density influence the rock mass deformation modulus, which in turn determines bedrock stress magnitudes (Martin 2007).

3.2.2 Rock types at Forsmark

In addition to the three fracture domains, bedrock at the proposed repository site also consists of two compositional rock domains (Stephens et al. 2007). The dominant domain is ~75 % composed of quartz-rich (24–46 %) metagranite. The subordinate rock domain, RFM045, is 65–70 % composed of altered and metamorphosed finer-grained granite. Other rock types include pegmatite and pegmatitic granite (13 % and 14 %, in each domain respectively), fine- to medium-grained metagranodiorite and tonalite (5 % and 9 %, respectively), and amphibolite (4 % and 7 %, respectively). Amphibolite occurs as sills and irregular inclusions that are elongate parallel to the mineral fabric, which plunges to the SE. Although some bodies of amphibolite are more than a few metres thick and, locally, are some tens of metres thick, most are thinner. Compositional variations are important to bedrock fracturing because they exert control on rock strength (Sklar and Dietrich 2001, Zhang 2002, Glamheden et al. 2007) and because rock mineral fabric and foliation may control fracture orientations and spacing (Beacom et al. 2001, Stephens et al. 2007). In the Forsmark bedrock, mean uniaxial compressive strengths range between 145 MPa for amphibolite and 373 MPa for albitized granite and granodiorite (Glamheden et al. 2007).

3.2.3 Stress fields

Bedrock is subjected to a three-dimensional stress field comprised of one vertical and two horizontal components. The vertical component is gravitational, and its magnitude increases with depth because of the increasing overlying rock mass. In contrast, the magnitudes of the horizontal components are at Forsmark controlled by far-field tectonic forces attributable to a mid-Atlantic ridge-push and isostatic rebound following the deglaciation of the last Fennoscandian Ice Sheet (Andersson et al. 2002, Stephens and Simeonov 2015). The magnitudes of the horizontal components progressively increase with depth beneath the ground surface because of the additive effects of gravity attributable to the progressively increasing mass of overlying rock. Under present conditions, the maximum compressive stress (σ_H) is oriented NW–SE and its magnitude is higher in the deeper, less fractured, domain FFM01 than in the superficial, more-fractured, domain FFM02 (Table 3-1; Martin 2007). In the uppermost 150 m, σ_H^t (i.e. the far-field horizontal compression due to tectonics and glacial history) averages 19 MPa, declines to 9.1 MPa at 150–400 m depth because of the presence of a gently-inclined deformation zone (ZFMA2), and then increases to 29.5 MPa below 400 m (Table 3-1) (Mas Ivars and Hakami 2005, Martin 2007). It deviates insignificantly in orientation from the surrounding rock in the Singö and Forsmark deformation zones but its magnitude is much higher in the Forsmark tectonic lens (Martin 2007). The minimum compressive stress (σ_h^t) is oriented NE–SW and displays much lower values than σ_H^t (Table 3-1; Martin 2007). The present magnitudes and orientations of the maximum and minimum compressive stresses, and their spatial variations, are important controls on the formation of new fractures and the opening of old ones.

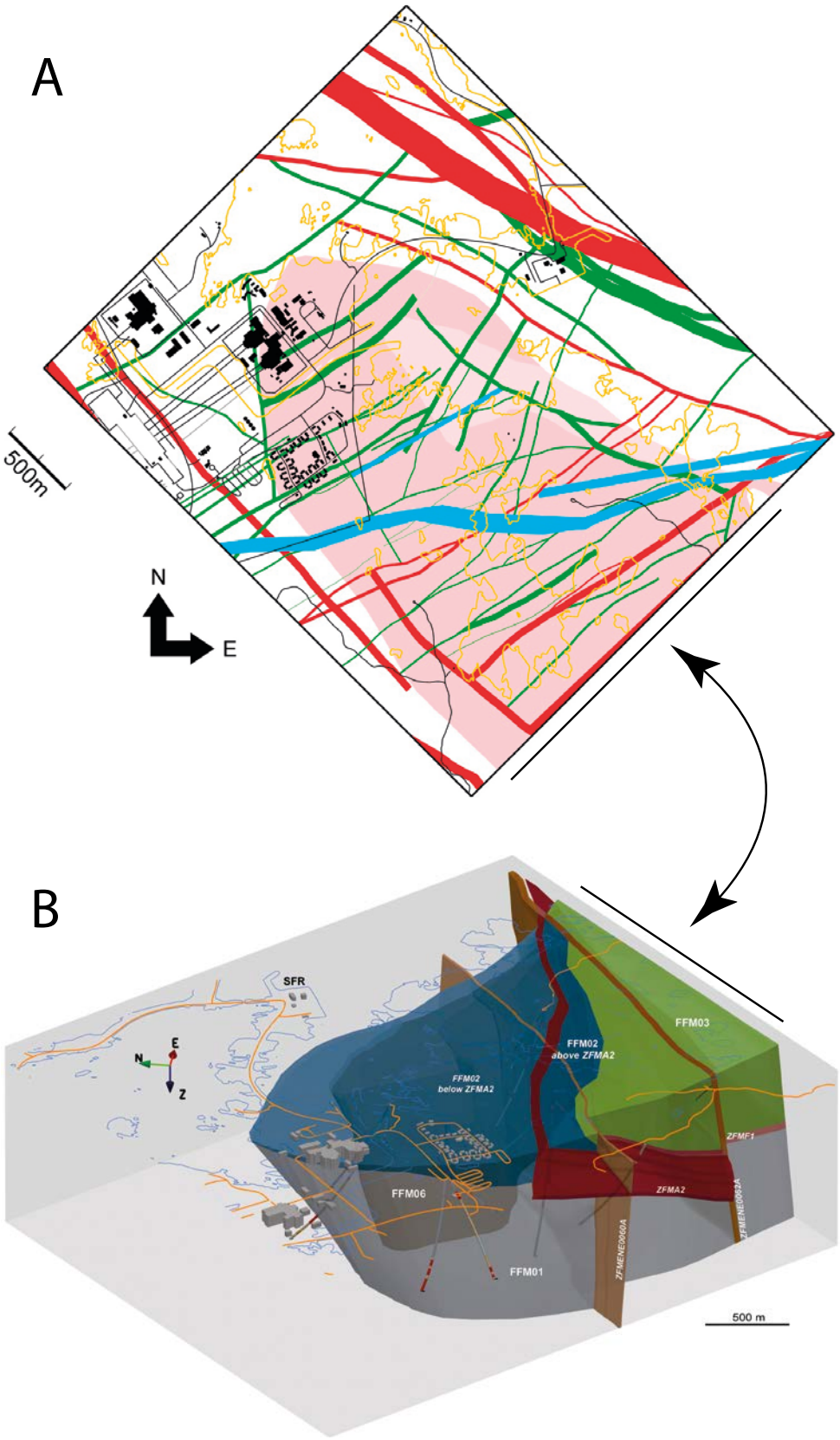

Figure 3-1. *Fracture domains at Forsmark. A. Plan-view of deformation zones at Forsmark with trace lengths greater than 1 km on a surface at 500 m depth (reproduced from Figure 5-4 in Stephens and Simeonov, 2015). B. 3D model of fracture domains FFM01 (grey), FFM02 (blue), and FFM03 (green) shown with deformation zones ZFMENE0060A and ZFMENE6062A (reproduced from Figure 5-4 in Olofsson et al. 2007). The orientations of the map in A and the model in B are rotated with respect to each other, as indicated by the double-headed arrow. The position of the SE margin of the map in A is shown by the black line in B.*

Table 3-1. Stress conditions used in model scenarios.

Topography	Model run	Ambient stress						
		σ_H^t	σ_h^t	Orientation of H	Vertical gradient of…			
					H $k_H\rho g$	h $k_h\rho g$	z ρg	Young's Modulus
		MPa	MPa	°	MPa/m	MPa/m	MPa/m	GPa
Reg 20 m	Scenario 1	19.0	11.0	N145°E	0.008	0.006	0.0265	65
	Scenario 2	9.1	6.8	N145°E	0.074	0.034	0.0265	65
	Scenario 3	29.5	9.2	N145°E	0.023	0.028	0.0265	65

An analysis of 10371 open fractures from Forsmark boreholes reveals that their abundance decreases with depth (Figure 3-2; Martin 2007). Gently dipping (<20°) open fractures, which comprise 32 % of the total, decrease dramatically in abundance below 200 m depth, whereas open steeply-dipping (more than 70°) fractures, which comprise 22 % of the total, are more evenly distributed with depth. Open fractures dipping at intermediate angles show a variable distribution with depth. These frequency distributions add further support to the contrast in fracture abundances and stresses between fracture domains FFM01 and FFM02–FFM03.

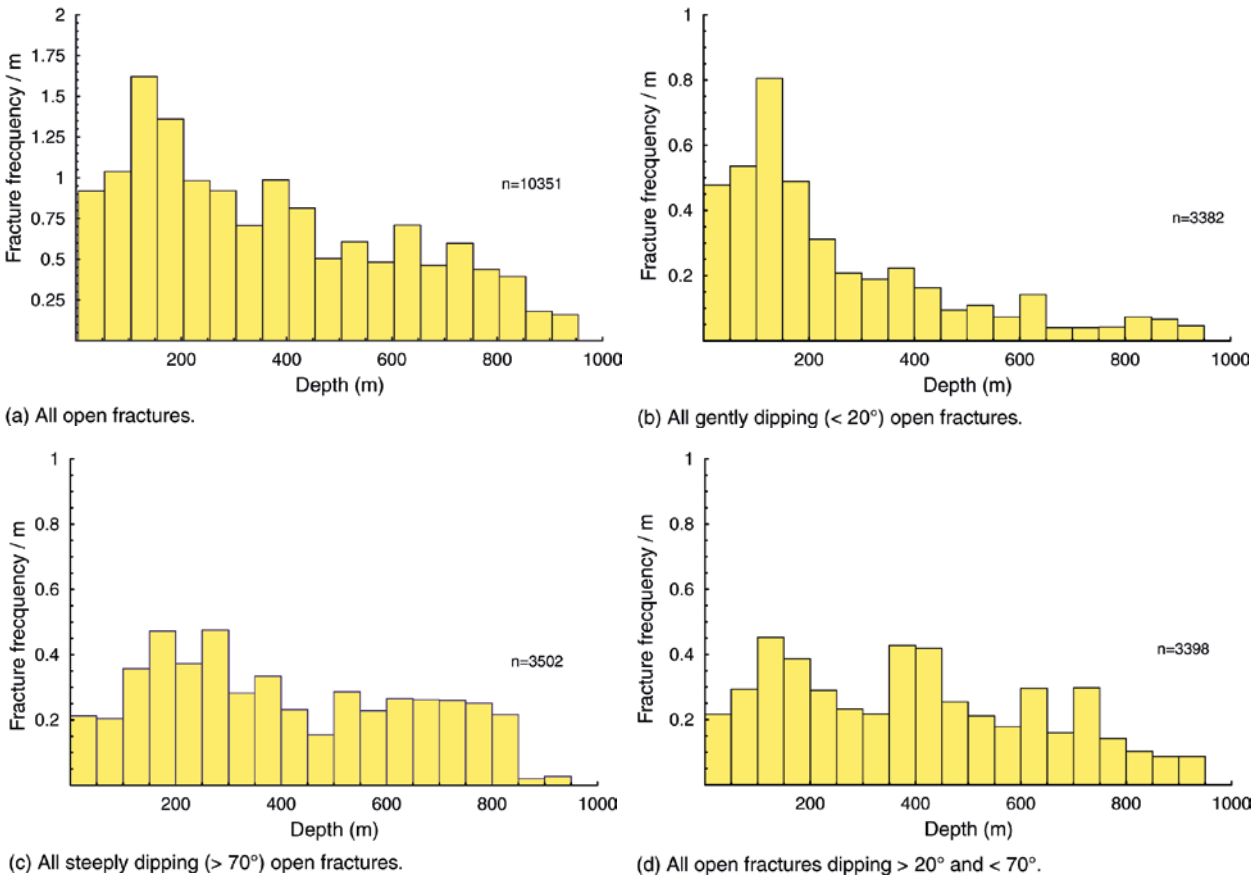

Figure 3-2. *Frequency distributions of open fractures with depth (reproduced from Figure 2-8 in Martin 2007).*

3.2.4 Hydraulic jacking of subhorizontal fractures during glaciation

Some steeply-dipping fractures in the uppermost few metres and some near-surface sub-horizontal joints may have formed during glaciations (Carlsson 1979, Leijon 2005). These appear frequently to have nucleated from existing, mineralized, fractures (Carlsson 1979, Leijon et al. 2005). Glacially-induced hydraulic jacking provides a key mechanism for opening sub-horizontal fractures at Forsmark, preferentially over vertical fractures (Hökmark et al. 2010, Lönnqvist and Hökmark 2013). This is because in sub-horizontal fractures pore pressures can be generated that exceed the vertical stress in rock subjected to a high σ_H^t. Conversely, in sub-vertical fractures, normal stress acting on fracture walls will exceed the pore pressure at a shallow depth below the ground surface, which will suppress fracture opening. Evidence for hydraulic jacking during the last glaciation at Forsmark is abundant (Figure 2-26), consisting of open sub-horizontal fractures, with apertures of centimetres to tens of centimetres, filled with glacifluvial sediments (Carlsson 1979, Carlsten et al. 2004, Hökmark et al. 2010). These filled fractures are concentrated in the uppermost metres but extend down some tens of metres beneath the ground surface (Hökmark et al. 2006, 2010). Where they occur, they are likely of high importance to preparing bedrock for glacial erosion. Modelling indicates that future hydraulic jacking at Forsmark will be confined to the uppermost 200 m (Hökmark et al. 2010, Lönnqvist and Hökmark 2013). However, sub-horizontal fractures may propagate for long distances (i.e. hundreds of metres, or more; Lönnqvist and Hökmark 2013). We highlight here only one mechanism for bedrock fracturing during glaciation, relating specifically to the opening of subhorizontal joints through hydraulic jacking. Others occur, and we refer the reader to Chapter 4 for information on those.

3.2.5 Topographic controls on fracturing

Perturbation of the ambient near-surface stress fields by bedrock surface topography may exert control on the opening of bedrock fractures, making them accessible to water and subject to erosive processes, and on the generation of new fractures (Miller and Dunne 1996, Slim et al. 2015, St Clair et al. 2015, Martel 2016). This is because theoretical calculations and field observations indicate that convex and concave landforms can cause vertical and lateral variations in the shallow subsurface stress field (Slim et al. 2015, St Clair et al. 2015, Martel 2016). These stress perturbations are highest at the surface and decrease with depth. Increases in each of topographic relief (i.e. amplitude), surface curvature (i.e. the derivative of slope), and the magnitude σ_H^t, with respect also to the magnitude σ_H^t, increase the topographic perturbation of the ambient stress field (St Clair et al. 2015). A decrease in topographic wavelength also increases this perturbation (St Clair et al. 2015). This topographic modification of near surface ambient stresses can influence which fractures open, where in the landscape they open, and the depth below the ground surface to which they open (St Clair et al. 2015).

The onshore topography of Forsmark is characterized by a low regional surface gradient and low relief (1 m/km and less than 20 m, respectively, on the subaerial part of the landscape). Both of these parameters increase in the adjacent offshore region. At a regional scale, the bedrock is fractured and faulted into rock blocks with areal extents of tens of km^2 and which dip gently to the east (Grigull et al. 2019). They provide notable relief in this otherwise almost flat landscape, particularly along their western flanks, which form scarps some tens of metres high. Despite the low relief, topographic curvatures are frequently high at the outcrop scale, in locations where glacial erosion of convex–concave parts of the landscape is more evident (Figure 3-3), and, at the regional scale, along the fault block scarps.

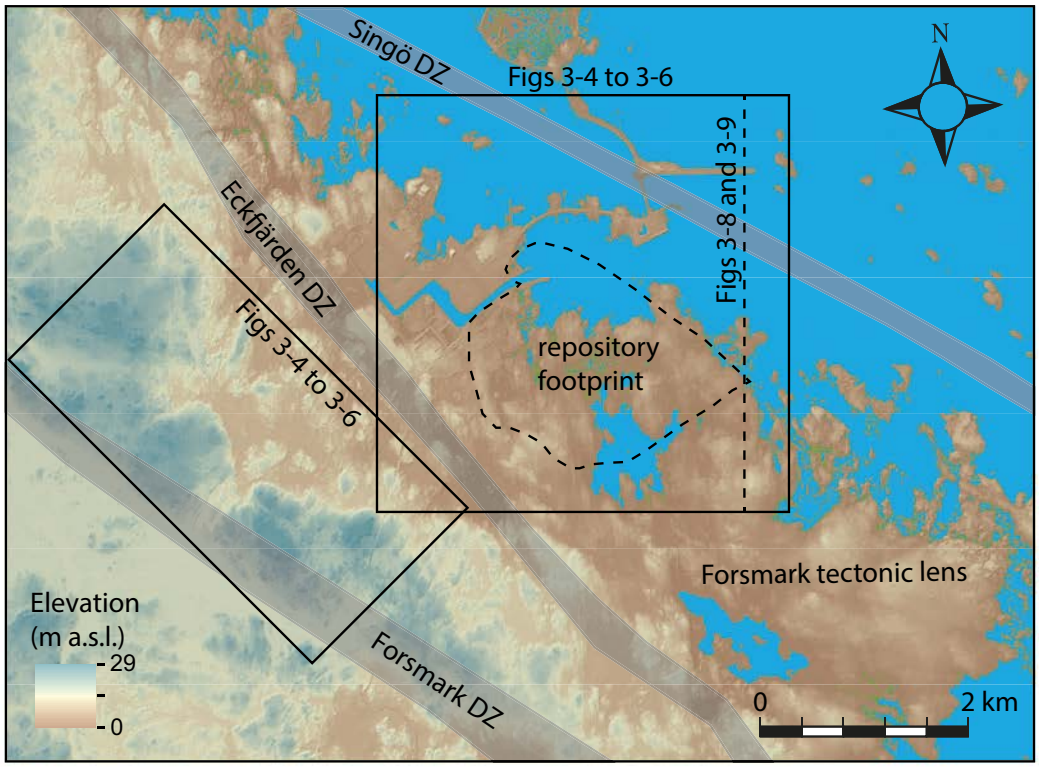

Figure 3-3. *LiDAR-based DEM of the glaciated basement terrain at Forsmark with major deformation zones (DZ) shown in grey. The areas analysed in the modelling of topographic perturbations of near surface stresses presented in Figures 3-4 to 3-6 are shown in the rectangles. The location of the vertical section presented in Figures 3-8 and 3-9 is illustrated by the N–S-oriented dashed line. The footprint of the planned repository is shown in the dashed outline.*

Although the Forsmark topography displays a low relief (amplitude), it still perturbs the near-surface ambient stress fields because the magnitude of σ_H^t is high in absolute terms and relative to σ_h^t (Table 3-1; Martin 2007) and because topographic curvatures are locally high. Following Martel (2016) for conditions where the amplitude (A) of relief is short relative to topographic wavelength (L), i.e. where A/L <0.04, regional horizontal compression (T) alone induces localized vertical tension beneath hillcrests. Combined with gravity, it induces surface-parallel compression beneath hillcrests. If T is about an order of magnitude more compressive than ρgA (where ρ is rock density and g is gravitational acceleration) regional compression dominates the near-surface stress field, resulting in formation and/or opening of sheeting joints parallel to the surface, particularly in hills. In contrast, gravity induces localized horizontal tension beneath valley bottoms. If T is about an order of magnitude less compressive than ρgA, gravity dominates the near-surface stress field, resulting in the opening of sub-vertical fractures at valley bottoms. The depth to which topography influences the stress field and bedrock fracturing is determined by the combination of horizontal compressive stresses and topographic wavelength. Higher values increase the depth of the topographic perturbation. The conditions explored by Martel (2016) are also applicable to the Forsmark landscape, because, similarly, A/L ratios are low.

3.2.6 Interactions between topography, fracturing and glacial erosion

If fracture openness at the land surface exerts control on glacial erosion, any controls on that openness, including topographic perturbation of the near-surface ambient stress field, may contribute to spatial variation of glacial erosion processes and rates. If the surface topography and near-surface stresses interact in ways that favour opening of steeply dipping fractures, then glacial abrasion and plucking might exploit these to deepen concavities and increase relief. If topography modulates near-surface stresses such that sub-horizontal joints preferentially open below convexities, then these might be exploited by glacial plucking or ripping to lower summits and reduce relief. In reality, both processes may be occurring, contributing to a complex spatial and temporal pattern of glacial erosion

that lies between the two end-member possibilities and which is also governed by other controls. This study investigates how topography might partly control glacial erosion at Forsmark through its possible influence on bedrock fracturing.

3.3 Modelling the perturbation of near-surface stresses by topography at Forsmark

High-quality data are available for modelling the topographic perturbation of near-surface stresses, including: ambient stress field measurements from 23 boreholes (with those derived from overcoring being the most appropriate); values for Young's modulus determined specifically for Forsmark; and DEMs including the subaerially exposed surface (including till and sediments), bathymetry, and the bedrock surface (with till and sediment deposits removed), at resolutions of 2 m, 20 m, and 20 m, respectively. Whereas stresses associated with marine transgression are not well constrained they can be handled in our recently-developed mechanically-based boundary element model (St Clair et al. 2015). In this model, the total stress field is calculated as the sum of the ambient stress due to gravity and tectonics and the stress perturbation from topography (Slim et al. 2015, St Clair et al. 2015, Martel 2016).

From the stress field, two scalar quantities may be calculated that act as proxies for two mechanisms that could influence the formation and opening of fractures. Firstly, a failure potential (ϕ) may be calculated as a proxy for shear fracturing or shear sliding on existing fractures. This is defined as $(\sigma_{mc} - \sigma_{lc})/(\sigma_{mc} + \sigma_{lc})$, where σ indicates a stress, and the subscripts denote the most compressive (*mc*) and least compressive (*lc*) principal stresses, with compression being positive. Secondly, the magnitude of *lc* may be used as a proxy for opening-mode displacement on fractures. Both quantities may represent the propensity for increasing fracture apertures above hairline, which likely generates open fractures. A larger ϕ indicates that new shear fractures are more likely to form, and that existing fractures oriented obliquely to the *mc* and *lc* directions are more likely to dilate because of sliding on the rough fracture surfaces. A smaller *lc* indicates that fractures oriented nearly perpendicular to the σ_{lc} direction will be more likely to open.

The model uses the present topography, bedrock properties, and the shallow subsurface far-field stress field as initial input. Both constant far-field stresses at the ground surface and their changes with depth are considered. The model has been developed at scales equivalent to 10^2 to 10^3 m horizontal distances and recent work shows that it is adaptable to the low amplitudes (i.e. less than 20 m) that characterize Forsmark (Martel 2016). To also meet our needs, the model has been adapted to three-dimensions and explicitly treats the development of surface parallel fractures.

The three-dimensional boundary element model Poly3D (Thomas 1993) was used to calculate stress fields beneath the topographic surface of the Forsmark area (St Clair et al. 2015, Moon et al. 2017). The model assumes linear-elastic, homogeneous, and isotropic rock beneath the Earth's surface. The topographic surface is treated as a traction-free boundary formed by the removal of overburden in a laterally confined, elastic body of rock (Martel 2000, Martel and Muller 2000). The total stress in the body is calculated as the sum of gravitational stress, regional horizontal far-field tectonic stresses, and the stress perturbation associated with the traction-free topographic surface. The ambient stresses due to gravity and tectonics are calculated as:

$$\sigma_H^a = -k_H \rho g z + \sigma_H^t \quad (3\text{-}1a)$$

$$\sigma_h^a = -k_h \rho g z + \sigma_h^t \quad (3\text{-}1b)$$

$$\sigma_v^a = -\rho g z \quad (3\text{-}1c)$$

$$\sigma_{Hh}^a = \sigma_{Hv}^a = \sigma_{hv}^a = 0 \quad (3\text{-}1d)$$

where *H* and *h* denote the directions of the most and least compressive horizontal stresses, *v* denotes the vertical direction, ρ is rock density, *g* is gravitational acceleration, and *z* is elevation above a reference point. Compressive stresses are positive. The terms σ^a and σ^t represent ambient stress and constant horizontal tectonic compression, respectively. The parameter *k* is the vertical gradient in horizontal normal stress relative to the vertical gradient in vertical normal stress, with k_H and k_h

representing the gradients in the most and least compressive horizontal stresses. The double-subscripted terms in *equation 3-1d* refer to shear stresses. For our simulations, three model scenarios were run with different stress conditions based on the compilations of *in-situ* hydrofracturing and overcoring stress measurements from within and adjacent to the study area (Table 3-1. Stress conditions used in model scenarios 3–1; Martin 2007).

The regolith surface of Forsmark (FM_REG_20m_RH2000; 20-m resolution), which is beneath soil and postglacial sediment, was used to construct a mesh of triangular elements that cover an area of ~80 km^2 centred on the Forsmark power stations and proposed repository site. The mean elevation was subtracted, and the edges of the grid were tapered outside the area of interest to zero elevation to ensure stress equilibrium. The elevation grid was then transformed into a triangular mesh with variable resolutions; finer triangular elements (~75 m) near the area of interest and coarser elements (100–300 m) near the edges of the grid. Observation points were arranged in three-dimensional grids with ~75 m horizontal spacing and approximately 10 m vertical spacing. This modelling was completed at relatively crude horizontal and vertical resolutions to gauge the importance of the topographic control on near surface stresses.

From the three-dimensional stress fields, the magnitudes and orientations of the three principal stresses were calculated: most compressive stress (σ_{mc}), intermediate compressive stress (*ICS*), and least compressive stress (σ_{lc}). The magnitude of σ_{lc} represents the potential for generating or dilating opening-mode fractures (Barton and Moos 1999, Min et al. 2004). A failure potential (F), which represents the potential for sliding on shear fractures (Iverson and Reid 1992, Yeo et al. 1998), was also calculated as (Iverson and Reid 1992):

$$\Phi = \left|\frac{\sigma_{mc} - \sigma_{lc}}{\sigma_{mc} + \sigma_{lc}}\right| \qquad (3\text{-}2)$$

The spatial distributions of σ_{lc}, σ_{mc}, and F near the surface (−100 m) and at depth (−400 m) for the three model scenarios are shown in Figures 3-4, 3-5 and 3-6. Overall stress patterns are consistent with predictions for strong, anisotropic stresses (Moon et al. 2017). The smaller σ_{lc} beneath landforms with negative curvatures (for example, convex ridges) indicates that fractures are more likely to open in these locations. These fractures are also more likely to be sub-horizontal and/or surface-parallel. In addition, σ_{lc} is smaller beneath topographic ridges oriented perpendicular to the *H* orientation (N145°E). The topographic perturbation of the ambient stress field, and therefore the control of fracture opening, is strongest near the surface and is much weaker at depth.

Because of strong horizontal tectonic compression with a large stress anisotropy, the orientations of principal stresses at −100 and −400 m barely differ and mostly follow the imposed orientations. High values of F (i.e. > ~0.55), likely attributable to large differential stresses, are predicted near the surface, but also at depth. This indicates an elevated potential for generating or reactivating shear fractures, especially those with an oblique dip, striking perpendicular to the σ_H orientation.

Low topographic relief and weakly undulating topography produce smaller curvatures over long wavelengths (hundreds of metres to kilometres) and less variable stresses than sites previously analyzed in the U.S.A. (Moon et al. 2017). Figure 3-7 shows a plot of the magnitudes of least, intermediate, and most compressive stresses with elevation for all observation grids. Without the influence of topographic stress perturbations, principal stresses would follow the imposed gradients of ambient stresses with depth. Deviations from the imposed gradients of near-surface principal stresses in the uppermost 50–80 m indicate a substantial influence of topographic perturbations in the near-surface. This effect is highest in model scenarios 1 and 3, which reflects the higher magnitude and more anisotrophic horizontal compressive stress fields. The effect is also highest on σ_{mc} and lowest on the ICS in all scenarios. The increase with depth in σ_{lc} is highest for scenario 1 and for σ_{mc} in scenario 2. However, in all scenarios, the influence of topographic perturbations dissipates with increasing depth and, consequently, principal stresses vary little at greater depths. At the depth of the proposed repository (around 450 m), stresses vary spatially by only ~2 MPa (6 % of the surface magnitudes).

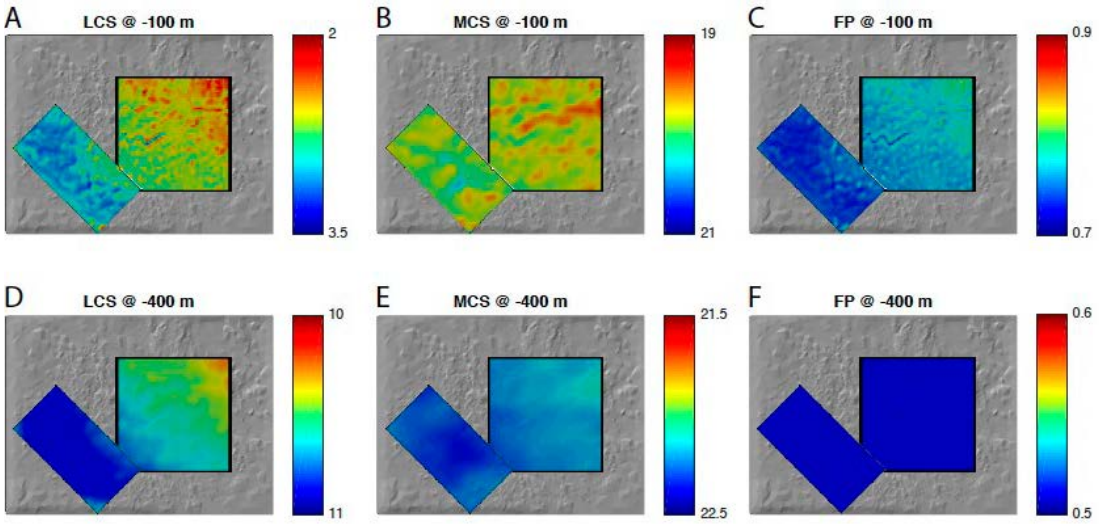

Figure 3-4. *Topographic control on the near surface stress field for Model scenario 1, which is based on measured stress conditions at Forsmark from 0 to 150 m depth below surface. The most compressive stress is oriented N145°E, and maximum and minimum horizontal compressive stress magnitudes are (σ_H^t = 19 MPa; σ_h^t = 11 MPa). Panels A to C show the least compressive ($\sigma_{lc,}$ MPa), most compressive (σ_{mc}, MPa) stress, and failure potential (ϕ =(σ_{mc}−σ_{lc})/(σ_{mc}+σ_{lc})), respectively, at 100 m depth. Panels D to F show σ_{lc}, σ_{mc}, and ϕ, respectively, at 400 m depth. Red indicates locations where the stress field is least compressive, resulting in a higher number of open bedrock factures, whereas blue indicates locations where the stress field is most compressive, resulting in fewer open bedrock fractures. See Figure 3-3 for location.*

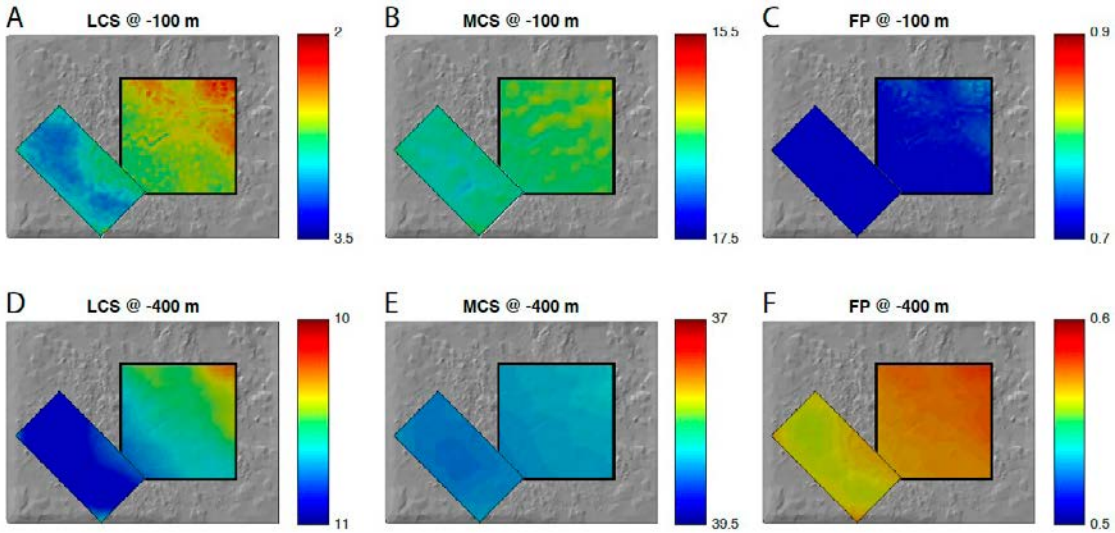

Figure 3-5. *Topographic control on the near surface stress field for Model scenario 2, which is based on measured stress conditions at Forsmark from 150 to 400 m depth below surface. The most compressive stress is oriented N145E, and maximum and minimum horizontal compressive stress magnitudes are (σ_H^t = 9.1 MPa; σ_h^t = 6.8 MPa. Figure descriptions and symbols are the same as Figure 3-4 and see Figure 3-3 for location.*

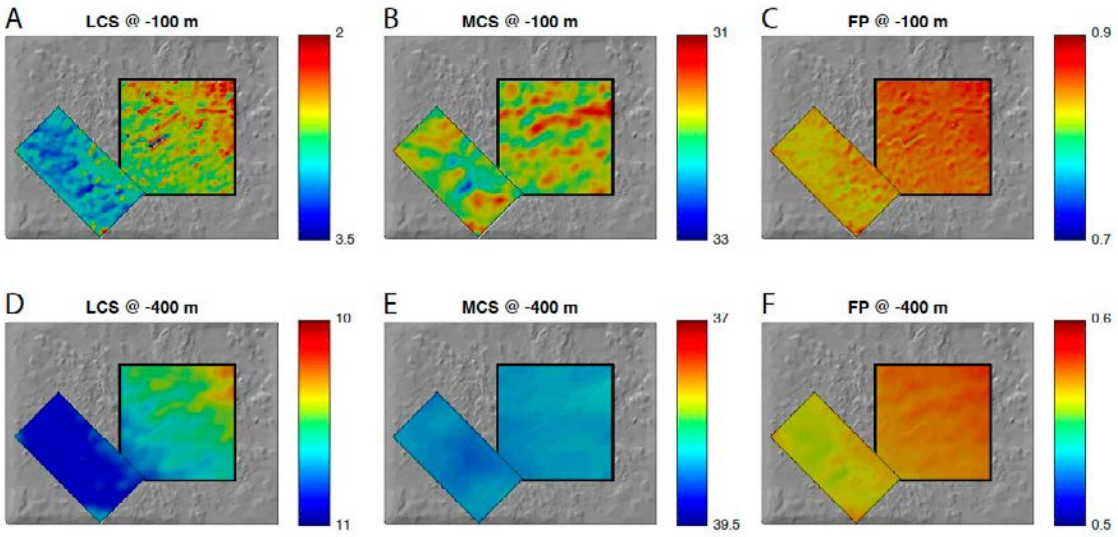

Figure 3-6. *Topographic control on the near surface stress field for Model scenario 3, which is based on measured stress conditions at Forsmark from 400 to 600 m depth below surface. The most compressive stress is oriented N145E, and maximum and minimum horizontal compressive stress magnitudes are (σ_H^t = 29.5 MPa; σ_h^t = 9.2 MPa). Figure descriptions and symbols are the same as Figure 3-4 and see Figure 3-3 for location.*

To examine the variation of stress fields in detail, we show the variation of σ_{lc} at depths from 0 to 600 m along a north-south oriented transect within the modelled domain (Figure 3-8). The results show that the topographic influence on σ_{lc} is significant in the near-surface (i.e. < 100 m) and decays with increasing depth. The model also predicts that one area along this transect, corresponding to a surface concavity, is likely in tension, which may cause opening of sub-vertical fractures in this location. The lower topographic perturbation of the near surface stresses offshore may reflect the lower resolution DEM and/or loading of the landscape by sediments.

In addition, we consider how spatially varying loading of the bedrock surface from overlying sediments and ocean water modifies shear and normal traction for each boundary element in our model and thus impact the subsurface stress fields. We calculate loading by sediments and water from densities of 2 000 kg/m^3 and 1 000 kg/m^3, respectively, and from present-day sediment and water column thicknesses (Sohlenius et al. 2013). We assume pore pressure as hydrostatic water pressure, which is dependent upon depth below the present-day sea level. Then, we calculate the effective stress fields by subtracting pore water pressure from total stress fields.

A model of these effects using the ambient stress conditions of scenario 1 indicates significant changes in near-surface stress fields (Figure 3-9). The effective stress that considers the pore pressure produces overall less compressive σ_{lc}. In addition, σ_{lc} is more variable near-surface and an additional concavity in the bedrock surface is in tension compared with predictions from the model scenario based only on bedrock surfaces (Figure 3-9). The horizontal variations of σ_{lc} at depths ranging from 100 m to 600 m below the sea level are shown in Figure 3-10. At 100 m below the ground surface, stress fields are perturbed by short wave-length topographic variations and so show more small-scale spatial variation. Conversely, with increasing depth beneath the ground surface, the ambient stress fields are increasingly affected by long wavelength topographic features, the large-scale topographic gradient, and the presence of the Baltic Sea. The resulting broader-scale spatial variations occur because in low relief topography (where A/L < 0.04) the depth to which topography influences the stress field increases with topographic wavelength (Martel 2016). The magnitude of σ_{lc} does, however, also increase with depth and the pattern of longer wavelength topographic perturbations of ambient stresses in plan-view remains imprinted on the declining topographic perturbation of the ambient stresses. Therefore, the strongest topographic control on near-surface stresses is imparted by shorter-wavelength landforms in the uppermost 100 m.

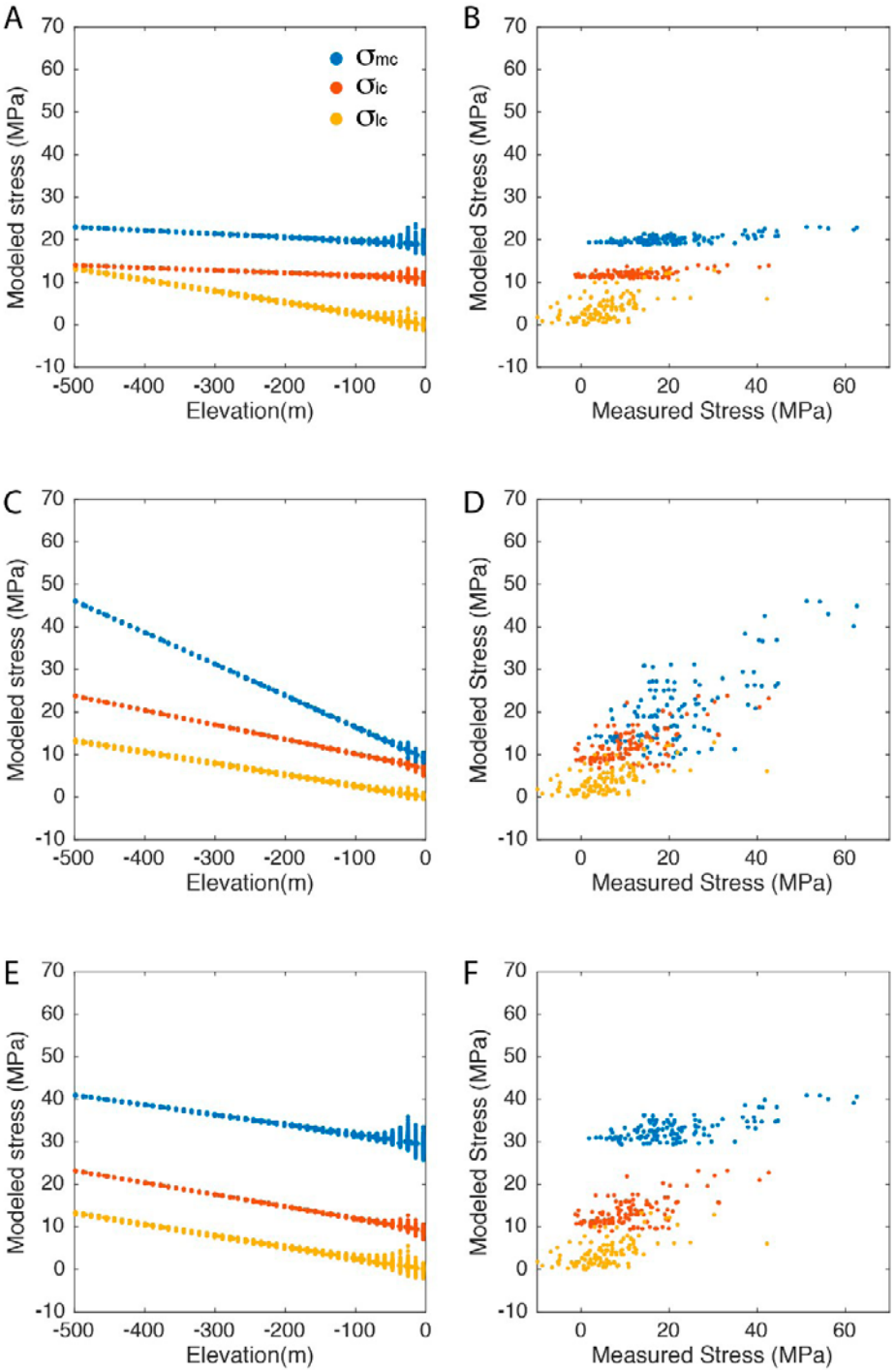

Figure 3-7. *Modelled principal stress magnitudes. Model stresses for Scenarios 1 to 3 are shown in panels A and B, C and D, and E and F, respectively. Left panels show modelled stresses against bedrock depth below surface (m) and right panels show modelled against measured stresses (in MPa). Blue, red, and orange data indicate most, intermediate, and least compressive stress, respectively.*

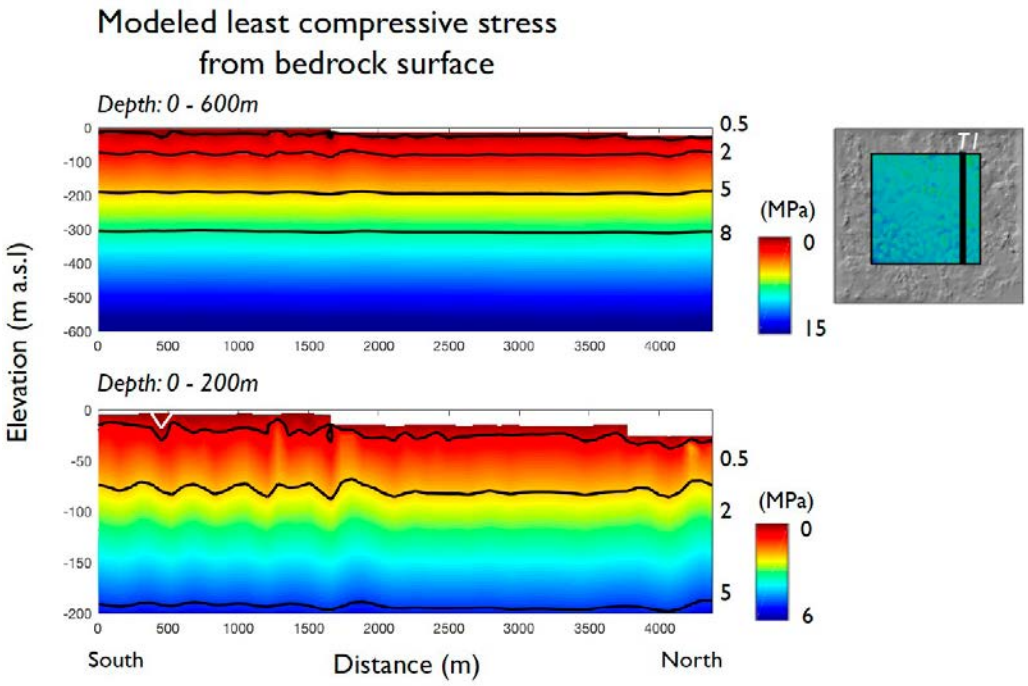

Figure 3-8. *Topographic control on the near surface stress field for Model scenario 1, which is based on measured stress conditions at Forsmark from 0 to 150 m below the surface. Top and bottom panels show the least compressive (σ_{lc}) stress at depths between 0–600 m and 0–200 m below surface, respectively. The white line represents a contour that the σ_{lc} equals to zero, which indicates that the area above will be in tension. The black lines represent contours for σ_{lc} = 0.5, 2, 5, and 8 MPa. See Figure 3-3 for the location.*

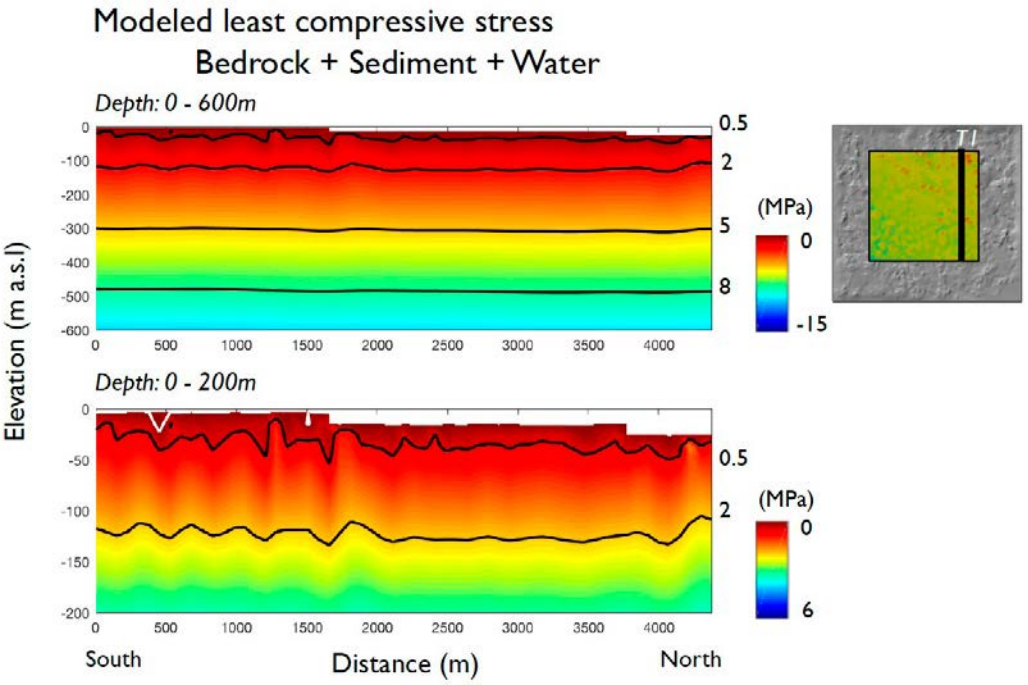

Figure 3-9. *Topographic control on the near-surface stress field for Model scenario 1, which is based on measured stress conditions at Forsmark from 0 to 150 m depth below the surface and includes influences from the bedrock surface, sediment and water loading, and water pore pressure effects. Top and bottom panels show the least compressive (σ_{lc}) stress at depths between 0–600 m and 0–200 m below surface, respectively. The white contour shows where σ_{lc} equals zero, so areas above that are in tension. The black contours show where σ_{lc} = 0.5, 2, 5, and 8 MPa. See Figure 3-3 for the location.*

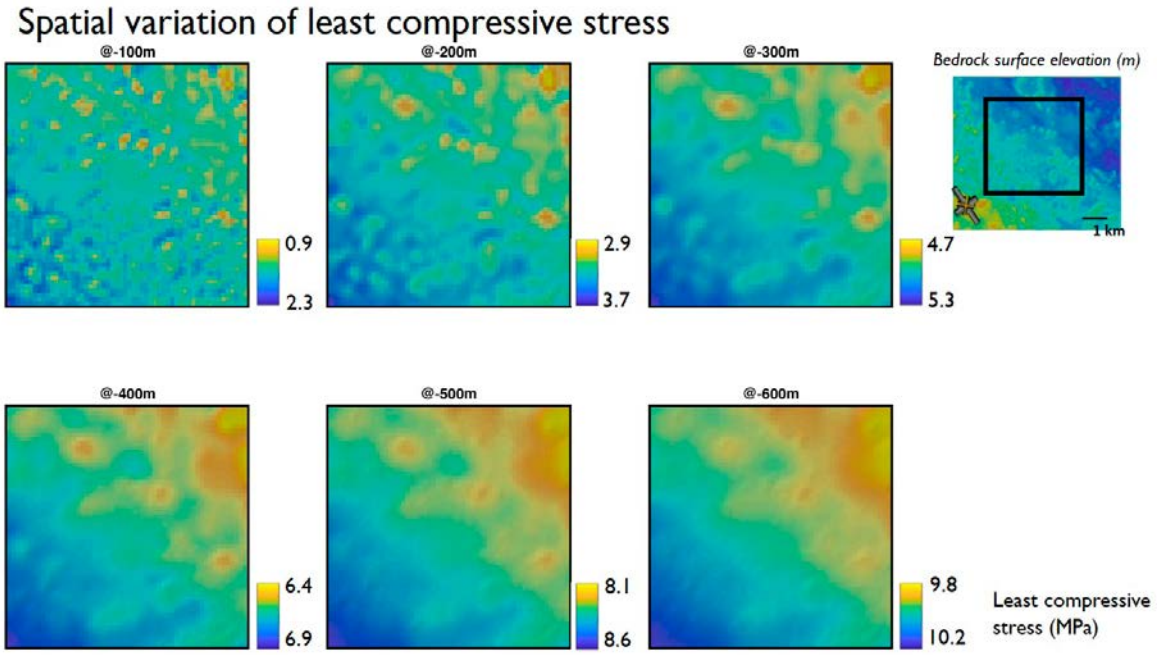

Figure 3-10. *Spatial variations of the least compressive stress field at different depths from 100 m to 600 below surface. The ambient stress condition is based on Model scenario 1, which is based on measured stress conditions at Forsmark at a depth of 0 to 150 m beneath the surface. The stress field calculation accounts for influences from the bedrock surface, sediment and water loading, and water pore pressure. The study location is shown in Figure 3-3.*

3.4 Implications of topographic perturbation of near surface stress fields for glacial erosion

Our model predictions of where topographic perturbation of near-surface stresses controls fracture opening may help us to predict the spatial pattern of erosion during the last glaciation and perhaps during the next one. This assumes that fracture opening does indeed exert control on glacial erosion. Our model predicts that sub-horizontal fractures will more likely open beneath convex landforms, particularly those with long axes oriented NE–SW (Figures 3-4 to 3-6), which is perpendicular to σ_H^t (Table 3-1; Martin 2007). This may produce higher erosion rates on ridges and lower erosion rates in valleys that display this orientation. Glacial erosion may reduce overall relief for these landforms. Conversely, the higher σ_{lc} magnitudes beneath ridges and valleys oriented parallel to the σ_H orientation may mean they are more resistant to glacial erosion and relief may persist, rather than increase or decrease. In addition, it appears that some valleys might be in tension, which would favour opening of sub-vertical fractures in these locations (Figures 3-5 and 3-6). Glacial erosion rates might therefore be higher in these valleys, potentially increasing local relief. Finally, our model also predicts an elevated potential for generating or reactivating shear fractures, especially those with an oblique dip, striking perpendicular to the σ_H orientation (Figures 3-4 to 3-6). Where these fractures intersect the bedrock surface those locations might also be more susceptible to glacial erosion. In summary, spatial variations in glacial erosion rates and resulting temporal changes in relief might partly reflect spatial variations in the near surface stress fields attributable to topographic perturbations.

Our model results also indicate that the topographic perturbation of the ambient stress fields is most important in the uppermost near-surface and declines with depth (Figures 3-4 to 3-7). The large spatial variations in the stress fields resulting from this perturbation occur over topographic wavelengths of a few hundred metres (Figure 3-10). However, the potential control on near-surface stresses exerted by shorter wavelength topography, such as that relating to individual roches moutonnées, remains uncertain. It is also difficult to test the erosion rate implications from a cosmogenic nuclide data set that displays wide spatial dispersion and is focussed primarily on bedrock outcrop summits (Chapter 6). While the model results indicate that topographic perturbations of near-surface stresses might exert control on glacial erosion rates of the bedrock surface, at least over certain topographic wavelengths, there is also little topographic influence on the opening of fractures at the planned repository depth.

There are several limitations of the stress modelling. These include: (i) we can only assess the effects of the present stress field on bedrock fracture opening; (ii) we do not account for spatial heterogeneities in stress magnitudes caused, for example, by faulting; (iii) we lack core data from the uppermost 50 m, which would allow us to better link model predictions of fracture opening with implications for glacial erosion, (v) the spatial resolution of the model is about 75 m, which is therefore the minimum outcrop dimension that can be directly assessed, and; (v) the model predicts which joints might be available for future glacial erosion based on the present topography. These results are not directly comparable to, or tested by, inferences of past glacial erosion rates from cosmogenic nuclides. Past glacial erosion has also modified the topography into its present form from an antecedent topography, which perhaps would have perturbed near surface stresses in ways that differ to those modelled for the present topography. Where curvatures have increased through erosion of outcrop flanks and/or of concavities, the topographic perturbation of the near surface stress fields is stronger now than in the past. However, where surface curvatures have decreased by, for example, the erosion of summit areas, then the topographic perturbation of near surfaces stresses is lower now than in the past. Work has been ongoing to address some of these limitations.

3.5 Summary

To further assess potential controls on glacial erosion at Forsmark, we assess how topography may perturb near-surface stress fields to control which fractures may open and where in the landscape they open. We did this using a three-dimensional boundary element model to calculate stress fields beneath the topographic surface of the Forsmark area. Influences from pore pressure and sediment loading on the near-surface stress fields are also considered. The following conclusions can be drawn:

- Topography may strongly perturb near-surface stress-fields in the uppermost 100 metres even in this low relief landscape. The topographic perturbation declines with depth and is minor at 400 m below the ground surface.
- The stress perturbation is apparent over topographic wavelengths of a few hundred metres in the uppermost 100 m but occurs over longer wavelengths (albeit with declining significance) as depth increases).
- The smaller σ_{lc} beneath landforms with negative curvatures (for example, convex ridges) indicates that fractures are more likely to open in these locations. These fractures are also more likely to be sub-horizontal and/or surface-parallel. In addition, σ_{lc} is smaller beneath topographic ridges oriented perpendicular to the orientation of σ_H^t (N145°E).
- High values for the failure potential (F), which represents the potential for sliding on shear fractures, are predicted in the uppermost 100 m, but also at −400 m depth. This indicates an elevated potential for generating or reactivating shear fractures, especially those with an oblique dip, striking perpendicular to the σ_H orientation.
- The model predicts that sub-horizontal fractures will more likely open beneath convex landforms, particularly those with long axes oriented NE–SW, which is perpendicular to σ_H^t. This may produce higher erosion rates on ridges and lower erosion rates in valleys that display this orientation. Glacial erosion may reduce overall relief for these landforms. Conversely, the higher *lc* magnitudes beneath ridges and valleys oriented parallel to the σ_H^t orientation may mean they are more resistant to glacial erosion and relief may persist, rather than increase or decrease. In addition, it appears that some valleys might be in tension, which would favour opening of sub-vertical fractures in these locations. Glacial erosion rates might therefore be higher in these valleys, potentially increasing local relief.

4 Glacial bedforms as indicators of patterns and depths of glacial erosion in NE Uppland

4.1 Introduction

Former ice sheet beds show assemblages of landforms and deposits that provide a record of ice flow, ice marginal positions and the processes that have shaped the glacier bed. In this research strand, we focus on how glacial bedforms may constrain processes, patterns and, particularly, depths of glacial erosion beneath the Fennoscandian Ice Sheet around Forsmark and in NE Uppland. Depths of glacial erosion in basement in Uppland are constrained in two ways: (i) by using the sub-Cambrian unconformity as a reference surface and (ii) by applying the ergodic hypothesis through regarding spatial variations in the forms of large glacial landforms as representing, in part, different stages in their development (Chorley et al. 1984).

The processes of glacial erosion acting through multiple glacial cycles on the hard, fractured Precambrian crystalline bedrock of the Fennoscandian Shield have produced a nested hierarchy of distinctive landscapes and landforms (Rudberg 1988). At landscape scales (10–100 km), glacial landscapes include distinct zones of glacial erosion linked to former ice sheet dynamics (Kleman and Stroeven 1997, Ebert et al. 2015). At regional scales (1–10 km), major landforms include glacial valleys (Rudberg 1988), rock basins (Johansson et al. 2001a, Roberts and Long 2005) and large hills, some streamlined in the direction of ice flow (Ebert and Hättestrand 2010). At local scales (0.1–1 km length) in Uppland, smaller hills, fracture-guided valleys and star- and box-shaped rock basins are common landforms of glacial erosion. Macro-scale (10–100 m) landforms have received particular attention previously and include roches moutonnées, whalebacks, small drumlins and crag and tails (Rudberg 1973, Glasser and Warren 1990). Glacially eroded bedrock surfaces at meso- (1–10 m) and micro- (< 1 m) scales are dominated by polished or smooth surfaces, striations and small grooves that are products of glacial abrasion and by small cliffs and sockets left when rock plates and blocks are excavated by glacial quarrying (Glasser and Warren 1990, Bennett and Glasser 2009). Structural control is pervasive at all scales on erosional forms, with eminences developed in basement rocks with low fracture densities and depressions excavated in fracture zones (Sugden and John 1976).

Basement terrain around Early Palaeozoic outliers in Sweden has landscape and regional scale features which are distinctive when compared to other lowland shields. These features have important implications for understanding how glacial erosion has modified the basement topography. Firstly, the Cambrian basement unconformity has been exhumed from beneath cover rocks over wide areas around sedimentary outliers and so represents inherited topography. In contrast, at locations distant from sedimentary outliers, present basement surfaces are likely to be entirely of epigene origin, products of processes active at or near the present Earth's surface (Twidale 2009) operating through the Neogene and Pleistocene. Secondly, Early Palaeozoic cover rocks have much lower rock mass strength than the underlying basement rocks. This implies that glacial erosion of the overlying cover rocks would have been rapid, but that the rate of glacial erosion would have slowed down once downwearing reached the hard basement unconformity. Thirdly, the Cambrian basement unconformity surface was formed by non-glacial processes. The glacial bedforms developed on the exposed basement have developed entirely since its re-exposure. Fourthly, U2 is generally flat and so it is unlike the exhumed hilly sub-Mesozoic unconformity surfaces of southern Sweden (Lidmar-Bergström et al. 2017) and epigene hilly terrains of Neogene age preserved beneath cold-based ice, such as in northern Finland (Hall et al. 2015). The flatness of the Cambro-Ordovician unconformity allows U2 to be used as a reference surface for glacial erosion (Johansson et al. 2001b). The depth of erosion below U2 is represented by height differences between bedrock highs on the edges of the buried unconformity and at increasing distances from outliers. Detailed evidence for the glacial transformation of the sub-Cambrian unconformity also comes from an analogue area around Trollhättan in Västergötland, where the original planar form and accordant elevation of the unconformity in the present landscape is closely constrained by Early Palaeozoic cover rocks found nearby (Johansson et al. 1999). A final key feature is apparent at the regional scale in Uppland and in parts of Västergötland - the sub-Cambrian unconformity surface lacked a thick weathering mantle (Elvhage and Lidmar-Bergström 1987). This situation contrasts with that found in most shield and platform areas at the onset of glaciation where epigene surfaces carried locally thick

weathering mantles (Hall and Migoń 2010). It also contrasts with conditions on the sub-Mesozoic unconformity in southernmost Sweden, where the basement was deeply weathered in fracture zones before its exhumation (Lidmar-Bergström 1995). In Uppland, roughening of U2 derives mainly from glacial erosion of variably fractured, hard bedrock whereas, in other basement terrains, glacial erosion has also included the removal of significant depths of weathered rock (Glasser and Hall 1997). Topographic roughness developed in response to glacial erosion of basement thus derives from at least two separate components: inherited roughness from an irregular weathering front and heterogeneity of fracture density of bedrock. Where U2 was flat and unweathered when exhumed by Pleistocene glacial erosion, roughness derives from exploitation of fracture patterns.

4.1.1 Aims

This section is focussed on glacial landforms in NE Uppland and the Forsmark area. The main aims of this research strand are to:

- Map landscapes and landforms of glacial erosion at the regional (1–10 km) and local (0.1–1 km) scales using LiDAR imagery in Digital Elevation Models (DEMs).
- Provide an inventory of smaller glacial landforms based on field observations at the macro (10–100 m), meso (1–10 m) and micro (< 1 m) scales.
- Link landforms to sets of glacial processes operating at different scales grouped as abrasion, plucking, ripping, thrusting and meltwater erosion.
- Assess the timing of re-exposure of the basement from beneath cover rocks and the likely depths of sedimentary rock removed during the Pleistocene.
- Estimate depths of glacial erosion in basement using the dislocated sub-Cambrian unconformity (U2) as a reference surface, and through morphological comparisons between and across large, flat-topped, exhumed fault blocks.
- Use field evidence from micro- to meso-forms on roche moutonnée surfaces to assess the likely processes operating on these surfaces in relation to erosion depths and rates estimated from cosmogenic nuclide inventories.

In the present study, we have identified a hitherto unrecognised process set of glacial erosion that has operated in the Forsmark area which we term *glacial ripping*. Mapping by the Swedish Geological Survey has shown that boulder spreads, with blocks 1 to 5 m long, are developed over wide areas in Uppland and eastern Sweden. At many localities, these blocks can be traced to nearby bedrock outcrops that have been disrupted and displaced by shallow glaciotectonics operating at the base of the Fennoscandian Ice Sheet. Hydraulic jacking of bedrock observed in excavations in and around the Forsmark site (Carlsson and Christiansson 2007) (Figure 2-26) is interpreted as a precursor to this disruption. Widespread glacial ripping of bedrock is an overlooked but important process of glacial erosion, capable of mobilising bedrock to depths of several metres late in a single glacial cycle. The glacial entrainment of bedrock blocks 1–20 m long and of different shapes has been modelled in a separate study under different ice thicknesses and glaciological conditions (Krabbendam and Hall 2019).

4.1.2 Controls on glacial erosion

The main controls on glacial erosion are summarised in Figure 4-1. Rock and topographic controls remain invariant or change slowly through time but glaciological controls vary within glacial cycles as an ice sheet builds up and decays. We summarise below the operation of these controls in the specific context of the Forsmark area.

Timing and duration of Pleistocene glaciation

The number, timing and duration of periods of glaciation determine the maximum period of time over which processes of glacial erosion may have acted on the glacier bed (Kleman et al. 2008). Since the onset of extensive glaciation on the Canadian shield at 3.5 Ma (Gao et al. 2012) and in Fennoscandia at 2.75 Ma (Laberg et al. 2012), the Forsmark area has undergone many cycles of ice sheet growth and retreat during the Late Cenozoic (Mangerud et al. 1996, Kleman et al. 1997).

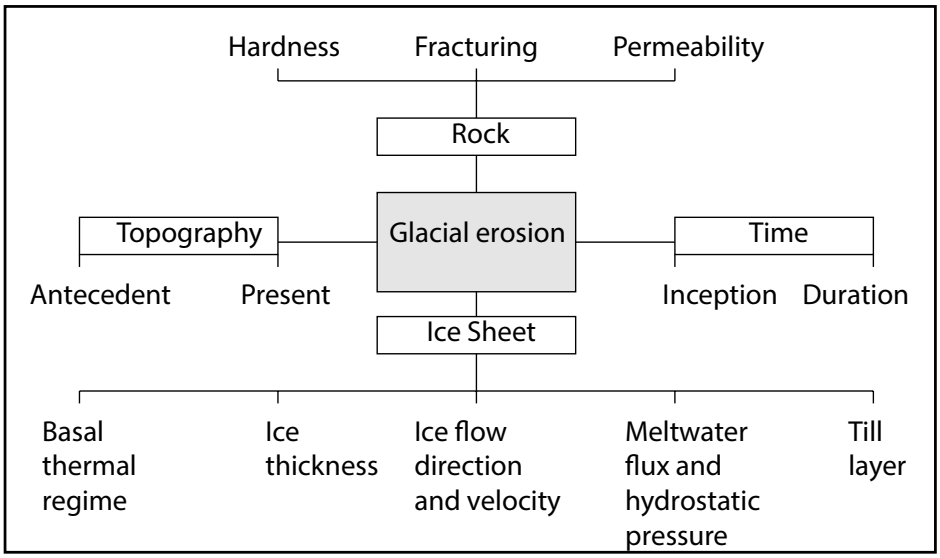

Figure 4-1. *Main controls on glacial erosion.*

The Laurentide Ice Sheet advanced close to Pleistocene maximum limits as early as 2.4 Ma (Balco et al. 2005), at around the same time as the first major climatic deterioration of the Pleistocene in northern and central Europe (Litt et al. 2008) and the first large influx of glacigenic debris from the Fennoscandian Ice Sheet in the Norwegian Sea (Mangerud et al. 1996). Marine isotope curves and offshore glacial sediments indicate a gap of around 1 Ma before the Laurentide Ice Sheet again reached close to Early Pleistocene maximum limits (Balco et al. 2005). In Fennoscandia, ice sheet glaciation extended onto the shelf off SW Norway and excavated or deepened the Norwegian Trench during the Menapian Stage (Marine Isotope Stage (MIS) 36 or 34) at ~−1.2–1.1 Ma (Sejrup et al. 2005, Reinardy et al. 2017, Ehlers et al. 2018). In the Netherlands and central North Sea, the Menapian cold stage is marked by the presence of marine foraminifera of high arctic affinities (Ekman 1999). The admixture of Palaeogene-Neogene and Pleistocene pollen in sediments from this cold stage (Laban and van der Meer 2011) is consistent with erosion of preglacial soils and deposits by an extensive Fennoscandian Ice Sheet. The Hattem gravels of the Menapian in the Netherlands carry major quantities of clasts from eastern Fennoscandian and central Swedish (Dalarna) source areas (Zandstra 1983, 1993). Menapian tills are recognised in Poland (Ber et al. 1998), where this cold stage has been placed at ~1.4 Ma (Lindner and Marks 2008). The Menapian ice advance, however, did not reach N Germany (Ehlers et al. 2011) or the Netherlands (Laban and van der Meer 2011). After this phase, the distinctive Baltic Gravel Assemblage, which largely consists of clasts derived from the Lower Palaeozoic rocks of southern Scandinavia (Gibbard and Lewin 2016), disappears from the Pleistocene sequences in Denmark and northern Germany (Bijlsma 1981). The change indicates destruction of the northern part of the Eridanos drainage, including the Bothnian river system (Overeem et al. 2001), and first excavation of the Skagerrak and Kattegat basins (Houmark-Nielsen 2004) by the Menapian ice sheet. The onset of excavation of the overdeepened basins of the Bothnian and Baltic Seas probably also dates from this time.

Full ice-sheet conditions became dominant in Fennoscandia under the 100 ka climate cycles of the Middle and Late Pleistocene. The ‘major’ worldwide events with substantial ice volumes that typify the later Pleistocene glaciations occurred over the last 1 Ma-800 ka or less (i.e. MIS 16, 12, 10, 6, 4–2) (Ehlers et al. 2018). Deep glacial erosion is recognised through this period in SW Norway (Sejrup et al. 2003) and NE Scotland (Glasser and Hall 1997). Till stratigraphy indicates that the Fennoscandian Ice Sheet extended into Poland during at least 7 separate phases of glaciation (Marks 2011). Tills recognised in Lithuania (MIS 16) (Baltrūnas et al. 2019) and in NE Poland (MIS 18) (Ber et al. 1998) date from the early Middle Pleistocene. The maximum extent of the Fennoscandian Ice Sheet in NW Europe was reached in the Elsterian (MIS 12) and Late Saalian (MIS 6) cold stages (Ehlers et al. 2011). Tills deposited during these glacial phases in Poland contain indicator erratic clasts sourced from Uppland (Czubla et al. 2019). The Elsterian glaciation represents a major phase of glacial erosion, with removal of almost all earlier sediment from around the present Bothnian

and Baltic Seas (Šliaupa and Hoth 2011), erosion of the Åland rapakivi granites as shown by large numbers of these clasts in tills in Poland (Czubla et al. 2019), cutting of tunnel valley networks in the southern Baltic (Flodén et al. 1997) and remodelling of the drainage systems of northern Germany (Ehlers et al. 2011).

The Weichselian glacial cycle started at 115 ka and is reviewed elsewhere (SKB 2010, Helmens 2019). The marine record for the Early Weichselian (MIS 5d–5a) shows two relatively warm interstadial periods at 105–93 ka (MIS 5c) and 85–74 ka (MIS 5a). Intervening interstadials are thought to have been accompanied by the development of mountain ice sheets (Kleman et al. 2008). At 90–80 ka, ice sheet models indicate that the Fennoscandian Ice Sheet was of sufficient extent to approach or cover the Forsmark area (Svendsen et al. 2004) and may have advanced over permafrost (Näslund et al. 2008). During the MIS 4 stadial, the Fennoscandian Ice Sheet covered large parts of or all of Sweden, Finland and Norway, including the Forsmark region (Schmidt et al. 2014). The duration of ice cover and the ice thickness at this time, however, remain uncertain (Mangerud et al. 2011). Another uncertainty is the thickness and distribution of till cover, a consideration in the interpretation of cosmogenic nuclide inheritance in rock surfaces. Climatic deterioration after 37–35 ka (Wohlfarth 2010) led to merging of mountain ice caps (Patton et al. 2016). The main Late Weichselian glaciation commenced in late MIS 3 after ~32 ka (Lundqvist 2004) and the Fennoscandian Ice Sheet was already at limits in Jutland by ~29–27 ka (Houmark-Nielsen and Kjaer 2003), requiring rapid build-up and advance of the ice sheet. The last glacial maximum (LGM) was reached in Denmark at 22–21 ka (Hughes et al. 2016, Stroeven et al. 2016). During the Younger Dryas stadial (12.9–11.7 ka), the Fennoscandian Ice Sheet margin extended across central Sweden (Lundqvist 1987) at a position ~150 km S of Forsmark. Deglaciation of the Forsmark site was complete by 10.8 ka (Persson 1992, Stroeven et al. 2016).

Modelling experiments for the Fennoscandian Ice Sheet have provided insights into the duration of ice cover in the Forsmark area. The duration of ice cover over the last 1 Ma was ~300 ka (Figure 4-2), leaving ~700 ka for denudation by non-glacial processes. Models for the Fennoscandian Ice Sheet in the last glacial cycle indicate ~40 ka of ice cover at Forsmark over the last 120 ka (Näslund 2006, Schmidt et al. 2014). The duration of ice cover is considered further in the next chapter in modelling of erosion rates based on cosmogenic nuclide inventories.

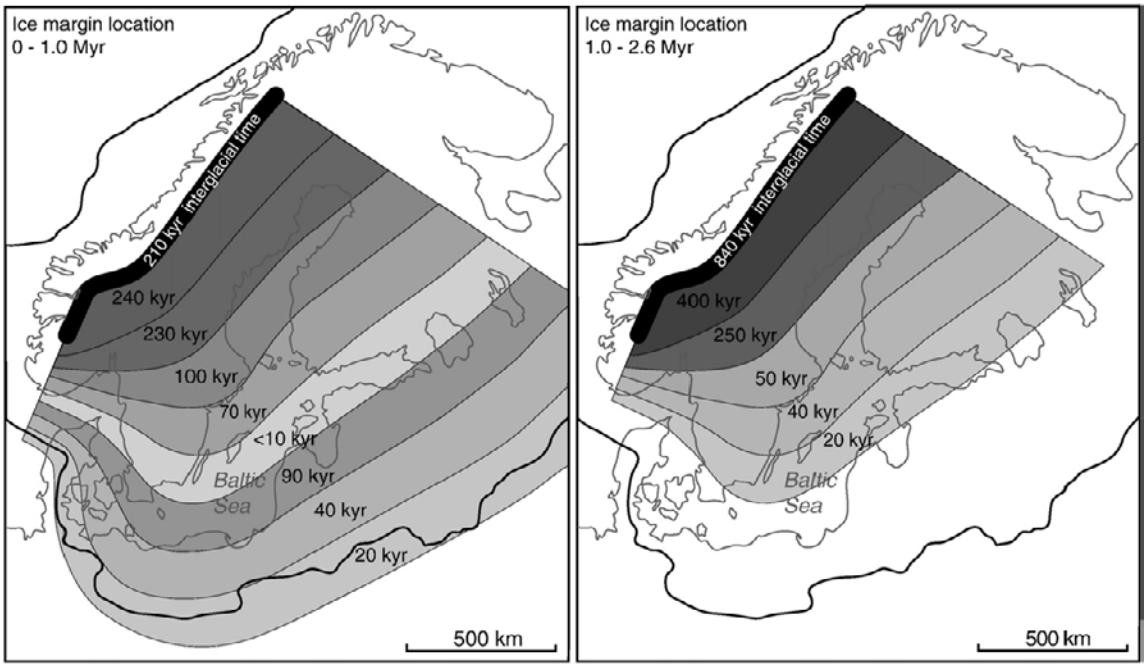

Figure 4-2. *The estimated length of time that the Fennoscandian Ice Sheet margin resided within different zones between 1.0–2.6 Ma and 0–1.0 Ma. The Forsmark area lay within the marginal zone for an estimated total duration of 100 ka and was covered by the Fennoscandian Ice Sheet for ~330 ka over the last 1 million years (reproduced from Kleman et al. 2008).*

Rock type and fracturing

Rock type and structure are important controls on patterns, processes and rates of glacial erosion. At the onset of Pleistocene glaciation, the substrate of the Fennoscandian Ice Sheet in the Forsmark area and its surroundings comprised two main rock types of contrasting resistance: Ordovician Limestone and Proterozoic crystalline rocks.

Today, Ordovician Limestone is confined to small outliers offshore from Forsmark (Figure 2-8) but formerly limestone covered the basement of Uppland and it likely remained much more extensive than today at the start of the Pleistocene. The Ordovician limestone is soft, near horizontally bedded, vertically jointed and highly permeable (Lindskog et al. 2018). The underlying, thin Alum Shale was thinly bedded and soft (Andersson et al. 1985).

The Svecokarelian crystalline rocks of Uppland include rocks derived from felsic, intermediate and mafic protoliths of diverse origin (Stephens 2010) (Figure 2-1). At Forsmark, four main rock domains are recognised, each of which subsumes a range of lithologies (Figure 4-3). The main sets of fractures at Forsmark as summarised in cross-section in Figure 4-4. The crystalline rocks provided a different substrate for the Fennoscandian Ice Sheet to the Ordovician limestones and shales. The crystalline rocks are hard, with a wide range of fracture spacings and orientations (Stephens 2010) (Figure 4-5). Permeability is generally low at Forsmark except in steeply and gently dipping deformation zones, in zones with horizontal fractures and in the uppermost part of the bedrock associated to the Fracture Domain 2 (FFM02) (Follin et al. 2007).

Topography of the ice sheet bed

Topography influences ice sheet flow through a direct influence on converging or diverging flow and through an indirect influence on basal temperatures (Sugden 1978). At the regional scale (1–10 km), relief amplitude in Uppland (less than 20 m) in relation to ice sheet thickness (more than 2 km) is negligible and likely exerted little influence in directing ice sheet flow. At the onset of Pleistocene glaciation, an antecedent topography likely existed on horizontal or gently dipping Ordovician limestone that may have included gentle slopes and homoclinal scarps, similar to that found on gently dipping Devonian strata in the Baltic States today (Baltrūnas et al. 2019). Progressive re-exposure of the underlying sub-Cambrian unconformity exhumed a basement surface of low relief broken by faults into a mosaic of rock blocks (Figure 2-21).

The marine basins of the Bothnian Sea and the wider Baltic Sea occupy depressions that extend below present sea level (Figure 2-6). The Åland Deep, a submarine basin that reaches a depth of −290 m between Åland and Uppland, is by far the largest rock basin in the region, a product of glacial overdeepening within a Jotnian half-graben (Amantov et al. 2011). The Deep and the developing Bothnian Sea depression likely exerted increasing topographic control over ice sheet flow through Middle to Late Pleistocene glaciations (Arnold and Sharp 2002).

Glaciological controls

Ice thickness

Ice thickness is an important control on overburden and groundwater pressure at and below the ice sheet bed (Hökmark et al. 2010, Vidstrand et al. 2013). The Late Saalian (MIS 6) ice sheet is estimated to have reached a thickness of 3.0–3.5 km in the Forsmark region in ice sheet models (Colleoni et al. 2014, Quiquet et al. 2016). Weichselian (MIS 5d-2) ice sheet simulations indicate that the Fennoscandian Ice Sheet at Forsmark reached a maximum thickness of 1.5 km in MIS 4 (Näslund 2006) and 2.4–3.0 km at the LGM (SKB 2010, Schmidt et al. 2014). During the Younger Dryas stadial, when the ice front stood south of Stockholm, the ice thickness at Forsmark is estimated as ~1 km (SKB 2010). Assuming similar ice sheet profiles in earlier glacial phases, the thickness of the Fennoscandian Ice Sheet at Forsmark was less than 1 km only in periods when the ice margin stood within its Younger Dryas limits. It is argued later that several processes of glacial erosion are enhanced beneath thin ice; hence, the Younger Dryas phase may provide a useful analogue for the glaciological drivers of effective erosion.

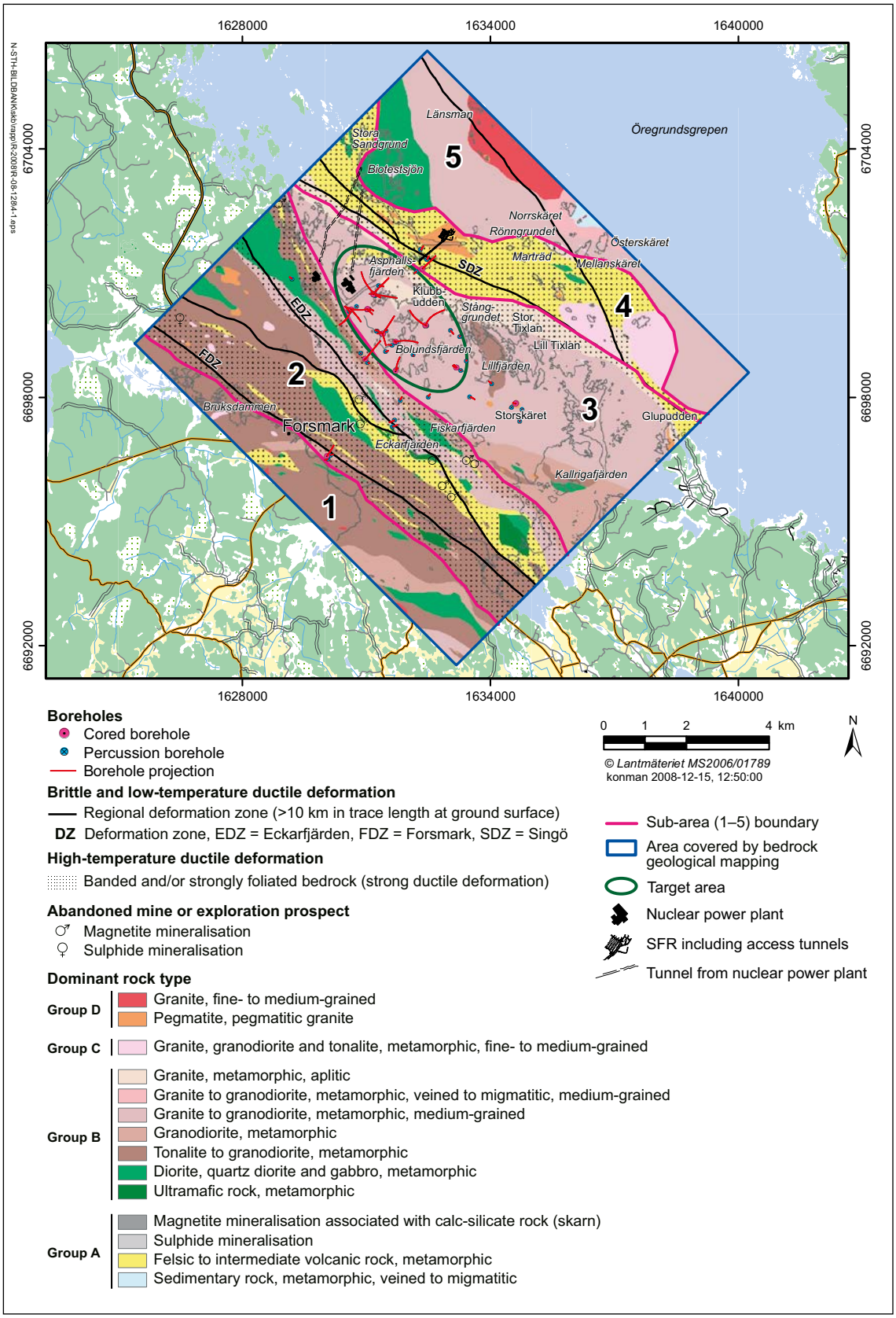

Figure 4-3. *Simplified bedrock geological map of the Forsmark area. Deformation zones with a trace length at the ground surface greater than 10 km, abandoned mines or exploration prospects and boreholes drilled during the site investigation programme are also shown on the map. The rock type subareas 1–5 are distinguished on the basis of the general character of the ductile deformation in combination with the degree of homogeneity of the bedrock, as revealed during geological mapping. Reproduced from Stephens et al. (2008a).*

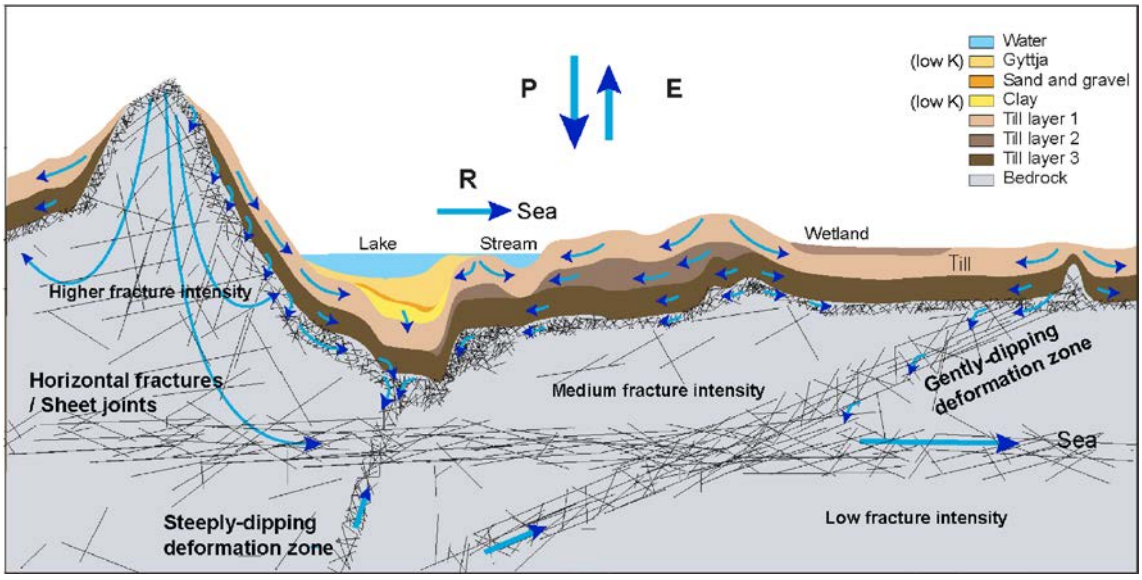

Figure 4-4. *Cross-section cartoon to illustrate fracture patterns, regolith and groundwater hydrology in the upper 150 m of the rock around the proposed repository at Forsmark. P = precipitation, E = evapotranspiration, and R = runoff. Reproduced from Follin et al. (2007).*

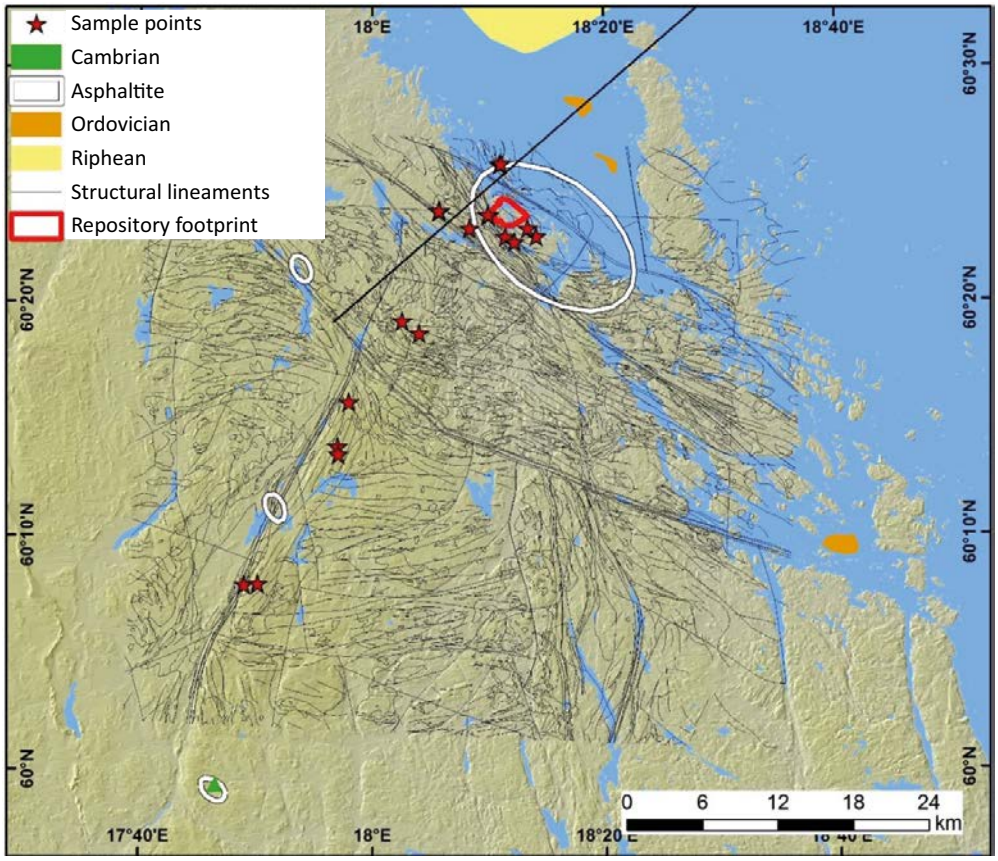

Figure 4-5. *Structural lineaments around Forsmark from SGU data. From N–S, the deformation zones oriented WNW–ESE are Singö, Eckarfjärden and Forsmark (see Figure 2-5). The ENE–WSW oriented fracture zone defines the W edge of the Ironworks block. Asphaltite is widely present in boreholes in the Forsmark area. Sample points refer to cosmogenic nuclide sample sites. Structural lineaments shown as thin black lines. SW-NE transect lines parallel to the thick black line are shown in Figure 2-11.*

Basal thermal regime

Glacier basal thermal regime is a fundamental control on glacial erosion (Kleman et al. 2008). In cold-based glaciers, the basal ice remains below the pressure melting point and movement takes place mainly through internal deformation of the ice rather than through sliding across the bed. Hence glacial erosion is negligible or zero in zones of permanently cold-based glacier ice. Repeated development of cold-based basal conditions below the Fennoscandian Ice Sheet is linked to the extensive preservation of periglacial and preglacial regolith and landforms in parts of northern Fennoscandia (Lagerbäck 1988a, Kleman 1992, Ebert et al. 2011, Ebert et al. 2012a) and at high elevations in the Scandes mountains (André 2004, Goodfellow et al. 2008). Such remnants are lacking in Uppland and instead the ubiquitous presence of striae, polished surfaces and crescentic marks on rock surfaces indicates that the Fennoscandian Ice Sheet was warm-based and sliding during at least the latter part of the last glacial cycle and likely also during earlier cycles (Figure 4-6). The Late Weichselian ice sheet advanced on to permafrost in the Forsmark area (Hartikainen et al. 2010) and likely remained cold-based for a short period during its build-up (SKB 2010), switching to dominantly warm-based conditions later (Arnold and Sharp 2002). A fast-flowing Baltic Ice Stream extended deep into the interior of the Fennoscandian Ice Sheet during ice sheet drawdown phases (Patton et al. 2016).

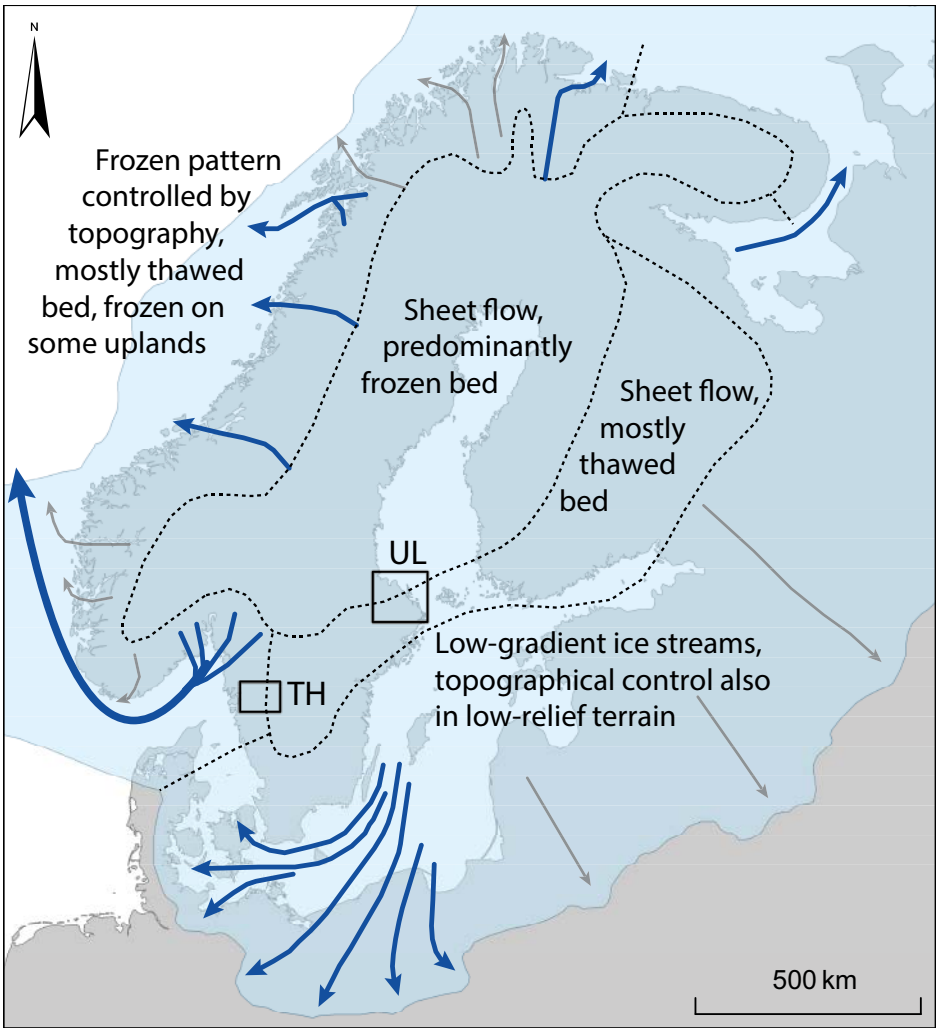

Figure 4-6. *Long term average Pleistocene basal thermal regime of the Fennoscandian Ice Sheet (Kleman and Glasser 2007). Forsmark lies at the boundary of zones with a predominantly frozen bed and a mostly thawed bed. UL Uppland. TH Trollhättan.*

Ice flow direction and velocity

Directions of former ice flow have been reconstructed in NE Uppland from striae, till fabrics and indicator erratics (Persson 1992, Sohlenius and Rudmark 2003, Sohlenius et al. 2004) (Figure 4-7). In the Forsmark area, a lower carbonate-rich till unit is overlain by one or two younger tills (Albrecht 2005). The lower till is over-consolidated, dark grey in colour, with a high (~15 %) clay content and a high (20–30 %) content of Palaeozoic limestone in the gravel fraction (Forssberg et al. 2007). Palynomorphs from thermophilous trees are present in the till matrix (Robertsson et al. 2005) and are also found in silt that fills open, sub-horizontal fractures at Forsmark (Robertsson 2004). The pollen is reworked and likely derived originally from vegetation cover that existed in MIS 5 (Robertsson et al. 2005). The lower till has been interpreted as a subglacial diamicton deposited during advance of the MIS 6 (Björnbom 1979) or MIS 4 ice sheet (Robertsson et al. 2005) by ice moving from the N (Sundh et al. 2004).

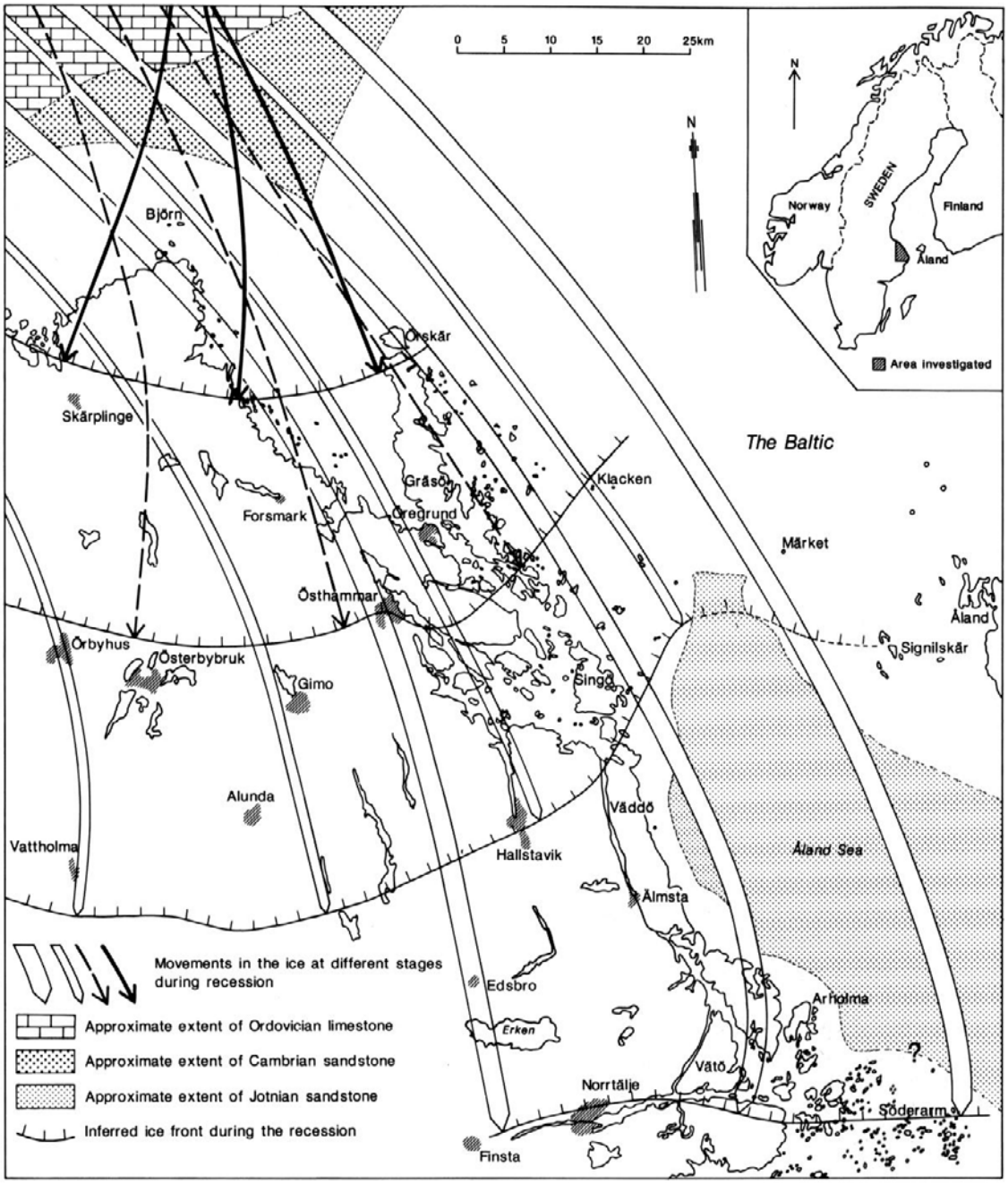

Figure 4-7. *Ice flow directions during Late Weichselian deglaciation in NE Uppland (Persson 1992).*

The upper tills are less hard to loose, sandy diamictons, with lower carbonate contents. In excavated trenches, underlying polished bedrock displays glacial striae with orientations from NW (300–320°) and N (345–20°), with the former set representing the oldest ice flow (Sohlenius et al. 2004). The younger striae from the north were mostly found at shallow depths, less than 1.5 m, and most likely the younger northerly ice flow influenced only the upper parts of the till deposits (Sundh et al. 2004). The upper till units were deposited by ice moving from the N through NNW during the youngest regional ice movement (Hedenström 2004). Similar flow directions during ice retreat are indicated by Mega-Scale Glacial Lineations (MSGLs) on the sea bed N and E of Forsmark (Greenwood et al. 2017).

Forsmark stands in a zone of scoured bedrock that stretches for 800 km along part of the Swedish east coast and across the Åland islands (Kleman et al. 2008). To an extent, this zone reflects wave washing and removal of till during emergence (Olvmo 2010) but the scoured bedrock is also located on the western edge of a zone of fast ice flow seen in ice sheet models to flow towards and through the Åland Deep (Holmlund and Fastook 1993, Arnold and Sharp 2002, Clason et al. 2016, Patton et al. 2016, Greenwood et al. 2017). Modelled cumulative sliding distances for the last ice sheet along the Bothnian depression were large (Figure 4-8; after Näslund et al. 2003), providing considerable potential for efficient glacial erosion in this depression.

Models of ice velocities and basal thermal regime have been developed for the Fennoscandian Ice Sheet in south-eastern Sweden during a dynamic phase of the deglaciation, around 14 300 years before present. Ice velocities remained below 150 m/yr except in the marginal zone where velocities of up to 500 m/yr are simulated, with associated high (more than 5 mm/yr) rates of basal melting (Näslund et al. 2005).

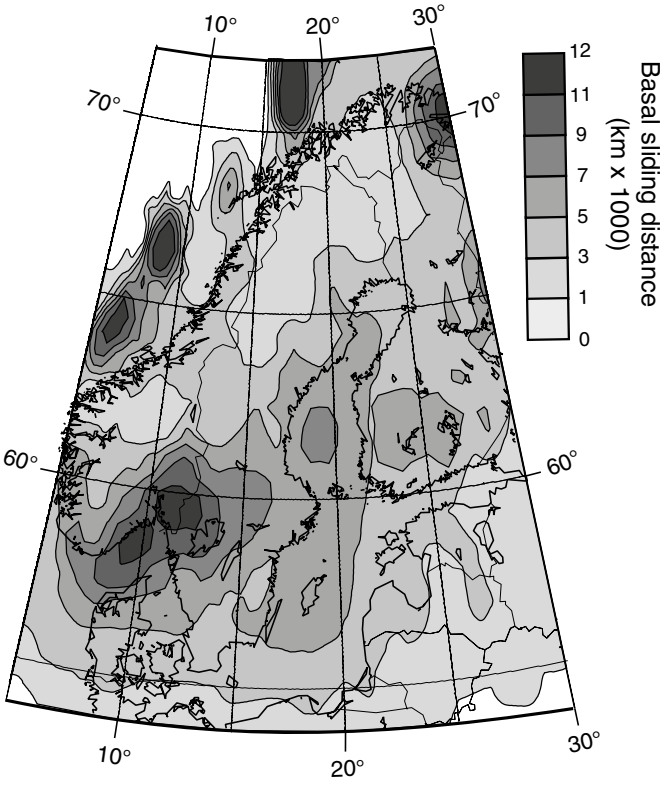

Figure 4-8. *Distribution of modelled cumulative basal sliding distance over Fennoscandia during the last glacial cycle (modified from Näslund et al. 2003). The parameter describes potential glacial erosion when considering the ice sheet basal thermal regime, amount of basal sliding and bed topography. The Uppland and Forsmark areas have intermediate values.*

Glacial hydrology

The drainage systems of present and past ice sheets and glaciers are highly dynamic and continually adjust to the available amount of melt water. The primary driving force for groundwater flow below and in front of an ice sheet is the hydraulic pressure gradient. This gradient is greatest close to the ice margin and particularly influenced by steepness of the ice margin and by the rate of ice advance and retreat (Vidstrand et al. 2013, Claesson Liljedahl et al. 2016). During the retreat from the Younger Dryas ice sheet limit (Lundqvist 1987), very large volumes of meltwater were generated that led to development of glacial erosion forms of regional and local extent in the Bothnian Sea (Greenwood et al. 2016, Holmlund et al. 2016), to the excavation of meltwater canyons in central Sweden (Jansen et al. 2014), and to formation of arrays of micro- and meso-forms in the Åland Sea archipelago (Strömberg 2010). Recent models of the subglacial hydrology of the Fennoscandian Ice Sheet indicate that large subglacial lakes and meltwater drainage pathways were abundant (Shackleton et al. 2018). Routing of subglacial meltwater was mainly via the Tierp-Uppsala trench and the Åland Deep under full ice sheet conditions but smaller ice sheets, such as those simulated for 30 ka and 11.6 ka routed meltwater through many smaller N–S orientated trenches across Uppland (Shackleton et al. 2018).

Basal debris

Debris at the ice sheet base provides the tools for abrasion but may also act as a protective barrier between the sliding glacier ice and the bedrock (Sugden and John 1976). Tills at Forsmark include high concentrations of sand, gravel and boulders derived from hard crystalline rocks indicating a high potential for abrasion across bedrock surfaces of equivalent or lesser hardness. High matrix carbonate concentrations in tills in E Uppland (Ingmar and Moreborg 1976) indicate that softer Ordovician limestones have been eroded from offshore in large volumes and strongly comminuted during glacial transport.

Present day till distribution around Forsmark has been strongly influenced by the large scale morphology of the bedrock surface and by washing of glacial deposits during post-glacial emergence (Sohlenius et al. 2013). Elevated areas of bedrock today have generally thin (less than 2 m) or no sediment covers. Around Forsmark, when areas with bedrock outcrops are excluded, the average modelled regolith depth is 6.5 m. The maximum depth of regolith is 42 m. The average regolith depth in the terrestrial area is 4.0 m at Forsmark but increases to 8.3 m in the marine part (Hedenström et al. 2008). The difference in thickness in terrestrial and marine settings indicates that an approximate thickness of more than 4 m of glacial deposits has been redistributed during emergence.

4.1.3 Processes of glacial erosion

We recognise five main sets of glacial processes that may have operated widely to erode the bedrock of the Forsmark area:

- Abrasion, whereby the glacier bed is scored by debris carried in the sole of the glacier.
- Plucking, the removal of fracture-bounded blocks of rock from small cliffs.
- Ripping, the entrainment of extensive rock layers by traction at the glacier base in response to the reduction of frictional resistance during build-up of overpressure in bedrock fractures.
- Thrusting, where thin-skinned glaciotectonics may have mobilised frozen or unfrozen bedrock.
- Meltwater erosion in rock channels.

The signatures of these processes are present in landforms of glacial erosion at different scales. Abrasion is evident from polished, striated and smoothed rock surfaces seen at the micro- to macro-scales (Glasser and Bennett 2004). The former action of plucking in block removal is apparent from sockets and small lee-side and flank cliffs at scales of 1–10 m (Glasser and Warren 1990, Krabbendam and Glasser 2011). The combined operation of abrasion and plucking is responsible for the characteristic stoss-lee form of roches moutonnées at scales of 10–250 m (Rastas and Seppälä 1981). Ripping produces boulder spreads that extend over distances of a few metres to kilometres. The markers for thrusting in sedimentary rocks and soft sediments include hill-hole pairs and glacial rafts (Seppälä 2016, Phillips 2018). It is uncertain whether or not thin-skinned glaciotectonics operated effectively in fractured basement during the Pleistocene, but this mechanism is one of

several considered later that may contribute to the glacial excavation of large rock basins. Meltwater is an important component in all erosion processes but meltwater moving at high velocities provides potential for erosion of large volumes of bedrock (Maizels 1989). Specifically, meltwater may play a dominant role in the cutting of channels and canyons in bedrock (Olvmo 1985, Jansen et al. 2014).

4.2 Methods

4.2.1 GIS mapping of glacial landscapes and landforms at the regional and local scales

Digital elevation and bathymetric data were combined to a common digital elevation model (DEM). The onshore elevation data has a horizontal grid resolution of 2 × 2 m and is based on the national elevation model (Nationella Höjdmodellen) produced by Lantmäteriet. Bathymetric contour lines from the Swedish Maritime Administration (Sjöfartsverket) were used to interpolate a sea floor surface using a combination of the Topo-to-Raster and Aggregate functions in ArcGIS with a final horizontal resolution of 50 × 50 m. This resolution was chosen in order to bridge the difference between the high-resolution terrestrial elevation and the contour-based bathymetric data. Existing SGU data, maps and reports on basement and Quaternary geology represent a fundamental resource for the generation of new maps and diagrams in this report.

Regional landscapes (1–10 km)

The main features of the relief on the dislocated U2 surface are described in Section 2.3. Mapping of glacial bedforms at the regional scale is focussed on NE Uppland. In this study, we map in LiDAR imagery the distribution and form of flat-topped, low relief bedrock surfaces on upstanding, 3–15 km wide, fault blocks, and large rock basins, with floors buried by till and post-glacial deposits, at lower elevations. The glacial landforms are later compared to the antecedent topography on U2 to identify patterns and to estimate depths of glacial erosion.

Local landforms (0.1–1 km)

Local landforms are mapped mainly from DEMs, with ground truthing, across NE Uppland and within the Forsmark area. Individual streamlined hills have been mapped over an area of ~1 000 km^2 using a national hill shade model at 1 m resolution. Fledermaus software is used for profile generation and analysis. The mapped landforms have been superimposed in ArcGIS on existing SGU datasets. The DEM's (2 m and 50 m) together with the soil cover, bedrock geology and bedrock depth maps were provided by SGU (available at https://zeus.slu.se/get/?drop=). The DEM's were resampled to a 1 m and 10 m resolution to improve visual interpretation, using ArcMap 10.6. The modified diagrams from previous studies were first georectified using the overview map provided by SGU as a base map. Features such as faults and lithologies were then superimposed as a separate layer and modified in ArcMap 10.6 and Adobe Illustrator CS 6.

Ground surface profiles were made by drawing transects over the DEMs covering the Uppland area, using ArcMap 10.6. The individual profiles were stacked in Excel for visual interpretation.

The geological lineaments were identified and mapped using the DEMs according to their morphological characteristics based on visual interpretation. A length-weighted rose diagram was produced on basis of the mapped features. The main orientations of the lineaments were determined by first assessing the geographical starting point (x1, y1) and end point (x2, y2) of each drawn polyline in an UTM grid. The angle between the two points was then calculated in the field calculator, using the following formula:

$$tan{-}1\ ((x2 - x1),(y2 - y1)) \times 180\ \pi \qquad (4\text{-}1)$$

In the attribute table, the angle of each drawn polyline relative to north was obtained. By inserting the length of each polyline into the attribute table, it was possible to plot the data into a length-weighted rose diagram, using MATLAB script available at https://se.mathworks.com/matlabcentral/fileexchange/65009-weighted-rose.

Around Forsmark and at all sample sites proposed or chosen for cosmogenic nuclide sampling in Uppland, the form of individual hills was examined in the field using DEMs as base maps. The presence or absence of 10 different landforms of glacial erosion at the local scale was logged at these and other key sites as part of a wider landform inventory (Appendix 1). Detailed maps of glacial sediments are available for the proposed repository footprint area at Forsmark and its immediate surroundings (Sohlenius et al. 2004).

Three terrain types were identified on the basis on landform assemblages mapped and observed at the local scale: glacially roughened, streamlined and disrupted terrain. Each terrain type is described in detail and linked later to processes of glacial erosion. To visualize terrain roughness in NE Uppland, mean, minimum and maximum elevation surfaces with 10 x10 cell search windows were created based on the 2 m LIDAR DEM from Lantmäteriet. The Relative Topographic Position (RTP), is an index of the local topographic position of a site relative to its surroundings (Newman et al. 2018). RTP is an index of topographic roughness, calculated using the Arc-GIS raster equation (MEAN-MIN)/(MAX-MIN) (Jenness 2004, Cooley 2013) To improve the visual output, a mean surface model based on a 50 × 50 cell search window was generated from the 10 × 10 cell based RTP map. (See Table 4-1 for more detailed workflow).

The frequency of boulder cover has been mapped in Uppland by SGU at 1:25 000 to 1: 100 000 scales using air photos and field mapping. Four boulder cover types are recognised: A. Block-rich to large block-rich surface (Blockrik till storblockig yta). B. Block-rich surface (Blockrik yta). C. High block frequency on different soil type than moraine (Hög blockfrekvens på annan jordart än morän). D. Large block-rich surface (Storblockig yta). South of Storfjärden (Figure 4-9), it is clear that different categories previously have been used to map similar boulder spreads on different map sheets. In this study, the boulder cover categories are merged for NE Uppland and for the Forsmark area. Field checking indicates that the boulder covers are largely composed of large, angular rock blocks that form extensive *boulder spreads* that locally mantle and mask rock surfaces. Boulder spreads provide important evidence of glacial ripping.

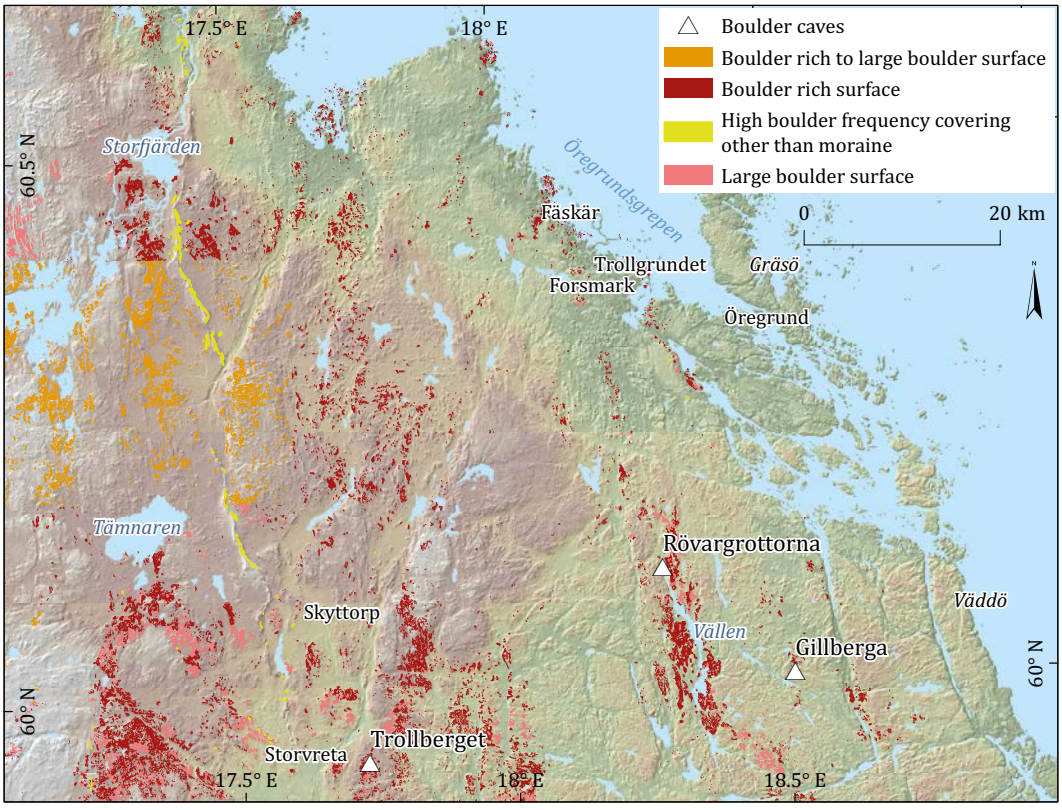

Figure 4-9. *SGU classifications of boulder spreads in Uppland. Continuity across map sheets indicates that the different categories can be grouped. One exception is the high boulder frequencies found on esker tops, such as the large esker (yellow) seen south of Storfjärden.*

4.2.2 Field mapping of glacial landforms at the macro to micro scales

We have gathered data for an inventory of the presence-absence of 60 features of glacial erosion at 49 sites across NE Uppland at four scales: local (0.1–1 km), macro (10–100 m), meso (1–10 m) and micro (< 1 m) scales (Appendix 1). Regional and local landforms were interpreted from DEMs based on LiDAR data whereas features at the macro- to micro- scales were recorded in the field. The field sites include almost all sites sampled for cosmogenic nuclide analysis. Presence-absence data is used widely in ecology (Manel et al. 2001). Typically, abiotic or biotic variables are used to predict the abundance, presence or absence of the target organisms. Applications in geomorphology are less common but are important in predictive models (Miska and Jan 2005). Presence-absence data are quick to collect and so allow landforms at multiple sites to be surveyed in a short time. Such data complements but does not replace geomorphological mapping (Thiery et al. 2007).

The data set indicates the frequency and distribution of different features of glacial erosion at each scale. Associations between features are also apparent across scales. Some glacial landforms can be regarded as diagnostic of particular processes of glacial erosion. For example, glacial abrasion produces striae, glacial plucking forms lee side cliffs on roche moutonnées and glacial ripping can lead to development of boulder spreads. Other landforms are products of the interaction of several processes of glacial erosion. A classic example is provided by roches moutonnées that are regarded as products of abrasion and plucking operating together to shape small rock obstructions under deforming basal ice layers (Sugden and John 1976). Some landforms, particularly those of negative relief, are of less certain origin. For example, box and prismatic sockets are common meso-forms on some rock surfaces in Uppland but have received little previous attention. Presence-absence data for glacial features is useful in this study of glacial erosion around Forsmark and also in other contexts (Bradwell 2013) as the data allow identification of the main landforms at different scales and point to the main processes involved. The presence-absence data can be related to depths of glacial erosion predicted from models and cosmogenic nuclide inventories.

Field recording of small features of glacial erosion involves a bias towards exposures on upstanding rock surfaces. This survey includes shallow subsurface micro- and mesoforms but where the sample site surroundings are obscured by soil and vegetation or where no sections are available in near-surface bedrock to check for then then the presence or absence of these features is unknown and *Don't know* was recorded.

Glacial disruption is a process set that involves the jacking, dilation and disintegration of rock in the near surface and the entrainment of the resultant rock blocks to form boulder spreads and boulder moraines. Evidence of bedrock disruption is apparent only in natural and man-made exposures. Evidence of entrainment of rock blocks is not well seen in air photos due to extensive and dense forest cover. Boulder spreads are also poorly imaged in 2 m DEMs based on LiDAR data due to smoothing of the ground surface during data processing. Such DEMs are valuable however in areas with boulder spreads for assessing the proximity of bedrock to the ground surface, for the mapping of bedrock structures and for the identification of meso-scale to local scale features such as transverse scarps. Mapping of micro- to macro-scale features associated with glacial disruption is strongly reliant on field observations and mapping.

4.2.3 Linking landforms to processes of glacial erosion

Landforms across scales are linked on the basis of diagnostic features to five groups of processes of glacial erosion: abrasion, plucking, ripping, thrusting and meltwater erosion. The influence of bedrock hardness on abrasion rates is examined on the basis of results of a Schmidt Hammer survey of 27 sites and 43 rock surfaces. Further data are given in Appendix 2. A summary of results is included from a separate desk-top study of the forces necessary to entrain rock blocks of different sizes and shapes under different glaciological conditions (Krabbendam and Hall 2019). Close attention is given to the macro- to meso-forms of glacial erosion present at potential or actual sample sites in the Forsmark area and along the sample transect towards Uppsala. Four areas were targeted for detailed investigation and were photographed in a drone survey by AMKVO AB that provided imagery at cm resolution. Wave-washed, newly emerged rock surfaces were photographed along the coast at Forsmark at Stora and Lilla Sandgrund, Klubbudden and Lilla Asphällan (Figure 1-1). Detailed maps of meso- and micro-forms on these surfaces allow identification of the main process of erosion operated during deglaciation. A clear-felled area of glacially disrupted terrain at Gunnarsbo was

also photographed to provide a base map for plotting of macro- to micro-forms including moraines, transverse scarps, gouges and boulder spreads that provide detailed evidence for the processes involved in glacial ripping at a key locality within the Forsmark site boundary.

4.2.4 Fracture patterns on outcrops sampled for cosmogenic nuclides at Forsmark

Fracture mapping was completed on 12 outcrops sampled for cosmogenic nuclides in the Forsmark area (Figure 4-10). Mapping was done in August 2018 using a Brunton compass over a maximum area of 20 m^2 that always included a cosmogenic nuclide sample site. To assist the mapping of these partly vegetated outcrops, strips of heavy plastic tape were used to create a grid of 1 × 1 m squares that was always aligned to the cardinal compass bearings. Additional 10 cm markings were also made on the tape to assist mapping accuracy and precision. Mosses and lichens that could be removed by hand were temporarily removed from the mapping areas and subsequently restored. However, areas of thick peat and vegetation remained a feature of most outcrops and limited the areal extent of the mapping. Final versions of the maps were drawn in Adobe Illustrator from scanned originals (Figure 4-39). Fracture spacing was calculated from the maps by summing all fractures along each of the metre-spaced northings and eastings comprising the outcrop map grid and dividing that sum by the total measurement lengths. Additional fracture data are given in Appendix 3.

During sampling for cosmogenic nuclides in 2016, a separate fracture survey was undertaken. Line transects ~50 m long were set out perpendicular and parallel to ice flow across rock surfaces that were largely free of vegetation and sediment cover. The spacing of open, major fractures was recorded, as indicated by clefts and rock steps, following the 'line method' (Davis and Reynolds 1996) used previously in studies of fracturing and glacial erosion (Dühnforth et al. 2010, Krabbendam and Bradwell 2011).

Figure 4-10. *A fracture mapping grid on the summit of Wave Rock. Heavy plastic tape, with 10 cm increments drawn on it, was laid out to form a maximum mapping area of 20 m^2, with a 1 m^2 grid-size. The mapped area of each outcrop was usually smaller because the bedrock was partly buried in peat and vegetation that was too thick to temporarily remove by hand.*

4.2.5 Estimating total depths of glacial erosion in basement using geomorphological evidence

A variety of methods have been used in other contexts to estimate depths of glacial erosion through all or part of the Quaternary period. These include

- Source-to-sink sediment budgets in which the volumes of Pleistocene sediment in the receiving basins are replaced within present topography that has been modified by glacial erosion (Bell and Laine 1985, Glasser and Hall 1997, Dowdeswell et al. 2010, Hall et al. 2013b).
- Estimates based on inherited cosmogenic nuclides in slowly eroding terrains. Examples include inventories of meteoric ^{10}Be and ^{26}Al in tills in mid-west USA (Balco et al. 2005), on Baffin Island (Willenbring Staiger et al. 2006) and in northern Sweden (Ebert et al. 2012b) and of cosmogenic nuclides in Baffin Island (Briner et al. 2005), northern Sweden (Stroeven et al. 2002b) and northern Finland (Darmody et al. 2008).
- Comparisons between antecedent and present topography in locations where the form and elevation of the antecedent topography is known and provides a reference surface. Such reference surfaces include exhumed unconformities (Olvmo et al. 1999, Bonow 2005) and pre-Pleistocene erosion surfaces (Godard 1961, Delmas et al. 2009).
- Modification of preglacial landforms of known form, including hills (Sugden et al. 1992, Ebert and Hättestrand 2010) and valleys (Hall and Gillespie 2017).

In this study, we use U2 as a reference surface, along with the fault-bounded blocks produced by its dislocation. We follow a method also used in a type area of the sub-Cambrian unconformity around Trollhättan (Hall et al. 2019a) that requires the following information:

- The form of the Early Palaeozoic unconformity, and depths of weathering across its surface before its re-exposure.
- The contribution, if any, of weathering and subaerial erosion to modification of the basement surface during the Phanerozoic but prior to the onset of Pleistocene glaciation.
- The form of the present bedrock surface.

In the Trollhättan area, the buried and exposed unconformity has a near planar form (Johansson et al. 2001b). Re-exposure of the basement in the vicinity of Early Palaeozoic outliers is a result of Pleistocene glacial erosion. In Uppland, U2 is buried by Ordovician limestone offshore from Forsmark and the exposed U2 forms a ramp that rises at a gradient of ~0.2 % towards Forsmark (Figure 2-11). Areas of rock topography with less than 5 m relief across NE Uppland are interpreted as little-modified fragments of U2 that provide pinning points for its reconstruction. Whilst the form of the buried and exposed unconformity in Trollhättan and across Västergötland is well constrained by the extent of the large outliers, in Uppland the absence of outliers on the present land area requires a greater reliance on morphological evidence.

In the Trollhättan area, the sub-Cambrian unconformity has been dislocated by post-Early Permian fault movements. The resultant fault blocks have vertical displacements of 5–50 m (Ahlin 1987, Hall et al. 2019a). The fault scarps at the edges of rock blocks can provide constraints on patterns and depths of glacial erosion. As the fault scarps are exhumed features, the edges of the raised rock blocks were sharp on re-exposure and so provide a simple, step-like reference surface for subsequent glacial modification. Glacial erosion of rock blocks has lowered top surfaces and edges and excavated trenches along bounding fracture zones (Figure 4-11). We explore similar rock block topography in the Närke district in this report. In Uppland, the terrain also includes a mosaic of dislocated fault-bounded rock blocks, originally sharp-edged where still buried beneath Ordovician limestone offshore (Winterhalter et al. 1981) but exhumed onshore from beneath a former cover of Alum Shale and limestone (Beckholmen and Tirén 2010a, Grigull et al. 2019) (Figure 2-21). The fault scarps and block tops are used here as reference surfaces for estimation of depths of glacial erosion. The present rock surface in profiles is compared to the estimated former positions of the scarp and block top (Figure 4-11).

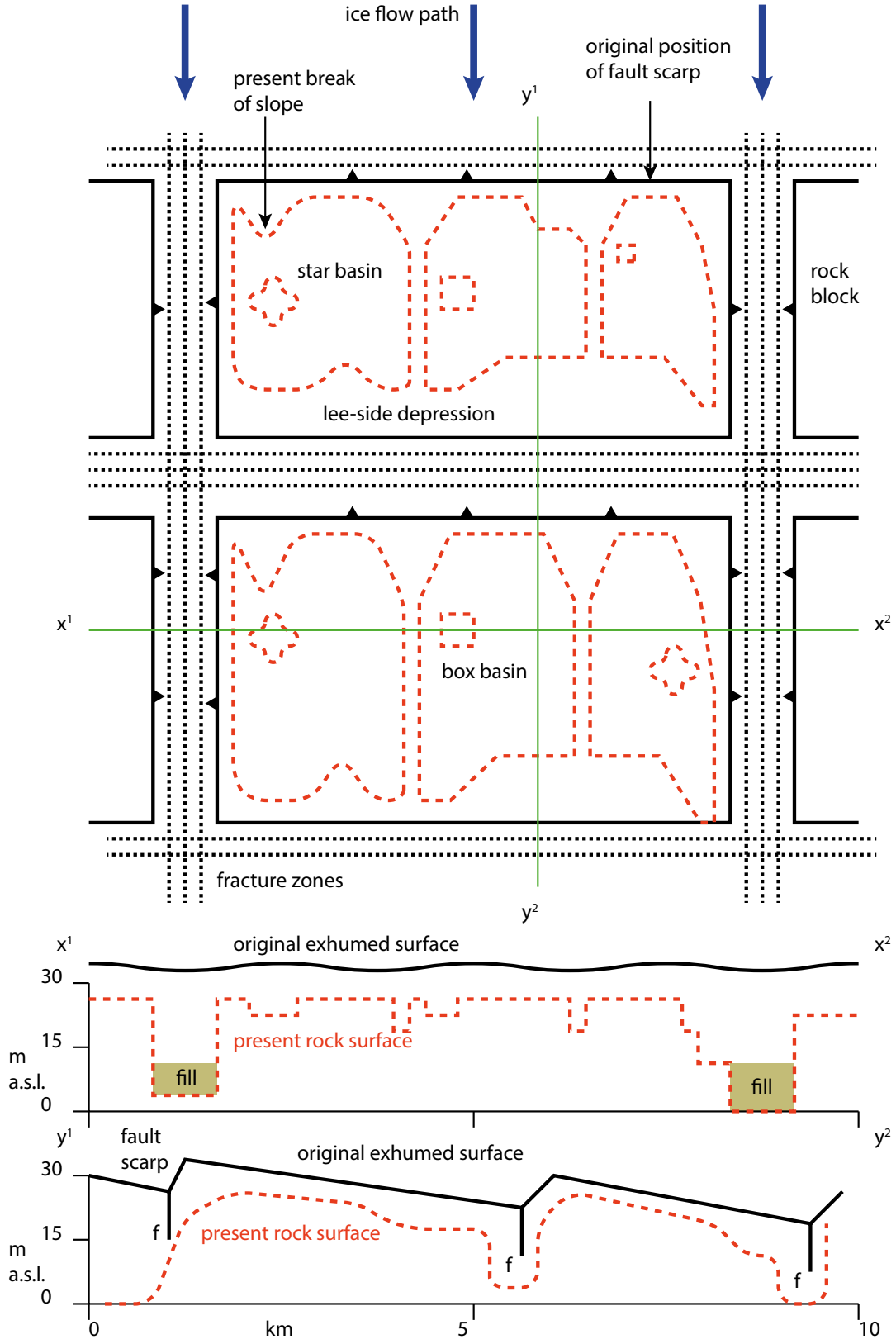

Figure 4-11. *Exhumed fault blocks as reference surfaces for glacial erosion in Uppland. The upper panel gives a schematic plan view; the lower panels provide schematic sections normal and parallel to former ice flow.*

Space-time substitutions have been used in a variety of geomorphic settings to assess the variable impacts of glacial erosion of ice sheets on shields (Hall et al. 2013a, Krabbendam and Bradwell 2013, Ebert 2015). Here we apply an ergodic hypothesis to explore progressive glacial modification of the dislocated surface of U2 by comparing in DEMs and profiles adjoining rock blocks with different surface forms in the Alunda area, 40 km S of Forsmark. We also examine more widely the spatial patterns of glacial erosion and its progression by comparing in topographic profiles the former position of U2 with that of the present rock surface.

Models of the former sub-Cambrian unconformity in Uppland (U2) were generated as summit envelope surfaces on the basis of a modelled DEM of the bedrock surface (Section 2.3.9). The procedure uses the present elevation of bedrock summits as pinning points and yields DEMs showing smoothed surfaces at different scales that represent models of U2 (the former bedrock surface). (See Table 2-1 for a step-by-step description). Additionally, to visualize terrain roughness, mean, minimum and maximum elevation surfaces with 10 × 10 cell search windows were created based on the 2 m LIDAR DEM from Lantmäteriet. The Relative Topographic Position was calculated using the raster equation (mean-min)/(max-min). To improve the visual output, a mean surface model based on a 50 × 50 cell search window was generated from the 10 × 10 cell based RTP map (Table 4-1). Terrain roughness was also calculated by the Standard Deviation (SD) method (Newman et al. 2018) using a standard deviation of elevation in neighbouring cells within a 100 m radius.

Table 4-1. Steps for generating a terrain roughness map using the RTP (Relative topographic position) roughness index.

Input Data (source)	Calculation(s)	Result
2 m LIDAR DEM (Lantmäteriet)	Focal statistics: Generating a mean elevation surface using a 10×10 cell search window. The GIS picks the mean pixel value within the search window.	mean DEM (mean)
2 m LIDAR DEM (Lantmäteriet)	Focal statistics: Generating a minimum elevation surface using a 10×10 cell search window. The GIS picks the minimum pixel value within the search window.	minimum DEM (min)
2 m LIDAR DEM (Lantmäteriet)	Focal statistics: Generating a maximum elevation surface using a 10×10 cell search window. The GIS picks the maximum pixel value within the search window.	maximum DEM (max)
Mean DEM Min DEM Max DEM	Raster calculator: (mean-min)/(max-min)	RTP map with 2 m resolution based on 10×10 cell search window
RTP map based on 10×10 cell search window	Focal statistics: Generating a mean surface using 50×50 cell (i.e. 100×100 m) search windows	RTP map with 2 m resolution based on the 50×50 cell mean (improved visual output)

We model erosion volumes in the Forsmark area by the creation of an envelope surface from local summits, using focal statistics, and subtraction of the DEM of the current land surface (Table 4-2). Firstly, we use a 20 m surface model that also includes the bathymetry of the Baltic Sea. Secondly, we employ a 20 m model that represents an interpolated model of the bedrock surface (with sediments removed). As a first approach, a smoothed envelope surface was created. To achieve this, firstly, a maximum surface was created using a search window of 1 km, where each pixel in the elevation model shows the highest value found in this search window. Secondly, to achieve a more realistic modelled land surface without circles, which still displays maximum elevations, the maximum surface was smoothed by creating a mean surface, with the same search window of 1 km, i.e. each pixel of the maximum surface shows the mean elevation within a circle of 1 km. The same operation was conducted for the bedrock surface resulting in a subtraction surface with higher values. The result also shows the pattern of erosion with defined corridors of higher magnitude of erosion.

Table 4-2. Steps for estimation of glacial erosion depths in GIS in Uppland.

Input Data (source)	Calculation(s)	Result
2 m LIDAR DEM (Lantmäteriet) 20 m soil depth (Swedish Geological Survey)	Resampling of the 20 m soil depth to 2 m Subtraction of the soil depth from the 2 m LIDAR DEM	2 m DEM of the present bedrock surface
2 m DEM of the present bedrock surface	Focal statistics: Generating a maximum surface using circular search windows of different radii. The GIS picks the highest pixel value within the circle of the given radius.	A 2 m maximum surface with circles and steps between them
2 m maximum surface	Focal statistics: Generating a mean surface using a circular search window with the identical radius that the input maximum surface was based on	A 2 m maximum-mean (smoothed) surface (a summit envelope surface)
2 m summit envelope surface 2 m DEM of the present bedrock surface	Subtraction of the bedrock surface from the summit envelope surface	A 2 m raster showing the elevation differences between the summit envelope surface and the bedrock surface for every pixel in the raster – the modelled erosion depth

Several potential sources of bias or error exist in using the modelled U2 surface, and the dislocated rock blocks derived from it, as reference surfaces for glacial erosion:

1. U2 is regarded as a near planar basement surface. Whilst this assumption matches available information from the buried unconformity offshore and the present basement terrain (UQ) has a relief of less than 10 m over wide areas in NE Uppland (Section 2.3.9), the wavelength and amplitude of relief on U2 is poorly constrained over distances of 0.1–1 km.
2. Topographic profiles emphasise summits and envelope surfaces use summits as pinning points. The generated profiles and envelope surfaces are smoothed surfaces and ignore valleys with widths less than the spacing of the sample grid. This error is likely to be small as valleys on the U2 surface in Uppland are km-wide features of shallow depth.
3. An estimate of 10 m is used for the rock lost from above basement summits on U2 based, in part, on equivalent height differences between still-buried U2 surfaces and exposed basement summits nearby around Early Palaeozoic outliers in southern Sweden. In Uppland, the Ordovician outliers are submerged and so the height difference between the buried and exposed unconformity can only be constrained to within 15 m. The 10 m erosion depth estimate for Uppland relies heavily on morphological evidence from the interpreted form of U2 and the glacial modification on its surface. Whilst this evidence appears incompatible with 50 m erosion depths below summits (Section 2.3.9), if integrated glacial erosion since exhumation has been spatially uniform then landforms could be maintained during lowering and the upper limit for basement summit erosion could potentially be higher than the 10 m erosion depth estimate. Alternatively, lower erosion of basement summits is possible where summits remain accordant in elevation and planar in form, indicating a closer proximity to U2.
4. In areas remote from cover rocks, the summits of the exhumed unconformity have been exposed to erosion for periods of uncertain and perhaps different duration. Erosion of separate summits of similar resistance to erosion at similar rates would lead to maintenance of a general accordance of summit elevations during lowering from the original unconformity. Uniform lowering across lines of former ice flow is however unlikely.
5. Models of U2 based on summit envelope surfaces derived from a 0.5 or 1 km grid will underestimate the former elevation of U2 where glacial erosion has lowered all summits across areas more than 1–2 km wide. Such areas are generally evident in DEMs as low elevation corridors or basins. Areas of apparent deeper erosion however may also resemble the little modified surfaces of fault blocks in low topographic positions.

4.3 Results

4.3.1 Regional landscapes and local landforms of glacial erosion

Landscapes of east central Sweden and south west Finland

At scales of 10–100 km, the basement terrain on the Åland ridge between east central Sweden and south-west Finland shows both inherited pre-Pleistocene features and distinctive glacial landscapes (Figure 4-12). Inherited elements include the re-exposed U2 unconformity, with its characteristic low roughness, in Uppland and SW Finland. Terrain of high roughness, with 20–100 m of local relief, is found to the west of N–S oriented faults in Uppland (Figure 2-19). This terrain has been interpreted as representing the eroded U2 unconformity that was re-exposed to fluvial erosion and deep weathering in the Mesozoic and later further modified by glacial erosion, including removal of regolith (Green et al. 2013). In Uppland and in SW Finland, there is a N–S transition from terrain of low to medium roughness, perhaps indicating longer basement re-exposure towards the south. The highest terrain roughness at this scale is found in the Åland archipelago, where deep, fracture-guided trenches separate low fracture-bound blocks that rise above present sea level. The Stockholm archipelago also shows high roughness but here the excavation of fault-bounded Jotnian, Cambrian and Ordovician basins (Hagenfeldt and Söderberg 1994) has contributed to the diversification of relief. High terrain roughness at this scale in areas surrounding Uppland includes components that derive from glacial excavation of fractured rock, pre-Pleistocene weathered rock, and Jotnian and Early Palaeozoic cover rocks. By far the largest rock basin is the −270 m Åland Deep, excavated in Jotnian sandstone in a half-graben.

Regional landscapes (1–10 km) in Uppland

Main topographic elements of regional landscapes

The terrain of NE Uppland has a low relative relief of less than 10–20 m per km largely inherited from U2 (Figure 2-22). The main features of the sub-Cambrian unconformity are its flatness and dislocation into low, tilted rock blocks. Glacial modification of this antecedent topography has been variable in its impact. Elevated fault block tops S of Forsmark retain substantial summit areas with less than 5 m bedrock relief per km that appear in DEMs as smooth surfaces without glacial lineations (Figure 4-13). Lower fault block tops, such as that around Griggebo (Figure 2-24), show similar bedrock relief. The smooth block tops show low (less than 2–3 m high) roches moutonnées that align with N–S fracture patterns and former ice flow. In contrast, at lower elevations, till-floored rock trenches and basins stand with floors up to 20 m below adjacent bedrock highs. Trenches are often elements within larger basins and linear depressions, with fracture-controlled bounding slopes. Rock basins are dominantly oriented N–S and so follow the flanks of rock highs but some are also aligned NW–SE and stand in the lee of bedrock highs (Figure 4-13). Basins at Fagerviken (Figure 4-13) and Forsmark are open-ended towards the north, the direction of former ice flow and, in the case of Forsmark, in the zone of high fracture density of the intersecting Singö Deformation Zone (Figure 4-3). Basins and linear depression floors include rock hills that reach elevations close to those in the surroundings. At Forsmark and also further west, the hills that rise from depression floors show weak streamlining due to the presence of rounded stoss faces, fracture-guided alignment with ice flow and the presence of till tails. Trenches and valleys continue below sea level in Öregrundsleden and in the Singö part of the Öregrund archipelago (Figure 4-13) but here the topographic lows are, in part, products of the glacial excavation of Jotnian and Ordovician sedimentary rocks from within small grabens and half grabens (Figure 2-8).

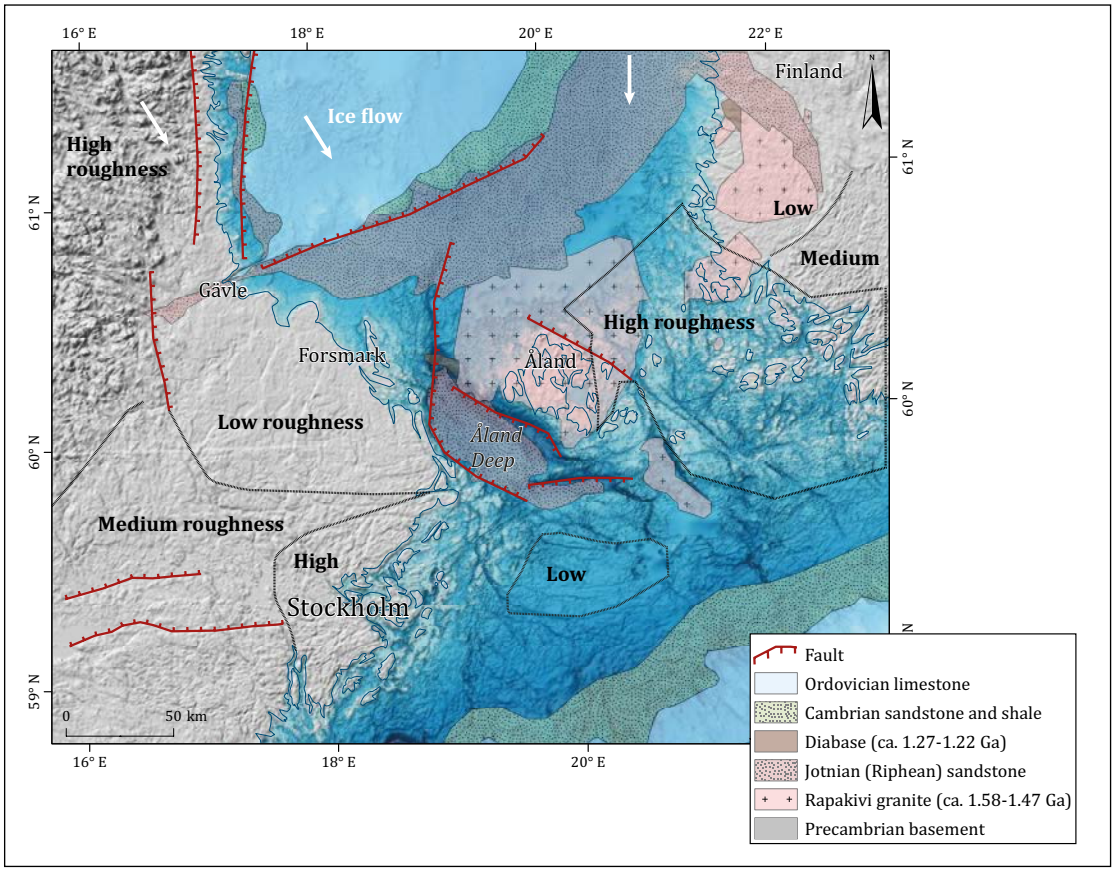

Figure 4-12. *Main elements of the bedrock topography and terrain roughness at the landscape scale in areas surrounding Åland.*

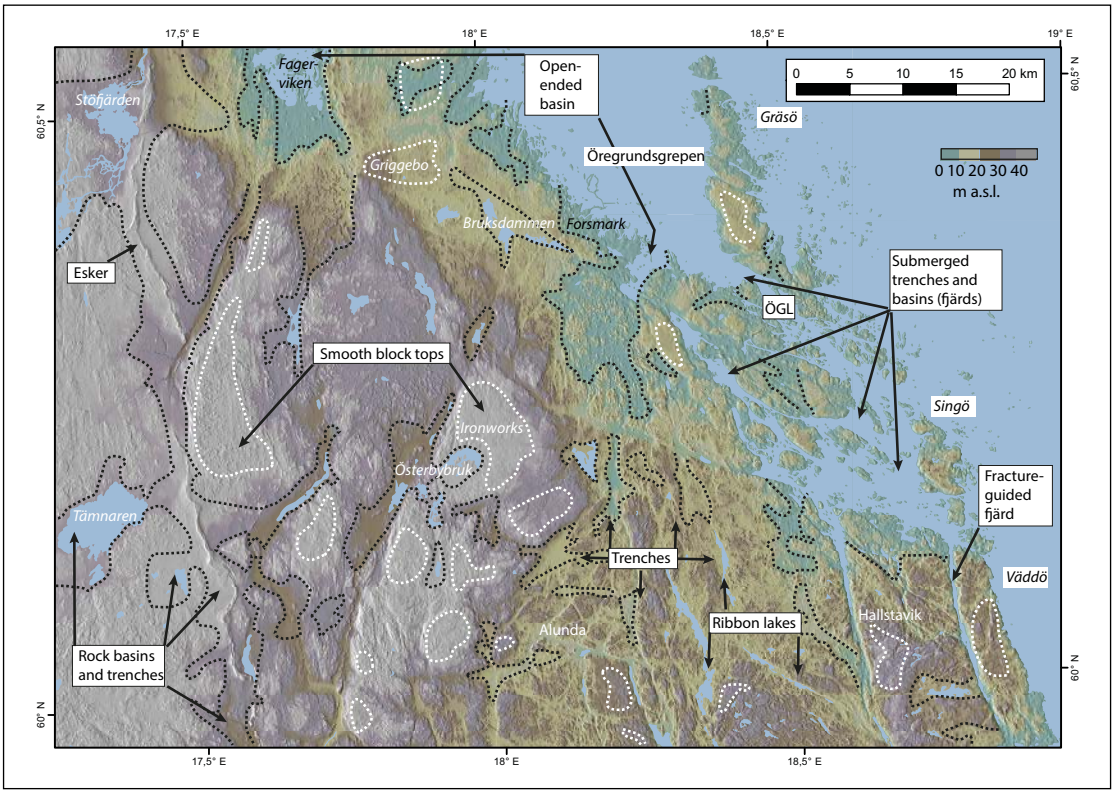

Figure 4-13. *Landscapes and landforms of glacial erosion at the regional scale in NE Uppland. ÖGL Öregrundsleden*

Trenches and rock basins

Rock trenches in Uppland can extend for many kilometres in length, locally holding ribbon lakes and fjärds, but widths are usually less than 1 km. *Fjärd* is part of many local place names on the low-lying Uppland coast. The term refers more widely to glacially eroded inlets and bays found on lowland rocky coasts (Werth 1908, Embleton 1982). Trenches typically follow major fracture zones mainly oriented ENE–WSW and between E–W and ESE–WNW (Figure 4-5) and delineate the edges of fault blocks (Figure 2-21). Interconnected, fracture-guided trenches likely acted as major melt-water pathways across Uppland (Figure 4-14), with very large flow volumes directed via the major trenches that border NE Uppland, the Tierp-Uppsala and Öregrundsleden channels (Shackleton et al. 2018). East of Forsmark and Alunda, several trenches follow WNW–ENE orientations, across the former line of ice flow (Figure 4-13). Drowned trenches with fjärds near Hallstavik occur along the edges of fault blocks with summits at 20–30 m a.s.l. These trenches are oriented roughly parallel to former ice flow. Depths of sediment beneath trench floors in NE Uppland are seen in SGU maps to widely reach 10 m but fills of more than 25 m are exceptional and confined to a few, less than 1 km wide, enclosed depressions.

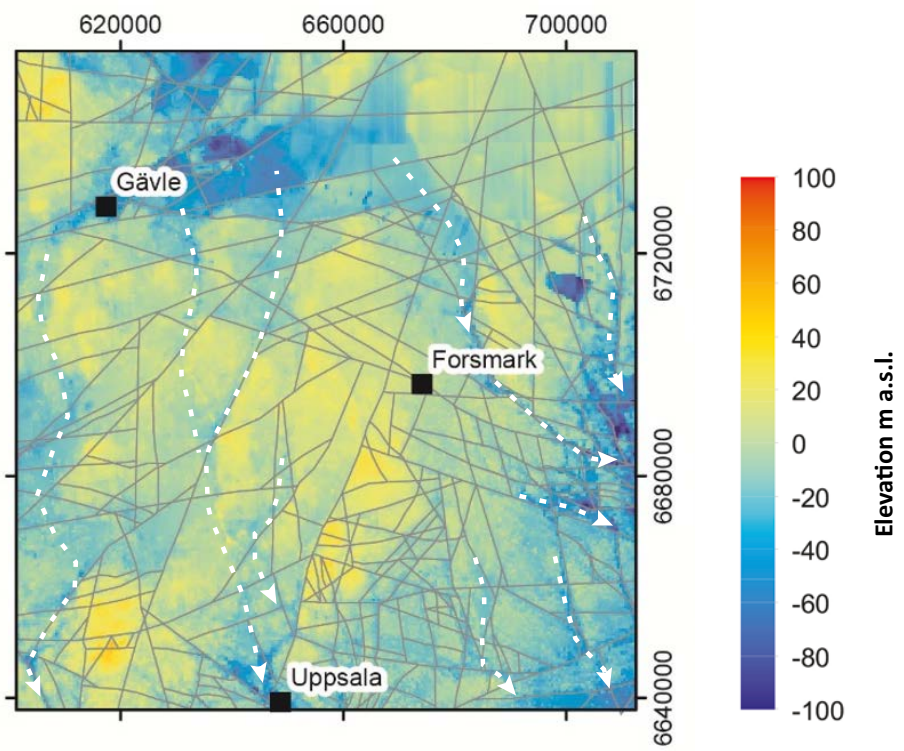

Figure 4-14. *Large trenches as major meltwater pathways across Uppland. Model for bedrock elevation relative to sea level and rock blocks, corrected for the gentle tilt to the north-east of the present regional topography (Grigull et al. 2019). High elevation topography in yellow; low elevation topography in blue. A system of inter-connected trenches crosses the region from N to S (dashed white lines) and likely marks major meltwater pathways. Similar pathways are identified in recent simulations of subglacial meltwater dynamics beneath the Fennoscandian Ice Sheet (Shackleton et al. 2018). Coordinated are in metres (SWEREF99TM).*

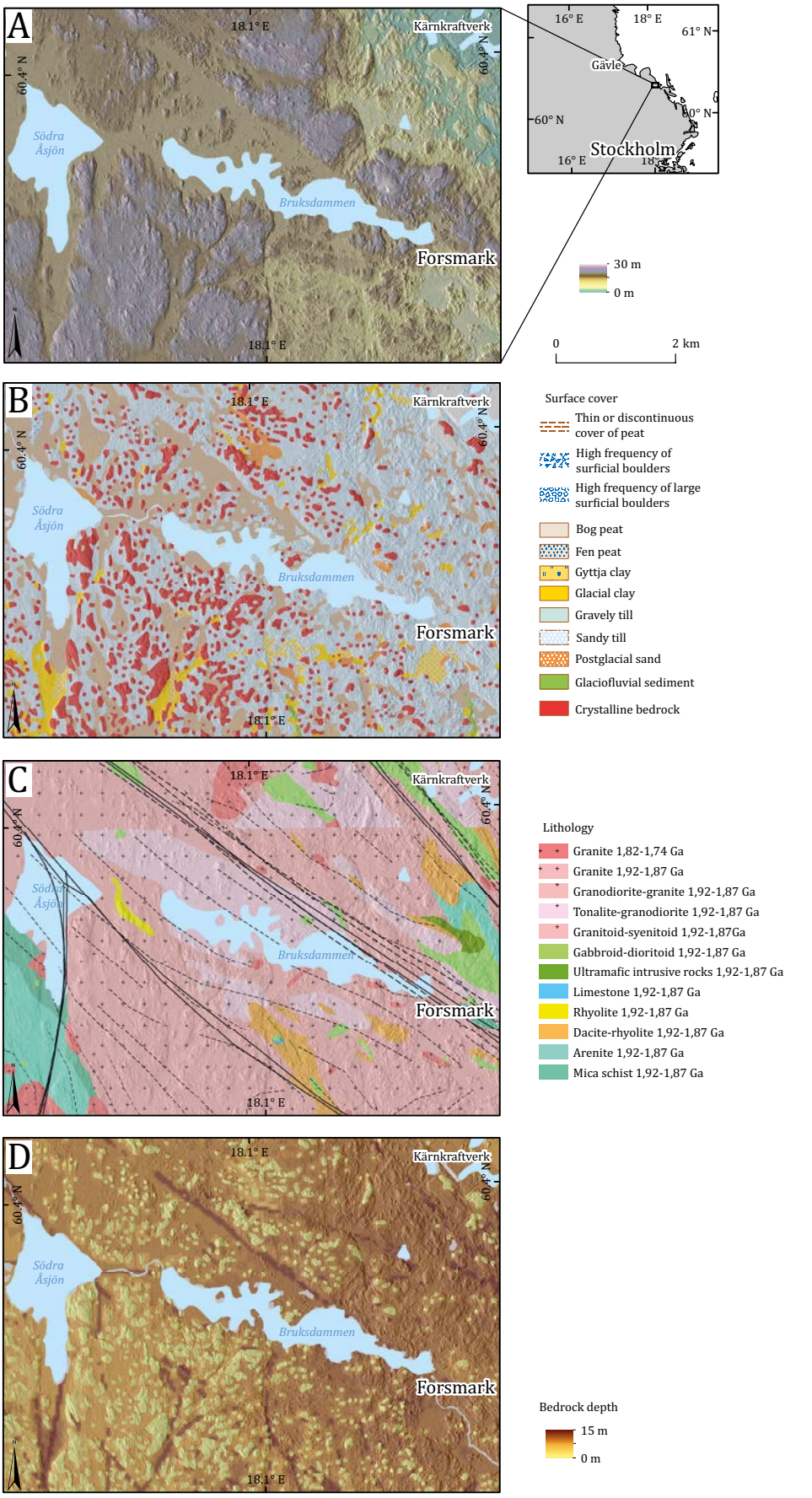

Figure 4-15. *Bruksdammen and Södra Åsjön rock basins. A. DEM of the low relief terrain around the basins. B. SGU data for the Quaternary geology. Note the limited extent of boulder spreads. C. Geology. Structural lineaments are from SGU data. D. SGU data on depth to bedrock. Fault- and fracture-guided rock trenches are up to 15 m deep. Elevations in panel A are in m a.s.l.*

Rock basins extend over areas of up to 30 km^2 in NE Uppland (Figure 4-13). Basin outlines give a wide variety of planforms, only a few of which are strongly rectilinear or box-shaped at this scale. Basin margins conform locally to major fractures at the edges of rock blocks but crossing fractures have been exploited by glacial erosion to form connecting trenches that give roughly cruciform planforms to some basins. SGU data indicates that sediment thickness beneath basin floors rarely exceeds 20 m (Figure 4-15). The frequent presence of bedrock hills on basin floors is a further indication that the basins are often of shallow depth.

The Bruksdammen basin, along with the connecting Södra Åsjön basin, lies W of Forsmark village (Figure 4-15). The basins are similar in extent and form to other broad, shallow rock basins in NE Uppland (Figure 4-13). The geology of the surrounding area includes a wide range of crystalline rock types of acid to ultrabasic composition. The Bruksdammen basin sits between the edges of two fault-bounded rock blocks with tops at ~20 m a.s.l. (Beckholmen and Tirén 2010b). The Forsmark Deformation Zone runs NW from Forsmark and marks the line of a narrow (up to 200 m wide) trench filled by 5–10 m of glacial and post-glacial sediments (Figure 4-15). The southern shore of Bruksdammen has a linear trend and may also follow a major structure in the basement at the edge of the southern rock block. A set of N–S oriented trenches, 50–500 m wide and several km in length, also likely follow fracture zones parallel to the deformation zone that crosses Södra Åsjön.

The Bruksdammen basin is ~5 km long and up to 1.5 km across at its western end. Along its axis are found isolated hills and hill masses that rise to 20 m a.s.l. The Södra Åsjön basin covers ~3 km^2 and is star-shaped around the diamond-shaped centre in which the lake sits. Basin margins are crenulated to indented, with rounded noses to hills on stoss faces. Individual hills and ridges, 50–400 m long, are oriented parallel to former ice flow and to bedrock fractures. The terrain is weakly streamlined, a combined result of streamlining of bedrock ridges and the presence of till tails. Bedrock edges to hills and ridges are rounded and sharp edges indicative of rock removal by glacial erosion late in the last glaciation appear to be missing. Patches of disrupted bedrock, a few hundred metres in width, occur locally (Figure 4-15). Erosion forms on the exposed, elevated bedrock around the basin are typical of these found on glacially roughened and streamlined terrain at slightly higher elevations in surrounding areas. The basin floors are hidden beneath water and sediment but rock hills have similar features to those in the vicinity of the basins. Clear evidence of recent major loss of rock mass to glacial erosion from the basins appears to be lacking, such as hill-hole pairs, sharp-edged rock scarps and the presence of rubble till or other thick till covers in a down-ice direction. Available evidence indicates excavation of these two basins was controlled not by variable rock type but by closer fracture spacing in the topographic lows. The processes involved in excavation, however, remain obscure. The varied geology of the area allows the possibility in future of using boulder counts to estimate half-distances of transport and thereby derive estimates of rock losses from the basins in the last glaciation (Salonen 1986).

Progressive glacial erosion of rock blocks in the Alunda area

Granite gneisses, along with small masses of basic and ultrabasic gneisses, dominate the geology of the Alunda area. Lineaments indicate the existence of three main vertical fracture sets (Figure 4-16). Topographic lineaments indicate that fracture spacing and orientation at different scales are key controls on the differentiation of the relief on the three blocks.

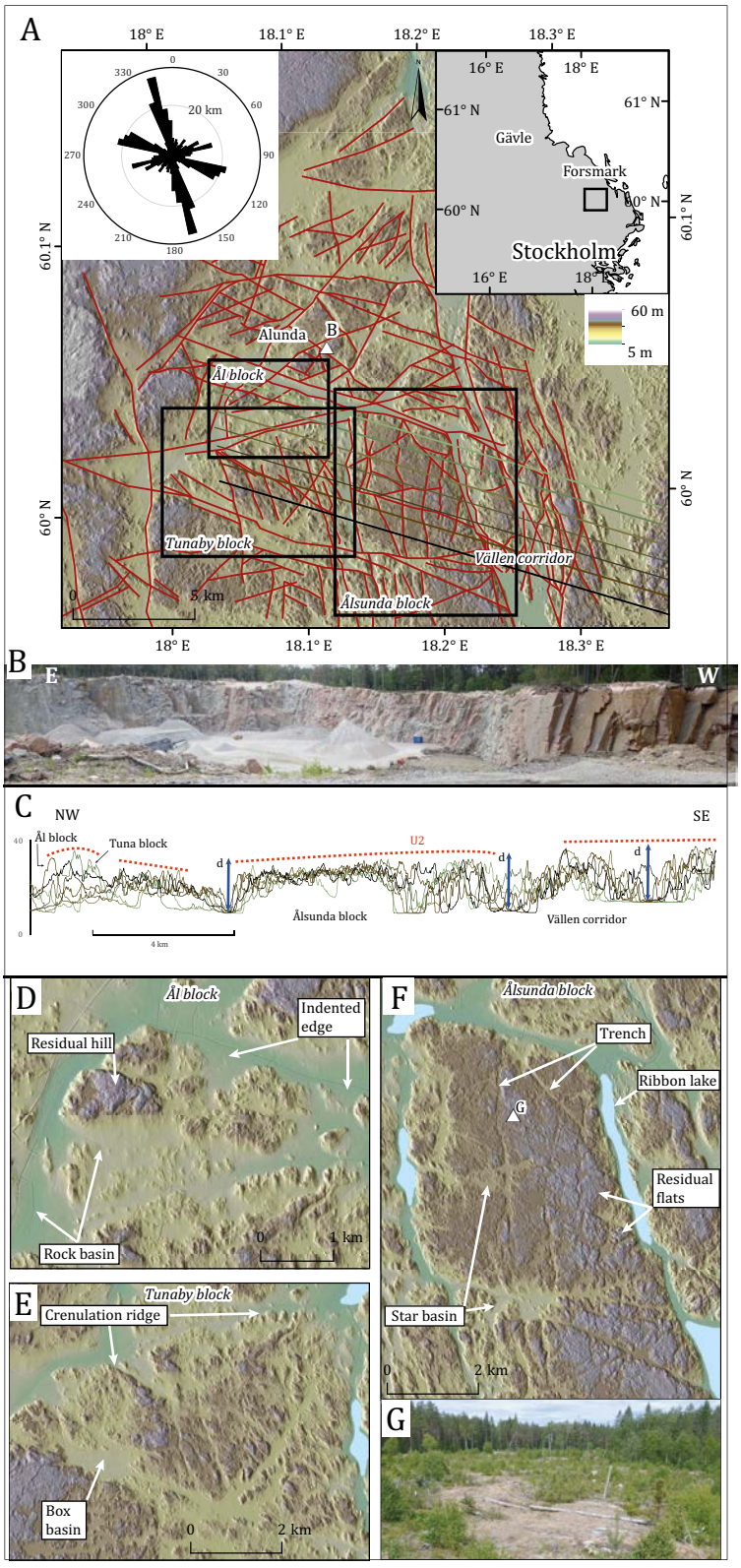

Figure 4-16. *Progressive glacial erosion of rock blocks in the Alunda area, Uppland. A. DEM of study area showing main fractures and dominant orientations. Three boxes delimit areas of distinctive basement topography around the settlements of Ål, Ålsunda and Tunaby and the Vällen corridor. Red lines are fractures inferred from topographic lineaments. The distance-weighted rose diagram shows the dominant fracture orientations. B. South face of a quarry near Alunda showing prominent vertical fractures. C. Superimposed topographic profiles (lines shown in A) running WNW–ENE. Interpreted original of position of U2 indicated. Maximum depth (d) of glacial erosion along fracture zones indicated by arrows. Thicknesses of sediment beneath valley floors are ignored. D. Ål block. E. Ålsunda block. F. Tunaby block. G. Low (less than 3 m) basement relief on the surface of the Ålsunda block. Total depths of till and postglacial clay here are 0–3 m.*

The Alunda area includes adjacent fault blocks which each display different bedrock surface morphology. Bedrock summits lie within a narrow elevation range at 25–35 m a.s.l where large areas of residual rock flats, with less than 4 m elevation range in summits, remain on the highest ground.

- On the *Ålsunda block,* the north-western part of the top surface has lost from wide areas a rock layer at least 3–5 m thick based on the height differences with its remaining high points and the smooth block top surface to the east (Figure 4-16F). Lowering of the wider block top has been uneven, with the excavation of narrow (less than 100 m wide) trenches along fractures, oriented both parallel and traverse to ice flow, and shallow star basins at fracture intersections. The edges of the block remain sharp with only small indentations from the loss of triangular-shaped rock layers of shallow (10 m) depth. The broad (up to 300 m wide) fracture zones that bound the block have been excavated to depths of more than 20 m. Roughness is low on this block top and high only along the edges of rock trenches (Figure 4-17).
- The *Tunaby block* shows a marked reduction in the extent of bedrock highs above 25 m a.s.l., an increase in the number and width of fracture-guided trenches and a greater areal extent of rock basins on the block surface (Figure 4-16E). The stoss edge of the block is crenulated, with streamlined stoss faces of roches moutonnées separated by fracture-guided clefts. The edges of the block are poorly defined with several large indentations. The extent of low roughness on this block top is reduced and a greater density of trenches and basins is indicated by high roughness (Figure 4-17).
- The *Ål block* shows only a small (1.5 km^2) area of bedrock rising above 25 m developed in a kernel of massive gneiss (Figure 4-16D). A rock basin of 0.65 km^2 area found in its lee is excavated to a depth of more than 15 m below the kernel summit. The edges of the Ål block are diffuse and the bounding trenches are up to 0.8 km wide. Roughness is high across this block (Figure 4-17).

Subglacial conditions were similar at these adjacent sites, although subtle differences may have existed below the Fennoscandian Ice Sheet in the routing of subglacial meltwater along bounding trenches (Figure 4-14). As topographic, geological and glaciological controls on glacial erosion across the three blocks are essentially identical, the contrasting morphologies of the three adjacent rock blocks are taken to represent the progressive modification of the former U2 surface. Block tops were first lowered by loss of rock sheets and the excavation of shallow basins and dissected by the excavation of fault-guided trenches. As the block top was lowered, residual high points became increasingly confined to the more massive rock compartments. The edges of the blocks were transformed from straight margins along fracture-guided trenches to crenulated and then indented edges where the outline of the original rock block was masked. The increase in relative relief between the three blocks, the lowering of the block tops and the absence of extensive rock flats at lower elevations indicate that progressive glacial modification led to an overall roughening of bedrock topography.

Local landforms (0.1–1 km) in Uppland

Types of landforms

At the local scale, various landforms typical of hills and hollows can be mapped in the bedrock topography. Common features are box hills, large roches moutonnées, lee cliffs and star and box basins. Box hills retain a fracture-guided planform, with cliffs on stoss, flank and lee faces (Figure 4-18). Other hills have a typical roche moutonnée form, with a smooth stoss face and lee cliff. Crag-and-tails occur at around half of sites inventoried but this high number includes numerous sites surveyed in the Forsmark area where weakly streamlined terrain is typical. Many hills are oriented roughly N–S in the general former direction of ice flow but hill flanks are frequently defined by fractures with similar orientations, indicating strong structural control. Large whalebacks are not recorded frequently. The contrasting morphologies indicate that box hills are mainly shaped by block removal from surrounding fracture zones whereas roches moutonnées and whalebacks have been shaped additionally by abrasion. The landform inventory indicates that *fracture-guided valleys* are the only ubiquitous local landforms. Valley lengths may extend over several km but widths generally fall into the range of 50–250 m. Small rock basins are classified as *star basins* and *box basins* on the basis of planforms. Shapes are determined by the orientations of the crossing and bounding fractures. Extensive *boulder spreads*, indicative of glacial disruption of bedrock, were observed at only 8 inventory sites.

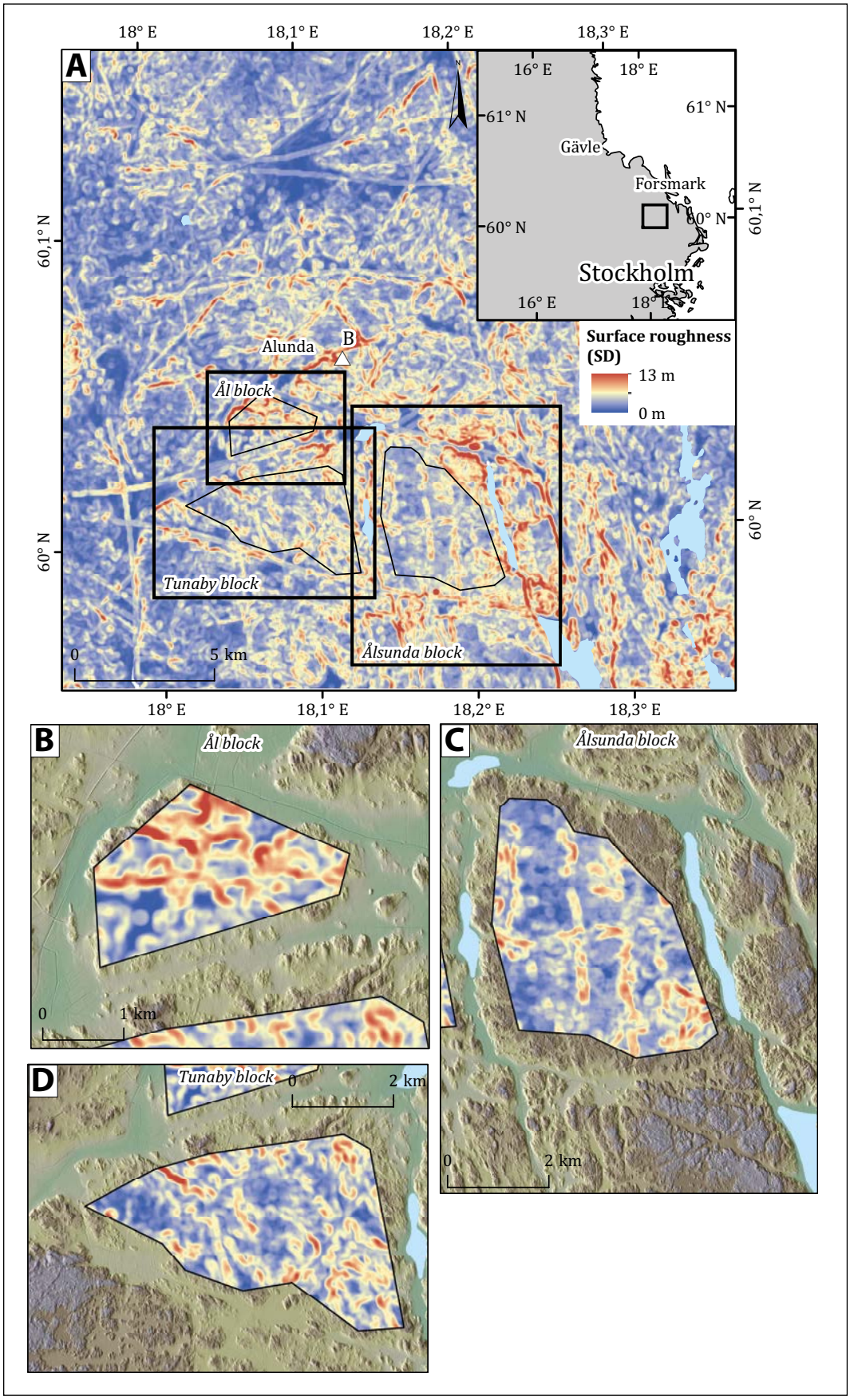

Figure 4-17. *Topographic roughness based on the Standard Deviation (SD) method on fault block surfaces at Alunda. A. Locations of the fault blocks. B. Ål block. C. Ålsunda block. D. Tuna block.*

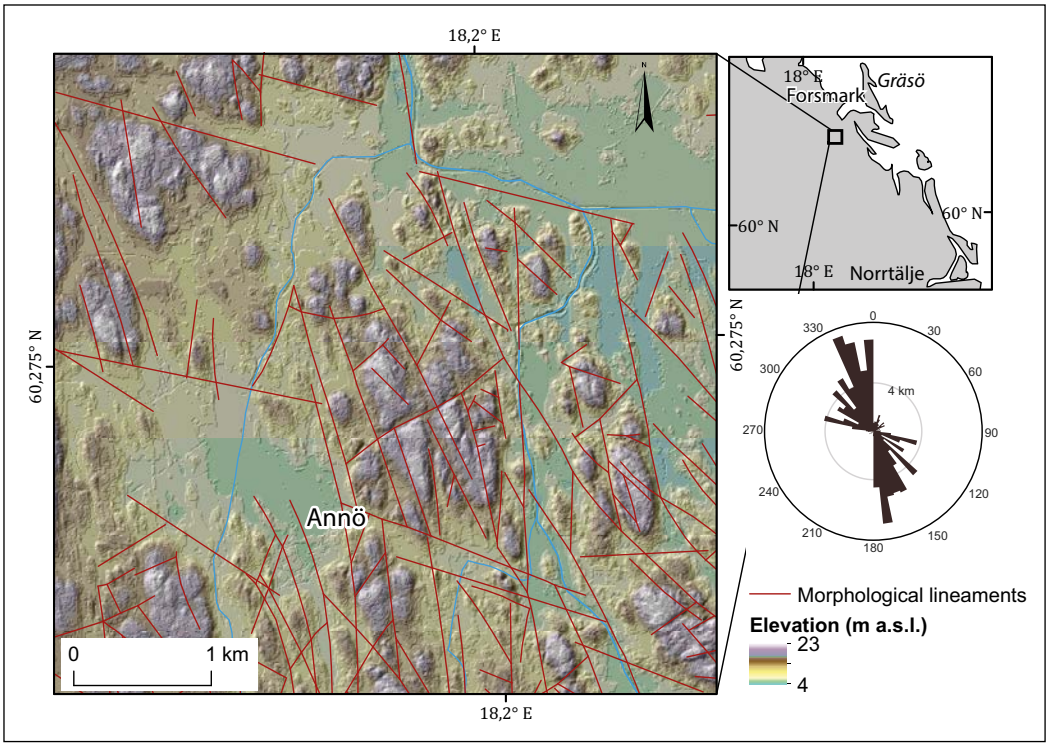

Figure 4-18. *Box hills and basins around Annö, 12 km S of Forsmark. Bedrock topography is controlled by two orthogonal sets of fractures. Hill and basin planforms approach box shapes. Hill stoss and flank faces are rounded.*

Landform assemblages and terrain types

The first phase of regional mapping from DEMs identified a zoned distribution of assemblages of glacial bedforms at 0.1–1 km scales in NE Uppland, including the Forsmark area. From Forsmark towards Öregrund (Figure 4-19), weakly streamlined glacial bedforms lie in two belts oriented NNW–SSE. West of this area, streamlined glacial bedforms occur in patches over areas of 1–5 km^2. Large areas, however, lack streamlined glacial bedforms, particularly in more elevated areas where bedrock lies at the surface or where till covers are thin. Boulder spreads, indicators of glacial disruption of bedrock and entrainment of blocks over short distances at the ice sheet base, also occur within belts and patches. Boulder spreads, however, are distributed separately from non-streamlined and streamlined glacial bedforms (Figure 4-19).

Zonation of landforms and landform assemblages provides the basis for the recognition of three different terrain types at the local scale:

1. *Ice-roughened terrain*. Exposed bedrock is extensive on topographic high points. Roches moutonnées and box hills are widespread. Fracture-guided valleys of varying widths and orientations are common. Till cover thickens in depressions and partly infills shallow rock basins with star- and box-shaped outlines. *Roughening* here refers to contrasts between smooth surfaces interpreted as inherited facets of U2 and the present bedrock surfaces.
2. *Weakly streamlined terrain*. Exposed bedrock is more restricted in extent. Drumlinoid hills are common, mainly of 50–300 m length and aligned parallel with former ice flow. Rock cores show rounded stoss faces and fracture-guided flanks. Small lee side and flank cliffs are seen in LiDAR-based imagery. Many hills have low till tails of 50–250 m length. Broad trenches, depressions and rock basins occur in fracture zones between hill groups. Here, thicknesses of glacial and marine deposits often exceed 5 m.
3. *Glacially disrupted terrain*. *In situ* bedrock is widely concealed by spreads of large, angular boulders that are mapped by SGU as occurring in extensive patches and belts (Figure 4-9). Surrounding undisrupted terrain, and enclaves within boulder spreads, show typical features of ice-roughening or weak streamlining.

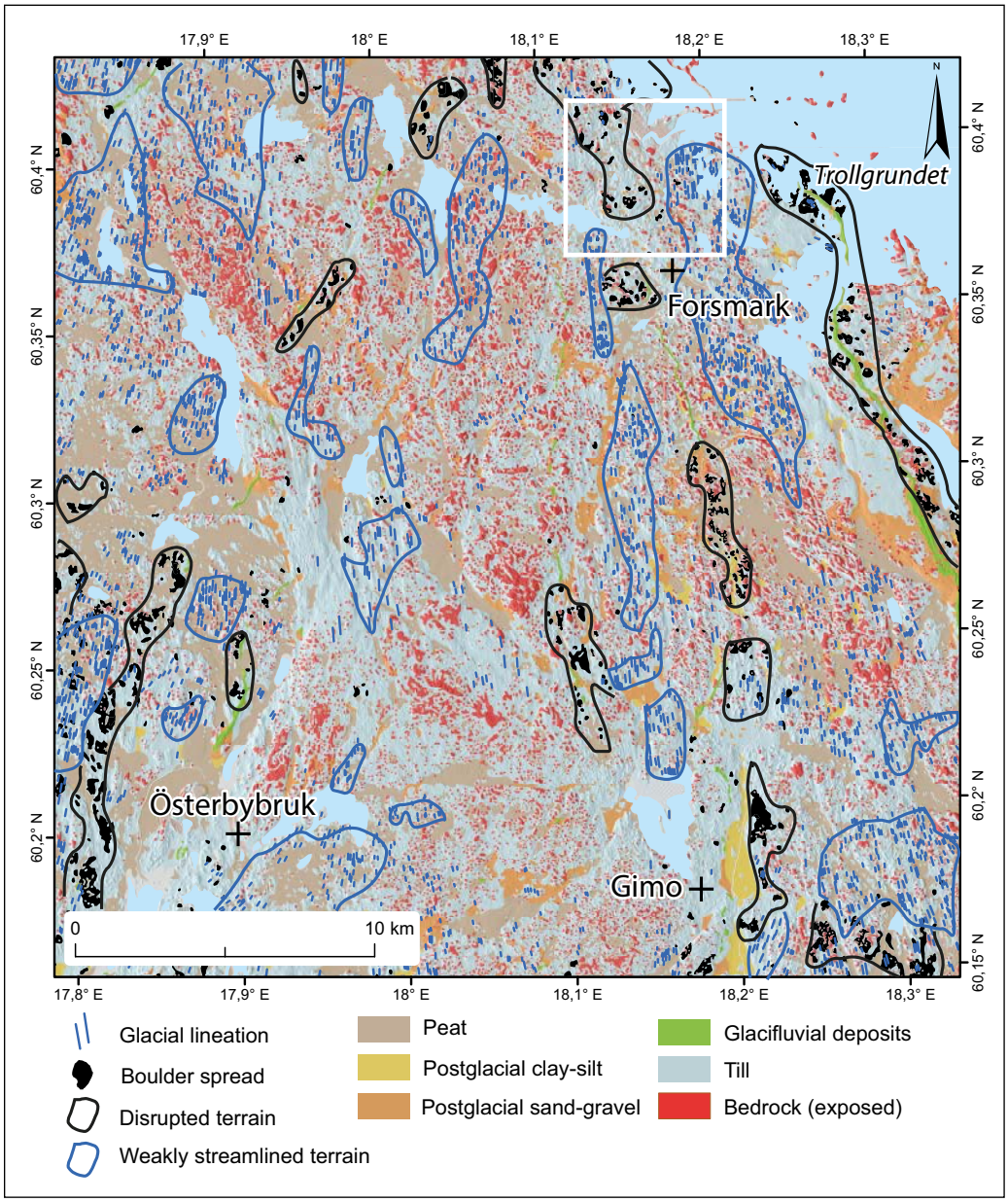

Figure 4-19. *Glacial lineations in NE Uppland overlain on an SGU map of rock outcrops, till cover, glacifluvial and post-glacial deposits. Glacial lineations delimit areas of weakly streamlined terrain. Boulder spreads delimit areas of glacially disrupted terrain. The white box is the area around Forsmark shown in Figure 4-27.*

Whilst the terrain types are distinct between core areas, the boundaries of the terrain types vary between sharp and gradational. Moreover, the basic elements of the bedrock topography are found across the terrain types, namely the positive relief features of box hills and roches moutonnées and the negative relief features of fracture-guided valleys and rock basins. Glacial streamlining derives in places largely from the presence of till tails. Glacial disruption of bedrock took place at different elevations, across the tops of box hills and roches moutonnées but also across the floors of trenches and basins. To varying extents, the glacially streamlined and disrupted terrains have developed by modification of pre-existing, non-streamlined terrain with asymmetric rock hills and fracture-guided trenches and basins. Case studies of the three terrain types are given below. The terrain types are compared later to an index of topographic roughness derived from LiDAR data.

Glacially roughened terrain

Large parts of NE Uppland show extensive exposure of bedrock on topographic highs (Figure 4-19) within terrain of variably spaced hills that are separated by fracture-aligned valleys and depressions. Similar terrain is found in western part of the Forsmark nuclear power station site. Perhaps the best exposure in this type of terrain is around Ballast Quarry, Skyttorp (Figure 4-20A). The Quarry is set into the top surface of a 10 km wide, eastward tilted, fault block, with summit elevations at 50–70 m a.s.l., that forms some of the highest ground in this part of Uppland. The Quarry lies ~1 km E of the edge of the fault scarp above Skyttorp that edges the sediment filled Fyrisån depression with a floor at ~24 m a.s.l. Bedrock is exposed widely on topographic highs (Figure 4-20B). Fracture-guided valleys and box basins are frequent. Lower ground is covered by sandy till and wave-washed gravel. Boulder spreads become extensive ~1 km E of the Quarry but do not occur in its vicinity.

Around the Quarry, bedrock highs are less than 5 m high, 100–250 m long and 50–100 m wide. These hills may be closely grouped but also may be isolated from each other over distances of several hundred metres (Figure 4-20A). Hills are oriented NW–SE and NNW–SSE, following fracture orientations and the general direction of former ice flow. Quarry exposures show that small bedrock highs are developed in rock kernels where vertical fractures are spaced at more than 4–5 m (Figure 4-20C) and that the flanks of these small hills follow narrow (less than 2 m wide) mafic dykes and closely fractured zones where granite gneiss blocks are widely less than 1 m in diameter (Figure 4-20D). Macro-scale (10–100 m) rock bumps show an unusually wide range of shapes, with roches moutonnées, whalebacks (Figure 4-20E) and crag-and-tails, with stoss- and lee-cliffs and clefts all represented. Abrasion forms dominate at the meso- and micro-scales (Figure 4-20F). Lee-side depressions are filled by up to 5 m of sandy till but till tails are short or absent. Approximately 100 m long quarry exposures indicate that underlying rock surfaces in depressions are abraded and rather smooth, with low, rounded rock edges and little evidence for recent quarrying of bedrock and incorporation of plucked blocks into the base of the till.

Glacially streamlined terrain

A belt of glacially streamlined terrain extends S for ~10 km from Forsmark (Figure 4-19). At Lilla Aspö, this belt is ~8 km wide (Figure 4-21) and contains landforms similar to those present in the planned repository site. The fault block surrounding Lilla Aspö stands S of the Forsmark Deformation Zone. The block top surface is near horizontal, with summit elevations falling within an elevation range of 10–19 m a.s.l. over an area of ~25 km^2. Fracture sets oriented to 350°N are prominent and have been picked out by glacial erosion.

Hills stand 5–15 m above wide rock basins and narrow trenches (Figure 4-21). A-axis lengths for hills are 200–400 m but widths vary widely from 50–200 m, with drumlinoid, box and prismatic shapes. Stoss faces of hills are prominent and rounded whilst lee faces are lower and widely masked by till. Streamlining of hill forms is seen in DEMs to include both rock and till tails, indicating the development of a range of crag-and-tail forms. Till tails are up to 250 m long, with length/width ratios of 10:1 but heights of less than 3 m. Trenches between hill groups are mainly ~100 m wide but reach widths of 0.5 km. Basins are larger, up to 1 km wide, but shallow, within floors up to 10 m below rock risers and sediment fills of less than 5 m thickness. Silt- and clay-rich, calcareous till reaches maximum depths of 10 m in trenches. In the northern part of the area, field stones include many erratic boulders of Ordovician limestone and lesser numbers of Cambrian sandstone derived from offshore.

Glacially disrupted terrain

Glacial disruption involves the jacking, dilation and disintegration of rock in the near surface and the entrainment of the resultant rock blocks to form boulder spreads and boulder moraines. Along the Lake Vällen corridor (Figure 4-22F), basic and ultrabasic gneisses dominate west of the lake whereas acid gneisses lie to the east. The topography is strongly oriented N–S along fracture-guided trenches, with sediment-covered floors of more than 20 m below summits. Summit areas maintain elevations of 25–35 m a.s.l. on 1 km wide rectangular bedrock highs. The contrasting morphology of the Vällen corridor compared with blocks further west (Figure 4-22) and east (Figure 4-43) appears to be a result of more closely-spaced (0.5–1.5 km) but wider (0.1–0.3 km) fracture zones aligned parallel to former ice flow.

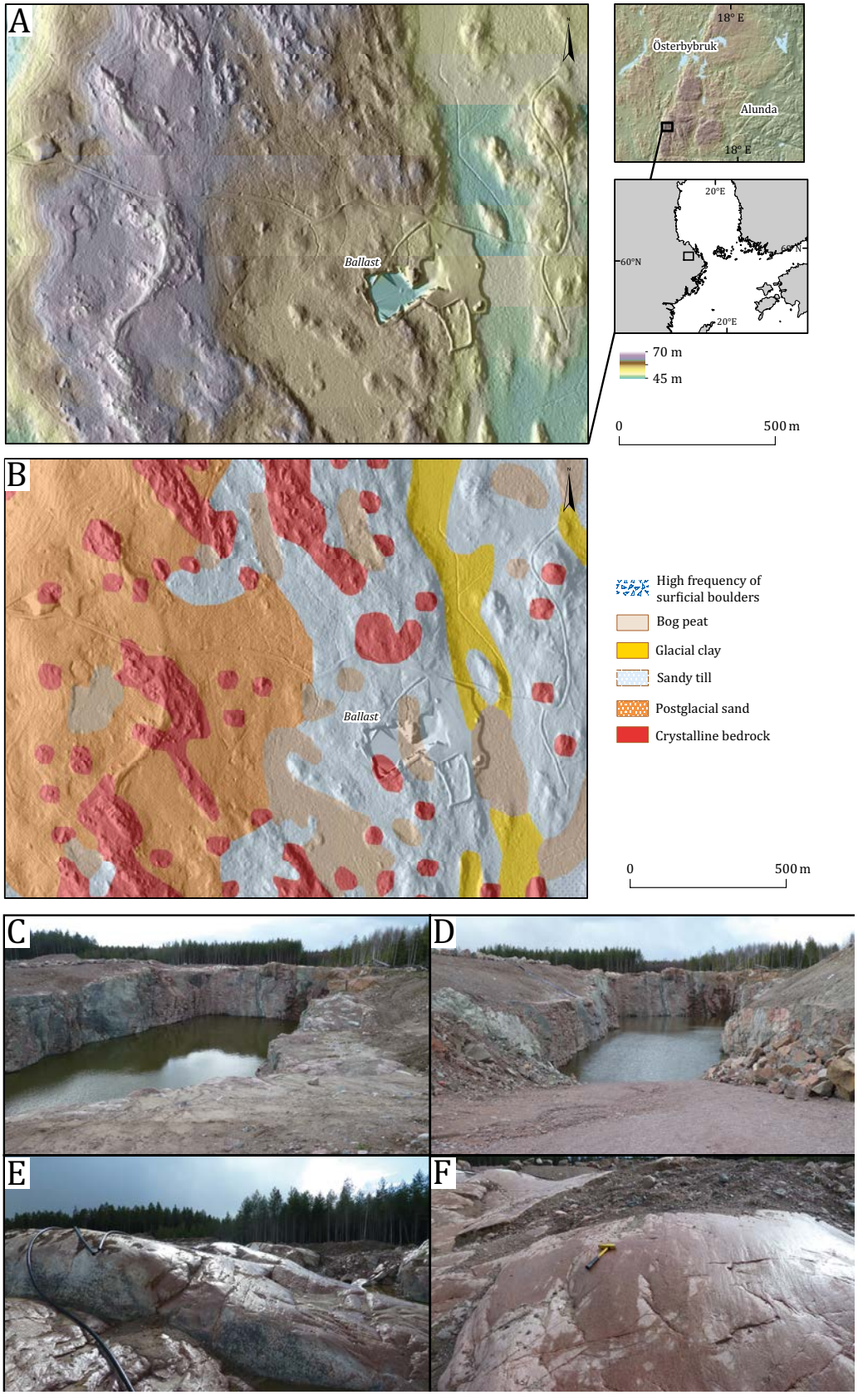

Figure 4-20. *Glacially roughened terrain around Ballast Quarry. A. LiDAR-based DEM of the area around the Quarry. B. Extract of SGU Quaternary map showing the distribution of bedrock outcrops and sediments. C. View to SW, showing the dominance of vertical fractures. Bedrock relief is < 5 m. D. Detail of C. The distant face shows a whaleback in section, bounded to the SE by a fracture zone. E. Surface of this whaleback, showing its smooth, abraded surface. F. Detail of a striated surface, with crescentic friction cracks. Boulder spreads are not mapped by SGU within this map area but become extensive at a distance of 1.2 km E of the Quarry.*

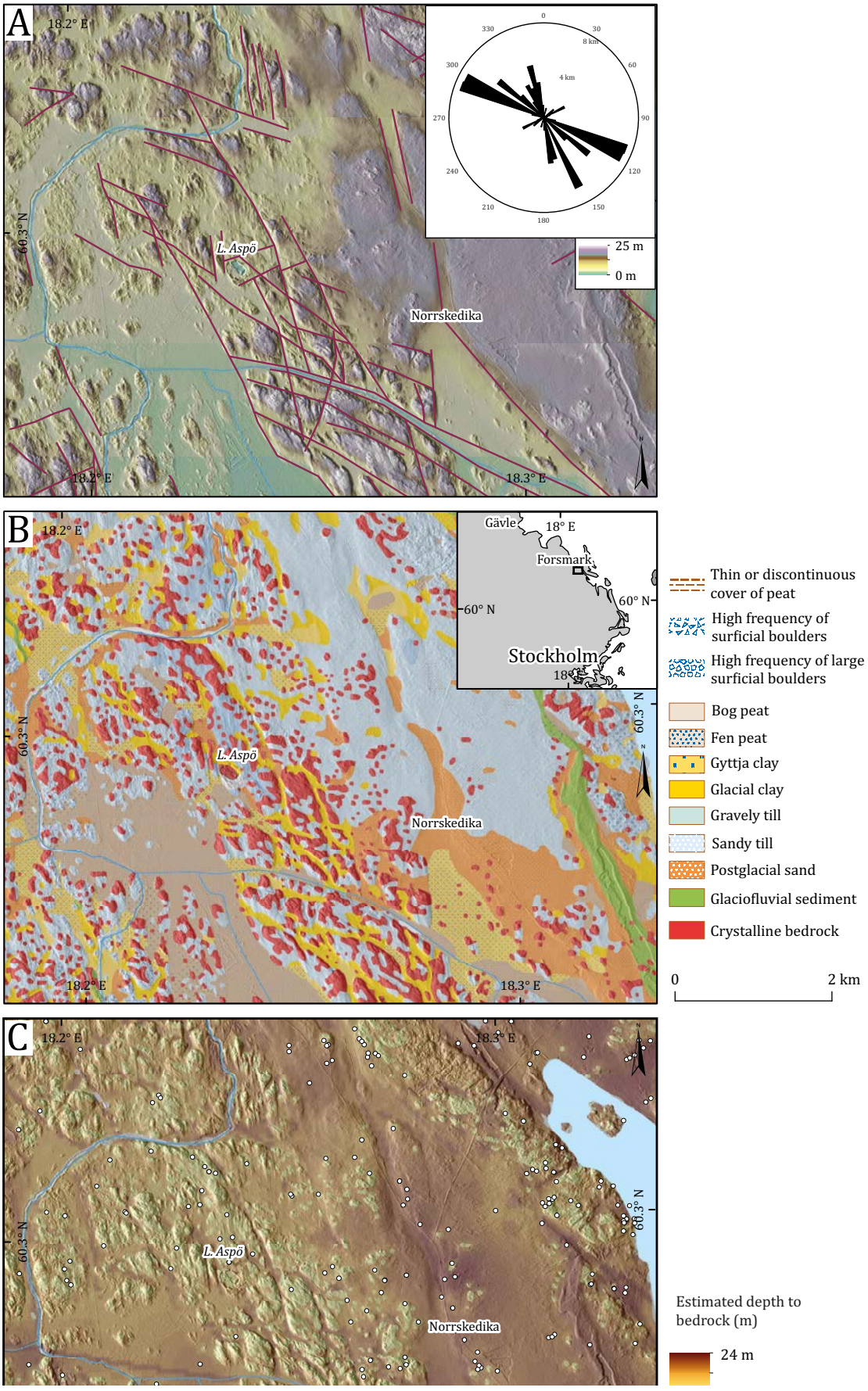

Figure 4-21. *Weakly glacially streamlined terrain around Lilla Aspö. A. DEM with main lineaments. Inset rose diagram shows fracture orientation based on these lineaments. B. Map of Quaternary geology based on SGU data. C. Depth to bedrock based on SGU data.*

The Vällen corridor (Figure 4-22) shows extensive development of disrupted bedrock and boulder spreads within a ~7 km wide belt (Lagerbäck et al. 2005). The belt is flanked by glacially roughened terrain with typical roches moutonnées (Lagerbäck et al. 2005), with smooth upper surfaces and plucked lee faces, separated by shallow till-filled rock basins and deeper NNW–SSE oriented trenches. In the disrupted zone, the terrain is irregular, with up to 15 m of relief between tops and basin floors, and includes box hills, roches moutonnées and rectilinear ridges and star and box basins. Reconnaissance mapping and available SGU data within the disrupted zone indicate that bedrock surfaces are extensively buried by spreads of large (1–5 m A-axis length), angular boulders of local rock types (Figure 4-22). The boulder spreads are locally piled into low moraine ridges. In LiDAR-based DEMs, boulder spreads are seen to cover the surfaces of box hills and roches moutonnées and also parts of the floors of shallow basins. Block covers are unlikely widely to exceed 2 m in thickness, however, as structural lineaments remain clearly visible in 2 m resolution DEMs. A distinctive feature is the presence of sharp-edged scarps, up to 5 m high and 250 m long, transverse and normal to former ice flow. The scarps appear to mark the edges of rock sheets lost to glacial plucking and ripping. Parallel lineaments, presumed to be grooves with metre-wide spacing, are apparent on the soles of these former rock sheets. At Grindstugan (Figure 4-22D), Fagervik (Figure 4-22E) and Gilberga (Agrell 1981), disrupted roches moutonnées occur with open fractures and boulder caves.

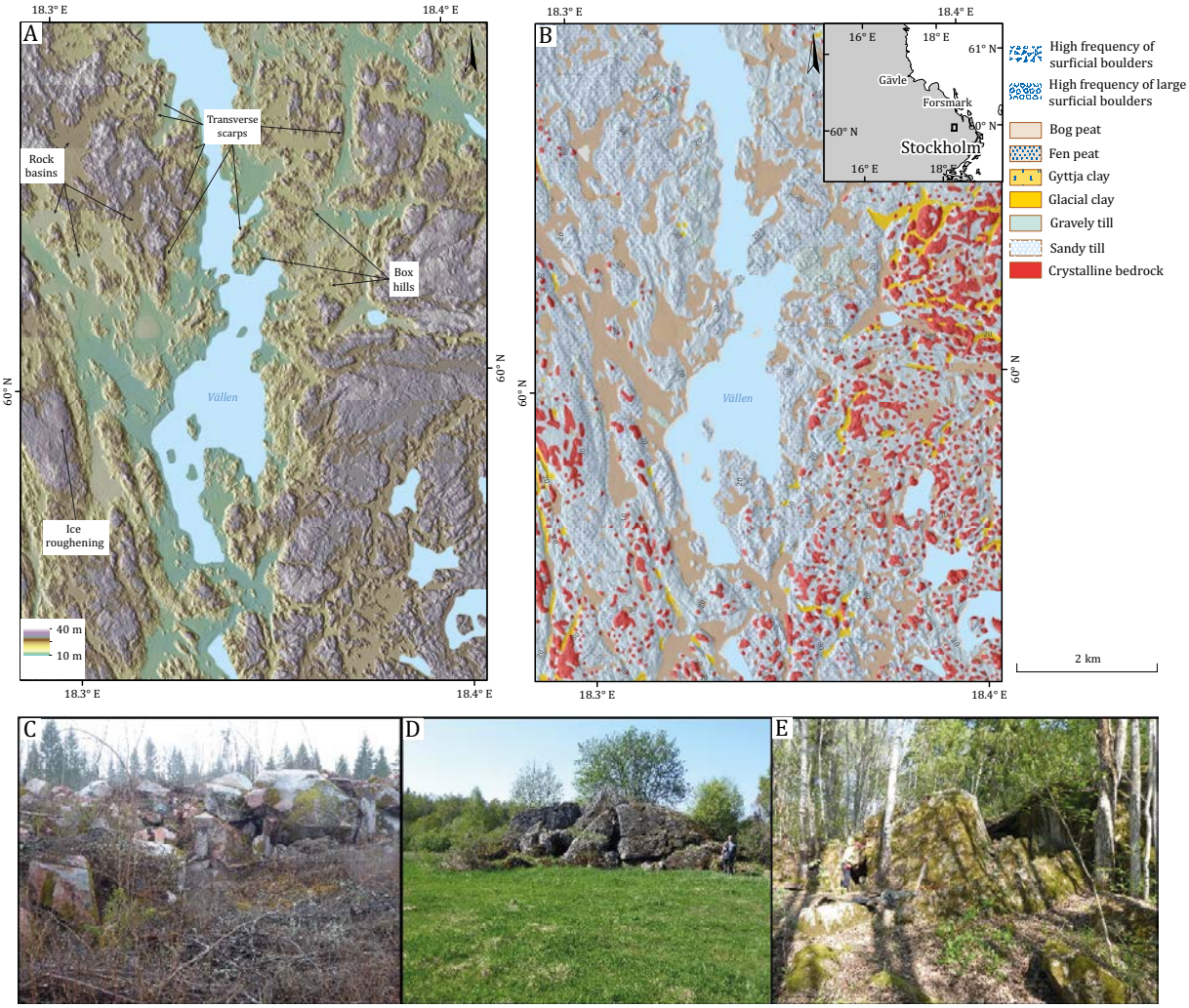

Figure 4-22. *Glacially-disrupted terrain along the Vällen corridor. A. DEM of part of the Vällen corridor, with key landforms. B. Extract of SGU Quaternary geology map showing extensive boulder spreads on both sides of the lake. C. Glacially disrupted granite gneiss bedrock blocks up to 5 m diameter at Nybygget (CN 682916; CE 6654977). D. Glacially disrupted roche moutonnée at Grindstugan (CN 679890; CE 6669734). E. Boulder cave in disrupted roche moutonnée at Fagervik (CN 681386; CE 6667691).*

Topographic roughness

Within Uppland, RTH, an index of topographic roughness calculated for 100 m windows, reveals different patterns of topographic roughness to those apparent at scales of more than 10 km (Figure 4-23). Moreover, RTP does not conform simply to the terrain types recognised above. High RTP in areas W of Österbybruk, S of Herräng and around Storvreta is an expression of high relative relief of 10–20 m between bedrock highs and closely spaced, fracture-guided trenches and basins, often lake-filled. Roughness is also high along the edges of topographic corridors, including ribbon lake-filled trenches E of Alunda. High RTP is seen in areas with extensive glacial disruption where large rock blocks, including mega-clasts >5 m b-axis length are present along Lake Vällen and in the Storvreta area. These differences are a reminder that terrain roughness is scale dependent (Falcini et al. 2018). Further refinement is needed to better assess how terrain roughness links to glacial erosion across scales.

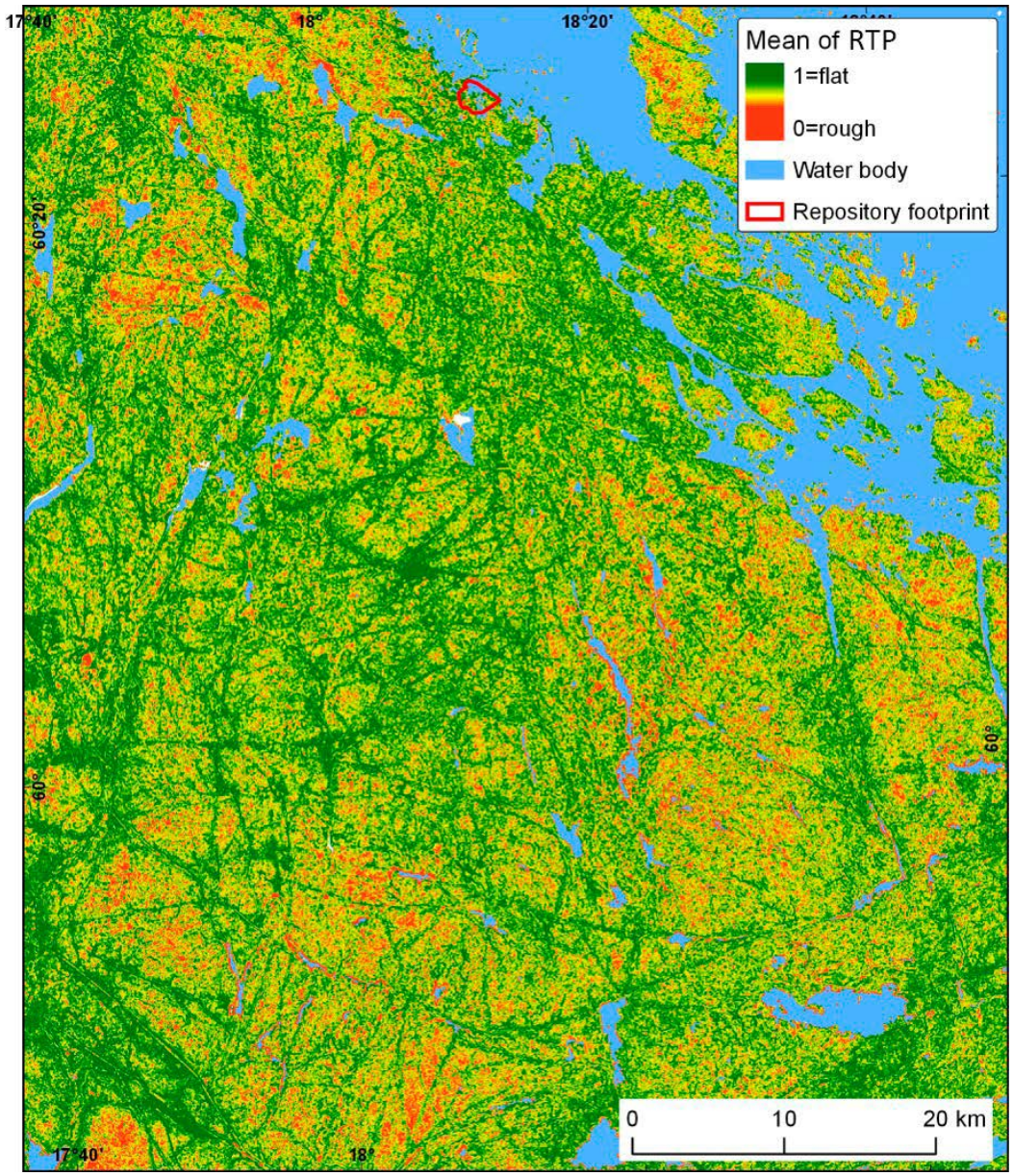

Figure 4-23. *Topographic roughness of the landscape in NE Uppland using the mean of the RTP (RTP calculation is explained in Table 4-1). The mean calculation is based on 50 × 50 cells (i.e. 100 × 100 m windows) and used to improve the visual impression.*

4.3.2 Macro to micro scale glacial landforms

The landform inventory at the macro- to micro-scales allows an assessment of the frequency of occurrence of minor glacial bedforms and the identification of assemblages of landforms of glacial erosion at these and other scales. Site inventories are available in Appendix 1.

Macroforms (10–100 m)

Common macroforms are small roches moutonnées and lee side and flank cliffs. Whalebacks and crags with till tails are less common. Disrupted bedrock and boulder spreads are present at only ~20 % of sites inventoried. Collectively, macroforms indicate that the shaping of bedrock hills by abrasion and plucking is important at this scale (Figure 4-24) and confirm that streamlining of the ice sheet bed is weakly developed and patchy in its occurrence in NE Uppland. Evidence of the operation of glacial ripping from disrupted bedrock and boulder spreads is spatially restricted in its distribution.

Mesoforms (1–10 m)

Common mesoforms include smooth rock surfaces, rounded stoss edges, lee-side and flank cliffs and lee-side blocks (Figure 4-25). These features indicate that abrasion and plucking also operate effectively at this scale. Diagnostic features of glacial ripping include sub-horizontal fracture fills, disrupted bedrock and hydro-fractures but are less common features. This lower representation may in part reflect the lack of sections at some sites where the immediate subsurface is not exposed. The absence, however, of most or all these features from some well-exposed sites indicates that the operation of glacial ripping was patchy in its distribution.

Microforms (less than 1 m)

Micro-scale landforms of glacial erosion are below 1 m in size, with low relief amplitude and are often found superimposed on larger landforms (Glasser and Bennett 2004). Some microforms are ubiquitous in the study area, or almost so, namely glacial polish, striae, conchoidal fractures, lee-side and flank cliffs and lee-side blocks. Polish and striae point to the widespread action of glacial abrasion on rock surfaces. Other features indicate that rock surfaces have been lowered by the removal of chips, flakes and small blocks. The frequency, extent and depth of these small cavities or *lacunae* can be large and cover surface areas equivalent to those of adjacent smooth or striated surfaces. Hence, development of lacunae is an important part of the erosion budget at this scale (Olvmo 2010). Sharp edges to many small cliffs and sockets and the presence of small blocks of very local origin indicate that plucking operated across fractured rock surfaces during the final stages of deglaciation. *Box sockets* and *prismatic sockets* found at the micro- and meso-scales appear to relate to the loss of blocks through the interaction of hydraulic jacking and fracture opening operating at depths of up to 0.5 m below the rock surface and are considered further below. Similar forms are recorded on islands E and SE of Forsmark (Holmlund et al. 2016).

Macroforms (10 - 100 m)

Järnboden (NE flank of large whaleback)

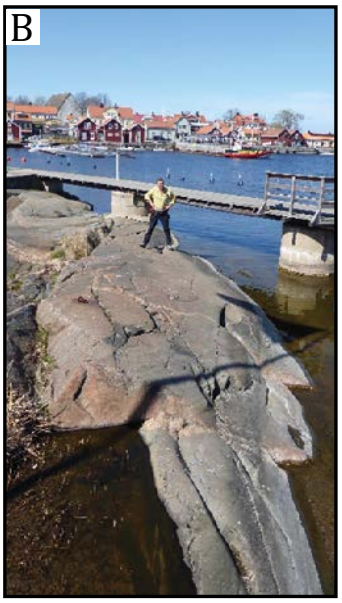

Öregrund Fiskehamn

Stenskar

Antenna View

Figure 4-24. *Typical glacial macroforms (10–100 m) in NE Uppland. A. Järnboden (CN 6676000; CE 690726) (Figure 4-52). NE flank of large whaleback, one of several along the northern, stoss edge of a rock block near Hargshamn. B. Surface of a small roche moutonnée at Öregrund Fiskehamn (CN 6694240; CE 689964) (Figure 1-1B), with extensive abraded surfaces and small lee side cliffs. Ice movement towards the camera. C. Stenskär, Öregrund (CN 6697008; CE 683061) (Figure 4-52). Complex abraded and quarried surface on closely fractured intermediate to basic gneiss. Ice movement away from camera. D. Antenna View, Forsmark (CN 6698218; CE 674127) (Figure 1-1B). Glacial disruption of orthogonally fractured amphibolite bedrock. Ice movement towards the camera.*

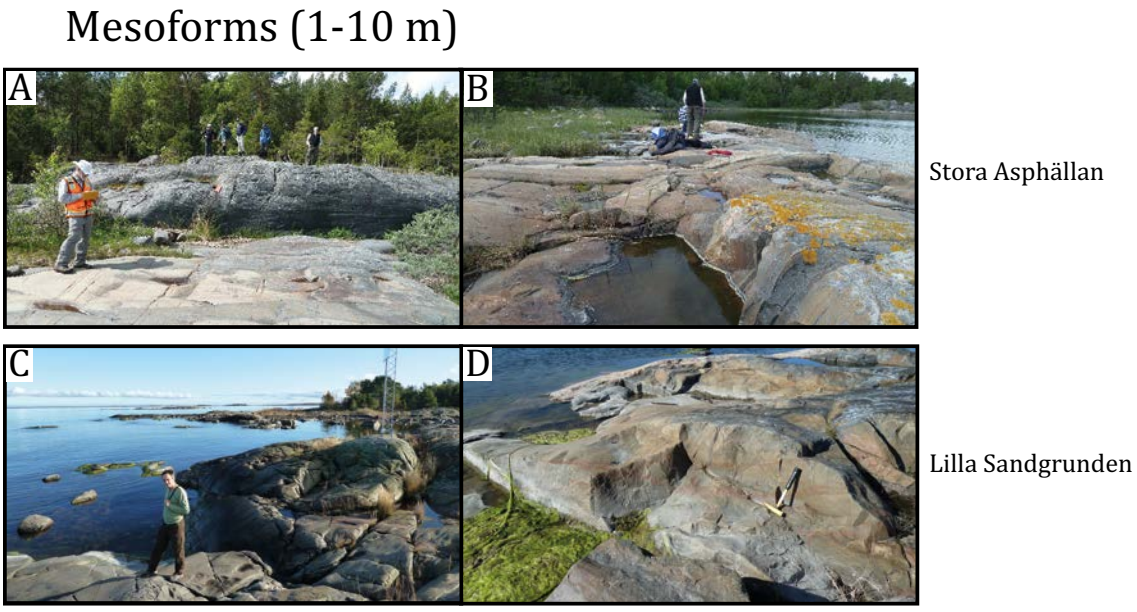

Figure 4-25. *Typical glacial meso-forms on coastal rock surfaces at Forsmark (Figure 1-1). A. Stora Asphällan. Abraded surfaces developed in granite gneiss and amphibolite. The more widely fractured amphibolite forms a small hill. Ice movement away from camera. B. Stora Asphällan. Abraded surface in intermediate banded gneiss, with rounded and sharp lee side cliffs and sockets Ice movement from R to L. C. Lilla Sandgrund. Small roches moutonnées with abraded surfaces and multiple edge rounded sockets. D. Lilla Sandgrund. Lee side cliffs and sockets with rounded and sharp edges.*

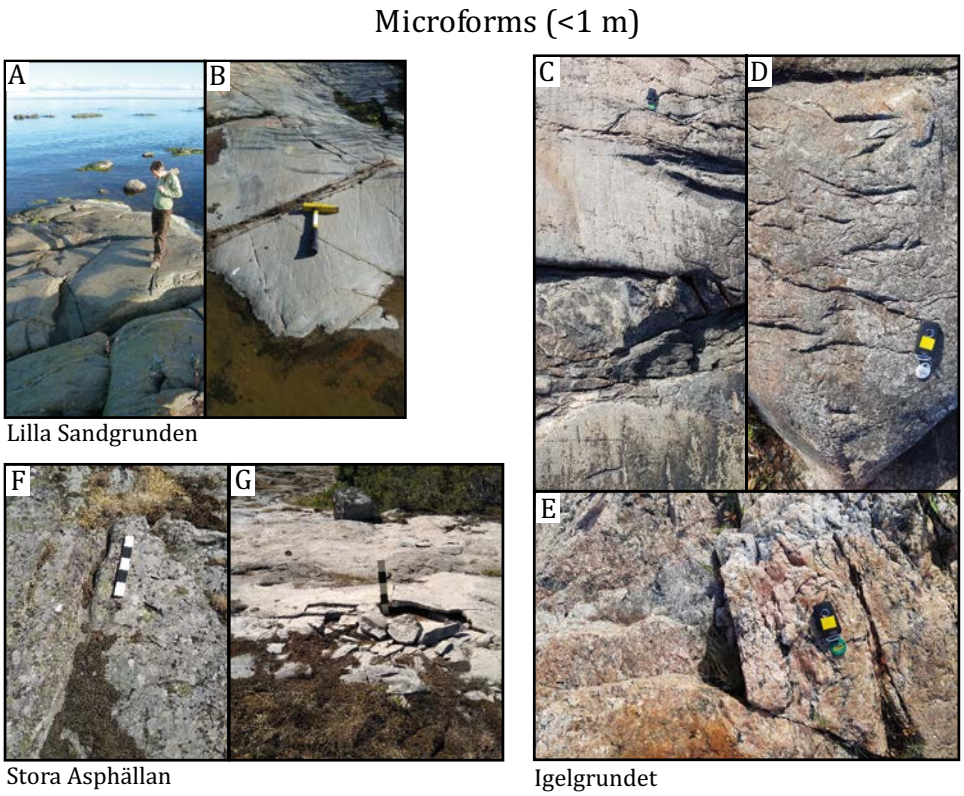

Figure 4-26. *Typical glacial micro-forms. A. Lilla Sandgrund (Figure 1-1). Multiple abraded and polished surfaces on intermediate gneiss. B Lilla Sandgrund. Crossing striae. C. Igelgrundet (Figure 1-1). Complex microforms on a single rock surface, with evidence of abrasion and loss of small rock fragments. D. Igelgrundet. Crescentic marks. E. Igelgrundet. Chipping and fracturing of a pegmatite dyke. F. Stora Asphällan (Figure 1-1). Small S-form. G. Stora Asphällan. Small A-tent pop-up indicative of high compressive stress in the rock surface.*

4.3.3 Glacial landforms and processes in the Forsmark area

Regional context

Forsmark stands in the tectonic hinge zone between Uppland and the Bothnian and Åland Seas (Beckholmen and Tirén 2009, Grigull et al. 2019). Two sets of regional fracture zones interfere in Forsmark area. One set, with a width of some tens of kilometres trends WNW–ESE. The other set consists of NNW–SSE to N–S trending faults (Figure 4-5). At Forsmark, the two fracture sets intersect to frame an elongate prismatic block (Beckholmen and Tirén 2010a). The Forsmark site is located in the north-western wedge of the Forsmark Block (Figure 4-3). At Forsmark, post-Ordovician reactivation of faults dislocated U2 mainly along the WNW–ESE set resulting in a local uplift of a lath-shaped block. The relative vertical component of the late displacement along the southern boundary of the Forsmark Block, the Forsmark Deformation Zone, is less than 20 m, while the relative vertical displacement along the north-eastern boundary, the Singö Deformation Zone, is ~5 metres. The upper surface of the Forsmark Block was tilted gently eastwards (Beckholmen and Tirén 2010a, Grigull et al. 2019). The Forsmark Block was formerly buried by Late Cambrian Alum Shale, Ordovician limestone and younger sedimentary rocks (Figure 2-20). At least several tens of metres of Early Palaeozoic rocks were removed by glacial erosion to over-deepen the present depression of Öregrundsgrepen, north-east of Forsmark. It is likely that glacial erosion has also re-exposed the basement surface of the Forsmark Block.

Glacial erosion forms at the local scale

Glacial erosion has made a significant impact on the surface of the Forsmark Block. The three terrain types recognised in Uppland can also be seen in the Forsmark area (Figure 4-27). Glacially roughened terrain occurs widely outside of a 2 km wide belt of weak glacial streamlining present over much of the repository footprint area. Boulder spreads occur widely within and beyond the Forsmark site. A belt of glacially disrupted bedrock and associated boulder spreads occurs below the large esker, named Börstil, that crosses Kallrigafjärden (Sohlenius et al. 2004). The landform inventory confirms that a wide variety of glacial landforms is present in the Forsmark area at the local (0.1–1 km) scale (Figure 4-28). In glacially roughened terrain, roches moutonnées are the dominant hill form but the Forsmark area has lower frequencies of box hills and more whalebacks than in this terrain type in other parts of Uppland. In glacially streamlined terrain, N–S oriented, elongate hills, 50–200 m long, are mainly crag-and-tail forms developed in weakly streamlined bedrock and with till tails. In the belts and patches of glacially disrupted terrain, there is widespread evidence of hydraulic jacking of bedrock, of resultant bedrock disruption and of the entrainment of bedrock sheets. As this evidence is linked to the newly recognised process set of glacial erosion, *glacial ripping*, the critical evidence is summarised below.

As in the wider area of Uppland, weak glacial streamlining and glacial disruption is superimposed on a basic geometry of glacially roughened terrain controlled by fracture patterns. The availability of detailed information of regolith thickness in the Forsmark site provides a rare window into the negative relief forms. A bedrock model created by removal of regolith (Figure 4-28) reveals a bedrock topography of 20 m relief and high roughness. Small hill masses and star and box basins cover roughly equivalent areas. Basins locally have an apparent relief of only a few metres but the floors of other depressions are rough, with closely-spaced bedrock risers. In the glacially streamlined area, the presence of bedrock streamlining parallel to N–S fracture orientations is clear. Glacially disrupted bedrock appears to be mainly distributed in areas of higher bedrock elevation (Figure 4-28) but may be concealed beneath post-glacial sediment in topographic lows.

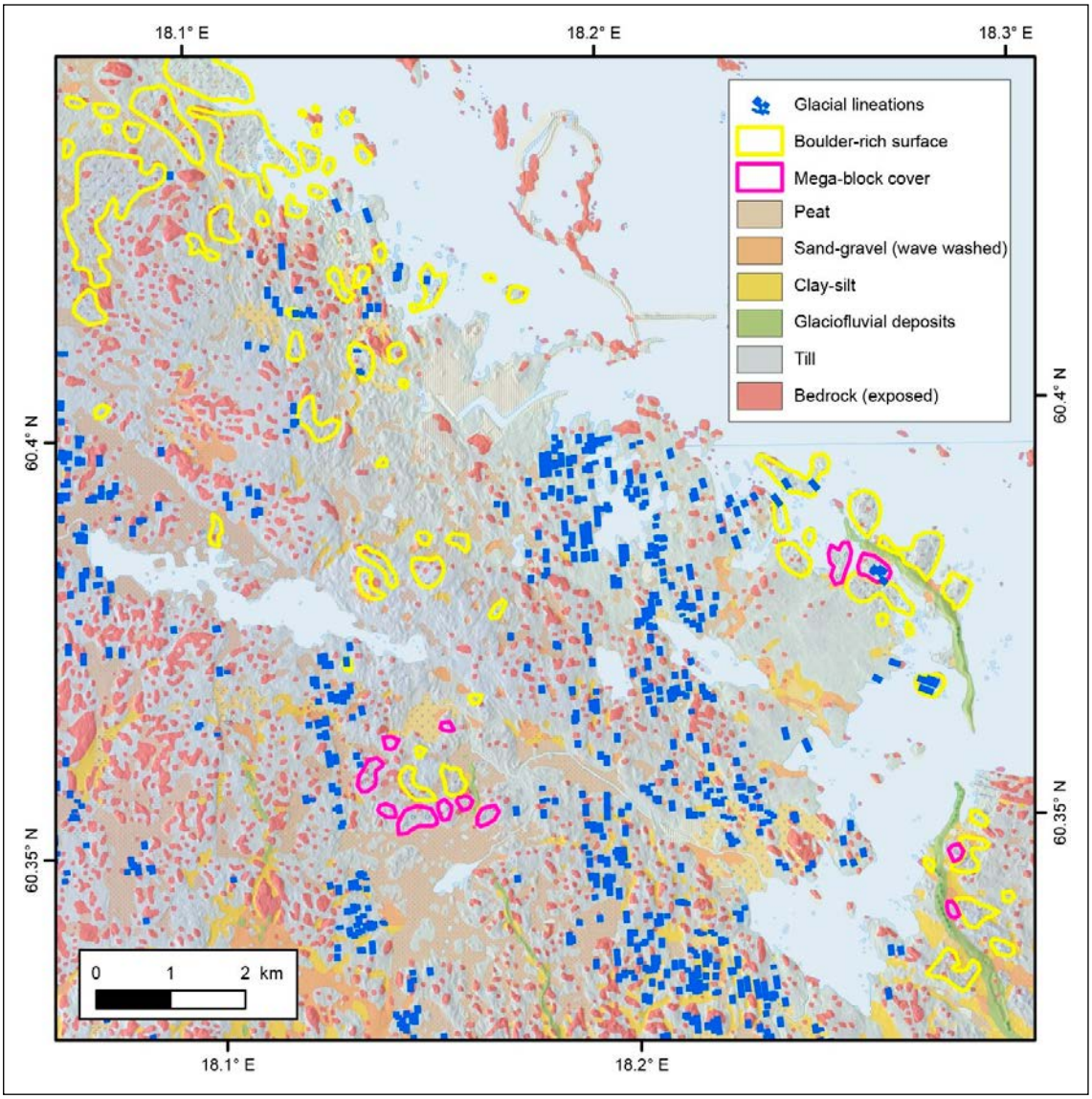

Figure 4-27. *Glacial lineations in the Forsmark area overlain on a map of bedrock outcrops, till cover and glacifluvial deposits. Areas with block-rich and mega-block covers are also shown. The distribution of glacial sediments in this area is also available in a revised soil model, where sediment depth data points have been established by trenching and drilling (Sohlenius et al. 2013).*

Glacial erosion forms at the macro- to microscales

Samples for cosmogenic nuclides come mainly from bedrock high points in the terrain around Forsmark and along a transect towards Uppsala (see Figure 5-2). The landform inventory at the micro- and meso-scales includes all cosmogenic nuclide sample sites and provides information on the presence and absence of features that can be related to different process sets (Table *4-3*). Forms of glacial abrasion are ubiquitous and include polish, striae and rounded edges. Small lacunae are also widespread on rock surfaces and indicate the loss of blocks and plates from small and shallow sockets. Forms derived from glacial plucking are also ubiquitous around the edges of rock hills, with the presence of large sockets on flank and lee slopes and detached, angular blocks in lee side positions. Features indicative of hydraulic jacking and bedrock disruption are generally missing but at several sites exposure of the subsurface is lacking.

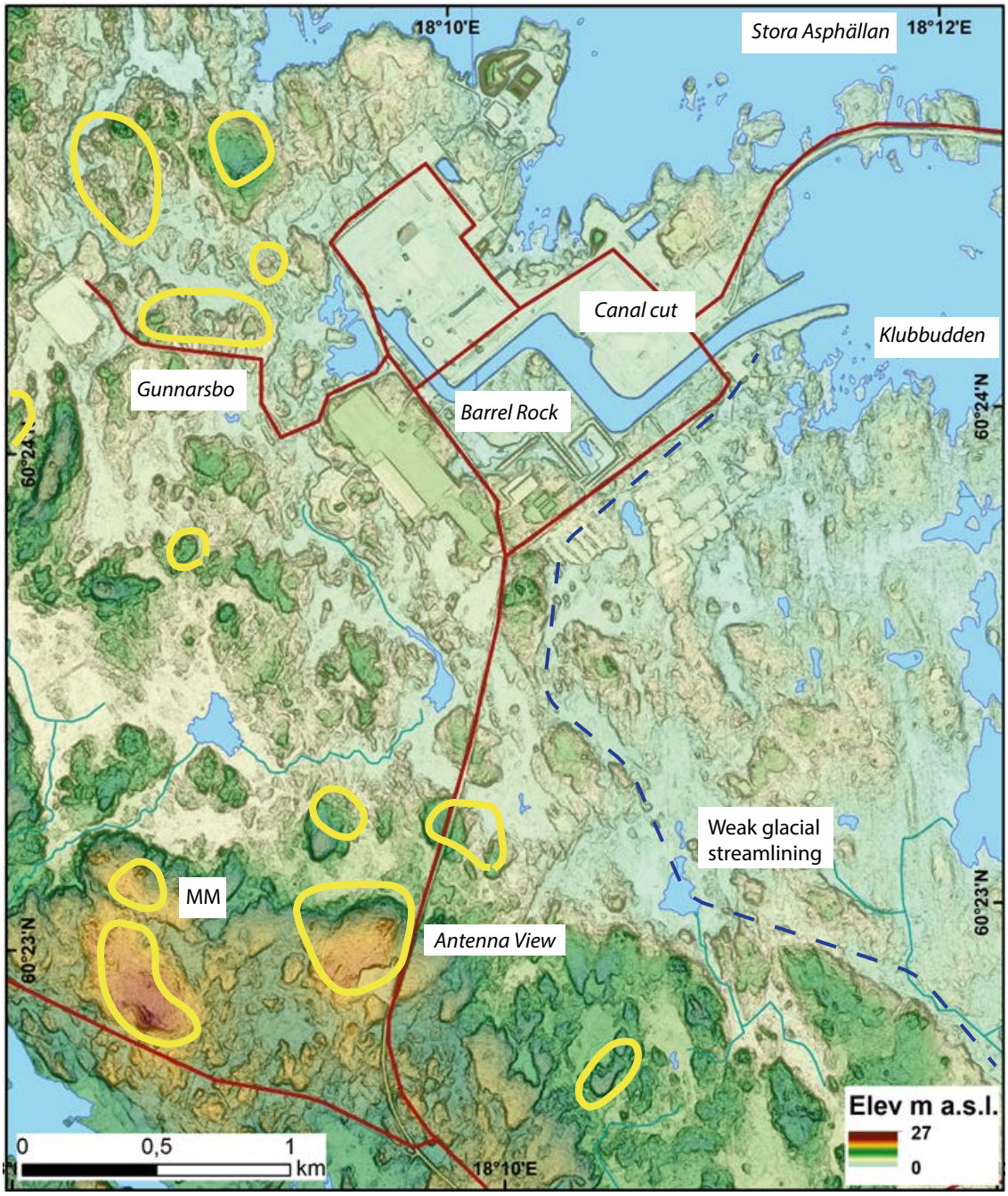

Figure 4-28. *DEM of the bedrock surface at Forsmark. Areas of disrupted bedrock with large numbers of angular boulders are shown in yellow, modified from SGU data with additional field observations on bedrock highs.*

Table 4-3. Presence or absence of micro- and meso-forms at 22 cosmogenic nuclide sample sites.

Micro-forms (0.1–1 m)	Polish	Striae	Grooves	Micro crag and tail	Conchoidal fractures	Edge fractures	Lee-side cliff	Stoss-side cliff	Flank cliff	Small blocks lost	Sub-horizontal fracture fills	Hydro fractures	Vertical displacement	Vertical fracture fills	Angular blocks	Box socket	Prismatic sockets	Lee-side blocks
Present	22	22	2	0	22	11	22	8	21	17	1	1	0	3	1	11	5	22
Absent	0	0	13	21	0	9	0	13	1	3	15	15	16	11	21	11	16	0
Don't know	0	0	7	1	0	2	0	1	0	2	6	6	6	8	0	0	1	0

Meso-forms (1–10 m)	Smoothed surface	Stoss edge rounding	S-form	Edge fractures	Lee-side cliff	Stoss-side cliff	Flank cliff	Sub-horizontal fracture fills	Disrupted bedrock	Hydro fractures	Box socket	Prismatic sockets	Lee-side blocks
Present	22	22	1	7	22	8	21	0	3	2	10	3	16
Absent	0	0	15	14	0	14	1	14	19	19	10	18	6
Don't know	0	0	6	1	0	0	0	8	0	1	2	0	0

Three contrasting, well exposed sites, Klubbudden, Wave Rock and Stora Asphällan (Figure 1-1), provide case studies for assessment of the main processes of erosion operating at the micro- to macro-scales on rock risers from which multiple samples were taken for cosmogenic nuclides.

Klubbudden

Klubbudden, with the adjacent Stånggrundet lighthouse headland, stands on the north-eastern edge of the repository footprint area (Figure 4-29).The bedrock here is a banded gneiss situated in the core of a folded ductile high-strain belt inside the Forsmark tectonic lens (Figure 4-3). The well-exposed bedrock along the coast slopes seawards and is dominated by a generally pale red, fine-grained and leucocratic metagranite (Stephens 2010). Metagranite is tectonically interleaved with dykes of amphibolite and pegmatite. The tectonic banding at Klubbudden is oriented approximately 115°/80° and a conspicuous mineral stretching lineation in all the rocks, except the pegmatite, is oriented 125°/35°. These fracture orientations are clearly evident in DEMs and drone images along with a N20E–S20W to N40E–S40W oriented fracture set (Figure 4-29A and B). Generally sub-horizontal fractures with varying inclinations locally divide the rocks into 0.3–1.3 m thick sheets (Figure 4-29). Mean feldspar crystal length is 1.9 mm (1σ = 0.9 mm). Mafic veins also occur. Mean spacing of fractures at the embayment cosmogenic nuclide sample site is 0.42 m (Figure 4-39).

The headlands reach a maximum elevation of 5 m a.s.l. Domes, whalebacks and roches moutonnées rise only 1–3 m above surrounding rock surfaces (Figure 4-29). Abraded surfaces are widespread especially on the highest ground. On the present shoreline, blocks up to 40 cm A-axis length have been removed from sockets by wave action and transported into adjacent hollows (Figure 4-29B). Larger sockets and low steps are common on rock surfaces with high fracture densities (Figure 4-29B). The presence of abraded edges and faces confirms that these sockets and steps are products of glacial erosion. Many sockets are sharp edged, with box and prismatic shapes, and resemble similar forms seen at Stora and Lilla Sandgrund (Figure 1-1). A measure of the depth of rock lost to late erosion is provided by an area of 200 m^2 where ~10 % of the surface has lost tabular blocks ~20 cm thick. In depressions, 10–30 cm thick, sandy and gravel-rich till layers remain but wave wash has also removed till and released boulders.

Figure 4-29. *Stånggrundet headland macro- to micro-forms. A. Drone image of part of the shoreline around the lighthouse at Stånggrundet. B. Same image showing areas of boulder accumulation after wave transport and locations where blocks have been lost from large sockets after glacial erosion. C Trench along western margin of the headland. Flank plucking, with rounded and sharp edges to rock steps that follow gently inclined fractures. D. View westwards along the shoreline towards the lighthouse. Abraded rock surfaces with mainly rounded edges and multiple sockets. E. View eastwards along the shoreline towards the lighthouse. Convex stoss surface with abraded facets and loss of small, cuboidal blocks. F. Closely fractured and rough rock surface from which small rock blocks and fragments have been removed, in part by wave action. G. Gently inclined fractures in pink, fine- to medium-grained and leucocratic metagranite. Stoss-side block loss. Note the sharp, unabraded edges to rock steps. H. Stoss- and flank-side rock steps with rounded and abraded upper surfaces.*

Abrasion has smoothed rock surfaces over wide areas. Closely spaced fractures have facilitated block removal. An important late phase of block removal is indicated by fresh edges to sockets and by the presence of box and prismatic sockets from which blocks appear to have removed under groundwater overpressure.

Wave Rock

Wave Rock is an informal name given to a rock riser with a summit at 11 m a.s.l. SW of Tixelfjärden that stands to the SE of the repository footprint area (Figure 4-30). The hill summit is developed in unusually massive porphyritic granite gneiss with spacing of vertical fractures that exceeds 10 m. In the surroundings, the dominant rock type is a grey, medium-grained and equigranular metatonalite with segregations and veins of pegmatite (Figure 4-3). The metatonalite shows a conspicuous, linear grain-shape fabric oriented 140°/30° and is also foliated (L > S tectonite) (Stephens 2010). In DEMs, the dominant fracture orientations are to NW–SE and NE−SW and oblique to northerly ice flow. On the mapped summit surface, the dominant fracture set is oriented W30N−E30S to W40N–E40S (see Figure 4-39). Sheeting joints with up to 1 m vertical spacing occur in places on the flanks of the outcrop, away from the mapped summit area.

Wave Rock is a convex rock hill, with a gently undulating top surface of less than 1.5 m relief over an area of ~6 000 m^2. Glacial polish is preserved in patches on phenocrysts on the lee slope. Hence, a maximum of 2 mm depth of the rock surface has been lost to weathering since emergence. Most edges to fractures are well-rounded and there are only occasional, widely spaced, cm deep, shallow sockets. The flanks of the hill show 0.5–3 m high rock steps and sockets where blocks have been removed by plucking. Fractures are more closely spaced on the stoss face of the hill and on the low whalebacks that are found to the south. Rock slabs from which samples were cut stand less than 3 m above their surroundings. On this lower ground, sockets up to 2 m deep are present below flank and lee faces, several with sharp edges and fresh faces indicating block removal during deglaciation. The southernmost sample site shows spalling of 5–10 cm thick sheets from the surface of a low whaleback.

The mapped fractures around the Wave Rock summit sample site form a 20 m^2 area in the total exposed outcrop. This part of the outcrop is formed in granitic gneiss that varies from fine-grained (mean feldspar crystal length of 0.8 mm; 1σ = 0.3 mm) to pegmatitic (mean feldspar length of 10.4 mm; 1σ = 4.9 mm). Pegmatites occur as veins and also appear on the outcrop surface as lenses. Sub-vertical fractures track the pegmatite veins and the cosmogenic nuclide sample site is located in this zone of pegmatites. The mean spacing of sub-vertical fractures is 1.1 m, which is the widest recorded for any of the 12 measured sample outcrops at Forsmark. Fracture spacing measured using the line method is much wider at 5.5 m (Section 4.3.4).

The upper surface of Wave Rock lacks micro- to macro-forms formed by processes other than abrasion. Hence, it is possible that the upper surface was eroded by abrasion alone during the time interval that the present rock surface developed. Plucking was likely suppressed on the upper surface by the wide spacing of the vertical and horizontal fractures. Plucking has been important in removing blocks from the stoss, flank and lee sides of Wave Rock, and also from around its base. On upstanding rock surfaces at lower elevations, abrasion was accompanied by processes which removed small rock fragments and plates. No evidence of ripping is seen at Wave Rock but extensive disrupted terrain with boulder spreads is found < 0.5 km NE of the site.

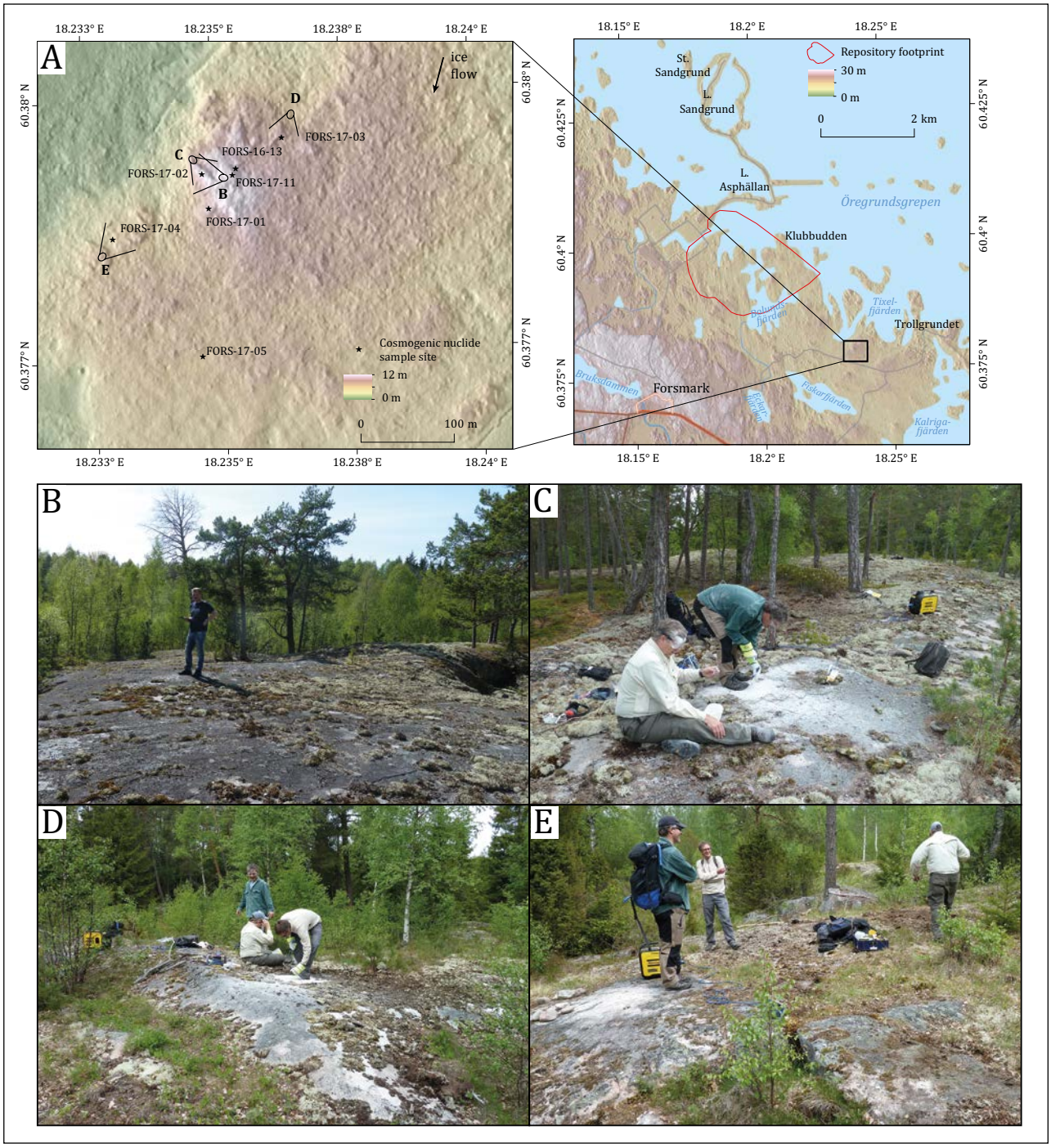

Figure 4-30. *Glacial macro- to micro-forms at Wave Rock. LiDAR image of Wave Rock, a small hill summit at 11 m a.s.l. E of the proposed repository site. A. Location and DEM of the Wave Rock locality, showing the locations of the rock surfaces sampled for cosmogenic nuclides. Locations and viewpoints of photographs B–E are indicated. B. Gently curved summit surface with few open, vertical fractures. C. Sample site FORS 17-02, showing the gently curved summit surface of the hill in the background. D. Sample site FORS 17-03 on the stoss side of the hill. Vertical fractures here are more closely spaced than on the hill top. E. Sample site FORS 17-04. Note the small cliffs, edges and sockets from which blocks have been removed.*

Stora Asphällan

This former small island lies N of the repository footprint area (Figure 4-31) and close to the Singö Deformation Zone (Figure 4-3). A tectonically banded gneiss sequence is exposed, with banding oriented 130°/90° (Stephens 2010) and main fractures oriented NW−SE and NE−SW (Figure 4-31). Grey, fine-grained and finely banded, felsic rock, possibly volcanic in origin, forms the dominant

rock type. Subordinate rock types include metadiorite, fine-grained amphibolite and pegmatite that occurs as both semi-concordant boudins and discordant, dyke-like bodies. On the felsic rock, vertical fractures are generally spaced at less than 1 m, whereas on large amphibolite masses, which form small hills (Figure 4-25A), the fracture vertical fracture spacing is more than 2 m. Closely spaced, gently inclined fractures in the felsic gneiss dip to NW. A small A-tent is seen in the felsic gneiss (Figure 4-26G). A-tents are pop-up micro- and meso-forms where a pair of abutting raised slabs, each roughly rectangular, meet in a crestal fracture, and enclose a prismatic void (Ericson and Olvmo 2004, Twidale and Bourne 2009). A-tents indicate high compressive stresses at the present rock surface.

The mapped area (Figure 4-39) shows low convexity and is located on a NW-sloping outcrop at the present shoreline in fine-grained granitic gneiss (mean feldspar length of 1.4 mm; $1\sigma = 0.7$ mm). This small area displays the most complex fracture pattern of the 12 mapped outcrops (Figure 4-39). The dominant fracture set is oriented N60E−S60W to N73E−S73W and frequently comprises closely spaced parallel fractures (~5 cm), which are the main contributor to the close fracture spacing observed on this outcrop (mean of 0.25 m). A second fracture set, oriented N32E−S32W, occurs in the northern part of the mapped area. Small mafic lenses (few 10s of cm^2) occur in the northernmost and southernmost parts of the mapped area.

Stora Asphällan is one of several N−S orientated roches moutonnées that rise to 6 m a.s.l. and are joined by the causeway road. The detailed form of Stora Asphällan is controlled by the different fracture spacing but common fracture orientations in the felsic gneiss and amphibolite (Figure 4-31). Differential glacial erosion has led to the emergence of amphibolite lenses as rock hills. Rock surfaces are extensively abraded, with smooth surfaces on finer-grained gneisses (Figure 4-31), but sockets are also widespread (Figure 4-31). Many large sockets and rock steps retain sharp edges and indicate block removal late in the last glaciation. Small blocks may have been removed from the rock surface by wave action. Blocks transported by waves occur as clusters in rock hollows.

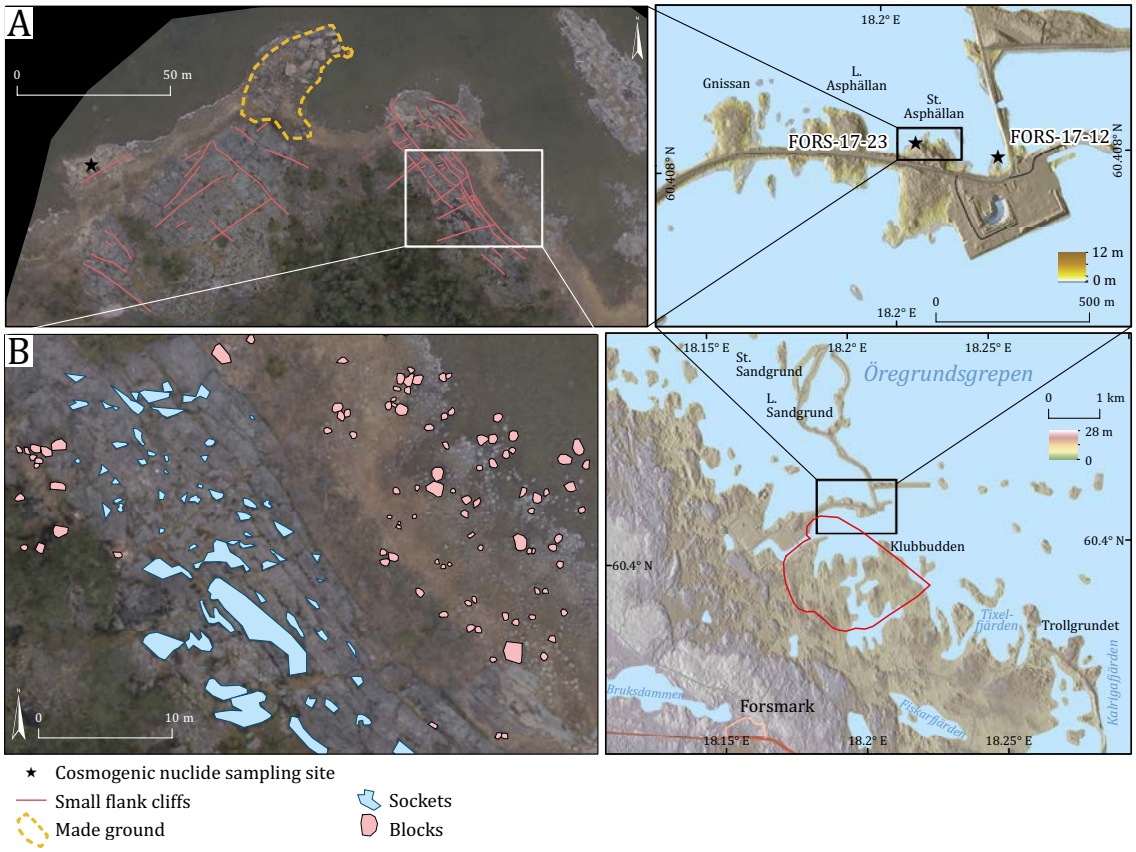

Figure 4-31. *Glacial meso- and micro-forms at Stora Asphällan, Forsmark. A. Main fracture lineaments and extent of exposed, glacially abraded surfaces. B. Distribution of sockets and blocks.*

Evidence for glacial disruption at Forsmark

Glacial disruption is a term used to describe a process set that involves components of hydraulic jacking, bedrock disruption, entrainment and transport of rock blocks and deposition. Evidence for hydraulic jacking of gneiss bedrock below the Fennoscandian Ice Sheet was first described in detail from excavations at Forsmark in the 1970s in a substantial body of work that remains the primary source of information for this phenomenon (Carlsson 1979, Carlsson and Olsson 1982a, b, Carlsson and Christiansson 1987, 2007). Subsequently, evidence for hydraulic jacking was observed in other parts of the Forsmark site (Leijon 2005). Detailed modelling of groundwater pressures under various scenarios beneath former ice sheets at Forsmark suggests that hydraulic jacking may be possible to depths of 200 m (Lönnqvist and Hökmark 2013), or even 400 m (Talbot 2014). Surveys of the Forsmark area revealed extensive spreads of large, locally-sourced, angular boulders (Sohlenius et al. 2004, Lagerbäck et al. 2005). Further field observations suggest that hydraulic jacking is linked explicitly to glacial disruption of bedrock and the entrainment and removal of rock blocks over wide areas. That research continues and what follows below is a short summary of current understanding of glacial disruption in the Forsmark area.

Hydraulic jacking and bedrock disruption

Critical evidence for the operation of *hydraulic jacking* at Forsmark comes from sets of sediment-filled, sub-horizontal fractures in granite gneisses exposed in excavations during the construction of the power plants and the canal (Figure 4-32). The sediment fills occur mainly in the upper 5 m of the rock pile but are recorded to a depth of 13 m (Carlsson and Olsson 1976). The sediment infills comprise mainly unconsolidated, laminated silt and sand. The sediment was introduced by glacial meltwater into fractures opened at very high subglacial water pressures (Pusch et al. 1990, Hökmark et al. 2006, Carlsson and Christiansson 2007, Hökmark et al. 2010).

Associated dilation is indicated by the opening of pre-existing, mineral-coated, sub-horizontal fractures and *hydrofracturing* is suggested by the development of parallel new, non-coated fractures (Carlsson 1979). Jacking and dilation also has been observed in temporary excavations below multiple till layers in the repository footprint area (Leijon 2005, Forssberg et al. 2007).

Glacial disruption of bedrock has been recorded at numerous localities at Forsmark including within the 1970s excavations (Figure 4-32), in temporary excavations (Leijon 2005, Forssberg et al. 2007) and in surface exposures (Figure 4-33). Glacially disrupted bedrock is marked by intense fracturing, the presence of sediment fills in fractures of various inclinations, the presence of crushed or fragmented rock fragments along dilated fractures and the slight movement and rotation of rock blocks in the near surface.

In photographs from the 1970s canal excavations (Figure 4-32), there is little evidence that jacking, hydrofracturing and disruption was followed by glacial entrainment. The photographs show till cover on parts of the bedrock surface but underlying disrupted bedrock has not been moved and few large blocks occur in the till base (Figure 4-32E and F). Boulder spreads are also absent from the immediate area around the canal cuts. Along the Forsmark cooling water inlet canal, hydraulic jacking and fracturing are identified as precursors to glacial ripping but the fractured bedrock surface was not moved by the overriding ice sheet. The presence of over-consolidated, carbonate-rich basal till units of possible MIS 4 or older age overlying jacked bedrock (Forssberg et al. 2007), over-consolidated silts in sub-horizontal fractures (Carlsson and Olsson 1976) and of palynomorphs of thermophilous trees in sediment found in fracture fills (Robertsson 2004) suggest that at least some hydraulic jacking at Forsmark predates the last deglaciation.

Glacial ripping

There is widespread evidence around the Forsmark site for *glacial ripping* of bedrock that occurred at a late stage during the last deglaciation. This takes the form of poorly exposed bedrock outcrops that show widespread disruption and displacement along horizontal, inclined and vertical fractures. Tilted and/or transported angular blocks of similar gneiss lithology are found in the immediate vicinity of source outcrops. More conspicuous are *boulder spreads* composed of mainly locally-derived blocks (more than 1 m A-axis) and mega-blocks (more than 5 m) that have been mapped over wide areas around Forsmark (Sohlenius et al. 2004).

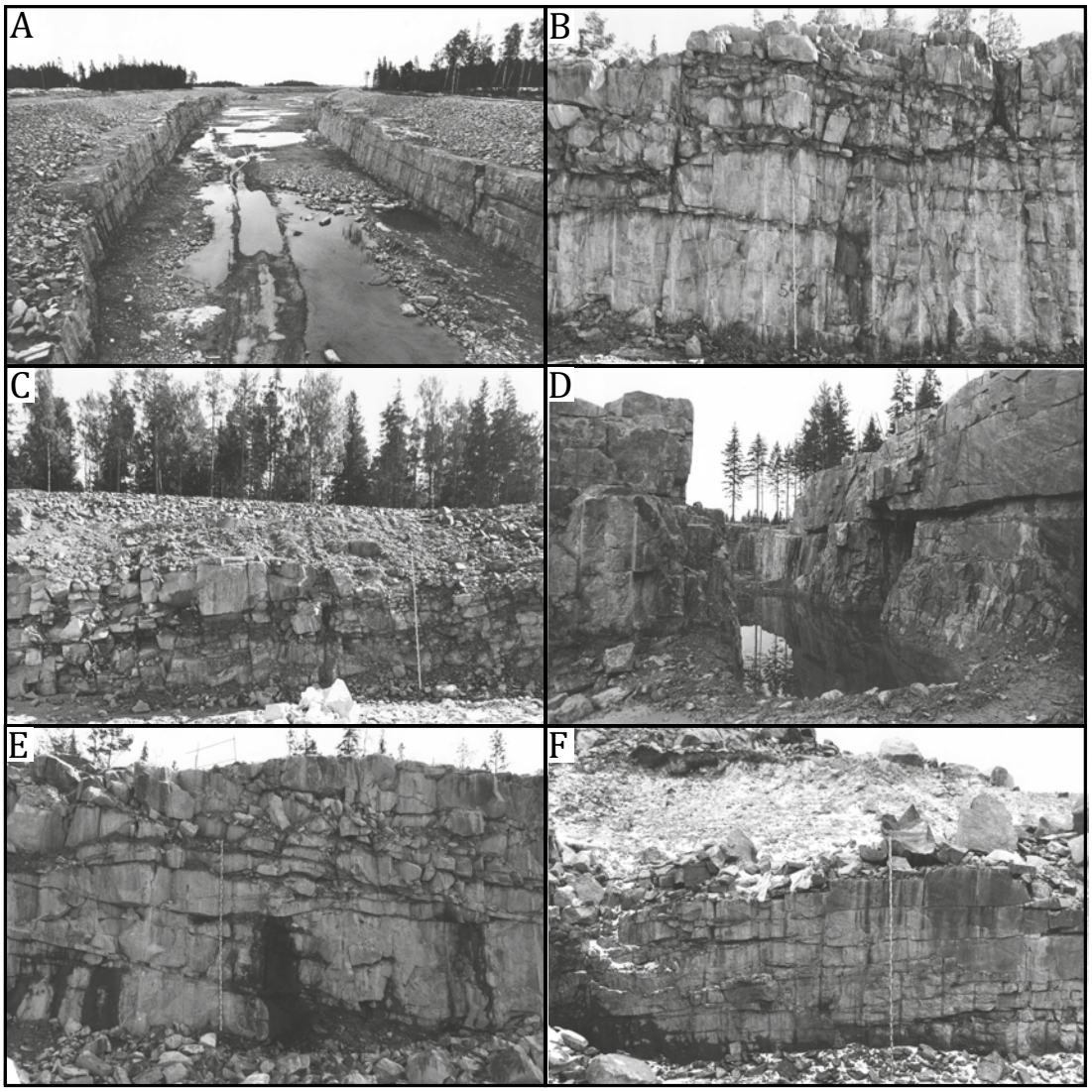

Figure 4-32. *Sediment-filled sub-horizontal fractures in excavations for the inlet canal at Forsmark in the 1970s (Photos by Anders Carlsson). A. View to seaward of the canal cut showing sub-horizontal fractures in granite gneiss. B. Hydraulic jacking along sub-horizontal fractures. C. Gently inclined and vertical open fractures with near-surface sediment fills. Broken rock fragments along open fractures. Measuring pole is 4 m long. D. Glacially disrupted bedrock with sediment fills and rock fragments in open fractures. The maximum thickness of the silt and sand fill in the face to the right is 0.8 m. E. Glacially disrupted bedrock showing no lateral disturbance below till. F. Hydraulically jacked bedrock showing no lateral disturbance below till.*

At the site named here as Barrel Rock (Figure 4-28), the onset of glacial ripping is apparent on the lee side of a large roche moutonnée developed in a massive amphibolite and gabbroic gneiss boss (Figure 4-33A and B). Vertical fracture spacing in the lee of the hill is less than 4 m. A rock sheet less than 2 m thick and 50 m long has been disrupted and detached but the transport distance for individual blocks is of the order of metres (Figure 4-33).

At 0.5–1 km west of Barrel Rock, at a site named Gunnarsbo (Figure 4-28), drone images and ground surveys indicate that bedrock surfaces have been disrupted and mobilised by ice moving across an area of ~0.1 km^2. The rock surface is generally concealed beneath a 1–2 m thick cover of angular blocks (Figure 4-34). Small areas of *in situ* bedrock are apparent from orientations of fractures, gneiss foliation and striae that are consistent with nearby bedrock outcrops. Blocks derived from these outcrops can be found at distances of 1–10 m. Amphibolite rock types dominate, likely derived from the less than 3 km wide band of amphibolite found at and N of the Gunnarsbo locality.

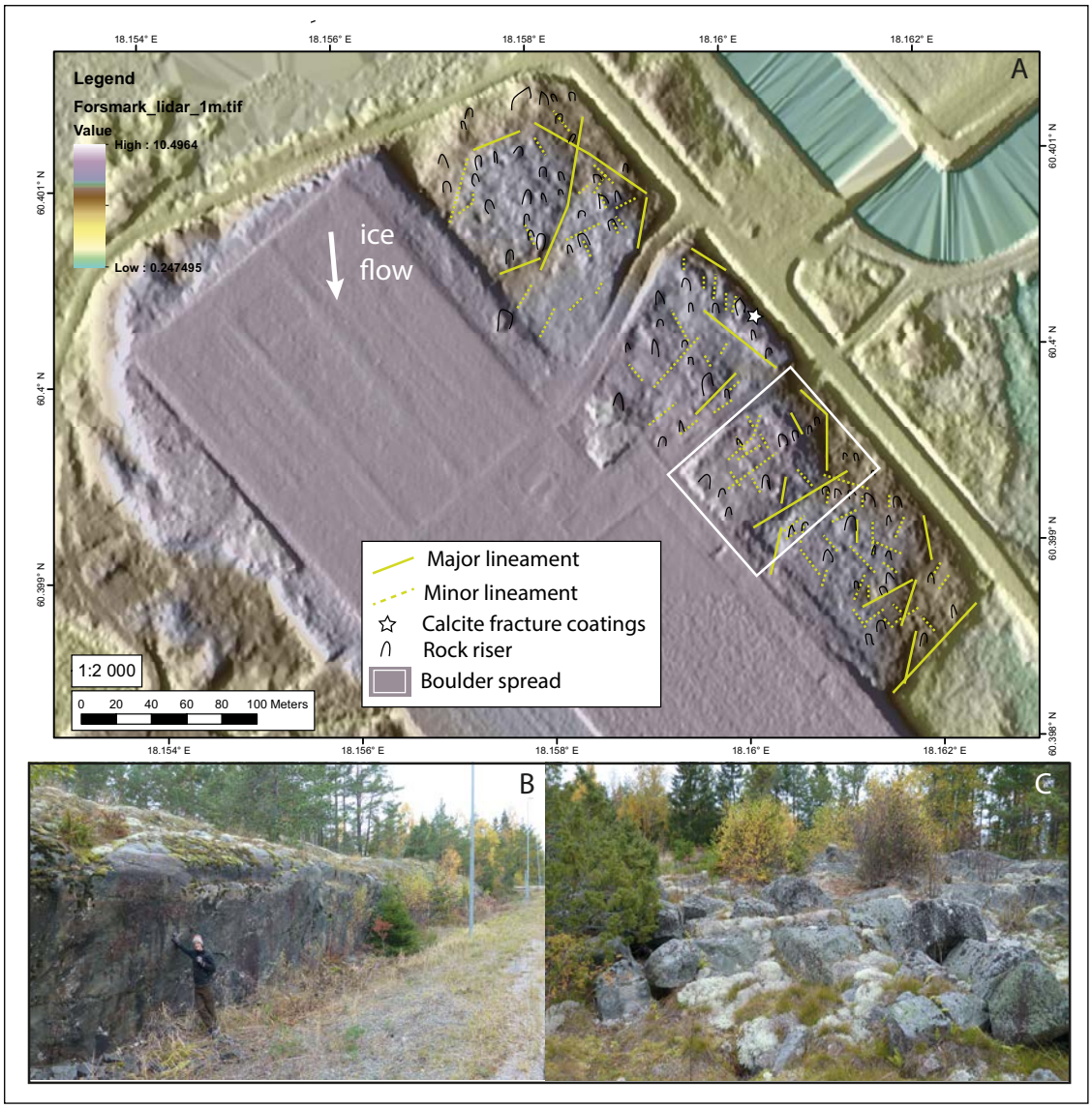

Figure 4-33. *Barrel Rock, Forsmark. A. LiDAR-based DEM of the context of the roadside outcrops. Fracture-guided lineaments interpreted from the image, along with low rock risers. e. B. Massive gabbroic gneiss on the stoss side of the hill mass. Vertical fractures close to the figure retain silt and sand fills and show calcite coatings. C. Angular boulders of gabbro carried a few metres from glacially disrupted bedrock. Location of calcite coatings and area of boulder spreads shown in A.*

Lineaments visible in DEMs (Figure 4-35) indicate that bedrock is present at shallow (less than 3 m) depth across the area. Various features are apparent in DEMs that show how glacial ripping has eroded the bedrock surface. Traverse scarps appear to represent the edges of missing rock sheets. Mega-erratics form a conspicuous boulder train, with a gouge developed in the rock surface along the track of one of the largest blocks. Displaced rock blocks are locally piled into ~2 m high boulder moraines.

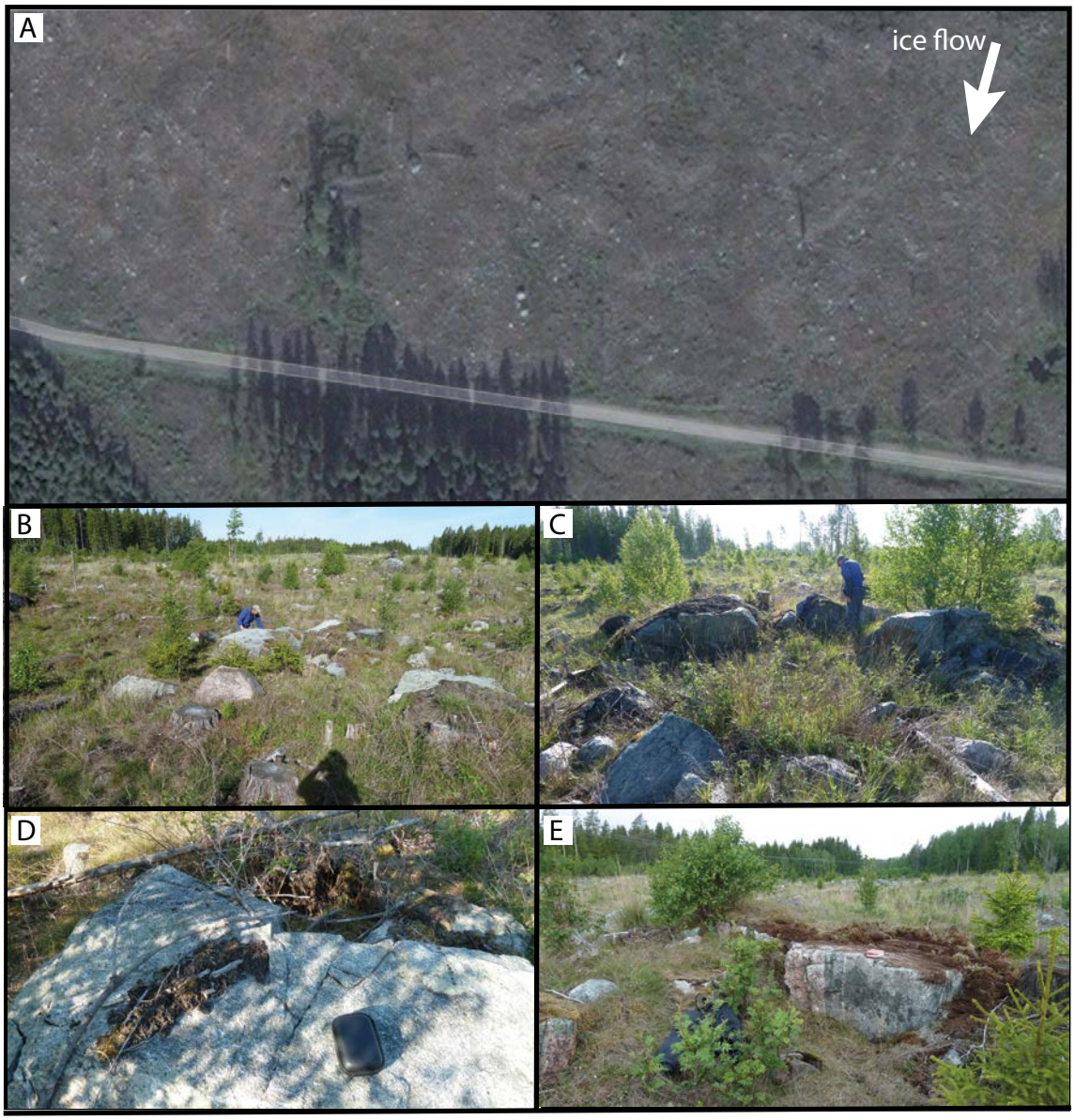

Figure 4-34. *Gunnarsbo. A. Vertical air photo showing large blocks on the till surface. B. Large angular blocks amid glacially disrupted bedrock. C. Glacially disrupted bedrock surface from which large blocks have been removed. D. Abraded top surface of a bedrock remnant. E. Plucked face of the same bedrock remnant.*

Further evidence in support of the development of groundwater overpressure beneath the edge of the Fennoscandian Ice Sheet

During survey of the landform inventory (Appendix 1), it became evident that 1–10 m long, shallow, box and prismatic sockets were frequent on rock surfaces in the Forsmark area. Detailed drone images from Stora Sandgrund, a small island N of Forsmark (Figure 4-36), reveal wave-washed rock surfaces where more than ~30 % of the surface area is covered in sockets. Many sockets have angular, fracture-controlled planforms (Figure 4-36).

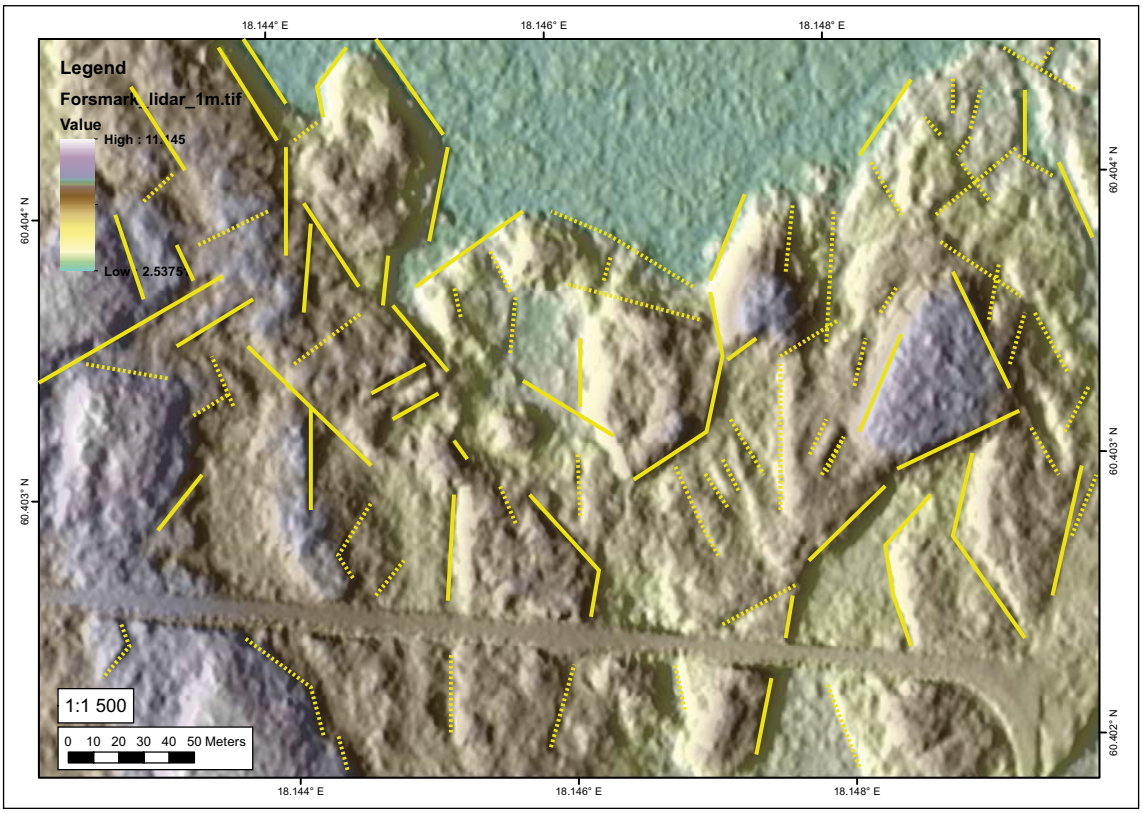

Figure 4-35. *Topographic lineaments in terrain with glacial ripping at Gunnarsbo, Forsmark. The parallelism of many lineaments is consistent with presence of fractures in bedrock. This suggests that undisrupted bedrock is present at shallow depth.*

Similar rock surfaces with numerous sockets are accessible on the neighbouring former island of Lilla Sandgrund (Figure 4-37), now joined to the mainland by a causeway that provides access to the cooling water outfalls. Here, newly emerged rock surfaces in acid to basic gneisses are exposed on low stoss faces across the abraded tops of whalebacks and roches moutonnées. The rock surfaces display multiple sockets parallel and traverse to the former ice flow direction, with A-axis lengths of up to 7 m and depths of up to 0.7 m. The quarrying of some small (< 0.5 m A-axis length) blocks from sockets by waves is indicated by the presence of angular blocks in adjacent hollows. Larger sockets, however, lack obvious displaced fragments in the vicinity and are interpreted as meso- and micro-forms developed by glacial erosion. Sockets are fracture-bounded and include pre-existing fractures that retain chlorite and calcite fracture coatings and new, uncoated, vertical and inclined fractures. New, still tight fractures on abraded rock surfaces show rough edges, branching and anastomosing traces, with localised cm-scale fragmentation of rock between fractures. Some large sockets display both abraded and sharp edges and appear to be products of multiple quarrying events.

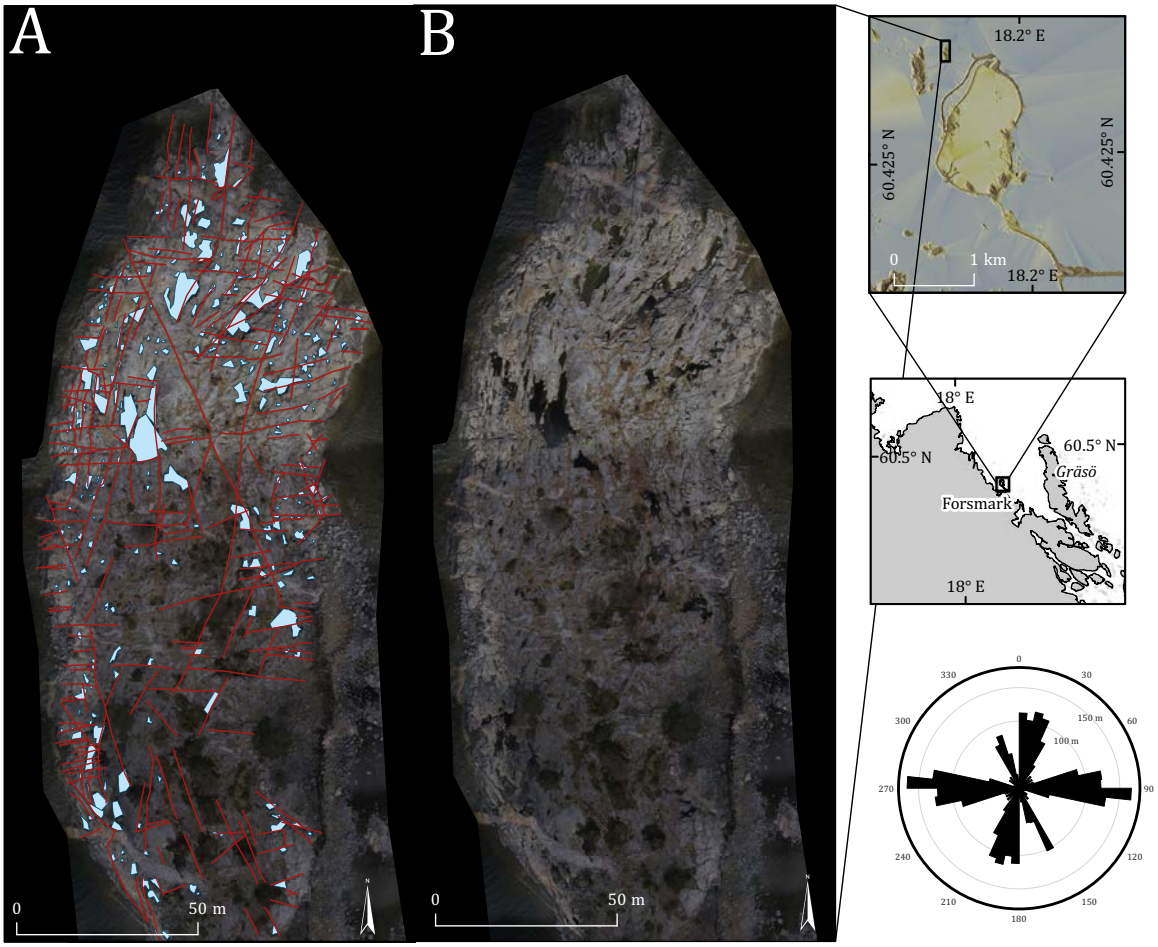

Figure 4-36. *Drone image of Stora Sandgrund showing wave-washed surfaces with numerous angular sockets. A. Socket locations and shapes (in blue). Fracture patterns interpreted from lineaments with strong W−E and N−S orientations. B. Vertical drone image of the same surface. The rose diagram shows the orientation of fracture-guided lineaments on the exposed surfaces.*

Sockets with sharp edges indicate the removal of blocks of rock late in the last glacial cycle. The blocks removed were up to several metres in length but of shallow (less than 1.2 m) depth, with shapes determined by bounding fractures. Block removal required the lifting of tabular and prismatic blocks out of sockets. Extraction of blocks at the glacier base would have required development of cavities at the ice sheet base. Lifting appears to have been associated with the development of new fractures with features consistent with hydrofracturing. The sockets are provisionally interpreted as products of block removal when cavities developed at the ice sheet bed under conditions of groundwater overpressure during final deglaciation. Unlike the jacking at Forsmark that may penetrate to depths of many metres, the sockets appear to relate to jacking close to the ice-rock contact. Such confinement may be due to restricted permeability in the subsurface. Further work is needed to understand the origins of these sockets and their potential importance as markers for former groundwater overpressure at the former bed of the Fennoscandian Ice Sheet.

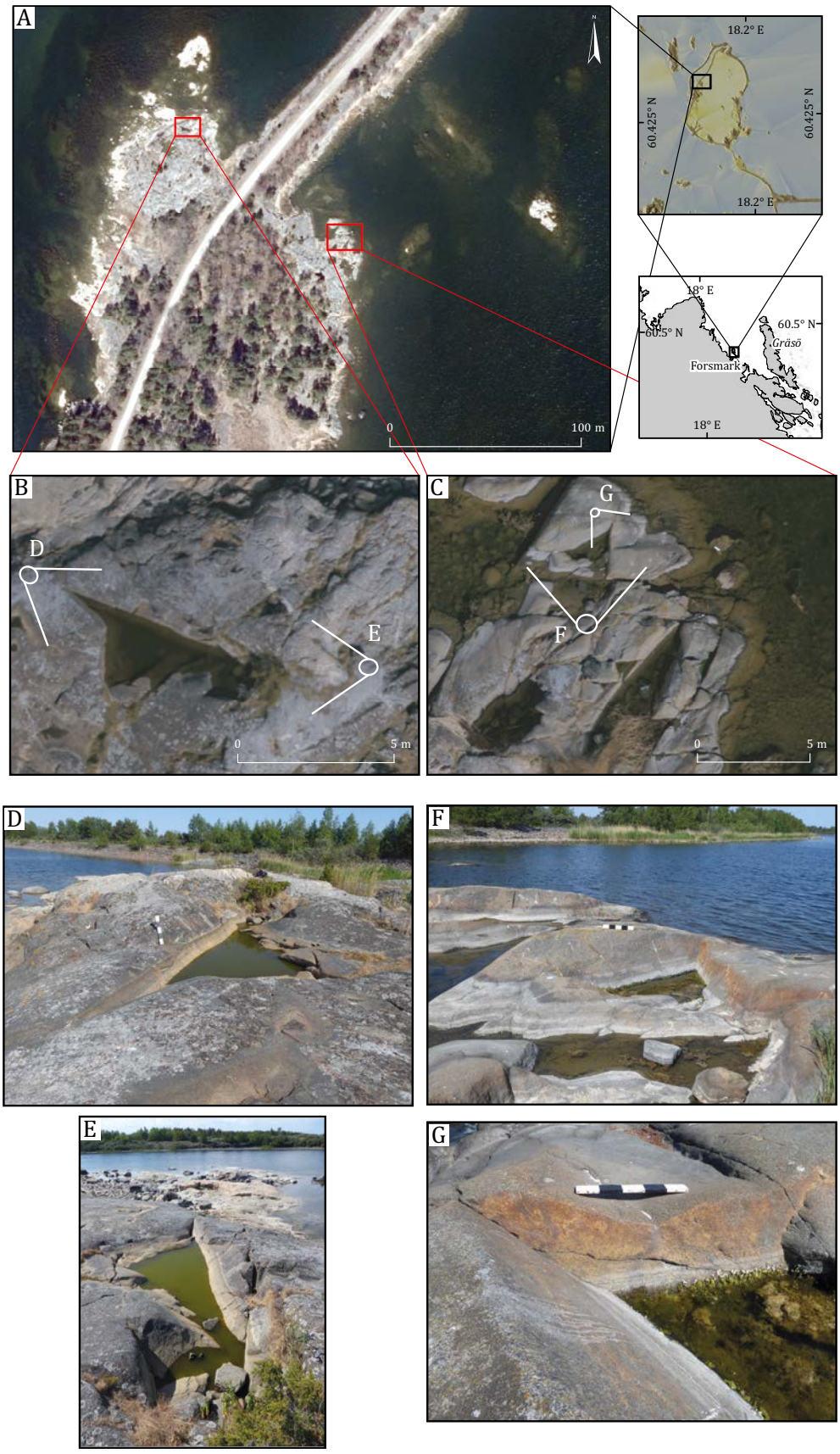

Figure 4-37. *Drone and surface images of box and prismatic sockets on Lilla Sandgrund. A. Location and vertical drone image. B. Large socket west of the road. C. Large sockets east of the road. D. Ground image of the socket in B. F & G. Ground images of the sockets in C. Note the surrounding abraded surfaces, the lack of abrasion within the socket, fracture coatings and the inclined hydro-fracture in G. Measuring stick is 50 cm long.*

4.3.4 Rock hardness, fracture spacing and glacial features on outcrops sampled for cosmogenic nuclides at Forsmark

A Schmidt Hammer testing survey was carried out on 43 rock surfaces at 27 sites (Appendix 2), including almost all sites sampled for cosmogenic nuclides, to assess the possible influence of rock hardness on abrasion of rock surfaces in the Forsmark area. Upper Quartile R-values for samples and sample sites represent the most reliable indicator of rock hardness as measured by Schmidt Hammer tests as these values are least likely to be affected by rock surface micro-roughness and micro-cracking. Mean and Upper Quartile R-values are generally > 59 and indicate that the gneiss bedrock is very hard. Only two sites provided R-values of < 50, interpreted as a result of post-glacial weathering. Testing of rock types found in the Forsmark Tectonic Lens also yielded high values for uniaxial compressive stress (SKB 2008). Mean R-values for sites show no apparent systematic variation in R-values from N to S and only a weak negative correlation with elevation. Plots of R-values against average erosion rates derived from cosmogenic nuclides indicate no correlation (Figure 5-13E). There is no firm evidence from the Schmidt Hammer data that small differences in rock hardness influence rates of glacial abrasion in the Forsmark area.

Fracture mapping was completed on 12 outcrops sampled for cosmogenic nuclides in the Forsmark area (Figure 4-38). Fracture maps are compiled in Figure 4-39. Additional data for each site are contained in Appendix 3.

Outcrop mapping (Figure 4-39) reveal three sets of steeply-dipping fractures, which conform with fracture sets previously identified by Saintot et al. (2011) from other outcrops at Forsmark. The NE–SW fracture set is the most commonly observed on these 12 outcrops, being present at Klubbudden, The Bornhardt, Neon Roundabout, Repository Footprint 2, Yonder Flats (FORS-16-07 only), and Mt Megantic (Appendix 4). If these fractures are also generally a component of the NE–SW set identified by Saintot et al. (2011) they are 1.7–1.6 Ga old. A second fracture set, oriented ENE–WSW, is best observed at Office View, Shimmering Flats, and Mount Megantic. A third fracture set, oriented NW–SE, occurs at Wave Rock (especially), Yonder Flats (both sites), and Mount Megantic. Steeply dipping fractures with these orientations at Forsmark are considered by Saintot et al. (2011) to be 1.8 Ga old, with the latter set reactivated 1.1–0.9 Ga ago. The gentle northwards slope of several outcrops is influenced by fractures dipping obliquely in this direction. Most of the mapped outcrops (9/12) exhibit gently inclined stoss-sides, and 10 of 12 display lee-side scarps, usually beyond the mapped areas, and so display morphologies similar to those of roches moutonnées developed where rock fractures dip up-ice (Gordon 1981).

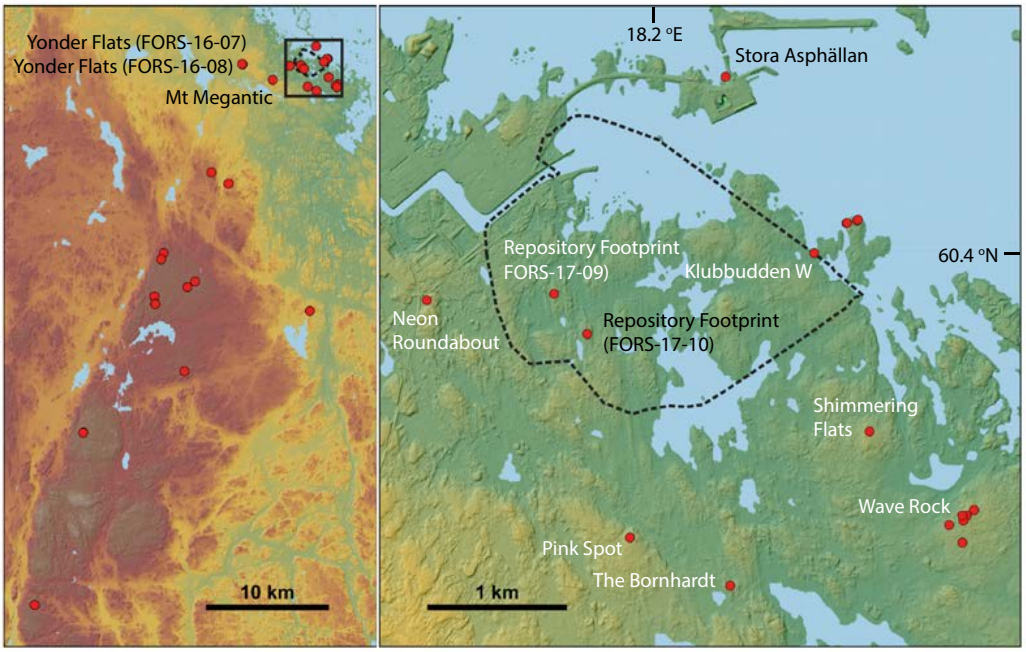

Figure 4-38. *Map showing outcrops sampled for cosmogenic nuclides (red dots) and named sites where fracture mapping of sample surfaces was carried out.*

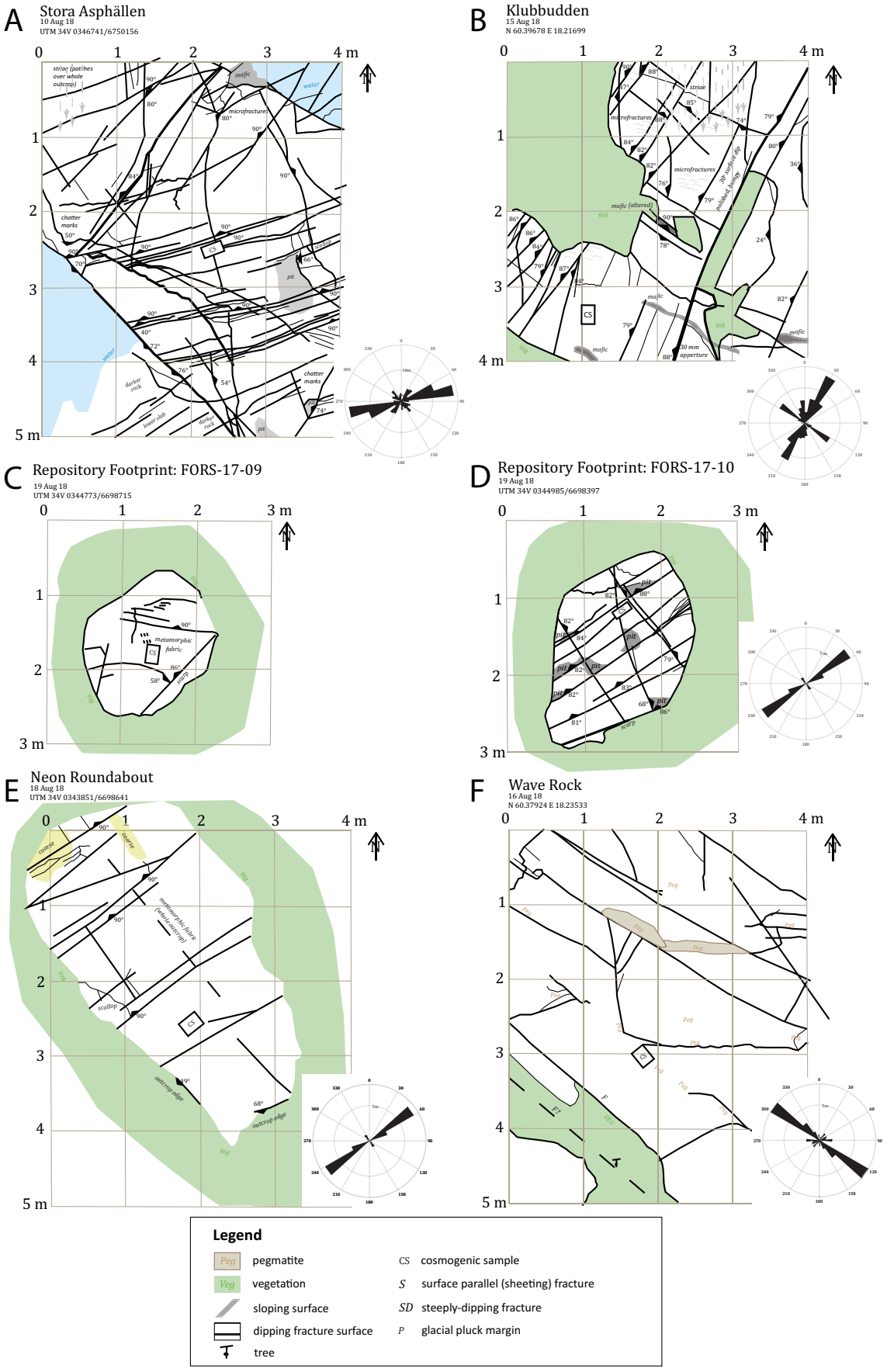

Figure 4-39. *Fracture maps for selected 25 m² summit areas around cosmogenic nuclide sample sites. A. Stora Asphällan. B. Klubbudden. C and D. Repository footprint area. E. Neon Roundabout. F. Wave Rock. G. Shimmering Flats. H. Pink Spot. I. The Bornhardt. J. Mt Megantic. K and L. Yonder Flats.*

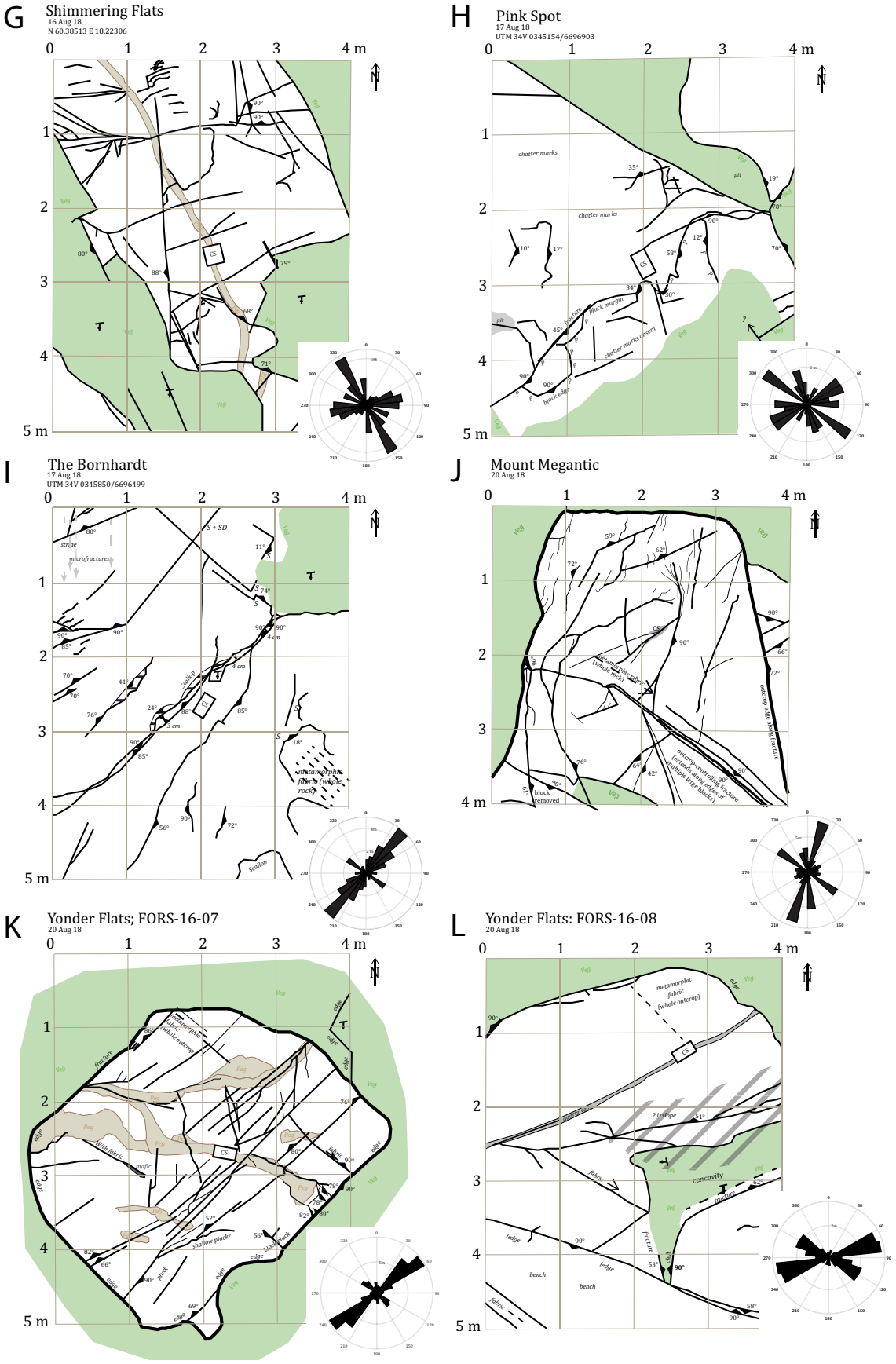

Figure 4-39. *Continued from previous page.*

The interpretation of these fracture sets is assisted by additional observations. The NE–SW orientation of the metamorphic fabric seen at Neon Roundabout (FORS 16-04); Repository 1 (FORS-17-09); Yonder Flats (FORS-16-07 and 16-08); and Mount Megantic (FORS 16-09) agrees with previous observations at Forsmark (Stephens et al. 2008a). With the exception of Repository 1, subordinate fracture sets occurred parallel to this fabric orientation at each of these sites. Fractures with apertures wider than hairline are extremely rare, with a fracture displaying a 3–4 cm aperture on The Bornhardt providing the key exception. Otherwise, the exposure of crack walls is limited to locations where formerly adjacent rock has been eroded. Mineral fills in fractures were not observed, although most displayed hairline apertures and the fractures were also not examined in detail for these. Where they occur, pegmatitic veins also frequently exert control on the orientations and termination and nucleation points of fractures.

The mean spacing of steeply dipping fractures varies from 0.24 m at Repository Footprint 2 to 1.14 m at Wave Rock (Figure 4-17). The mean for the 12 sites is 0.6 m (1σ = 0.3 m). On the line transects, the mean fracture spacings are greater, ranging from vary from 1.1 to 7.7 m (Figure 4-40). The mean for the 12 sites is 3.8 m (1σ = 1.4 m). The line transects are 50 m long and so are 10 times longer than equivalent lines across the outcrop maps. Only major, open fractures were recorded on the line transects whereas fractures with hairline apertures were also recorded on the maps. The large difference between the values is likely a reflection of fractal properties of fracture distributions (Bonnet et al. 2001).

The inventory of glacial micro- and meso-forms confirms that features of glacial abrasion and plucking are ubiquitous on or adjacent to surfaces sampled for cosmogenic nuclides (Table *4-3*). Plucking is well evidenced on many of these sample outcrops, even though none of the three major fracture sets aligns with the N–S direction of ice flow as evidenced in striae. Shallow pluck sites tend to occur on the summit areas of the outcrops on the lee sides (with respect to former ice flow) of the ENE–WSW set of sub-vertical fractures. In addition, the flanks of the rock risers are frequently defined by vertical steps to lower bedrock, often mantled in sediment and vegetation. The flank characteristics are consistent with plucking, usually of larger blocks, along the NW–SE and NE–SW sets of steeply dipping fractures. The edges of the plucking sites are usually angular to sub-rounded, which indicates that plucking widely occurred late during the last glaciation. At Pink Spot (Figure 4-9), the absence of crescentic marks and glacial polish from the plucked summit surface may also point to erosion late in deglaciation.

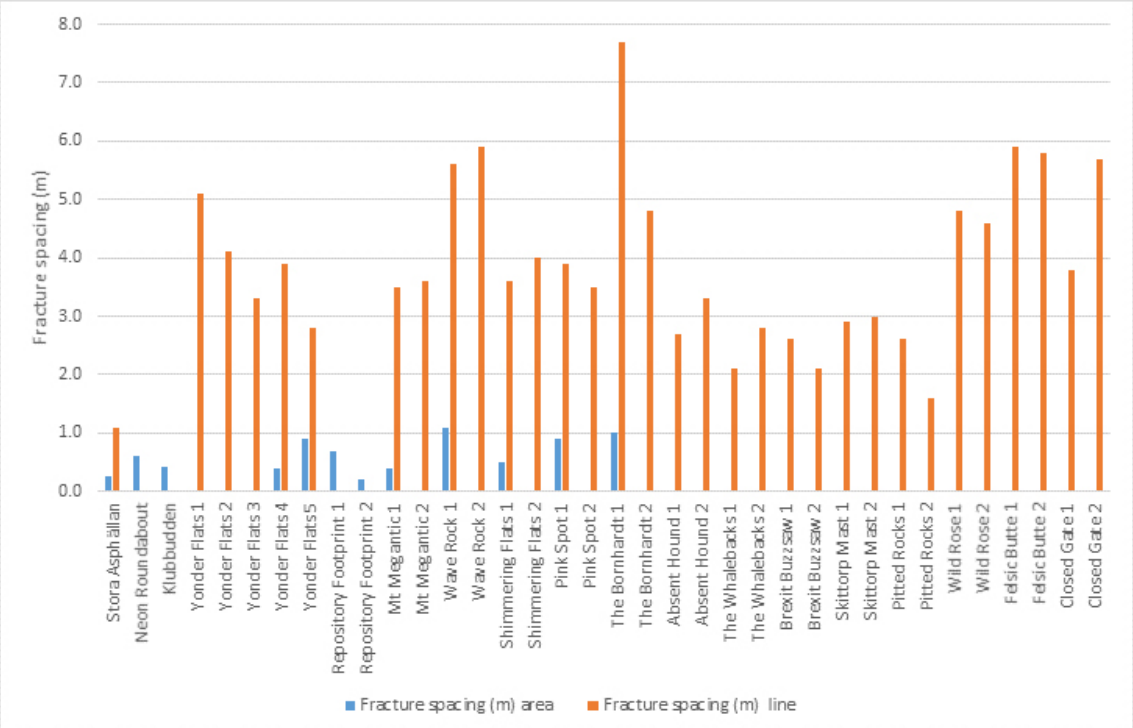

Figure 4-40. *Histogram showing the mean fracture spacing for each mapped outcrop for detailed (5 × 5 m area) maps of summit outcrops sampled for cosmogenic nuclides and 50 m line transects across the sample sites. Apart from Stora Asphällan, each site surveyed for 50 m line transects has two perpendicular transects.*

The three sites with the largest fracture spacing on summit maps, Wave Rock, The Bornhardt, and Yonder Flats (FORS-16-08), display the highest surface convexities at the outcrop-scale (Figure 4-41). Mount Megantic has a summit surface that displays low convexity but its lee side comprises a vertical scarp a few metres high from which blocks have been removed by ripping or plucking to form 150 m long erratic trains. In general, the spacing of steeply dipping fractures appears to control the convexity of these outcrops, with lower-convexity outcrops occurring where the spacing of steeply dipping fractures is ≤0.86 m.

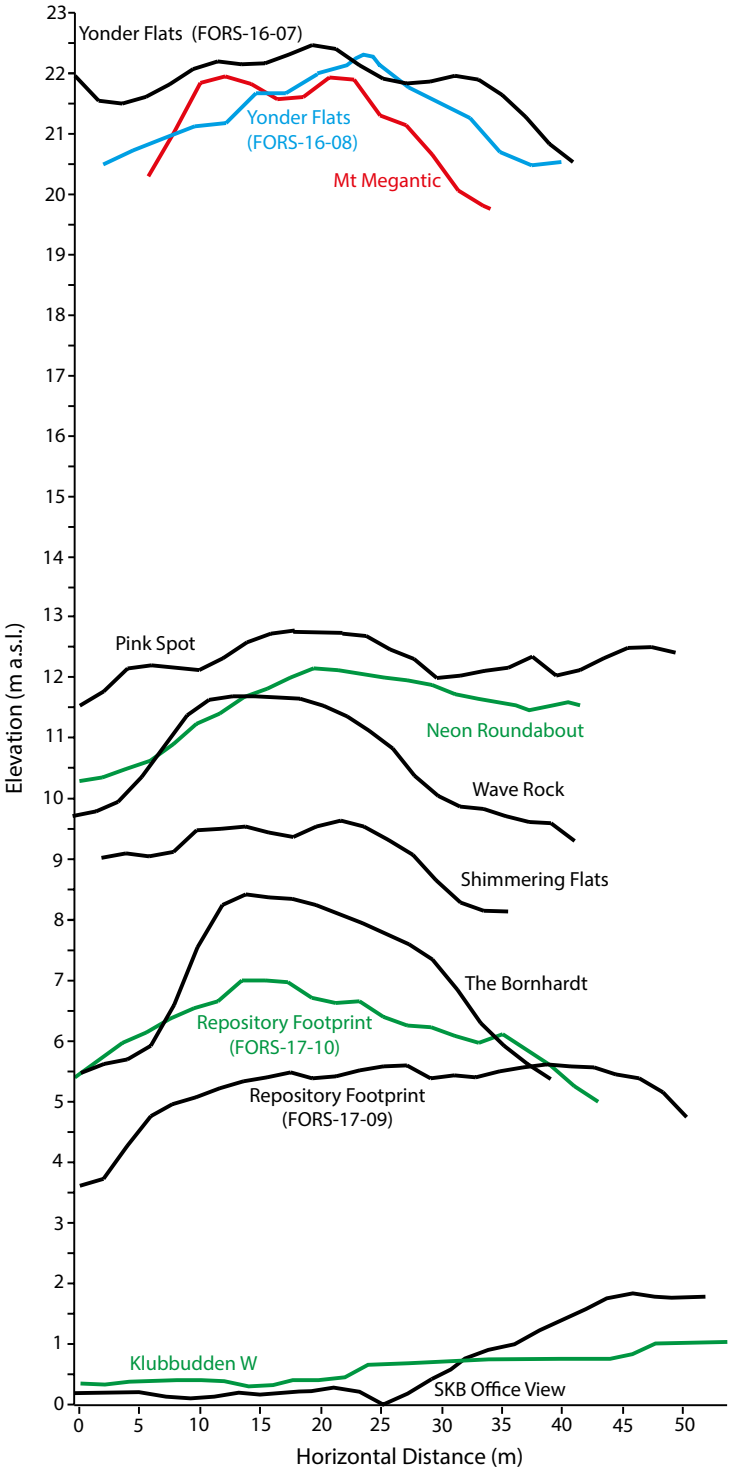

Figure 4-41. *Two-dimensional profiles centered on each mapped outcrop, showing elevation versus horizontal distance transverse to former ice-flow direction. The profiles were generated using the profile tool in ArcGIS from the 2 m resolution LIDAR elevation model (source: Lantmäteriet).*

Evaluating the more general potential contribution of glacial erosion of sub-horizontal fractures to the present forms of these outcrops is difficult. Sub-horizontal fractures within the mapped outcrop areas were observed only on The Bornhardt. In addition, sub-horizontal fractures were observed outside mapped areas on Wave Rock and at Shimmering Flats. The comparative rarity of these fractures in the outcrops may be an artefact of the mapping, because mapping was done in plan-view on small areas of outcrop summits. Lower flanks of the outcrops, where sub-horizontal fractures might be located, are usually covered in sediment and vegetation. Sub-horizontal joints are abundant below the ground surface in fracture domains FFM01 and FFM02, as revealed in excavations and in bedrock cores (Carlsson 1979, Lejon et al. 2005, Martin 2007). They therefore likely occur beneath at least some of the outcrops mapped here. The notably flat tops of the Neon Roundabout, Repository Footprint 1 and Repository Footprint 2 outcrops may, for example, reflect glacial erosion along sub-horizontal fractures. In addition, sub-horizontal fractures might control the vertical dimensions of the outcrops, by determining the depths to which surrounding bedrock has been eroded, as evidenced in Figures 53–57 from Carlsson (1979). Further detailed work is needed to establish how fracture spacing and orientation controls the detailed form of bedrock surfaces and how the various processes of glacial erosion interact with fracture patterns at the micro- to meso-scales.

4.3.5 Depths of glacial erosion based on geomorphological criteria

Glacial erosion of cover rocks and basement

Glacial erosion by the Fennoscandian Ice Sheet through the Pleistocene has two basic components in Uppland and across large areas of lowland Sweden:

1. Removal of Early Palaeozoic and any younger sedimentary cover rocks from above U2 and
2. Erosion of basement rocks from below the former Early Palaeozoic unconformity.

Total depths of glacial erosion can be estimated from geomorphological evidence, particularly by using the dislocated surface of U2 as a reference surface (Section 2.3.10). The height difference between U2 modelled in summit envelope surfaces and the present bedrock surface indicates the depth of rock lost to glacial erosion since re-exposure of the basement surface.

Removal of cover rocks and excavation of marine basins

The Bothnian, Åland and Baltic Seas fill marine basins that have been excavated by Pleistocene glacial erosion (Amantov 1995). The present Seas are generally shallow, with 86 % of the combined marine basins having depths of < 100 m (Jakobsson et al. 2019), but with localised overdeepenings. The marine basins occupy Mesoproterozoic intracratonic basins from which the rocks lost to glacial erosion include mainly Jotnian, Early Palaeozoic and younger sedimentary rocks (Figure 2-6). Hence the origins of the marine basins involve deep erosion of Early Palaeozoic cover rocks, an erosion history that has direct bearing on the timing and pace of the removal of Early Palaeozoic sedimentary cover from basement in areas along the western margins of these Seas, including across Uppland.

Whilst information is accumulating on the configuration and environments around the Baltic Sea in the last interglacial (Miettinen et al. 2002), little is yet known about earlier events (Kalm et al. 2011). The continuous operation of the Bothnian River and the larger Eridanos drainage system through the Neogene and Early Pleistocene until 1.1 Ma (Gibbard and Lewin 2016) indicates, however, that before this date the present marine basins did not exist. Hence the removal of Early Palaeozoic cover rocks to create marine basins in the Bothnian and Åland Seas likely post-dates 1.1 Ma and the termination of the operation of the Bothnian river system. Excavation below present sea level may relate to increases in the duration of ice cover and the thickness of the Fennoscandian Ice Sheet under the 100 ka glacial cycles during and after the Middle Pleistocene Transition (Kleman et al. 2008) (Figure 4-2). However, the oldest marine interglacial sediments known in the Baltic basin, including the former strait between the Gulf of Finland and the White Sea, are Holsteinian (MIS11) in age (Raukas 1991). The absence of older marine sediment may be simply an expression of the efficiency of erosion by the previous Elsterian ice sheet (MIS 12), the most extensive Fennoscandian ice sheet in the Pleistocene (Ehlers et al. 2011). Alternatively, the deepening of the Bothnian, Åland and Baltic basins may date mainly from the large ice sheets that developed in cold stages including and after MIS 16. The minimum total depths of sedimentary rocks removed from the present marine

basins are indicated by present mean water depths of ~50 m (Marmefelt and Omstedt 1993). If deep erosion commenced at 1.1 Ma then a minimum average thickness of more than 4.5 m of sedimentary rock was removed in each 100 ka glacial cycle.

In the Öregrund archipelago, sedimentary cover rests locally on basement on single fault blocks (Figure 2-8). This allows estimation of the minimum depth of glacial excavation of sedimentary rock from basins by subtracting the height of basement hills on neighbouring islands from water depths in the sounds. Singöfjärden has a maximum depth of 49 m and an average depth of 11 m whilst neighbouring basement tops rise above 20 m a.s.l. Maximum depth of excavation in Jotnian and Ordovician sedimentary rocks is ~70 m, with an average depth of 30 m. At Raggaröfjärden, the surrounding basement tops reach elevations of 15 m whereas the submerged Ordovician outlier has a surface at −16 m, indicating removal of more than 30 m of limestone. In the eastern part of the Öregrundsleden, near the island of Vässarön, >45 m of Jotnian and Ordovician cover is missing. A minimum of 40 m of Ordovician limestone is missing from NW of the Gräsö block (Figure 2-11). The depths of erosion of sedimentary rocks from these small grabens and basins are approximately twice the depths of rock basins with basement floors in Uppland. If deep erosion commenced at 1.1 Ma then minimum average thicknesses of more than 3–6 m of sedimentary rock were removed in each 100 ka glacial cycle. To these totals should be added unknown thicknesses of sedimentary cover removed from above the upper surfaces of upstanding basement fault blocks that remain at or close to the level of the U2 unconformity.

Erosion of re-exposed fault scarps and fault block tops in Uppland

Fault-bounded and locally tilted rock blocks produced by dislocation of the surface of U2 provide reference surfaces for estimation of glacial erosion on basement block edges and summits (Figure 4-11). Where still buried by Ordovician limestones on the bed of the Bothnian Sea, the fault scarps are sharp-edged and flat-topped (Winterhalter et al. 1981). The exhumed Gräsö block stands ~30 m higher than the block on the bed of the Öregrundsgrepen to the W but only 10 m higher than blocks to the E (Beckholmen and Tirén 2010b, Grigull et al. 2019). Assuming an initial position of a sharp-edged scarp along the West Gräsö Fault, a triangular rock wedge has been removed along the edge of the fault scarp of ~20 m depth and tapering to zero across a width of 1–1.5 km. The base of the dip slope on the unnamed block to the W of the Ironworks Block rises to 32 m a.s.l. whereas the scarp crest reaches 52 m on the Ironworks Block itself. The north-western edge of the Ironworks Block has been eroded back over a distance of ~0.5 km, with up to 10–20 m of lowering. In W–E profiles near Hallstavik, fault scarps have been eroded back to a depth of 15 m over distances of up to 0.75 km (Figure 4-43). Around Alunda (Figure 4-16), the northern edge of the Alsunda block is linear and stands at the same elevation as the block immediately to the N which appears have provided protection for the block edge from glacial erosion. The northern edges of the Tuna and Ål blocks to the W are more exposed along wider, fault-guided trenches and have indented block edges that have been lowered by 10–20 m in rock basins along these edges. Maximum rock block elevations relative to adjacent blocks across Uppland and offshore are low, with 65 % standing within 20 m (Grigull et al. 2019). Some fault scarps stand only 10 m above the edges of neighbouring rock blocks (Figure 2-9). Lowering of the scarp crests by glacial erosion has been insufficient to remove low fault scarps. More widely, glacial erosion depths have been insufficient to erase the inherited bedrock topography across the mosaic of exhumed fault blocks (Figure 2-21).

Fault block tops at Ironworks (Figure 4-42), Alunda (Figure 4-16) and Hallstavik (Figure 4-43) retain extensive areas on the highest parts of the blocks with low relief and lacking in glacial landforms indicative of deep erosion. These flats are interpreted from morphological evidence as little-modified facets of U2 that stand less than 10 m below its original level. Lower rock surfaces have greater relative relief, developed through isolation of box hills and roches moutonnées and entrenchment of fracture-guided valleys and excavation of star and box basins. Glacial erosion has acted progressively to modify and destroy the inclined, near planar tops of exhumed fault blocks rather than to maintain the original near planar form. Across the Ironworks Block (Figure 4-42), the maximum depth of basement lowering is in lee-side basins and bounding trenches and amounts to ~20 m. On roughened parts of the block top, lowering is restricted to ~10 m. At Alunda, the depth of erosion of basins and trenches on the Ålsunda Block is similar but parts of the adjoining tops of the Ål and Tuna Blocks have been lowered by 15–20 m. Near Forsmark, the basins of the Södra Åsjön and Bruksdammen have been excavated to maximum depths of 20 m (Figure 4-15).

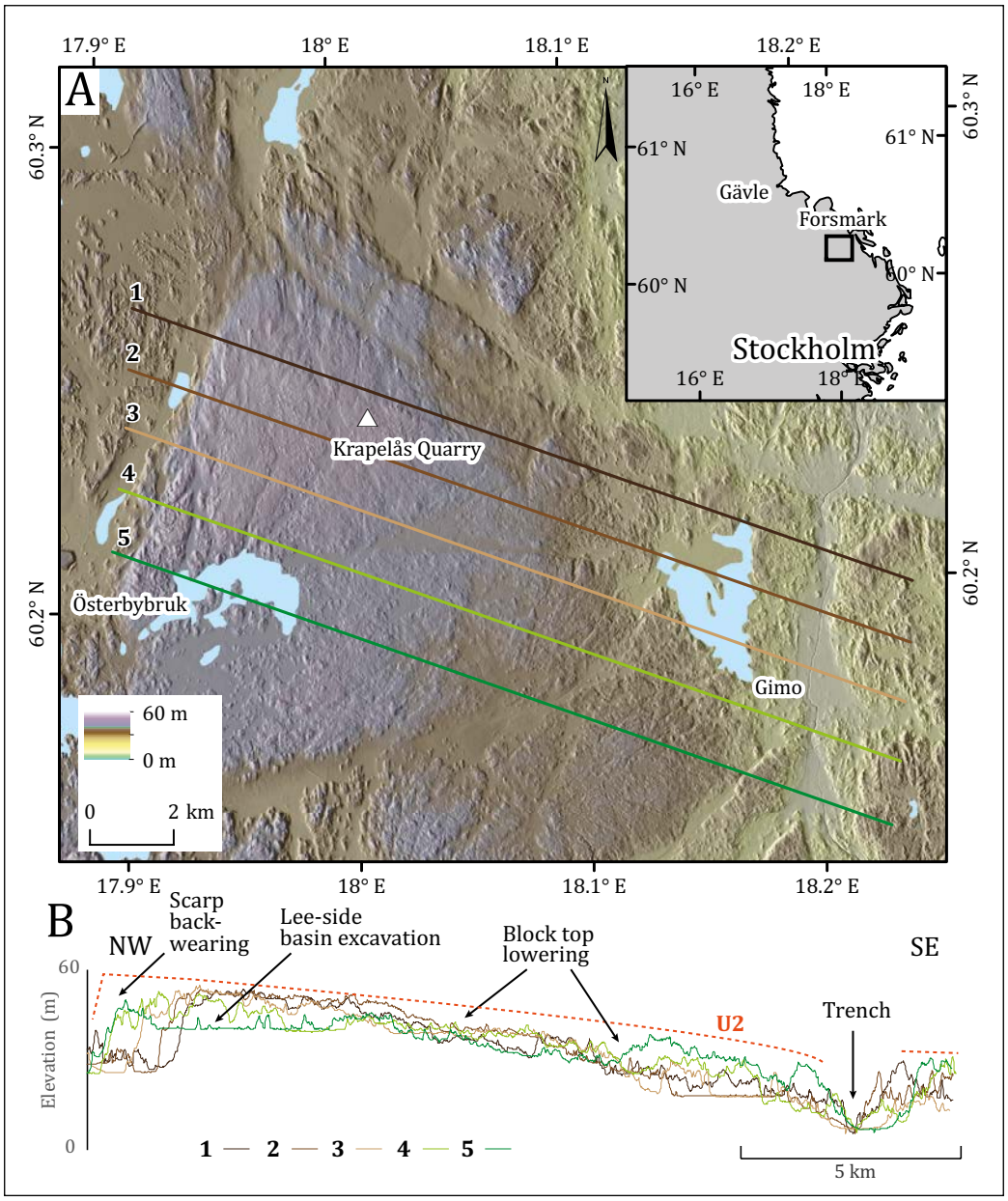

Figure 4-42. *Glacial erosion of the Ironworks fault block. A. DEM is metres a.s.l. Profiles are numbered 1–5. B. Superimposed NW–SE profiles across the block. Approximate position of U2 shown above summits on the inclined block, with the former position of the exhumed fault scarp to the NW.*

Around Hallstavik, profiles indicate extensive block top lowering of 10–15 m (Figure 4-43). The depth of erosion increases to 20 m in southern Väddö and exceeds 25 m in fracture-controlled W–E rock basins. Fault block top erosion of basement spans the periods since removal of Early Palaeozoic cover from each fault block top. When compared to likely erosion depths derived from cosmogenic nuclides (Section) of 1.6–3.5 m for the last glacial cycle (100 ka) (Section 5.4.2), the assumption of <10 m summit erosion for these fault block tops suggests re-exposure of these surfaces in the last 500 ka, As stripping of Ordovician cover was likely diachronous across the U2 surface, the duration of basement exposure to glacial erosion likely varied across the Uppland and the least modified fault block tops likely represent areas of most recent re-exposure.

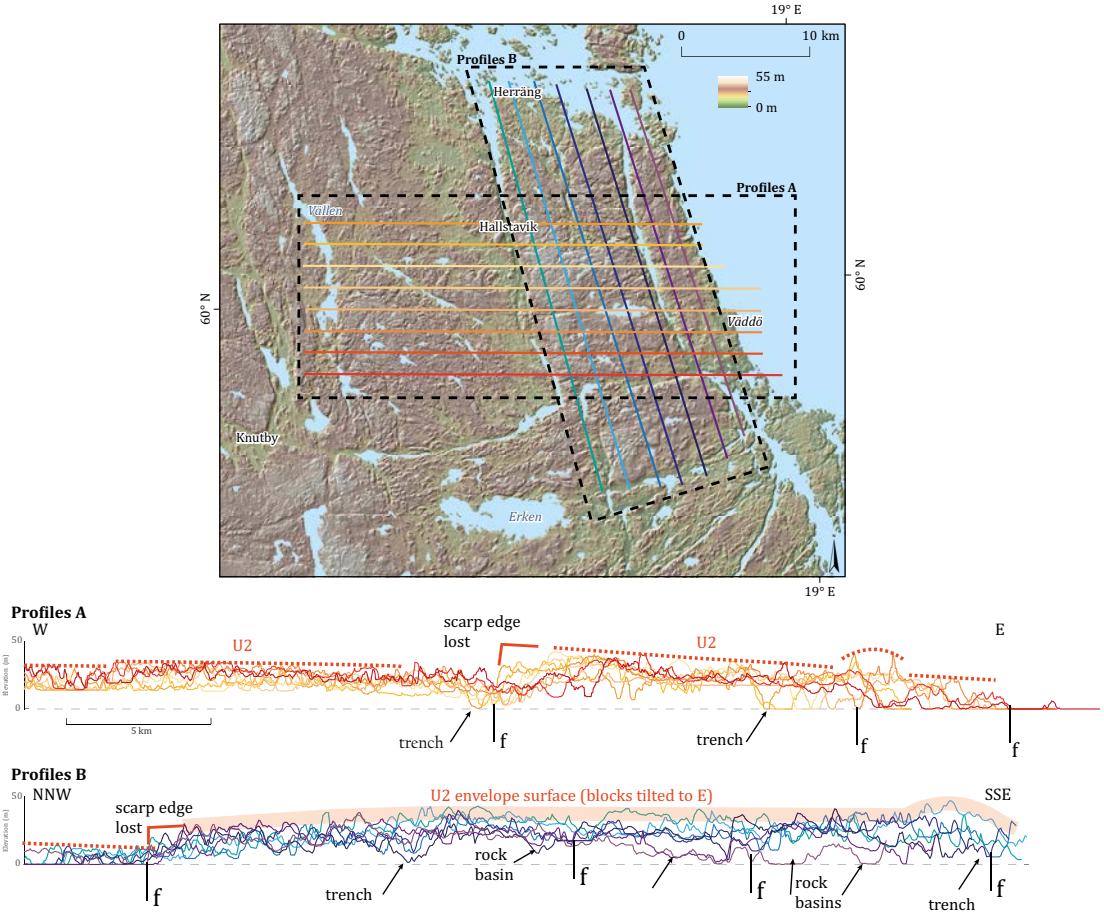

Figure 4-43. *Glacial modification of exhumed fault blocks around Hallstavik. DEM in m a.s.l. Profiles A run W–E; Profiles B run NW–SSE parallel to the coastline. Approximate position of U2 shown above summits, with the positions of exhumed fault scarp and faults (f). DEM in m a.s.l. Profiles A run W–E; Profiles B run NNW–SSE parallel to the coastline. Approximate position of U2 shown above summits, with the positions of exhumed fault scarps and faults (f).*

Erosion of re-exposed fault scarps and fault block tops at Närke

Patterns and depths of glacial modification of exhumed fault blocks are perhaps most clearly seen at Närke where basement blocks emerge from beneath Early Palaeozoic cover (Figure 2-16 and Figure 2-17). The minimum depth of sedimentary rock removed by erosion to re-expose the faulted basement unconformity is indicated by the elevation of fault scarp crests relative to that of the sedimentary cover found at the base of dip slopes lying immediately to the N. Where scarp height is low (less than 20 m), as along the northern edges of the basement inliers, roughness of the block top is also low (Figure 4-44). Where scarp height is high (more than 50 m), as south of the edge of the Early Palaeozoic cover, the elevation range and roughness of the block top is high (Figure 4-44). Erosion depths derived by abstracting the present basement relief from summit envelope surfaces are low when scarp height is low and higher when scarp height is greater (Figure 4-45). Assuming that glacial erosion rates were uniform across the former surfaces of the gently inclined Early Palaeozoic cover rocks, the approximately threefold difference in scarp heights indicates a similar difference in the duration of exposure to glacial erosion between cuestas with low and high scarps. The contrasts in roughness and depth of glacial erosion appear to reflect these differences in cumulative exposure to glacial erosion (Figure 4-44 and 4-45). Fault scarp form also varies with scarp height. Low fault scarps display less erosion and retreat along scarp edges, linear depressions perpendicular to the scarp crest are shallow and short compared with similar features along high fault scarps (Figure 4-44). These differences in glacial modification of fault scarps likely represent not only the duration of glacial erosion but also the greater prominence of higher scarps. The pattern of progressive glacial erosion of fault scarps and block tops at Närke is directly comparable to erosion patterns seen on exhumed fault blocks in Uppland.

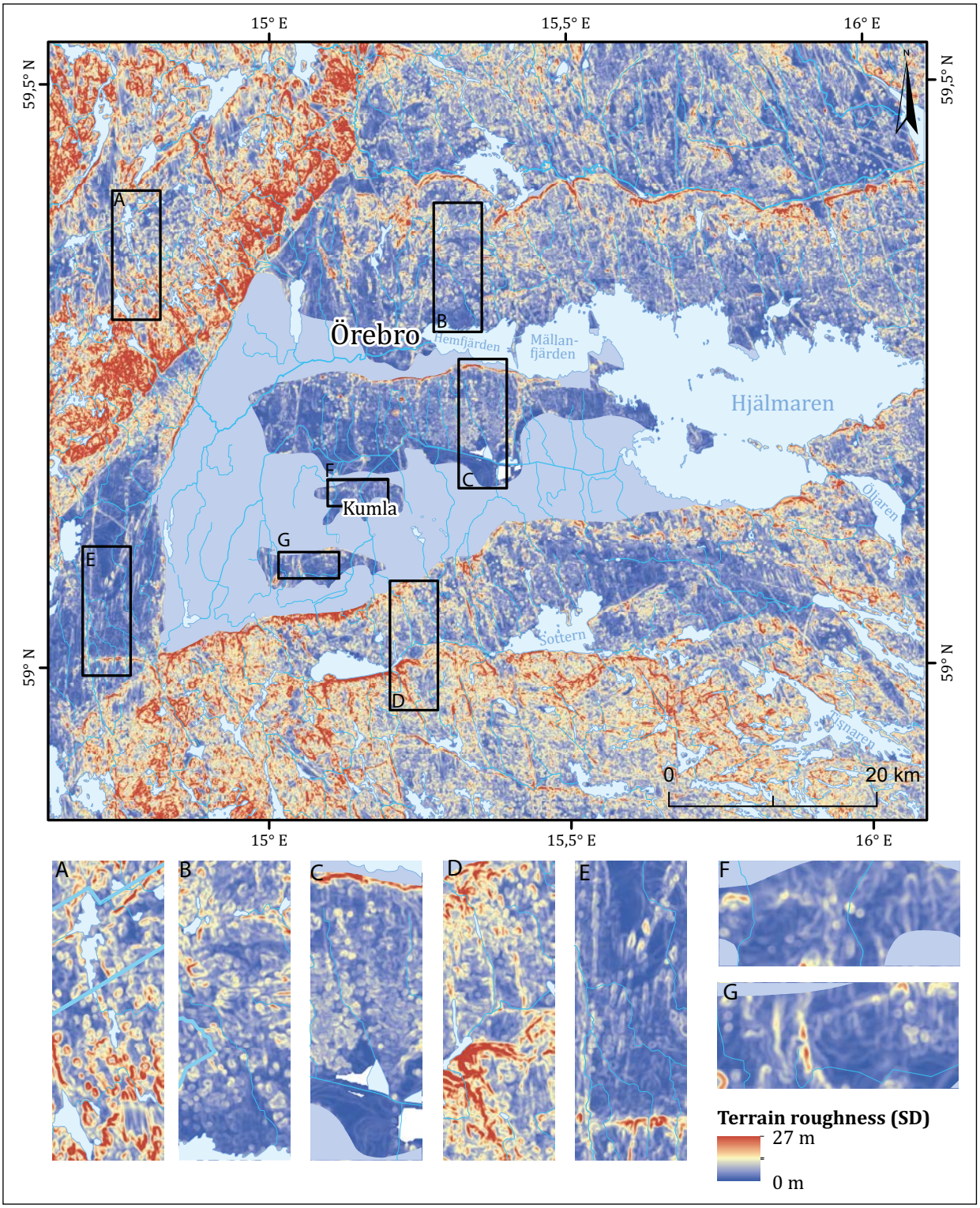

Figure 4-44. *Bedrock terrain roughness (in m) calculated using the SD method across exhumed fault blocks in the Närke district. The lower panels A–G show details of topographic roughness in the bedrock across fault blocks. Former ice flow from the N.*

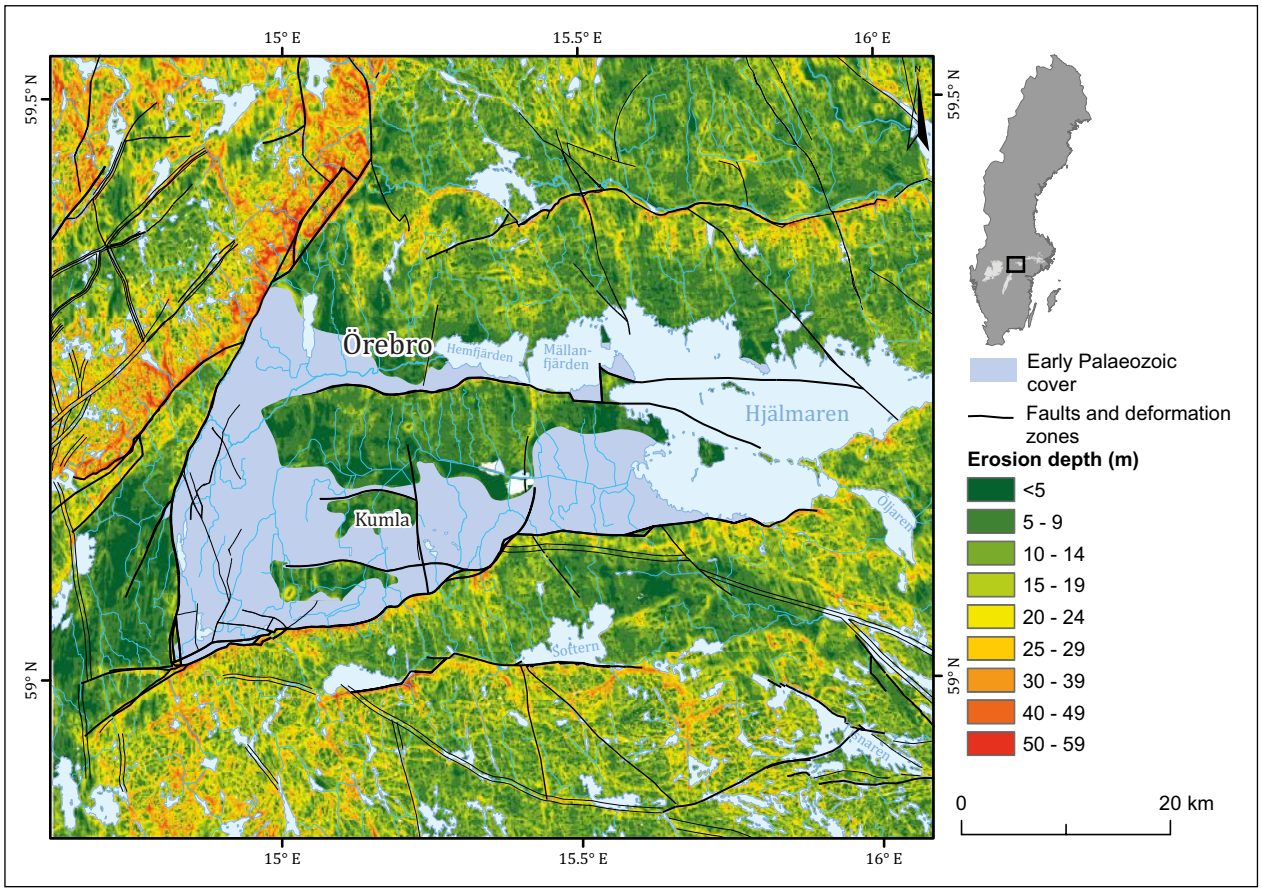

Figure 4-45. *Glacial erosion of basement on exhumed fault blocks at Närke derived from a model of the summit envelope surface. Erosion depths are not shown for the Early Palaeozoic cover. Estimated erosion depths across blocks, with greatest erosion along exhumed fault block edges. Estimated erosion depths also vary between blocks, with lowest erosion depths on blocks interpreted to have been exhumed most recently.*

Depths of glacial erosion of basement in Uppland based on summit envelope surface models of U2

The present bedrock summits provide pinning points for models of U2 and allow estimation of depths of basement erosion below U2 (Section 2.4).

GIS modelling of glacial erosion of basement in NE Uppland

The pattern and depth of glacial erosion below the summit envelope surface is presented for an area of 4 000 km^2 in NE Uppland (Figure 4-46). Depths of erosion increase southwards, with a greater number, closer spacing and increased depth of trenches and basins and a greater frequency of lakes. Large areas have less than 10 m of basement erosion below the regional summit envelope surface and include locations west of Forsmark, including Griggebo, the Ironworks Blocks and its northward continuation, terrain in central Uppland that extends in a belt east of Alunda towards Väddö and northern Gräsö. On the northern edges of fault blocks near Herräng, the depth of basement erosion may be underestimated, as here the entire block edge over a distance of 3 km may have been lowered by ~10 m below U2. Where glacial erosion has significantly lowered summits below U2 that are spaced more than 1–2 km apart, the total depth of glacial erosion is underestimated. The estimated mean erosion depth in basement across NE Uppland is 14 m below the summit envelope surface.

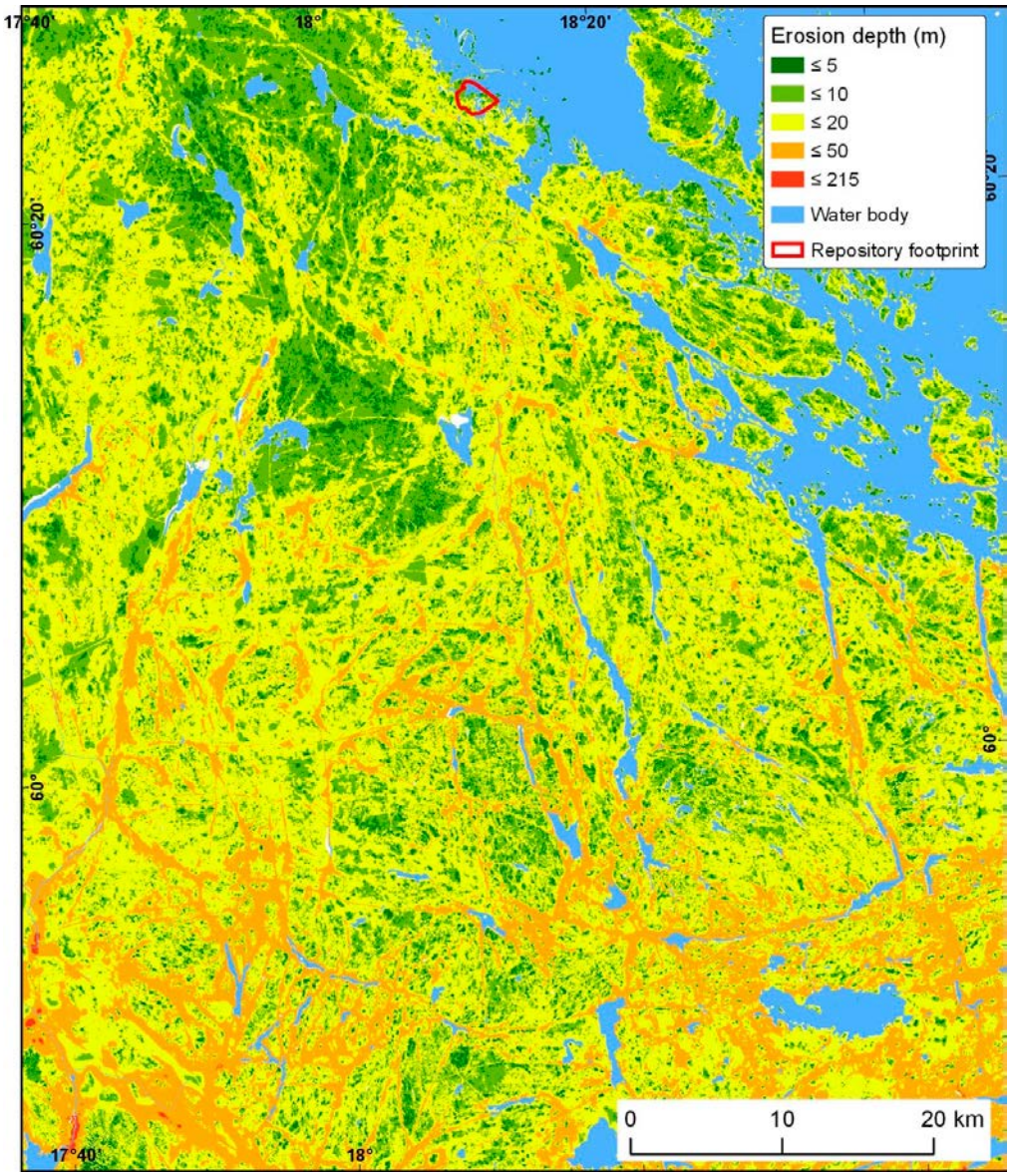

Figure 4-46. *Erosion depth (m) across NE Uppland. Modelled by subtracting the bedrock surface from the MAX MEAN surface of the bedrock surface (the summit envelope surface), based on a circular window with 500 m radius* (Table 4-2)*. Category values selected to emphasise the distribution of end members of minimum and maximum erosion.*

GIS modelling of glacial erosion in the Forsmark area

A similar approach is used in the Forsmark area but with inclusion of the offshore area (Figure 4-47). The highest erosion depths of 70 m are found in a trench along the West Gräsö Fault. Erosion depths are high along the edge of the Gräsö block and increase southwards towards the Öregrundsgrepen (Figure 4-13), from which Jotnian and Ordovician sedimentary cover also has been deeply eroded. On the present land area around Forsmark, basement erosion is greatest in trenches and basins aligned with major structures. Average total basement erosion depth across the area is 12 m. Again, where glacial erosion has significantly lowered summits below U2 that are spaced more than 1–2 km apart the total depth of glacial erosion is underestimated. The errors are likely to be small, however, because maximum summit heights at 1 km spacing in the Forsmark area vary by less than 5 m.

GIS modelling of glacial erosion in the repository footprint area

Total depths of basement erosion were also modelled for the footprint area of the repository site. Figure 4-48 shows the modelled erosion depth, using the same method i.e. the mean of the max

within 1 km circles. Maximum erosion depth is 23 m. Mean erosion values are 6 m for the DEM with sediments (A), and 8 m for the bedrock surface model (B). Again, where glacial erosion has significantly lowered summits below U2 that are spaced more than 1–2 km apart, the total depth of glacial erosion is underestimated. The errors on these estimates are again likely to be small because maximum summit heights at 1 km spacing in the repository footprint area vary by less than 5 m.

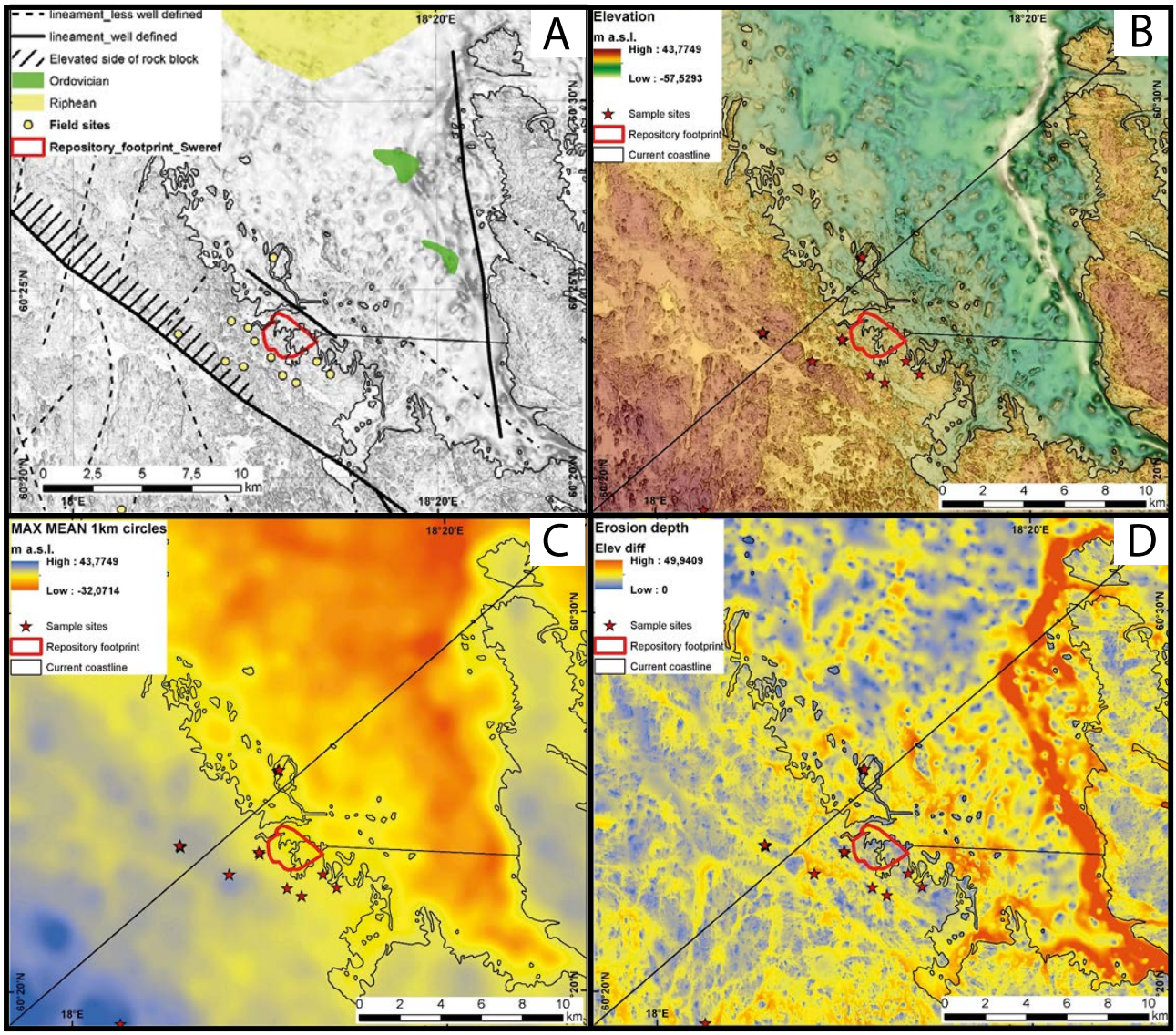

Figure 4-47. *Glacial erosion in the Forsmark area based on a summit envelope surface. A. Major lineaments and cover rock remnants in the Forsmark region. Lineaments from Ahlbom and Tirén (1991). Jotnian and Ordovician from Söderberg and Hagenfeld (1995). Today's coastline is shown. B. Current surface elevation of the Forsmark area including bathymetry. C. Reconstruction of an envelope surface from local summits using the minimum values within a circular search window of 1 km diameter with the maximum surface as base. D. Reconstructed erosion depths (m) in the Forsmark area using the mean of the maximum within search windows with 1 km diameter. The pattern represents the subtraction surface where the current land surface was subtracted from the mean of the envelope surface. E. Bedrock surface model of the Forsmark area (provided by SKB). Highest elevations, represented by bedrock outcrops, are the same as in B. Lowest areas in the Baltic are more than 30m deeper than in the DEM with sediments. F. Erosion depths modelled using the same parameters in the GIS-analysis as for the DEM with sediments (D): the bedrock surface was subtracted from the mean of the maximum using circular search fields of 1 km diameter. Average erosion depth is 12 m, highest erosion depth is 70 m. This model likely shows more correct erosion depths; it should be noted though that the bedrock surface is a model, created from interpolation of point values, so this calculation is based on the reconstruction of a model. G. Profile lines SW–NE (indicated by black line in A–D) of the mean of the maximum surface (red), the present land surface (green) and the subtraction surface representing rock erosion. The mean basement erosion value here is 8 metres.*

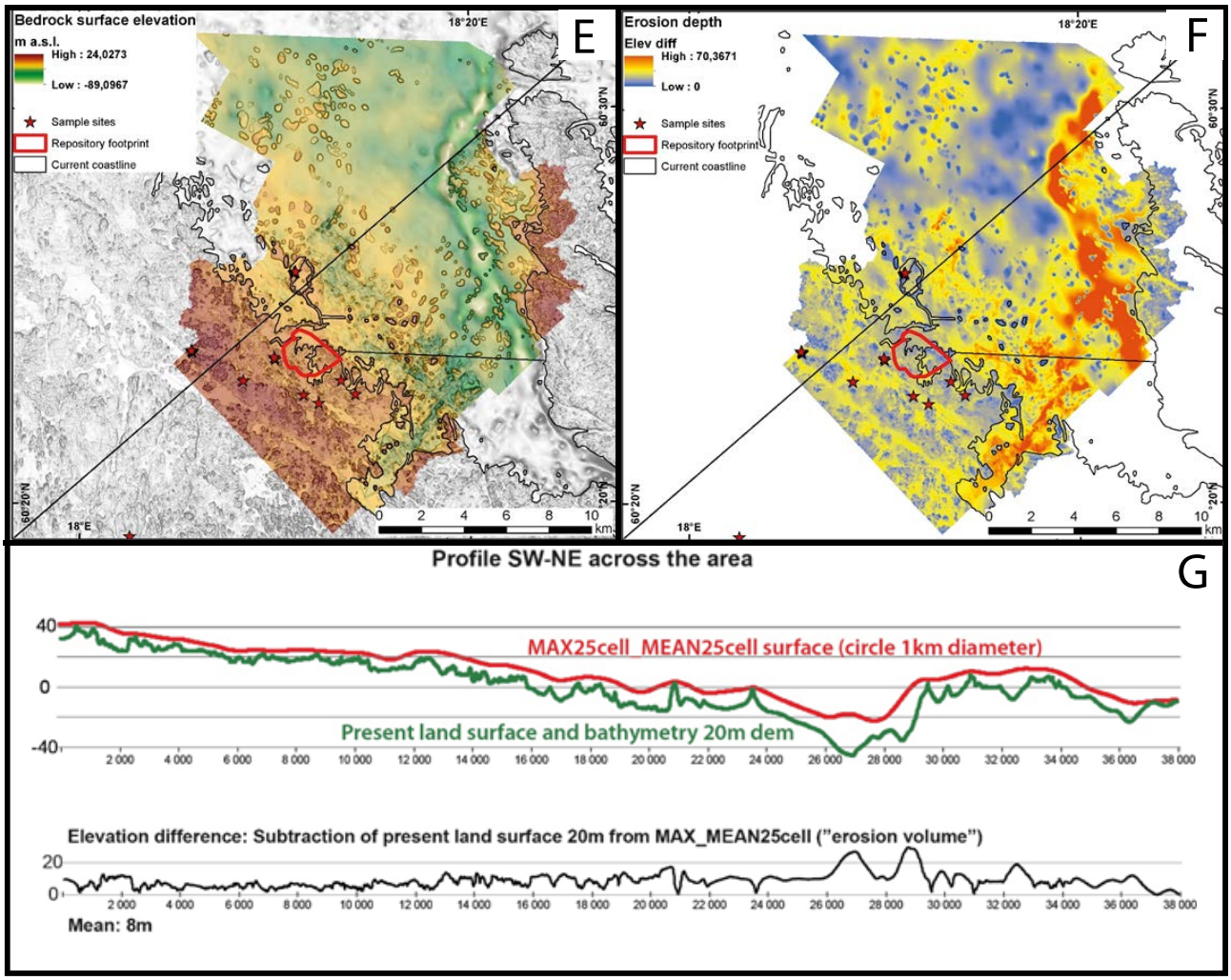

Figure 4-47. *Continued from previous page..*

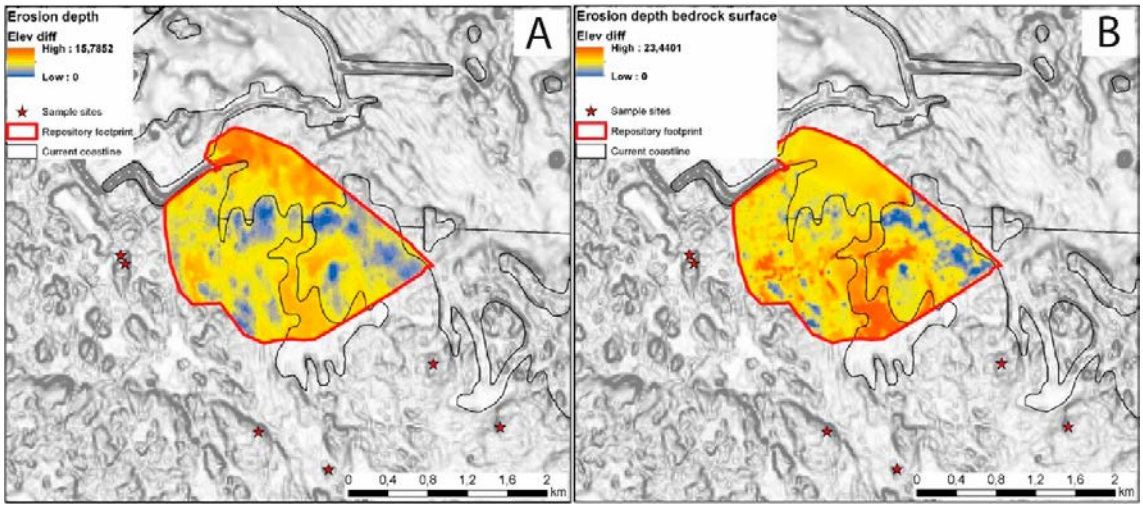

Figure 4-48. *Glacial erosion model for the Forsmark repository footprint area. A. Erosion depths (m) reconstructed for basement across the footprint of the repository site, using the DEM of the current land surface. Mean erosion across the footprint: 6 m. Max erosion: 16 m. B. Erosion depths reconstructed for the footprint of the repository site, using the bedrock surface model, and assuming zero erosion of high points.*

4.4 Discussion

A striking feature of the present basement topography at the landscape scale around Early Palaeozoic outliers in south central Sweden is its smoothness and flatness (Figure 2-15). Similar topography is seen in SW Finland (Figure 4-12). As smooth, flat basement topography occurs widely beneath Ediacaran to Ordovician cover rocks in southern Fennoscandia and emerges from beneath cover around outliers, the presently exposed, smooth basement topography in Sweden has long been interpreted as largely inherited after re-exposure of the sub-Cambrian unconformity (Högbom 1910, Rudberg 1954, Lidmar-Bergström 1988). A corollary of this interpretation is that the impact of Pleistocene glacial erosion has been insufficient to erase an inherited form (Lidmar-Bergström 1997). Little attention has been given, however, to alternative hypotheses that the smooth basement topography in shield lowlands may have been formed through ice sheet planation or that surface smoothness or a general hill summit accordance has been maintained during uniform lowering of the exhumed unconformity surface through depths of many tens of metres.

Formation and maintenance of low relative relief in crystalline terrain by glacial erosion has been explored in the context of the formation of high plateaux fragments in southern Norway and on other glaciated passive margins in the Northern Hemisphere. One mechanism invoked is the glacial buzzsaw hypothesis that recognises the potential for mountain glaciers to rapidly denude topography at and above the glacier Equilibrium Line Altitude (ELA), irrespective of uplift rates, rock type or pre-existing topography (Brozović et al. 1996, Mitchell and Montgomery 2006). The apparent correspondence between the vertical distribution of the high-elevation, low-relief surfaces in Norway and long-term glacier equilibrium line altitude has been used as evidence to support the idea that effective erosion in extensively glaciated passive margins limits topographic height (Steer et al. 2012). ELAs in Norway, however, moved through large vertical ranges during the Quaternary and glacial erosion has been focussed on valley deepening and scalping of inner shelves (Hall and Kleman 2014). In the setting of lowland Sweden, far below ELAs, the glacial buzzsaw, as currently conceived, cannot operate.

A second mechanism with greater relevance to our study derives from computational experiments that suggest that high-elevation, low relief surfaces are products of long-term ice-sheet erosion (Egholm et al. 2017). Relief planation in these experiments arises dynamically from evolving feedbacks between topography, ice dynamics and erosion over million-year timescales. In these experiments, channelled ice flow deepens valleys but faster sliding over ridges on plateaux increases erosion and therefore reduces local topographic relief. This modelling, however, ignored the heterogeneity of bedrock (for example in fractures and fracture zones) that are known to induce a rough landscape once glacially eroded (Johansson et al. 2001b, Dühnforth et al. 2010, Krabbendam and Bradwell 2014). Also, the model assumes that glacial erosion on topographic highs is higher than on topographic lows. This ignores model results indicating that abrasion rates are strongly controlled by debris content (Hallet 1981). Debris even in the subglacial setting will concentrate in topographic lows, because it is denser than water and ice. As a potential result, topographic lows may tend to become enhanced under glacial abrasion (Krabbendam et al. 2016), contributing to roughening. On the larger scale, fjord incision brings erosional unloading and induces flexural isostatic uplift, increasing plateaux elevation. We note that the ice sheet planation process set seems unable to account for the greater extent and falling elevation of plateaux E of the main ice shed in Scandinavia (Hall et al. 2013b) and also the presence of plateaux at different elevations in individual mountain areas (Ebert et al. 2011). In lowland basement terrain in Sweden, ice sheet flow was not strongly channelled, valleys are generally shallow and flexural isostatic uplift was limited. Faster sliding over bedrock highs, however, has potential to reduce summit height and thereby maintain low relative relief across such terrain. This possibility is explored below using evidence from landforms, geological controls and cosmogenic nuclides.

4.4.1 Landscapes and landforms of glacial erosion

Glacial modification of pre-existing topography is widespread on crystalline shields and platforms in the Northern Hemisphere. Evidence of topographic inheritance commonly includes situations where smooth surfaces which lack extensive and well-developed glacial forms and which retain non-glacial features such as blockfields, tors and saprolite (Hall et al. 2019b) are incised by major landforms of glacial erosion, such as cirques and glacial valleys. Pleistocene glacial modification of

pre-existing Neogene fluvial topography is commonplace across large parts of Norway (Bonow et al. 2003, Fjellanger and Etzelmüller 2003, Fjellanger and Sørbel 2007, Hall et al. 2013b, McDermott et al. 2015, Schermer et al. 2017), Sweden (Kleman and Stroeven 1997, Lidmar-Bergström et al. 2012, Ebert et al. 2015), northern Finland (Söderman 1985, Hall et al. 2015) and north-west Russia (Amantov 1995). Preservation of old relief forms and associated weathering covers is most evident where the Fennoscandian Ice Sheet was cold-based and largely non-erosive (Lagerbäck 1988a, b, Hirvas 1991, Hättestrand and Stroeven 2002, Donner 2005, Kleman et al. 2008, Hall et al. 2015). Palaeoforms, such as inselbergs and valley segments (Olvmo et al. 1999, Bonow et al. 2003, Ebert et al. 2015), and weathering remnants (Lidmar-Bergström 1995, Olvmo et al. 2005, Olesen et al. 2012, Gilg et al. 2013), however, are also recognised widely in zones of former warm-based, erosive ice flow in Fennoscandia. Similar landform inheritance beneath warm-based ice is recognised in crystalline bedrock terrain is recognised widely in Scotland (Godard 1961, Krabbendam and Bradwell 2014, Hall et al. 2019b), Greenland (Peulvast et al. 2011, Medvedev et al. 2013) and on the Laurentian shield (Sugden 1978, Peulvast et al. 1996, Briner et al. 2006, Bouchard et al. 2007). Widespread inheritance indicates that the impact of Pleistocene glacial erosion even under warm-based ice generally has been insufficient to erase pre-existing regional scale topography.

Glacial modification of extensive, exhumed pre-Cenozoic unconformities is a special case of topographic inheritance. Glacial erosion of exhumed unconformities has been widely observed in Fennoscandia and includes erosion of unconformities of Neoproterozoic (Laajoki 2002), Ediacaran to Cambrian (Lidmar-Bergström 1997, Jarsve et al. 2014) age. Glacial erosion after exhumation of low relief basement unconformities is also found on parts of the Canadian shield along the edges of Cambrian to Ordovician sedimentary covers in Quebec (Bouchard and Jolicoeur 2000), Ontario (Corcoran 2008), Hudson Bay (Nelson and Johnson 2002), Baffin Island (Ebert 2015) and in other parts of the Canadian Arctic (Bird 1967). In each case, the continuity of these exhumed unconformities in the present shield landscape indicates limited Pleistocene glacial erosion.

The bedrock topography of Uppland at the regional scale closely resembles in its smoothness, hill summit accordance and low relief that around other Early Palaeozoic outliers in southern and eastern Sweden (Figure 2-15). Bedrock relief, summit elevation range and roughness increase across Uppland west of Uppsala and south towards Stockholm (Figure 4-12). These transitions are unlikely to relate to some form of ice sheet planation (i.e. a decrease in roughness by glacial erosion; Egholm et al. 2017) as this would require glacial erosion to produce both relatively smooth and rough topography across similar rock types and structures in adjacent areas. In the absence of geomorphological evidence of former sliding boundaries, former glaciological conditions across Uppland can be assumed to have been broadly similar throughout the Pleistocene (Figure 4-8). The absence of big hills and hill masses from NE Uppland also cannot have been a product of ice sheet planation as such hills are present west of Uppsala and south towards Stockholm. The changes in roughness across Uppland and its surroundings may also relate in part to differences in the timing of basement exposure (Lidmar-Bergström and Näslund 2002). The mosaic of low elevation rock blocks recognised in Uppland (Figure 4-13) closely resembles similar dislocated basement terrain around Early Palaeozoic outliers in Västergötland (Jansson et al. 2011) and in SE Sweden (Lidmar-Bergström 1997). At Närke, basement and cover rocks have been dislocated across a series of W–E faults, with tilting of block tops to the south (Tirén 1993) (Figure 2-17). Stripping of Early Palaeozoic cover has exposed fault scarps in basement (Figure 2-16). Rock block tops in Uppland have various inclinations, fault scarps have different orientations with respect to former ice flow and the overall block shapes are not streamlined parallel to former ice flow (Figure 2-21), features that are not typical of landscapes of advanced glacial erosion.

Glacial modification of the block-faulted unconformity surface is most evident at the regional (1–10 km) scale. Upstanding fault blocks have become isolated and fragmented by the excavation of km-long, fracture-guided trenches (Figure 4-13) and up to km-wide, box- and star-shaped rock basins. The raised edges of exhumed fault blocks have been rounded, lowered and indented by glacial erosion (Figure 4-11 and Figure *4-44*). Narrow trenches and shallow rock basins of different sizes have been excavated on block tops (Figure 4-16). Rock basins of kilometre length were formed in zones of high fracture density on the flanks and lee sides of fault-bounded rock blocks (Figure 4-15).

The presence of inherited and glacial forms and the development of structurally controlled trenches and basins are typical features of landscapes of areal scouring on glaciated shields (Linton 1963,

Johansson et al. 2001b, Lagasquie et al. 2001, Krabbendam and Bradwell 2014, Krabbendam et al. 2016). When compared to a type area of areal scouring, the cnoc-and-lochain terrain developed in Lewisian gneiss in Assynt, Scotland (Krabbendam and Bradwell 2014), the present basement topography at the regional scale in NE Uppland shows many similarities but also key differences. Fracture-aligned trenches and star basins are common to both areas (Krabbendam and Bradwell 2014). The hills or *cnocs* show pronounced stoss and lee asymmetry (Bradwell 2013). The low Uppland hills found within glacially roughened terrain also show asymmetry in the widespread development of roches moutonnées. Stoss and lee asymmetry is a characteristic feature of large hills developed in crystalline rocks after glacial erosion (Jahns 1943, Olvmo and Johannson 2002, Ebert and Hättestrand 2010). However, the cnocs that are prominent in cnoc-and-lochain landscapes have summit elevations that vary by more than 50 m in Assynt. Comparable large hills are absent from NE Uppland where hills are instead low and locally flat-topped, with widely accordant summits that fall within an elevation range of < 10 m (Figure 4-13). The distinctive glacial hill forms in Uppland reflect the inheritance and glacial modification of flat bedrock topography from the sub-Cambrian unconformity.

The Uppland landscape has developed beneath episodically warm-based ice sheets (Näslund et al. 2003) where ice flow was laterally extensive and not focused into narrow channels. Streamlined, smooth rock hills and ridges, with few plucked faces, have been associated elsewhere with high erosion rates beneath fast-flowing, former ice streams (Roberts and Long 2005, Bradwell 2013). Glacial streamlining is, however, only weakly and locally developed in Uppland (Figure 4-19). Only on Åland (Lindström 1988) and in other parts of SW Finland (Rastas and Seppälä 1981) are whalebacks common. Instead, in Uppland, stoss and lee forms predominate (Figure 4-13). Development in intervals with high sliding velocities, thin ice and low effective normal pressure may be inferred (Glasser and Bennett 2004). The terrain types identified across NE Uppland indicate significant variations in the impact of glacial erosion on the basement surface, with locally weak development of erosional forms on fault block tops (Figure 2-23). This variability may relate to differences in the timing of basement re-exposure. Alternatively, zones of low glacial modification may link to glaciological controls at different scales, perhaps relating to inter-stream areas within the Fennoscandian Ice Sheet (Punkari 1997), persistent “sticky patches” on the ice sheet bed (Kleman and Glasser 2007), spatial variations in the duration of cold-based conditions (Näslund et al. 2005), or to recurrent spatial variations in subglacial hydrogeology (Jaquet and Siegel 2003).

Glacial landforms at local (0.1–1 km) scales include various hill forms, mainly box hills, roches moutonnées, crag-and-tails and whalebacks, and hollows, mainly fault-guided valleys and box- and star basins. This assemblage of rock landforms provides a common substrate across Uppland on which terrain types and glacial and postglacial deposits are superimposed. Three terrain types are recognised: glacially-roughened, weakly-streamlined and disrupted terrain. Glacially-roughened terrain is representative of the wider substrate and includes box hills isolated by the removal of fracture-bounded blocks (Figure 4-18). Glacial streamlining is developed along N–S belts (Figure 4-19) and comprises two elements, weak streamlining of low rock ridges and hills and deposition of long, low and thin till tails. Bedrock streamlining was facilitated by the near coincident orientation of N–S ice flow (Figure 4-7) and subparallel fracture sets (Figure 4-5) (see also Krabbendam et al. 2016). Deposition on till tails included sandy till units formed late in the last glaciation (Albrecht 2005). Glacial disruption is part of a newly recognised process set that is based on evidence provided by a distinctive assemblage of landforms linked to glacial ripping. Observational evidence for development of subglacial groundwater overpressure comes from sockets on rock surfaces, dilated, extended and new fractures in bedrock and sediment fills in fracture. Glacial disruption of near-surface bedrock is marked by intense fracturing, dilation and minor displacement within the rock mass. Entrainment and transport of disrupted bedrock generates block trains and boulder spreads that include boulder moraine ridges. The three terrain types tend to occur in discrete belts or patches (Figure 4-19), a distribution that indicates important differences in the process sets that operated across the ice sheet bed.

Macro- (10–100 m) to micro- (< 1 m) forms in Uppland include many stoss and lee forms typical of glaciated shield terrain (Glasser and Warren 1990). The landform inventory indicates that whalebacks have a restricted development and that s-forms are not widespread. Arrays of lacunae (Section 4.3.2) are recognised on rock surfaces close to the present coastline that represent a significant component of total rock surface lowering by glacial erosion at the end of the last glacial cycle.

Lee-side block concentrations of similar lithology to local outcrops are also common (Lidén 1975). A significant late phase of plucking beneath the Fennoscandian Ice Sheet is indicated, as at locations in eastern Scotland (Sugden et al. 2019), but, in Uppland, mainly as part of the ripping process set.

There are similarities and differences between the glacial landforms found in Uppland and those reported recently from the beds of the adjacent Bothnian and Åland Seas (Greenwood et al. 2017). Unlike in Uppland, the present sea floor retains extensive areas floored by sedimentary rocks (Figure 2-6) and here sediment covers tend to be thick and to display soft-sediment erosional and depositional forms shaped by a range of processes that operated towards the close of deglaciation. In basement rocks, the main erosional forms found offshore are the mega-scale glacial lineations (MSGLs) with lengths of 1–9 km within Flow Set A, oriented roughly N–S. MSGLs terminate in the central-southern Bothnian Sea and mark the track of one or more palaeo-ice streams that followed the axis of the Bothnian Sea basin (Greenwood et al. 2017). Similar MSGLs are absent in Uppland, indicating that ice streams did not operate for long periods and consistent with more limited glacial erosion of basement. Weakly-streamlined bedforms in Uppland are oriented roughly N–S (Figure 4-19) and represent the onshore continuation of Flow Set C found off the north Uppland coast. This landform assemblage of drumlins and crag and tails formed during retreat of the Fennoscandian Ice Sheet from its ice marginal position in the Younger Dryas (Greenwood et al. 2017). Glacial modification on a submerged rock block surface E of Gräsö, outside the MSGL zone (Figure 4G in Greenwood et al. 2017), shows strikingly similar features to those found in the Alsunda and Hallstavik areas (Figure 4-16 and Figure 4-43). Prominent in the offshore record is a rich assemblage of glacial meltwater landforms, comprising both eskers and meltwater channels across a range of spatial scales. Meltwater corridors, oriented roughly N–S and ~600–3 800 m wide, ~8–80 m deep and ~20–40 km long, exploit large-scale bedrock fracture patterns (Greenwood et al. 2017). These meltwater corridors are generally larger in all dimensions than the trenches identified in Uppland (Figure 4-13), and may have been widened by other processes of glacial erosion, but the roughly parallel orientation and strong structural guidance indicate a similar origin to trenches in Uppland.

4.4.2 Lithological and structural controls on glacial erosion

A fundamental contrast in rock hardness exists in NE Uppland between relatively soft Mesoproterozoic and Early Palaeozoic cover rocks and hard basement. In small, fault-bounded grabens and half-grabens in the archipelago SE of Forsmark in which Jotnian and Ordovician sedimentary rocks are down-faulted, glacial erosion has selectively removed softer cover rocks to depths at least twice that of basins formed in basement (Section 4.3.5).

The crystalline bedrock in NE Uppland is generally very hard. Schmidt Hammer R-values for gneisses have mean and Upper Quartile R-values that are generally > 59 (Section 4.3.4). The general hardness of the gneisses indicates that fracturing is the fundamental control on rock resistance to glacial erosion in Uppland. The significance of fracture patterns is apparent across scales through links between fracturing, glacial landscapes and landforms. At the regional scale (1–10 km), large trenches, many with ribbon lakes and fjärds, are associated with the main regional structures (Figure 4-5). Such trenches include the Öregrundsleden, developed along the Singö Deformation Zone and the Bruksdammen basin developed in part along the Forsmark Deformation Zone. The trenches that demarcate the main rock blocks in Uppland also appear to follow bounding fault and fracture zones. The large rock basins eroded in basement are preferentially located at intersections of major structures (Figure 4-15), indicating that these are zones of high fracture density, but this association has not been demonstrated by fracture analysis. At the local scale (0.1–1 km), box- and star-basins and box hills and low hill masses with many individual roches moutonnées have rectilinear planforms that are clearly fracture-aligned (Figures 4-18 and 4-21). At the macro- to micro-scales (< 1–100 m), fracturing is a major control on the detailed morphology of rock surfaces. Vertical fracture spacing varies by three orders of magnitude from 0.1 − > 10 m (Figures 4-29 to 4-31). Horizontal and inclined fractures are more closely spaced and generally lack spacings wider than 5 m (Figure 4-32). Vertical fracture spacing appears to determine the location, size and form of many small roche moutonnées.

When R-values are plotted against fracture spacing for cosmogenic nuclide sample localities on a model of abrasion and plucking (Krabbendam and Glasser 2011), important relationships are revealed (Figure 4-49). These localities are on tops of roches moutonnées where the spacing of major, open vertical fractures recorded in line transects fall within the abrasion dominant domain where fracture spacing exceeds 4 m and within the shared plucking and abrasion domain at closer spacings. The range of fracture spacings recorded across surfaces around the Wave Rock, Ironworks and Pitted Rock sample sites also generally fall into these domains. The Klubbudden surface includes areas with dense fractures that fall entirely into the plucking domain. These plots are consistent with observations of micro- and meso-forms found on these surfaces. For example, a dominance of abrasion forms on the sample surfaces at Wave Rock (Figure 4-30) contrasts with the locally extensive development of sockets of various sizes at sites such Klubbudden (Figure 4-29). Fracture spacings for the summit fracture maps for sample sites (Figure 4-39) plot entirely within the plucking domain (Figure 4-49) but this is likely a methodological artefact of detailed mapping of fractures over areas of only 25 m^2 that included short, closed, hairline cracks. This model (Figure 4-49) is important for interpretation of erosion rates derived from cosmogenic nuclide inventories because some cosmogenic nuclide sample sites come from summits, like Wave Rock, with rock surfaces where long, open vertical fractures are spaced at more than 4 m and abrasion is dominant. Hence, erosion rates for those sites are dominantly from glacial abrasion. At sites with closer fracture spacing, plucking (and/or whatever micro-erosional processes are responsible for the lacunae on these surfaces) becomes important. Similar conclusions have been reached in zones of former fast ice flow in Kongsfjorden, Svalbard, where evidence of micro- and meso-scale plucking and other processes may extend across entire rock surfaces where the rock is closely fractured (van Boeckel 2018). It is apparent that, as in other hard, crystalline bedrock terrain (Krabbendam and Bradwell 2011, Krabbendam and Glasser 2011), the relative contributions of plucking and abrasion can be constrained in Uppland by comparing sites with fracture spacings that fall into the different process domains. Such approaches complement studies of cosmogenic nuclides across the surfaces of large roches moutonnées (Briner and Swanson 1998, Colgan et al. 2002).

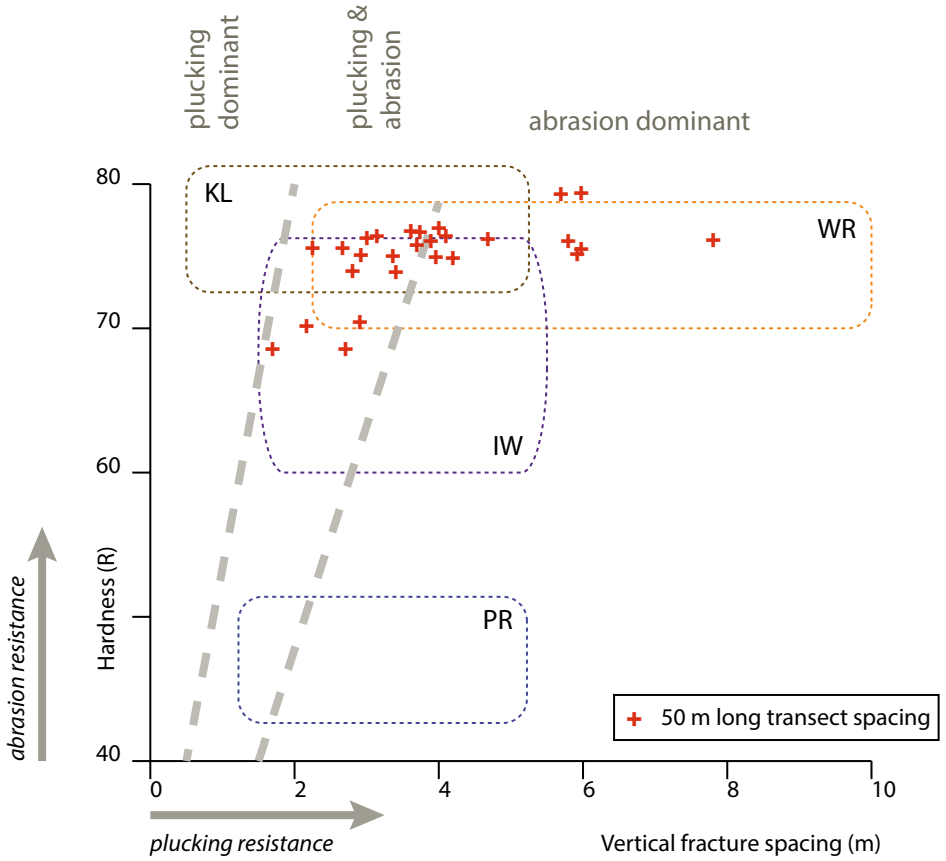

Figure 4-49. *Model of abrasion and plucking in relation to rock hardness and fracture spacing based on joint spacing in line transects (Krabbendam and Glasser 2011). Envelopes show hardness (R values) and vertical fracture spacing at 4 sites sampled for cosmogenic nuclides in the Forsmark area. IW Ironworks; KL Klubbudden; PR Pitted Rocks: WR Wave Rock.*

4.4.3 Linking landscapes and landforms to glacial processes

A nested hierarchy of landforms of glacial erosion exists in Uppland and across other lowland shield terrains that spans the regional to micro scales. Individual landforms reflect the controls from rock type and fracturing, topography, former glaciological conditions and time (Figure 4-1). Individual features of certain landforms or the landform itself, however, may be diagnostic of the former operation of a specific process of glacial erosion but in many cases landforms of glacial erosion are products of the interaction of different processes through time (Bennett and Glasser 2009). Moreover, palaeo-glaciological inferences based on the extant landform record give undue emphasis to those process sets that have operated most recently (Bradwell 2013). In this section, glacial landforms are linked to erosional processes across scales in an attempt to better understand the impacts of different processes on erosion patterns.

Modelling of block removal at the glacier bed

A short, desktop modelling study (Krabbendam and Hall 2019) has provided a first-order analysis of the forces required to move a block of bedrock at the bed of an ice sheet, and the glaciological conditions under which these forces may occur. This problem is relevant for analysis of glacial erosion beneath an ice sheet over a glacial cycle. Around Forsmark, we can view the terrain simply as one of upstanding rock blocks of different sizes separated by rectilinear basins and clefts. The analysis deals with forces acting to remove upstanding blocks 0–20 m in length. It does not deal directly with plucking, where individual blocks are removed from fracture-bounded sockets along rock cliffs that fringe upstanding rock masses.

The problem basically concerns the balance between the resisting force of the block in question versus the driving force exerted by the ice onto the block (Figure 4-50). If the driving force is greater than the resisting force, the block will move; conversely if the resisting force exceeds the driving force then the block stays in place. Intuitively, one would expect that larger blocks are more difficult to move than smaller blocks: the physical basis of this may be that the resisting force rises faster with increasing block size than the driving force.

Glaciological conditions may vary at a site throughout a glacial cycle. Hence 4 different scenarios were modelled: cold-based ice, warm-based ice, ice stream, slowing ice flow and freeze on (Krabbendam and Hall 2019).

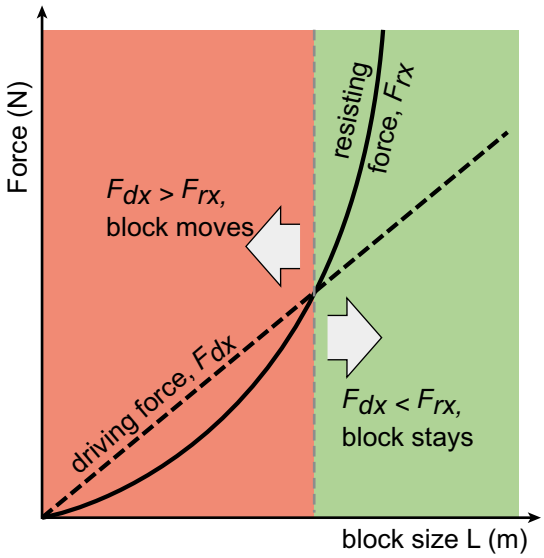

Figure 4-50. *Driving force and resisting force plotted against block size. If the driving force (dotted line) exceeds the resisting force (solid line), a block will move (red zone).*

The rock block was first considered as a cube, with equal sides, so that $V = L^3$ (Figure 4-51). The block rests on a horizontal surface, separated from the underlying bedrock by a fracture. Next, block shape was examined. Geomorphological evidence from hard rock terrains shaped beneath warm-based, sliding ice shows that variously streamlined, non-cubic bedforms (whalebacks, roche moutonnées) are common (Bennett and Glasser 2009). Hence, three different block geometries were explored: (i) flattened cuboids ('slab') with a square top area, but variable height; (ii) elongate cuboids (akin to whalebacks or rock ridges), with a square stoss side, but variable length; and (iii) we look at streamlined forms, mimicked by varying the slope of the stoss side on an elongate cuboid. No consideration was made at this stage for rock masses made up of multiple blocks, for abrasion or for lee-side plucking.

Despite significant uncertainties, a number of trends and conclusions emerged from the study (Krabbendam and Hall 2019). Overall, one conclusion is that block removal is more likely beneath thin ice than under thick ice under all three scenarios for which this is calculated (cold-based, warm-based and ice-stream scenarios). The reason behind this is that the resisting force increases with increasing ice thickness: the weight of the ice, which is linearly dependent on ice thickness, is a significant contributing factor and rises faster with ice thickness than the driving forces.

Under cold-based conditions, block removal is not likely. The resisting forces are high, firstly because there is no water pressure, and secondly because the friction-coefficient between the block and the bed are high. Equally, the driving forces are probably fairly low. If block removal occurs, there is little dependency on block size, since the curves of driving and resisting forces are near parallel. In simple terms: either all blocks stay, or all blocks move and there is no significant 'sorting' effect.

In the warm-based scenario, the uncertainty is arguably largest. If the driving forces are calculated using the basal shear stress, block removal is only likely at high shear stresses and thin ice. Such conditions may possibly develop during the growth of an ice sheet and the temporal change from cold-to-warm based conditions. On the other hand, if the forces are dependent on viscous drag around the obstacle, then block removal is significantly more likely for small blocks than for larger ones, indicating a significant sorting effect. Whether or not block removal occurs depends largely on the ice viscosity, which is poorly constrained.

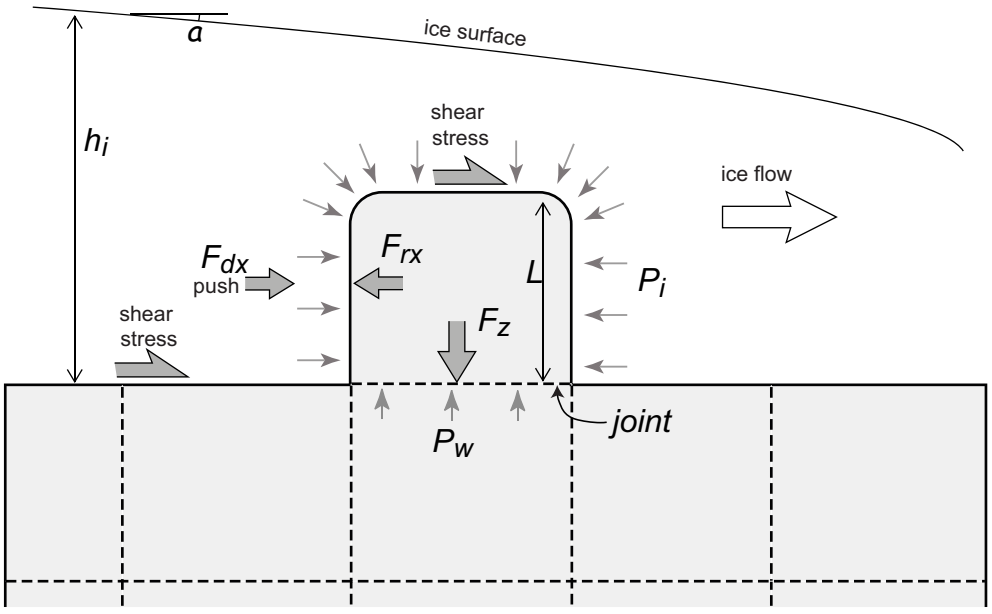

Figure 4-51. *Schematic drawing showing different forces, stresses and pressures on a block at the bed of an ice sheet – not to scale. Fdx = driving force; Frx = resisting force; Fz = normal force on basal joint; hi = ice thickness; L = size of block; Pi = cryostatic pressure; Pw is water pressure.*

In the ice-stream scenario, block removal is likely. At high basal sliding velocities (e.g. 400 m yr^{-1}), all upstanding blocks are removed; at somewhat more modest velocities (50–100 m yr^{-1}), smaller blocks are removed (< 5–10 m); there is a strong 'sorting effect' with smaller blocks removed earlier than larger blocks. It is likely that abundant water is present at and near the base, with likely high water pressures: these are likely to lower the effective friction coefficient beneath the block.

Block shape and streamlining is important under fast-flowing ice. A flat cuboid ('slab') has a much lower driving force applied to it than a cubic block, whereas an elongate cuboid has a much higher resisting force: in either case, they have significantly less probability of moving than cubic blocks. Equally, a sloping ('streamlined') stoss-side decreases the driving force applied to the block and lowers the probability of removal. These conclusions are consistent with geomorphological observations of streamlined bedrock features (rock ridges, roches moutonnées, whalebacks etc.) preserved beneath areas of presumed fast palaeo-ice flow.

In the slow-down with freeze-on scenario, the top of the block becomes frozen onto the overlying ice, whereas the base of block may remain thawed. This scenario is highly effective in block removal, particularly if accompanied by high water pressure (Pw > 90 %). Even at relatively modest driving stresses (50 kPa), almost all blocks are removed. There is little or no sorting effect: larger blocks have nearly the same chance of removal as smaller ones. Block shape and streamlining are not very relevant for the slow-down scenario: streamlined blocks have as much probability of moving as cubic block shapes. This is basically because if these slow-down and freeze-on conditions occur, the frozen ice-bed affects the entire top surface of the block and is thus independent of block shape.

The model indicates that upstanding rock blocks of 0–10 m length may be removed from rock surfaces under all scenarios except beneath cold-based ice. This is consistent with the absence of upstanding, isolated blocks, with heights more than 2 m, from rock risers across the Forsmark area. The model also indicates that upstanding streamlined bedforms of > 10 m length are highly resistant to block removal under all conditions except, perhaps, for slow down with freeze-on at the ice margin. This result is entirely consistent with the widespread occurrence of roches moutonnées and other rock hills at the macro scale and above in glaciated shield terrain, including that in Uppland (Figure 4-20). At four known sites in glacially disrupted terrain in Uppland, there is evidence for the disruption of large roches moutonnées (20–60 m long, 10 m high) (Figure 4-22). Here and elsewhere in glacially ripped terrain, subglacial groundwater overpressure is likely to be the driving factor in reducing frictional resistance to entrainment of large rock masses. The likelihood of block removal beneath thin glacier ice directs attention to the potential importance of glacial erosion during advance and decay of the Fennoscandian Ice Sheet.

Abrasion process set

The former operation of glacial abrasion in Uppland is evident from polished and striated rock surfaces at the micro-scale, smoothed surfaces and rounded edges at the meso-scale and rounding of stoss faces on roches moutonnées and across whalebacks and rock basin floors at the macro-scale. Abrasion microforms are very extensive on newly exposed rock surfaces, often absent only from the floors of sockets from which various sizes of rock blocks and plates have been removed late in the last glacial cycle. Weathering micro-forms may survive periods of glacial erosion (Hall and Phillips 2006). Small weathering pits, however, have been observed at only one site in NE Uppland (Pitted Rocks) indicating that any such features that existed before the last glaciation were erased by erosion during that glaciation. Striae and polished surfaces are destroyed by postglacial weathering but meso-scale smoothing of rock surfaces is typical away from the present coastline and confirms the ubiquity of abrasion across rock surfaces.

Abrasion is conventionally regarded as a process in which debris in the glacier sole scores and scours rock surfaces at the glacier bed (Bennett and Glasser 2009). At many sites, however, in the Forsmark area and in NE Uppland, rock surfaces are seen at the meso- and micro-scales to carry lacunae where chips, plates and small fragments have been removed by glacial erosion. The origins of these lacunae are poorly understood but whilst some, like conchoidal fractures (Krabbendam et al. 2017), relate to the stick-slip motion of clasts across the glacier bed, others seem to require dislodgement of rock fragments. Additionally, sites at the present coastline carry many metre-scale box and prismatic sockets (Figure 4-36), apparently products of block removal under high subglacial

groundwater pressure. The surface area covered by lacunae and sockets can be large, as at sites like Klubbudden (Figure 4-29), indicating that, whatever the origins of these various features, the removal of rock fragments contributes significantly to the lowering of the rock surface. The rock surfaces sampled for cosmogenic nuclides on roches moutonnées summits include sites that locally carry many lacunae (Figure 4-29) and sockets (Figure 4-31).

Mathematical modelling indicates that coupling between bedrock form and ice flow causes relief to increase due to faster ice flow and higher abrasion rates around bedrock hills (Hindmarsh 1999). Abrasion of the edges of massive rock compartments that form hills and, locally, the edges of trenches and basins, combined with excavation of surrounding more fractured rocks also leads to increased topographic curvature that in turn may generate new rock fractures on these edges (Section 3.2.6). Limited observations from trench and basin floors indicate widespread abrasion that is consistent with high ice flow velocities through bedrock lows. Abrasion rates are also strongly influenced by the availability of debris in basal ice to act as abrasive tools (Sugden and John 1976). As the density of rock is higher than ice and water and under conditions of basal melting, rock clasts tend to migrate towards low points on the glacier bed (Hallet 1981), providing a further mechanism for enhanced abrasion across rock surfaces in topographic lows, provided that sediment accumulation does not then protect the rock from erosion (Dreimanis and Vagners 1969).

Plucking process set

Glacial plucking or quarrying refers to the removal of fracture-bounded rock blocks from sockets along steps on the glacier bed (Bennett and Glasser 2009). Evidence for the operation of plucking in Uppland is provided by the presence of low rock steps seen widely at the micro- to meso-scales. The edges of steps may be rounded by abrasion after plucking and block removal or remain sharp as a consequence of block removal late in deglaciation. Associated sockets may also have floors and sides without and with abraded surfaces. At the macro-scale and above large sockets are preferentially located in flank and lee locations on box hills and roches moutonnées. Linear scarps or cliffs more than 100 m in length, however, are largely confined to the edges of trenches. Evidence for plucking from topographic lows is limited by exposure but suggests that plucking may be of much more restricted distribution than on topographic highs.

Plucking is localised in its operation on lee and flank slopes (Boulton 1979), where it is strongly influenced by existing fracture orientation and spacing (Krabbendam and Glasser 2011, Hooyer et al. 2012). In Uppland, a prominent fracture set is oriented roughly N–S (Figure 2-5). This alignment sub-parallel to ice flow has facilitated lateral plucking along hill flanks and the sides of trenches and contributed to streamlining, as in other glaciated hard rock terrains (Krabbendam et al. 2016). Where sharp discontinuities exist in fracture spacing in NE Uppland, there is little evidence for retreat of the hill flank or trench edge. At the local scale, box hills and large roches moutonnées also retain rectilinear outlines that appear to generally conform to sharp discontinuities in fracture spacing (Figure 4-18). At macro-scales and below, quarry exposures (Figure 4-32) indicate that vertical fracture spacing varies by three orders of magnitude whereas horizontal and inclined fractures are generally confined to two orders of magnitude. The locations and low height of rock risers at this scale appears to be partly controlled by the presence of rock bosses where vertical fracture spacing is wide but sub-horizontal and inclined fracture spacing is closer, and usually is less than 2 m in the near surface. Further mapping is required to establish how rock knob locations and forms link to fracture patterns.

Ripping process set

During this investigation, a new process set, glacial ripping, was identified for glacial erosion, building on ideas from Lagerbäck et al. (2005). Current understanding indicates that glacial ripping involves jacking and dilation of the near surface bedrock combined with traction from the overriding ice sheet. The landform inventory suggests that glacial ripping may have a diagnostic landform assemblage (Figure 4-52). This assemblage includes features indicative of jacking and fracture dilation seen at outcrop and the more conspicuous disrupted bedrock and boulder spreads found at the meso-scale and above. Links between stoss sockets and glacial ripping remain to be demonstrated. The large numbers of sockets found on smooth rock surfaces near to the present Forsmark coastline are associated locally with hydro-fractures at sites such as Lilla Sandgrund (Figure 4-26) and so

probably relate to the development of groundwater overpressure at the ice sheet bed. The operation of glacial ripping during final deglaciation is indicated by the angularity and short transport distances for boulders within boulder spreads. Around Trollgrundet, E of Forsmark (Figure 1-1), boulder spreads and moraine ridges are overlain by a section of the Börstil esker (Sohlenius et al. 2004), indicating that disruption and glacial transport predate esker sedimentation. Much remains to be understood about the timing, sequence, and operation of the glacial ripping process set. Available evidence, however, strongly supports a glacial origin for disrupted roches moutonnées and boulder spreads (Lagerbäck et al. 2005), rather than an alternative origin during major late- and post-glacial earthquakes (Mörner 2011).

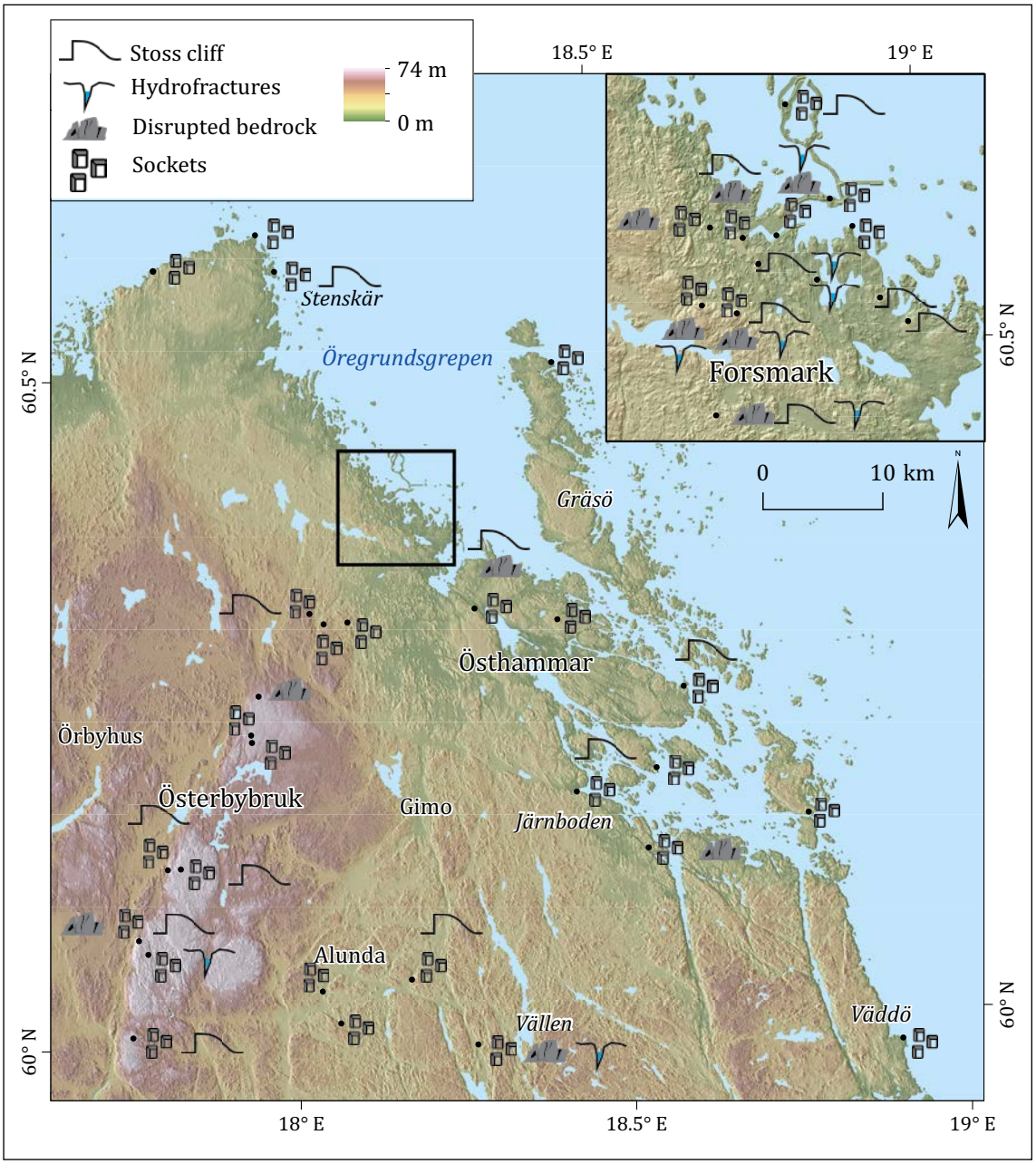

Figure 4-52. *Distribution of meso- to micro-scale features interpreted as elements of the glacial ripping landform assemblage.*

Potential significance of glacial ripping as a component of glacial erosion at Forsmark

The glacial ripping process set involves several connected processes. Geomorphic and subsurface evidence from the Forsmark site, other locations in Uppland and more widely across eastern lowland Sweden indicate that jacking, disruption, ripping and transport operated widely beneath the Fennoscandian Ice Sheet during the last glacial cycle. Hence, glacial ripping is potentially an important component of glacial erosion. At Forsmark, fracture fillings reach depths of at least 13 m, and may extend to some tens of metres (Hökmark et al. 2006, Follin et al. 2007), and indicate the potential depth over which bedrock is jacked and may be mobilised by ripping. At Gunnarsbo (Figure 4-34) and in the Vällen corridor (Figure 4-22), however, boulder spreads appear to extend to depths of only a few metres and indicate that glacial ripping operated mainly to mobilise thin rock sheets. At many localities, the short distances of block transport, the angularity of transported blocks and the sharpness of fractured edges in bedrock indicate the operation of glacial ripping immediately prior to final deglaciation. Groundwater pressures beneath retreating ice margins may attain overpressure that are sufficient to jack and open sub-horizontal fractures (Vidstrand et al. 2013) and to provide the necessary reduction in frictional resistance that allows brief mobilisation of fractured bedrock at the ice sheet bed. Depths of rock mobilised are at least equal to estimates of 1.6–3.5 m of erosion through the last 100 ka glacial cycle indicated by cosmogenic nuclide inventories (Section 5.4.2). Hence glacial ripping during final deglaciation may represent in places a major or dominant component of glacial erosion through the last glacial cycle, particularly if conditions during ice advance also favour the development of groundwater overpressure.

Thrusting process set

Glacial thrusting is known to be capable of the displacement and transport of large (10 m to 1 km long) rafts of sedimentary rock and soft sediment over long distances (Aber 1985). Thrusting is an element of thin-skinned glaciotectonics that operates at ice margins and at the base of advancing ice sheets. Two main conditions are required for massive, intact blocks of material to be incorporated: (1) the sediment or rock being overridden by the glacier should contain permeable beds confined by less permeable layers and (2) elevated groundwater pressure should occur in the less permeable beds. Ice advance over permafrost may provide an impermeable, confining layer and allow glacial transport of frozen rafts with little deformation (Bluemle and Clayton 1984). Incorporation of large blocks of material into the glacier base requires compressive flow within the glacier itself close to the ice margin (Rychel et al. 2015). When compressing flow occurs, the flow lines within the glacier have an upward component of motion (Nye 1952). This generally occurs where ablation exceeds accumulation and on reverse slopes where the bed beneath the glacier is concave upward (Merritt 1992). Under these conditions, large blocks of material may be sheared upward into the base of the ice as a result of the decreased effective stress caused by elevated pore-water pressure (van der Wateren 1985). Rafts may be transported, essentially intact, for many kilometres (Merritt et al. 2017).

Glacial thrusting and thin-skinned glaciotectonics are not processes generally associated with hard, crystalline bedrock. Glacial thrusting is recognised, however, in hard sedimentary rocks in Dakota, USA (Bluemle and Clayton 1984) and in northern England (Evans et al. 2018). Glaciotectonic disturbance is also reported from within Alum Shale (Thorslund and Jaanusson 1960) and Ordovician limestones in Sweden (Lundqvist 1987, Lindskog et al. 2018). Large, shallow rock basins in basement in Uppland mark locations where the largest volumes of rock have been removed from below U2. It is important to explore the possibility that glacial thrusting and related glaciotectonics have been involved in the excavation of these basins.

Evidence for thrusting in other contexts mainly comprises large holes from which rafts have been removed, the raft themselves, hills or ridges formed from deposited rafts and any sediments reworked after disintegration of rafts. Hill-hole pairs, separated by distances of 5 km or more, are key indicators (Aber et al. 1989, Rychel et al. 2015). In the bedrock topography of NE Uppland, holes are widely present as basins of various sizes and shapes. The edges of basins are often not sharp, as might be expected if rock had been extracted by recent thrusting but variably rounded and indented (Figure 4-13). The Bruksdammen basin, with its irregular outline and axial rock ridge, appears instead to be a product of incremental erosion by abrasion, plucking and ripping (Figure 4-15). Moreover, paired hill-holes and large glacial rafts of gneiss bedrock that retain rock structure internally have not been recognised during reconnaissance mapping. Available evidence does not support a major role for glacial thrusting in the formation of rock basins in Uppland.

An important caveat should be applied to this working conclusion. Glacial thrusting is a process that can operate effectively when an ice front advances over permafrost (Boulton and Caban 1995, Harris and Murton 2005). Such conditions existed during the advance of the last, and likely earlier ice sheets in Uppland (Vidstrand et al. 2013). Thrusting may also have been facilitated where bedrock had been disrupted at the close of a previous glacial phase. Hence, evidence for thrusting of gneiss bedrock during ice advance may have been destroyed by later glacial erosion.

Glacial meltwater process set

Glacial meltwater may be directly involved in glacial erosion through sheet and channelled flow at the ice-rock interface (Boulton et al. 1995) and indirectly through its importance in generating high hydrostatic pressures (Boulton and Caban 1995). Landform evidence for direct involvement of meltwater sheet flow in erosion of hard bedrock is provided by a range of sculpted micro- to meso-forms (termed *s-forms*) (Kor et al. 1991) which include various transverse and longitudinal troughs, furrows and cavities (Ljungner 1930). Channelled meltwater flow is responsible for the cutting of meltwater channels that include rock canyons (Olvmo 1985).

In NE Uppland, limited evidence appears to exist for erosion by meltwater through sheet flow. S-forms have not been recognised widely. Narrow, sinuous rock troughs formed by meltwater (classed in the landform inventory as s-forms) are only a minor component of the meso-forms found on exposed rock surfaces. Polished flutes however are recognised on islands in the Åland Sea (Strömberg 2010) and westwards towards Forsmark (Holmlund et al. 2016) and have been linked to high discharges of meltwater moving across parts of the ice sheet bed during final deglaciation (Holmlund et al. 2016). In contrast, rock trenches are widely developed across Uppland at the macro- to regional scales (Figure 4-16). The trenches have been compared to tunnel valleys (Talbot 1999, 2014) and to meltwater canyons of *kursu*-type (Olvmo 1985, Tirén et al. 2001). Similarities include the high length/width ratio and the flat floors, but important differences exist. Firstly, trenches run both parallel and traverse to former ice flow, whereas tunnel valleys (Kehew et al. 2012) and meltwater canyons (Johansson 2003) usually only run subparallel to former ice flow direction. Secondly, the trenches in lowland Sweden and Finland are developed in hard, fractured gneiss bedrock and so differ markedly from tunnel valleys that are most common in soft sediments with much lower rock resistance found beneath ice sheet beds in areas such as the North Sea (Huuse and Lykke-Andersen 2000, Stewart and Lonergan 2011). On the floor of the Baltic Sea, tunnel valleys are found only in softer substrates beyond the edge of the exposed Precambrian basement (Flodén et al. 1997). Thirdly, integrated networks of rock-cut meltwater canyons have not been identified in Uppland, unlike in other parts of Fennoscandia (Olvmo 1985, Tirén et al. 2001, Johansson 2005). Fourthly, the rock floors of the trenches are relatively shallow, with depths that are generally less than 20 m in NE Uppland, increasing to < 50 m further south (Figure 4-46), whereas tunnel valleys beneath the bed of the southern Baltic Sea have depths of 50–100 m (Flodén et al. 1997). These differences indicate somewhat separate origins for the rock trenches in Uppland.

Trench location, orientation and spacing is primarily controlled by deformation zones and faults and does not generally match the location, N–S orientation and ~ 25 km spacing of major eskers in NE Uppland (Boulton et al. 2001). That trenches have acted as meltwater conduits seems likely, as in the Bothnian Sea (Greenwood et al. 2017), particularly where deep trenches run parallel to former ice flow (Figure 4-14). Yet direct evidence of meltwater erosion is elusive. The sides of trenches are typically rounded and indented, with lee-side cliffs on hills, indicating modification by glacial abrasion and plucking. Moreover, reconnaissance mapping has not identified along trench sides the micro- and meso-forms (potholes, sichelwannen etc.) diagnostic of large volumes of meltwater flowing under high pressure (Holtedahl 1967). Trenches in Uppland also appear to lack glaciofluvial boulder fans at exits, unlike in Småland (Persson 1969). One possibility is that meltwater erosion occurred mainly prior to the last deglaciation so that its effects have been largely effaced by subsequent erosion across the ice sheet bed. A second possibility is that meltwater erosion operates on trench floors in combination with other processes of glacial erosion under conditions of high sub-glacial water pressure. A third possibility is that narrow trenches are first incised in fractured bedrock by meltwater but subsequent widening is achieved mainly other processes of glacial erosion. Much remains to be understood about the processes responsible for the excavation of bedrock trenches in Uppland.

Interaction of processes of glacial erosion

Evidence for the former operation of different processes of glacial erosion should be considered alongside that which indicates the combined operation of those processes. One way to evaluate process interaction is within a framework of two major controls on the effectiveness of glacial erosion: fracture spacing and subglacial groundwater pressure (Figure 4-53). Abrasion operates largely irrespective of fracture spacing (Krabbendam and Glasser 2011) but it is affected indirectly by groundwater pressure through its effects on basal sliding velocity (Ugelvig et al. 2018). Plucking is particularly effective at fracture spacings of less than 3 m (Figure 4-49) and the process is enhanced by high subglacial groundwater pressure (Ugelvig et al. 2016). Hydraulic jacking and fracture dilation, both likely precursors to glacial ripping, require the build-up of groundwater overpressure in fractured rock beneath the ice sheet bed. Preliminary interpretations indicate the importance of sub-horizontal fractures in jacking but suggest that ripping operates in rock with both widely-spaced fractures (Figure 4-22) and closely-spaced-fractures (Figure 4-33). Thrusting, if it operates, is similar, except that fracture orientation and spacing in gneiss bedrock determine zones of low and high permeability. Glacial meltwater erosion requires high discharges and flow velocities to be effective, conditions that may develop during supraglacial lake drainage (Bartholomew et al. 2011) and during deglaciation (Jansen et al. 2014). High meltwater fluxes at the ice sheet base are likely to be associated with high groundwater pressures or short periods of overpressure (Claesson Liljedahl et al. 2016). The evacuation of fracture zones along trenches suggests selective erosion of closely fractured rocks that included the action of subglacial meltwater streams. The two main areas of overlap for the process envelopes are in rocks that are closely fractured and under conditions of high to over pressure when plucking, ripping and meltwater each operate. Highly effective glacial erosion can be predicted under these circumstances.

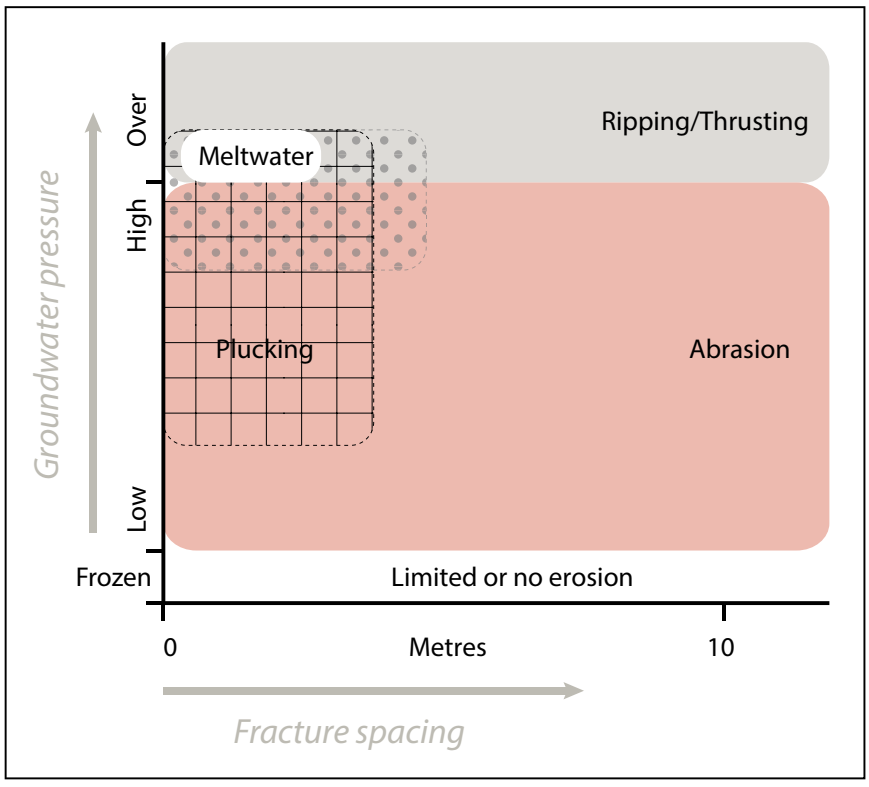

Figure 4-53. *Schematic model of the interaction of processes of glacial erosion indicated by overlapping domains in relation to subglacial groundwater pressure and fracture spacing.*

A second way to consider interaction between different processes of glacial erosion is in terms of spatial variation. Different processes may be more or less effective in different parts of the basement landscape of Uppland. Abrasion operates across the entire ice sheet bed whenever the basal ice is sliding. Abrasion rates may be highest where ice is forced to deform around obstacles (Hindmarsh 1999) and where debris is concentrated at the ice sheet base in rock hollows. Plucking operates along rock cliffs and steps. Observational evidence of plucking operating on bedrock surfaces in topographic lows or beneath till cover is sparse (Figure 4-20) but this situation may be merely a result of limited exposure. Ripping operates on km-wide patches and belts but apparently left large areas of NE Uppland unaffected during the last deglaciation (Figure 4-27). Thrusting, if it operated, was likely focussed on zones of high fracture density across the sites of larger rock basins. Meltwater erosion was largely confined to the main routeways of meltwater discharge along N–S trenches (Figure 4-14). Hence, in Uppland, different sets of processes likely had different impacts across topographic highs and lows on the former ice sheet bed.

When different processes of glacial erosion are considered in the spatial context of glacially-roughened terrain that forms the substrate for the glacial topography across Uppland then spatially varied and scale dependent impacts become apparent. Abrasion operated mainly to smooth and lower rock surfaces across the entire terrain at the macro- to micro-scales. Plucking acts to remove blocks from rock steps along hill flanks and lee slopes and along the edges of trenches and basins, again at the macro- to micro-scales. Ripping eroded both bedrock highs and lows but apparently only within restricted areas where it operated mainly at the macro- and local scales. Prismatic and box sockets, together with other lacunae, indicate a wider influence for block loss from rock surfaces at the micro- to meso-scales. Any thrusting was focussed on basins at the local and regional scale. Meltwater erosion was largely confined to trenches. Combined operation of different processes was most likely in zones of close fracturing and where high groundwater pressures developed.

A third way to consider process interaction is through time. The erosional processes operating on a rock surface may vary between and through glacial cycles as subglacial conditions change (Hubbard et al. 2009, Cowton et al. 2012). Close to zero erosion is expected when the ice sheet is cold-based (Sugden 1968). Abrasion can be expected to operate continuously whenever the debris-laden sole of the ice sheet is sliding across bedrock but at different rates according to ice flow velocity, overburden thickness and groundwater pressure, supply of abrasive material to the glacier base and protection afforded by a basal till layer (Sugden and John 1976). Plucking is favoured under thin ice and high groundwater pressure (Sugden et al. 2019). Ripping requires development of groundwater overpressure and operated efficiently under ice marginal environments during the retreat of the last Fennoscandian Ice Sheet. Models of subglacial groundwater pressures indicate that the advance of the last ice sheet over permafrost provided conditions necessary for development of over pressure at the ice margin (Vidstrand et al. 2013). Hence, whilst there is strong geomorphological evidence that ripping operated effectively during the last deglaciation (Section 4.3.3), it is plausible that ripping and other erosional processes that were facilitated by groundwater overpressure operated during advances of the Fennoscandian Ice Sheet. Recent models of the subglacial hydrology of the Fennoscandian Ice Sheet indicate that routing of meltwater through the many N–S orientated trenches in Uppland also occurred mainly during ice sheet build-up and decay, when the Fennoscandian Ice Sheet margin stood in the Stockholm area (Shackleton et al. 2018). Thrusting is widely associated with rafting of frozen soft sediments during ice advance (Bluemle and Clayton 1984, Lee and Phillips 2013, Merritt et al. 2019) and may have operated in zones of fractured basement during advance of the last Fennoscandian Ice Sheet. The episodic and perhaps short-lived operation of some of these different process sets is shown schematically in Figure 4-54. Aside from abrasion, other processes of glacial erosion are likely to operate most effectively at the start and end of glacial phases when an ice sheet is thin and groundwater pressure is high.

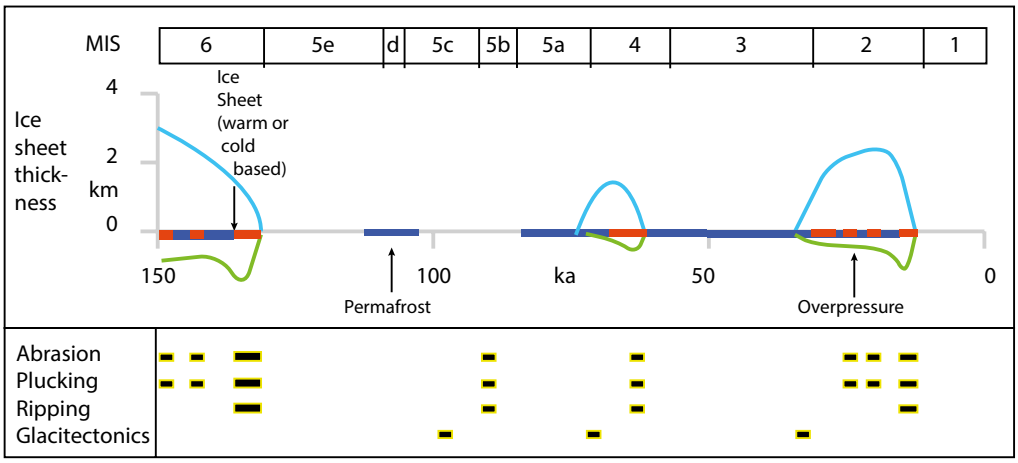

Figure 4-54. *Schematic model of the suggested episodic operation of different processes of glacial erosion beneath the Fennoscandian Ice Sheet over the last 150 ka in the Forsmark area. Data on ice thickness and permafrost from SKB (2010). The Fennoscandian Ice Sheet also may have advanced S of Forsmark in MIS 5b (Svendsen et al. 2004) but the thickness and duration of any ice cover is unknown.*

4.4.4 Progressive glacial modification

Available evidence from Uppland and the southern Bothnian Sea given in Chapter 2 indicates that the Cambrian basement unconformity, prior to dislocation and exhumation, was a smooth surface of very low relief. The continued operation of the Bothnian River system until ~1.1 Ma indicates the persistence until that time of Early Palaeozoic sedimentary cover around the margins of what is now the Åland Sea. Hence, the initial stages of glacial erosion likely involved the removal of cover rocks from U2 in the Forsmark area and across large parts of NE Uppland. Re-exposure of U2 in NE Uppland, and also unconformities around other Early Palaeozoic outliers in S-C Sweden, has provided unusual opportunities to examine the progressive modification across scales of hard, variably fractured and originally smooth basement surfaces beneath successive Fennoscandian ice sheets.

Landscape (10–100 km) scale

Topographic roughness and relative relief vary at the landscape scale across east central Sweden (Figure 4-12). Roughness and relief are low in northern Uppland, indicating limited erosion of the U2 surface, compared to areas to the west and south. Ice sheet models, however, indicate broadly similar dynamics for the former Fennoscandian Ice Sheet at this scale outside the former Bothnian Ice Stream zone (Näslund et al. 2003). Rock type (Figure 2-1) and major fracture patterns (Figure 4-14) also do not change systematically southwards across Uppland (Figure 4-8). Hence the observed differences between northern Uppland and neighbouring terrain must involve factors other than ice sheet dynamics and geology. One possibility is that U2 in southern and western areas was exhumed and exposed to weathering prior to the Pleistocene (Lidmar-Bergström and Olvmo 2015) or in the Early Pleistocene. Deep weathering developed along fracture zones but was later removed by glacial erosion. In contrast, the basement in NE Uppland was re-exposed later during the Pleistocene and so any weathering remained shallow or insignificant. In this scenario, the differences in roughness and relative relief relate to former pre-glacial weathering patterns. A second scenario is that whilst Early Palaeozoic cover persisted into the Pleistocene across large parts of Uppland, it was removed first in the south and west, exposing the basement to glacial erosion through a greater number of glacial cycles than in areas further north. Further work is needed to test these and other alternative scenarios.

Regional (1–10 km) scale

Modification of the exhumed unconformity

In Uppland, topographic roughness also varies at the regional scale (Figure 4-23). The dimensions, frequency and interconnectivity of trenches and basins increase southwards (Figure 4-46), as does lake density (Figure 2-19). Topographic roughness (Falcini et al. 2018), valley interconnectivity (Haynes 1977) and lake density (Sugden 1977, Briner et al. 2008, Ebert 2015) are each potential proxies for the intensity of glacial erosion. Hence, a general southward increase is indicated in the impact of glacial erosion across Uppland. The proxies relate in a general way to variations in the spacing, number and volume of trenches and rock basins. These negative relief forms represent locations where erosion below the former unconformity has been deepest and where the greatest volumes of rock have been removed. In contrast, the summit areas have lost much less rock mass and are estimated to generally remain within 10 m elevation of the former unconformity surface.

Modification of exhumed fault blocks

The main topographic features found at the regional scale in Uppland are the variably inclined, flat-topped fault blocks on the dislocated U2 surface (Figure 2-21). The progressive glacial modification of the fault blocks is seen in the Alunda area (Figure 4-16), on the Ironworks Block (Figure 4-42) and around Hallstavik (Figure 4-43). Rock block tops are lowered initially through the loss of thin layers of gneiss from sites of close fracture spacing. Deeper erosion on block tops is focussed along and at the intersections of minor fracture zones. Rock block edges are first rounded and later indented and eroded backward. Deep erosion between rock blocks is confined initially to bounding fault zones through the excavation of trenches. Similar progressive erosion is apparent on exhumed fault block tops and edges at Närke (Figure 4-44). Comparison of adjacent blocks of similar size and elevation around Alunda between Ål and Väddö (Figures 4-16, 4-22 and 4-43) indicates that progressive erosion involved the deepening of trenches and extension of rock basins on the block surfaces. Summit heights within and across adjoining fault blocks between Ål and Väddö remain accordant even where summits become isolated on bosses of massive gneiss.

Smooth fault block tops and sharp fault scarps at Närke are indicators of relatively recent re-exposure of basement to glacial erosion (Figure 4-44). Smooth fault block tops in NE Uppland are found at both relatively high elevations, such as at Väddö, Ironworks and Alsunda, and at low elevations, as at Griggebo (Figure 4-13). At Ironworks, the block top surface across large areas of gneiss with vertical fracture spacing of less than 3 m (Figure 4-42). Its high elevation is not a function of rock resistance but likely rather of recent re-exposure, and hence short time of exposure to glacial erosion. The smooth block tops together appear to indicate where patches of sedimentary cover persisted longest in Uppland. Uneven but progressive glacial erosion of sedimentary outliers is also evident across Västergötland, where the Lugnås outlier has been stripped of dolerite cap rock (Calner et al. 2013) and so has been prepared for final removal in future glaciations.

Modification by headward erosion

Attention has been drawn previously to the possibility that headward glacial erosion may in future glaciations extend towards Forsmark, a process that could significantly increase local rates and depths of glacial erosion at the proposed repository site. The possible mechanisms involved are uncertain but include the headward extension of meltwater canyons, tunnel valleys and major incisions during jökulhaups (Talbot 1999). Trenches oriented NW–SE occur as fjärds, ribbon lakes and linear basins to the SE of Forsmark (Figure 4-13), with deeps offshore reaching −57 m off Gräsö. In the archipelago around Singö, several trenches and basins occur in small half grabens floored by Jotnian sedimentary rocks (Söderberg and Hagenfeldt 1995) (Figure 2-8). Glacial erosion has exploited these fracture zones and the sandstones that formerly filled them to create the sounds that run between Gräsö and the Öregrund and SE of Östhammar (Figure 4-55). The landform assemblages at the head of these sounds and associated lakes include each of the terrain types recognised for the Forsmark area and across NE Uppland (Figure 4-55). Almost all bedrock highs have elevations below 20 m a.s.l. and the sediment infills for trenches and basins rarely exceed 10–20 m. High rock steps that might indicate onset zones for headward erosion are not

apparent along the trenches. We note also that the supposed zones of headward erosion are oriented obliquely to ice flow at the end of the last glaciation (Figure 4-7), as also shown by the orientation of drumlins (Figure 3-10) and to earlier phases of ice flow, as indicated by weak bedrock streamlining (Figure 4-19). Available evidence supports the glacial exhumation of small horsts and grabens in this part of the archipelago but the potential for headward erosion seems limited.

Local (0.1–1 km) scale

Progressive erosion is apparent at this scale from differences between terrain types. Flat-topped parts of fault blocks show low surface roughness with low roches moutonnées and shallow fracture-guided clefts (Figure 4-23). The weak development of glacial roughening indicates that these areas represent patches of limited glacial erosion depth. Bedrock landforms with greater relief found elsewhere across other rock blocks developed through glacial roughening, weak streamlining and ripping represent more advanced glacial modification. For each terrain type, however, the bedrock summits remain at similar elevations as relative relief increases. .

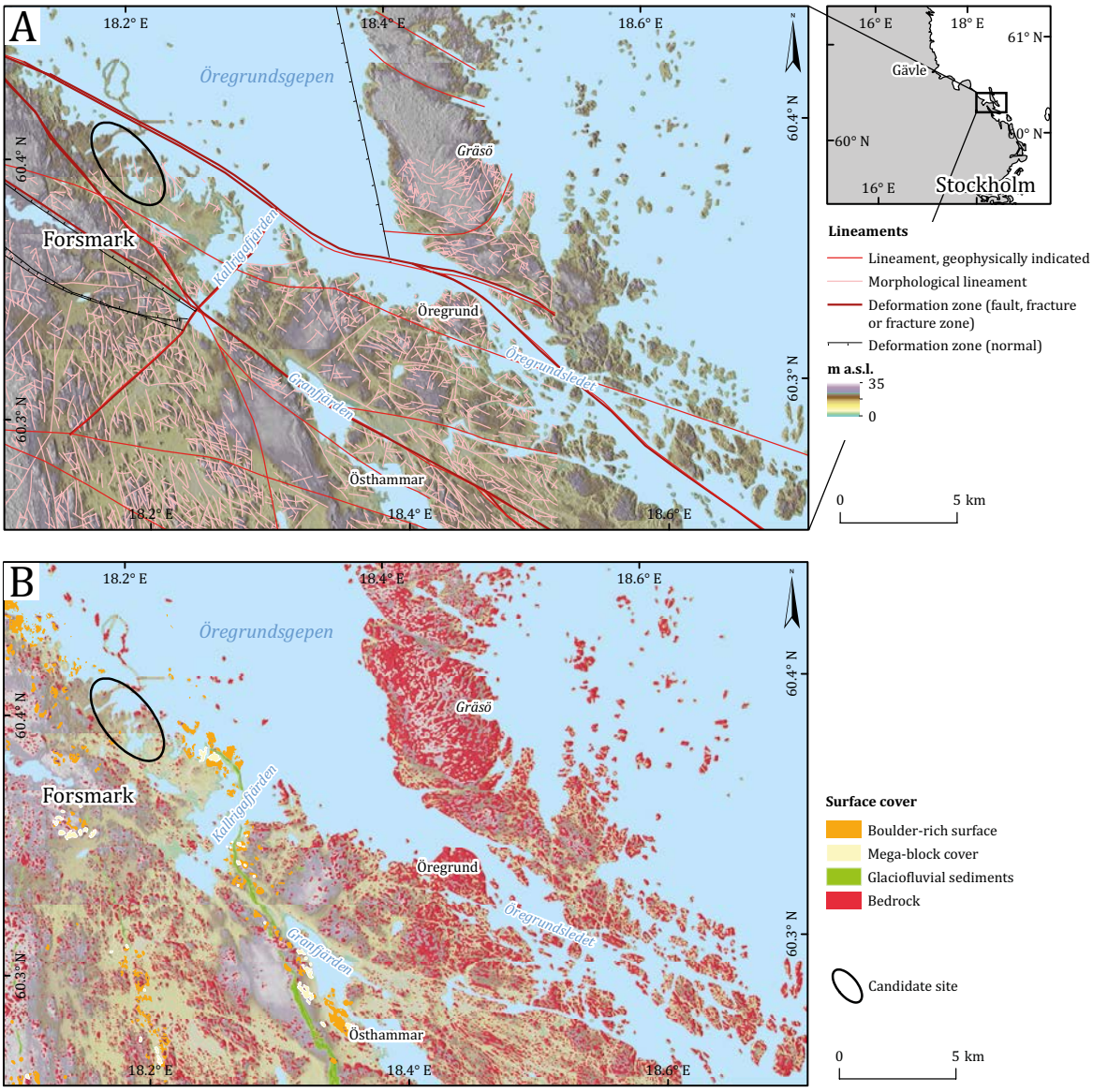

Figure 4-55. *Topography in the supposed headward erosion zone south-east of Forsmark. A. DEM based on Lantmäteriet data with lineaments based on SGU data. B. DEM overlain by SGU data on boulder spreads, glaciofluvial deposits and exposed bedrock.*

Glacial ripping has potential to reduce, maintain or increase relative relief. In the Vällen corridor, several large roches moutonnées have been disrupted (Figure 4-22), with opening of fractures and caves. These massive, but now disintegrated, bedrock bosses have been prepared for erosion and removal in the next glacial advance. Whilst future loss of these hills would reduce local relief, only a few examples of disrupted roches moutonnées with block caves are known from Uppland (Figure 4-9). Much more extensive are boulder spreads (Figure 4-9), which often appear to be shallow rooted (Figure 4-35). Removal of thin layers of fractured gneiss from flat-topped fault blocks, such as Ironworks (Figure 4-42), and low relief hill summits, as at locations around Forsmark (Figure 4-28), would maintain low summit relief. Also, in the Vällen corridor, glacial ripping has contributed to an increase in relief by block excavation on broad trench floors (Figure 4-22). Evidence for former operation of the glacial ripping process set is strongly zoned. Little geomorphological evidence is yet available for the wide operation of ripping within glacially roughened and streamlined terrain types. Hence, the net effect of glacial ripping on the relative relief of basement surfaces remains to be properly evaluated.

Macro (10–100 m) to micro (< 1 m)-scales

Macro- to micro-scale landforms of glacial erosion represent the products of different sets of processes of glacial erosion operating on variably fractured but hard gneiss. At the macro-scale, glacial landforms approach a steady state morphology with features that are maintained during glacial erosion unless glaciological conditions change. Modelling reported in the previous Section indicates that low, streamlined rock surfaces and slabs are highly resistant to removal. Erosion of such surfaces was piecemeal and involved the development of meso- and micro-forms. Roches moutonnées, and also small rock basins, are strongly controlled in plan form by fracture patterns, indicating that plan form is maintained during glacial erosion.

Meso- and micro-forms develop in response to prevailing subglacial conditions. Micro-forms such as striae on exposed bedrock surfaces are aligned with directions of ice flow during deglaciation (Sohlenius et al. 2004) and probably were mainly produced towards the end of the last glacial cycle. We note, however, that crossing striae have been recorded in the Forsmark area (Sohlenius et al. 2004) and that carbonate-rich tills occur at depth locally that are of possible MIS 6 (Björnbom 1979) or MIS 4 age (Lundqvist 1973, Robertsson et al. 2005). Such occurrences point to spatially variable erosion and to locations where till cover may have protected bedrock from erosion throughout the last glacial cycle.

Changes in landforms of glacial erosion through time

Development of glacial landforms through time varies with scale. At the landscape scale (10–100 km), the main impact of glacial erosion has been to roughen the bedrock surface and to increase relative relief. There is no evidence that the sub-Cambrian unconformity was glaciated during the final stages of its formation during Cambro-Ordovician times. Hence, the characteristics of the presently exposed basement in Uppland do not include inherited pre-Cambrian glacial bedforms. The U2 basement surface found beneath and around Early Palaeozoic outliers in Västergötland, Närke and Uppland is flat and lacks large hills and deep valleys. The present low relief and low elevation range of the basement in these areas is a result of direct inheritance of topography from the unconformity. The small elevation differences between the basement on the buried unconformity and at distances of 1–40 km from the edges of these outliers indicate that present basement summits stand close in elevation to the former unconformity. At the landscape scale in Uppland, the main impact of Pleistocene glacial erosion has been to exhume the sub-Cambrian unconformity but erosion of the basement has been insufficient to obscure its original form.

At the regional scale, the variable inclinations, low fault scarps and lack of glacial streamlining on the exhumed fault block surfaces in Uppland represent inherited erosional and tectonic features. Inheritance of low, flat topped, variably tilted, rock block topography is not consistent with deep glacial erosion in basement. The southward increase in Uppland in topographic roughness, relative relief, valley connectivity and lake density mark an increasing glacial impact. Comparisons between adjacent fault blocks provide evidence of progressive modification with erosion of edges, roughening and lowering of tops and excavation of bounding trenches along fracture zones. The overall impact of glacial erosion at this scale also has been to increase and roughen relief.

This situation is in direct contrast to models of ice sheet planation where undulating bed topography is reduced through time (Egholm et al. 2017). The critical parameter in the ice sheet planation model is the basal sliding rate. The basic assumption in the modelling of Egholm et al. (2017) is that sliding is faster over ridges because thinner ice reduces the contribution of creep to the total velocity and sliding must accelerate to compensate. Faster sliding over ridges increases erosion and thereby reduces local topographic relief. There are several reasons why landform evidence in the shield lowland around Forsmark diverges from these model results. The rock landform record represents the cumulative result of spatially and temporally variable interactions between different processes of glacial erosion. The ice sheet planation model is, however, rooted in abrasion (Egholm et al. 2017). Abrasion contributes to the streamlining of rock surfaces (Hubbard et al. 2000) but thereby reduces frictional resistance to ice flow through time (Hindmarsh 1999). On low hills, such as in Uppland, the increase in sliding velocity in response to ice deformation may remain low (Boulton 1979) and have limited influence on abrasion rates. Furthermore, the greater availability of basal debris in lows on the ice sheet bed (Boulton and Eyles 1979) due to density sorting may increase abrasion rates in these locations (Krabbendam 2016). Abrasion also may contribute only 10–40 % of the total rock removed by all processes of glacial erosion (Iverson 2002, Melanson et al. 2013). Other glacial processes, including plucking (Boulton 1979), are more effective than abrasion, at least locally and periodically, and so may be quantitatively more important for glacial erosion budgets through a glacial cycle (Benn and Evans 2010). Critically, the ice sheet planation model ignores the widely observed heterogeneity in fracture density and, hence, spatial variability of glacial erosion rates across the former ice sheet bed that are manifest across scales in Uppland. Hills and valleys persist in hard shield bedrock due to large differences in fracture spacing. Fracture patterns are major controls on erosion rates through multiple glacial cycles for all processes of glacial erosion, other than abrasion (Krabbendam and Glasser 2011, Iverson 2012).

At the local scale, increases in topographic roughness and relative relief on the ice sheet bed may be modulated by processes which suppress valley deepening or which preferentially erode hills. Thick sediment fills may protect valley floors from erosion over long time periods (Preusser et al. 2010). At the macro-scale and below, the presence of a till layer may transfer the plane of subglacial slip from the bedrock to the till surface (Iverson et al. 2003) and thereby suppress erosion. On large roches moutonnées, up-ice migration of small rock steps lowers rock surfaces (Briner and Swanson 1998), plucking can extend beyond lee and flank faces (Rastas and Seppälä 1981) and sheet joints in granites may be exploited through the removal of fractured pieces of rock slabs (Sugden et al. 1992). Glacial ripping is a special case, capable of disrupting and removing large roches moutonnées but also of deepening trenches. The operation of the jacking-disruption-ripping process set was also spatially and temporally restricted at the end of the last glaciation in eastern Sweden.

Local scale roughness influences patterns of ice flow across the ice sheet bed. On flat surfaces, basal sliding rates are uniform. As ice sheet bed relief increases, basal sliding rates diverge as ice starts to deform around obstacles and pressure differentials increase between the stoss and lee sides of hills (Glasser and Warren 1990). Greater bed roughness influences basal ice flow (Schoof 2005) and the main processes of glacial erosion (Boulton 1982). Abrasion rates may increase around hills and in hollows where deformation leads to faster sliding rates (Glasser and Bennett 2004). Larger obstacles provide greater opportunities for flow separation at the glacier bed and for the opening of cavities, increasing potential for plucking (Hallet 1996). Glacial meltwater flow is most likely to be channelled through clefts and trenches. Thin-skinned glacitectonics and glacial ripping may, however, be insensitive to local bed topography. Understanding the changing contributions of different glacial processes through a glacial cycle (Figure 4-54) to erosion rates and to the shaping of hills and hollows on the ice sheet bed remains a major challenge.

4.4.5 Depths of glacial erosion

Sedimentary cover

Glacial overdeepening of the marine basins the Bothnian and Åland Seas indicate minimum average losses of 50 m thicknesses of Mesoproterozoic and Early Palaeozoic sedimentary cover rocks (Section 4.3.1). Deep erosion likely commenced after termination of the operation of the Bothnian River system at 1.1 Ma (Overeem et al. 2001) when successive Fennoscandian Ice Sheets reached their maximum extents and thicknesses in the Middle and Late Pleistocene (Ehlers et al. 2018,

Batchelor et al. 2019). An onset for overdeepening at 1.1 Ma suggests that an average thickness of more than 4.5 m of sedimentary rock was removed from these basins in each glacial cycle through the late Early and Middle Pleistocene. Average Pleistocene sediment thicknesses on the East European Plain are 49 m (Gorlach et al. 2015). The sediments are Elsterian and younger in age and include large volumes of Early Palaeozoic rocks excavated from the Baltic basin. If deep erosion mainly dates from MIS 12 commencing at 478 ka then depths of Early Palaeozoic rocks removed from the marine basins in each glacial cycle are roughly doubled. Small grabens in the archipelago SE of Forsmark have lost thicknesses more than 30–40 m of Jotnian and Ordovician sedimentary fill. Basement surfaces on fault block tops representing the exhumed U2 surface between these grabens have also lost Early Palaeozoic cover rocks. Hence additional, unknown thicknesses of sedimentary rocks may have been lost from above the sites of these grabens. South of the Gulf of Finland, it has been estimated using pre-Pleistocene planation surfaces as reference surfaces that ~ 40 m of mainly Devonian cover was removed in the Pleistocene (Amantov 1995). Whilst these broad estimates are subject to high uncertainties, a minimum thickness of several tens of metres of Ordovician limestone was likely eroded by the Fennoscandian Ice Sheet from large parts of Uppland through the Middle and Late Pleistocene.

Basement gneisses

Estimates of depths of glacial erosion in basement across Uppland in this chapter are based on the use of U2 as a reference surface in profiles and models. The models of U2 rest on assumptions that U2 was originally a near planar surface, without deep Neoproterozoic weathering at the time of burial, overlain by Ordovician limestone and broken by minor, post-Ordovician faulting. An estimate of 10 m is used for the maximum height difference between present summits on flat-topped blocks and the former position of U2. This height difference is consistent with elevation ranges across rock highs on some fault block tops of less than 5 m (Figure 2-21), the relative relief of the basement in proximity to the Ordovician outliers offshore from Forsmark (Figure 2-11) and the identification of fault scarps along the edges of fault blocks with elevations less than 10 m above dip slopes on adjacent blocks (Beckholmen and Tirén 2010b). Limited lowering from U2 is also consistent with the smooth bedrock topography developed across rock blocks of diverse gneiss types at the regional scale. The 10 m estimate may be too low if the pattern of glacial erosion since exhumation is spatially uniform and capable of maintaining landforms inherited from the U2 surface or capable of forming and maintaining similar features during deeper erosion. Both possibilities are considered unlikely because of the evidence for progressive modification of the U2 surface in Uppland (e.g. Figure 4-16) and around other Early Palaeozoic outliers (e.g. Figure 4-45). Glacial erosion also shows marked spatial variability in erosion depths with significant control by fracture spacing at the regional (Figure 4-23), local (Figure 4-17), macro- (Figure 4-18), meso- (Figure 4-25) and micro- (Figure 4-26) scales.

U2 is modelled using bedrock summits as pinning points for profiles and summit envelope surfaces. On roughened fault block tops, depths of erosion in basement are less than 5–10 m below summit envelope surfaces (Figure 4-42), increasing locally to 15–20 m for rock basins opened within blocks such as the Ål Block (Figure 4-16). The greatest depths of erosion in NE Uppland rarely exceed 20 m in trenches that bound rock blocks and for basins at block edges or on blocks with high fracture densities (Figure 4-43). Variable depths of erosion below the former U2 surface indicate that average rates of erosion in basement were at least 2–3 times higher in trenches than on summits. Large triangular wedges of rock missing from formerly sharp block edges. Along the upstanding edge of the Gräsö block, a rock volume of ~0.01–0.03 km^3 is missing. Based on models of the smoothed surface of U2 using 0.5 and 1 km search windows, the estimated mean erosion depth of basement is 14 m across NE Uppland (Figure 4-46), 12 m (Figure 4-47) in the Forsmark area and is 8 m in the repository footprint area (Figure 4-48). A preliminary estimate of 10 m should be added to these estimates that represents basement rock lost from summits below U2. Basement erosion is slightly underestimated across search windows of more than 1 km where glacial erosion has lowered all summits below U2, as is likely in the shallow basin of the repository footprint area (Figure 4-13). If the onset of basement erosion dates from 1.1 Ma then average erosion depths per glacial cycle are ~2 m.

In northern Sweden, depths of glacial erosion have been estimated using a space-time transformation that compared three similar granite terrains with inselbergs, palaeo-surfaces and valleys that showed different morphological impacts of glacial erosion. Average depths of erosion in zones of fast ice

flow with large flyggbergs were 27 ± 11 m, of which 10–20 m likely represents the original depth of saprolite or fractured rock (Hall et al. 2013a). In southern Sweden, on scoured, unweathered bedrock, depths of Pleistocene erosion have been estimated as 0–30 m, with the upper figure confined to joint valleys and including the loss of formerly thick saprolite (Lidmar-Bergström 1997). These estimates also are broadly consistent with those for Uppland based on geomorphological evidence. Limited Pleistocene glacial erosion of granite and gneiss hills has been widely recognised in other glaciated crystalline terrains (Jahns 1943, Sugden et al. 1992, Olvmo et al. 1999, Ebert and Hättestrand 2010, Ebert et al. 2012a)

Broad constraints on depths of glacial erosion across eastern Fennoscandia are provided by thicknesses of Pleistocene sediments along the southern margin of the Fennoscandian Ice Sheet. The upland or mountain edge south of the North European plain provided a barrier to sediment dispersal so that the plain became a regional trap for sediment transported by the Fennoscandian Ice Sheet. An earlier source-sink sediment budget estimated the total thicknesses of sediment across Sweden, the Swedish part of the Baltic, the Kattegat and Denmark (Påsse 2004). After correction for pore space, the total sediment volume was compared to the total area of Sweden to provide an estimate of average Pleistocene erosion of the bedrock of 12 m. Glacial erosion during a full glacial cycle is estimated to be between 0.2 m and 4 m. Whilst the approach has much potential, the present estimates have errors which are difficult to constrain closely on current evidence. Likely overestimation of glacial erosion of basement in Sweden may derive from deep erosion of sedimentary rocks in the Skaggerak, Kattegat and Jutland adjacent to and within the sink areas. Likely sources of underestimation of glacial erosion include (i) the loss of Ordovician limestone debris in solution, (ii) sediment losses to the eastern North Sea in periods when the Fennoscandian Ice Sheet flowed westwards through the Kattegat and Skaggerak and (iii) the detritus derived from glacial erosion in Sweden that are now present in Pleistocene sediments in the Baltic states (Gorlach et al. 2015) and in N Germany and N Poland (Woźniak and Czubla 2015, Czubla et al. 2019). The latter volumes are considerable and comparable to those in Denmark, with average sediment thicknesses in northern Germany (Ehlers et al. 2011), Poland (Czerwonka and Krzyszkowski 1994) and on the East European Plain (Gorlach et al. 2015) reaching several tens of metres. Further research is needed to constrain sources and volumes of Swedish sediment in these sinks.

4.5 Summary

During the Pleistocene, erosion by the Fennoscandian Ice Sheet in Uppland removed Early Palaeozoic sedimentary cover rocks, re-exposed the low relief Cambrian basement unconformity and eroded underlying hard and fractured basement, modifying its surface. The resultant glacial landscapes of Uppland compromise a nested hierarchy of landforms at different scales set mainly within an altitudinal range of less than 20 m.

Mapping of landscapes and landforms of glacial erosion at the regional (1–10 km) and local (0.1–1 km) scales using DEMs reveals the pattern of modification of the exhumed unconformity and the development of new glacial landforms. Progressive erosion of basement blocks involved the lowering and roughening of block tops through the excavation of trench and shallow basins along fracture zones, the crenulation and indentation of block edges and the excavation of more than 20 m deep bounding trenches and basins. Mapping of local landforms shows a strong zonation of features within three glacial landform assemblages, roughened, streamlined and ripped terrain. An inventory of smaller glacial landforms is provided based on field observations at the macro (10–100 m), meso (1–10 m) and micro (< 1 m) scales. Landform assemblages and landforms across scales are linked to sets of glacial processes grouped as abrasion, plucking, ripping, thrusting and meltwater erosion. Glacial ripping is a newly recognised process set that involves the jacking, disruption and entrainment of rock blocks, with the formation of extensive spreads of large, angular rock blocks. Ripping is linked to development of groundwater overpressure beneath the retreating margin of the Fennoscandian Ice Sheet. The ripping process set is an important, perhaps locally dominant agent of glacial erosion in parts of the Forsmark area that operates to depths of at least several metres. Widespread glacial thrusting of fractured gneiss bedrock in NE Uppland is not supported by available geomorphological evidence. Glacial meltwater erosion is confined to rock trenches and likely operated in combination with other erosional processes under conditions of high subglacial groundwater pressure.

Field evidence from micro to meso forms on roche moutonnée surfaces allows assessment of the likely processes operating on these surfaces in relation to erosion depths and rates estimated from cosmogenic nuclide inventories. Abrasion microforms, including polished and striated surfaces, are ubiquitous but the frequency and lacunae on rock surfaces indicates that other processes are important for micro-erosion budgets. Plucking has generated rock steps and sockets on roche moutonnée flank and lee slopes. Freshly exposed rock surfaces along the coastline display numerous 0.5–5 m wide prismatic and box sockets that probably relate to block removal under high groundwater pressure. The micro to macro forms currently displayed on rock surfaces mainly reflect the operation of the erosional processes late in the last glacial cycle. The presence of crossing striae (Figure 4-26) and old till covers, however, may indicate areas of bedrock that may have escaped significant erosion by the last Fennoscandian Ice Sheet.

Removal of soft, bedded and jointed sedimentary cover involved the loss of at least several tens of metres of cover rock based on the depths of sub-Jotnian and -Ordovician basins in the archipelago E of Forsmark. Estimates of depths of glacial erosion in basement were derived using the dislocated sub-Cambrian unconformity as a reference surface. Dislocated rock blocks that remain buried offshore have sharp edges to fault scarps. On the re-exposed unconformity these edges have lost triangular rock wedges up to 30 m deep on fault scarp faces. The tops of rock blocks are estimated to have lost less than 10 m of rock over wide areas. This estimate is supported by geomorphological evidence in Uppland and from other basement terrains around early Palaeozoic outliers in S-C Sweden but subject to uncertainties that derive from the assumptions that underpin models of U2 and from the possibility that glacial erosion has been spatially uniform and so maintained an antecedent topography or formed similar landforms. The greatest volumes of eroded rock come from more than 20 m deep trenches and basins excavated along fracture zones. Subtraction of the present bedrock surfaces from a summit envelope surface model for U2 created using present summit elevations as pining points provides estimates of depths of glacial erosion. An average of 14 m of rock has been lost to glacial erosion of basement across NE Uppland, with increasing depths of erosion towards the south. In the Forsmark area and across the repository footprint, the equivalent depths are 12 m and 8 m, respectively. To these estimates should be added a maximum of 10 m of rock depth lost from summits. Estimated maximum thicknesses of average total basement erosion of 24 m at Forsmark are consistent with estimates for other lowland shield areas in Sweden and with Pleistocene sediment volumes on the North European plain.

Geomorphological evidence at the regional and local scales supports a general increase in relative relief and topographic roughness across the former unconformity surface under progressive glacial erosion. At the local scale, increases in relative relief and roughness may be linked to the former operation of plucking, thrusting and meltwater erosion beneath the last Fennoscandian Ice Sheet. Glacial abrasion rates, if uniform across the low relief of the ice sheet bed, may act to maintain existing bed forms during erosion. The glacial ripping process set may have acted to reduce, maintain or increase relative relief and bed roughness. At the macro- to micro-scales the glacial bedforms probably approach a steady state in which subglacial erosion processes act on hard, variably fractured bedrock. Glacial erosion rates derived from cosmogenic nuclides can provide tests for different models of glacial erosion of the basement surfaces. Uniform erosion rates on summits, sustained through multiple glaciations, point to maintenance of accordant summit altitudes whereas non-uniform erosion rates indicate eventual divergence. Different erosion rates between high and low points, if sustained through multiple glacial cycles, indicate trends towards increasing or decreasing relief. Different erosion rates between surfaces with closely and widely spaced fractures may constrain the importance of fracture control on erosion. Such tests are considered in Chapter 5.

5 Glacial erosion: estimates from cosmogenic nuclides

5.1 Introduction

Cosmogenic nuclides have been used frequently to study the dynamics and history of former ice sheets, including the Fennoscandian (Brook et al. 1996, Fabel et al. 2002, Stroeven et al. 2002a, b, Anjar et al. 2014, Blomdin et al. 2016, Jansen et al. 2019). Here, we measure cosmogenic nuclide concentrations to infer glacial erosion rates for bedrock in the Forsmark area, eastern Sweden, during the late Quaternary.

Our methodology builds on the production of cosmogenic nuclides in quartz in rock surfaces that are exposed to cosmic rays (Lal 1991, Gosse and Phillips 2001). Cosmic ray interactions with the Earth's atmosphere yield a cascade of secondary particles, primarily neutrons but also muons, that bombard the Earth's surface (Figure 5-1). When these secondary cosmic rays interact with rock minerals radioactive nuclides are produced, with half-lives relevant to the timescales of geologic processes. The cosmogenic nuclide that is most widely-applied in the study of Earth-surface processes is ^{10}Be, and it has a half-life of 1.39 Ma (Chmeleff et al. 2010, Korschinek et al. 2010). Another commonly used isotope produced in quartz is ^{26}Al, with a half-life of 705 ka (Nishiizumi 2004). These isotopes are often measured together because their different half-lives allow a comparison of processes over different timescales and because they can both be extracted using the same laboratory procedures. Other potentially useful isotopes include ^{14}C (half-life of 5.73 ka) and ^{21}Ne (stable). The production rates of these isotopes in quartz (especially ^{10}Be) are well-constrained. Production rates vary spatially and temporally because of differences in atmospheric pressure and the strength of the Earth's magnetic field (production rates increase with both latitude and altitude; Lal 1991, Gosse and Phillips 2001). Cosmic ray particles penetrating a rock surface are rapidly attenuated, so the production of cosmogenic nuclides is almost entirely constrained to the uppermost few metres (Figure 5-1). Hence, given a known local rate of cosmogenic nuclide production in rock minerals (e.g., ^{10}Be in quartz: (Nishiizumi et al. 1989, Stroeven et al. 2015), a measured nuclide concentration indicates the total duration of exposure to cosmic rays.

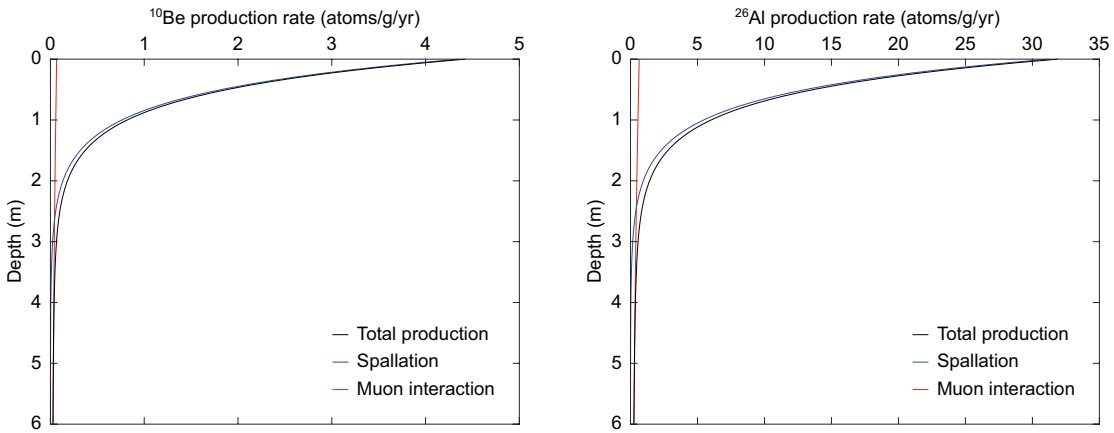

Figure 5-1. *Production rate in bedrock at Wave Rock (Figure 1-1B), sample FORS-16-13 10 (Figure 5-96), for ^{10}Be and ^{26}Al at an elevation of 12 m a.s.l. and assuming a density of 2.65 g cm^{-3}. Because the production rate from spallation (blue curve) varies over time, although minimally at this latitude, the long-term average production rate is plotted. In the uppermost 2.5 m of bedrock almost all cosmogenic nuclide production is through spallation processes. Below that depth, production rates are very low and dominated by muon interaction. The production rate depth profiles have been calculated based on the production rate computations in the expage calculator (http://expage.github.io/calculator).*

In formerly glaciated regions, such as the Forsmark area, a cosmogenic nuclide concentration in quartz at the Earth's surface may be interpreted as a deglaciation age provided the last ice sheet removed a thick enough (typically more than 3 m) layer of rock so that the new surface started with a cosmogenic nuclide concentration near zero and there has been minimal to no erosion of the new surface since it was exposed to cosmic radiation.. Where apparent exposure ages exceed deglaciation age, the incomplete removal of bedrock with previously accumulated cosmogenic nuclides results in the inheritance of nuclides from one, or more, preceding ice-free exposure periods. The production of nuclides at shallow depths below the surface (Figure 5-1) commonly introduces geologic uncertainty in deriving surface exposure ages (Putkonen and Swanson 2003, Balco 2011, Heyman et al. 2011). This uncertainty may relate to post-exposure erosion or temporary burial by sediments, water or snow, each of which will decrease nuclide abundances, thereby causing underestimations in ages. While we must always account for geologic-, nuclide production rate-, laboratory-, and measurement uncertainties (Gosse and Phillips 2001), the concentration of cosmogenic nuclides in surface rock minerals offers a powerful tool for inferring timing and rates of Earth surface processes. This is because such concentrations are fundamentally the integrated result of depth-dependent production rates and the surface erosion rate. As an alternative to calculating duration of exposure, a cosmogenic nuclide concentration can therefore be used to infer the rate of erosion (Lal 1991).

5.2 Methods

5.2.1 Sampling and sample preparations

Our sampling strategy was primarily designed to locate and target sites of lowest glacial erosion. This is because they would most likely contain inheritance (concentrations higher than those expected for postglacial exposure duration) in the inventories of two cosmogenic nuclides, ^{10}Be and ^{26}Al. The presence of inheritance would allow us to calculate glacial erosion depths and rates over recent glaciations, based on reconstructed durations of ice cover. Where the Fennoscandian Ice Sheet eroded rock sufficiently thick to essentially remove the entire cosmogenic nuclide inventory, typically a few metres, no further insight on glacial erosion rate can be gleaned using this technique. An obvious shortcoming in our primary sampling strategy is that we are perhaps biasing our results towards lower erosion rates because lower parts of the landscape may have undergone more glacial erosion. To test for this suspected bias, we have also collected bedrock samples on two coastal embayments (i.e. in long wave-length bedrock concavities) where water currents and waves have removed sediments prior to bedrock emergence above sea level and where organic material has not yet accumulated. We then compared nuclide inventories from these expected low-inventory sites with other sites to gain a more complete picture of glacial erosion across this landscape.

To target suspected locations of least erosion and highest nuclide inheritance, we primarily sampled exposed bedrock summits in the Forsmark region and along a low ridge extending ~50 km south of Forsmark (Figure 5-2). In addition to satisfying our aim of locating samples with nuclide inheritance, sampling summits also allowed us to minimize errors caused by potential past surface burial by sediments. Surface burial would decrease nuclide inventories and thereby provide for erroneously high erosion rate inferences. Twenty bedrock summit samples have been measured within 5 km of the planned repository (Table A4-1), covering an elevation range of 0–24 m a.s.l., including two samples located directly above the repository footprint (Figure 5-2b; Table A4-2). Thirteen samples (25–67 m a.s.l.) scatter along the gently-elevated ridge protruding southwards of the Forsmark area of investigation (Figure 5-2a; Table A4-2). Two samples were taken from concave locations adjacent to the present shoreline (FORS-17-12 and 17-21). We additionally sampled three large boulders from a nearby headland (FORS-17-17, 17-18, and 17-20), to potentially test their recent emergence from water and to contrast them to cosmogenic nuclide data from two bedrock samples there (FORS-17-14 and 17-19, Figure 5-2b; Table A4-2). Finally, we collected four samples from a steeply-dipping quartz vein exposed in a road cut located c. 1 km south of the power plant (immediately below site FORS-16-04 in Figure 5-2b). We did this to further constrain erosion histories over multiple glaciations from ^{10}Be and ^{26}Al depth profiles. Two samples yielded results, from depths of 8 cm and 250 cm below the top of the road cut (NRD-001 and NRD-003, Table A4-2). This dataset forms the basis for inferences of erosion rates and depths attributable to the Quaternary glaciations in, and around, Forsmark.

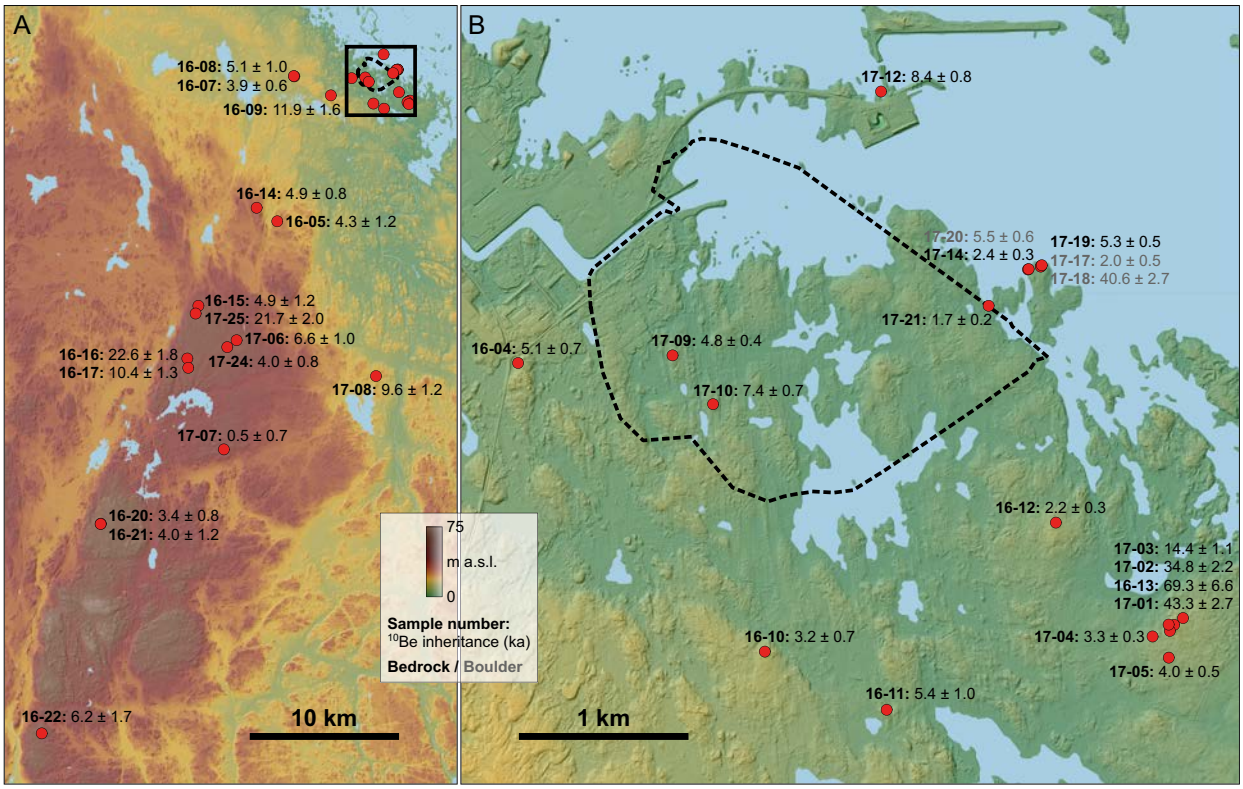

Figure 5-2. *Topographic maps over the investigation area around Forsmark including the distribution of cosmogenic nuclide samples with sample names and calculated ^{10}Be inheritance (defined as the difference between simple exposure age and the expected exposure age based upon the reconstructed deglaciation age (Stroeven et al. 2016) and a reconstructed history of shoreline displacement (Figure 5-3). A) Distribution of cosmogenic nuclide sample locations across the wider study area, from the planned repository location (black box; right panel) and along an NNE–SSW directed ridge. B) The repository footprint area (dashed line) and cosmogenic nuclide sample locations within and immediately beyond this area. Two depth profile samples were taken from a quartz vein exposed in a road cut adjacent to sample FORS-16-04 (NRD-001 and NRD-003, not shown). The topographic maps are derived from the 2 m resolution LiDAR elevation model.*

Samples were collected during the summers of 2016 and 2017 with a rock saw, hammer, and chisel. We measured shielding (Dunne et al. 1999) for three sample locations because some sections of the topographic horizon were more than 10° above a horizontal plane. These measurements of topographic shielding are used to correct local nuclide production rates.

To calculate erosion based on inheritance, it is imperative that we know the duration of exposure following deglaciation. The timing of deglaciation is well-constrained through the Fennoscandian Ice Sheet retreat reconstruction by Stroeven et al. (2016), with the timing of ice retreat in the Forsmark area being especially well-constrained through local clay-varve data (Strömberg 1989). However, there is an additional complication in that the study area around Forsmark is located below the highest marine limit (Hedenström and Risberg 2003). All samples in this study have initially, after the last deglaciation, been submerged due to glacial isostatic adjustment, and calculated exposure ages need to be corrected for the duration of submergence We use a single shoreline displacement curve for all samples, based on a recent SKB reconstruction of the local shoreline displacement at Forsmark (Figure 5-3). This shoreline displacement curve generally agrees with an independent shoreline displacement reconstruction based on radiocarbon dating of lake isolation basins in a region 60–100 km west and northwest of Forsmark (Berglund 2005).

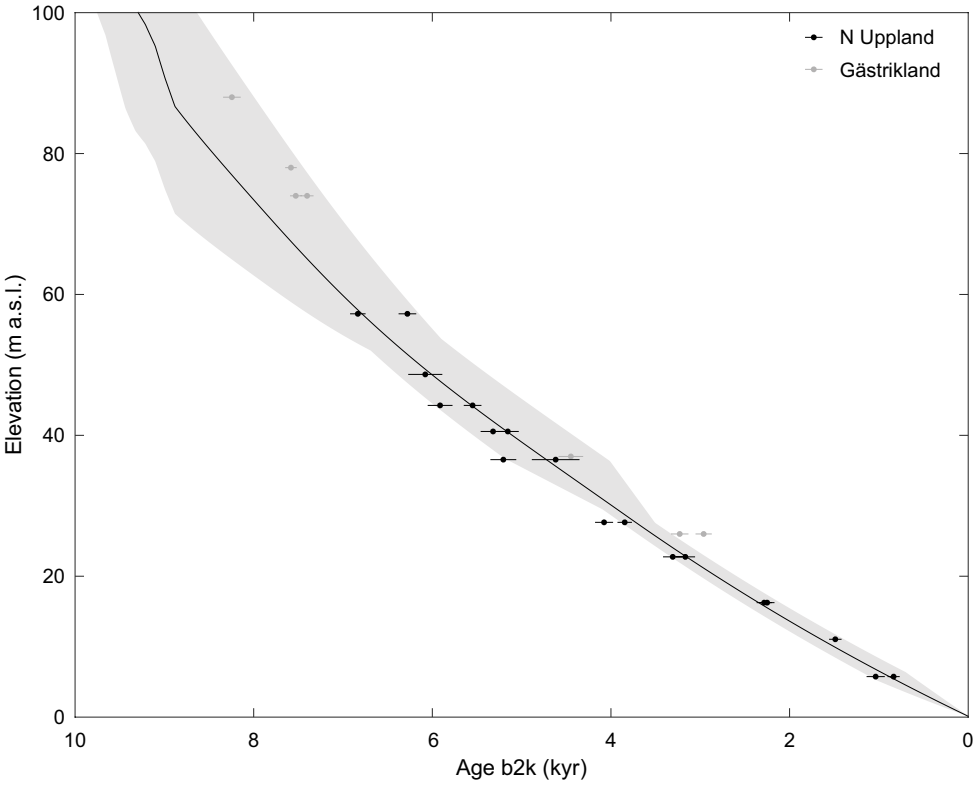

Figure 5-3. *Reconstructed shoreline displacement for the Forsmark region made by SKB based on radiocarbon dating of isolation events (Hedenström and Risberg 2003) and the shoreline displacement from Påsse and Daniels (2015). All ages are related to year 2000 (b2k) CE and all elevations are given in height reference system RH2000. The grey area shows the estimated uncertainty for the shoreline displacement. The black and grey points show calibrated radiocarbon ages for isolation events in northern Uppland (Robertsson and Persson 1989, Risberg 1999, Bergström 2001, Hedenström and Risberg 2003) and in Gästrikland (Berglund 2005). The radiocarbon ages have been re-calibrated using the IntCal13 calibration curve and OxCal 4.3. The Gästrikland samples are located some 60–100 km inland from Forsmark.*

For our study on the long-term imprint of glacial erosion, it is crucial that the adopted shoreline displacement curve is reliable. Hence, we amended our strategy in an attempt to test the validity of the reconstructed shoreline displacement. Firstly, by sampling a suite of locations along the gently elevated ridge extending ~50 km south of Forsmark (the elevated margin of a rock block that dips gently to the ESE: see Figure 5-2A), we can test for the progressive emergence of this landscape above sea level up to an elevation of 67 m a.s.l. We do this assuming that there has been no recent uplift of this block margin, for example, through post-glacial faulting, and that the shoreline displacement has been principally uniform over the entire study region. This assumption appears reasonable based on recent studies (Lagerbäck et al. 2005). Secondly, we sampled three glacial erratic boulders located just above the present shoreline with the expectation that, if these were sourced from bedrock at depths large enough to have escaped prior exposure, their nuclide concentrations would accurately reflect exposure acquired while uplifted through the water column and subaerial exposure following emergence above sea level. Thirdly, we measured ^{14}C produced *in situ* in quartz from 5 samples along the elevation gradient. Because of its short half-life relative to the duration of previous ice cover, there should be no inheritance from previous exposure periods. Each of these three strategies offers an independent test of the shoreline displacement curve.

The nuclide ^{10}Be was selected on the basis of it being the most widely applied, and best understood, nuclide in the study of Earth-surface processes (Dunai 2010). Additionally, ^{26}Al was selected because it has a shorter half-life than ^{10}Be, a known production rate, and can be measured with equal precision. Hence, apart from providing an independent constraint upon erosion rates inferred from ^{10}Be concentrations, the $^{26}Al/^{10}Be$ ratio may provide additional information on how long rock

surfaces may have been buried by glacial ice or sediments after first exposure. In using ^{26}Al we also take advantage of significant recent advances in the accelerator mass spectrometry (AMS) measurement of this nuclide resulting from the use of a gas-filled magnet at PRIME lab (Granger et al. 2014), which allows the efficient separation of ^{26}Al from Mg, resulting in highly accurate ^{26}Al measurements.

Sample preparation and measurement of ^{10}Be and ^{26}Al concentrations in our samples were completed at PRIME Lab, Purdue University, following standard procedures (Kohl and Nishiizumi 1992). Sample preparation includes quartz separation followed by ^{9}Be and ^{27}Al carrier addition, extraction of ^{10}Be and ^{26}Al, and AMS measurements of ^{10}Be/^{9}Be and ^{26}Al/ ^{27}Al ratios. Total Al concentrations were determined by ICP measurements. Isotope measurements were standardized against the 07KNSTD standard for ^{10}Be (Nishiizumi et al. 2007), and the KNSTD standard for ^{26}Al (Nishiizumi 2004). For five samples, repeat measurements of separate aliquots were completed to test measurement reproducibility. For these samples, we use uncertainty-weighted mean concentrations and uncertainties (unbiased estimator for reliability weights) with a minimum limit of 3 % of the concentration for the uncertainty based on the full set of measurements (3 % limit applied for two repeat ^{26}Al measurements).

It was generally difficult to extract clean quartz from the samples because the quartz was frequently subordinate to feldspar and was fine-grained, which meant that much of it crushed finer than the requisite 250–500 µm grain size. It was also difficult to purify through standard HF leaching. We suspect that these issues reflect the long history of the basement rocks at Forsmark, characterized by multiple episodes of metamorphism (Chapter 1). The resulting recrystallized fine-grained quartz may contain fluid inclusions and/or is intercalated with other minerals. This is a particular problem in quartz veins because they crystallized from residual fluids and indeed quartz vein samples presented the most problems. Because of the resulting difficulties in cleaning the quartz, six samples ultimately yielded insufficient quartz for Accelerator Mass Spectrometry (AMS) measurements. Of those measured, many samples ended up being small (down to a few grams; Table A4-1) which increased the AMS errors on the measurement of ^{10}Be and ^{26}Al (Table A4-2).

The impact of the long metamorphic history on the Forsmark bedrock appears to have been significant to the measurement of ^{14}C. Five samples measured for ^{14}C at ETH, Zurich did not yield the expected pattern of older apparent exposure ages with increasing elevation along the sample transect. Three samples yielded ages that were far younger than expected from regional deglaciation and the existing sea level displacement curve and two were saturated, which means that no age inferences can be made from those measurements. These results reflect that this technique remains in a pioneering phase and/or they reflect the complex bedrock chemistry. For example, ^{14}C may have been produced in the two saturated samples through U decay in adjacent rock minerals. We exclude these measurements from our results and discussion because we consider these data to be unreliable.

5.2.2 Exposure age calculations

We calculate simple apparent exposure ages from the measured ^{10}Be and ^{26}Al concentrations using the expage calculator (http://expage.github.io/calculator.html v. 201902). This calculator is based on the original CRONUS calculator of Balco et al. (2008) but adopts the nuclide-specific LSD production rate computations (Lifton et al. 2014). Production rate from spallation varies over time and is calibrated against a global set of ^{10}Be and ^{26}Al production rate calibration sites. Production rate from muons is constant over time (Marrero et al. 2016). In our study this includes a minor modification to reduce a potential near-surface artefact (Balco 2017), and is calibrated against the Beacon Heights ^{10}Be and ^{26}Al sandstone bedrock core data (Borchers et al. 2016, Marrero et al. 2016, Phillips et al. 2016, Balco 2017).

We followed the approach of Stroeven et al. (2015) in also taking account for shielding during glacial isostatic uplift through the water column in the expage calculator (expage_sealevel.m: Appendix 5). We calculate the mismatch in time (yr) between a simple exposure age and an expected exposure age given a reconstructed deglaciation age and the shoreline displacement curve. The deglaciation age is based on the Stroeven et al. (2016) deglaciation reconstruction and ranges from 10 800 to 10 950 years before sampling.

The attenuation length of spallogenic production of ^{10}Be and ^{26}Al is calculated from atmospheric pressure and a time-dependent geomagnetic rigidity cut-off, similar to the CRONUScalc calculator (Marrero et al. 2016). For the Forsmark region, this results in an average attenuation length of 152 g cm^{-2}. We use a rock density of 2.65 g cm^{-3} and a water density of 1.0 g cm^{-3} in our calculations. We assume that there has been no post-emergence shielding by vegetation, snow, or sediments.

5.2.3 Glacial erosion simulations

To simulate site-specific glacial erosion based on ^{10}Be and ^{26}Al concentrations, we use a modified version of the expage glacial erosion calculator by also including shielding by sea water after deglaciation (glacialE_sealevel.m: Appendix 5). In this calculator, a glaciation history is defined by a cut-off value for the benthic δ^{18}O record from the LR04 stack of Lisiecki and Raymo (2005). We assume that the growth and decay of the Fennoscandian Ice Sheet has followed this proxy for global ice volume. Because the duration of cosmic ray exposure since the last glaciation is of major importance for the erosion rate estimate, local last deglaciation is set independently by the Stroeven et al. (2016) reconstruction. During periods of ice coverage, the ^{10}Be and ^{26}Al production rates are assumed to be zero. During ice-free periods the production rates are computed from sample shielding depth, which is a function of glacial erosion, non-glacial subaerial erosion, submergence, and the densities of rock and water.

Glacial erosion simulations are run in two modes of operation: (1) constant erosion rate and (2) constant erosion depth. In the first case, the glacial erosion depth of each ice cover period scales with the duration of ice coverage. In the second case, the glacial erosion depth of each ice cover period is constant, independent of the duration of ice coverage, and instead scales with the number of ice coverage periods. Whereas the former may mimic the effect of wet-bed glaciation, the latter may mimic glaciations dominated by dry-bed conditions, but experiencing erosion during wet-bed deglaciation (Kleman 1992, Harbor et al. 2006, Cowton et al. 2012, Sugden et al. 2019). We acknowledge that this is a simplification of natural conditions under ice sheets. For example, conditions conducive for either mode of operation may have co-occurred or have switched-on or switched-off within any single glaciation (Figure 4-54).

Subaerial erosion is assumed to operate at a constant rate for all ice-free periods. Again, this is a necessary simplification of a complex reality, but one which appears reasonable for an area which has most likely remained low relief over the course of Pleistocene glaciation. Inundation by sea water occurs following each ice cover period because of glacial isostatic depression. While submerged, the samples experience neither glacial nor subaerial erosion. To calculate emergence through the water column, we use the shoreline displacement curve for Forsmark for the last deglaciation (Figure 5-3) and a filtering approach-derived displacement curve following previous ice cover periods. For the latter, the ice cover history of the preceding 30 ka determines the sea level displacement curve. This filtering approach (subfunction uplift_preLGM) is calibrated against the shoreline displacement curve for Forsmark for the last deglaciation and modelled sea level displacement in Forsmark following the MIS 4 glaciation (SKB 2010).

Erosion rates have been calculated in two ways. First, in a simple calculation for single nuclides (^{10}Be or ^{26}Al), glacial erosion is computed for a specific ice cover (δ^{18}O cut-off value) and subaerial erosion rate couple, based on an interpolation of 50 simulated nuclide concentrations derived from a suite of glacial erosion rates or suite of glacial erosion depths (cf. Fu et al. 2018). We use this method to investigate the sensitivity of glacial erosion to perturbations of specific model parameters.

Second, following a more sophisticated approach, predefined minimum and maximum values for glacial erosion, subaerial erosion, and δ^{18}O cut-off values are all imposed to allow for a search of the parameter space yielding the target nuclide concentration within measurement uncertainties plus propagated production rate uncertainties. This is done iteratively to approach the minimum and maximum parameter values that yield the target nuclide concentrations. The iterative search for the parameter space yielding the measured cosmogenic nuclide concentrations is done with repeat computations of cosmogenic nuclide production for a range of scenarios, with the minimum and maximum values for each of the three parameters searched with decreasing step size down to a maximum of 0.01 mm/ka or 0.01 cm/ice cover period for glacial erosion, 0.01 mm/ka for subaerial erosion, and 0.01 ‰ for the δ^{18}O cut-off value. Because the relation between the input

parameters values and the resulting cosmogenic nuclide concentration is potentially non-linear and discontinuous, we use a guided Monte Carlo approach to search for the full range of parameter limits and potential erosion depths over time. This is done first focused around the iteratively-determined minimum and maximum parameter values searching actively for lower minimum values and higher maximum values for each of the three parameters using five Monte Carlo runs with 150 scenarios each for each of the six parameter limits. Finally, Monte Carlo runs with 150 random scenarios using parameters drawn from ranges defined by the determined minimum and maximum parameter limits each decreased and increased, respectively, by 10 %, are run iteratively to generate at least 1 000 cosmogenic nuclide concentration solutions or for a maximum of 100 runs. For full details of the erosion simulations, we refer to the supplementary function glacialE_sealevel.m (Appendix 5). With this method, we can find the range of glacial erosion rates that satisfies the measurements for assumed subaerial erosion rates and reasonable ice cover histories (see below). This method also enables the calculation of erosion histories for $^{26}Al/^{10}Be$ pairs. Specifically, only certain scenarios will yield a match with both measured nuclide concentrations, and we use this method to simulate the erosion history of the Forsmark surfaces.

To calculate interquartile ranges of the simulated erosion ranges, we use the function range_percentile.m (Appendix 5). This function calculates summed percentiles from a number of minimum-maximum ranges assuming uniform probability distribution between the individual minimum and maximum values and equal weight of each individual minimum-maximum range.

For the two depth profile samples we use the same sophisticated simulation approach as for the surface samples that includes the same scenarios as for the surface bedrock samples to simulate glacial erosion. This is done by specifying the parameter “burialdepth” to 8 cm and 250 cm in glacialE_sealevel.m (Appendix 5). To investigate the nuclide concentration depth profile, we also use the simple exposure depth profile calculator (depthcalc.m: Appendix 5) of the expage calculator, which calculates the best-fit simple exposure age assuming only one period of exposure with no erosion.

5.2.4 Input parameter constraints

To constrain the potential ice cover history of the Forsmark region, we use a minimum $\delta^{18}O$ cut-off value of 4.4 ‰ and a maximum value of 4.6 ‰ (Figure 5-4). For the last glacial cycle, this yields glaciation from MIS 4 to MIS 2 with an ice free period in MIS 3, as indicated by ice sheet modelling and proxy data (Svendsen et al. 2004, SKB 2010, Wohlfarth 2010, Femke Helmens 2019). These two cut-off values allow for a range of possible glaciation histories. Through the last glacial cycle (from ~115 ka) and the Quaternary ((from ~2.6 Ma) the total duration of ice cover become 23–49 ka and 162–340 ka, respectively. This corresponds well with previous interpretations of average Quaternary ice sheet extent, and indicates that the Forsmark region has remained ice free for most of the Quaternary (Porter 1989, Kleman et al. 1997, Kleman et al. 2008, SKB 2010).

Subaerial erosion is assumed to operate at a constant rate for all ice-free periods. For the subaerial erosion rate, we set the minimum and maximum values to 0 and 5 mm/ka, respectively. The upper limit of 5 mm/ka is somewhat higher than estimated Holocene erosion rates (André 1996, 2002) to account for higher average subaerial erosion rates if weathering accelerates under longer ice free periods.

We run the simulations starting from various points back in time with the cosmogenic nuclide samples starting at zero nuclide concentration. For a case where the sample starts at depths with a minimal cosmogenic nuclide production rate, this zero nuclide assumption is perfectly valid. For a case where the sample starts a shallow depth with a notable cosmogenic nuclide production rate (Figure 5-1), the zero nuclide assumption implies that the bedrock must have been shielded from cosmic rays prior to the point in time when the simulation starts. In such a situation, we can mentally equate the start of our simulation to follow a sudden and instantaneous erosion of the sedimentary cover rocks that completely shielded the underlying basement rock surface from cosmic rays (Section 4.3.4). Because it is difficult to determine the timing of cover rock removal with certainty, we ran the simulations starting from 130 ka, 0.5 Ma, 1.0 Ma, 2.588 Ma, and 10 Ma. These starting points cover a wide range of scenarios, including likely end-members where cover rock removal occurred as recently as the penultimate glaciation (130 ka) or before 10 Ma ago, through non-glacial processes.

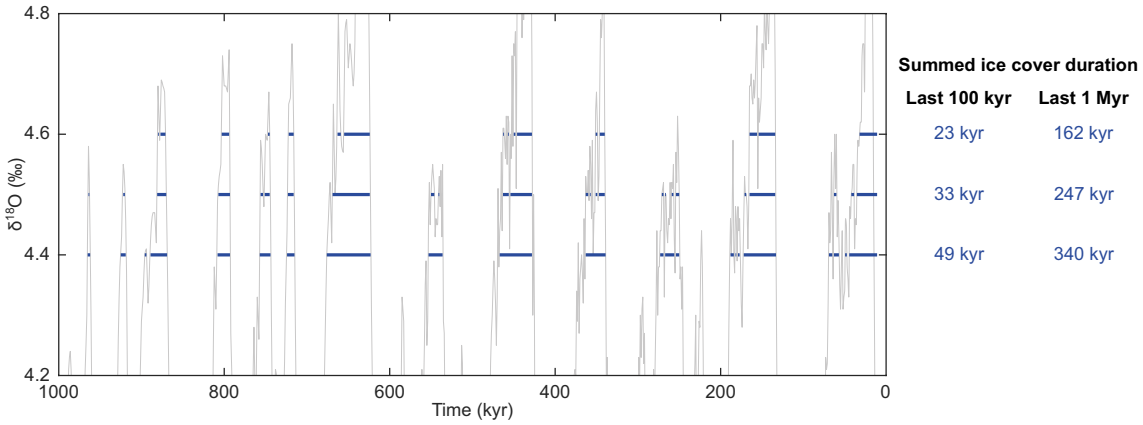

Figure 5-4. *A truncated marine oxygen isotope record (Lisiecki and Raymo 2005) defines the timing and duration of the Forsmark area ice cover histories for cut-off values of 4.4 ‰, 4.5 ‰, and 4.6 ‰. The integrated duration of ice coverage is tabulated to the right for the last 100 ka and 1 Ma given these three ice cover histories.*

It is crucially important to explore the full range of possible depths and rates of Quaternary glacial erosion for the Forsmark area from ^{10}Be and ^{26}Al data. This is because of uncertainties in our data and incomplete understanding of glacial erosion, we considered two end-member scenarios starting at 10 Ma which assume no glacial erosion (1) between 10 Ma and 130 ka and (2) after 55 ka. We do not consider these end-members to be particularly likely, but they are chosen simply to explore the boundaries of our model space. In the first scenario, all glaciations prior to the last glacial cycle are non-erosive and the only glacial erosion is that which occurs in the last glacial cycle. This scenario requires intense glacial erosion during the last glacial cycle up to the late Weichselian to account for measured concentrations. In the second scenario there is no glacial erosion in the ice cover period(s) after MIS 4. Because the samples will be exposed at or close to the surface for the full subaerial period after MIS 4, glacial erosion in MIS 4 and earlier ice cover periods will be higher than in the constant glacial erosion scenarios. Similar to the other simulations, we ran these extreme scenarios with both constant glacial erosion rate and constant glacial erosion depth. Table 5-1 specifies simulation specific parameters for all 14 simulation scenarios.

Table 5-1. Glacial erosion simulations. All simulations have the same predetermined parameter boundaries for the δ^{18}O cut-off value (4.4–4.6 ‰) and the subaerial erosion rate (0–5 mm/ka).

Simulation	Starting point	Glacial erosion
1	130 ka	Constant glacial erosion rate
2	130 ka	Constant glacial erosion depth
3	0.5 Ma	Constant glacial erosion rate
4	0.5 Ma	Constant glacial erosion depth
5	1.0 Ma	Constant glacial erosion rate
6	1.0 Ma	Constant glacial erosion depth
7	2.588 Ma	Constant glacial erosion rate
8	2.588 Ma	Constant glacial erosion depth
9	10 Ma	Constant glacial erosion rate
10	10 Ma	Constant glacial erosion depth
11	10 Ma	10 Ma-130 ka: no glacial erosion; 130–0 ka: constant glacial erosion rate
12	10 Ma	10 Ma-130 ka: no glacial erosion; 130–0 ka: constant glacial erosion depth
13	10 Ma	10 Ma-55 ka: constant glacial erosion rate; 55–0 ka: no glacial erosion
14	10 Ma	10 Ma-55 ka: constant glacial erosion depth; 55–0 ka: no glacial erosion

5.2.5 Sensitivity tests of the glacial erosion simulations

To test the sensitivity of the glacial erosion simulations to specific scenario parameters, we ran a set of simulations for four particular samples (FORS-16-13, 16-21, 17-08, and 17-21) in which we varied one parameter at a time. The four samples were chosen to cover a range of sample elevations (time of emergence from water) and cosmogenic nuclide inheritance. As reference scenario, we use a $\delta^{18}O$ cut-off value of 4.5 ‰, a subaerial erosion rate of 2.5 mm/ka, and we start the simulation from 1 Ma. We varied the $\delta^{18}O$ cut-off value, the subaerial erosion rate, the simulation starting point, the shoreline displacement curve, and also the sediment cover of previous ice-free periods (Figure 5-4), and we ran simulations in the constant erosion rate and the constant erosion depth modes. These tests help us to evaluate the reliability of derived glacial erosion rates.

5.3 Results

5.3.1 Cosmogenic nuclide concentrations and repeat measurements

Sample data, ^{10}Be and ^{26}Al concentrations, simple apparent exposure ages, and simulated erosion rates and depths are displayed in Supplementary Tables A4-1 to A4-4. Measured sample concentrations of ^{10}Be (^{26}Al) are 9–303 $\times 10^3$ (69–2 060 $\times 10^3$) atoms/g. The number of ^{10}Be (^{26}Al) blank atoms are 0–33 % (0–22 %) of the total number of atoms in the samples, with all samples but one yielding < 12 % (< 14 %) blank atoms of the total number of atoms in the samples. For the five samples with repeat nuclide measurements, four samples yield concentrations that agree within two standard deviations. The fifth sample, FORS-17-11 (Wave Rock; Figure 5-2b), returned concentrations for both ^{10}Be (46.5 ± 4.5 and 29.2 ± 1.9 × 10^3 atoms/g) and ^{26}Al (115 ± 15 and 219 ± 14 × 10^3 atoms/g) that were incompatible with each other. We cannot explain this mismatch and we therefore disregard this sample in all further calculations and discussions. For FORS-17-01 (Wave Rock; Figure 5-2b), the ^{26}Al concentration uncertainty exceeds the concentration, and we therefore also disregard this ^{26}Al measurement in all further calculations and discussions. All disregarded ^{10}Be and ^{26}Al sample measurements are, however, within the full range of measured concentrations and would therefore yield single nuclide output within the full range of measurements for exposure age and erosion simulations.

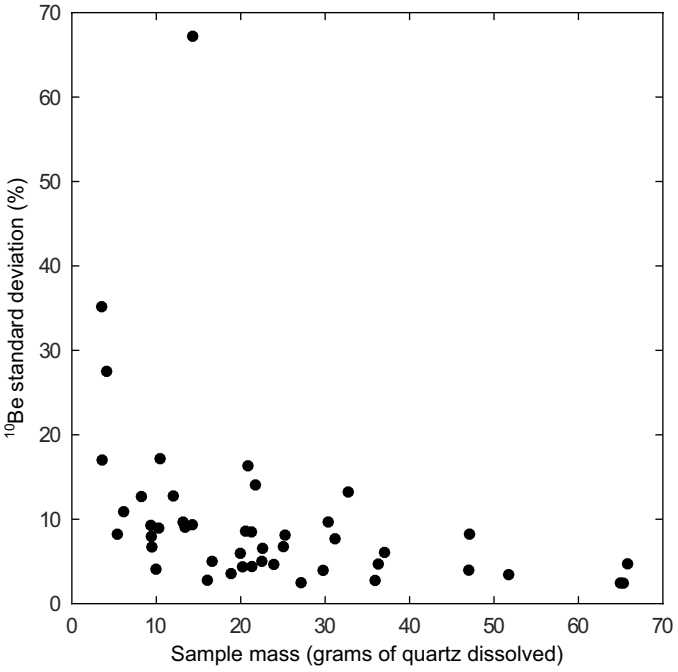

Figure 5-5. *^{10}Be standard deviation, expressed in percent of measured ^{10}Be abundances, versus the mass of quartz dissolved from each sample. Our measurements show that ^{10}Be, ^{26}Al, and $^{26}Al/^{10}Be$ ratios all show increasing standard deviations (2σ) with decreasing sample size. Quartz was frequently hard to isolate and clean for samples collected in this study and therefore the resulting amount of clean quartz (sample size) became smaller than anticipated.*

AMS errors on the measurement of ^{10}Be and ^{26}Al increase for small samples (<20 g; Figure 5-5). However, while errors are larger for small samples, glacial erosion rate estimates from our ^{10}Be and ^{26}Al data remain robust.

5.3.2 Exposure ages and inheritance

Even though we explicitly sought locations in the landscape that might have evaded severe ice sheet erosion, such that we could use the inheritance signal to tease out bedrock erosion histories, it is nonetheless surprising that we were successful in 40 out of 41 locations. Figure 5-6 displays simple ^{10}Be and ^{26}Al exposure ages against sample elevation. Simple exposure ages for ^{10}Be (^{26}Al) range from 2.1±0.2 ka (2.2±0.6 ka) to 71.2±5.4 ka (68.4±5.4 ka) (Table A4-2). Considering the reduced exposure to cosmic rays due to glacial isostatic rebound and shielding by water following deglaciation (solid curve, Figure 5-6), all samples yield exposure ages older than expected from only postglacial exposure to cosmic rays. Converted into full exposure at the surface, the ^{10}Be (^{26}Al) data displays 0.5–69.3 ka (1.6–66.0 ka) of prior exposure (inheritance) with a median at 5.1 ka (5.1 ka) and an interquartile range of 4.0–10.0 ka (3.4–9.2 ka) (Figure 5-2a; Table A4-2). There is an overlap within uncertainty between the measured and the expected post-glacial ^{10}Be concentration for one sample (FORS-17-07). The three boulder samples, all located close to present-day sea level and sampled to provide an independent test of the shoreline displacement curve, have similar amounts of inheritance as the bedrock samples, with ^{10}Be (^{26}Al) yielding 2.0, 5.5, and 40.6 ka (1.6, 5.5, and 37.4 ka) of prior exposure.

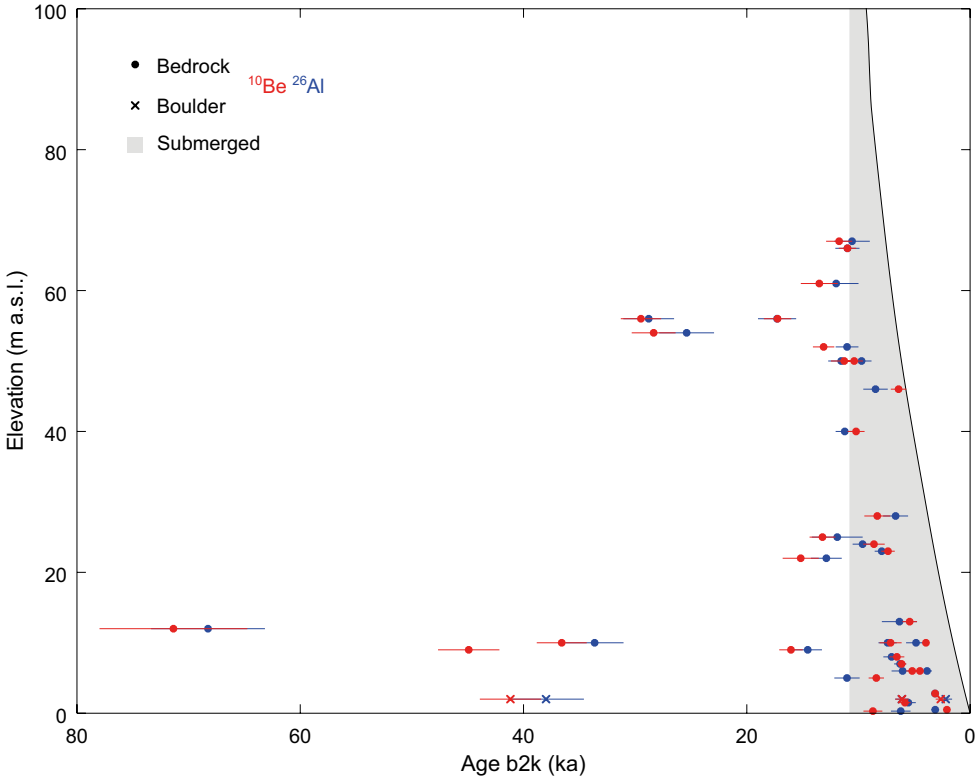

Figure 5-6. *Simple ^{10}Be and ^{26}Al exposure ages, assuming one period of full exposure to cosmic rays, and sample elevation. The black line shows the reconstructed shoreline displacement (Figure 5-3) and the grey area shows the post-glacial period of submergence. Surfaces that experienced glacial erosion during the last ice cover period deep enough to remove the inventory of cosmogenic nuclides would overlap within uncertainty with the shoreline displacement curve. Because all samples have experienced prior exposure, the simple exposure ages are higher than expected for fully reset samples.*

5.3.3 Glacial erosion simulation sensitivity

Within the specified parameter boundaries, perturbations in the subaerial erosion rate (±2.5 mm/ka) and the shoreline displacement curve (upper and lower boundaries in Figure 5-3) yield minor differences in glacial erosion depths (Figure 5-7). Similarly, 50 cm of sediment cover during the MIS 3 ice-free period(s) or during the full pre-LGM ice-free periods only yield slight differences compared to the scenario with no sediment cover. Perturbations of the ice cover history, as determined by ±0.1 ‰ in the $\delta^{18}O$ cut-off value, and the simulation starting point (130 ka, 10 Ma) both yield larger differences in simulated glacial erosion depths. Shorter and fewer durations of ice cover, and longer simulation durations (earlier starting points), yield higher glacial erosion depths. The choice of the mode of operation of glacial erosion also has an impact on simulated erosion depths, with constant glacial erosion depths generally yielding more vertical lowering of the rock surface over the simulated periods than constant glacial erosion rates.

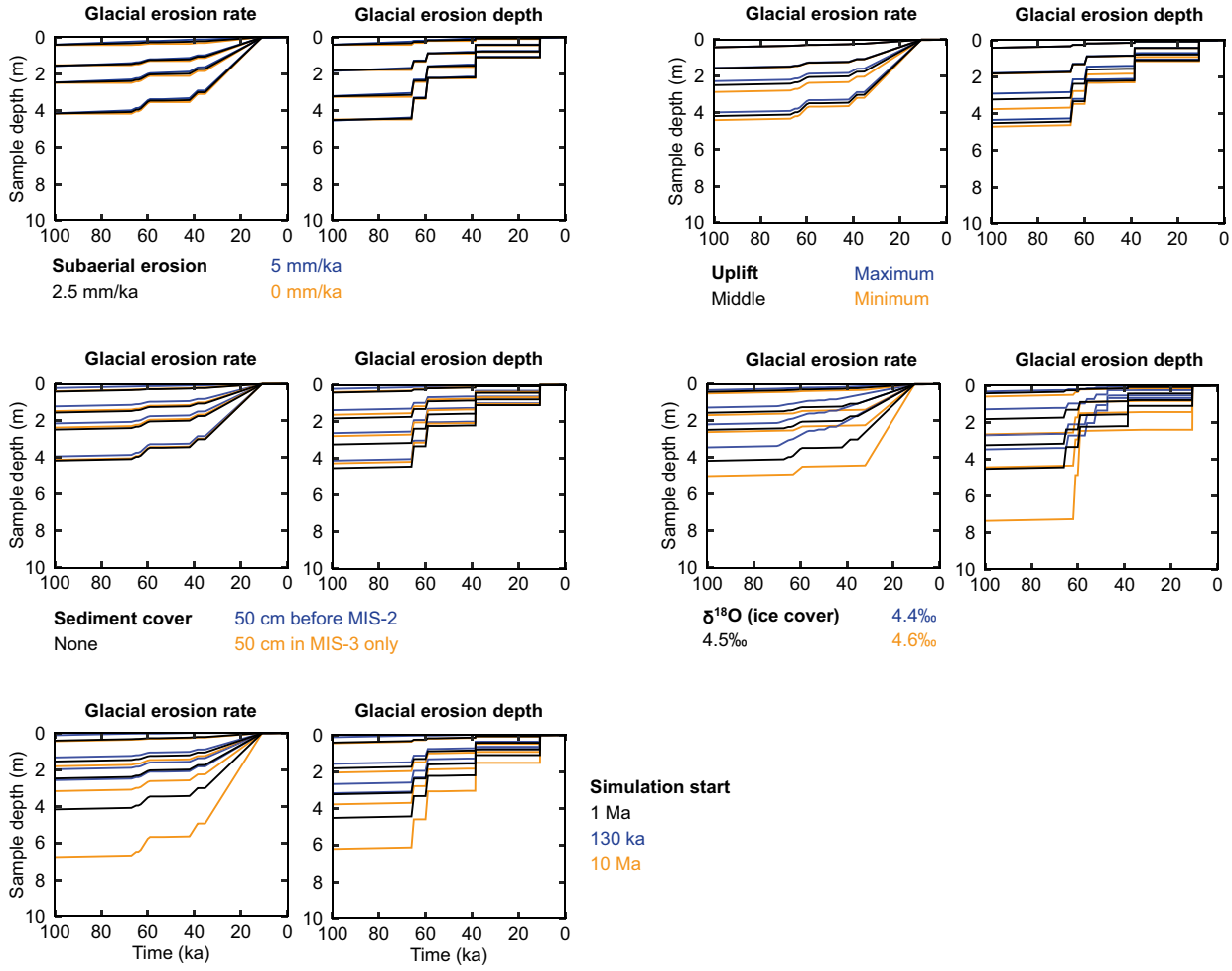

Figure 5-7. *Sensitivity tests of the erosion simulation. Each panel shows the simulated erosion (sample depth history) over the last 100 ka for four samples (FORS-16-13, 16-21, 17-08, and 17-21) and three scenarios. The black lines show the erosion of the reference scenario, as defined by the five reference parameters, with constant glacial erosion rate (left panels) and constant glacial erosion depth (right panels). The red and blue lines show the erosion when perturbing one of the four parameters: subaerial erosion rate, uplift model (Figure 5-3), sediment cover, $\delta^{18}O$ cut-off value, and simulation start. For the predetermined parameter space, the erosion is generally more sensitive to perturbations of the ice cover history and simulation start point than to perturbations of the interglacial erosion rate, the uplift model and modest (< 50 cm) sediment cover.*

5.3.4 Erosion simulations

Figure 5-8 and Figure 5-9 display the outcome of single nuclide erosion simulations from bedrock surface samples. Considering the full suite of simulations (scenarios 1–14), glacial erosion estimates based on ^{10}Be measurements range from zero to unlimited (Table A4-3). If the one sample with the lowest ^{10}Be inheritance is excluded (FORS-17-07), calculated glacial erosion rates fall below 0.39 m/ka (for constant glacial erosion rates) and below 3.3 m per ice cover period (for constant glacial erosion depths). For the full suite of constant glacial erosion simulations (scenarios 1–10) calculated glacial erosion rates for ^{26}Al concentrations fall below 0.33 m/ka (for constant glacial erosion rates) and 3.5 m per ice cover period (for constant glacial erosion depths).

Figure 5-10 displays the outcome of erosion simulations for bedrock samples that satisfy both ^{10}Be and ^{26}Al constraints with single erosion scenarios. For scenarios 1–10, 81 % to 90 % of the 31 samples yielded a solution (Table A4-3). For the full suite of bedrock samples and for scenarios 1–10, 84 % yielded a solution. These samples yield glacial erosion rate estimates for constant glacial erosion rates (constant glacial erosion depths) of 0–0.24 m/ka (2.5 m per ice cover period), with interquartile ranges of 0.04–0.09 m/ka (0.4–1.1 m per ice cover period). The interquartile range of simulated total erosion depths for scenarios 1–10 over the last 100 ka is 1.6–3.5 m. For erosion simulations starting at 1 Ma or earlier (scenarios 5–10), the interquartile range of simulated total erosion over the last 1 Ma is 13–27 m. The interquartile range of simulated total erosion depths for scenarios 1-10 over the last 35 ka, including the last ice cover period, is 0.6-1.6 m.

Simulations without glacial erosion between 10 Ma and 130 ka (scenarios 11–12) result in intense glacial erosion during the last glacial cycle, with interquartile range of total erosion over the last 100 ka for single nuclide simulations between 3.6 and 16.4 m (Table A4-3). Because glacial erosion prior to the last glacial cycle is preset to zero, total erosion over the last 1 Ma is slightly higher because of the minor contribution of subaerial erosion during ice-free periods. The simulations without glacial erosion after 55 ka (scenarios 13 and 14) result in intense glacial erosion for the preceding glaciations. For the single nuclide simulations, 20 and 21 ^{10}Be samples and 21 and 23 ^{26}Al samples overlap with full resetting of the cosmogenic nuclide signal from prior glacial erosion for the cases of constant erosion rate and constant erosion depth, respectively. For each of the four scenarios with varying glacial erosion, relatively few samples (20–22) yield solutions in the combined nuclide simulations.

The two samples located above the planned repository footprint (FORS-17-09/10; Figure 5-2) yield 1.0–5.6 m total erosion over the last 100 ka and 6.1–41.7 m total erosion over the last 1.506 Ma, based on single nuclide ^{10}Be and ^{26}Al simulations (sample FORS-17-10 yields no solution in the combined ^{10}Be and ^{26}Al simulations). The 19 bedrock samples located at 0–24 m a.s.l. within 5 km of the planned repository yield a total erosion over the last 100 ka (1 Ma) of 0–8.6 m (2.0–61.5 m), based on the combined ^{10}Be and ^{26}Al simulations. The 13 bedrock samples located at 25–67 m a.s.l. along the ridge south of Forsmark yield a total erosion over the last 100 ka (1 Ma) of 0.6–8.1 m (4.6–55.7 m), based on the combined ^{10}Be and ^{26}Al simulations.

Figure 5-11 displays the production rate normalized ^{26}Al/^{10}Be ratios in a commonly used isotope ratio plot (Lal 1991). Measured isotope ratios generally fall around the expected simple exposure and constant erosion end-point ratios, although there is a large scatter (5.1–10.7) in the isotope ratios (Table A4-2). The largest scatter in isotope ratios occurs for samples with low concentrations, whereas the samples with the highest concentrations generally fall close to expected ratios for simple exposure.

Model results for the ^{10}Be and ^{26}Al depth profile, taken from a steeply-dipping quartz vein exposed in the road cut near where the surface sample FORS-16-04 (Figure 5-2) was located are presented in

Figure 5-11 (Table A4-4). The theoretical simple surface exposure age, which assumes a single period of exposure with no erosion, is 8.0 ± 4.4 ka (8.5 ± 3.2 ka) based on the ^{10}Be (^{26}Al) concentrations. These results overlap well with the exposure age of 6.6 ± 0.7 ka (7.0 ± 0.7 ka) for ^{10}Be (^{26}Al) (Table A4-2) for ^{10}Be (^{26}Al) for sample FORS-16-04. For both ^{10}Be and ^{26}Al, however, the nuclide concentration of the sample at 250 cm is too high for such a simple scenario (Figure 5-12). Rather, combined ^{10}Be and ^{26}Al glacial erosion simulations show that scenarios 5–6, with 1 Ma simulation duration, yield the best overlap with both depth profile samples. Scenarios 1–2 (130 ka simulation duration) and 11–14 (extreme scenarios) poorly match both depth profile samples.

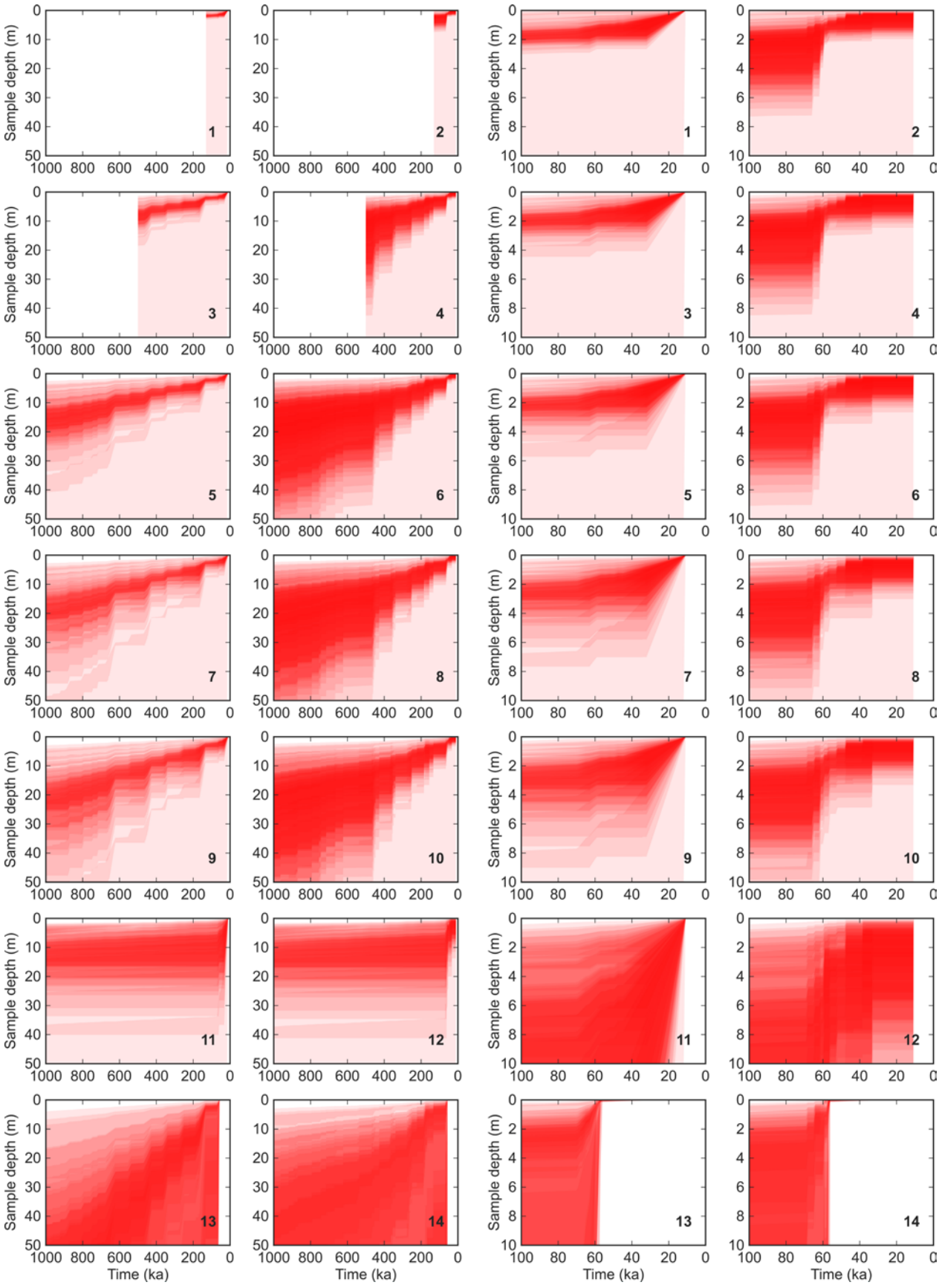

Figure 5-8. *Erosion simulation output for ^{10}Be simulations. Each simulated individual sample depth range is shown with 90 % transparency so that overlapping sample depths yield darker areas. The bold number in the lower right corner of each panel shows the simulation scenario number (Table 5-1). The left panels show the sample depth history over the last 1 Ma and the right panels show the sample depth history over the last 100 ka.*

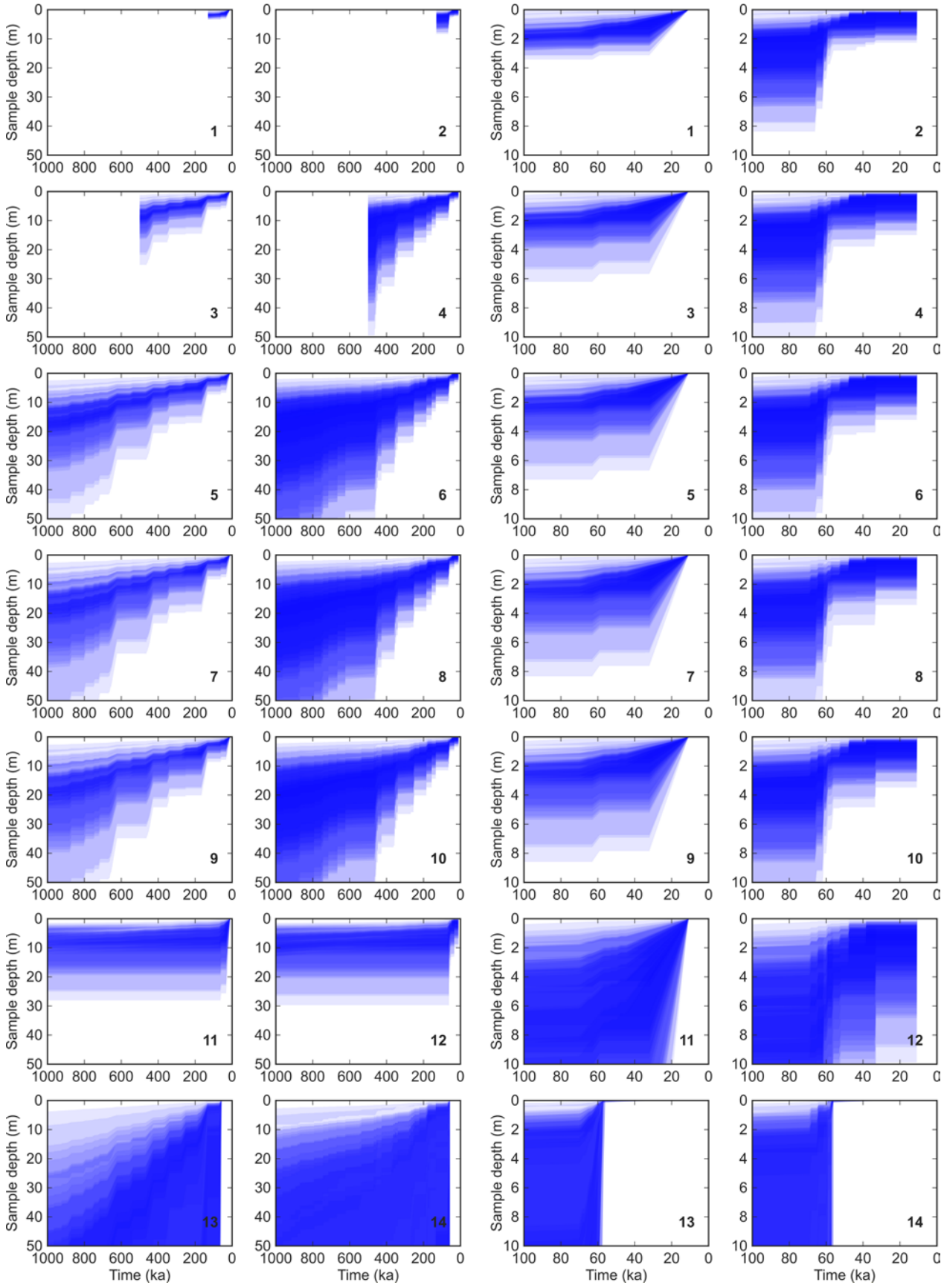

Figure 5-9. *Erosion simulation output for ^{26}Al simulations. Each simulated individual sample depth range is shown with 90 % transparency so that overlapping sample depths yield darker areas. The bold number in the lower right corner of each panel shows the simulation scenario number (Table 5-1). The left panels show the sample depth history over the last 1 Ma and the right panels show the sample depth history over the last 100 ka.*

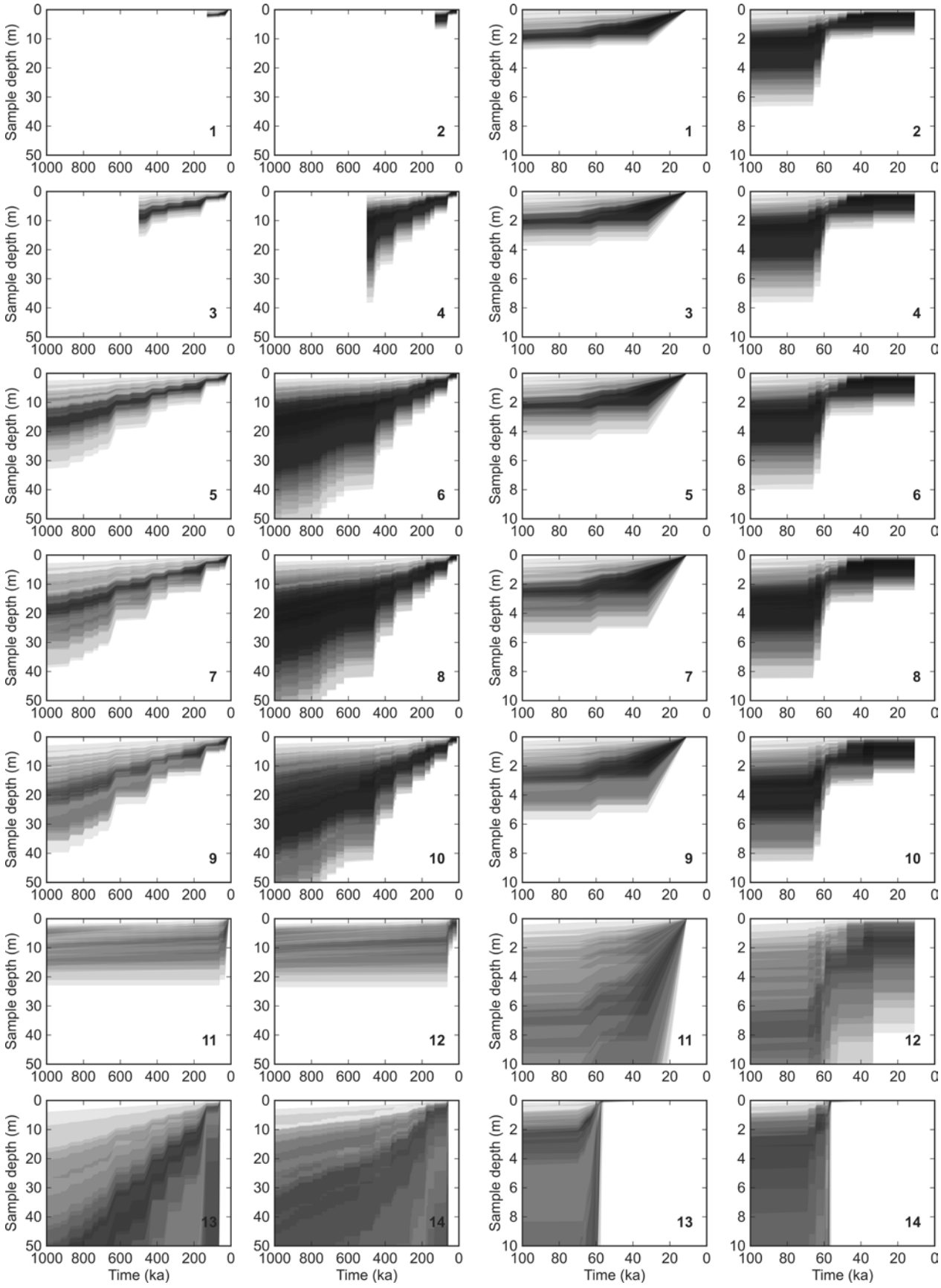

Figure 5-10. *Erosion simulation output for combined ^{10}Be and ^{26}Al simulations. Each simulated individual sample depth range is shown with 90 % transparency so that overlapping sample depths yield darker areas. The bold number in the lower right corner of each panel shows the simulation scenario number (Table 5-1). The left panels show the sample depth history over the last 1 Ma and the right panels show the sample depth history over the last 100 ka.*

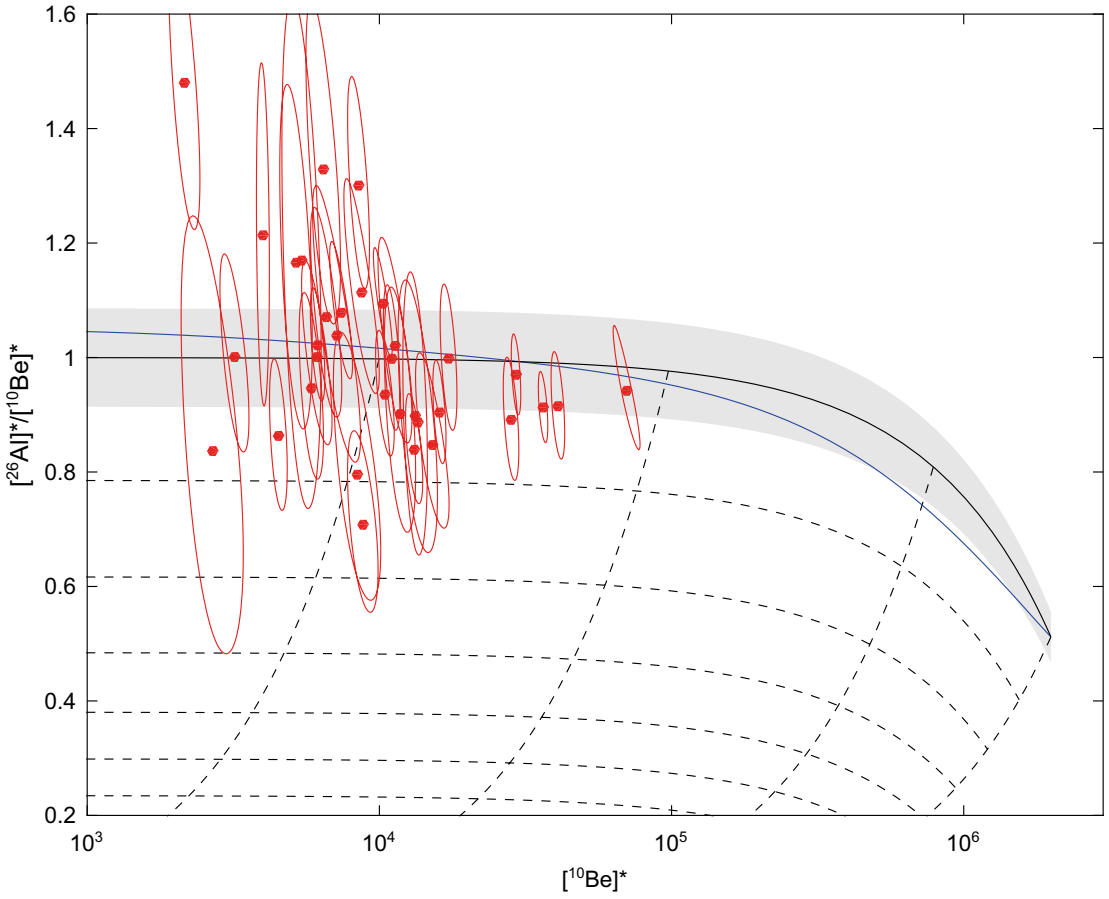

Figure 5-11. *Bedrock sample $^{26}Al/^{10}Be$ ratios with sample ^{10}Be and ^{26}Al concentrations normalized against long-term average surface ^{10}Be and ^{26}Al production rates. The solid black curve shows the theoretical path under full exposure at the surface. The blue curve shows the theoretical constant erosion end-point line. The sub-horizontal dashed curves show theoretical $^{26}Al/^{10}Be$ ratios after periods of burial (no production) with steps of 0.5 Ma. The sub-vertical dashed curves show the path of $^{26}Al/^{10}Be$ ratios if buried after 10 ka, 100 ka, 1 Ma, and 10 Ma of exposure. The grey area shows the uncertainty of the full exposure $^{26}Al/^{10}Be$ ratios, based on uncertainties of ^{10}Be and ^{26}Al production rates and assuming that their uncertainties are independent.*

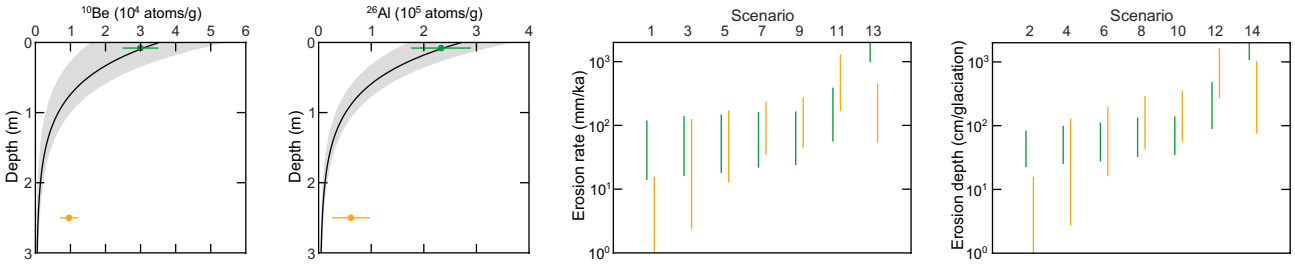

Figure 5-12. *Model results for the depth profile from the road cut at FORS-16-04. The two left panels display the ^{10}Be and ^{26}Al concentrations against sample depth, and a modelled simple exposure depth profile with 2s uncertainties. The deep sample (NRD-003) has ^{10}Be and ^{26}Al concentrations that exceed those expected for a simple exposure scenario. The two right panels display the range of modelled glacial erosion for the two depth profile samples, using the combined ^{10}Be and ^{26}Al simulation scenarios 1–14. Scenarios 5–6, with 1 Ma simulation duration, yield the best glacial erosion overlap for the two samples. The full output from the glacial erosion simulations, including single nuclide simulations, is available in Table A4-4.*

5.4 Discussion

5.4.1 Variation in sample inheritance/glacial erosion and their controlling local factors

To investigate if local factors such as bedrock hardness, bedrock fracture spacing, relief, and elevation can explain the variation of simulated glacial erosion rates (based on inheritance), we have analyzed such relations using one modelled erosion rate scenario (Figure 5-13). Across the board, there appear to be no significant correlations. For example, none can be seen between elevation and inheritance, nor, therefore, with the amount of glacial erosion (Figure 5-13A). Low-lying sites have both high inheritance (e.g., Wave Rock [12 m a.s.l.] and Mount Megantic [22 m a.s.l.]) and slight inheritance (e.g., Klubbudden [0.5–2.8 m a.s.l.] and Yonder Flats [23–24 m a.s.l.]). Similar variations in inheritance occur along the higher-elevation Uppland transect. For example, both Ironworks Quartz Bleb (54 m a.s.l.), and The Whalebacks (56 m a.s.l.) have high inheritance, whereas the Ironworks Whaleback (46 m a.s.l.) and Pitted Rocks (66–67 m a.s.l.) do not (Table A4-2). These similarities in inheritance, and inferred glacial erosion rates (Figure 5-13), occur despite the Ironworks Block (located on the Uppland transect) displaying somewhat lower relief than the other sampled blocks.

The relationships of inheritance and erosion rate with local elevation differences (relief) are also ambiguous (Figure 5-13C). We tested the assumption that erosion during the last glaciation was lower on bedrock summits than in lower parts of the landscape most thoroughly at Wave Rock (Figure 4-30), where initial measurements of one sample (FORS-16-13) yielded high inheritance. As anticipated, the highest inheritance (^{10}Be: 69 ka; ^{26}Al: 66 ka) indeed occurs at the outcrop summit (12 m a.s.l.). Lower down, at 9–10 m a.s.l. on the outcrop flanks, three samples displayed lower, but still considerable, inheritance (13–43 ka). The two lowermost samples, located at 6 m a.s.l. and 150–200 m southwest and south of the summit, displayed the least inheritance (2.6–4.8 ka). This systematic pattern of decreasing inheritance with decreasing elevation indicates that higher erosion rates have occurred at the base of the outcrop than at the summit, consistent with glacial erosion locally increasing relief through either vertical or lateral erosion.

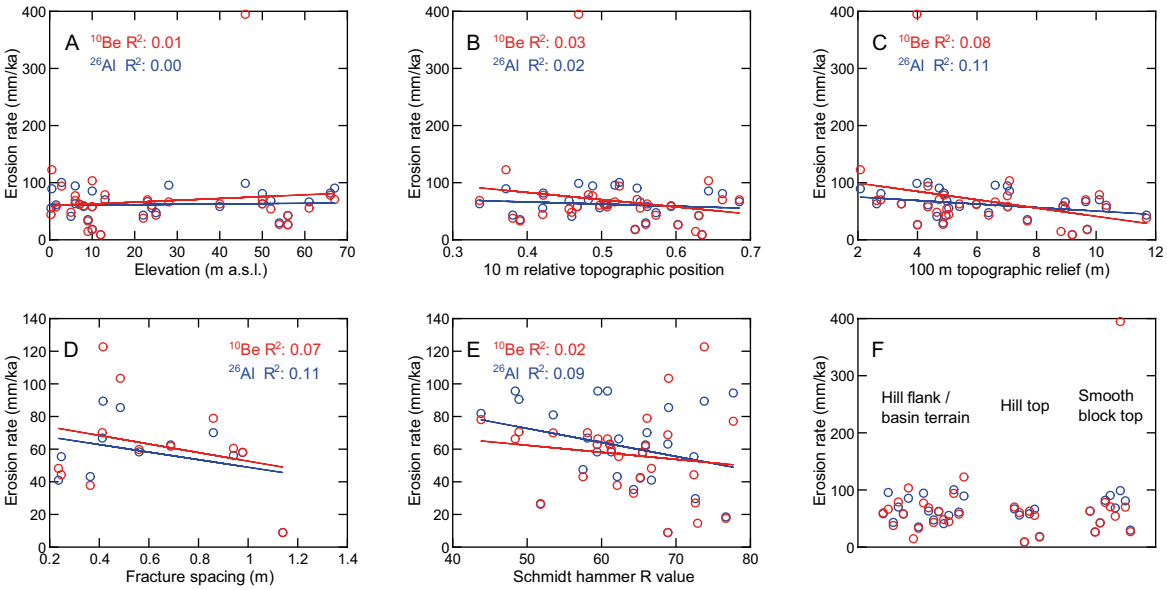

Figure 5-13. *Relation between local factors and simulated glacial erosion rate using a specific scenario ($\delta^{18}O$ cut-off value of 4.5 ‰, subaerial erosion rate of 2.5 mm/ka, and simulation start at 1 Ma). Glacial erosion rate appears to be unrelated to A) sample elevation, B) relative topographic position, C) topographic relief, D) fracture spacing at sample sites (area method; Section 4.2.4), and E) bedrock hardness using Schmidt Hammer R-values. F) simulated glacial erosion rates divided into three groups; similar to the other local factors, there is no clear relation between sample setting and glacial erosion rate.*

While our results, which primarily reflect glacial erosion during the last glaciation, show that erosion can increase relief at a local scale, ambiguity arises when considering how glacial erosion might control relief development more broadly across the landscape, over multiple glacial cycles. For example, in apparent contrast to the Wave Rock results, the coastal embayment at Stora Asphällan displays significantly more inheritance (8.4 ± 0.8 ka) than any of the Klubbudden bedrock sites, low lying summits including Neon Roundabout (FORS-16-04), Yonder Flats (FORS-16-07), Pink Spot (FORS-16-10), The Bornhardt (FORS-16-11), Shimmering Flats (FORS-16-12), and Repository Footprint (FORS-17-09), and an additional five summits along the Uppland transect (Figures 5-2, 5-6). Therefore, the lowest site we sampled, located in a concave position in a coastal embayment, has eroded more slowly during recent glaciation(s) than 13 of the sampled summits.

We have previously introduced a new process of glacial erosion, glacial ripping (Section 4.3.3), which may explain why parts of low relief landscapes may be prone to relief reduction by glacial erosion. Glacial ripping exploits sub-horizontal and gently dipping fractures and has potentially been a widespread process at Forsmark and elsewhere in Uppland (Section 4.3.3). An example of how potent glacial ripping is and how it may ultimately reduce local relief is provided at Mt Megantic (FORS-16-09). This summit underwent one of the lowest inferred rates of erosion during the last glaciation, yet it is located 2 m from a vertical scarp, south of which rock exceeding 3 m in thickness is interpreted to have been ripped or plucked at the termination of the last glaciation (Section 4.3.3). Nearby blocks with A-axis lengths of 5 m sourced from this outcrop also indicate glacial transport of large boulders (Section 4.3.3). It is possible and perhaps reasonable to expect that parts of the remaining summit area, including our sample site, may also be eroded to a depth of more than 3 m during the next glaciation. If so, this site, which experienced low erosion during the last glaciation, will instead see an erosion rate sufficiently high to be unconstrained by cosmogenic nuclides during the next glaciation, resulting in further lowering across the hill summit and potentially resulting in reduced local relief. We interpret boulder spreads in the vicinity of at least one other cosmogenic nuclide sample site (FORS-17-09, which overlies the planned repository footprint, and also perhaps at FORS-16-12) as evidence for ripping during the last deglaciation. We note however that the cosmogenic nuclide data from most bedrock surfaces indicate a total removal of < 3.5 m of rock in the last glaciation, a depth equal to or less than that lost to ripping on the lee side of Mt Megantic. Because our sampling was not explicitly designed to test for the newly recognised process of glacial ripping, we cannot draw more general conclusions.

Our modelling of topographic perturbations of the near surface ambient stress fields has similar implications (Chapter 3). We show that for ambient stress conditions at Forsmark, sub-horizontal joints are expected to generally open beneath convex landscape elements (hills; Figures 3-4 to 3-6), which may stimulate enhanced glacial erosion of these sites by plucking and ripping and reduce local relief. At the same time, steeply dipping joints may open in some concave landscape elements (valleys), which may also promote glacial erosion of these and result in an increase in local relief (Figures 4-8 and 4-9). While our study highlights a range of erosion rates across the Forsmark study area and has illuminated many potential controls on relief evolution through glacial erosion, including new ones, the balance between glacial erosion processes that increase relief, and those that decrease relief, could potentially shift in a stochastic manner between glaciations to favour persistence of a low relief landscape.

A more complete understanding of relief generation at Forsmark was hampered by our sampling strategy, which primarily targeted summits. A more thorough testing of low-lying and concave locations is desirable, but highly constrained by the presence of continuous sedimentary covers.

Furthermore, we find no support for bedrock fracture spacing as a control on rates and depths of glacial erosion at our cosmogenic nuclide sample sites (Figure 5-13). An apparent absence of a control of fracture spacing on rates of glacial erosion contrasts with studies of fracture control on glacial erosion rates in Yosemite (Dünhforth et al. 2010) and glacial erosion processes in Scotland (Krabbendam and Glasser 2011). This difference may reflect one, or several, factors. Firstly, comparing study results is complicated by measurements being made by different methods and researchers. In the detailed area fracture survey, all fractures, including those with hairline apertures, intersecting lines comprising a grid up to 25 m^2 were counted (Sections 4.2.4 and 4.3.4). Grid axes were oriented with ice flow and perpendicular to it. This method contrasts with Dünhforth et al.

(2010) and Krabbendam and Glasser (2011) who each used line surveys. However, while the latter study only counted open fractures, the former study defined a fracture as: 'any structure in the rock that showed either a crack leading to surface irregularities or that displayed signs of adjacent rock weathering or alteration which is comparable to the definition of fractures used in this study. Furthermore, they counted these fractures parallel, and perpendicular, to ice flow, as done here. Because of these similarities, and because measurements of fracture spacing using a grid or a line survey should not inherently differ if the definition of a fracture is comparable, we consider a comparison of our study results with those of Dünhforth et al. (2010) to be both valid and potentially illustrative of how glacial erosion rates at Forsmark may relate to fracture spacing. Our results from the 50 m line surveys however yielded much wider vertical fracture spacings (Figure 4-40).

Using Dünhforth et al. (2010) as a comparison leads us to a potential second reason for why fracture spacing did not correlate with glacial erosion rate in this study. The absence of correlation between these parameters at Forsmark may reflect the relatively close spacing of sub-vertical fractures on our sampled outcrops. The mean fracture spacing of 1.1 m at Wave Rock (Section 4.3.4), which is the highest measured at Forsmark using the grids is the same as the close spacing recorded for rapidly eroded sites in Yosemite (1.1 ± 0.03 m; Dühnforth et al. 2010). In comparison, the spacing of wide fractures in Yosemite is 3.3 ± 0.1 m. These differences between Forsmark and Yosemite may reflect the long history of the basement rock at Forsmark, during which it has undergone multiple episodes of orogeny, burial and exhumation, metamorphism, and associated fracturing (Chapter 2). This history contrasts with the much shorter, and straightforward, history of the particularly massive granite plutons at Yosemite (Dühnforth et al. 2010). The 1.89 billion-year history of basement at Forsmark is reflected in the presence of three main fracture sets (Section 3.2) and other fractures, including those that relate to compositional variations, such as pegmatites (Section 4.3.4) and Quaternary glaciation (Leijon 2005). The spacing of fractures on the measured outcrops at Forsmark (with a maximum mean of 1.1 m) further contrasts with measurements of fracture spacing at Fågelmara (mean of 0.9 m) in SE Sweden and at Trollhättan (mean range of 1.0 to 12.5 m) and Nordkroken (mean range of 7.7 to 20.0 m) in SW Sweden, using the same definition of fractures as used in this study (Goodfellow et al. 2019). The absence of correlation between fracture spacing and the rates and depths of glacial erosion at Forsmark may reflect the scarcity of rock-kernels that display mean fracture spacing wider than 1 m.

A third reason for the absence of correlation between fracture spacing and glacial erosion rate is that long, outcrop-bounding fractures may be a key control on glacial erosion rates and depth. The characteristics of these fractures, such as orientation relative to ice flow directions, dip, and openness may be the key control on glacial erosion rates and depths at Forsmark, rather than the spacing of all fractures. Alternatively, or in addition, our data might indicate an importance of glacial erosion along surface parallel or subhorizontal fractures. These fractures are not easily mapped and our data are also consistent with sheets of rock of different thickness having been removed at the various locations, as illustrated by the glacial erosion simulations assuming constant depth of erosion per ice cover period. Characteristics of outcrop-bounding fractures may be partly evaluated from aerial imagery, DEMs, and ground-penetrating radar, but a thorough evaluation requires field observations and is usually constrained by the presence of sediments and vegetation, even for convex locations (cf. Section 4.3).

A fourth potential reason for absence of correlation between glacial erosion and fracture spacing at Forsmark is that erosion rates have been low and so may not have been greatly controlled by fracture spacing. Streamlining of landforms is weak and basal sliding rates have been modelled to be low (Näslund et al. 2003).

While our data indicate that fracture spacing at Forsmark is less than at other measured sites in southern Sweden (Goodfellow et al. 2019) and less than measured in a similar study at Yosemite (Dünhforth et al. 2010), the spacing of all fractures, as measured here, may be typical of shield rocks that display ages extending beyond hundreds of millions of years, particularly in the uppermost meters to tens of meters of basement that were present prior to glacial erosion. The fracture spacing, which appears lower than some other landscapes, may also be reflected in the generally low relief of Forsmark (less than 20 m on the onshore part of the landscape) and the small outcrop summit areas (square meters to a few tens of square meters). While certain fractures (open, outcrop

bounding) may reasonably be expected to exert control on glacial erosion, other fractures may also be important, as reflected for example in the presence of micro and meso glacial erosion forms (Section 4.3) and in summit convexities and curvatures that appear to vary with fracture spacing (Figure 4-41).

Similar to fracture-spacing, a very weak negative correlation with erosion rate is obtained for Schmidt Hammer R-values, indicating that small differences in rock hardness at Forsmark provide an apparently insignificant control on glacial erosion rates at our sample sites. Hence, although we would expect some relationship between depth of glacial erosion with local bedrock characteristics and with short and long wavelength topography (Chapter 4), we have been unable to demonstrate such.

Finally, we fail to identify a relationship between stress model predictions for bedrock erosion rates and erosion rates inferred from the cosmogenic nuclide simulations. Stress model predictions of erosion potential for the three sites illustrated in Figure 5-14 is that their summits would be approximately equally susceptible to erosion through opening of sub-horizontal fractures. However, cosmogenic nuclide modelling reveals that Wave Rock, at least during the last glaciation, has eroded at a much slower rate than the other two sites. While subhorizontal joints are visible at some locations on Wave Rock and Shimmering Flats (Section 4.2), their extents beneath the outcrops remain unknown. In addition to an uncertainty regarding the presence (Pink Spot) and extents of subhorizontal joints beneath these outcrops, the apparent absence of correlation between stress model predictions and inferred modelled cosmogenic nuclide erosion rates may reflect several factors. Firstly, the model is based on stress values calculated for a depth of 50 m below the ground surface. Stresses will be lower at the surface than at 50 m depth, but the positive topographic perturbation of the near-surface stresses will be stronger. Exactly how this unfolds as a control on bedrock fracturing at the surface remains undetermined. Secondly, our cosmogenic nuclide sampling strategy was not designed to explicitly test this model and, as previously stated, included only two concave sites because of burial by sediments. Thirdly, stress model predictions of bedrock susceptibility to glacial erosion is strictly valid for upcoming glaciation(s), not for the history of glacial erosion inferred from cosmogenic nuclide modelling. Fourthly, topographic perturbation of near surface stresses will have varied temporally as glacial erosion increased or decreased local and regional relief and modified surfaces curvatures. Lastly, topographic perturbation of near surface stresses is only one potential control of many on glacial erosion. Therefore, identifying its role as a potential control on glacial erosion through selected point measurements is, at best, difficult. However, despite the inability of our study to test the predictions of the stress model on glacial erosion rates, given the above caveats, topographic perturbations of near surfaces stresses are likely to be an important but understudied component. The interaction of strong horizontal compression with bedrock hydrology during glaciations has induced spectacular hydrofracturing and jacking of bedrock sheets at Forsmark (Hökmark et al. 2010). Hence, topographic perturbation of near surface stresses may be an important control on glacial ripping, plucking, and erosion along sub-vertical fractures located in valleys that are in tension, and may also induce feedbacks between abrasion, which rounds bedrock surfaces, and the formation of sheeting joints, through its control on outcrop morphology. Further study of feedbacks between topographic perturbations of near-surface stresses and glacial erosion processes and rates may be revealing.

Our data set, with its limitations, may indicate that glacial erosion across variably fractured low-relief bedrock landscapes is a complex, stochastic process. Because we have not been , to demonstrate a clear relationship between glacial erosion rate and local bedrock, topographic, and stress state characteristics, but rather demonstrate stochastic erosion, ice sheet dynamics may have been the driving process. This tentative conclusion must be evaluated against the spatial bias of our sampling, which overwhelmingly targeted summit areas. Our findings are compatible with the relief of the landscape being too low and the spacing of fractures being too tight for those factors to exert clear control on glacial erosion. Indeed, the uppermost tens to hundreds of metres of bedrock is generally fracture-saturated, throughout Forsmark and much more broadly over the Sub-Cambrian peneplain (Chapter 2). Perhaps in such landscapes, glacial erosion becomes stochastic, removing bedrock where fracture systems and subglacial conditions align for effective erosion in one location but not in another, and where the glacially-modified topography subsequently may induce new fracture opening to maintain a fracture-saturated landscape (Chapter 4) and stimulate glacial erosion in new locations and persistence of low relief.

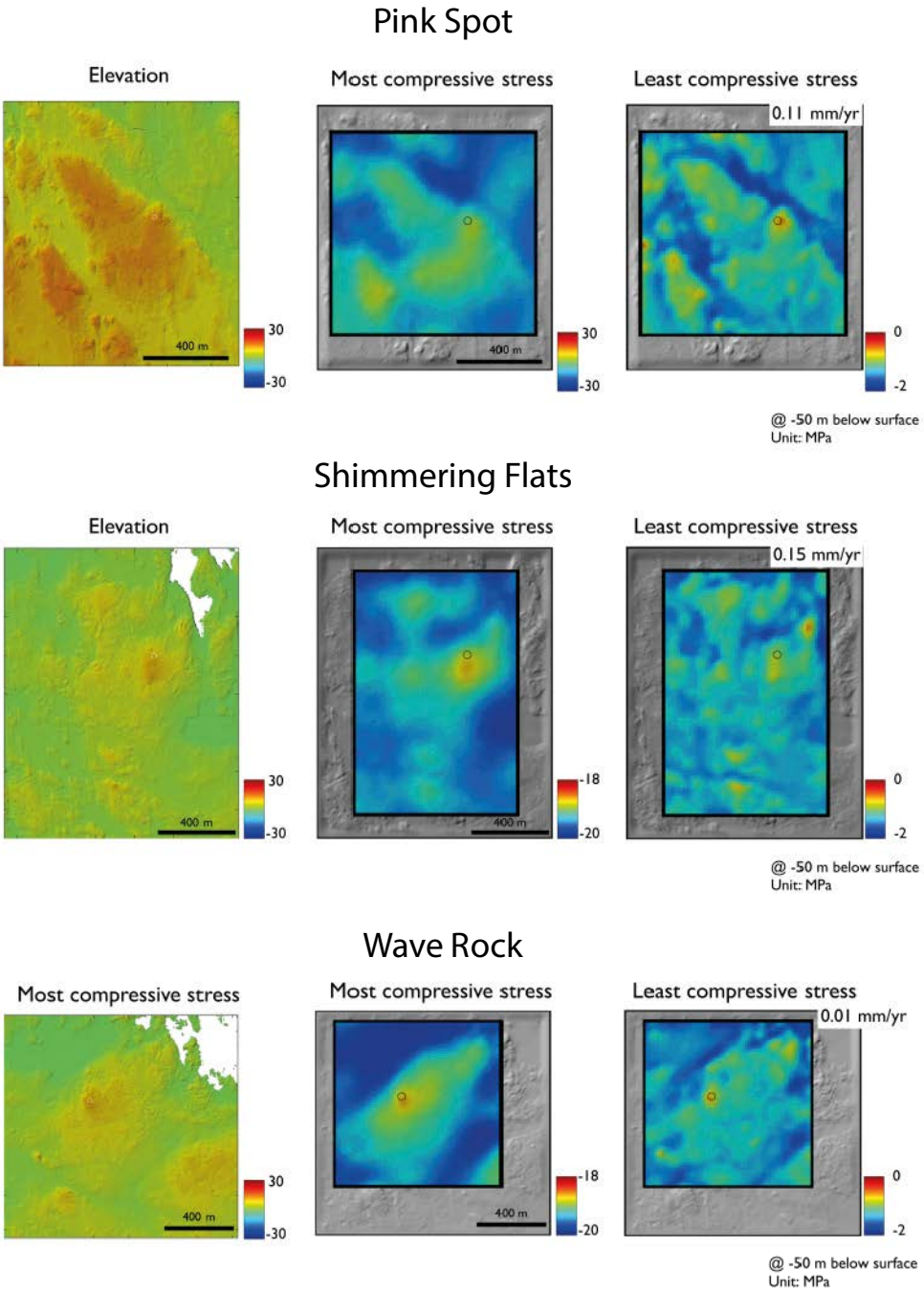

Figure 5-14. *Glacial erosion rates (in mm/yr) inferred from ^{10}Be concentrations for three bedrock summits. Black circle indicates the location of the sample site. The underlying horizontal compression is anisotropic, and while σ_H is high it reaches local minima beneath the summits. These stress conditions favour opening of subhorizontal joints below the sample locations. The panels show stress values at 50 m depth below the ground surface.*

5.4.2 Glacial erosion rates and depths per ice cover period and integrated over multiple periods

In our simulations, glacial erosion varies from 0 m to more than 3 m per ice cover period. Total erosion over the last 100 ka and 1 Ma varies from 0 m to more than 8 m and 60 m, respectively. Thus, there is a quantifiable variation in simulated rates and totals of erosion. However, given the temporally and spatially variable nature of glacial erosion (Kleman et al. 1999, Harbor et al. 2006, Stroeven et al. 2013), and the shallow depths to which measurable, cosmogenic nuclide production occurs (0–3 m; Figure 5-1), the simulated erosion depths are remarkably well-clustered, with typical

values for simulations with constant glacial erosion rate ranging between 1.6 m and 3.5 m over the last 100 ka (simulations 1–10) and between 13 m and 27 m over the last 1 Ma (simulations 5–10) (Figures 5-8 to 5-10). Glacial erosion rates are generally higher than subaerial erosion rates in the simulations, with the latter limited to a maximum of 5 mm/ka. A higher total erosion during the last 100 ka (per ice cover period) compared to the average erosion of the full 1 Ma period, reflects increasingly intense glaciation with respect to duration and frequency.

Depths of erosion vary between the simulations, particularly regarding the choice of the simulation period (130 ka to 10 Ma) and the glacial erosion mode (constant erosion rate or constant erosion depth). Mid-range erosion depths over the last 100 ka vary between 1.3 m and 3.9 m for simulations starting at 130 ka (simulations 1–2), and between 1.7 m and 5.5 m for simulations starting at 10 Ma (simulations 9–10). This difference is the effect of the longer duration of cosmogenic nuclide production (ice-free conditions) for the 10 Ma simulations, implying that more erosion is required to reach down to depths with equivalent cosmogenic nuclide concentrations. For simulations starting at 1 Ma (simulations 5–6), those with constant glacial erosion rate (erosion scaled against duration of ice cover) typically yields erosion depths of 1.5 m to 2.9 m over the last 100 ka and 11 m to 21 m over the last 1 Ma. Simulations with constant erosion depths (erosion scaled against number of ice cover periods), yield instead mid-range erosion depths of 1.9 m to 4.7 m over the last 100 ka and 12 m to 33 m over the last 1 Ma. This is an effect of the ice cover history, with longer durations of glaciation and fewer glaciations, typical for the past 700 ka or so (Tziperman and Gildor 2003), leading to lower integrated glacial erosion depths when assuming constant erosion rate than when assuming constant erosion depth. Inferred rates and depths of erosion are similar to those inferred from previous studies in glaciated regions. Simulated glacial erosion rates from the combined ^{10}Be and ^{26}Al measurements, with a mid-range of 0.04–0.09 m/ka, falls in the lower range of global compilation of glacial erosion rates between 0.0001 and 10 m/ka (Delmas et al. 2009).

For both the duration of simulation and the glacial erosion mode, it is difficult to determine which is more likely to be correct. If thick layers of sedimentary cover rocks were removed during the penultimate glaciation, the 130 ka simulation duration would best reflect the glacial erosion of basement rocks. If the sedimentary cover rocks were removed long before the Quaternary glaciations, however, the 10 Ma simulation duration would better reflect the glacial erosion of basement rocks. There are currently no precise constraints on the timing of cover rock removal in the investigation area but the absence of sedimentary cover rock outliers in NE Uppland is an argument for cover rock removal well before the penultimate glaciation (130 ka). If so, glacial erosion estimates using longer timescales yield perhaps the best representation of reality. The progressive deepening of the Baltic Basin by glacial processes since 1.1 Ma (Chapter 3) may be the best estimate for the re-exposure of and onset of glacial erosion in basement in the Forsmark area after removal of Early Palaeozoic cover rocks, perhaps rendering 1 Ma erosion reconstructions to be those of most interest. This view is also supported by the road cut depth profile samples, which, although with large uncertainties, yield the best overlap for the 1 Ma simulation scenarios (Figure 5-12).

For the mode of glacial erosion, it is difficult to determine which of the two end-member scenarios is more realistic but both may apply. From glacially eroded landforms in the region, it is clear that glacial abrasion, plucking, ripping and meltwater erosion have affected different parts of the landscape. While glacial abrasion is commonly seen as a more continuous process, provided basal ice was at the pressure melting point, plucking (or ripping and other erosion processes) may be thought of as episodic. The constant erosion rate mode may therefore be taken as a measure of continuous abrasion and the constant erosion depth mode as more representative of punctuated s plucking or ripping. However, it is difficult to determine how much of the total glacial erosion has been caused by continuous abrasion and how much of the total glacial erosion has been caused by episodic bedrock removal through plucking or ripping. Indeed, even if abrasion occurs over longer duration than a sudden plucking event, it does not automatically imply that it is persistent throughout a full ice cover period. Similarly, it is highly conceivable, and demonstrated in this report, that plucking may be followed by abrasion which perhaps occurs for a relatively short duration towards the end of an ice cover period. We see the two glacial erosion modes as end-member scenarios that capture a far more complex spectrum of glacial erosion (Glasser and Hall 1997, Lidmar-Bergström 1997, Stroeven et al. 2002a, Riihimaki et al. 2005, Goehring et al. 2011).

The cosmogenic nuclide concentrations will only be affected by surface erosion and shielding at the specific sample location. Hence, when thinking about erosion at the regional and landscape scale, one should be wary to draw firm conclusions from extreme values. However, the fact that such a large part of the dataset supports erosion histories in the same range offers good support for two conclusions on glacial erosion. First, there has been some erosion of most (and potentially all) sites, and the overall landscape is lowering. Second, while glacial erosion has affected all of the Forsmark region landscape, it has been limited to c. 1.6–3.5 m during the past 100 ka and 13–27 m over the past 1 Ma.

5.4.3 Development of cosmogenic nuclide inventories

When interpreting cosmogenic nuclide data in terms of long-term glacial erosion, it is important to keep in mind that the most recent erosion event is typically by far the most important in terms of the cosmogenic nuclide inventory (and strongly guides inferences on glacial erosion and shielding by water/sediment). Intense erosion during the last glaciation would result in a low nuclide concentration while a lack of erosion during the last glaciation would result in a relatively high nuclide concentration. Given the spatially and temporally variable pattern of erosion for the last glaciation that emerges from our data, it is entirely possible that similarly variable erosion patterns characterized earlier glaciations, but which differed at each site. Hence, it could be that a low concentration sample is the effect of 2–3 m of erosion during the last glaciation, but that average erosion over multiple glaciations has been lower. Alternatively, a high concentration sample could be the result of the last glaciation being non-erosive, but that earlier glaciations have eroded more. This leads to two considerations. First, if glacial erosion rates have structurally changed over time (increasing or decreasing), our output could be skewed towards either too low erosion or too high erosion estimates. Second, if glacial erosion rates have instead fluctuated over time (for example, removing a bedrock sheet in one erosion event but not in another), then perhaps our spatially variable pattern yields a landscape-wide informed picture of the spreads of erosion rates that one might expect in any one glaciation back in time. Currently, we lack good quantitative methods to determine how glacial erosion has changed over time and we cannot, based on our data, say which would be more likely.

5.4.4 $^{26}Al/^{10}Be$ ratios and burial

The $^{26}Al/^{10}Be$ ratios range from 5.1 to 10.7 with a median value of 7.1 (which basically equates to 1 on the normalized scale of Figure 5-11). Most of the ratios overlap within uncertainty with the simple exposure curve in the classic $^{26}Al/^{10}Be$ ratio plot (solid black curve, Figure 5-11). The implication of this is that there is no support for extended periods of burial under non-erosive ice while the samples are at or close to the surface. These results are in-line with expectation. If there had been significant durations of burial beneath cold-based ice (ratios falling below the exposure island outlined by the black and blue curves in Figure 5-11), ice cover periods had to last hundreds of thousands of years, with only short ice-free periods (sub-horizontal dashed curves in Figure 5-11 (Fabel and Harbor 1999) denote ratios after multiples of 0.5 Ma of burial). While one estimate of the integrated duration of ice cover over our research area during the last 1 Ma is in excess of 230 ka (Kleman et al. 2008), marine oxygen isotope records indicate that glaciation events were regularly interspersed with ice-free conditions (Figure 5-4; Lisiecki and Raymo 2005). These short burial periods are undetectable in $^{26}Al/^{10}Be$ ratios because of the slow decay of the $^{26}Al/^{10}Be$ ratio given the long half-lives of c. 0.7 and 1.4 Ma, respectively, for each of these nuclides.

In addition to excluding extensive burial of bedrock surfaces by non-erosive glacial ice, the full $^{26}Al/^{10}Be$ ratios also exclude long periods of burial by sediments. However, short periods of burial by sediments during isostatic rebound of our sampled bedrock surfaces through shallow water and post-subaerial exposure could still theoretically have occurred. If so, this would be a primary reason why surface exposure periods inferred from ^{10}Be and ^{26}Al must be interpreted as minima and simple erosion rates interpreted as maxima. A number of lines of circumstantial evidence, however, indicate that burial by sediments is unlikely to have significantly influenced our inferred erosion rates and depths. Firstly, in the landscape classification of Kleman et al. (2008), this area is characterized as "mostly scoured bedrock with thin patchy drift". Secondly, we primarily sampled bedrock summits, which were free of sediments. Thirdly, summits at the coast are already free of sediments, indicating that any sediment redistribution occurs prior to and during emergence above sea level. Fourthly, all

of our data, with the exception of one site, show inheritance of cosmogenic nuclides. None of our sampled summits indicates an age that postdates deglaciation and emergence above sea-level, which would lead us directly to suspect surface burial by sediments. Fifthly, our Monte Carlo simulations explore a range of possible histories across a large number of samples, rather than our erosion rate inferences being dependent upon single histories from a small number of samples, in which sediment burial might consequently be more important. Finally, there is no trend in cosmogenic nuclide inheritance with elevation. If there had been burial of our sampled summits during isostatic rebound through shallow water, then a trend towards less inheritance with declining elevation may have occurred. This is because the rate of rebound has declined markedly over the Holocene (Figure 5-3), resulting in a longer duration in which sediment might shield nuclide production for low-lying bedrock under shallow water than for higher elevation samples. We therefore conclude that while simple exposure histories based on our cosmogenic nuclide data are minima, we have no reason to suspect that real exposure histories are significantly longer. Our inferences of erosion rates and depths therefore remain robust.

In addition to dispersion of $^{26}Al/^{10}Be$ ratios attributable to low abundances of these nuclides in many of our samples (Figure 5-12), the ratios may be skewed towards higher values because of the increased importance of production of these nuclides from muons at depth. Nuclide production from muons yields higher $^{26}Al/^{10}Be$ ratios than nuclide production through spallation, and this may partly explain why seven samples have $^{26}Al/^{10}Be$ ratios larger than 8. While there might be some general contribution of nuclide production from muons to higher $^{26}Al/^{10}Be$ ratios, all of these samples that deviate from the full exposure ratio have relatively low cosmogenic nuclide concentrations and most of these samples still overlap within uncertainties with the simple surface exposure path. In fact, if production rate uncertainties are also taken into account (the grey-shaded area in Figure 5-11), only three samples have $^{26}Al/^{10}Be$ ratios that are inconsistent with a simple exposure history. Two of these samples (FORS-17-21 and 17-07) lie above the uncertainty zone on the exposure curve and one (FORS-17-12) lies below. The two high-ratio samples, which are located in the Klubbudden embayment (17-21) and at Ironworks Whaleback (FORS-17-07), could possibly be explained if they resided at a depths much deeper than at 3 m depth over multiple glacial cycles, thus acquiring a reservoir of high $^{26}Al/^{10}Be$ before having been exhumed rapidly through the uppermost 3 m of bedrock and therefore acquiring a smaller component of spallation-ratio $^{26}Al/^{10}Be$. The other, low-ratio, sample (FORS-17-12), located in an embayment at Stora Asphällan, is consistent with long-term burial while the sample resided in the upper 3 m of the bedrock column. It is also consistent with the constant erosion scenarios 8–10 with shorter durations of burial and the low ratio caused by the more rapid decay of ^{26}Al compared to ^{10}Be (cf. Knudsen et al. 2019). These $^{26}Al/^{10}Be$ ratio data further highlight the spatially and temporally variable nature of glacial erosion at Forsmark.

The $^{26}Al/^{10}Be$ ratios are useful in testing that most of our samples provide robust estimates of glacial erosion rates and depths. Only the two samples with the highest $^{26}Al/^{10}Be$ ratios are associated with simulations that do not yield a solution. However, for 25 samples, all simulation scenarios with invariant glacial erosion yield solutions (simulations 1–10). This indicates that the measured ^{10}Be and ^{26}Al concentrations for these samples are generally in agreement with each other and with spallation $^{26}Al/^{10}Be$ ratios, and that the simulation scenarios, despite their simplistic assumptions, can explain most of the cosmogenic nuclide dataset. For the extreme scenarios (simulations 11–12), eleven samples lack a combined nuclide solution. This indicates that the extreme scenarios with major changes of the glacial erosion during the last glacial cycle have larger problems in explaining the full cosmogenic nuclide data, and that the invariant glacial erosion scenarios are likely closer to the reality.

5.4.5 Future glacial erosion

Safety assessments for the planned spent nuclear fuel repository requires consideration of glacial erosion under future ice sheets. Estimated depths of past glacial erosion based on cosmogenic ^{10}Be and ^{26}Al inventories in bedrock exposures described above are 13–27 m over the last 1 Ma.

To estimate the potential future depths of glacial erosion at the Forsmark site, we combine the simulated glacial erosion (erosion rate and erosion depth) for the combined ^{10}Be and ^{26}Al simulations with output from numerical models projecting future ice sheet cover at Forsmark over the coming 1 Ma based on IPCC emission scenarios and future variations in insolation (Lord et al. 2019). The

total time of ice sheet coverage over the Forsmark site (with "higher confidence") over the coming 1 Ma is 247 ka, 207 ka, 104 ka, and 254 ka given the IPCC RCP2.6, RCP4.5, and RCP8.5 emission scenarios and a case without anthropogenic carbon emissions, respectively. We use the interquartile range of the full set of simulated glacial erosion rates and depths from scenarios 1–10 as a mid-range of future glacial erosion, and percentile 5–95 as a wider range of potential future glacial erosion rates and depths. We simulate the future erosion by combining these erosion values with the higher confidence projected future ice cover from Lord et al. (2019) for the four different emission scenarios. We apply a range of subaerial erosion rates of 0–5 mm/ka similar to the glacial erosion simulations for the cosmogenic nuclide data. Projected depths of total erosion for the Forsmark site over the coming 100 ka is less than 1 m (Figure 5-15). The mid-range total erosion depth over the coming 1 Ma is 5–28 m, and the wider range of depth of total erosion is 2–43 m (Table 5-2). While erosion estimates for basins are underrepresented in this dataset, there remains some uncertainty whether slightly higher depths of erosion might be expected over depressions. Future work is required to shed light on this. It is also important to note that these projected depths of erosion are highly dependent on the assumption that glacial erosion in the past is representative of glacial erosion in the future.

Table 5-2. Projected future total erosion of the Forsmark region over the coming 1 Ma based on cosmogenic nuclide-derived simulated glacial erosion values and projected future ice cover periods (Lord et al. 2019).

	Most likely 1 Ma erosion depth (m)		Wider range 1 Ma erosion depth (m)	
Emission scenario	**Glacial erosion rate: 40–89 mm/ka**	**Glacial erosion depth: 39–109 cm/glaciation**	**Glacial erosion rate: 16–144 mm/ka**	**Glacial erosion depth: 14–166 cm/glaciation**
Natural	11–28 m	7–24 m	4–43 m	3–35 m
RCP 2.6	11–27 m	8–25 m	4–42 m	3–37 m
RCP 4.5	9–24 m	7–22 m	4–36 m	2–32 m
RCP 8.5	5–15 m	5–18 m	2–21 m	2–24 m

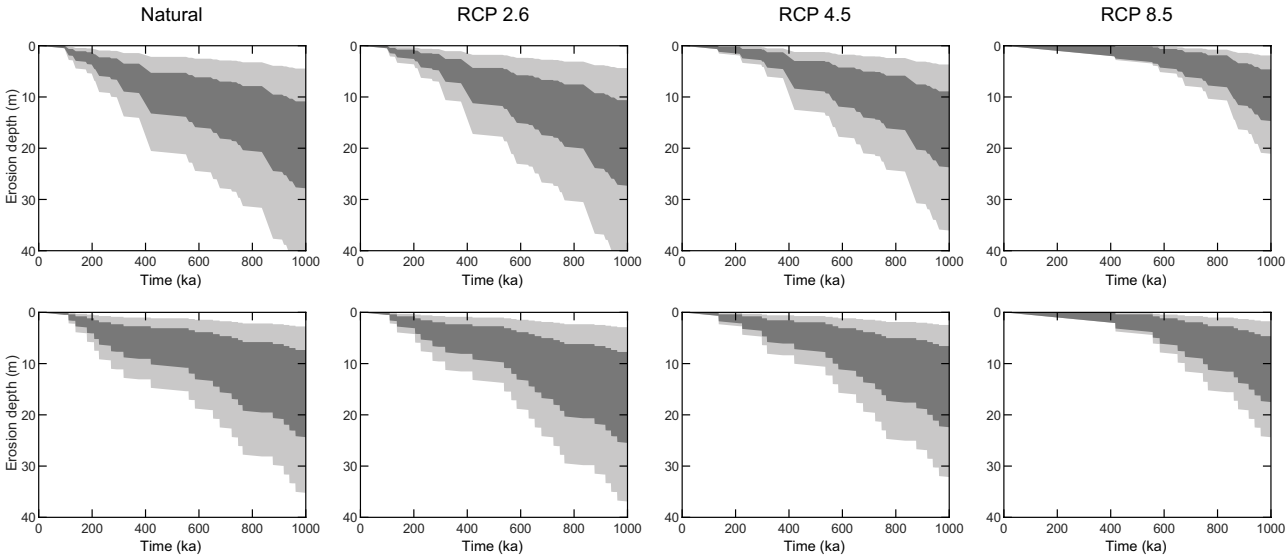

Figure 5-15. *Projected future total erosion depths of the Forsmark region based on simulated past glacial erosion rates and depths and projected future ice cover periods over Forsmark over the coming 1 Ma. (Lord et al. 2019). The upper panels show the total erosion (glacial and non-glacial) for scenarios with constant glacial erosion rates and the lower panels shows the total erosion (glacial and non-glacial) for scenarios with constant glacial erosion depth at the end of each ice cover period. The dark grey areas show a mid-range of future total erosion depths based on the interquartile range of simulated past combined ^{10}Be and ^{26}Al erosion values. The light grey areas show a wider range of projected erosion depths based on the 5–95 percentile range of the simulated past combined ^{10}Be and ^{26}Al erosion values. All projections yield less than 1 m erosion over the coming 100 ka and less than 43 m erosion over the coming 1 Ma.*

5.5 Summary

To investigate glacial erosion of low-relief topography in Uppland beneath the Fennoscandian Ice Sheet we have measured ^{10}Be and ^{26}Al in 32 surface bedrock samples, three boulder samples, and two depth profile samples. The timing and rates of regional deglaciation and isostatic rebound are well-constrained. Simple surface bedrock exposure ages range from 2 to 71 ka. Taking the shielding by water during isostatic rebound into account, all samples but one have ^{10}Be and ^{26}Al concentrations higher than commensurate for deglaciation, with the mid-range samples being 3.4–9.6 ka too old. This cosmogenic nuclide inheritance due to prior exposure enables us to explore model space for past glacial erosion. Tracking the cosmogenic nuclide production rate over time and depth, we simulate the build-up of ^{10}Be and ^{26}Al under a range of scenarios with varying ice cover durations, subaerial erosion rates, and modes of glacial erosion (constant erosion rate or constant erosion depth for each ice cover period). Under these assumptions, and if excluding one sample, the simulations yield glacial erosion lower than 0.4 m/ka or 3.5 m per ice cover period. For most of the samples for which we yield a solution for both ^{10}Be and ^{26}Al, glacial erosion was restricted to 0.04–0.09 m/ka or 0.4–1.1 m per ice cover period. Over the last 100 ka, this translates into a total erosion of only 1.6–3.5 m. The amount of cosmogenic nuclide inheritance / glacial erosion in the surface bedrock samples scatters across the landscape with an apparent stochastic nature. For one hill with the highest inheritance and with multiple samples, cosmogenic nuclide inheritance decreases, and glacial erosion increases with distance from and height below the summit. For the full set of samples, there is, however, no correlation with local topography (elevation, relative topography, relief) or with geological factors (fracture spacing, rock hardness). Considering the complexity of glacial erosion processes and the non-linear depth dependence of cosmogenic nuclide production rates, the glacial erosion is still well-clustered and relatively low.

To project glacial erosion in future glaciations, we use the simulated glacial erosion rates/depths together with the output from a study modelling future glaciations over Forsmark under a set of greenhouse gas emission scenarios. For the coming 100 ka, projected total erosion is less than 1 m, and for the coming 1 Ma, the most likely total erosion range from 5 to 28 m.

Ancillary data (Appendix 5)

As part of this study we wrote two new functions based on the expage calculator and one function for calculating summed percentiles from a number of minimum-maximum ranges.

1. expage_sealevel.m
2. glacialE_sealevel.m
3. range_percentile.m

6 Conceptual understanding of erosion in Uppland

The motivation for the glacial erosion study was to assess the past and future impact of glacial erosion on the site of the planned geological repository for spent nuclear fuel at Forsmark. The research undertaken in this study informs safety assessments in relation to future periods of glaciation over the next 0.1–1 Ma. The study relates to four research strands and the main findings, limitations and next steps for each strand are summarised below.

6.1 Erosion and burial history of the basement in Uppland

This study has identified the importance of the sub-Jotnian (U1) unconformity as a fundamental surface for understanding the erosion history of Uppland. A close proximity of U1, U2 (the sub-Cambrian unconformity) and the present erosional level of the basement (UQ) is manifest close to the edge of the Jotnian sedimentary cover on the seabed off north Uppland (Figure 2-7) and in the Öregrundsgrepen (Figure 2-11). Here, flat-lying Jotnian and Ordovician sedimentary outliers rest on low relief basement surfaces at similar elevations within a distance of 4 km (Figure 2-6). West of Singö, several small grabens, half-grabens and basins retain Jotnian sandstones (Figure 2-8). Displacement of overlying Ordovician limestones indicate Phanerozoic fault reactivation. Thick Jotnian sedimentary rocks formerly covered the basement of Uppland, including the Forsmark area, but had been largely eroded by the end of the Late Neoproterozoic, when extensive areas of basement were re-exposed. Uncertainties remain over the position of U1 in relation to the present basement, particularly in areas further south and west in Uppland where post-U1 basement erosion of several hundred metres is likely around the Björkö impact structure. Potential fracture development beneath U1 and the formation of fracture coatings below Jotnian red beds have received little attention. The Uppland area also has yet to be examined in the wider context of Precambrian basement erosion around the margins of the Mesoproterozoic basin of the Bothnian Sea.

Little detailed attention has been given previously to the sub-Cambrian unconformity in Uppland and to the significance of the Ordovician outliers found in the vicinity of Forsmark and in the Singö archipelago. Seismic surveys of the sea bed date mainly from the 1970s and 1980s (Flodén 1980, Flodén et al. 1980, Winterhalter et al. 1981) and there is a need for new work to check for the presence of unrecognised outliers and to better understand the geology of known occurrences. Recent advances in understanding of Cambrian and Ordovician sequence stratigraphy (Nielsen and Schovsbo 2011, 2015) have highlighted a important difference between the sedimentary sequence on the Åland ridge and in other parts of Sweden. On this ridge, which extends westward to include Uppland, Early Cambrian sands and silts were removed by erosion during the Hawke Bay regression prior to renewed marine transgression and deposition of Alum Shale and Ordovician limestone. The Cambrian basement unconformity (U2) is here recognised in Uppland as a diachronous planation surface of polygenetic origin. U2 first developed as a subaerial planation surface in the Neoproterozoic but was graded and re-exposed by shoreline erosion during the Early Cambrian before burial. The significance of long phases of basement exposure during the late Neoproterozoic for fracture development, opening and mineralization beneath U2 remains to be further explored.

The sub-Cambrian unconformity in Uppland is part of a much wider unconformity on Baltica. U2 is a product of three main phases of denudation: (i) prolonged and deep denudation of basement and cover through the Neoproterozoic, including glacial erosion in the Cryogenian, (ii) weathering, fluvial erosion and extensive planation in the Ediacaran after ~584 Ma as Baltica drifted from high to low latitudes and (iii) shoreline erosion through the Cambrian in multiple transgressive-regressive cycles as Baltica was flooded under generally rising sea levels. Further work is required to better understand the timings of these phases and the processes and rates of erosion operating during each phase. Such work would allow comparisons with the coeval Great Unconformity on Laurentia (Peters and Gaines 2012, Keller et al. 2019).

6.2 Morphology of the sub-Cambrian unconformity

Near planar surfaces are typical of the buried sub-Cambrian unconformity in Västergötland and around Närke (Figure 2-13). Extensive low relief basement surfaces extend away from these outliers and become progressively more dissected and rougher with distance (Figure 2-15). Large hills are absent over wide areas, unlike in areas of basement that were exposed to Mesozoic and Cenozoic deep weathering and where undulating hilly relief is typical (Lidmar-Bergström 1995). Another characteristic feature of the sub-Cambrian unconformity in southern Sweden is the dislocation of near planar basement surfaces by post-Ordovician, partly post-Early Permian faulting, to produce tilted fault blocks. The emergence of the faulted, near planar U2 surface from below Cambrian to Ordovician cover is manifest at Närke (Figures 2-16 and 2-17).

Inheritance of the low relief on the exposed basement in Uppland from the sub-Cambrian (U2) unconformity is indicated by the presence of similar basement relief below Ordovician limestones in the Bothnian Sea and the emergence of this relief off Forsmark. The low elevation ranges of basement summits and the numerous post-Ordovician fault blocks are features that are typical of the sub-Cambrian unconformity in south-central Sweden. New fault block maps allow more precise examination of differences in form and elevation across adjoining fault blocks in Uppland (Grigull et al. 2019). Previous interpretations are supported of the present basement surface (UQ) in Uppland as representing the re-exposed and block-faulted U2 surface, modified by glacial erosion. The models of U2 rest, however, on assumptions that U2 was originally a near planar surface, without deep Neoproterozoic weathering at the time of burial, overlain by Ordovician limestone and broken by minor, post-Ordovician faulting. Further research is required to better constrain the morphology, weathering characteristics and dislocation of the U2 surface across Uppland to allow comparisons with basement surfaces of similar age and origin elsewhere in Fennoscandia (Lidmar-Bergström et al. 2012) and in former parts of Laurentia (Parnell et al. 2014).

The elevation differences between the original position of U2 and present basement summit is difficult to constrain precisely in Uppland because of the restricted number and areal extent of submerged Ordovician outliers. Where Ordovician cover remains on the tilted fault block that rises towards Forsmark (Figure 2-11), the elevation range of basement summits is ~10 m. Small elevation differences between the buried and exposed basement surface are consistent with the inheritance of low relief from the Cambrian uniformity around outliers. Further work is underway to constrain height differences between U2 and UQ around the edges of other Early Palaeozoic outliers that lie further S in Sweden (Hall et al. 2019a).

6.3 Pleistocene re-exposure of the basement

The re-exposure of the basement in Uppland has been loosely assigned to the Cenozoic (Sandström and Tullborg 2009, Sandström et al. 2009) but in Section 4.1.2 it is suggested that final removal of Ordovician limestone cover in the Forsmark area dates from after 1.1 Ma. This hypothesis recognises that overdeepening of Mesoproterozoic and Early Palaeozoic basins offshore and in the Öregrund archipelago must have been a product of erosion by the Fennoscandian Ice Sheet. Before 1.1 Ma, the Fennoscandian Ice Sheet was of restricted extent and expanded to cover the Forsmark area only for brief periods (Kleman et al. 2008). As the Bothnian River appears to have operated until 1.1 Ma, basin excavation below present sea level is younger. In Fennoscandia, the Menapian cold stage is recognised as perhaps the first period when the Fennoscandian Ice Sheet extended close to the maximum limits reached subsequently in the Middle Pleistocene (Ehlers et al. 2018). Accelerated erosion from this time links the onset of excavation of the Bothnian and Baltic Sea basins to overdeepening in the Kattegat (Houmark-Nielsen 2004), Skagerrak and the Norwegian Trench (Sejrup et al. 2000). The history of the Eridanos river system from the Eocene onwards is, however, poorly known in areas surrounding the Bothnian basin (Gibbard and Lewin 2016). One approach to constraining the timing of final removal of Ordovician limestone cover across Uppland may be in further analyses of calcite and other late coatings in basement fractures at Forsmark. An abundant supply of carbonate from solution of the thinning limestone cover ended with its final removal. A second approach is to trace detritus sourced from basement in Uppland and around other areas around the Bothnian Sea in Neogene to Late Pleistocene sediments in the southern parts of the Baltic basin on the East European Plain by using clast lithology (Czubla et al. 2019), heavy minerals and detrital zircon ages (Overeem et al. 2001, Knudsen et al. 2005, Gibbard and Lewin 2016).

6.4 Topographic perturbations of near-surface bedrock stresses, fracture development, and possible links to glacial erosion at Forsmark

We assessed how present topography may perturb near-surface stress fields at Forsmark to impart control on which fractures may open and where in the landscape and subsurface they open. We did this using a three-dimensional boundary element model and considered influences from pore pressure and sediment loading on the near-surface stress fields. This modelling showed that topography may strongly perturb near-surface stress-fields in the uppermost 100 m, even in this low relief landscape. The topographic perturbation declines with depth and is minor at depths below 400 m. The model predicts that sub-horizontal fractures will more likely open beneath convex landforms perpendicular to the maximum horizontal compressive stress (directed NW–SE), i.e. particularly those landforms with long axes oriented NE–SW. This may produce higher erosion rates on ridges and lower erosion rates in valleys that display this orientation and might result in overall relief reduction through glacial erosion. Conversely, the higher magnitudes of the least compressive horizontal stress beneath ridges and valleys oriented parallel to the maximum horizontal compressive stress may mean they are more resistant to glacial erosion and relief may persist or increase, rather than decrease. Finally, it appears that some valleys might be in tension, which would favour opening of sub-vertical fractures in these locations. Glacial erosion rates might therefore be higher in these valleys, potentially increasing local relief. In summary, even in this low-relief landscape, topography may exert control on near-surface bedrock fracturing and patterns and depths of glacial erosion. Further research is needed to explore other controls on present fracture openness including contributions of antecedent conditions as far back as 1.9 Ga. Topographic stress perturbations are also likely to have interacted with groundwater overpressure underneath the Fennoscandian Ice Sheet, which has been modelled previously to extend to depths of 500 m. Future work on elucidating how perturbations of ambient stresses through surface effects such as topography and pore water pressure should be based on data sets on fracturing from the uppermost tens of meters and include a temporal component regarding ice sheet loading, unloading, and its effects on pore water pressures. It should also target explicit testing of model predictions of fracture opening and glacial erosion through cosmogenic nuclides in locations favorable to the application of this technique, such as minimal shielding of bedrock by sediments.

6.5 Glacial bedforms and erosional processes in NE Uppland

Geomorphological evidence presented here confirms strong control of fracture patterns on landforms of glacial erosion across scales in Uppland. The availability of detailed fracture data for the rock surface and at depth at Forsmark provides future opportunities to quantify the links between fracturing and glacial erosion processes. The near-planar form of U2 across broad areas provides unusual opportunities in south-central Sweden to explore the emergence of distinctive glacial relief forms during progressive glacial erosion. Improved understanding of patterns and origins of the roughness of glaciated bedrock terrain across scales in Uppland may provide further insights into patterns and processes of glacial erosion. At the regional and local scales, glacial erosion has acted to lower and roughen the surface of the former U2 unconformity. The largest features of glacial erosion in Uppland are the rock trenches, many km long, and basins up to 30 km^2 in area, that have been excavated within fracture zones to depths of 20 m or more. Analysis of detailed subsurface data available for Forsmark, combined with information on fracturing provided from boreholes and excavation may allow further investigations of the origins of these features. The excavation of trenches can also be explored using models of subglacial hydrology below the Fennoscandian Ice Sheet (Shackleton et al. 2018). Three discrete terrain types – glacially-roughened, weakly-streamlined and disrupted terrain (Figure 4-19) – are identified in Uppland but the glaciological controls on their distributions are not yet clear. The potential impact of headward erosion through the extension of fjärd heads towards Forsmark also has yet to be properly evaluated. Landforms at the local scale and below have been logged mainly in inventories and there is a need for further detailed mapping of glacial erosion forms at different scales and to link the bedrock morphology of the present onshore and offshore areas. Initial modelling of the forces required to move bedrock blocks at the ice sheet base have yielded promising results (Krabbendam and Hall 2019) but further work is needed to consider more complex rock block shapes and the role of internal fracture patterns. The models can

also be tested in glaciated granite terrains, such as the Cairngorms (Goodfellow et al. 2014) or the Ross of Mull (Petronis et al. 2012), Scotland, where orthogonal fracture sets are associated with the development of upstanding bedrock blocks of different sizes but simple shapes. Further understanding of spatial and temporal variations in glacial erosion by the Fennoscandian Ice Sheet at the local and regional scales in the Forsmark area requires the development of ice sheet models dedicated to exploring the controls on processes and rates of glacial erosion that operate across scales.

Glacial ripping involves the combined operation of hydraulic jacking, fracture dilation and bedrock disruption, and local glacial transport of large boulders. The process set appears to operate effectively during deglaciation where groundwater overpressure develops beneath the ice margin. As hydraulic jacking is modelled to operate at considerable depths in fractured basement at Forsmark (Lönnqvist and Hökmark 2013, Hökmark and Lönnqvist 2014) and as physical evidence of jacking is widely present in the upper ~ 10 m of the rock pile (Carlsson 1979, Carlsson and Christiansson 2007), associated disruption and glacial entrainment has the potential, at least locally, to remove rock sheets of considerable depth over wide areas. The physical evidence for bedrock disruption includes spreads of large, angular boulders that have previously been cited as critical evidence of mega-earthquakes (Mörner 2004). Available evidence reported previously (Lagerbäck et al. 2005) and in this report, however, strongly supports a glacial origin for disrupted roches moutonnées and boulder spreads. Further detailed geomorphological mapping of features associated with glacial ripping is required in order to constrain the extent, depth and context of the operation of this process set. Better understanding may also emerge from modelling of dynamic subglacial hydrogeology in relation to jacking and fracture dilation and of the tractive forces operating on rock surfaces at the bed of the Fennoscandian Ice Sheet.

6.6 Pleistocene glacial erosion in NE Uppland: depths and patterns based on geomorphological evidence

Initial phases of erosion by the Fennoscandian Ice Sheet likely involved the thinning and removal of more extensive Early Palaeozoic cover. Small grabens in the archipelago SE of Forsmark have lost thicknesses more than 30–40 m of Jotnian and Ordovician sedimentary fill and similar thickness may have been removed from the Forsmark area. Further investigation is needed to establish the total thicknesses of sedimentary rock removed by overdeepening of the Bothnian and Baltic basins through the Pleistocene.

Removal of sedimentary cover re-exposed the low relief basement surface of the U2 unconformity. The continuity of low relief and the consistently narrow elevation range of summits across wide areas (Figure 2-15) indicates limited erosion of basement since the re-exposure of U2. Consideration of scenarios of 1, 10 and 50 m erosion of summits below U2 suggest that the 10 m erosion estimate, whilst lacking precise constraints in Uppland, provides the best fit to the geomorphological evidence. A 50 m erosion estimate would imply that the present basement topography is not inherited from U2 and that the landforms on the present landsurface are entirely of glacial origin. This high estimate is considered unlikely as the basement surface of Uppland lacks features such as high roughness (Taylor et al. 2004, Falcini et al. 2018) or advanced streamlining (Bradwell et al. 2008) typical of landscapes of deep glacial erosion in crystalline bedrock. Laterally-extensive, accordant summit elevations also appear incompatible with sustained, deep differential erosion across variably fractured basement. Comparisons of present bedrock topography with summit envelope surfaces provide estimates of depths of glacial erosion. The estimated mean erosion depth of basement is 14 m across NE Uppland (Figure 4-46), 12 m (Figure 4-47) in the Forsmark area and is 8 m in the repository footprint area (Figure 4-48). A preliminary estimated thickness of 10 m of summit erosion on fault block tops should be added to these estimates. The original elevation of U2 above present summits perhaps represents the main uncertainty for these estimates. This estimate for summit erosion is less than modelled erosion depths with mid-range constant glacial erosion over the last 1 Ma of 13–27 m based on cosmogenic nuclide inventories. The difference may indicate underestimation of the depth of summit erosion in basement using geomorphological evidence, or post-1 Ma erosion of cover rocks to re-expose basement or model limitations.

Glacial modification of the sub-Cambrian unconformity surface has varied with scale. At the landscape (10–100 km) scale, the main impact of the Fennoscandian Ice Sheet has been to lower and roughen the unconformity but the marked differences in roughness between Uppland and areas to the west and south indicate that differences in the timing of basement re-exposure may be important controls on topographic roughness at this scale. At the regional (1–10 km) scale, glacial erosion has increased relative relief and roughness. Progressive glacial modification is evident from the contrasting morphologies of adjacent fault blocks (Figure 4-16). On five high points on the Ironworks block, differences in cosmogenic nuclide inheritance indicate spatially variable depths of glacial erosion in the last glacial cycle but no comparable data is available for low points. At the local scale (0.1–1 km), glacial modification of hills has involved a range of erosional processes. The strong control of fracture spacing on glacial erosion rates has increased relative relief and topographic roughness, with slower erosion on resistant rock knobs than along trenches and in basins where fractures are closely spaced. Low relief may have been maintained locally during glacial erosion, however, at sites affected by glacial ripping, a process capable of both the disruption and removal of large roches moutonnées and the removal of thin (a few metres-thick) layers of fractured rock. The overall pattern of glacial modification of the U2 surface in Uppland indicates that roughening generally dominates and is quite different to the smoothing proposed in recent models (Egholm et al. 2017).

6.7 Glacial erosion in the last glacial cycle: estimates from cosmogenic nuclides

To investigate glacial erosion of low-relief topography in Uppland beneath the Fennoscandian Ice Sheet we have measured ^{10}Be and ^{26}Al in 32 bedrock samples. The timing and rates of regional deglaciation and isostatic rebound are well-constrained. Simple exposure ages range from 2 to 71 ka. Taking the shielding by water due to isostatic rebound into account, all samples but one have ^{10}Be and ^{26}Al concentrations higher than commensurate with the concentrations being simple measures of exposure after deglaciation, with most samples being 3.5–10 ka too old. This cosmogenic nuclide inheritance due to prior exposure enables us to explore model space for past glacial erosion. Tracking the cosmogenic nuclide production rate over time and depth, we simulate the build-up of ^{10}Be and ^{26}Al under a range of scenarios with varying ice cover durations, subaerial erosion rates, and modes of glacial erosion (constant erosion rate or constant erosion depth for each ice cover period). Under these assumptions and if excluding one sample with minimal cosmogenic nuclide inheritance, the simulations yield Quaternary glacial erosion lower than 0.4 m/ka or a thickness of 3.3 m per ice cover period. For a mid-range of the samples for which there is a solution for both ^{10}Be and ^{26}Al, glacial erosion was restricted to 0.04–0.09 m/ka or 0.4–1.1 m per ice cover period. For the last glacial cycle (last 100 ka), this translates into a total erosion of only 1.6–3.5 m. A comparison with previously published ^{10}Be and ^{26}Al data from bedrock samples in low-relief regions of Fennoscandia lends support to limited glacial erosion, with a large number of samples displaying cosmogenic nuclide inheritance (Stroeven et al. 2016).

Further work is needed to extend our coverage of erosion estimates based on cosmogenic nuclide inventories. Our sample set was reduced in size because of difficulties in cleaning quartz and because micro-crystalline quartz was abundant. Both factors may reflect the long metamorphic history of these basement rocks. Our sample strategy was also focussed on rock summits but the assumption that these are the slowest eroding parts of the landscape requires further testing. Results from around Wave Rock are consistent with low erosion rates across this low hill summit relative to its immediate surroundings. Other summits, flanks and bases of other hills should be sampled however, and sampling should include depth profiles from drill cores beneath summits in order to better understand patterns of erosion operating over individual hills during the last glaciation and earlier periods. Future cosmogenic nuclide analyses may focus on providing erosion estimates on rock surfaces in topographic lows, and on testing further how fracture spacing links to glacial erosion rates across the landscape (Dühnforth et al. 2010),. Shielding by present or former sediment is, however, problematic in topographic lows. Such estimates would better constrain the variability of glacial erosion across bedrock highs and lows. The potential of headward erosion to extend NW towards Forsmark can also be explored by providing erosion rates estimates around fjärd heads.

6.8 Future glacial erosion

Future glacial erosion at the Forsmark site may be considered on the basis of evidence for past erosion from geomorphology and cosmogenic nuclides. Assuming re-exposure of basement at 1.1 Ma before present and steady erosion rates, estimated average depths of glacial erosion of basement are ~2 m per glacial cycle. In basins and trenches, erosion rates may exceed 3 m per glacial cycle. Hydraulic jacking and fracture dilation have potential to prepare greater depths of rock for removal by glacial ripping but the past extent and impact of the ripping process set requires detailed investigation to constrain potential future erosion depths.

Potential future depths of glacial erosion at the Forsmark site can be derived through a combination of simulations of glacial erosion based on cosmogenic ^{10}Be and ^{26}Al nuclides with simulated scenarios of future ice sheet cover at Forsmark over the coming 1 Ma based on IPCC emission scenarios and future variations in insolation (Lord et al. 2019). Projected depths of total erosion for the Forsmark site over the coming 100 ka are less than 1 m. Over the coming 1 Ma, the mid-range total erosion depth range is 5–28 m, and the wider range of total erosion depth is 2–43 m. It is important to note that these projected depths of erosion are highly dependent on the assumption that glacial erosion in the past is representative of glacial erosion in the future.

7 Conclusions

In this final section, the scientific results and interpretations of this study are presented in terms relevant to assessing the long-term safety of the planned geological repository for spent nuclear fuel in Forsmark.

The Fennoscandian craton first stabilised after the Svecokarelian orogeny in east central Sweden. The basement was reduced to low relief by 1.5 Ga at the sub-Jotnian (U1) unconformity. The proximity of U1 to the present-day erosion level offshore from Forsmark in Öregrundsgrepen indicates that total Neoproterozoic and Phanerozoic denudation of basement has been negligible. Depths of basement erosion over the last 1.5 Ga in Uppland are amongst the lowest known on the Earth's cratons, a product of tectonic stability and prolonged burial.

During the Neoproterozoic, a km thick Jotnian sandstone cover was removed to re-expose the basement. A peneplain formed during a period of more than 40 Ma of subaerial weathering and erosion close to base level. This surface formed the sub-Cambrian unconformity (U2) and was later graded by shoreline erosion during marine transgression in the Early Cambrian, re-exposed to minor erosion and later reburied beneath Middle Cambrian Alum Shale and Early Ordovician limestone. Our reconstructions support previous interpretations that the present basement surface across large parts of Uppland represents the re-exposed sub-Cambrian unconformity, modified by Pleistocene glacial erosion. The basement summits in the vicinity of Forsmark lie close to the former unconformity and indicate very limited erosion of basement since 541 Ma.

Sediment eroded from the Caledonide orogenic belt buried the basement to depths of up to 2 km in the Palaeozoic. Cover rocks were thinned by erosion through the Mesozoic and Cenozoic but there is no evidence that the basement in the Forsmark area was exposed to weathering prior to Pleistocene glaciation. Over-deepening of Mesoproterozoic basins in the Åland Sea and small grabens in the Öregrund archipelago and final removal of Early Palaeozoic cover from the Forsmark area probably dates from the Menapian glaciation at 1.1 Ma, when the Bothnian River system ceased to operate after erosion by the Fennoscandian Ice Sheet.

New fracture sets and fracture coatings may have developed at Forsmark during exposure of U1 and U2. Dislocation of the U2 unconformity is post-Ordovician in age and may be coeval with Late Carboniferous-Early Permian rifting in the Oslo graben. Previous and new reconstructions of fault block location and tilt are supported by topographic profiles, with vertical displacement of blocks by, at most, a few tens of metres. The dislocated, re-exposed U2 surface is most closely represented by fault blocks with tops that show < 5 m bedrock relief over km-wide areas.

Pleistocene glacial erosion at Forsmark led to removal of Ordovician limestone and lowering of the underlying hard, fractured basement surface. Removal of soft, bedded and jointed sedimentary cover involved the loss of at least several tens of metres of cover rock based on the 30–40 m depths of glacially excavated sub-Jotnian and Cambrian basins in the archipelago E of Forsmark.

The preservation of low, exhumed fault scarps and fault block tops with < 5 m relief in Uppland indicate a proximity of basement highs that is likely within 10 m to the U2 surface. Summit envelope surface models indicate that an average of 14 m of rock has been lost to glacial erosion of basement across NE Uppland, with increasing depths of erosion towards the south. In the Forsmark area, the equivalent depth is 12 m. To these estimates should be added the < 10 m depth of rock lost from summits below the original modelled level of U2. The greatest volumes of glacially eroded rock came from rock trenches and basins, 10–20 m deep, excavated along fracture zones. These estimates rest on assumptions that U2 was originally a near planar surface, without deep Neoproterozoic weathering at the time of burial, overlain by Ordovician limestone and broken by minor, post-Ordovician faulting. The estimates also may be too low if glacial erosion has been spatially uniform, allowing maintenance of exhumed fault blocks, with inclined tops with accordant summit elevations, during lowering of > 10 m by glacial erosion.

Glacial erosion by the Fennoscandian Ice Sheet led to the development of a nested hierarchy of glacial landforms. Three types of glacial terrain are recognised at the local scale: (i) ice-roughened, (ii)

weakly streamlined and (iii) disrupted terrain. Ice-roughened terrain is dominated by roches moutonnées and box hills, with fracture-guided trenches and box and star basins. Weakly streamlined terrain includes elongate hills, with till tails, and parallel trenches aligned with fracture sets and former ice flow. Glacially disrupted terrain is characterised by extensive spreads of large, angular boulders that mask underlying bedrock. Landform assemblages seen at different scales are linked to sets of glacial processes grouped as abrasion, plucking, ripping and meltwater erosion.

Glacial ripping is a newly recognised process set that involves the jacking, disruption and entrainment of rock blocks, with the formation of extensive spreads of large, angular boulders. The process of ripping requires groundwater overpressure, possibly with high volumes of meltwater, beneath the retreating margin of the Fennoscandian Ice Sheet. The ripping process set is an important, perhaps locally dominant agent of glacial erosion in the Forsmark area that operated locally to depths of at least several metres during deglaciation.

The evolving topography beneath the re-exposed U2 unconformity may have contributed to fracturing in ways that influenced further glacial erosion in the Pleistocene. A mechanically-based boundary element model is applied in which the total stress field is calculated as the sum of the ambient stress due to gravity and tectonics and the stress perturbation from topography and groundwater pressure. Whereas the regional surface gradient and present topographic relief are low (1 m/km and < 20 m, respectively), both parameters increase in the adjacent offshore region and topographic curvatures are frequently high, particularly on the flanks of trenches and basins and on hills and ridges. In addition, Forsmark is characterized by high maximum horizontal compressive stresses (15–24 MPa) in the shallow subsurface. The model predicts that sub-horizontal fractures will more likely open beneath convex landforms perpendicular to the maximum horizontal compressive stress (directed NW–SE), i.e. particularly those landforms with long axes oriented NE–SW. This may produce higher erosion rates on ridges and lower erosion rates in valleys that display this orientation and might result in overall relief reduction through glacial erosion. Conversely, the higher magnitudes of the least compressive horizontal stress beneath ridges and valleys oriented parallel to the maximum horizontal compressive stress may mean they are more resistant to glacial erosion and relief may persist or increase, rather than decrease. It further appears that some valleys might be in tension, which would favour opening of sub-vertical fractures in these locations. Glacial erosion rates might therefore be higher in these valleys, potentially increasing local relief. The topographic influence on stress fields is strongest in the uppermost 100 m. and the present topography may exert control on near-surface bedrock fracturing, even in this low relief landscape.

Paired cosmogenic ^{10}Be and ^{26}Al nuclide concentrations were measured for 32 surface bedrock samples along a transect that extends 50 km ~ 50 km SSW from Forsmark, and three boulder samples at the coast. The samples are primarily collected from local high points in the landscape because these sites are least impacted by shielding effects caused by sediment covers. Compared to the expected cosmogenic nuclide concentration based on the timing of deglaciation and emergence from water, all cosmogenic nuclide samples show inheritance from prior exposure equivalent to 0.5–69 ka surface exposure, with most samples being 4–10 ka too old. For a suite of ice-cover, submergence and weathering scenarios and assuming that each glaciation eroded with a similar erosion mode (constant erosion rates or constant incremental depth erosion), a mid-range of the paired ^{10}Be and ^{26}Al data yield 1.6–3.5 m erosion over the last 100 ka, and 13–27 m erosion over the last 1 Ma. For simulations starting at 1 Ma, those with constant glacial erosion rate (erosion scaled against duration of ice cover) typically yields erosion depths of 1.4 m to 2.5 m over the last 100 ka and 11 m to 18 m over the last 1 Ma. Simulations with constant erosion depths (erosion scaled against number of ice cover periods), yield instead typical erosion depths of 1.9 m to 4.3 m over the last 100 ka and 12 m to 30 m over the last 1 Ma. From one hill with seven analysed samples, the pattern of cosmogenic nuclide inheritance indicates lowest erosion across the hill top and more intense erosion around its base. Nineteen samples from low elevation (0–24 m a.s.l.) within 4 km of the power plant and proposed repository site yield total erosion since 100 ka of 0–8.6 m. The three boulder samples all yield inheritance of similar magnitude to the bedrock samples equivalent to 2–41 ka of surface exposure. The three boulder samples all yield inheritance of similar magnitude to the bedrock samples equivalent to 2–40 ka of surface exposure. The results support an interpretation of limited glacial erosion as the boulders must have experienced exposure prior to the last ice-cover period and thereby have been located at shallow depth. The erosion depths over 1 Ma are larger than the estimate of up to 10 m lowering of basement summits below U2 based on geomorphological evidence. The

higher 1 Ma erosion depths derived from cosmogenic nuclides may include removal of cover rocks or simply reflect erosion of basement rock. If the latter, the 10 m estimate for U2 lowering based on geomorphological evidence is too low. Both options are consistent with re-exposure of basement from below Early Palaeozoic cover rocks by glacial erosion within the last 1.1 Ma.

Safety assessment for the proposed nuclear waste repository site requires consideration of glacial erosion under future ice sheets. To estimate potential future depths of glacial erosion at the Forsmark site, we combine simulations of glacial erosion based on ^{10}Be and ^{26}Al cosmogenic nuclides with projections of future ice sheet cover at Forsmark over the coming 1 Ma from ice sheet modelling based on IPCC emission scenarios and future variations in insolation (Lord et al. 2019). Projected depths of total erosion for the Forsmark site over the coming 100 ka is less than 1 m. Over the coming 1 Ma, the mid- range of total erosion depth is 5–28 m, and the wider range of total erosion depth is 2–43 m. It is important to note that these projected depths of erosion are highly dependent on the assumption that glacial erosion depths in the past are representative of glacial erosion depths in the future.

References

SKB's (Svensk Kärnbränslehantering AB) publications can be found at www.skb.com/publications.

Abels A, Mannola P, Lehtinen M, Bergman L, Pesonen L J, 1998. New observations of the properties of the Lumparn impact structure, Åland Islands, southwestern Finland. Meteoritics and Planetary Science Supplement 33, A7.

Abels A, Plado J, Pesonen L J, Lehtinen M, 2002. The impact cratering record of Fennoscandia. In Plado J, Pesonen L J (eds). Impacts in Precambrian Shields. Berlin: Springer, 1–58.

Aber J S, 1985. The character of glaciotectonism. Geologie en Mijnbouw 64, 389–395.

Aber J S, Croot D G, Fenton M M, 1989. Hill-hole pair. In Aber J S, Croot D G, Fenton M M. Glaciotectonic landforms and structures. Dordrecht: Springer, 13–28.

Agrell H, 1981. Gillberga Gryt – En sentida sprickgrotta i Uppland. Sveriges Speleolog-Förbund, Grottan Nr 4. (In Swedish.)

Ahlbom K, Tirén S A, 1991. Overview of geologic and geohydrologic conditions at the Finnsjön site and its surroundings. SKB TR 91-08, Svensk Kärnbränslehantering AB.

Ahlbom K, Andersson P, Ekman L, Gustafsson E, Smellie J, Tullborg E-L, 1986. Preliminary investigations of fracture zones in the Brändan area, Finnsjön study site. SKB TR 86-05, Svensk Kärnbränslehantering AB.

Ahlin S, 1987. Phanerozoic faults in the Västergötland basin area, SW Sweden. GFF 109, 221–227.

Albrecht J, 2005. Forsmark site investigation. study of Quaternary sediments in connection with investigations of bedrock lineaments. SKB P-05-138, Svensk Kärnbränslehantering AB.

Alm E, Huhma H, Sundblad K, 2005. Preliminary Palaeozoic Sm-Nd ages of fluorite-calcite-galena veins in the southeastern part of the Fennoscandian Shield. SKB R-04-27, Svensk Kärnbränslehantering AB.

Amantov A, 1995. Plio Pleistocene erosion of Fennoscandia and its implications for Baltic area. In Proceedings of the Third Marine Geological Conference "The Baltic". Warszawa, 47–56. (Prace Panstwowego Instytutu Geologicznego 149)

Amantov A, Fjeldskaar W, 2013. Geological-geomorphological features of the Baltic region and adjacent areas: imprint on glacial-postglacial stages of development. Regional Geology and Metallogeny 53, 90–104.

Amantov A, Hagenfeldt S, Soderberg P, 1995. The Mesoproterozoic to lower Palaeozoic sedimentary bedrock sequence in the northern Baltic proper, Aland Sea, Gulf of Finland and Lake Ladoga. In Proceedings of the Third Marine Geological Conference "The Baltic". Warszawa, 19–25. (Prace Panstwowego Instytutu Geologicznego 149)

Amantov A, Laitakari I, Poroshin Y, 1996. Jotnian and Postjotnian: sandstones and diabases in the surroundings of the Gulf of Finland. Geological Survey of Finland, Special Paper 21, 99–114.

Amantov A, Fjeldskaar W, Cathles L, 2011. Glacial erosion/sedimentation of the Baltic region and the effect on the postglacial uplift. In Harff J, Björck S, Hoth P (eds). The Baltic Sea basin. Berlin: Springer, 53–71.

Andersson A, Dahlman B, Gee D G, Snäll S, 1985. The Scandinavian alum shales. Uppsala: Sveriges geologiska undersökning. (Ser. Ca 56)

Andersson J, Christiansson R, Hudson J, 2002. Site investigations. Strategy for Rock Mechanics Site Descriptive Model. SKB TR-02-01, Svensk Kärnbränslehantering AB.

Andersson M, Malehmir A, Troll V R, Dehghannejad M, Juhlin C, Ask M, 2013. Carbonatite ring-complexes explained by caldera-style volcanism. Scientific Reports 3, 1677. doi:10.1038/srep01677

Andersson U B, 1997. The sub-Jotnian Strömsbro granite complex at Gävle, Sweden. GFF 119, 159–167.

André M-F, 1996. Rock weathering rates in arctic and subarctic environments (Abisko Mts, Swedish Lappland). Zeitschrift für Geomorphologie 40, 499–517.

André M-F, 2002. Rates of Postglacial rock weathering on glacially scoured outcrops (Abisko–Riksgränsen area, 68° N). Geografiska Annaler: Series A, Physical Geography 84, 139–150.

André M-F, 2004. The geomorphic impact of glaciers as indicated by tors in North Sweden (Aurivaara, 68º N). Geomorphology 57, 403–421.

Anjar J, Larsen N K, Håkansson L, Möller P, Linge H, Fabel D, Xu S, 2014. A ^{10}Be-based reconstruction of the last deglaciation in southern Sweden. Boreas 43, 132–148.

Arnold N, Sharp M, 2002. Flow variability in the Scandinavian ice sheet: modelling the coupling between ice sheet flow and hydrology. Quaternary Science Reviews 21, 485–502.

Artyushkov E A, Lindström M, Popov L E, 2000. Relative sea-level changes in Baltoscandia in the Cumbrian and early Ordovician: the predominance of tectonic factors and the absence of large scale eustatic fluctuations. Tectonophysics 320, 375–407.

Asklund B, 1930. Nyupptäckta kambrosilurlokaler i Östergötland, Södermanland och Uppland. Geologiska Föreningens i Stockholm Förhandlingar 52, 147–153. (In Swedish.)

Augustinus P C, 1991. Rock resistance to erosion: some further considerations. Earth Surface Processes and Landforms 16, 563–569.

Axberg S, 1980. Seismic stratigraphy and bedrock geology of the Bothnian Sea, northern Baltic. Stockholm: Almqvist & Wiksell, 153–213. (Stockholms Contributions in Geology 36.)

Aydin A, Basu A, 2005. The Schmidt hammer in rock material characterization. Engineering Geology 81, 1–14.

Balco G, 2011. Contributions and unrealized potential contributions of cosmogenic-nuclide exposure dating to glacier chronology, 1990–2010. Quaternary Science Reviews 30, 3–27.

Balco G, 2017. Production rate calculations for cosmic-ray-muon-produced ^{10}Be and ^{26}Al benchmarked against geological calibration data. Quaternary Geochronology 39, 150–173.

Balco G, Stone J O, Mason J A, 2005. Numerical ages for Plio-Pleistocene glacial sediment sequences by ^{26}Al/^{10}Be dating of quartz in buried paleosols. Earth and Planetary Science Letters 232, 179–191.

Balco G, Stone J O, Lifton N A, Dunai T J, 2008. A complete and easily accessible means of calculating surface exposure ages or erosion rates from ^{10}Be and ^{26}Al measurements. Quaternary Geochronology 3, 174–195.

Baltrūnas V, Karmaza B, Pukelytė V, Karmazienė D, 2019. Pleistocene architecture and stratigraphy in the contact zone of ice streams and lobes in the south-eastern part of the Baltic Region. Quaternary International 501, 21–32.

Bartholomew I, Nienow P, Sole A, Mair D, Cowton T, Palmer S, Wadham J, 2011. Supraglacial forcing of subglacial drainage in the ablation zone of the Greenland ice sheet. Geophysical Research Letters 38. doi:10.1029/2011GL047063

Barton C A, Moos D, 1999. In situ stress measurements can help define local variations in fracture hydraulic conductivity at shallow depth. In Powers M H, Cramer L, Bell R S (eds). Proceedings of the Symposium on the Application of Geophysics to Engineering and Environmental Problems, 14–18 March 1999. Wheat Ridge, CO: Society of Exploration Geophysicists, 1–10.

Batchelor C L, Margold M, Krapp M, Murton D K, Dalton A S, Gibbard P L, Stokes C R, Murton J B, Manica A, 2019. The configuration of Northern Hemisphere ice sheets through the Quaternary. Nature Communications 10, 3713. doi:10.1038/s41467-019-11601-2

Beacom L E, Holdsworth R E, McCaffrey K J W, Anderson T B, 2001. A quantitative study of the influence of pre-existing compositional and fabric heterogeneities upon fracture-zone development during basement reactivation. Geological Society, London, Special Publications 186, 195–211.

Becker R A, Tikoff B, Riley P R, Iverson N R, 2014. Preexisting fractures and the formation of an iconic American landscape: Tuolumne Meadows, Yosemite National Park, USA. GSA Today 24, 4–10.

Beckholmen M, Tirén S A, 2009. The geological history of the Baltic Sea, a review of the literature and investigation tools. SSM report 2009:21, Swedish Radiation Safety Authority.

Beckholmen M, Tirén S A, 2010a. Rock-block configuration in Uppland and the Ålands-hav basin, the regional surroundings of the SKB site in Forsmark, Sea and land areas, eastern Sweden. SSM report 2010:41, Swedish Radiation Safety Authority.

Beckholmen M, Tirén S A, 2010b. Displacement along extensive deformation zones at the two SKB sites: Forsmark and Laxemar. SSM report 2010:43, Swedish Radiation Safety Authority.

Bell M, Laine E P, 1985. Erosion of the Laurentide region of North America by glacial and glacio-fluvial processes. Quaternary Research 23, 154–174.

Benn D I, Evans D J A, 2010. Glaciers and glaciation. 2nd ed. London: Hodder Education.

Bennett M R, Glasser N F, 2009. Glacial geology: ice sheets and landforms. 2nd ed. Chichester: Wiley-Blackwell.

Ber A, Janczyk-Kopikowa Z, Krzyszkowski D, 1998. A new interglacial stage in Poland (Augustovian) and the problem of the age of the oldest Pleistocene till. Quaternary Science Reviews 17, 761–773.

Berglund M, 2005. The Holocene shore displacement of Gästrikland, eastern Sweden: a contribution to the knowledge of Scandinavian glacio-isostatic uplift. Journal of Quaternary Science 20, 519–531.

Bergman L, 1982. Clastic dykes in the Åland islands, SW Finland and their origin. Geological Survey of Finland, Bulletin 317, 7–33.

Bergman L, Lindberg B, 1979. Phanerozoic veins of galena in the Åland rapakivi area, southwestern Finland. Bulletin of the Geological Society of Finland 51, 55–62.

Bergström E, 2001. Late Holocene distribution of lake sediment and peat in NE Uppland, Sweden. SKB R-01-12, Svensk Kärnbränslehantering AB.

Berner R A, 1992. Weathering, plants, and the long-term carbon cycle. Geochimica et Cosmochimica Acta 56, 3225–3231.

Bijlsma S, 1981. Fluvial sedimentation from the Fennoscandian area into the north-west European Basin during the Late Cenozoic. Geologie en Mijnbouw 60, 337–345.

Bingen B, Nordgulen Ø, Viola G, 2008. A four-phase model for the Sveconorwegian orogeny, SW Scandinavia. Norsk geologisk tidsskrift 88, 43–72.

Bird J B, 1967. The physiography of Arctic Canada: with special reference to the area south of Parry Channel. Baltimore: Johns Hopkins Press.

Björnbom S, 1979. Clayey basal till in central and northern Sweden: a deposit from an old phase of the Würm glaciation. Uppsala: Sveriges geologiska undersökning. (Serie C 753)

Blomdin R, Fu P, Goodfellow B W, Gribenski N, Heyman J, Newall J C, Stroeven A P (eds), 2016. Third Nordic Workshop on cosmogenic nuclide techniques: celebrating 30 years of counting cosmogenic atoms, Stockholm university, 8–10 June 2016. Svensk Kärnbränslehantering AB.

Bluemle J P, Clayton L, 1984. Large-scale glacial thrusting and related processes in North Dakota. Boreas 13, 279–299.

Bonnet E, Bour O, Odling N E, Davy P, Main I, Cowie P, Berkowitz B, 2001. Scaling of fracture systems in geological media. Reviews of Geophysics 39, 347–383.

Bonow J M, 2005. Re-exposed basement landforms in the Disko region, West Greenland – disregarded data for estimation of glacial erosion and uplift modelling. Geomorphology 72, 106–127.

Bonow J M, Lidmar-Bergström K, Näslund JO, 2003. Palaeosurfaces and major valleys in the area of the Kjølen Mountains, southern Norway – consequences of uplift and climatic change. Norsk Geografisk Tidsskrift 57, 83–101.

Borchers B, Marrero S, Balco G, Caffee M, Goehring B, Lifton N, Nishiizumi K, Phillips F, Schaefer J, Stone J, 2016. Geological calibration of spallation production rates in the CRONUS-Earth project. Quaternary Geochronology 31, 188–198.

Bouchard M, Jolicoeur S, 2000. Chemical weathering studies in relation to geomorphological research in southeastern Canada. Geomorphology 32, 213–238.

Bouchard M A, Jolicoeur S, Peulvast J P, 2007. Altération et évolution géomorphologique du bouclier canadien dans le sud-ouest de Québec. In André M-F (ed). Du continent au bassin versant : theories et practiques en géographie physique (Hommage au Professeur Alain Godard). Lyon: Presses Universitaires Blaise-Pascal, 39–54. (In French.)

Boulton G S, 1979. Processes of glacier erosion on different substrata. Journal of Glaciology 23, 15–38.

Boulton G S, 1982. Processes and patterns of glacial erosion. In Coates D R (ed). Glacial geomorphology. Springer, 41–87.

Boulton G S, Caban P, 1995. Groundwater flow beneath ice sheets: Part II – Its impact on glacier tectonic structures and moraine formation. Quaternary Science Reviews 14, 563–587.

Boulton G S, Eyles N, 1979. Sedimentation by valley glaciers: a model and genetic classification. In Schlüchter C (ed). Moraines and varves: origin, genesis, classification: proceedings of an INQUA symposium on genesis and lithology of quarternary deposits, Zürich, 10–20 September 1978. Rotterdam: Balkema, 11–23.

Boulton G S, Caban P, Van Gijssel K, 1995. Groundwater flow beneath ice sheets: Part I – Large scale patterns. Quaternary Science Reviews 14, 545–562.

Boulton G S, Zatsepin S, Maillot B, 2001. Analysis of groundwater flow beneath ice sheets. SKB TR-01-06, Svensk Kärnbränslehantering AB.

Bradwell T, 2013. Identifying palaeo-ice-stream tributaries on hard beds: Mapping glacial bedforms and erosion zones in NW Scotland. Geomorphology 201, 397–414.

Bradwell T, Stoker M, Krabbendam M, 2008. Megagrooves and streamlined bedrock in NW Scotland: the role of ice streams in landscape evolution. Geomorphology 97, 135–156.

Briner J P, Swanson T W, 1998. Using inherited cosmogenic ^{36}Cl to constrain glacial erosion rates of the Cordilleran ice sheet. Geology 26, 3–6.

Briner J P, Miller G H, Davis P T, Finkel R C, 2005. Cosmogenic exposure dating in arctic glacial landscapes: implications for the glacial history of northeastern Baffin Island, Arctic Canada. Canadian Journal of Earth Sciences 42, 67–84.

Briner J P, Miller G H, Davis P T, Finkel R C, 2006. Cosmogenic radionuclides from fiord landscapes support differential erosion by overriding ice sheets. Geological Society of America Bulletin 118, 406–420.

Briner J P, Miller G H, Finkel R, Hess D P, 2008. Glacial erosion at the fjord onset zone and implications for the organization of ice flow on Baffin Island, Arctic Canada. Geomorphology 97, 126–134.

Brook E J, Nesje A, Lehman S, Raisbeck G, Yiou F, 1996. Cosmogenic nuclide exposure ages along a vertical transect in western Norway: implications for the height of the Fennoscanidan ice sheet. Geology 24, 207–210.

Brown E T, 1981. Suggested method for rock characterization, testing and monitoring, ISRM Commission on Testing Methods. Oxford: Pergamon Press.

Brozović N, Burbank D, Meigs A, 1996. Glacial buzzsaws, topographic lightning rods and landscape development in the northwestern Himalaya and Karakoram. Eos, Transactions, American Geophysical Union 77, 252.

Buntin S, Malehmir A, Koyi H, Högdahl K, Malinowski M, Larsson S Å, Thybo H, Juhlin C, Korja A, Górszczyk A, 2019. Emplacement and 3D geometry of crustal-scale saucer-shaped intrusions in the Fennoscandian Shield. Scientific Reports 9, 10498. doi:10.1038/s41598-019-46837-x

Calner M, Ahlberg P, Lehnert O, Erlström M (eds), 2013. The Lower Palaeozoic of southern Sweden and the Oslo Region, Norway: field guide for the 3rd Annual Meeting of the IGCP project 591. Uppsala: Sveriges geologiska undersökning. (Rapporter och meddelanden 133)

Carlsson A, 1979. Characteristic features of a superficial rock mass in southern central Sweden – horizontal and subhorizontal fractures and filling material. PhD thesis. Uppsala university. (Striae 11)

Carlsson A, Christiansson R, 1987. Geology and tectonics at Forsmark, Sweden. Report 1987/42, Vattenfall, Swedish State Power Board.

Carlsson A, Christiansson R, 2007. Construction experiences from underground works at Forsmark. Compilation report. SKB R-07-10, Svensk Kärnbränslehantering AB.

Carlsson A, Olsson T, 1976. Joint fillings at Forsmark, Uppland, Sweden: A discussion. Geologiska Föreningen i Stockholm Förhandlingar 98, 75–77.

Carlsson A, Olsson T, 1982a. High rock stresses as a consequence of glaciation. Nature 298, 739–742.

Carlsson A, Olsson T, 1982b. Rock bursting phenomena in a superficial rock mass in southern central Sweden. Rock Mechanics 15, 99–110.

Carlsten S, Petersson J, Stephens M, Mattsson H, Gustafsson J, 2004. Forsmark site investigation. Geological single-hole Interpretation of KFM02A and HFM04-05 (DS2). SKB P-04-117, Svensk Kärnbränslehantering AB.

Cederbom C, 2001. Phanerozoic, pre-Cretaceous thermotectonic events in southern Sweden revealed by fission track thermochronology. Earth and Planetary Science Letters 188, 199–209.

Chmeleff J, von Blanckenburg F, Kossert K, Jakob D, 2010. Determination of the ^{10}Be half-life by multicollector ICP-MS and liquid scintillation counting. Nuclear Instruments and Methods in Physics Research Section B: Beam Interactions with Materials and Atoms 268, 192–199.

Chorley R J, Schumm S A, Sugden D E, 1984. Geomorphology. London: Methuen.

Claesson Liljedahl L, Munier R, Sandström B, Drake H, Tullborg E-L, 2011. Assessment of fractures classified as non-mineralised in the Sicada database. SKB R-11-02, Svensk Kärnbränslehantering AB.

Claesson Liljedahl L, Kontula A, Harper J, Näslund J-O, Selroos J-O, Pitkänen P, Puigdomenech I, Hobbs M, Follin S, Hirschorn S, Jansson P, Kennell L, Marcos N, Ruskeeniemi T, Tullborg E-L, Vidstrand P, 2016. The Greenland Analogue Project: Final report. SKB TR-14-13, Svensk Kärnbränslehantering AB.

Clason C C, Greenwood S L, Selmes N, Lea J M, Jamieson S S, Nick F M, Holmlund P, 2016. Controls on the early Holocene collapse of the Bothnian Sea Ice Stream. Journal of Geophysical Research: Earth Surface 121, 2494–2513.

Cocks L R M, Torsvik T H, 2005. Baltica from the late Precambrian to mid-Palaeozoic times: the gain and loss of a terrane's identity. Earth-Science Reviews 72, 39–66.

Colgan P M, Bierman P R, Mickelson D M, Caffee M, 2002. Variation in glacial erosion near the southern margin of the Laurentide Ice Sheet, south-central Wisconsin, USA: Implications for cosmogenic dating of glacial terrains. Geological Society of America Bulletin 114, 1581–1591.

Colleoni F, Wekerle C, Masina S, 2014. Long-term safety of a planned geological repository for spent nuclear fuel in Forsmark–estimate of maximum ice sheet thicknesses. SKB TR-14-21, Svensk Kärnbränslehantering AB.

Cooley S W, 2013. GIS4 Geomorphology. Available at: http://gis4geomorphology.com/roughness-topographic-position/ [20 October 2017].

Corcoran P L, 2008. Ordovician paleotopography as evidenced from original dips and differential compaction of dolostone and shale unconformably overlying Precambrian basement on Manitoulin Island, Canada. Sedimentary Geology 207, 22–33.

Cowton T, Nienow P, Bartholomew I, Sole A, Mair D, 2012. Rapid erosion beneath the Greenland ice sheet. Geology 40, 343–346.

Czerwonka J A, Krzyszkowski D, 1994. Pleistocene stratigraphy and till petrography of the central Great Poland Lowland, western Poland. Folia Quaternaria 65, 7–71.

Czubla P, Terpiłowski S, Orłowska A, Zieliński P, Zieliński T, Pidek I A, 2019. Petrographic features of tills as a tool in solving stratigraphical and palaeogeographical problems – A case study from Central-Eastern Poland. Quaternary International 501, 45–58.

Darmody R G, Thorn C E, Seppala M, Campbell S W, Li Y K, Harbor J, 2008. Age and weathering status of granite tors in Arctic Finland (~68° N). Geomorphology 94, 10–23.

Davis G H, Reynolds S J, 1996. Structural geology of rocks and regions. 2nd ed. New York: Wiley.

Davis W M, 1902. Baselevel, Grade and Peneplain. The Journal of Geology 10, 77–111.

Deere D U, Miller R P, 1966. Engineering classification and index properties for intact rock. Technical Report AFWL-TR-65-116, Air Force Weapons Laboratory (WLDC), New Mexico 87117.

Degeai J-P, Peulvast J-P, 2006. Calcul de l'érosion à long terme en région de socle autour de grands astroblèmes du Québec et de France. Géographie physique et Quaternaire 60, 131–148. (In French.)

Delmas M, Calvet M, Gunnell Y, 2009. Variability of Quaternary glacial erosion rates – A global perspective with special reference to the Eastern Pyrenees. Quaternary Science Reviews 28, 484–498.

DeLucia M S, Guenthner W R, Marshak S, Thomson S, Ault A, 2017. Thermochronology links denudation of the Great Unconformity surface to the supercontinent cycle and snowball Earth. Geology 46, 167–170.

Donner J, 2005. The Quaternary history of Scandinavia. Cambridge: Cambridge University Press.

Dott R H Jr, 2003. The importance of eolian abrasion in supermature quartz sandstones and the paradox of weathering on vegetation-free landscapes. The Journal of Geology 111, 387–405.

Dowdeswell J A, Ottesen D, Rise L, 2010. Rates of sediment delivery from the Fennoscandian Ice Sheet through an ice age. Geology 38, 3–6.

Drake H, Tullborg E-L, MacKenzie A B, 2009a. Detecting the near-surface redox front in crystalline bedrock using fracture mineral distribution, geochemistry and U-series disequilibrium. Applied Geochemistry 24, 1023–1039.

Drake H, Tullborg E-L, Page L, 2009b. Distinguished multiple events of fracture mineralisation related to far-field orogenic effects in Paleoproterozoic crystalline rocks, Simpevarp area, SE Sweden. Lithos 110, 37–49.

Drake H, Heim C, Roberts N M W, Zack T, Tillberg M, Broman C, Ivarsson M, Whitehouse M J, Åström M E, 2017. Isotopic evidence for microbial production and consumption of methane in the upper continental crust throughout the Phanerozoic eon. Earth and Planetary Science Letters 470, 108–118.

Drake H, Ivarsson M, Tillberg M, Whitehouse M, Kooijman E, 2018. Ancient microbial activity in deep hydraulically conductive fracture zones within the Forsmark target area for geological nuclear waste disposal, Sweden. Geosciences 8, 211.

Dreimanis A, Vagners U J, 1969. Lithological relation of till to bedrock. In Wright H E Jr (ed). Quaternary geology and climate: the proceedings, vol. 16, of the 7th Congress of the International Association for Quaternary Research (INQUA), Boulder/Denver, 1965.

Dreyer T, 1988. Late Proterozoic (Vendian) to Early Cambrian sedimentation in the Hedmark Group, southwestern part of the Sparagmite Region, southern Norway. Norges geologiske undersøkelse Bulletin 412, 1–27.

Dunai T J, 2010. Cosmogenic nuclides: principles, concepts and applications in the earth surface sciences. Cambridge: Cambridge University Press.

Dunne J, Elmore D, Muzikar P, 1999. Scaling factors for the rates of production of cosmogenic nuclides for geometric shielding and attenuation at depth on sloped surfaces. Geomorphology 27, 3–11.

Dühnforth M, Anderson R S, Ward D, Stock G M, 2010. Bedrock fracture control of glacial erosion processes and rates. Geology 38, 423–426.

Ebert K, 2009. Terminology of long-term geomorphology: a Scandinavian perspective. Progress in Physical Geography 33, 163–182.

Ebert K, 2015. GIS-analyses of ice-sheet erosional impacts on the exposed shield of Baffin Island, eastern Canadian Arctic. Canadian Journal of Earth Science 52, 966–979.

Ebert K, Hättestrand C, 2010. The impact of Quaternary glaciation on inselbergs in northern Sweden. Geomorphology 115, 56–66.

Ebert K, Hättestrand C, Hall A M, Alm G, 2011. DEM identification of macroscale stepped relief in arctic northern Sweden. Geomorphology 132, 339–350.

Ebert K, Hall A M, Hättestrand C, 2012a. Pre-glacial landforms on a glaciated shield: the inselberg plains of northern Sweden. Norsk geologisk tidsskrift 92, 1–17.

Ebert K, Willenbring J K, Norton K P, Hall A M, Hättestrand C, 2012b. Meteoric ^{10}Be concentrations from saprolite and till in northern Sweden saprolite: Implications for genesis and age. Quaternary Geochronology 12, 11–22.

Ebert K, Hall A M, Kleman J, Andersson J, 2015. Unequal ice sheet erosional impacts across low-relief shield terrain in northern Fennoscandia. Geomorphology 233, 64–74.

Egholm D L, Jansen J D, Brædstrup C F, Pedersen V K, Andersen J L, Ugelvig S V, Larsen N K, Knudsen M F, 2017. Formation of plateau landscapes on glaciated continental margins. Nature Geoscience 10, 592–597.

Ehlers J, Grube A, Stephan H-J, Wansa S, 2011. Pleistocene glaciations of North Germany – New results. In Ehlers J, Gibbard P L, Hughes P D (eds). Quaternary glaciations: extent and chronology: a closer look. Amsterdam: Elsevier, 149–162. (Developments in Quaternary Sciences 15)

Ehlers J, Gibbard P L, Hughes P D, 2018. Quaternary glaciations and chronology. In Past glacial environments. 2nd ed. Elsevier, 77–101.

Ekman S R, 1999. Early Pleistocene pollen biostratigraphy in the central North Sea. Review of Palaeobotany and Palynology 105, 171–182.

Elo S, Kuivasaari T, Lehtinen M, Sarapää O, Uutela A, 1993. Iso-Naakkima, a circular structure filled with Neoproterozoic sediments, Pieksämäki, south-eastern Finland. Bulletin of the Geological Society of Finland 65, 3–30.

Elvhage C, Lidmar-Bergström K, 1987. Some working hypotheses on the geomorphology of Sweden in the light of a new relief map. Geografiska Annaler: Series A, Physical Geography 69, 343–358.

Embleton C, 1982. Fiord, fjord; Fiard, fjärd. In Schwartz M L (ed). Beaches and coastal geology. Boston, MA: Springer, 426–427.

Ericson K, 2004. Geomorphological surfaces of different age and origin in granite landscapes: an evaluation of the Schmidt hammer test. Earth Surface Processes and Landforms 29, 495–509.

Ericson K, Olvmo M, 2004. A-tents in the central Sierra Nevada, California: a geomorphological indicator of tectonic stress. Physical Geography 25, 291–312.

Erlström M, 1987. Complex fracture-filling material from the Singö fault zone at Forsmark, central Sweden. Geologiska Föreningen i Stockholm Förhandlingar 109, 55–57.

Evans D J A, Archer S, Wilson D J H, 1999. A comparison of the lichenometric and Schmidt hammer dating techniques based on data from the proglacial areas of some Icelandic glaciers. Quaternary Science Reviews 18, 13–41.

Evans D J A, Dinnage M, Roberts D H, 2018. Glacial geomorphology of Teesdale, northern Pennines, England: Implications for upland styles of ice stream operation and deglaciation in the British-Irish Ice Sheet. Proceedings of the Geologists' Association 129, 697–735.

Fabel D, Harbor J, 1999. The use of in-situ produced cosmogenic radionuclides in glaciology and glacial geomorphology. Annals of Glaciology 28, 103–110.

Fabel D, Stroeven A P, Harbor J, Kleman J, Elmore D, Fink D, 2002. Landscape preservation under Fennoscandian ice sheets determined from in situ produced ^{10}Be and ^{26}Al. Earth and Planetary Science Letters 201, 397–406.

Fairbridge R W, Finkl C W, 1980. Cratonic erosional unconformities and peneplains. Journal of Geology 88, 69–86.

Falcini F A M, Rippin D M, Krabbendam M, Selby K A, 2018. Quantifying bed roughness beneath contemporary and palaeo-ice streams. Journal of Glaciology 247, 822–834.

Femke Helmens K F, 2019. The last 130 000 years in Fennoscandia reconstructed based on a long and fossil-rich sediment sequence preserved at Sokli, northern Finland: new evidence for highly dynamic environmental and climate conditions. SKB TR-18-04, Svensk Kärnbränslehantering AB.

Fjellanger J, Etzelmüller B, 2003. Stepped palaeosurfaces in southern Norway – interpretation of DEM-derived topographic profiles. Norsk geografisk tidsskrift 57, 102–110.

Fjellanger J, Sørbel L, 2007. Origin of the palaeic landforms and glacial impact on the Varanger Peninsula, northern Norway. Norsk geologisk tidsskrift 87, 223–238.

Flodén T, 1977. Tectonic lineaments in the Baltic from Gävle to Simrishamn. KBS TR 59, Kärnbränslesäkerhet.

Flodén T, 1980. Seismic stratigraphy and bedrock geology of the central Baltic. Stockholm: Almqvist & Wiksell. (Stockholm Contributions in Geology 35)

Flodén T, Jacobsson R, Kumpas M G, Wadstein P, Wannäs K, 1980. Geophysical investigation of western Bothnian Bay. Geologiska Föreningen i Stockholm Förhandlingar 101, 321–327.

Flodén T, Söderberg P, Wickman F E, 1993. Björkö, a possible Middle Proterozoic impact structure west of Stockholm, Sweden. Geologiska Föreningen i Stockholm Förhandlingar 115, 25–38.

Flodén T, Bjerkéus M, Sturkell E, Gelumbauskaitė Ž, Grigelis A, Endler R, Lemke W, Flodén T, Bjerkéus M, Sturkell E, 1997. Distribution and seismic stratigraphy of glacially incised valleys in the southern part of the Baltic. In Proceedings of the Fourth Marine Geological Conference "The Baltic". Uppsala: Sveriges geologiska undersökning. (Ser. Ca 86)

Flowers R M, Bowring S A, Reiners P W, 2006. Low long-term erosion rates and extreme continental stability documented by ancient (U-Th)/He dates. Geology 34, 925–928.

Follin S, Levén J, Hartley L, Jackson P, Joyce S, Roberts D, Swift B, 2007. Hydrogeological characterisation and modelling of deformation zones and fracture domains, Forsmark modelling stage 2.2. SKB R-07-48, Svensk Kärnbränslehantering AB.

Follin S, Hartley L, Rhén I, Jackson P, Joyce S, Roberts D, Swift B, 2014. A methodology to constrain the parameters of a hydrogeological discrete fracture network model for sparsely fractured crystalline rock, exemplified by data from the proposed high-level nuclear waste repository site at Forsmark, Sweden. Hydrogeology Journal 22, 313–331.

Forssberg O, Mærsk Hansen L , Koyi S, Vestgård J, Öhman J, Petersson J, Albrecht J, Hedenström A, Gustavsson J, 2007. Forsmark site investigation. Detailed fracture and bedrock mapping, Quaternary investigations and GPR measurements at excavated outcrop AFM001264. SKB P-05-269, Svensk Kärnbränslehantering AB.

Friese N, Vollbrecht A, Leiss B, Jacke O, 2011. Cambrian sedimentary dykes in the Proterozoic basement of the Västervik area (southeast Sweden): episodic formation inferred from macro-and microfabrics. International Journal of Earth Sciences 100, 741–752.

Fu P, Stroeven A P, Harbor J M, Heyman J, Hättestrand C, Caffee M W, 2018. Ice cap erosion patterns from bedrock ^{10}Be and ^{26}Al, southeastern Tibetan Plateau. Earth Surface Processes and Landforms 44, 918–932.

Gabrielsen R H, Nystuen J P, Jarsve E M, Lundmark A M, 2015. The Sub-Cambrian Peneplain in southern Norway: its geological significance and its implications for post-Caledonian faulting, uplift and denudation. Journal of the Geological Society 172, 777–791.

Gabrielsen R H, Nystuen J P, Olesen O, 2018. Fault distribution in the Precambrian basement of South Norway. Journal of Structural Geology 108, 269–289.

Gao C, McAndrews J H, Wang X, Menzies J, Turton C L, Wood B D, Pei J, Kodors C, 2012. Glaciation of North America in the James Bay Lowland, Canada, 3.5 Ma. Geology 40, 975–978.

Gibbard P L, Lewin J, 2016. Filling the North Sea Basin: Cenozoic sediment sources and river styles. Geologica Belgica 19, 201–217.

Gilg H A, Hall A M, Ebert K, Fallick A E, 2013. Cool kaolins in Finland. Palaeogeography, Palaeoclimatology, Palaeoecology 392, 454–462.

Glamheden R, Fredriksson A, Roeshoff K, Karlsson J, Hakami H, Christiansson R, 2007. Rock mechanics Forsmark. Site descriptive modelling Forsmark stage 2.2. SKB R-07-31, Svensk Kärnbränslehantering AB.

Glasser N F, Bennett M R, 2004. Glacial erosional landforms: origins and significance for palaeoglaciology. Progress in Physical Geography 28, 43–75.

Glasser N F, Hall A M, 1997. Calculating Quaternary erosion rates in North East Scotland. Geomorphology 20, 29–48.

Glasser N F, Warren C R, 1990. Medium scale landforms of glacial erosion in south Greenland; process and form. Geografiska Annaler: Series A, Physical Geography 72, 211–215.

Godard A, 1961. L'efficacité de l'erosion glaciare en Écosse du Nord. Revue de Géomorphologie Dynamique 12, 32–42. (In French.)

Goehring B M, Schaefer J M, Schluechter C, Lifton N A, Finkel R C, Jull A T, Akçar N, Alley R B, 2011. The Rhone Glacier was smaller than today for most of the Holocene. Geology 39, 679–682.

Goodfellow B W, Stroeven A P, Hättestrand C, Kleman J, Jansson K N, 2008. Deciphering a non-glacial/glacial landscape mosaic in the northern Swedish mountains. Geomorphology 93, 213–232.

Goodfellow B W, Skelton A, Martel S J, Stroeven A P, Jansson K N, Hättestrand C, 2014. Controls of tor formation, Cairngorm Mountains, Scotland. Journal of Geophysical Research: Earth Surface 119, 225–246.

Goodfellow B W, Stroeven A P, Martel S J, Heyman J, Rossi M, Cafee M W, 2019. The Subcambrian peneplain in southern Sweden: Morphology, formation, and glacial erosion. SKB TR-19-22, Svensk Kärnbränslehantering AB.

Gorbatschev R, 1967. Petrology of Jotnian rocks in the Gävle area, east central Sweden. Stockholm: Sveriges geologiska undersökning. (Serie C 621)

Gordon J E, 1981. Ice-scoured topography and its relationships to bedrock structure and ice movement in parts of northern Scotland and west Greenland. Geografiska Annaler: Series A, Physical Geography 63, 55–65.

Gorlach A, Kalm V, Hang T, 2015. Thickness distribution of Quaternary deposits in the formerly glaciated part of the East European plain. Journal of Maps 11, 625–635.

Gosse J C, Phillips F M, 2001. Terrestrial in situ cosmogenic nuclides: theory and application. Quaternary Science Reviews 20, 1475–1560.

Gradstein F M, Ogg J G, Schmitz M, Ogg G, 2012. The geologic time scale. Amsterdam: Elsevier.

Grahn Y, Nõlvak J, Paris F, 1996. Precise chitinozoan dating of Ordovician impact events in Baltoscandia. Journal of Micropalaeontology 15, 21–35.

Granger D E, Caffee M W, Woodruff T E, 2014. A tenfold increase in ^{26}Al currents at PRIME Lab: Revisiting old ideas and exploring new possibilities with a gas-filled-magnet. Proceedings of GSA Annual Meeting in Vancouver, British Columbia, 19–22 October 2014. Available at: https://gsa.confex.com/gsa/2014AM/finalprogram/abstract_245480.htm

Grazhdankin D, 2003. Structure and depositional environment of the Vendian Complex in the southeastern White Sea area. Stratigraphy and Geological Correlation 11, 313–331.

Green P F, Lidmar-Bergström K, Japsen P, Bonow J, Chalmers J A, 2013. Stratigraphic landscape analysis, thermochronology and the episodic development of elevated, passive continental margins. Geological Survey of Denmark and Greenland Bulletin 30.

Greenwood S L, Clason C C, Jakobsson M, 2016. Ice-flow and meltwater landform assemblages in the Gulf of Bothnia. Geological Society, London, Memoirs 46, 321–324.

Greenwood S L, Clason C C, Nyberg J, Jakobsson M, Holmlund P, 2017. The Bothnian Sea ice stream: early Holocene retreat dynamics of the south-central Fennoscandian Ice Sheet. Boreas 46, 346–362.

Greiling R O, Jensen S, Smith A G, 1999. Vendian-Cambrian subsidence of the passive margin of western Baltica – application of new stratigraphic data from the Scandinavian Caledonian margin. Norsk geologisk tidsskrift 79, 133–144.

Grigull S, Peterson G, Nyberg J, Öhrling C, 2019. Phanerozoic faulting of Precambrian basement in Uppland. SKB R-19-22, Svensk Kärnbränslehantering AB.

Hadding A R, 1929. The pre-Quaternary sedimentary rocks of Sweden. III: The Paleozoic and Mesozoic sandstones of Sweden. Lund: Gleerup.

Hagenfeldt S E, 1995. Erratics and Proterozoic-Lower Palaeozoic submarine sequences between Åland and mainland Sweden. Uppsala: Sveriges geologiska undersokning. (Serie C 84)

Hagenfeldt S E, Söderberg P, 1994. Lower Cambrian sandstone erratics and geophysical indications of sedimentary rock in the Stockholm area, Sweden. GFF 116, 185–190.

Hall A M, Gillespie M R, 2017. Fracture controls on valley persistence: the Cairngorm Granite pluton, Scotland. International Journal of Earth Sciences 106, 2203–2219.

Hall A M, Kleman J, 2014. Glacial and periglacial buzzsaws: fitting mechanisms to metaphors. Quaternary Research 81, 189–192.

Hall A M, Migoń P, 2010. The first stages of landscape modification by ice sheets: evidence from central Europe. Geomorphology 123, 349–363.

Hall A M, Phillips W M, 2006. Weathering pits as indicators of the relative age of granite surfaces in the Cairngorm Mountains, Scotland. Geografiska Annaler: Series A, Physical Geography 88, 135–150.

Hall A M, Ebert K, Hättestrand C, 2013a. Pre-glacial landform inheritance in a glaciated shield landscape. Geografiska Annaler: Series A, Physical Geography 95, 33–49.

Hall A M, Ebert K, Kleman J, Nesje A, Ottesen D, 2013b. Selective glacial erosion on the Norwegian passive margin. Geology 41, 1203–1206.

Hall A M, Sarala P, Ebert K, 2015. Late Cenozoic deep weathering patterns on the Fennoscandian shield in northern Finland: a window on ice sheet bed conditions at the onset of Northern Hemisphere glaciation. Geomorphology 246, 472–488.

Hall A M, Krabbendam M, Van Boeckel M, Ebert K, Hättestrand C and Heyman J, 2019a. The sub-Cambrian unconformity in Västergötland, Sweden: Reference Surface for Glacial Erosion of Basement. SKB TR-19-21, Svensk Kärnbränslehantering AB.

Hall A M, Connell E R, Merrit J W, Hubbard A, 2019b. Early and Middle Pleistocene environments, landforms and sediments in Scotland. Earth and Environmental Science Transactions of The Royal Society of Edinburgh 110, 5–37.

Hallet B, 1981. Glacial abrasion and sliding: their dependence on the debris concentration in basal ice. Annals of Glaciology 2, 23–28.

Hallet B, 1996. Glacial quarrying: a simple rheoretical model. Annals of Glaciology 22, 1–8.

Haq B U, Schutter S R, 2008. A chronology of Paleozoic sea-level changes. Science 322, 64–68.

Harbor J, Stroeven A P, Fabel D, Clarhäll A, Kleman J, Li Y, Elmore D, Fink D, 2006. Cosmogenic nuclide evidence for minimal erosion across two subglacial sliding boundaries of the late glacial Fennoscandian ice sheet. Geomorphology 75, 90–99.

Harris C, Murton J B, 2005. Interactions between glaciers and permafrost: an introduction. Geological Society, London, Special Publications 242, 1–9.

Hartikainen J, Kouhia R, Wallroth T, 2010. Permafrost simulations at Forsmark using a numerical 2D thermo-hydro-chemical model. SKB TR-09-17, Svensk Kärnbränslehantering AB.

Haynes V M, 1977. The modification of valley patterns by ice sheet activity. Geografiska Annaler: Series A, Physical Geography 59, 195–207.

Hedenström A, 2004. Forsmark site investigation. Stratigraphical and analytical data of Quaternary deposits. SKB P-04-148, Svensk Kärnbränslehantering AB.

Hedenström A, Risberg J, 2003. Shore displacement in northern Uppland during the last 6500 calender years. SKB TR-03-17, Svensk Kärnbränslehantering AB.

Hedenström A, Sohlenius G, Strömgren G, Brydsten L, Nyman H, 2008. Depth and stratigraphy of regolith at Forsmark: site descriptive modelling SDM-Site Forsmark. SKB R-08-07, Svensk Kärnbränslehantering AB.

Henkel H, 1992. Geophysical aspects of meteorite impact craters in eroded shield environment, with special emphasis on electric resistivity. Tectonophysics 216, 63–89.

Heyman J, Stroeven A P, Harbor J M, Caffee M W, 2011. Too young or too old: Evaluating cosmogenic exposure dating based on an analysis of compiled boulder exposure ages. Earth and Planetary Science Letters 302, 71–80.

Hindmarsh R C, 1999. Coupled ice–till dynamics and the seeding of drumlins and bedrock forms. Annals of Glaciology 28, 221–230.

Hirvas H, 1991. Pleistocene stratigraphy of Finnish Lapland. Geological Survey of Finland, Bulletin 354, 1–123.

Holmlund P, Fastook J, 1993. Numerical modelling provides evidence of a Baltic Ice Stream during the Younger Dryas. Boreas 22, 77–86.

Holmlund P, Clason C, Blomdahl K, 2016. The effect of a glaciation on East Central Sweden: case studies on present glaciers and analyses of landform data. SSM report 2016:21, Swedish Radiation Safety Authority.

Holtedahl H, 1967. Notes on the formation of fjords and fjord-valleys. Geografiska Annaler: Series A, Physical Geography 49, 188–203.

Hooyer T S, Cohen D, Iverson N R, 2012. Control of glacial quarrying by bedrock joints. Geomorphology 153–154, 91–101.

Houmark-Nielsen M, 2004. The Pleistocene of Denmark: a review of stratigraphy and glaciation history. In Ehlers J, Gibbard P L, Hughes P D (eds). Quaternary glaciations: extent and chronology. Part I: Europe. Amsterdam: Elsevier, 35–46. (Developments in Quaternary Sciences 2)

Houmark-Nielsen M, Kjaer K H, 2003. Southwest Scandinavia, 40–15 kyr BP: palaeogeography and environmental change. Journal of Quaternary Science 18, 769–786.

Hubbard A, Bradwell T, Golledge N R, Hall A M, Patton H, Sugden D E, Cooper R, Stoker M S, 2009. Dynamic cycles, ice streams and their impact on the extent, chronology and deglaciation of the British–Irish ice sheet. Quaternary Science Reviews 28, 758–776.

Hubbard B, Siegert M J, McCarroll D, 2000. Spectral roughness of glaciated bedrock geomorphic surfaces: implications for glacier sliding. Journal of Geophysical Research: Solid Earth 105, 21295–21303.

Hughes A L, Gyllencreutz R, Lohne Ø S, Mangerud J, Svendsen J I, 2016. The last Eurasian ice sheets – a chronological database and time-slice reconstruction, DATED-1. Boreas 45, 1–45.

Huuse H, Lykke-Andersen H, 2000. Overdeepened Quaternary valleys in the eastern Danish North Sea: morphology and origin. Quaternary Science Reviews 19, 1233–1253.

Hättestrand C, Stroeven A P, 2002. A relict landscape in the centre of Fennoscandian glaciation: Geomorphological evidence of minimal Quaternary glacial erosion. Geomorphology 44, 127–143.

Högbom A G, 1910. Precambrian geology of Sweden. Bulletin of the Geological Institutions of Upsala 10, 1–80.

Högbom A G, Ahlström N G, 1924. Über die subkambrische Landflache am Fusse vom Kinnekulle. Bulletin of the Geological Institutions of the University of Uppsala 19, 55–88. (In German.)

Hökmark H, Lönnqvist M, 2014. Reply to comment by Christopher Talbot on "Approach to estimating the maximum depth for glacially induced hydraulic jacking in fractured crystalline rock at Forsmark, Sweden". Journal of Geophysical Research: Earth Surface 119, 955–959.

Hökmark H, Fälth B, Wallroth T, 2006. T-H-M couplings in rock. Overview of results of importance to the SR-Can safety assessment. SKB R-06-88, Svensk Kärnbränslehantering AB.

Hökmark H, Lönnqvist M, Fälth B, 2010. THM-issues in repository rock. Thermal, mechanical, thermo-mechanical and hydro-mechanical evolution of the rock at the Forsmark and Laxemar sites. SKB TR-10-23, Svensk Kärnbränslehantering AB.

Ingmar T, Moreborg K, 1976. The leaching and original content of calcium carbonate in till in northern Uppland, Sweden. Geologiska Föreningen i Stockholm Förhandlingar 98, 120–132.

Iverson N R, 2002. Processes of glacial erosion. In Menzies J (ed). Modern and past glacial environments. Elsevier, 131–145.

Iverson N R, 2012. A theory of glacial quarrying for landscape evolution models. Geology 40, 679–682.

Iverson N R, Cohen D, Hooyer T S, Fischer U H, Jackson M, Moore P L, Lappegard G, Kohler J, 2003. Effects of basal debris on glacier flow. Science 301, 81–84.

Iverson R M, Reid M E, 1992. Gravity-driven groundwater flow and slope failure potential: 1. Elastic Effective-Stress Model. Water Resources Research 28, 925–938.

Jahns R H, 1943. Sheet structure in granites: its origin and use as a measure of glacial erosion in New England. Journal of Geology 51, 71–98.

Jakobsson M, Stranne C, O'Regan M, Greenwood S L, Gustafsson B, Humborg C, Weidner E, 2019. Bathymetric properties of the Baltic Sea. Ocean Science Discussions 15, 905–924.

Jansen J D, Codilean A T, Stroeven A P, Fabel D, Hättestrand C, Kleman J, Harbor J M, Heyman J, Kubik P W, Xu S, 2014. Inner gorges cut by subglacial meltwater during Fennoscandian ice sheet decay. Nat Communications 5, 3815. doi:10.1038/ncomms4815

Jansen J D, Knudsen M F, Andersen J L, Heyman J, Egholm D L, 2019. Erosion rates in Fennoscandia during the past million years. Quaternary Science Reviews 207, 37–48.

Jansson K N, Stroeven A P, Alm G, Dahlgren K I T, Glasser N F, Goodfellow B W, 2011. Using a GIS filtering approach to replicate patterns of glacial erosion. Earth Surface Processes and Landforms 36, 408–418.

Japsen P, Green P F, Bonow J M, Erlström M, 2016. Episodic burial and exhumation of the southern Baltic Shield: Epeirogenic uplifts during and after break-up of Pangaea. Gondwana Research 35, 357–377.

Jaquet O, Siegel P, 2003. Groundwater flow and transport modelling during a glaciation period. SKB R-03-04, Svensk Kärnbränslehantering AB.

Jarsve E M, Krøgli S O, Etzelmüller B, Gabrielsen R H, 2014. Automatic identification of topographic surfaces related to the sub-Cambrian peneplain (SCP) in southern Norway – Surface generation algorithms and implications. Geomorphology 211, 89–99.

Jenness J S, 2004. Calculating landscape surface area from digital elevation models. Wildlife Society Bulletin 32, 829–839.

Johansson M, 1999. Analysis of digital elevation data for palaeosurfaces in south-western Sweden. Geomorphology 26, 279–295.

Johansson M, Olvmo M, Söderström M, 1999. Application of digital elevation and geological data in studies of morphotectonics and relief–a case study of the sub-Cambrian peneplain in southwestern Sweden. Zeitschrift für Geomorphologie 43, 505–520.

Johansson M, Migon P, Olvmo M, 2001a. Development of joint-controlled rock basins in Bohus granite, SW Sweden. Geomorphology 40, 145–161.

Johansson M, Olvmo M, Lidmar-Bergström K, 2001b. Inherited landforms and glacial impact of different palaeosurfaces in southwest Sweden. Geografiska Annaler 83A, 67–89.

Johansson P, 2003. Eskers and bedrock gorges (tunnel valleys) in the Pakasaivo area, western Finnish Lapland. Bulletin of the Geological Society of Finland 75, 5–15.

Johansson P, 2005. Meltwater canyon lakes (saivos) in western Finnish Lapland. In Ojala A E K (ed). Quaternary studies in the northern and Arctic regions of Finland. Espoo: Geological Survey of Finland, 33–39. (Geological Survey of Finland, Special Paper 40)

Juhlin C, Stephens M B, 2006. Gently dipping fracture zones in Paleoproterozoic metagranite, Sweden: Evidence from reflection seismic and cored borehole data and implications for the disposal of nuclear waste. Journal of Geophysical Research: Solid Earth 111, B09302.

Juhlin C, Sturkell E, Ebbestad J O R, Lehnert O, Högström A E S, Meinhold G, 2012. A new interpretation of the sedimentary cover in the western Siljan Ring area, central Sweden, based on seismic data. Tectonophysics 580, 88–99.

Kalm V, Raukas A, Rattas M, Lasberg K, 2011. Pleistocene glaciations in Estonia. In Ehlers J, Gibbard P L, Hughes P D (eds). Quaternary glaciations: extent and chronology: a closer look. Amsterdam: Elsevier, 95–104. (Developments in Quaternary Sciences 15)

Karhu J, 2000. Carbon, oxygen and strontium isotopic characteristics of late-stage fracture calcites at Olkiluoto and Romuvaara. Posiva Working Report 2000-19, Posiva Oy, Finland.

Kehew A E, Piotrowski J A, Jørgensen F, 2012. Tunnel valleys: Concepts and controversies – A review. Earth-Science Reviews 113, 33–58.

Keller C B, Husson J M, Mitchell R N, Bottke W F, Gernon T M, Boehnke P, Bell E A, Swanson-Hysell N L, Peters S E, 2019. Neoproterozoic glacial origin of the Great Unconformity. Proceedings of the National Academy of Sciences 116, 1136–1145.

Kenny G G, Schmieder M, Whitehouse M J, Nemchin A A, Morales L F, Buchner E, Bellucci J J, Snape J F, 2019. A new U-Pb age for shock-recrystallised zircon from the Lappajärvi impact crater, Finland, and implications for the accurate dating of impact events. Geochimica et Cosmochimica Acta 245, 479–494.

Kirsimäe K, Kalm V, Jørgensen P, 1999. Low-temperature diagenetic illite-smectite in Lower Cambrian clays in North Estonia. Clay Minerals 34, 151–163.

Klein R, Salminen J, Mertanen S, 2015. Baltica during the Ediacaran and Cambrian: A paleomagnetic study of Hailuoto sediments in Finland. Precambrian Research 267, 94–105.

Kleman J, 1992. The palimpsest glacial landscape in northwestern Sweden: Late Weichselian deglaciation landforms and traces of older west-centered ice sheets. Geografiska Annaler: Series A, Physical Geography 74, 305–325.

Kleman J, Glasser N F, 2007. The subglacial thermal organisation (STO) of ice sheets. Quaternary Science Reviews 26, 585–597.

Kleman J, Stroeven A P, 1997. Preglacial surface remnants and Quaternary glacial regimes in northwestern Sweden. Geomorphology 19, 35–54.

Kleman J, Hättestrand C, Borgström I, Stroeven A, 1997. Fennoscandian palaeoglaciology reconstructed using a glacial geological inversion model. Journal of Glaciology 43, 283–299.

Kleman J, Hättestrand C, Clarhäll A, 1999. Zooming in on frozen-bed patches: scale-dependent controls on Fennoscandian ice sheet basal thermal zonation. Annals of Glaciology 28, 189–194.

Kleman J, Stroeven A P, Lundqvist J, 2008. Patterns of Quaternary ice sheet erosion and deposition in Fennoscandia and a theoretical framework for explanation. Geomorphology 97, 73–90.

Knudsen C, Frei D, Rasmussen T, Rasmussen E S, McLimans R, 2005. New methods in provenance studies based on heavy minerals: an example from Miocene sands in Jylland, Denmark. Geological Survey of Denmark and Greenland Bulletin 7, 29–32.

Knudsen M F, Egholm D L, Jansen J D, 2019. Time-integrating cosmogenic nuclide inventories under the influence of variable erosion, exposure, and sediment mixing. Quaternary Geochronology 51, 110–119.

Kohl C P, Nishiizumi K, 1992. Chemical isolation of quartz for measurement of *in-situ*-produced cosmogenic nuclides. Geochimica et Cosmochimica Acta 56, 3583–3587.

Kohonen J, Rämö O T, 2005. Sedimentary rocks, diabases, and late cratonic evolution. In Lehtinen M, Nurmi P A, Rämö O T (eds.). Precambrian geology of Finland: key to the evolution of the Fennoscandian shield. Amsterdam: Elsevier, 563–603.

Kor P S G, Shaw J, Sharpe D R, 1991. Erosion of bedrock by subglacial meltwater, Georgian Bay, Ontario: a regional view. Canadian Journal of Earth Sciences 28, 623–642.

Korja A, Heikkinen P, Aaro S, 2001. Crustal structure of the northern Baltic Sea palaeorift. Tectonophysics 331, 341–358.

Korschinek G, Bergmaier A, Faestermann T, Gerstmann U C, Knie K, Rugel G, Wallner A, Dillmann I, Dollinger G, Lierse von Gostomski C, Kossert K, Maiti M, Poutivtsev M, Remmert A, 2010. A new value for the half-life of ^{10}Be by Heavy-Ion Elastic Recoil Detection and liquid scintillation counting. Nuclear Instruments and Methods in Physics Research Section B: Beam Interactions with Materials and Atoms 268, 187–191.

Krabbendam M, 2016. Sliding of temperate basal ice on a rough, hard bed: creep mechanisms, pressure melting, and implications for ice streaming. The Cryosphere 10, 1915–1932.

Krabbendam M, Bradwell T, 2011. Lateral plucking as a mechanism for elongate erosional glacial bedforms: explaining megagrooves in Britain and Canada. Earth Surface Processes and Landforms 36**,** 1335–1349.

Krabbendam M, Bradwell T, 2013. Glacial erosion of gneiss terrains: a re-assessment of the landscape of areal scouring and implications for bed roughness below ice sheets. EGU General Assembly Conference Abstracts, 4102.

Krabbendam M, Bradwell T, 2014. Quaternary evolution of glaciated gneiss terrains: pre-glacial weathering vs. glacial erosion. Quaternary Science Reviews 95, 20–42.

Krabbendam M, Glasser N F, 2011. Glacial erosion and bedrock properties in NW Scotland: abrasion and plucking, hardness and joint spacing. Geomorphology 130, 374–383.

Krabbendam M, Hall A M, 2019. Subglacial block removal – a preliminary analysis of driving and resisting forces under different glaciological scenarios. SKB TR-19-18, Svensk Kärnbränslehantering AB.

Krabbendam M, Eyles N, Putkinen N, Bradwell T, Arbelaez-Moreno L, 2016. Streamlined hard beds formed by palaeo-ice streams: A review. Sedimentary Geology 338, 24–50.

Krabbendam M, Bradwell T, Everest J D, Eyles N, 2017. Joint-bounded crescentic scars formed by subglacial clast-bed contact forces: Implications for bedrock failure beneath glaciers. Geomorphology 290, 114–127.

Krall L, Evins L Z, Kooijman E, Whitehouse M, Tullborg E-L, 2018. Tracing the palaeoredox conditions at Forsmark, Sweden, using uranium mineral geochronology. Chemical Geology 506, 68–78.

Krall L, Sandström B, Tullborg E-L, Evins L Z, 2015. Natural uranium in Forsmark, Sweden: The solid phase. Applied Geochemistry 59, 178–188.

Kresten P, Chyssler J, 1976. The Götemar massif in south-eastern Sweden: a reconnaissance survey. Geologiska Föreningen i Stockholm Förhandlingar 98, 155–161.

Kresten P, Troll V R, 2018. The Alnö Carbonatite Complex, Central Sweden. Berlin: Springer.

Laajoki K, 2002. New evidence of glacial abrasion of the late Proterozoic unconformity around Varangerfjorden, Northern Norway. Precambrian Sedimentary Environments: A Modern Approach to Ancient Depositional Systems, 405–436.

Laajoki K, 2003. The Larajæg'gi outcrop – a large combined Neoproterozoic/Pleistocene roche moutonnée at Karlebotn, Finnmark, North Norway. Norwegian Journal of Geology 84, 107–115.

Laban C, van der Meer J J M, 2011. Pleistocene glaciation in The Netherlands. In Ehlers J, Gibbard P L, Hughes P D (eds). Quaternary glaciations: extent and chronology: a closer look. Amsterdam: Elsevier, 247–260. (Developments in Quaternary Sciences 15)

Laberg J S, Andreassen K, Vorren T O, 2012. Late Cenozoic erosion of the high-latitude south-western Barents Sea shelf revisited. Geological Society of America Bulletin 124, **77**–88.

Lagasquie J-J, Lageat Y, Godard A, 2001. Rock resistance and its influence on landforms in basement terrains. In Godard A, Lagasquie J-J, Lageat Y (eds). Basement regions. Berlin: Springer, 93–116.

Lagerbäck R, 1988a. Periglacial phenomena in the wooded areas of northern Sweden – relicts from the Tärendö interstadial. Boreas 17, 487–499.

Lagerbäck R, 1988b. The Veiki moraines in northern Sweden: widespread evidence of an Early Weichselian deglaciation. Boreas 17, 469–486.

Lagerbäck R, Sundh M, Svedlund J-O, Johansson H, 2005. Forsmark site investigation Searching for evidence of late-or post-glacial faulting in the Forsmark region. Results from 2002–2004. SKB R-05-51, Svensk Kärnbränslehantering AB.

Lal D, 1991. Cosmic ray labeling of erosion surfaces: in situ nuclide production rates and erosion models. Earth and Planetary Science Letters 104, 424–439.

Larson S-A, Tullborg E-L, Cederbom C, Stiberg J-P, 1999. Sveconorwegian and Caledonian foreland basins in the Baltic Shield revealed by fission-track thermochronology. Terra Nova 11, 210–215.

Lassen A, Thybo H, 2012. Neoproterozoic and Palaeozoic evolution of SW Scandinavia based on integrated seismic interpretation. Precambrian Research 204–205, 75–104.

Lee J R, Phillips E, 2013. Glacitectonics – a key approach to examining ice dynamics, substrate rheology and ice-bed coupling. Proceedings of the Geologists' Association 124, 731–737.

Lehtovaara J J, 1982. Stratigraphical section through Lower Cambrian at Söderfjärden, Vaasa, western Finland. Bulletin of the Geological Society of Finland 54, 35–43.

Leijon B (ed), 2005. Forsmark site investigation. Investigations of superficial fracturing and block displacements at drill site 5. SKB P-05-199, Svensk Kärnbränslehantering AB.

Leith K, Moore J R, Amann F, Loew S, 2014. Subglacial extensional fracture development and implications for Alpine Valley evolution. Journal of Geophysical Research: Earth Surface 119, 62–81.

Lidén A, 1975. Till petrographical studies in an Archaen bedrock area in southern central Sweden. (Striea 1)

Lidmar-Bergström K, 1988. Denudation surfaces of a shield area in south Sweden. Geografiska Annaler: Series A, Physical Geography 70, 337–350.

Lidmar-Bergström K, 1991. Phanerozoic tectonics in southern Sweden. Zeitschrift für Geomorphologie, Supplementband 82, 1–16.

Lidmar-Bergström K, 1993. Denudation surfaces and tectonics in the southernmost part of the Baltic Shield. Precambrian Research 64, 337–345.

Lidmar-Bergström K, 1994. Morphology of the bedrock surface. In Fredén C (ed). National atlas of Sweden. Stockholm: Almqvist and Wiksell International, 44–54.

Lidmar-Bergström K, 1995. Relief and saprolites through time on the Baltic Shield. Geomorphology 12, 45–61.

Lidmar-Bergström K, 1996. Long term morphotectonic evolution in Sweden. Geomorphology 16, 33–59.

Lidmar-Bergström K, 1997. A long-term perspective on glacial erosion. Earth Surface Processes and Landforms 22, 297–306.

Lidmar-Bergström K, 1999. Uplift histories revealed by landforms of the Scandinavian domes. In Smith B J, Whalley W B, Warke P A (eds). Uplift, erosion and stability: perspectives on long-term landscape development. London: Geological Society, 85–91. (Special publication 162.)

Lidmar-Bergström K, Näslund J O, 2002. Landforms and uplift in Scandinavia. Geological Society, London, Special Publications 196, 103–116.

Lidmar-Bergström K, Olvmo M, 2015. Plains, steps, hilly relief and valleys in northern Sweden – review, interpretations and implications for conclusions on Phanerozoic tectonics. Uppsala: Sveriges geologiska undersökning. (SGU Research Paper C 838.)

Lidmar-Bergström K, Bonow J M, Japsen P, 2012. Stratigraphic Landscape Analysis and geomorphological paradigms: Scandinavia as an example of Phanerozoic uplift and subsidence. Global and Planetary Change 100, 153–171.

Lidmar-Bergström K, Olvmo M, Bonow J M, 2017. The South Swedish Dome: a key structure for identification of peneplains and conclusions on Phanerozoic tectonics of an ancient shield. GFF 139, 244–259.

Lifton N, Sato T, Dunai T J, 2014. Scaling *in situ* cosmogenic nuclide production rates using analytical approximations to atmospheric cosmic-ray fluxes. Earth and Planetary Science Letters 386, 149–160.

Liivamägi S, 2015. Neoproterozoic Baltic paleosol: geology and paleoenvironmental interpretation. PhD thesis. University of Tartu, Estonia.

Liivamägi S, Somelar P, Vircava I, Mahaney W C, Kirs J, Kirsimäe K, 2015. Petrology, mineralogy and geochemical climofunctions of the Neoproterozoic Baltic paleosol. Precambrian Research 256, 170–188.

Lindner L, Marks L, 2008. Pleistocene stratigraphy of Poland and its correlation with stratotype sections in the Volhynian Upland (Ukraine). Geochronometria 31, 31–37.

Lindskog A, Lindskog A M L, Johansson J V, Ahlberg P, Eriksson M E, 2018. The Cambrian-Ordovician succession at Lanna, Sweden: stratigraphy and depositional environments. Estonian Journal of Earth Sciences 67, 133–148.

Lindström E, 1988. Are roches moutonnées mainly preglacial forms? Geografiska Annaler: Series A, Physical Geography 70, 323–332.

Lindström M, Flodén T, Grahn Y, Kathol B, 1994. Post-impact deposits in Tvären, a marine Middle Ordovician crater south of Stockholm, Sweden. Geological Magazine 131, 91–103.

Linton D L, 1963. The forms of glacial erosion. Transactions and Papers (Institute of British Geographer) 33, 1–28.

Lisiecki L E, Raymo M E, 2005. A Pliocene-Pleistocene stack of 57 globally distributed benthic $\delta^{18}O$ records. Paleoceanography and Paleoclimatology 20, PA1003. doi:10.1029/2004PA001071

Litt T, Schmincke H-U, Frechen M, Schlüchter C, 2008. Quaternary. In McCann T (ed). The geology of Central Europe. Vol 2. Mesozoic and Cenozoic. London: Geological Society, 1287–1340.

Ljungner E, 1930. Spaltentektonik und Morphologie der schwedischen Skagerrak-Küste. Teil 111. Die Erosionsformen. Bulletin of the Geological Institutions of the University of Uppsala 21, 255–475. (In German.)

Lord N S, Lunt D, Thorne M, 2019. Modelling changes in climate over the next 1 million years. SKB TR-19-09, Svensk Kärnbränslehantering AB.

Lundmark A M, Lamminen J, 2016. The provenance and setting of the Mesoproterozoic Dala Sandstone, western Sweden, and paleogeographic implications for southwestern Fennoscandia. Precambrian Research 275, 197–208.

Lundqvist J, 1973. Dark bluish boulder-clay: A possible deposit from the first Würm glaciation. Bulletin of the Geological Institutions of the University of Uppsala, New Series 5, 19–20.

Lundqvist J, 1987. Glaciodynamics of the Younger Dryas Marginal zone in Scandinavia: implications of a revised glaciation model. Geografiska Annaler: Series A, Physical Geography 69, 305–319.

Lundqvist J, 2004. Glacial history of Sweden. In Ehlers J, Gibbard P L, Hughes P D (eds). Quaternary glaciations: extent and chronology. Part I: Europe. Amsterdam: Elsevier, 401–412. (Developments in Quaternary Sciences 2.)

Löfgren A, Laufeld S, 2007. Ordovician limestone in Hälsingland, Sweden. GFF 129, 113–116.

Lönnqvist M, Hökmark H, 2013. Approach to estimating the maximum depth for glacially induced hydraulic jacking in fractured crystalline rock at Forsmark, Sweden. Journal of Geophysical Research: Earth Surface 118, 1777–1791.

Maizels J, 1989. Sedimentary, palaeoflow dynamics and flood history of jökulhlaup deposits: palaeohydrology of Holocene sedimentary sequences in the southern Iceland sandur deposits. Journal of Sedimentary Petrology 59, 204–223.

Manel S, Williams H C, Ormerod S J, 2001. Evaluating presence–absence models in ecology: the need to account for prevalence. Journal of Applied Ecology 38, 921–931.

Mangerud J, Jansen E, Landvik J Y, 1996. Late Cenozoic history of the Scandinavian and Barents Sea ice sheets. Global and Planetary Change 12, 11–26.

Mangerud J, Gyllencreutz R, Lohne Ø, Svendsen J I, 2011. Glacial history of Norway. In Ehlers J, Gibbard P L, Hughes P D (eds). Quaternary glaciations: extent and chronology: a closer look. Amsterdam: Elsevier, 279–298. (Developments in Quaternary Sciences 15.)

Marks L, 2011. Quaternary glaciations in Poland. In Ehlers J, Gibbard P L, Hughes P D (eds). Quaternary glaciations: extent and chronology: a closer look. Amsterdam: Elsevier, 299–303. (Developments in Quaternary Sciences 15.)

Marmefelt E, Omstedt A, 1993. Deep water properties in the Gulf of Bothnia. Continental Shelf Research 13, 169–187.

Marrero S M, Phillips F M, Borchers B, Lifton N, Aumer R, Balco G, 2016. Cosmogenic nuclide systematics and the CRONUScalc program. Quaternary Geochronology 31, 160–187.

Martel S J, 2000. Modeling elastic stresses in long ridges with the displacement discontinuity method. Pure and Applied Geophysics 157, 1039.

Martel S J, 2016. Effects of small-amplitude periodic topography on combined stresses due to gravity and tectonics. International Journal of Rock Mechanics and Mining Sciences 89, 1–13.

Martel S J, Muller J R, 2000. A two-dimensional boundary element method for calculating elastic gravitational stresses in slopes. Pure and Applied Geophysics 157, 989–1007.

Martin C D, 2007. Quantifying in situ stress magnitudes and orientations for Forsmark. Forsmark stage 2.2. SKB R-07-26, Svensk Kärnbränslehantering AB.

Martinsson A, 1968. Cambrian palaeontology of Fennoscandian basement fissures. Lethaia 1, 137–155.

Martinsson A, 1974. The Cambrian of Norden. In Holland C H (ed). Lower Palaeozoic rocks of the world. Vol 2. Cambrian of the British Isles, Norden, and Spitsbergen. London: Wiley, 185–283.

Mas Ivars D, Hakami H, 2005. Effect of a sub-horizontal fracture zone and rock mass heterogeneity on the stress field in Forsmark area – A numerical study using 3DEC. Preliminary site description Forsmark area – version 1.2. SKB R-05-59, Svensk Kärnbränslehantering AB.

Mattsson Å, 1962. Morphologische Studien in Südschweden und auf Bornholm über die nichtglaciale Formenwelt der Felsenskulptur. PhD thesis. Lund: Gleerup. (Meddelanden från Lunds universitets geografiska institiution. Avhandlingar 39). (In German.)

McCarroll D, 1991. The Schmidt hammer, weathering and rock surface roughness. Earth Surface Processes and Landforms 16, 477–480.

McDermott J, Redfield T, Terje Osmundsen P, Arnhold C, Conrad D, 2015. A geomorphological analysis of the Cenozoic rejuvenation of the Southwestern Norwegian ‘passive’ margin. EGU General Assembly Conference Abstracts, 3098.

Medvedev S, Souche A, Hartz E H, 2013. Influence of ice sheet and glacial erosion on passive margins of Greenland. Geomorphology 193, 36–46.

Meidla T, 2017. Ediacaran and Cambrian stratigraphy in Estonia: an updated review. Estonian Journal of Earth Sciences 66, 152–160.

Melanson A, Bell T, Tarasov L, 2013. Numerical modelling of subglacial erosion and sediment transport and its application to the North American ice sheets over the Last Glacial cycle. Quaternary Science Reviews 68, 154–174.

Merritt J W, 1992. The high-level marine shell-bearing deposits of Clava, Inverness-shire, and their origin as glacial rafts. Quaternary Science Reviews 11, 759–779.

Merritt J W, Connell E R, Hall A M, 2017. Middle to Late Devensian glaciation of north-east Scotland: implications for the north-eastern quadrant of the last British-Irish ice sheet. Journal of Quaternary Science 32, 276–294.

Merritt J W, Hall A M, Gordon J E, Connell E R, 2019. Late Pleistocene sediments, landforms and events in Scotland: a review of the terrestrial stratigraphic record. Earth and Environmental Science Transactions of the Royal Society of Edinburgh 110, 39–91.

Miettinen A, Rinne K, Haila H, Hyvärinen H, Eronen M, Delusina I, Kadastik E, Kalm V, Gibbard P, 2002. The marine Eemian of the Baltic: new pollen and diatom data from Peski, Russia, and Pohja-Uhtju, Estonia. Journal of Quaternary Science 17, 445–458.

Migoń P, Lidmar-Bergström K, 2001. Weathering mantles and their significance for geomorphological evolution of central and northern Europe since the Mesozoic. Earth-Science Reviews 56, 285–324.

Mikko H, Smith C A, Lund B, Ask M V S, Munier R, 2015. LiDAR-derived inventory of post-glacial fault scarps in Sweden. GFF 137, 334–338.

Miller D J, Dunne T, 1996. Topographic perturbations of regional stresses and consequent bedrock fracturing. Journal of Geophysical Research: Solid Earth 101, 25523–25536.

Milnes A G, 2002. Swedish deep repository siting programme. Guide to the documentation of 25 years of geoscientific research (1976–2000). SKB TR-02-18, Svensk Kärnbränslehantering AB.

Min K-B, Rutqvist J, Tsang C-F, Jing L, 2004. Stress-dependent permeability of fractured rock masses: a numerical study. International Journal of Rock Mechanics and Mining Sciences 41, 1191–1210.

Miska L, Jan H, 2005. Evaluation of current statistical approaches for predictive geomorphological mapping. Geomorphology 67, 299–315.

Mitchell S G, Montgomery D R, 2006. Influence of a glacial buzzsaw on the height and morphology of the Cascade Range in central Washington State, USA. Quaternary Research 65, 96–107.

Moon S, Goodfellow B W, Perron J T, Martel S J, Caffee M W, Ebert K, Hall A, Hättestrand C, Heyman J, Mas Ivars D, Näslund J-O, Stroeven A, 2017. Interaction of strong compressive stresses with topography: Implications for bedrock fractures in Forsmark, Sweden. Geological Society of America Abstracts with Programs 49. doi:10.1130/abs/2017AM-300641

Mörner N-A, 2004. Active faults and paleoseismicity in Fennoscandia, especially Sweden. Primary structures and secondary effects. Tectonophysics 380, 139–157.

Mörner N-A, 2011. Paleoseismology: The application of multiple parameters in four case studies in Sweden. Quaternary International 242, 65–75.

Mörner N-A, Einar Tröften P, Sjöberg R, Grant D, Dawson S, Bronge C, Kvamsdal O, Sidén A, 2000. Deglacial paleoseismicity in Sweden: the 9663 BP Iggesund event. Quaternary Science Reviews 19, 1461–1468.

Munier R, Talbot C, 1993. Segmentation, fragmentation and jostling of cratonic basement in and near Äspö, southeast Sweden. Tectonics 12, 713–727.

Müller N, Hartung J B, Jessberger E K, Reimold W U, 1990. ^{40}Ar-^{39}Ar ages of Dellen, Jänisjärvi, and Sääksjärvi impact craters. Meteoritics 25, 1–10.

Nelson S J, Johnson M E, 2002. Jens Munk Archipelago: Ordovician-Silurian islands in the Churchill area of the Hudson Bay lowlands, northern Manitoba. The Journal of Geology 110, 577–589.

Newman D R, Lindsay J B, Cockburn J M H, 2018. Evaluating metrics of local topographic position for multiscale geomorphometric analysis. Geomorphology 312, 40–50.

Nielsen A T, Schovsbo N H, 2006. Cambrian to basal Ordovician lithostratigraphy in southern Scandinavia. Bulletin of the Geological Society of Denmark 53, 47–92.

Nielsen A T, Schovsbo N H, 2011. The Lower Cambrian of Scandinavia: Depositional environment, sequence stratigraphy and palaeogeography. Earth-Science Reviews 107, 207–310.

Nielsen A T, Schovsbo N H, 2015. The regressive Early-Mid Cambrian 'Hawke Bay Event'in Baltoscandia: epeirogenic uplift in concert with eustasy. Earth-Science Reviews 151, 288–350.

Nironen M, 2017. Guide to the geological map of Finland–Bedrock 1: 1 000 000. Geological Survey of Finland, Special Paper 60, 41–76.

Nishiizumi K, 2004. Preparation of ^{26}Al AMS standards. Nuclear Instruments and Methods in Physics Research Section B: Beam Interactions with Materials and Atoms 223, 388–392.

Nishiizumi K, Winterer E L, Kohl C P, Klein J, Middleton R, Lal D, Arnold J R, 1989. Cosmic ray production rates of ^{10}Be and ^{26}Al in quartz from glacially polished rocks. Journal of Geophysical Research: Solid Earth 94, 17907–17915.

Nishiizumi K, Imamura M, Caffee M W, Southon J R, Finkel R C, McAninch J, 2007. Absolute calibration of ^{10}Be AMS standards. Nuclear Instruments and Methods in Physics Research Section B: Beam Interactions with Materials and Atoms 258, 403–413.

Nye J F, 1952. The mechanics of glacier flow. Journal of Glaciology 2, 82–93.

Nyström J O, Levi B, 1980. Pumpellyite-bearing Precambrian rocks and post-Svecokarelian regional metamorphism in central Sweden. Geologiska Föreningen i Stockholm Förhandlingar 102, 37–39.

Nystuen J P, Andresen A, Kumpulainen R A, Siedlecka A, 2008. Neoproterozoic basin evolution in Fennoscandia, East Greenland and Svalbard. Episodes 31, 35–43.

Näslund J-O, 2006. Climate and climate-related issues for the safety assessment SR-Can. SKB TR-06-23, Svensk Kärnbränslehantering AB.

Näslund J-O, Rodhe L, Fastook J L, Holmlund P, 2003. New ways of studying ice sheet flow directions and glacial erosion by computer modelling – examples from Fennoscandia. Quaternary Science Reviews 22, 245–258.

Näslund J-O, Jansson P, Fastook J L, Johnson J, Andersson L, 2005. Detailed spatially distributed geothermal heat-flow data for modeling of basal temperatures and meltwater production beneath the Fennoscandian ice sheet. Annals of Glaciology 40, 95–101.

Näslund J-O, Wohlfarth B, Alexanderson H, Helmens K, Hättestrand M, Jansson P, Kleman J, Lundqvist J, Brandefelt J, Houmark-Nielsen M, Kjellström E, Strandberg G, Knudsen K L, Krog Larsen N, Ukkonen P, Mangerud J, 2008. Fennoscandian paleo-environment and ice sheet dynamics during Marine Isotope Stage (MIS) 3. Report of a workshop held September 20–21, 2007 in Stockholm, Sweden. SKB R-08-79, Svensk Kärnbränslehantering AB.

Olesen O, Bering D, Brönner M, Dalsegg E, Fabian K, Fredin O, Gellein J, Husteli B, Magnus C, Rønning J S, Solbakk T, Tønnesen J F, Øverland J A, 2012. Tropical weathering in Norway, TWIN final report. NGU-report 2012.005, Geological Survey of Norway.

Olofsson I, Simeonov A, Stigsson M, Stephens M, Follin S, Nilsson A C, Röshoff K, Lindberg U, Lanaro F, Fredriksson L, Persson L, 2007. Site descriptive modelling Forsmark, stage 2.2, a fracture domain concept as a basis for the statistical modelling of fractures and minor deformation zones, and interdisciplinary coordination. SKB R-07-15, Svensk Kärnbränslehantering AB.

Olvmo M, 1985. Meltwater canyons of the "kursu" and the "skura" type. Geografiska Annaler: Series A, Physical Geography 67, 133–137.

Olvmo M, 2010. Review of denudation processes and quantification of weathering and erosion rates at a 0.1 to 1 Ma time scale. SKB TR-09-18, Svensk Kärnbränslehantering AB.

Olvmo M, Johannson M, 2002. The significance of rock structure, lithology and pre-glacial deep weathering for the shape of intermediate-scale glacial erosional landforms. Earth Surface Processes and Landforms 27, 251–268.

Olvmo M, Lidmar-Bergström K, Lindberg G, 1999. The glacial impact on an exhumed sub-Mesozoic etchsurface in south-western Sweden. Annals of Glaciology 28, 153–160.

Olvmo M, Lidmar-Bergstrom K, Ericson K, Bonow J M, 2005. Saprolite Remnants as Indicators of Pre-Glacial Landform Genesis in Southeast Sweden. Geografiska Annaler: Series A, Physical Geography 87, 447–460.

Ormö J, Nielsen A T, Alwmark C, 2017. The Vakkejokk Breccia: An Early Cambrian proximal impact ejecta layer in the North-Swedish Caledonides. Meteoritics & Planetary Science 52, 623–645.

Overeem I, Weltje G J, Bishop-Kay C, Kroonenberg S B, 2001. The Late Cenozoic Eridanos delta system in the Southern North Sea Basin: a climate signal in sediment supply? Basin Research 13, 293–312.

Page L, Hermansson T, Söderlund P, Stephens M, 2007. Forsmark site investigation. $^{40}Ar/^{39}Ar$ and (U-Th)/He Geochronology: Phase 2. SKB P-06-211, Svensk Kärnbränslehantering AB.

Parnell J, Mark D F, Frei R, Fallick A E, Ellam R M, 2014. $^{40}Ar/^{39}Ar$ dating of exceptional concentration of metals by weathering of Precambrian rocks at the Precambrian–Cambrian boundary. Precambrian Research 246, 54–63.

Patton H, Hubbard A, Andreassen K, Winsborrow M, Stroeven A P, 2016. The build-up, configuration, and dynamical sensitivity of the Eurasian ice-sheet complex to Late Weichselian climatic and oceanic forcing. Quaternary Science Reviews 153, 97–121.

Paulamäki S, Kuivamäki A, 2006. Depositional history and tectonic regimes within and in the margins of the Fennoscandian Shield during the last 1300 million years. Posiva Working Report 2006-43, Posiva Oy, Finland.

Pehr K, Love G D, Kuznetsov A, Podkovyrov V, Junium C K, Shumlyanskyy L, Sokur T, Bekker A, 2018. Ediacara biota flourished in oligotrophic and bacterially dominated marine environments across Baltica. Nature Communications 9, 1807.

Persson C, 1985. Beskrivning till jordartskartan Östhammar NO. Beskrivning till jordartskartan Östhammar NO – Description to the Quaternary map Östhammar NO. Uppsala: Sveriges geologiska undersökning. (Ae 73)

Persson C, 1992. The latest ice recession and till deposits in northern Uppland, eastern central Sweden. SGU Bulletin 81, 217–224.

Persson K S, Sjöström H, 2003. Late-orogenic progressive shearing in eastern Bergslagen, central Sweden. GFF 125, 23–36.

Persson T, 1969. Skuror och andra erosionsrännor inom Smålands högland. Svensk geografisk årsbok 45, 73—98. (In Swedish.)

Peters S E, Gaines R R, 2012. Formation of the `Great Unconformity' as a trigger for the Cambrian explosion. Nature 484, 363–366.

Petronis M S, O'Driscoll B, Stevenson C T E, Reavy R J, 2012. Controls on emplacement of the Caledonian Ross of Mull Granite, NW Scotland: Anisotropy of magnetic susceptibility and magmatic and regional structures. GSA Bulletin 124, 906–927.

Peulvast J-P, Bouchard M, Jolicoeur S, Pierre G, Schroeder J, 1996. Palaeolandforms and morphotectonic evolution around the Baie des Chaleurs (eastern Canada). Geomorphology 16, 5–32.

Peulvast J-P, Bonow J M, Japsen P, Wilson R W, McCaffrey K J W, 2011. Morphostructural patterns and landform generations in a glaciated passive margin: the Kobberminebugt-Qaqortoq region of South Greenland. Geodinamica Acta 24, 1–19.

Phillips E R, 2018. Glacitectonics. In Menzies J, van der Meer J J M (eds). Past glacial environments. 2nd ed. Amsterdam: Elsevier, 467–502.

Phillips F M, Argento D C, Balco G, Caffee M W, Clem J, Dunai T J, Finkel R, Goehring B, Gosse J C, Hudson A M, Jull A J T, Kelly M A, Kuz M, Lal D, Lifton N, Marrero S M, Nishiizumi K, Reedy R C, Schaefer J, Stone J O H, Swanson T, Zreda M G, 2016. The CRONUS-Earth project: a synthesis. Quaternary Geochronology 31, 119–154.

Pokki J, Kohonen J, Lahtinen R, Rämö O, Andersen T, 2013a. Petrology and provenance of the Mesoproterozoic Satakunta sandstone, SW Finland. Geological Survey of Finland, Report of Investigation 204, 1–61.

Pokki J, Kohonen J, Rämö O T, Andersen T, 2013b. The Suursaari conglomerate (SE Fennoscandian shield; Russia) – Indication of cratonic conditions and rapid reworking of quartz arenitic cover at the outset of the emplacement of the rapakivi granites at ca. 1.65Ga. Precambrian Research 233, 132–143.

Porter S C, 1989. Some geological implications of average Quaternary conditions. Quaternary Research 32, 245–261.

Preeden U, Mertanen S, Elminen T, Plado J, 2009. Secondary magnetizations in shear and fault zones in southern Finland. Tectonophysics 479, 203–213.

Preusser F, Reitner J M, Schlüchter C, 2010. Distribution, geometry, age and origin of overdeepened valleys and basins in the Alps and their foreland. Swiss Journal of Geosciences 103, 407–426.

Punkari M, 1997. Subglacial processes of the Scandinavian Ice Sheet in Fennoscandia inferred from flow-parallel features and lithostratigraphy. Sedimentary Geology 111, 263–283.

Pusch R, Börgesson L, Knutsson S, 1990. Origin of silty fracture fillings in crystalline bedrock. Geologiska Föreningen i Stockholm Förhandlingar 112, 209–213.

Putkonen J, Swanson T, 2003. Accuracy of cosmogenic ages for moraines. Quaternary Research 59, 255–261.

Puura V, Amantov A, Tikhomirov S, Laitakari I, 1996. Latest events affecting the Precambrian basement, Gulf of Finland and surrounding areas. In Koistinen T J (ed). Explanation to the map of Precambrian basement of the Gulf of Finland and surrounding area 1:1 mill. Espoo: Geological Survey of Finland, 115–125. (Geological Survey of Finland, Special Paper 21)

Påsse T, 2004. The amount of glacial erosion of the bedrock. SKB TR-04-25, Svensk Kärnbränslehantering AB.

Påsse T, Daniels J, 2015. Past shore-level and sea-level displacements. Uppsala: Sveriges geologiska undersökning. (Rapporter och meddelanden 137)

Quiquet A, Colleoni F, Masina S, 2016. Long-term safety of a planned geological repository for spent nuclear fuel in Forsmark, Sweden and Olkiluoto, Finland. Phase 2: impact of ice sheet dynamics, climate forcing and multi-variate sensitivity analysis on maximum ice sheet thickness. SKB TR-16-02, Svensk Kärnbränslehantering AB.

Rastas J, Seppälä M, 1981. Rock jointing and abrasion forms on *roches moutonnées*, southwest Finland. Annals of Glaciology 2, 159–163.

Raukas A, 1991. Eemian interglacial record in the northwestern European part of the Soviet Union. Quaternary International 10, 183–189.

Reinardy B T I, Hjelstuen B O, Sejrup H P, Augedal H, Jørstad A, 2017. Late Pliocene-Pleistocene environments and glacial history of the northern North Sea. Quaternary Science Reviews 158, 107–126.

Riihimaki C A, MacGregor K R, Anderson R S, Anderson S P, Loso M G, 2005. Sediment evacuation and glacial erosion rates at a small alpine glacier. Journal of Geophysical Research: Earth Surface 110. doi:10.1029/2004JF000189

Risberg J, 1999. Strandförskjutningen i nordvästra Uppland under subboreal tid. In Segerberg A (ed). Bälinge mossar: kustbor i Uppland under yngre stenålder. PhD thesis. Uppsala University, Appendix 4. (In Swedish.)

Roberts D H, Long A J, 2005. Streamlined bedrock terrain and fast ice flow, Jakobshavns Isbrae, West Greenland: implications for ice stream and ice sheet dynamics. Boreas 34, 25–42.

Robertsson A-M, 2004. Forsmark site investigation. Microfossil analyses of till and sediment samples from Forsmark, northern Uppland. SKB P-04-110, Svensk Kärnbränslehantering AB.

Robertsson A-M, Persson C, 1989. Biostratigraphical studies of three mires in northern Uppland, Sweden. Uppsala: Sveriges geologiska undersökning. (Serie C 821.)

Robertsson A-M, Lundqvist J, Brunnberg L, 2005. Dark clayey till in central and northern Sweden – microfossil content and stratigraphical importance. GFF 127, 169–178.

Rosendahl H, 1934. The geology of the Finse district. Proceedings of the Geologists' Association 45, 367–372, IN15–IN16.

Rudberg S, 1954. Västerbottens berggrundsmorfologi: ett försök till rekonstruktion av preglaciala erosionsgenerationer i Sverige. PhD thesis. Uppsala university. (Geographica 25) (In Swedish.)

Rudberg S, 1970. The sub-Cambrian peneplain in Sweden and its slope gradient. Zeitschrift für Geomorphologie 9, 157–167.

Rudberg S, 1973. Glacial erosion forms of medium size: a discussion based on four Swedish case studies. Zeitscrift für Geomorphologie NF Supplementband 17, 33–48.

Rudberg S, 1988. Gross morphology of Fennoscandia – six complementary ways of explanation. Geografiska Annaler: Series A, Physical Geography 70, 135–167.

Rychel J, Woronko B, Karasiewicz M T, Szymczuk P, Morawski M, 2015. Ice-sheet dynamics of warta glaciation (Saale) in the marginal zone of Knyszewicze area, Northeastern Poland. Studia Quaternaria 32, 79–90.

Saintot A, Stephens M, Viola G, Nordgulen Ø, 2011. Brittle tectonic evolution and paleostress field reconstruction in the southwestern part of the Fennoscandian Shield, Forsmark, Sweden. Tectonics 30. doi:10.1029/2010TC002781

Salonen V-P, 1986. Glacial transport distance distributions of surface boulders in Finland. Espoo: Geological Survey of Finland. (Geological Survey of Finland, Bulletin 338.)

Sandström B, Tullborg E-L, 2009. Episodic fluid migration in the Fennoscandian Shield recorded by stable isotopes, rare earth elements and fluid inclusions in fracture minerals at Forsmark, Sweden. Chemical Geology 266, 126–142.

Sandström B, Page L, Tullborg E-L, 2006a. Forsmark site investigation. $^{40}Ar/^{39}Ar$ (adularia) and Rb-Sr (adularia, prehnite, calcite) ages of fracture minerals. SKB P-06-213, Svensk Kärnbränslehantering AB.

Sandström B, Tullborg E-L, Torres T D, Ortiz J E, 2006b. The occurrence and potential origin of asphaltite in bedrock fractures, Forsmark, central Sweden. GFF 128, 233–242.

Sandström B, Tullborg E-L, Smellie J, MacKenzie A B, Suksi J, 2008. Fracture mineralogy of the Forsmark site. SDM-Site Forsmark. SKB R-08-102, Svensk Kärnbränslehantering AB.

Sandström B, Tullborg E-L, Larson S Å, Page L, 2009. Brittle tectonothermal evolution in the Forsmark area, central Fennoscandian Shield, recorded by paragenesis, orientation and $^{40}Ar/^{39}Ar$ geochronology of fracture minerals. Tectonophysics 478, 158–174.

Sandström B, Annersten H, Tullborg E-L, 2010. Fracture-related hydrothermal alteration of metagranitic rock and associated changes in mineralogy, geochemistry and degree of oxidation: a case study at Forsmark, central Sweden. International Journal of Earth Sciences 99, 1–25.

Schermer E R, Redfield T F, Indrevær K, Bergh S G, 2017. Geomorphology and topography of relict surfaces: the influence of inherited crustal structure in the northern Scandinavian Mountains. Journal of the Geological Society 174, 93–109.

Schmidt P, Lund B, Näslund J-O, Fastook J, 2014. Comparing a thermo-mechanical Weichselian Ice Sheet reconstruction to reconstructions based on the sea level equation: aspects of ice configurations and glacial isostatic adjustment. Solid Earth 5, 371–388.

Schoof C, 2005. The effect of cavitation on glacier sliding. Proceedings of the Royal Society A: Mathematical, Physical and Engineering Sciences 461, 609–627.

Sejrup H P, Larsen E, Landvik J, King E L, Haflidason H, Nesje A, 2000. Quaternary glaciations in southern Fennoscandia: evidence from southwestern Norway and the northern North Sea region. Quaternary Science Reviews 19, 667–685.

Sejrup H P, Larsen E, Haflidason H, Berstad I M, Hjelstuen B O, Jonsdottir H E, King E L, Landvik J, Longva O, Nygård A, Ottesen D, Raunholm S, Rise L, Stalsberg K, 2003. Configuration, history and impact of the Norwegian Channel Ice Stream. Boreas 32, 18–36.

Sejrup H P, Hjelstuen B O, Dahlgren K T, Haflidason H, Kuijpers A, Nygård A, Praeg D, Stoker M S, Vorren T O, 2005. Pleistocene glacial history of the NW European continental margin. Marine and Petroleum Geology 22, 1111–1129.

Selonen O, Ehlers C, Luodes H, Karell F, 2011. Magmatic constraints on localization of natural stone deposits in the Vehmaa rapakivi granite batholith, southwestern Finland. Bulletin of the Geological Society of Finland 83, 25–39.

Selonen O, Ehlers C, Luodes H, Härmä P, 2014. Exploration methods for granitic natural stones – geological and topographical aspects from case studies in Finland. Bulletin of the Geological Society of Finland 86, 5–22.

Seppälä M V J, 2016. Lidar-based detection and interpretation of glaciotectonic features of the morainic topography of Finland. Journal of Geological Research 2016, 4292806. doi:10.1155/2016/4292806

Shackleton C, Patton H, Hubbard A, Winsborrow M, Kingslake J, Esteves M, Andreassen K, Greenwood S L, 2018. Subglacial water storage and drainage beneath the Fennoscandian and Barents Sea ice sheets. Quaternary Science Reviews 201, 13–28.

SKB, 2008. Site description of Forsmark at completion of the site investigation phase SDM-site Forsmark. SKB TR-08-05, Svensk Kärnbränslehantering AB.

SKB, 2010. Climate and climate-related issues for the safety assessment SR-Site. SKB TR-10-49, Svensk Kärnbränslehantering AB.

SKB, 2013. Site description of the SFR area at Forsmark at completion of the site investigation phase. SDM-PSU Forsmark. SKB TR-11-04, Svensk Kärnbränslehantering AB.

SKB, 2019. Post-closure safety for the final repository for spent nuclear fuel at Forsmark – Climate and climate related issues, PSAR version. SKB TR-18-15, Svensk Kärnbränslehantering AB.

Sklar L S, Dietrich W E, 2001. Sediment and rock strength controls on river incision into bedrock. Geology 29, 1087–1090.

Slater B J, Harvey T H P, Butterfield N J, 2018. Small carbonaceous fossils (SCFs) from the Terreneuvian (lower Cambrian) of Baltica. Palaeontology 61, 417–439.

Šliaupa S, Hoth P, 2011. Geological evolution and resources of the Baltic Sea Area from the Precambrian to the Quaternary. In Harff J, Björck S, Hoth P (eds). The Baltic Sea basin. Berlin: Springer, 13–51.

Slim M, Perron J T, Martel S J, Singha K, 2015. Topographic stress and rock fracture: a two-dimensional numerical model for arbitrary topography and preliminary comparison with borehole observations. Earth Surface Processes and Landforms 40, 512–529.

Smellie J, Tullborg E-L, Nilsson A-C, Sandström B, Waber N, Gimeno M, Gascoyne M, 2008. Explorative analysis of major components and isotopes. SDM-Site Forsmark. SKB R-08-84, Svensk Kärnbränslehantering AB.

Sohlenius G, Rudmark L, 2003. Forsmark site investigation. Mapping of unconsolidated Quaternary deposits. Stratigraphical and analytical data. SKB P-03-14, Svensk Kärnbränslehantering AB.

Sohlenius G, Hedenström A, Rudmark L, 2004. Forsmark site investigation. Mapping of unconsolidated Quaternary deposits 2002–2003. Map description. SKB R-04-39, Svensk Kärnbränslehantering AB.

Sohlenius G, Strömgren M, Hartz F, 2013. Depth and stratigraphy of regolith at Forsmark. SKB R-13-22, Svensk Kärnbränslehantering AB.

Sopher D, Juhlin C, 2013. Processing and interpretation of vintage 2D marine seismic data from the outer Hanö Bay area, Baltic Sea. Journal of Applied Geophysics 95, 1–15.

St Clair J, Moon S, Holbrook W S, Perron J T, Riebe C S, Martel S J, Carr B, Harman C, Singha K, Richter D, 2015. Geophysical imaging reveals topographic stress control of bedrock weathering. Science 350, 534–538.

Steer P, Huismans R S, Valla P G, Gac S, Herman F, 2012. Bimodal Plio-Quaternary glacial erosion of fjords and low-relief surfaces in Scandinavia. Nature Geoscience 5, 635–639.

Stephens M B, 2010. Forsmark site investigation. Bedrock geology – overview and excursion guide. SKB R-10-04, Svensk Kärnbränslehantering AB.

Stephens M B, Simeonov A, 2015. Description of deformation zone model version 2.3, Forsmark. SKB R-14-28, Svensk Kärnbränslehantering AB.

Stephens M B, Fox A, La Pointe P, Simeonov A, Isaksson H, Hermanson J, Öhman J, 2007. Geology Forsmark. Site descriptive modelling Forsmark-stage 2.2. SKB R-07-45, Svensk Kärnbränslehantering AB.

Stephens M B, Bergman T, Isaksson H, Petersson J, 2008a. Bedrock geology Forsmark. Modelling stage 2.3. Description of the bedrock geological map at the ground surface. R-08-128, Svensk Kärnbränslehantering AB.

Stephens M B, Simeonov A, Isaksson H, 2008b. Bedrock geology Forsmark. Modelling stage 2.3. Implications for and verification of the deterministic geological models based on complementary data. SKB R-08-64, Svensk Kärnbränslehantering AB.

Stephens M B, Follin S, Petersson J, Isaksson H, Juhlin C, Simeonov A, 2015. Review of the deterministic modelling of deformation zones and fracture domains at the site proposed for a spent nuclear fuel repository, Sweden, and consequences of structural anisotropy. Tectonophysics 653, 68–94.

Stewart A D, 2002. The later Proterozoic Torridonian rocks of Scotland: their sedimentology, geochemistry and origin. London: Geological Society of London. (Geological Society Memoir 24)

Stewart M A, Lonergan L, 2011. Seven glacial cycles in the middle-late Pleistocene of northwest Europe: Geomorphic evidence from buried tunnel valleys. Geology 39, 283–286.

Stroeven A P, Fabel D, Harbor J, Hättestrand C, Kleman J, 2002a. Quantifying the erosional impact of the Fennoscandian ice sheet in the Torneträsk–Narvik corridor, northern Sweden, based on cosmogenic radionuclide data. Geografiska Annaler: Series A, Physical Geography 84, 275–287.

Stroeven A P, Fabel D, Hättestrand C, Harbor J, 2002b. A relict landscape in the centre of Fennoscandian glaciation: cosmogenic radionuclide evidence of tors preserved through multiple glacial cycles. Geomorphology 44, 145–154.

Stroeven A P, Harbor J, Heyman J, 2013. Erosional landscapes. In Shroder J, Giardino R, Harbor J (eds). Treatise on Geomorphology. Vol 8. San Diego, CA: Academic Press, 100–112.

Stroeven A P, Heyman J, Fabel D, Björck S, Caffee M W, Fredin O, Harbor J M, 2015. A new Scandinavian reference ^{10}Be production rate. Quaternary Geochronology 29, 104–115.

Stroeven A P, Hättestrand C, Kleman J, Heyman J, Fabel D, Fredin O, Goodfellow B W, Harbor J M, Jansen J D, Olsen L, Caffee M W, Fink D, Lundqvist J, Rosqvist G C, Strömberg B, Jansson K N, 2016. Deglaciation of Fennoscandia. Quaternary Science Reviews 147, 91–121.

Strömberg B, 1989. Late Weichselian deglaciation and clay varve chronology in east-central Sweden. Uppsala: Sveriges geologiska undersökning. (Ser. Ca 73)

Strömberg B, 2010. Rare forms of meltwater erosion on bedrock: Polished flutes in the Åland Sea area, Sweden-Finland. Helsinki: Suomalainen tiedeakatemia. (Annales Academiae Scientiarum Fennicae, Geologica-Geographica 169)

Sturkell E, Lindström M, 2004. The target peneplain of the Lockne impact. Meteoritics & Planetary Science 39, 1721–1731.

Sugden D E, 1968. The selectivity of glacial erosion in the Cairngorm Mountains, Scotland. Transactions of the Institute of British Geographers 45, 79–92.

Sugden D E, 1977. Reconstruction of the morphology, dynamics, and thermal characteristics of the Laurentide ice sheet at its maximum. Arctic and Alpine Research 9, 21–47.

Sugden D E, 1978. Glacial erosion by the Laurentide ice sheet. Journal of Glaciology 20, 367–391.

Sugden D E, John B S, 1976. Glaciers and landscape: a geomorphological approach. London: Edward Arnold.

Sugden D E, Glasser N, Clapperton C M, 1992. Evolution of large roches moutonnées. Geografiska Annaler: Series A, Physical Geography 74, 253–264.

Sugden D E, Hall A M, Phillips W M, Stewart M A, 2019. Plucking enhanced beneath ice sheet margins: evidence from the Grampian Mountains, Scotland. Geografiska Annaler: Series A, Physical Geography 101, 34–44.

Sundh M, Sohlenius G, Hedenström A, 2004. Forsmark site investigation. Stratigraphical investigation of till in machine cut trenches. SKB P-04-34, Svensk Kärnbränslehantering AB.

Svendsen J I, Alexanderson H, Astakhov V I, Demidov I, Dowdeswell J A, Funder S, Gataullin V, Henriksen M, Hjort C, Houmark-Nielsen M, Hubberten H W, Ingólfsson Ó, Jakobsson M, Kjaer K H, Larsen E, Lokrantz H, Lunkka J P, Lysså A, Mangerud J, Matiouchkov A, Murray A, Möller P, Niessen F, Nikolskaya O, Plyak L, Saarnisto M, Siegert C, Siegert M J, Spielhagen R F, Stein R, 2004. Late Quaternary ice sheet history of northern Eurasia. Quaternary Science Reviews 23, 1229–1271.

Söderberg P, 1993. Seismic stratigraphy, tectonics and gas migration in the Åland Sea, northern Baltic proper. Stockholm: Almqvist & Wiksell. (Stockholm Contributions in Geology 43)

Söderberg P, Hagenfeldt S E, 1995. Upper Proterozoic and Ordovician submarine outliers in the archipelago northeast of Stockholm, Sweden. GFF 117, 153–161.

Söderbäck B (ed), 2008. Geological evolution, palaeoclimate and historical development of the Forsmark and Laxemar-Simpevarp areas. Site descriptive modelling SDM-Site. SKB R-08-19, Svensk Kärnbränslehantering AB.

Söderlund U, 2006. U–Pb baddeleyite ages of Meso-and Neoproterozoic dykes and sills in central Fennoscandia: a review. In Hanski E, Mertanen S, Rämö T, Vuollo J (eds). Dyke swarms: time markers of crustal evolution. London: Taylor & Francis, 75–84.

Söderlund U, Elming S-Å, Ernst R E, Schissel D, 2006. The central Scandinavian dolerite Group—Protracted hotspot activity or back-arc magmatism?: Constraints from U–Pb baddeleyite geochronology and Hf isotopic data. Precambrian Research 150, 136–152.

Söderman G, 1985. Planation and weathering in eastern Fennoscandia. Fennia 163, 347–352.

Sømme T O, Martinsen O J, Lunt I, 2013. Linking offshore stratigraphy to onshore paleotopography: The Late Jurassic–Paleocene evolution of the south Norwegian margin. Geological Society of America Bulletin 125, 1164–1186.

Talbot C J, 1999. Ice ages and nuclear waste isolation. Engineering Geology 52, 177–192.

Talbot C J, 2014. Comment on "Approach to estimating the maximum depth for glacially induced hydraulic jacking in fractured crystalline rock at Forsmark, Sweden" by M. Lönnqvist and H. Hökmark. Journal of Geophysical Research: Earth Surface 119, 951–954.

Taylor J, Siegert M J, Payne A J, Hubbard B, 2004. Regional-scale bed roughness beneath ice masses: measurement and analysis. Computers & Geosciences 30, 899–908.

Thiery Y, Malet J-P, Sterlacchini S, Puissant A, Maquaire O, 2007. Landslide susceptibility assessment by bivariate methods at large scales: Application to a complex mountainous environment. Geomorphology 92, 38–59.

Thomas A L, 1993. Poly3D: a three-dimensional, polygonal element, displacement discontinuity boundary element computer program with applications to fractures, faults, and cavities in the Earth's crust. MSc thesis. Department of Geology, Stanford University.

Thorslund P, Axberg S, 1979. Geology of the southern Bothnian Sea. Part I. Uppsala: Uppsala university, 35–62. (Bulletin of the geological institutions of the University of Uppsala NS 8)

Thorslund P, Jaanusson V, 1960. The Cambrian, Ordovician, and Silurian in Västergötland, Närke, Dalarna, and Jämtland, central Sweden. Guide to excursions Nos A 23 and C 18. Stockholm: Geological Survey of Sweden.

Tirén S A, 1991. Geological setting and deformation history of a low-angle fracture zone at Finnsjön, Sweden. Journal of Hydrology 126, 17–43.

Tirén S A, 1993. Planning of infrastructures and the role of remote analysis of structural elements in the bedrock. Geologiska Föreningen i Stockholm Förhandlingar 115, 275–277.

Tirén S A, Beckholmen M, 1989. Block faulting in southeastern Sweden interpreted from digital terrain models. Geologiska Föreningen i Stockholm Förhandlingar 111, 171–179.

Tirén S A, Beckholmen M, 1992. Rock block map analysis of southern Sweden. Geologiska Föreningen i Stockholm Förhandlingar 114, 253–269.

Tirén S A, Wänstedt S, Sträng T, 2001. Moredalen — a canyon in the Fennoscandian Shield and its implication on site selection for radioactive waste disposal in south-eastern Sweden. Engineering Geology 61, 99–118.

Torsvik T H, Cocks L R M, 2013. New global palaeogeographical reconstructions for the Early Palaeozoic and their generation. Geological Society, London, Memoirs 38, 5–24.

Tullborg E-L, Drake H, Sandström B, 2008. Palaeohydrogeology: A methodology based on fracture mineral studies. Applied Geochemistry 23, 1881–1897.

Tullborg E L, Suksi J, Geipel G, Krall L, Auqué L, Gimeno M, Puigdomenech I, 2017. The occurrences of $Ca_2UO_2(CO_3)_3$ complex in Fe(II) containing deep groundwater at Forsmark, eastern Sweden. Procedia Earth and Planetary Science 17, 440–443.

Tuuling I, 2017. Paleozoic rocks structure versus Cenozoic cuesta relief along the Baltic Shield – East European Platform transect. Geological Quarterly 61, 396–412.

Tuuling I, Flodén T, 2016. The Baltic Klint beneath the central Baltic Sea and its comparison with the North Estonian Klint. Geomorphology 263, 1–18.

Twidale C R, 1982. The Evolution of Bornhardts: The nature of these dramatic landforms that rise abruptly from flat plains is now beginning to be more fully understood. American Scientist 70, 268–276.

Twidale C R, 2009. Differentiating etch, epigene, and subaerial landforms. Zeitschrift für Geomorphologie 53, 1–21.

Twidale C R, Bourne J A, 2009. On the origin of A-tents (pop-ups), sheet structures, and associated forms. Progress in Physical Geography 33, 147–162.

Tynni R, 1982. On Paleozoic microfossils in clastic dykes on the Åland Islands and in the core samples of Lumparn. Geological Survey of Finland, Bulletin 317, 34–132.

Tziperman E, Gildor H, 2003. On the mid-Pleistocene transition to 100-kyr glacial cycles and the asymmetry between glaciation and deglaciation times. Paleoceanography 18, 1–8.

Ugelvig S V, Egholm D L, Iverson N R, 2016. Glacial landscape evolution by subglacial quarrying: A multiscale computational approach. Journal of Geophysical Research: Earth Surface 121, 2042–2068.

Ugelvig S V, Egholm D L, Anderson R S, Iverson N R, 2018. Glacial erosion driven by variations in meltwater drainage. Journal of Geophysical Research: Earth Surface 123, 2863–2877.

Uutela A, 1990. Proterozoic microfossils from the sedimentary rocks of Lappajärvi impact crater. Bulletin of the Geological Society of Finland 62, 115–121.

Uutela A, 2001. Proterozoic and early Palaeozoic microfossils in the Karikkoselkä impact crater, central Finland. Bulletin of the Geological Society of Finland 73, 75–85.

van Boeckel M, 2018. Identifying the controlling factors on variable glacial modification of bedrock dominated areas in Kongsfjorden, Svalbard. MSc thesis. Department of Geosciences, UiT the Arctic University of Tromsø.

van der Wateren F M, 1985. A model of glacial tectonics, applied to the ice-pushed ridges in the Central Netherlands. Bulletin of the Geological Society of Denmark 34, 55–74.

Vidstrand P, Follin S, Selroos J-O, Näslund J-O, Rhén I, 2013. Modeling of groundwater flow at depth in crystalline rock beneath a moving ice-sheet margin, exemplified by the Fennoscandian Shield, Sweden. Hydrogeology Journal 21, 239–255.

Viles H, Goudie A, Grab S, Lalley J, 2011. The use of the Schmidt Hammer and Equotip for rock hardness assessment in geomorphology and heritage science: a comparative analysis. Earth Surface Processes and Landforms 36, 320–333.

von Eckermann H, 1937. The Jotnian Formation and the sub-Jotnian unconformity. Geologiska Föreningen i Stockholm Förhandlingar 59, 19–58.

Wahlgren C-H, 2010. Oskarshamn site investigation. Bedrock geology – overview and excursion guide. SKB R-10-05, Svensk Kärnbränslehantering AB.

Welin E, 1964. Uranium disseminations and vein fillings in iron ores of northern Uppland, central Sweden. Geologiska Föreningen i Stockholm Förhandlingar 86, 51–82.

Welin E, 1966. The occurrence of asphaltite and thucholite in the Precambrian bedrock of Sweden. Geologiska Föreningen i Stockholm Förhandlingar 87, 509–526.

Welin E, 1992. Isotopic results of the Proterozoic crustal evolution of south-central Sweden; review and conclusions. Geologiska Föreningen i Stockholm Förhandlingar 114, 299–312.

Werth E, 1908. Fjorde, Fjärde und Föhrden. Zeitschrift für Geomorphologie 3, 346–358.

Willenbring Staiger J W, Gosse J, Little E C, Utting D J, Finkel R, Johnson J V, Fastook J, 2006. Glacial erosion and sediment dispersion from detrital cosmogenic nuclide analyses of till. Quaternary Geochronology 1, 29–42.

Williams R, Robinson D, 1983. The effect of surface texture on the determination of the surface hardness of rock using the Schmidt hammer. Earth Surface Processes and Landforms 8, 289–292.

Wiman C, 1918. Kambrisk sandsten anstående i trakten af Upsalas. Geologiska Föreningen i Stockholm Förhandlingar 40, 726–730. (In Swedish.)

Wiman E, 1942. Studies of the morpho-tectonics of the Mälar depression, Sweden. Bulletin of the Geological Institute of the University of Uppsala 29, 287–303.

Winterhalter B, 1972. On the geology of the Bothnian Sea, an epeiric sea that has undergone Pleistocene glaciation. Otaniemi: Geologinen tutkimuslaitos.

Winterhalter B, Flodén T, Ignatius H, Axberg S, Niemistö L, 1981. Geology of the Baltic Sea. In Voipio A (ed). The Baltic Sea. Amsterdam: Elsevier, 1–121. (Elsevier Oceanography Series 30.)

Wohlfarth B, 2010. Ice-free conditions in Sweden during Marine Oxygen Isotope Stage 3? Boreas 39, 377–398.

Woźniak P P, Czubla P, 2015. The Late Weichselian glacial record in northern Poland: A new look at debris transport routes by the Fennoscandian Ice Sheet. Quaternary International 386, 3–17.

Yeo I W, De Freitas M H, Zimmerman R W, 1998. Effect of shear displacement on the aperture and permeability of a rock fracture. International Journal of Rock Mechanics and Mining Sciences 35, 1051–1070.

Zandstra J G, 1983. Fine gravel, heavy mineral and grain-size analyses of Pleistocene, mainly glacigenic deposits in the Netherlands. In Ehlers J (ed). Glacial deposits in North- West Europe. Rotterdam: Balkema, 361–377.

Zandstra J G, 1993. Nördliche kristalline Leitgeschiebe und Kiese in der Westfälischen Bucht und angrenzenden Gebieten. In Skupin K, Speetzen E, Zandstra J G (eds). Die Eiszeit in Nordwest-deutschland. Zur Vereisungsgeschichte der Westfälischen Bucht und angrenzender Gebiete, 43–106. (In German.)

Zhang Z, 2002. An empirical relation between mode I fracture toughness and the tensile strength of rock. International Journal of Rock Mechanics and Mining Sciences 39, 401–406.

Öhrling C, Peterson G, Mikko H, 2018. Detailed geomorphological analysis of LiDAR derived elevation data, Forsmark. Searching for indicatives of late- and postglacial seismic activity. SKB R-18-10, Svensk Kärnbränslehantering AB.

Øvretveit K, 2016. Depositional and structural relationships along the basement-Cambrian contact in the Hardangervidda area. MSc thesis. The University of Bergen.

Appendix 1

Glacial landform inventory

Appendix 1 provides tables of results from an inventory survey of the presence-absence of 60 features of glacial erosion at 55 sites across NE Uppland at four scales: micro (< 1 m), meso (1–10 m), macro (10–100 m) and local (0.1–1 km) scales. Features at the micro- to macro- scales were mapped in the field whereas local landforms were interpreted from DEMs based on 2 m resolution LiDAR data. The field sites include all sites within the Schmidt Hammer rock hardness survey (Appendix 2) and almost all sites selected for fracture mapping (Appendix 3) and sampled for cosmogenic nuclide analyses (Appendix 4).

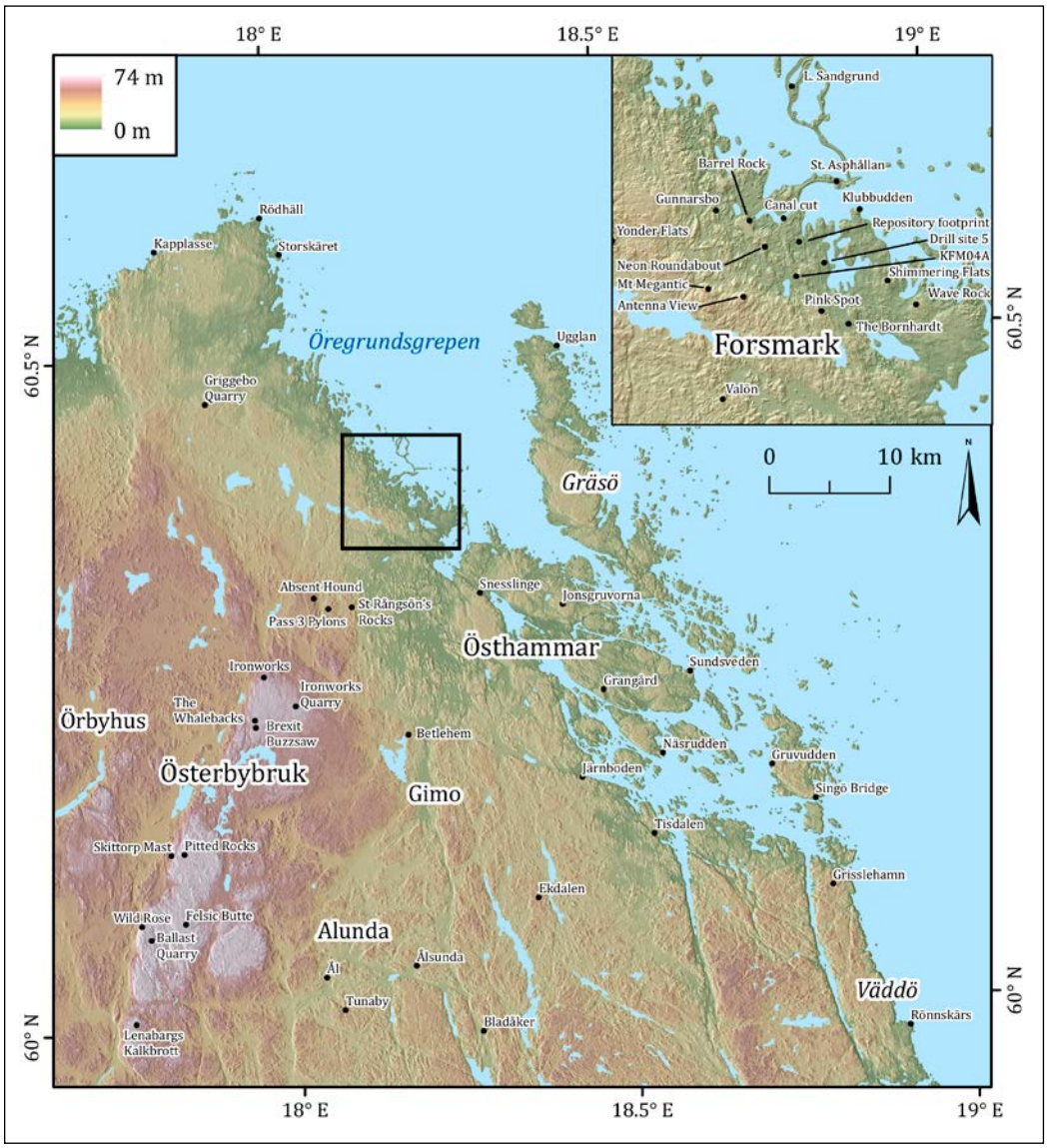

Figure A1-1. *Sites surveyed in the glacial landform inventory in Uppland and the Forsmark area. 1. Lilla Sandgrund. 2. Stora Asphällan. 3. Gunnarsbo. 4. Klubbudden. 5. Canal cut. 6. Barrel Rock. 7. Repository Footprint. 8. St Rångsön's Rocks 9. Neon Roundabout. 10. Drill Site KFM04A. 11. Antenna View. 12. Shimmering Flats. 13. Yonder Flats. 14. Mt Megantic. 15. Wave Rock. 16. Pink Spot. 17. The Bornhardt. 18. Valön.*

Table A1-1. Micro-erosion forms.

		Feature	Polish	Striae	Grooves	Micro crag and tail	Chatter marks	Edge fractures	Lee-side cliff	Stoss-side cliff	Flank cliff	Small blocks lost	Sub-horizontal fracture fills	Hydro fractures	Vertical displace-ment	Vertical fracture fills	Angular blocks	Box socket	Prismatic sockets	Lee-side blocks
		Process inferred	Abrasion				Micro-fracturing		Plucking				Jacking			Disruption		Hydraulic lift		Various
Sites	Lat N	Long E																		
Rödhäll	60.60353	17.99015	1	1	1	0	1	0	1	0	1	1	0	0	0	0	0	1	1	1
Kapplasse	60.58147	17.82838	1	1	1	0	1	1	1	1	1	1	0	0	0	0	0	1	1	1
Storskäret	60.57565	18.01679	1	1	1	0	1	0	1	1	1	1	0	0	0	0	0	1	0	1
Ugglan	60.49816	18.43032	1	1	1	0	1	1	1	1	1	1	0	0	0	0	1	1	1	1
Griggebo Quarry	60.46636	17.8953	1	1	0	0	1	0	1	0	1	1	0	0	0	0	0	0	0	1
Lilla Sandgrund	60.4305	18.18286	1	1	0	0	1	1	1	1	1	1	0	1	0	0	0	1	1	1
Stora Asphällan	60.40830	18.20155	1	1	1	0	1	1	1	1	1	1	0	0	0	1	0	1	1	1
Gunnarsbo	60.40296	18.14518	1	1	0	0	1	1	1	1	1	?	1	?	1	1	1	1	0	1
Klubbudden	60.40168	18.21159	1	1	1	0	1	1	1	0	1	1	0	1	0	0	0	1	1	1
Canal cut	60.40042	18.17607	1	1	?	0	1	1	1	1	1	?	1	1	1	1	1	1	1	1
Barrel Rock	60.40023	18.16038	1	1	0	0	1	1	1	1	1	1	1	1	0	1	1	1	0	1
Yonder Flats	60.39707	18.0964	1	1	0	0	1	1	1	1	1	1	0	0	0	?	0	0	1	1
Repository Footprint	60.39485	18.18275	1	1	?	0	1	?	1	?	1	?	?	?	?	?	0	1	?	1
Neon Roundabout	60.39412	18.16689	1	1	0	0	1	1	1	1	1	1	0	0	0	0	0	1	0	1
Drill Site 5	60.38978	18.19383	1	1	0	0	1	1	1	0	1	1	1	1	1	1	0	0	1	1
KFM04A	60.38702	18.18054	1	1	0	0	1	1	1	0	1	1	0	0	0	?	1	0	0	1
Mt Megantic	60.38507	18.13968	1	1	0	0	1	1	1	0	1	1	1	?	?	1	1	1	0	1
Shimmering Flats	60.38498	18.22279	1	1	0	0	1	1	1	0	1	1	0	0	0	?	0	0	0	1
Antenna View	60.38289	18.15586	1	1	0	0	1	1	1	1	1	1	?	1	?	?	1	1	0	1
Wave Rock	60.37923	18.23529	1	1	0	0	1	0	1	0	1	0	0	0	0	0	0	0	0	1
Pink Spot	60.37878	18.19159	1	1	0	0	1	1	1	0	1	1	0	0	0	0	0	1	0	1
The Bornhardt	60.37553	18.20389	1	1	0	0	1	0	1	0	1	0	0	0	0	?	0	0	0	1
Valön	60.35973	18.14395	1	1	0	0	1	1	1	1	1	?	1	?	?	?	1	0	0	1
Absent Hound	60.31866	18.04589	1	1	?	0	1	1	1	1	1	1	0	0	0	0	0	0	0	1
Snesslinge	60.31689	18.29536	1	1	?	0	1	1	1	1	1		1	?	1	?	1	1	0	1
St Rångsön's Rocks	60.31098	18.10266	1	1	0	0	1	1	1	0	1	0	?	?	0	?	0	0	1	1
Pass 3 Pylons	60.31042	18.06714	1	1	0	0	1	0	1	0	1	0	0	0	0	1	0	0	1	1
Jonsgruvorna	60.30553	18.41934	1	1	?	0	1	0	1	0	1	0	0	0	0	0	0	1	0	1
Ironworks	60.26160	17.96627	1	1	0	0	1	0	1	0	1	1	0	0	0	0	0	0	0	1

		Feature	Polish	Striae	Grooves	Micro crag and tail	Chatter marks	Edge fractures	Lee-side cliff	Stoss-side cliff	Flank cliff	Small blocks lost	Sub-horizontal fracture fills	Hydro fractures	Vertical displace-ment	Vertical fracture fills	Angular blocks	Box socket	Prismatic sockets	Lee-side blocks
		Process inferred	Abrasion				Micro-fracturing		Plucking				Jacking			Disruption		Hydraulic lift		Various
Sites	**Lat N**	**Long E**																		
Sundsveden	60.25098	18.60422	1	1	0	0	1	0	1	1	1	1	0	0	0	0	0	1	1	1
Grangård	60.24056	18.47358	1	1	1	0	1	0	1	1	1	1	0	0	0	0	0	1	0	1
Ironworks Quarry	60.23889	18.01150	1	1	0	0	1	0	1	0	1	1	0	0	0	0	0	0	0	1
The Whalebacks	60.22967	17.95	1	1	?	0	1	1	1	1	1	1	0	0	0	0	0	1	0	1
Brexit Buzzsaw	60.22425	17.95046	1	1	0	0	1	0	1	0	1	?	0	0	0	0	0	1	0	1
Betlehem	60.21399	18.1783	1	1	0	0	1	1	1	0	1	1	0	0	0	0	0	0	0	1
Näsrudden	60.19121	18.55727	1	1	?	0	1	0	1	0	1	1	0	0	0	?	0	1	0	1
Gruvudden	60.17847	18.71922	1	1	0	0	1	0	1	1	1	0	0	?	0	0	0	0	0	1
Järnboden	60.17613	18.43519	1	1	0	0	1	?	1	1	1	1	0	0	0	0	0	1	0	1
Singö Bridge	60.15162	18.78136	1	1	0	0	1	0	1	1	1	1	0	0	0	0	0	1	1	1
Pitted Rocks	60.13199	17.83570	1	1	?	0	1	0	1	1	1	1	?	?	?	?	0	1	1	1
Tisdalen	60.13176	18.53846	1	1	0	0	1	?	1	1	1	1	0	0	0	0	1	1	1	1
Skittorp Mast	60.13165	17.81607	1	1	0	0	1	0	1	1	1	1	?	0	0	0	0	1	0	1
Ekdalen	60.08826	18.36079	1	1	0	0	1	1	1	0	1	1	0	0	0	0	0	0	0	1
Grisslehamn	60.08674	18.80021	1	1	0	0	1	0	1	0	1	0	0	0	0	1	0	0	0	1
Felsic Butte	60.08001	17.83310	1	1	?	0	1	1	1	0	0	1	?	?	?	?	0	0	0	1
Wild Rose	60.07960	17.76809	1	1	?	0	1	0	1	1	1	1	?	?	?	?	0	1	0	1
Ballast Quarry	60.0692	17.78147	1	1	0	0	1	1	1	0	0	0	0	1	0	0	0	0	1	1
Ålsunda	60.04169	18.17412	1	1	0	0	1	0	1	1	1	0	0	1	0	0	0	1	0	1
Granholm	60.03681	18.3701	1	1	0	0	1	?	1	1	1	1	?	?	?	?	1	1	0	1
Ål	60.03605	18.03997	1	1	0	0	1	1	1	1	1	1	0	?	0	?	0	1	0	1
Tunaby	60.01131	18.06536	1	1	0	0	1	1	1	1	1	1	0	?	0	?	0	1	0	1
Closed Gate	60.00691	17.75368	1	1	?	?	1	?	1	0	1	1	?	?	?	?	0	1	0	1
Bladåker	59.99086	18.26866	1	1	0	0	1	1	1	1	1	1	?	1	?	?	1	1	1	1
Rönnskärs	59.97887	18.90329	1	1	0	0	1	1	1	1	1	1	0	0	0	0	0	1	1	1
Trollberget	59.94067	17.72701	1	1	0	0	1	1	1	1	1	1	0	1	1	0	1	0	0	1
		Present	**55**	**55**	**7**	**0**	**55**	**30**	**55**	**31**	**53**	**40**	**7**	**10**	**5**	**8**	**13**	**35**	**18**	**55**
		Absent	**0**	**0**	**37**	**54**	**0**	**20**	**0**	**23**	**2**	**9**	**38**	**31**	**40**	**29**	**42**	**20**	**36**	**0**
		Don't know	**0**	**0**	**11**	**1**	**0**	**5**	**0**	**1**	**0**	**5**	**10**	**14**	**10**	**18**	**0**	**0**	**1**	**0**

Cosmogenic nuclide sample sites indicated by grey shading. Where the sample site surroundings are obscured by soil and vegetation or where no sections are available in near-surface bedrock to check for shallow subsurface features then *Don't know* was recorded.

Table A1-2. Meso-erosion forms.

Mesoforms	1–10 m	A-axis length													
		Feature	Smooth rock surface	Stoss edge rounding	S-form	Edge fractures	Lee-side cliff	Stoss-side cliff	Flank cliff	Sub-horizontal fracture fills	Disrupted bedrock	Hydro fractures	Box socket	Prismatic sockets	Lee-side blocks
		Process inferred	Abrasion		Meltwater	Fracturing	Plucking			Jacking	Disruption		Hydraulic lift		
Sites	Lat N	Long E													
Rödhäll	60.60353	17.99015	1	1	1	0	1	0	0	0	0	0	1	0	1
Kapplasse	60.58147	17.82838	1	1	0	1	0	0	0	0	0	0	0	1	0
Storskäret	60.57565	18.01679	1	1	1	0	1	1	1	0	0	0	1	0	0
Ugglan	60.49816	18.43032	1	1	1	1	1	0	1	0	0	0	1	1	1
Griggebo Quarry	60.46636	17.8953	1	1	0	0	1	0	0	0	0	0	0	0	1
Lilla Sandgrund	60.4305	18.18286	1	1	1	1	1	1	1	0	0	0	1	1	1
Stora Asphällan	60.40830	18.20155	1	1	0	1	1	0	1	0	0	0	1	0	1
Gunnarsbo	60.40296	18.14518	1	1	?	1	1	0	1	1	1	?	1	0	1
Klubbudden	60.40168	18.21159	1	1	1	1	1	0	1	0	0	0	1	1	1
Canal cut	60.40042	18.17607	1	1	?	1	1	?	1	1	1	1	1	0	1
Barrel Rock	60.40023	18.16038	1	1	0	0	1	1	1	1	1	?	1	0	1
Yonder Flats	60.39707	18.0964	1	1	0	0	1	0	1	0	0	0	0	0	0
Repository Footprint	60.39485	18.18275	1	1	0	1	1	0	1	?	0	?	?	0	1
Neon Roundabout	60.39412	18.16689	1	1	0	1	1	1	1	0	0	1	?	0	1
Drill Site 5	60.38978	18.19383	1	1	1	1	1	0	1	1	0	1	0	0	
KFM04A	60.38702	18.18054	1	1	0	1	1	0	1	0	0	0	0	0	1
Mt Megantic	60.38507	18.13968	1	1	0	?	1	0	1	?	1	1	1	0	1
Shimmering Flats	60.38498	18.22279	1	1	0	1	1	1	1	0	0	0	0	0	1
Antenna View	60.38289	18.15586	1	1	0	1	1	1	1	?	1	1	1	0	1
Wave Rock	60.37923	18.23529	1	1	0	0	1	1	1	0	0	0	0	0	0
Pink Spot	60.37878	18.19159	1	1	0	0	1	0	1	0	0	0	0	0	0
The Bornhardt	60.37553	18.20389	1	1	0	0	1	0	1	0	0	0	0	0	0
Valön	60.35973	18.14395	1	1	0	1	1	1	1		1	1	0	0	1
Absent Hound	60.31866	18.04589	1	1	0	0	1	1	1	0	0	0	1		1
Snesslinge	60.31689	18.29536	1	1	?	1	1	1	1	?	1	0	1	0	1
St Rångsön's Rocks	60.31098	18.10266	1	1	0	1	1	0	1	?	0	?	0	1	1
Pass 3 Pylons	60.31042	18.06714	1	1	0	0	1	0	1	0	0	0	0	1	1
Jonsgruvorna	60.30553	18.41934	1	1	?	0	1	0	1	?	0	0	1	0	1
Ironworks	60.26160	17.96627	1	1	0	0	1	0	1	0	1	0	0	0	1

Mesoforms	1–10 m	A-axis length													
		Feature	Smooth rock surface	Stoss edge rounding	S-form	Edge fractures	Lee-side cliff	Stoss-side cliff	Flank cliff	Sub-horizontal fracture fills	Disrupted bedrock	Hydro fractures	Box socket	Prismatic sockets	Lee-side blocks
		Process inferred	Abrasion		Meltwater	Fracturing	Plucking			Jacking	Disruption		Hydraulic lift		
Sites	**Lat N**	**Long E**													
Sundsveden	60.25098	18.60422	1	1	0	0	1	1	1	0	0	0	1	1	1
Grangård	60.24056	18.47358	1	1	0	0	1	0	1	0	0	0	0	0	1
Ironworks Quarry	60.23889	18.01150	1	1	0	0	1	0	1	0	0	0	0	0	1
The Whalebacks	60.22967	17.95	1	1	?	0	1	0	1	?	0	0	1	1	1
Brexit Buzzsaw	60.22425	17.95046	1	1	?	0	1	0	1	?	0	0	1	0	1
Betlehem	60.21399	18.1783	1	1	0	1	1	0	1	0	0	0	0	0	1
Näsrudden	60.19121	18.55727	1	1	?	0	1	0	1	?	0	0	1	0	1
Gruvudden	60.17847	18.71922	1	0	0	0	1	0	1	0	0	0	0	0	1
Järnboden	60.17613	18.43519	1	1	0	0	0	1	1	0	0	0	1	0	1
Singö Bridge	60.15162	18.78136	1	0	0	0	1	1	1	0	0	0	1	1	1
Pitted Rocks	60.13199	17.83570	1	1	?	0	1	1	1	?	0	0	1	0	1
Tisdalen	60.13176	18.53846	1	1	0	0	1	0	1	0	1	0	1	0	1
Skittorp Mast	60.13165	17.81607	1	1	0	0	1	1	1	0	0	0	1	0	1
Ekdalen	60.08826	18.36079	1	1	0	0	1	0	1	0	0	0	0	0	1
Grisslehamn	60.08674	18.80021	1	1	?	0	1	0	1	0	0	0	0	0	1
Felsic Butte	60.08001	17.83310	1	1	?	0	1	0	0	?	0	0	0	0	0
Wild Rose	60.07960	17.76809	1	1	?	0	1	1	1	?	1	0	1	0	1
Ballast Quarry	60.0692	17.78147	1	1	1	0	1	0	1	0	0	1	0	1	1
Ålsunda	60.04169	18.17412	1	1	0	0	1	1	1	0	0	0	1	0	1
Granholm	60.03681	18.3701	1	1	0	0	1	1	1	?	1	?	1	0	1
Ål	60.03605	18.03997	1	1	?	0	1	0	1	?	0	0	1	0	1
Tunaby	60.01131	18.06536	1	1	?	0	1	0	1	?	0	0	1	0	1
Closed Gate	60.00691	17.75368	1	1	?	1	1	1	1	?	0	0	1	0	0
Bladåker	59.99086	18.26866	1	1	0	1	1	0	1	?	1	1	1	0	1
Rönnskärs	59.97887	18.90329	1	1	0	0	1	1	1	0	0	0	0	1	1
Trollberget	59.94067	17.72701	1	1	0	1	1	1	1	0	1	1	0	0	1
		Present	**55**	**53**	**7**	**20**	**53**	**21**	**51**	**4**	**13**	**9**	**30**	**11**	**46**
		Absent	**0**	**2**	**34**	**34**	**2**	**33**	**4**	**33**	**42**	**41**	**23**	**43**	**8**
		Don't know	**0**	**0**	**14**	**1**	**0**	**1**	**0**	**17**	**0**	**5**	**2**	**0**	**0**

Cosmogenic nuclide sample sites indicated by grey shading. Where the sample site surroundings are obscured by soil and vegetation or where no sections are available in near-surface bedrock to check for shallow subsurface features then *Don't know* was recorded.

Table A1-3. Macro-erosion forms.

Macroforms	10–100 m	A-axis length										
		Feature	Whaleback	Roche moutonnée	Crag-and-tail	Cleft	Lee-side cliff	Stoss-side cliff	Flank cliff	Gouge	Disrupted bedrock	Block spread
		Process inferred				Plucking				Ploughing	Disruption	Ripping
Sites	**Lat N**	**Long E**										
Rödhäll	60.60353	17.99015	0	0	0	0	0	0	0	0	0	0
Kapplasse	60.58147	17.82838	1	0	0	1	1	0	0	0	0	0
Storskäret	60.57565	18.01679	0	0	0	0	0	0	0	0	0	0
Ugglan	60.49816	18.43032	0	1	0	0	1	0	1	0	0	0
Griggebo Quarry	60.46636	17.8953	0	0	0	0	0	0	0	0	0	0
Lilla Sandgrund	60.4305	18.18286	1	1	0	0	0	0	1	0	0	0
Stora Asphällan	60.40830	18.20155	1	1	0	0	1	1	1	0	0	0
Gunnarsbo	60.40296	18.14518	0	1	0	0	1	1	1	1	1	1
Klubbudden	60.40168	18.21159	1	1	1	1	0	0	1	0	0	0
Canal cut	60.40042	18.17607	1	1	0	0	0	0	1	?	1	0
Barrel Rock	60.40023	18.16038	0	1	0	0	1	0	1	0	0	0
Yonder Flats	60.39707	18.0964	0	1	0	0	1	0	1	0	0	0
Repository Footprint	60.39485	18.18275	0	1	1	0	0	0	0	0	0	0
Neon Roundabout	60.39412	18.16689	0	1	1	1	1	0	0	0	0	0
Drill Site 5	60.38978	18.19383	1	1	1	0	1	0	0	0	1	0
KFM04A	60.38702	18.18054	0	1	0	0	1	0	1	0	0	0
Mt Megantic	60.38507	18.13968	0	1	0	1	0	0	0	0	1	1
Shimmering Flats	60.38498	18.22279	0	1	0	0	1	0	0	0	0	0
Antenna View	60.38289	18.15586	0	1	1	1	1	1	1	0	1	1
Wave Rock	60.37923	18.23529	1	1	0	0	0	0	1	0	0	0
Pink Spot	60.37878	18.19159	0	1	0	0	1	0	1	0	0	0
The Bornhardt	60.37553	18.20389	0	1	0	0	1	0	1	0	0	0
Valön	60.35973	18.14395	0	1	0	0	1	1	1	1	1	1
Absent Hound	60.31866	18.04589	0	1	0	1	1	0	1	0	0	0
Snesslinge	60.31689	18.29536	0	1	0	0	0	0	0	1	1	1
St Rångsön's Rocks	60.31098	18.10266	0	1	1	0	1	0	1	?	1	1
Pass 3 Pylons	60.31042	18.06714	0	1	0	0	1	0	1	1	0	0
Jonsgruvorna	60.30553	18.41934	0	0	0	0	0	0	0	0	0	0
Ironworks	60.26160	17.96627	1	1	0	0	0	0	0	0	0	0
Sundsveden	60.25098	18.60422	0	1	0	1	1	0	1	0	0	0
Grangård	60.24056	18.47358	0	1	0	1	1	0	1	0	0	0
Ironworks Quarry	60.23889	18.01150	1	1	0	0	0	0	0	0	0	0
The Whalebacks	60.22967	17.95	0	1	0	0	1	1	1	0	0	0
Brexit Buzzsaw	60.22425	17.95046	0	1	0	0	1	0	1	0	0	0
Betlehem	60.21399	18.1783	0	1	0	0	0	0	0	0	0	0
Näsrudden	60.19121	18.55727	0	0	0	0	0	0	0	0	0	0
Gruvudden	60.17847	18.71922	0	1	0	0	0	0	0	0	0	0
Järnboden	60.17613	18.43519	0	1	0	0	0	0	0	0	0	0
Singö Bridge	60.15162	18.78136	0	1	0	0	1	0	0	0	0	0
Pitted Rocks	60.13199	17.83570	0	1	1	1	1	0	1	0	0	0
Tisdalen	60.13176	18.53846	1	1	0	0	0	0	1	0	0	1
Skittorp Mast	60.13165	17.81607	0	1	0	0	1	1	0	1	0	0
Ekdalen	60.08826	18.36079	1	1	0	0	0	0	0	0	0	0
Grisslehamn	60.08674	18.80021	0	1	0	0	0	0	0	?	0	0
Felsic Butte	60.08001	17.83310	0	1	0	0	0	0	0	?	0	0
Wild Rose	60.07960	17.76809	0	1	0	1	0	0	0	?	0	0
Ballast Quarry	60.0692	17.78147	1	1	1	1	1	1	1	0	0	0

Macroforms	10–100 m	A-axis length										
		Feature	Whaleback	Roche moutonnée	Crag-and-tail	Cleft	Lee-side cliff	Stoss-side cliff	Flank cliff	Gouge	Disrupted bedrock	Block spread
		Process inferred				Plucking				Ploughing	Disruption	Ripping
Sites	**Lat N**	**Long E**										
Ålsunda	60.04169	18.17412	0	1	0	1	1	1	1	0	0	0
Granholm	60.03681	18.3701	0	1	0	0	0	0	0	0	1	1
Ål	60.03605	18.03997	0	1	0	0	0	0	0	?	0	0
Tunaby	60.01131	18.06536	0	1	0	0	1	0	1	?	0	0
Closed Gate	60.00691	17.75368	0	1	0	1	1	0	1	?	0	0
Bladåker	59.99086	18.26866	0	1	0	0	1	0	1	0	1	1
Rönnskärs	59.97887	18.90329	0	1	0	0	0	0	0	0	0	0
Trollberget	59.94067	17.72701	0	1	0	0	1	0	1	0	1	1
		Present	**12**	**49**	**8**	**13**	**30**	**8**	**29**	**5**	**11**	**10**
		Absent	**43**	**6**	**47**	**42**	**25**	**47**	**26**	**42**	**44**	**45**
		Don't know	**0**	**0**	**0**	**0**	**0**	**0**	**0**	**8**	**0**	**0**

Cosmogenic nuclide sample sites indicated by grey shading. Where the sample site surroundings are obscured by soil and vegetation or where no sections are available in near-surface bedrock to check for shallow subsurface features then *Don't know* was recorded.

Table A1-4. Local erosion forms.

Local landform assemblage		0.1–1 km										
		Feature	Box hill	Large roche moutonnée	Large whaleback	Crag-and-tail	Streamlined rock hill	Lee cliff	Fracture-guided valley	Star basin	Box basin	Block Spreads
		Process inferred										Ripping
Sites	**Lat N**	**Long E**										
Rödhäll	60.60353	17.99015	1	0	0	0	0	1	1	1	0	0
Kapplasse	60.58147	17.82838	0	1	0	1	1	1	1	1	0	0
Storskäret	60.57565	18.01679	0	1	0	1	0	1	1	1	0	0
Ugglan	60.49816	18.43032	1	1	0	0	0	1	1	1	0	0
Griggebo Quarry	60.46636	17.8953	0	0	1	1	0	0	1	1	0	0
Lilla Sandgrund	60.4305	18.18286	0	0	1	0	0	0	1	0	?	0
Stora Asphällan	60.40830	18.20155	0	1	1	0	0	1	1	?	?	0
Gunnarsbo	60.40296	18.14518	1	0	0	0	0	1	1	0	1	1
Klubbudden	60.40168	18.21159	0	1	0	1	0	0	1	0	1	0
Canal cut	60.40042	18.17607	0	1	0	1	0	0	1	0	1	0
Barrel Rock	60.40023	18.16038	0	1	0	1	0	1	1	1	0	1
Yonder Flats	60.39707	18.0964	0	1	0	1	0	1	1	1	0	0
Repository Footprint	60.39485	18.18275	0	0	0	1	0	0	1	0	1	0
Neon Roundabout	60.39412	18.16689	1	1	0	1	0	1	1	0	1	0
Drill Site 5	60.38978	18.19383	0	1	1	1	0	1	1	1	0	0
KFM04A	60.38702	18.18054	0	1	0	1	0	0	1	1	0	0
Mt Megantic	60.38507	18.13968	1	0	0	1	0	1	1	0	1	1
Shimmering Flats	60.38498	18.22279	0	1	0	1	1	1	1	0	1	0
Antenna View	60.38289	18.15586	0	1	0	0	0	1	1	1	1	0
Wave Rock	60.37923	18.23529	0	0	1	0	0	0	0	0	1	0
Pink Spot	60.37878	18.19159	0	1	0	1	0	1	1	1	0	0

Table A1-4. Continued from previous page.

Local landform assemblage		0.1–1 km										
		Feature	Box hill	Large roche moutonnée	Large whaleback	Crag-and-tail	Streamlined rock hill	Lee cliff	Fracture-guided valley	Star basin	Box basin	Block Spreads
		Process inferred										Ripping
Sites	Lat N	Long E										
The Bornhardt	60.37553	18.20389	0	1	0	1	0	1	1	0	1	0
Valön	60.35973	18.14395	1	0	0	0	1	1	1	1	0	1
Absent Hound	60.31866	18.04589	0	1	0	0	1	1	1	1	1	0
Snesslinge	60.31689	18.29536	1	1	0	0	0	1	1	1	1	1
St Rångsön's Rocks	60.31098	18.10266	1	1	0	1	0	0	1	0	1	1
Pass 3 Pylons	60.31042	18.06714	1	1	0	0	0	1	1	1	1	0
Jonsgruvorna	60.30553	18.41934	1	1	0	0	0	1	1	1	0	0
Ironworks	60.26160	17.96627	0	0	0	1	0	0	1	0	1	0
Sundsveden	60.25098	18.60422	0	1	0	0	0	1	1		1	0
Grangård	60.24056	18.47358	1	1	0	0	0	0	1		1	1
Ironworks Quarry	60.23889	18.01150	1	0	0	0	0	0	1	0	1	0
The Whalebacks	60.22967	17.95	0	1	0	0	?	0	1	1	1	0
Brexit Buzzsaw	60.22425	17.95046	0	1	0	0	0	0	1	1	1	0
Betlehem	60.21399	18.1783	1	1	0	1	0	1	1	1	0	0
Näsrudden	60.19121	18.55727	0	1	0	0	0	1	1	1	1	0
Gruvudden	60.17847	18.71922	0	1	0	0	0	1	1	1	0	0
Järnboden	60.17613	18.43519	0	1	1	0	0	0	1		0	1
Singö Bridge	60.15162	18.78136	0	1	0	0	0	1	1	1	1	0
Pitted Rocks	60.13199	17.83570	0	1	0	0	0	1	1	0	1	0
Tisdalen	60.13176	18.53846	1	1	0	0	0	1	1		1	1
Skittorp Mast	60.13165	17.81607	0	1	0	0	0	1	1	0	0	0
Ekdalen	60.08826	18.36079	0	1	0	0	1	1	1		1	0
Grisslehamn	60.08674	18.80021	1	1	0	0	0	1	1	1	0	0
Felsic Butte	60.08001	17.83310	1	0	0	0	0	1	1	0	1	0
Wild Rose	60.07960	17.76809	0	1	0	0	0	1	1	1	1	0
Ballast Quarry	60.0692	17.78147	0	1	0	1	0	1	1	1	0	0
Ålsunda	60.04169	18.17412	1	1	0	1	0	1	1	1	0	0
Granholm	60.03681	18.3701	0	1	0	0	1	0	1		0	1
Ål	60.03605	18.03997	1	1	0	1	1	1	1	1	1	0
Tunaby	60.01131	18.06536	1	0	0	0	1	0	1	0	1	0
Closed Gate	60.00691	17.75368	0	1	0	0	0	1	1	0	1	0
Bladåker	59.99086	18.26866	1	0	0	0	0	1	1	1	0	1
Rönnskärs	59.97887	18.90329	0	1	0	0	0	0	1	0	1	0
Trollberget	59.94067	17.72701	1	1	0	0	0	0	1	1	1	1
		Present	**21**	**42**	**6**	**21**	**8**	**37**	**54**	**29**	**32**	**12**
		Absent	**34**	**13**	**49**	**34**	**46**	**18**	**1**	**19**	**21**	**43**
		Don't know	**0**	**0**	**0**	**0**	**1**	**0**	**0**	**1**	**2**	**0**

Cosmogenic nuclide sample sites indicated by grey shading.

Appendix 2

Schmidt hammer rebound values on crystalline outcrops in north-east Uppland

Introduction

The Schmidt hammer (SH) has been used by geomorphologists in studies of relative dating (Evans et al. 1999), weathering phenomena (McCarroll 1991), and the links between rock strength and landforms (Ericson 2004). The instrument measures the distance of rebound of a controlled impact on a rock surface (Viles et al. 2011). Harder rocks have higher rebound (R) values. Over a range of rock types, R values correlate closely with tensile strength, uniaxial compressive strength, and abrasion hardness (Aydin and Basu 2005). The 'N' type Schmidt hammer can provide data on a range of rock types from weak to very strong with compressive strengths that range from c. 20 to 250 MPa. Schmidt hammer measurements are non-destructive to the rock surface and can be performed rapidly at multiple sample sites.

Rock hardness is an important control on the resistance of a rock surface to glacial abrasion (Augustinus 1991, Krabbendam and Bradwell 2011). In this study, 'N' type Schmidt hammer rebound values are used as a semi-quantitative proxy for abrasion resistance of Precambrian gneisses in the Forsmark area. Estimates of depths and rates of glacial erosion on bedrock summits with abraded surfaces derived from cosmogenic nuclides indicate order of magnitude variations across this area (Chapter 5). Constraining abrasion resistance is important for assessing the importance of rock hardness on abrasion rates.

Method

Sample strategy

The rock surfaces sampled were from high points on roches moutonnées and whalebacks in NE Uppland. The sample set includes 27 sites along a belt transect that runs SW from islands offshore of Forsmark towards Uppsala (Figure A2-1). Sampling of rock surfaces includes 43 rock surfaces sampled previously for cosmogenic nuclide analyses, from which 32 surfaces provided results. A further 11 rock summits were sampled to improve areal coverage.

Schmidt hammer measurements

A significant limitation on the use of the Schmidt hammer is its high sensitivity to discontinuities on a rock surface. Hence, fissile, closely foliated and laminated rocks cannot easily be investigated by this method. Results also may be influenced by surface texture, with smooth planar surfaces giving higher readings than rough or irregular surfaces (Williams and Robinson 1983). Surface irregularities are often crushed before the hammer plunger tip reaches the main rock surface, resulting in some loss of impact energy. Both the magnitude and repeatability of hammer readings increases with the degree of surface polishing.

A minimum of 25 R-values were taken at each site except at locations where exposed rock surfaces were of very restricted extent. All rock surfaces sampled in this survey were smooth, locally retaining glacial polish and fine striae. All measurements were taken more than 20 cm away from fractures and more than 1 m away from edges to minimise edge effects. As the presence of lichen and soil significantly lowers the Schmidt hammer values, only clean surfaces were sampled. Early in the survey, it became apparent that R-values varied widely at some sites and appeared to be influenced by differences in micro-roughness of the rock surface and the presence of sub-horizontal micro-fractures at depths of 1–5 cm below the sample surface. As high R-values are least likely to be affected by micro-roughness and other effects and so most likely to represent the hardness of fresh rock at each site, the upper quartile of the R-values was calculated for each sample and site. Measurements of R-values for fresh gneiss exposed in road cuttings and quarries were found to be unreliable due to the high micro-roughness of rock surfaces on newly exposed, sub-horizontal fractures.

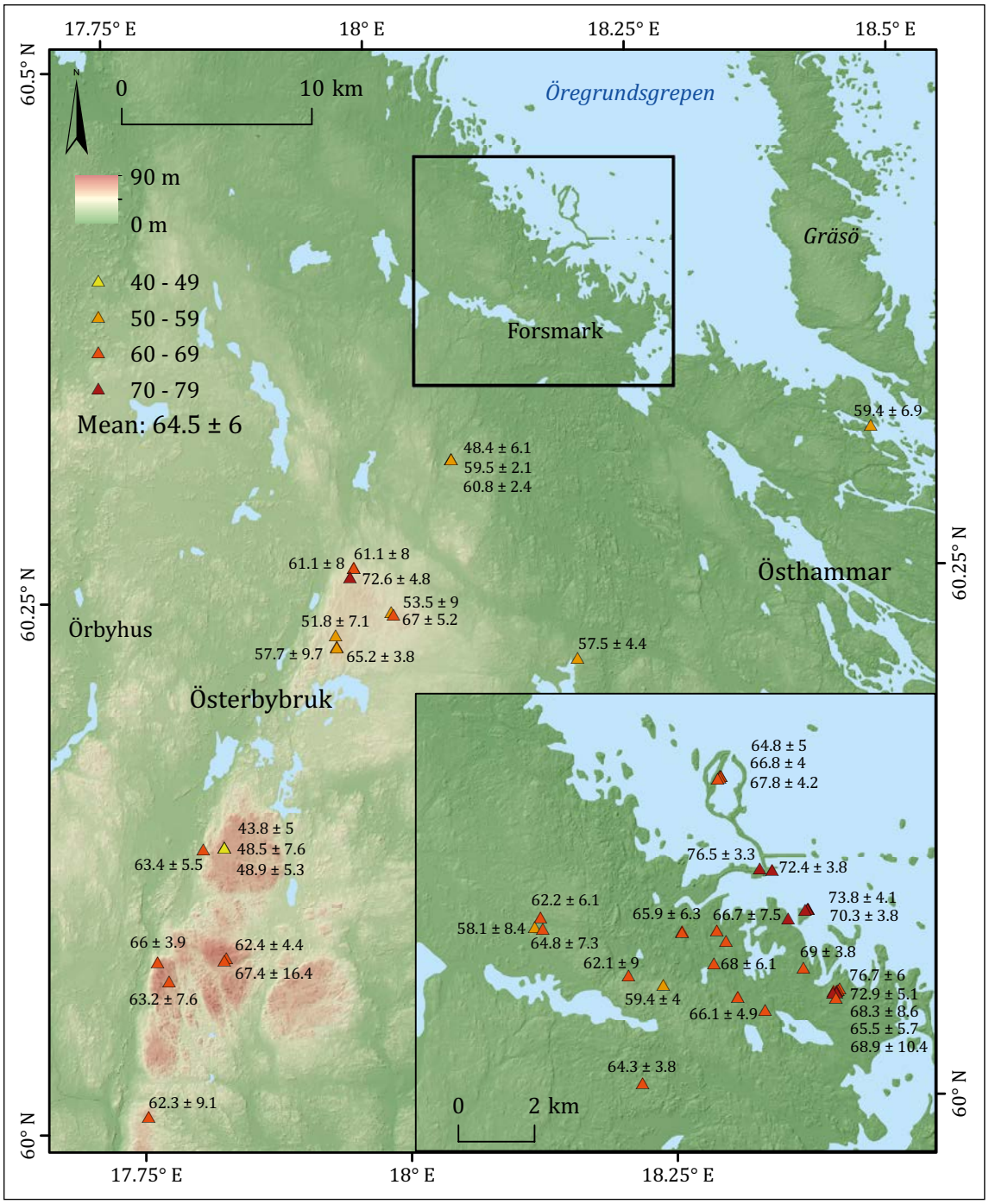

Figure A2-1. *R-values (mean and standard deviation) for bedrock surfaces in NE Uppland. Inset: R-values around Forsmark.*

Table A2-1. R-values for sample sites. (Some site names are changed to match local place names). Site Codes refer to sample sites for cosmogenic nuclides (Appendix 4).

Location	Site Code	Lat. N	Long. E	n	mean	SD	Upper Quartile
Lilla Sandgrund	FORS 16-03	60.43103	18.18812	25	64.8	5.0	68
Lilla Sandgrund		60.43103	18.18752	22	64.6	5.1	68
Lilla Sandgrund		60.43103	18.18812	24	67.5	4.3	71
Lilla Sandgrund	FORS 16-01	60.4307	18.18752	23	67.8	4.2	71
Lilla Sandgrund	FORS 16-02	60.43045	18.18665	29	66.8	4.0	70
Stora Asphällan	FORS 17-23	60.40885	18.20452	24	76.5	3.3	78
Stora Asphällan	FORS 17-12	60.40842	18.21043	25	72.4	3.8	74
Klubbudden		60.39886	18.22658	25	78.6	2.8	81
Klubbudden		60.39883	18.22654	25	79.3	5.4	83
Klubbudden		60.3987	18.2264	25	71.6	10.2	77
Klubbudden		60.39854	18.22506	23	70.3	3.8	72
Klubbudden	FORS 17-21	60.396774	18.216991	35	73.8	4.1	77
Björnbo	FORS 16-08	60.3998	18.09904	34	64.8	7.3	70
Björnbo	FORS 16-07	60.39761	18.09614	31	58.1	8.4	62
Björnbo	FORS 16-06	60.39706	18.09993	25	62.2	6.1	66
Neon Roundabout	FORS 16-04	60.39497	18.1661	32	61.3	6.4	66
Neon Roundabout	FORS 16-04	60.39487	18.1661	32	61.3	6.5	66
Repository Footprint	FORS-17-09	60.39485	18.18275	20	65.9	6.3	70
Repository Footprint	FORS 17-10	60.39219	18.18685	52	66.7	7.5	73
Borehole KFM04	KFM04	60.38702	18.18054	35	68.0	6.1	73
Mount Megantic	FORS 16-09	60.38507	18.13968	22	62.1	9.0	70
Shimmering Flats	FORS 16-12	60.38499	18.22309	25	69.0	3.8	71
Antenna View		60.382589	18.156024	25	59.4	4.0	60
Wave Rock	FORS 17-03	60.37965	18.23979	25	64.3	7.4	71
Wave Rock	FORS 17-11	60.37929	18.23893	25	68.3	8.6	75
Wave Rock	FORS 16-13	60.37925	18.23681	27	68.9	5.1	71
Wave Rock	FORS 17-02	60.37925	18.23817	27	76.7	6.0	80
Wave Rock	FORS 17-01	60.37887	18.23825	30	72.9	5.1	76
Wave Rock	FORS 17-04	60.37875	18.23655	27	77.7	4.5	81
Wave Rock	FORS 17-05	60.37757	18.23786	27	68.9	10.4	78
Pink Spot	FORS 16-10	60.37888	18.19113	25	66.1	4.9	70
The Bornhardt	FORS 16-11	60.37547	18.20393	33	65.5	5.7	69
Valön		60.359727	18.143947	25	64.3	3.8	67
Absent Hound	FORS 16-14	60.316807	18.4672	31	59.4	6.9	64
Pass 3 Pylons	FORS 16-05	60.310502	18.066966	5	60.8	2.4	62
Pass 3 Pylons	FORS 16-05	60.310501	18.066966	34	48.4	6.1	52
Pass 3 Pylons	FORS 16-05	60.310501	18.066967	2	59.5	2.1	60
Ironworks	FORS 16-15	60.26152	17.96972	21	61.1	8.0	67
Ironworks	FORS 16-15	60.26152	17.96972	21	61.1	8.0	67
Ironworks	FORS 17-25	60.25689	17.96591	52	72.6	4.8	76
Ironworks	FORS 17-24	60.23969	18.00361	51	53.5	9.0	61
Ironworks		60.23838	18.0057	52	67.0	5.2	71
The Whalebacks	FORS 16-16	60.2299	17.94989	33	51.8	7.1	55
Brexit Buzzsaw	FORS 16-17	60.224622	17.95046	31	65.2	3.8	68
Brexit Buzzsaw	FORS 16-17	60.22425	17.95046	31	57.7	9.7	67
Betlehem	FORS 17-08	60.21399	18.1783	29	57.5	4.4	60
Pitted Rocks	FORS 16-20	60.13226	17.83591	26	43.8	5.0	48
Pitted Rocks	FORS 16-19	60.13214	17.83588	25	48.5	7.6	53
Pitted Rocks	FORS 16-21	60.13208	17.8357	24	48.9	5.3	52
Skittorp Mast	FORS 16-18	60.13167	17.81605	32	63.4	5.5	69
Felsic Butte	FORS 16-24	60.08001	17.8331	25	62.4	4.4	67
Katthavet	FORS 16-24	60.0796	17.76809	26	66.0	3.9	69
Släsby		60.07911	17.831412	35	67.4	16.4	74
Ballast Quarry		60.070318	17.77846	26	63.2	7.6	70
Closed Gate	FORS 16-22	60.00691	17.75368	26	62.3	9.1	68.0
				Mean	64.5	6.0	68.6

Results

R-values for individual samples are given in Table 2-1 and shown on maps in Figure A2-1. The mean R-value for the sample set is 64.5 ± 6.0. Standard deviations rise to a maximum of 10.4 and indicate high variability in R-values at some sites.

R-values for sample sites are shown in Figure A2-1. Only two sites, Pass 3 Pylons and Pitted Rocks, have mean R-values of less than 50. The first site is in amphibolite and low hardness may be a result of incipient weathering of the rock surface. The second site is in granite gneiss and named after distinctive small weathering pits seen on the sides of roches moutonnées, indicating high susceptibility to weathering. Other sites have mean R-values > 59, reaching a maximum of 74.

Mean R-values for sites show no apparent systematic variation in R-values from N to S (Figure A2-2).

A weak negative correlation is seen between elevation and R-values (Figure A2-3). As higher elevation sites were the first to emerge above sea level during deglaciation, the correlation suggests that hardness of the rock surfaces may be linked to the total time of exposure to weathering.

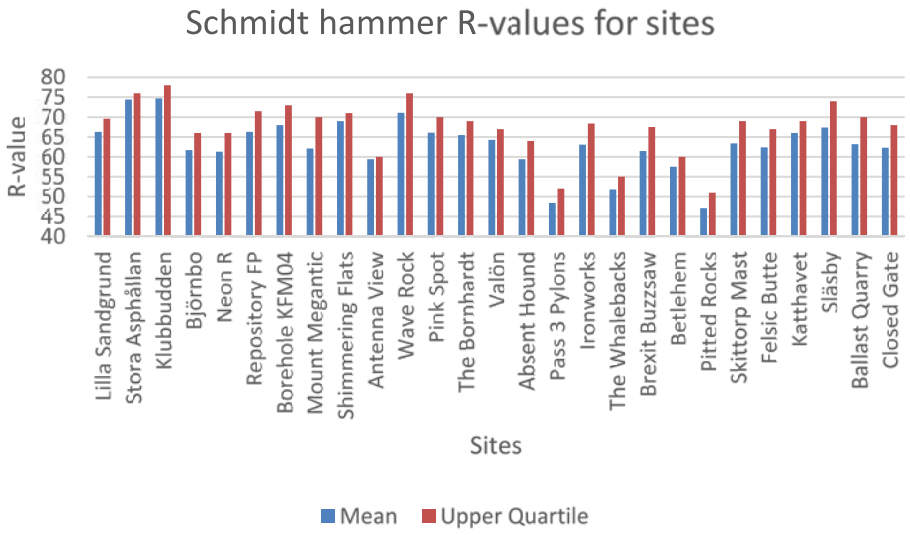

Figure A2-2. *Mean R-values for sample sites along a N–S transect from Forsmark towards Uppsala.*

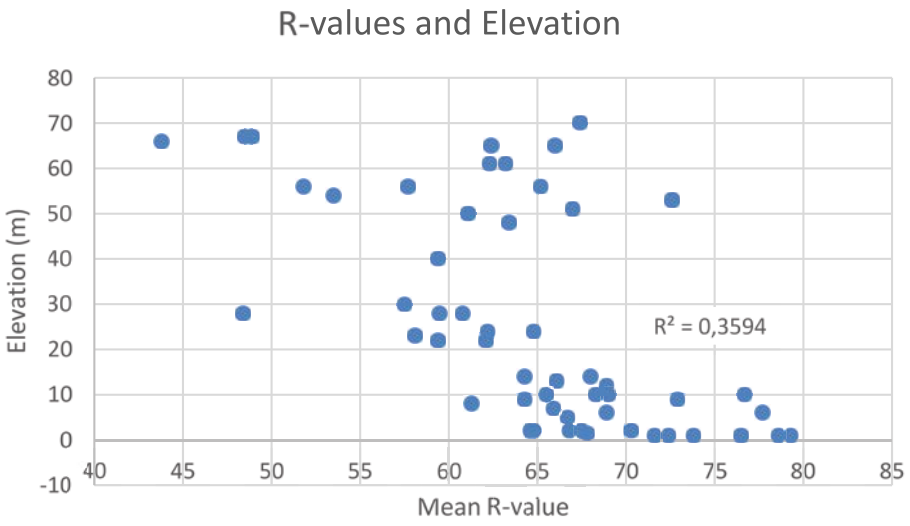

Figure A2-3. *Mean R-values and elevation for all samples.*

Discussion and Conclusions

SKB report (SKB 2008) summarizes results from a large testing programme for intact rock properties for the rock types found in the Forsmark Tectonic Lens during the site investigations for the Final Repository for spent fuel. Summary data are given in Table 4-2. The intact rock strength for all samples is rated as Very Strong (R5) to Extremely Strong (R6) according to the ISRM Suggested Method (Brown 1981). The range of values for uniaxial compressive strength indicate however significant variations in hardness within these ratings (SKB 2013).

Table 4-2. Properties for discrete fractures. From SKB (2013, Table 6-6).

Parameter					
Rock Code* Mean/StDev Min–Max**	**101057**	**101061**	**111058**	**103076**	**102017**
Uniaxial compressive strength (MPa)	226/50 126–326	183/45 90–270	280/45 210–350	139/45 100–200	142/45 60–230
Crack initiation stress (MPa)	116/26 64–168	114/22 64–166	148/22 104–192	–	–
Indirect tensile strength (MPa)	13/2 10–18	12/3 8–16	16/2 12–20	9/2 5–13	9/2 5–13
Young's modulus (GPa)	75/3 69–81	74/4 66–82	74/2.5 70–79	99***/3 93–105	81/4 73–89
Poisson's ratio	0.23/0.04 0.14–0.30	0.30/0.03 0.26–0.35	0.28/0.03 0.22–0.32	0.35***/0.03 0.29–0.41	0.22/0.04

* 101057 – Granite to granodiorite, 101061 – Pegmatite, pegmatitic granite, 111058 – Fine to medium-grained granite, 103076 – Felsic to intermediate metavolcanic rock, 102017 – Amphibolite.

** Parameters are described as normal distribution with truncations at the given Min–Max values. The most likely parameter value is the mean value.

*** Only 2 tested samples.

Mean and Upper Quartile R-values for Schmidt hammer tests on abraded rock surfaces in the Forsmark are generally > 59 but also show variation within and between samples and sites. In comparison to reported values from other rocks, these R-values values are high (Deere and Miller 1966). The hardness of the Precambrian gneisses in the Forsmark place these rocks mainly in the abrasion process domain of glacial erosion, except where fractures are closely spaced (Figure A2-4).

Upper Quartile R-values for samples and sample sites represent the most reliable indicator of rock hardness as measured by Schmidt hammer tests as these values are least likely to be affected by surface micro-roughness and micro-cracking. Plots of R-values against average erosion rates derived from cosmogenic nuclides indicate no correlation (Figure 5-13). There is no firm evidence from the Schmidt hammer data that rock hardness as measured by this method influences rates of glacial abrasion in gneisses in Uppland.

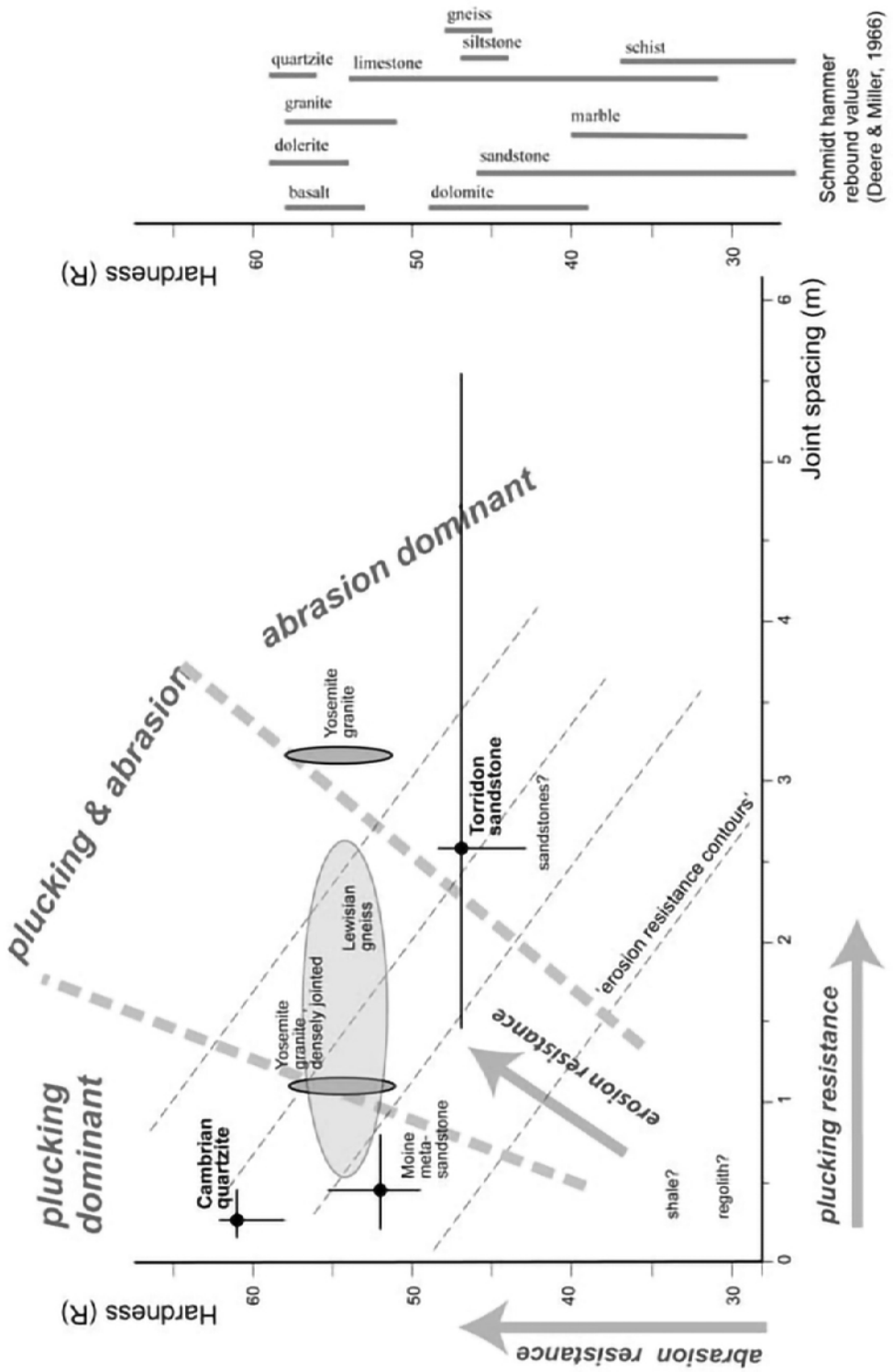

Figure A2-4. *R-values and glacial processes (from Krabbendam and Bradwell 2011).*

Appendix 3

Fracture data for cosmogenic nuclide sample sites

Fracture mapping was completed for 5 ×5 m areas on 12 outcrops sampled for cosmogenic nuclides in the Forsmark area (Section 4.2.4). A spreadsheet file (SKBdoc 1878017 – Supplementary information Appendix 3 TR-19-07.zip[*]) gives data for fracture spacing and length on these outcrops.

[*] Can be downloaded from www.skb.se/publications. Direct link: http://www.skb.com/publication/2493679/

Appendix 4

Cosmogenic nuclide data

This appendix contains cosmogenic nuclide sample data, cosmogenic nuclide measurements, and calculated exposure ages and erosion rates. The data is available in a spreadsheet file (SKBdoc 1878018 – Supplementary information Appendix 4 TR-19-07.zip[**]) which contains the following four spreadsheets:

A4-1 Cosmogenic nuclide measurement data (including blank measurements) and calculated ^{10}Be and ^{26}Al concentrations.

A4-2 Sample data (input for expage_sealevel.m and glacialE_sealevel.m; Appendix 5) and calculated ^{10}Be and ^{26}Al simple exposure ages and exposure age deviation from the expected simple exposure age taking shielding during glacial isostatic uplift through the water column into account (calculated using expage_sealevel.m).

A4-3 Simulated erosion data for all bedrock surface samples calculated using glacialE_sealevel.m.

A4-4 Simulated erosion data for the two road cut samples (NRD) calculated using glacialE_sealevel.m.

[**] Can be downloaded from www.skb.se/publications. Direct link: http://www.skb.com/publication/2493679/

Appendix 5

Cosmogenic nuclide calculation code

This appendix contains the functions used for cosmogenic nuclide exposure age calculations, erosion simulations, and interquartile range calculations. The functions are included in a file (SKBdoc 1878016 – Supplementary information Appendix 5 TR-19-07.zip[***]) which includes the following files:

expage_sealevel.m	Function for calculating simple exposure age and deviation from expected simple exposure age taking shielding during glacial isostatic uplift through the water column into account.
glacialE_sealevel.m	Function for simulation of glacial erosion taking shielding during glacial isostatic uplift through the water column into account (based on glacialE.m from expage-201902).
depthcalc.m	Function for calculating depth profile exposure ages (derived from expage-201902).

Associated files used by expage_sealevel.m, glacialE_sealevel.m, and depthcalc.m:

antatm.m
ERA40.mat
ERA40atm.m
glacialE_LR04.txt
interpolate.m
LSD_fix.m
LSDspal.m
make_consts_expage.m
Muons.m
Neutrons.m
PMag_Sep12.mat
P_mu_expage.m
Protons.m
rawattenuationlength.m
Reference.mat
SKB_RSL.txt
stone2000.m
XSectsReedyAll.mat

range_percentile.m	Function for calculating summed percentiles from a number of minimum-maximum ranges, assuming uniform probability distribution between the individual minimum and maximum values and equal weight of each individual minimum-maximum range.

All functions have been used in Octave 5.1. Most of the functions are expected to work with MATLAB but some difference has been noted for the function glacialE_sealevel.m which does not work properly when used in MATLAB.

[***] Can be downloaded from www.skb.se/publications. Direct link: http://www.skb.com/publication/2493679/

Arkitektkopia AB, Bromma, 2019

SKB is responsible for managing spent nuclear fuel and radioactive waste produced by the Swedish nuclear power plants such that man and the environment are protected in the near and distant future.

skb.se